UNIVERSITA' DEGLI STUDI DI VERONA

DEPARTMENT OF

Biotechnology

GRADUATE SCHOOL OF

Natural Sciences and Engineering

DOCTORAL PROGRAM IN

Biotechnology

Cycle / year: XXXIII/2017-2020

Genetic and phenotypic analysis of *Chlamydomonas* pale green mutants

S.S.D. BIO/04 Plant Physiology

Coordinator: *Prof. Matteo Ballottari*

Tutor: *Prof. Luca Dall'Osto*

Doctoral Student: *Valeria Vecchi*

Index

Abstract

In this thesis it was performed the characterization of different *Chlamydomonas reinhardtii* pale green mutants, both to investigate some important photosynthetic mechanisms and to identify mutations which result in enhanced productivity, to be exploitable for industrial applications. In the introduction chapters, it was first enlightened the importance of the study of photosynthesis in microalgae and the main challenges and constrains to deal with to increase biomass productivity. In this context different strategies were underlined, as the reduction of light harvesting antenna size to diminish the optical density, the bioengineering of the light stress response and the RuBisCO activity enhancement. Moreover, it was discussed about the novel approaches used to increase lipids and isoprenoid synthesis in different microalgae for both biofuels and industrial compounds production. Second, it was presented the potential of microalgae as feedstock for sustainable biofactories. It was discussed about the technical and biological challenges to make the largescale cultivation cost-effective and the genetic tools available to obtain highly productive strains. Third, it was enlightened the state of art of research on the so called pale green mutants in *Chlamydomonas*, strains characterized by a reduced optical density. These can be employed both for basic and applied research. Depending on the growth phenotype, indeed, these mutants could be promising candidate for large-scale industrial cultivation, or can be impaired in growth, thus useful to investigate important biological processes. In particular it was focused on CpSRP pathway defective strains, that are impaired in Light Harvesting Proteins (LHCs) insertion in thylakoids membrane, and on Chlorophyll a oxygenase (*cao*) mutants, that lost chlorophyll *b* and consequently have an altered peripheral antenna system. At the end of the introduction it was presented also the importance of genome editing tools and in particular of the CRISPR-Cas9 system to obtain specific mutants, avoiding side-mutations effects.

In the first part of the thesis, it was presented the *Chlamydomonas* pale mutant *as2.1*, characterized by an increased high light resistance and a faster growth in photoautotrophic conditions, compared to the WT. Sequencing data from this strain revealed a large deletion/insertion rearrangement including the gene *CpFTSY*, a soluble receptor belonging to the CpSRP pathway. Through a targeted mutagenesis by CRISPR-Cas9 genome editing approach, we aimed to understand if the growth advantage was related to the lack of CpFTSY . Unexpectedly, the CpFTSY-knock out (KO) mutants were unable to grow photoautotrophycally and showed a diminished abundance of LHCs and supercomplexes content than the control genotype; moreover, in mutant lines carotenoids biosynthesis was up-regulated, thus suggesting a higher susceptibility to excess light stress. To clarify these differences between *as2.1* and the genome edited strains, all these mutants were complemented by the CDS of *CpFTSY*, demonstrating that this gene is responsible for the high-growth phenotype of *as2.1*; however, characterization of complemented lines revealed *CpFTSY* was not the only actor involved in growth phenotype, rather a side mutation likely contributes to this feature.

The characterization of the first two *cpftsy* KO strains we obtained by genome editing revealed differences in LHC composition and in the relative abundance of monomeric vs. trimeric antennae, therefore additional KO lines were produced targeting this locus by a different sgRNA. The screening of several independent lines revealed a huge variation in the composition of the photosynthetic apparatus, that could tentatively be ascribed to an additional pathway or gene affecting the

biogenesis of antenna systems, that might possibly compensate the missing *CPFTSY* during the strain propagation.

cpftsy genome edited strains were also analyzed in comparison with *Chlamydomonas cao* mutants, to compare the effects of an impairment in LHCs insertion systems vs. chlorophyll biosynthesis, on the assembly of peripheral antenna system. Moreover, to understand which system is more important for light harvesting capacity, it was also produced a double mutant *cpftsy-cao* and the effects of the combined mutations were compared with those of the single ones. *cao* single mutants, despite a strong reduction in PSII functional antenna size and LHCII content, showed a remarkable resistance to excess light conditions, and a faster growth in photoautotrophic conditions compared to the wild type under saturating irradiances. *Chlorophyll b* biosynthetic pathway therefore appears crucial in the supramolecular organization of the photosystems, in the regulation of LHCII and LHCI relative abundance and in the structural stability of the LHCs, while its depletion does not significantly affect the core functionality. Instead, *cpftsy* single mutants were less affected in LHCII composition and in PSII functional antenna size than *cao* lines, however their photoautotrophic growth was impaired. Unexpectedly *CpFTSY* gene plays a minor role in regulating LHC system biogenesis, while the lower PsaA (PSI core-complex subunit) and CP47 (PSII core-complex subunit) contents suggested an involvement in the insertion of core proteins. The phenotype of *cpftsy-cao* double mutant is a cumulative result of the phenotypes of single mutants, thus it confirmed that *CAO* and *CpFTSY* regulate different steps of photosynthetic machinery biogenesis, and differently contributes to light-harvesting function.

The second part of the thesis is focused on the optimization of the CRISPR-Cas9 system in *Chlamydomonas*. The system was based on the direct electroporation of the purified Cas9 protein and the sgRNA in the cell. The first challenge was the identification of a method to purify the nuclease Cas9, with sufficient purity and quantity for experimental trials and working *in vivo*. Secondly, it was developed a method for synchronizing the cell, to allow tuning the relative frequency of non-homologous end joining (NHEJ) vs. homologous recombination (HR), according to experimental needs.

As appendix, two papers about the expression of hypertermophilic hydrolases in two different model organisms were presented. In *E.coli* were expressed two hemicellulase from *Thermotoga neapolitana* (endo-1,4-β-galactanase and α-L-arabinofuranosidase). They showed a higher activity compared to homologous isoforms present in other thermophilic organisms. These enzymes were combined with three additional *T. neapolitana* hyperthermophilic hemicellulases previously characterized, to form a promising highly thermostable hemi-cellulolytic blend. In the second paper, the cellobiohydrolase CBM3GH5 from *Caldicellulosiruptor saccharolyticus*, was expressed in the storage vacuole of *Nicotiana tabacum*. Cell wall-degrading enzymes are indeed toxic for plants if expressed in apoplast, while the storage vacuole expression maintained the proteins compartmented. Moreover, when extracted from plants the enzyme maintained its activity and both leaves and stems from transgenic plants were characterized by an improved temperature-dependent saccharification profile.

CHAPTER 1
Introduction: Potential and Challenges of Improving Photosynthesis in Algae

This paper was published in January 2020:

Vecchi V, Barera S, Bassi R, Dall'Osto L. Potential and Challenges of Improving Photosynthesis in Algae. Plants (Basel). 2020;9(1):67. Published 2020 Jan 3.

Abstract: Sunlight energy largely exceeds the energy required by anthropic activities, and therefore its exploitation represents a major target in the field of renewable energies. The interest in the mass cultivation of green microalgae has grown in the last decades, as algal biomass could be employed to cover a significant portion of global energy demand. Advantages of microalgal vs. plant biomass production include higher light-use efficiency, efficient carbon capture and the valorization of marginal lands and wastewaters. Realization of this potential requires a decrease of the current production costs, which can be obtained by increasing the productivity of the most common industrial strains, by the identification of factors limiting biomass yield, and by removing bottlenecks, namely through domestication strategies aimed to fill the gap between the theoretical and real productivity of algal cultures. In particular, the light-to-biomass conversion efficiency represents one of the major constraints for achieving a significant improvement of algal cell lines. This review outlines the molecular events of photosynthesis, which regulate the conversion of light into biomass, and discusses how these can be targeted to enhance productivity through mutagenesis, strain selection or genetic engineering. This review highlights the most recent results in the manipulation of the fundamental mechanisms of algal photosynthesis, which revealed that a significant yield enhancement is feasible. Moreover, metabolic engineering of microalgae, focused upon the development of renewable fuel biorefineries, has also drawn attention and resulted in efforts for enhancing productivity of oil or isoprenoids.

1.1 Introduction

1.1.1 Why Study Photosynthesis in Microalgae?

Oxygenic photosynthesis is the process by which photoautotrophs capture sunlight efficiently and converts it into organic molecules and biomass with an efficiency which is, instead, variable, depending on species and environmental conditions (Barber 2009). Oxygenic photosynthetic organisms, namely plants, algae and cyanobacteria, store into biomass the solar energy that reaches the Earth's surface at a rate of 120,000 terawatt/year (TW-y) (Stephenson et al. 2011). The current global energy demand of 14.9 TW-y, although it is projected to increase to 23.4 TW-y by 2030, yet falls greater than three orders of magnitude behind the solar energy on Earth. Therefore, exploitation of this potential by culturing photoautotrophs could satisfy at least part of the energy required for anthropic activities.

Among photosynthetic organisms, cyanobacteria and eukaryotic microalgae are the most promising feedstocks for the sustainable production of bulk bio-based materials such as food, feed, fuel and high-value metabolites; moreover, they can be used for wastewater treatments and in mitigation processes for CO_2-emissions (Benedetti et al. 2018). Algae can grow autotrophically, heterotrophically or mixotrophically in massive cultures for industrial purposes, in either open ponds or closed photobioreactors (PBRs). In contrast with land plants, algae do not require arable land and need far less fresh water for their growth. Moreover, the culture biomass devoid of stems and roots, which consumes metabolic energy, is fully photosynthetically active. Finally, biomass productivity is far less affected by the seasonal cycle (Benedetti et al. 2018). However, while microalgae represent a promising source of valuable bio-based products, an optimization of cultivation technologies is required in order to enhance growth rates and cell densities at saturation, thus making the process profitable (Georgianna and Stephen 2012). Indeed, productivity in photobioreactors is reduced by the inefficient light-to-biomass conversion, that leads to a photosynthetic efficiency significantly lower than the theoretical maximum of 9–10%, corresponding to ~80 g of biomass/m^2/day or 280 ton/ha/year (Melis 2009). In the industrial scale PBRs, algae light conversion yield falls between 3% and 5% (Melis 2009). Filling the gap that originates from light-use inefficiency, and that makes the controlled cultivation of microalgae still far from being commercially viable, is therefore essential. Comprehension of the mechanism regulating photosynthesis will allow researchers to identify the targets for genetic improvement and ultimately to enhance biomass yield, thus counterbalancing the costs for cultivation systems and downstream biomass processing.

1.1.2 Microalgal Species of Interest for Research on the Regulatory Mechanisms of Photosynthesis

Eukaryotic microalgae are classified according to their pigment content into *Rhodophyta* (red algae), *Chrysophyceae* (golden algae), *Phaeophyceae* (brown algae) and *Chlorophyta* (green algae) (Guiry 2012). *Chlorophyta* includes most genera currently employed for biotechnological applications (Benedetti et al. 2018). The best studied green microalgal species is certainly the model organism *Chlamydomonas reinhardtii*. The major reasons for this preeminent position in photosynthesis research resides in its haploid genetic organization, allowing the mutant phenotypes to be detected at the first generation without the need for segregation; moreover, sexual reproduction can be induced by modulating the growth conditions, it can be transformed in all its genomes (nuclear, chloroplastic and mitochondrial), and it is mixotrophic, thus allowing for the isolation of mutants with impaired photosynthesis (Harris 2001). Finally, a short life cycle makes it a good platform to study light-to-biomass conversion efficiency and to optimize photosynthesis (Grossman 2000). Besides *Chlamydomonas*, genetic tools have been developed for other species of green algae, which have an exploitation potential for high-value chemicals production (Benedetti et al. 2018). Among those, *Chlorella zofigiensis* accumulates high-value carotenoids and has high biomass and lipid productivity (Ip and Chen 2005); several species belonging to the genus *Chlorella* are of interest for human health supplements (García et al. 2017)and biofuel production (Guccione et al. 2014). Moreover, domestication strategies have been developed in *C. sorokiniana* to generate mutant strains with enhanced biomass productivity (Cazzaniga et al. 2014). In other *Chlorophyta*, limitations related to the lack of optimized genetic tools still exist, and particularly concern strains relevant for industrial applications: *Dunaliella salina*, extensively cultured in open ponds and photobioreactor for β-carotene (Xu et al. 2018)and lipids production (Ahmed et al. 2017) and *Haematococcus pluvialis*, an

industrial source of astaxanthin (Shah et al. 2016). Members of the *Nannochloropsis* genus, and the diatom *Phaeodactylum tricornutum*, all belonging to Heterokonta, are obligate photoautotrophs that have been intensively characterized, and are also well-developed models for studying microalgal molecular physiology and genetic engineering. The photosynthetic mechanisms of different species such as *Nannochloropsis gaditana*, *N. oceanica* or *N. oculata* have been investigated because of their unique photosynthetic architecture among Heterokonta, characterized by Chl *a* as the only primary pigment and high content of violaxanthin and vaucheriaxanthin (Basso et al. 2014); moreover, light regimes and nutrient starvation induce rapid *triacylglycerols* (TAGs) biosynthesis in these oleaginous strains, that are therefore considered promising for biodiesel production (Simionato et al. 2013). *Phaeodactylum tricornutum*, a species with a fully sequenced genome, is interesting for its high lipid content and for a peculiar light-harvesting system, binding the xanthophyll fucoxanthin (Fx), Chls *a* and *c* (Bowler et al. 2008; Wang et al. 2019).

In this review we mainly focused on green microalgae and diatoms, citing other species whenever it is considered relevant.

1.2 Photosynthesis

In both green algae and higher plants, the process of oxygenic photosynthesis can be divided into light and dark phases. In the former, photons are absorbed and utilized to drive Linear and Cyclic Electron Transfer (LET and CET, respectively), to form adenosine triphosphate (ATP) and the reduced form of Nicotinamide adenine dinucleotide phosphate (NADPH), which power the Calvin–Benson–Bassham cycle to produce carbohydrates in the dark phase (Figure 1.1).

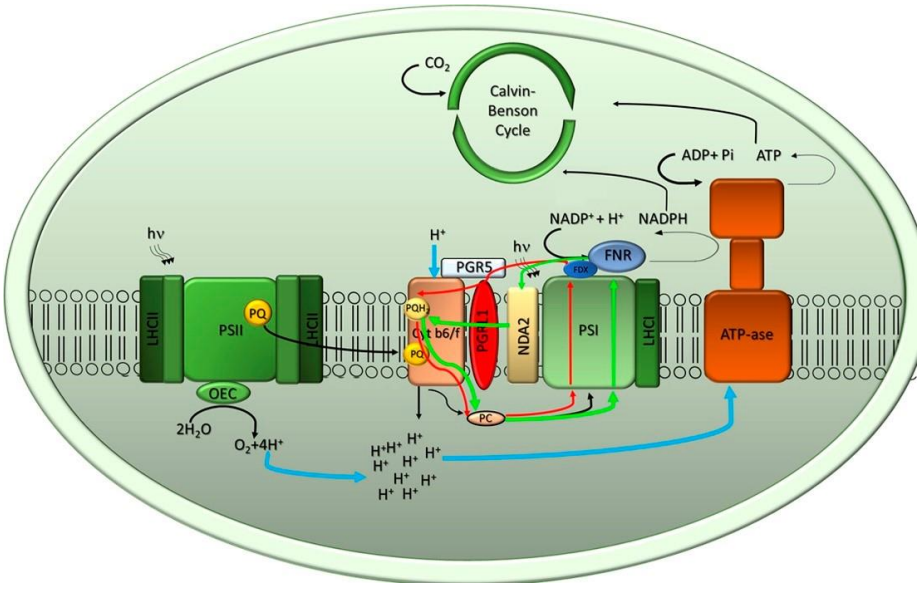

Figure 1.1 Schematic representation of photosynthetic electron transport. Arrangement of Photosystem I (PSI), Photosystem II (PSII), cytochrome b6f and adenosine triphosphate (ATP) synthase complexes within the thylakoid membranes is shown. The light-driven water splitting reaction leads to O_2 evolution and originates linear electron transport (LET), indicated with black arrows, from water to nicotinamide adenine dinucleotide phosphate ($NADP^+$), which is coupled to proton translocation from stroma into the luminal side of thylakoids during the light phase. The electrochemical gradient formed is used by the ATP synthase to produce ATP from Adenosine diphosphate (ADP) and Pi in the stroma. The NADPH and ATP formed during the light phase drive the

Calvin–Benson–Bassham cycle reactions in the stroma. Two pathways of cyclic electron transport (CET) around PSI are indicated with red (Ferredoxin-dependent pathway) and green (NDA2-dependent pathway) arrows, respectively.

1.2.1 The Light Phase of Photosynthesis

The linear electron transport (LET) reaction starts with the water-splitting complex Photosystem II (PSII), that captures sunlight and utilizes excitation energy to oxidize water molecules into protons (H^+) and molecular oxygen (O_2). The electrons removed from water are transferred via the Plastoquinone (PQ) pool to the Cytochrome b_6f (Cyt b_6f) complex and then utilized to translocate protons across the thylakoid membrane. The cytochrome *f* subunit reduces the soluble electron carriers' plastocyanin (PC), the electron donors of PSI. Absorption of photons by Photosystem I (PSI) promotes oxidation of its reaction centre (RC) P700. The electron removed by the oxidation event finally reduces ferredoxin (FDX) and the electron hole in $P700^+$ is filled by electrons from PC (Nelson and F Yocum 2006), while at the stromal side the ferredoxin $NADP^+$ reductase (FNR) transfers the electrons from FDX to $NADP^+$ to yield NADPH + H^+. This electron transport is coupled to the build-up of a proton gradient across the thylakoid membrane, with contributions from water splitting and PQH_2 oxidation by the Cyt b_6f. The return of protons to the stromal compartment is coupled to ATP synthesis (Nelson and F Yocum 2006).

The ATP:NADPH ratio is regulated by modulating LET and CET, the latter being the reaction which reduces PQ with excess reducing equivalent from FDX or NADPH (Munekage et al. 2004) (Figure 1.1). In *C. reinhardtii*, two CET pathways around PSI are suggested: The NADPH-dependent pathway involves type II NAD(P)H-dehydrogenase (NDA2), which recycles electrons from PSI into the intersystem chain via NADPH (Jans et al. 2008). The secondary FDX dependent pathway is mediated by two proteins: PROTON GRADIENT REGULATION 5 (PGR5) and PGR5-LIKE PHOTOSYNTHETIC PHENOTYPE 1 (PGRL1) (Jokel et al. 2018) (Figure 1.1).

Light-Harvesting Systems: PSI-LHCI and PSII-LHCII Supercomplexes Organization in Microalgae

Capture of light energy by both photosystems, which drives charge separation in RC and fuels LET and CET, is enhanced by pigment-binding proteins, the light-harvesting complexes (LHC). Various LHCs form the peripheral antenna system in both photosystems (Dall'Osto et al. 2015). While RC subunits were strongly conserved, the antenna complexes diversified through evolution (Ballottari et al. 2012; Dall'Osto et al. 2015), yet maintained a common architecture (Ben-Shem et al. 2003; Liu et al. 2004). The most represented member is the major antenna LHCII, a 22 kDa polypeptide which binds 14 chlorophylls (Chl) *a* and *b*, and four xanthophylls (Lutein, Neoxanthin, Violaxanthin and, upon high light exposure, Zeaxanthin) (Dall'Osto et al. 2013)(LHC)-like antenna proteins, which were present in a cyanobacterial ancestor, carried out photoprotective functions (Rochaix and Bassi 2019), while they later evolved into isoforms fulfilling either light-harvesting or energy-dissipative responses. The LHC superfamily consists of some 30 proteins, the most conserved being the subunits of PSI and PSII through the *Chlorophyta* (Alboresi et al. 2008), which have pre-eminently a light-harvesting role, while the light-harvesting complex stress-related (LHCSR) subunits have an energy-dissipative role, enabling photoprotection in excess light (EL) conditions through the non-photochemical quenching (NPQ) mechanism (Peers et al. 2009)(see Section 1.2.3). In *C. reinhardtii*,

the LHCI subunits, forming the PSI peripheral antenna system, and the monomeric subunits of the PSII supercomplex Lhcb4 (CP29) and Lhcb5 (CP26), are the most conserved antenna proteins. Trimeric LHCIIs, the major antennae of photosynthetic membranes of *C. reinhardtii*, are encoded by *Lhcbm* genes (*Lhcbm1–9*).

PSII-LHCII

The core complex of PSII is highly conserved in all organisms and consists of 40 different protein subunits. The RC is composed by subunits D1, D2 and cytochrome b_{559} and hosts P680, the PSII RC where the primary charge separation event occurs. Light-dependent transfer of reducing equivalents to PQ leads to $P680^+$ formation. The positive charges accumulated by four events of charge separation drive the water splitting reaction within the oxygen evolving complex (OEC), composed by the extrinsic polypeptides PsbO, PsbQ, PsbP and PsbR. Chl *a*- and β-carotene-binding inner antennae CP43 and CP47 enlarge the light harvesting capacity of the supercomplex. The PSII core is organized into dimers (C2), which, in turn coordinate a peripheral antenna system (see above). In higher plants, this LHC system is made of two layers: The inner, composed by the monomeric LHC proteins CP24, CP26 and CP29 (Miloslavina et al. 2011), which are bound, respectively, to the CP43 and CP47 core subunits, and the outer layer is made by the trimeric LHCII complexes (Su et al. 2017). In *C. reinhardtii*, the largest PSII-LHCII supercomplex characterized contains three LHCII trimers (named S, M and N) per monomeric core, and it is characterized by the absence of the monomeric antennae protein CP24. In mosses and higher plants, the N trimer has been substituted for by an additional monomeric LHC, CP24 (Lhcb6), LhcbM1, LhcbM2/7 and LhcbM3, which are the major components of LHCII trimers in the PSII supercomplex of *C. reinhardtii* (Drop et al. 2014)(Figure 1.2). Recently, Shen and co-workers reported a cryo-electron microscopy structure of a complete, $C_2S_2M_2N_2$-type PSII–LHCII supercomplex from *C. reinhardtii* at 3.37-A resolution. The high-resolution structure allowed not only locating the LHCII trimers in the complex, but also the plausible energy transfer pathways from the peripheral antennae to the PSII core. Moreover, a number of small core subunits (PsbE, PsbF, PsbH, PsbI, PsbJ, PsbK PsbL, PsbM, PsbTc, PsbW, PsbX and PsbZ) has been elucidated (Shen et al. 2019).

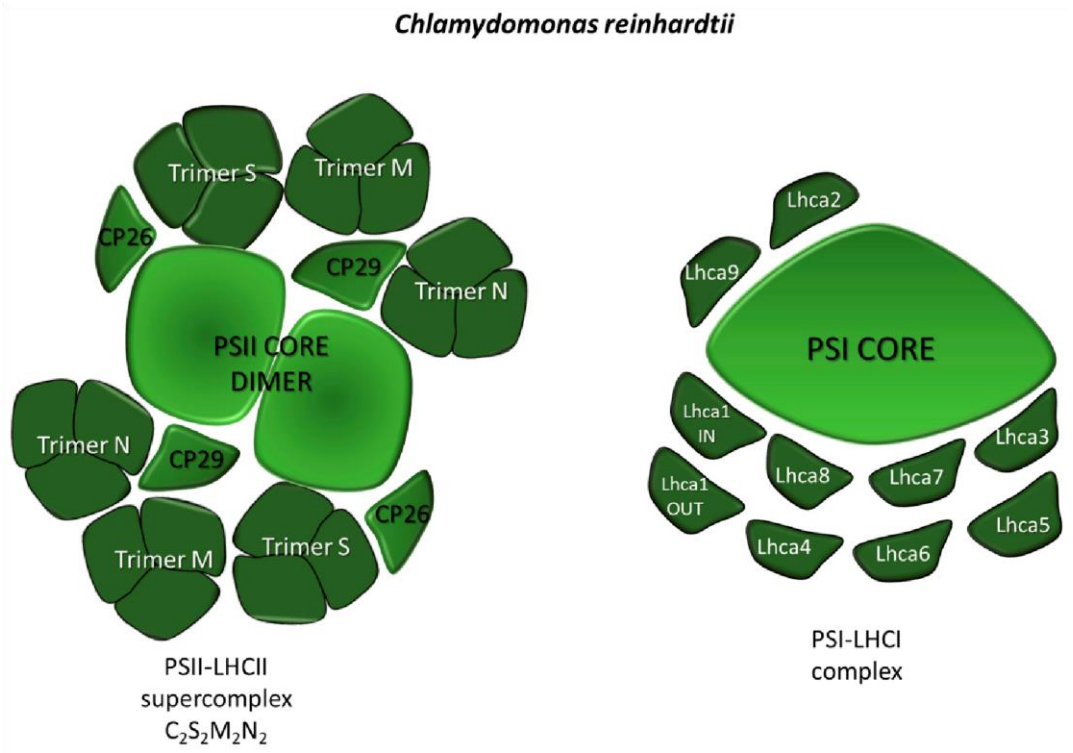

Figure 1.2 Supramolecular organization of PSII-LHCII and PSI-LHCI supercomplexes in the model alga *Chlamydomonas reinhardtii*. The schematic representations are based upon data from (Su et al. 2017)for PSII-LHCII and from (Drop et al. 2011)for PSI-LHCI. The core complexes of both PSs are shown in light green while the antenna complexes are shown in dark green.

PSI-LHCI

The organization of PSI-LHCI of *C. reinhardtii* was investigated by negative stain electron microscopy and single particle analysis, which revealed that the supercomplex is larger but less stable than that from higher plants. The Lhca1-9 antenna proteins loosely bind to the core, where this can explain the large variation in antenna composition of PSI-LHCI from *C. reinhardtii* found in the literature. The isolation of several PSI-LHCI supercomplexes with different antenna size allowed to precisely determine the position of Lhca2 and Lhca9 proteins and led to a model of whole PSI-LHCI supercomplex antenna organization (Drop et al. 2011). Moreover, a megacomplex constituted by a Cyt b_6f interacting with the PSI-LHCI complex was identified under anaerobic conditions, a treatment that promotes CET in *C. reinhardtii* (Steinbeck et al. 2018). More recently, the structure of *C. reinhardtii* PSI–LHCI supercomplex has been solved by cryo-electron microscopy, showing that up to ten LHCIs are associated with the PSI core (Su et al. 2019) (Figure 1.2).

1.2.2 The Dark Phase of Photosynthesis

In green algae and higher plants, the carbon dioxide reduction occurs in the dark phase of photosynthesis, which also occurs in the light, and is powered by the NADPH and ATP from the light phase. The whole process can be described with the general reaction:

$$2NADPH + H + 3ATP$$
$$\xrightarrow{\text{Enzymes}}$$
$$CO_2 + 4H^+ + 4e \longrightarrow (CH_2O) + H_2O$$

The entire process of carbon fixation, discovered by Calvin, Benson and Bassham in the early 1950s, requires two molecules of NADPH and three of ATP for each CO_2 fixed into sugars. This energy complement is supplied by the absorption of eight photons in the light phase.

Dark Reactions of Photosynthesis: The Calvin-Benson-Bassham Cycle

The conversion of CO_2 into sugar (or other compounds) is performed by three distinct phases (carboxylation, reduction and regeneration phases) within the Calvin–Benson–Bassham cycle (CBBc) (Figure 1.3). During the carboxylation phase, one molecule of CO_2 is added to the 5-carbon sugar ribulose bisphosphate (RuBP) by the enzyme ribulose bisphosphate carboxylase/oxygenase (RuBisCO) to form two molecules of phosphoglycerate (3-PGA). The enzyme is controlled by the RuBisCO-activase, which carboxylates a Lys residue in the presence of the substrate CO_2, thus preventing wasteful reaction with O_2 under CO_2-depleted conditions. The subsequent reduction phase catalyses the conversion of 3-PGA into 3-carbon (Triose-P) products glycerhaldeide-3-P (G3P) in two steps, by consuming ATP and NADPH. The regeneration phase restores the initial RuBP reactant from Triose-P, through a complex series of reactions which involves eight distinct enzymes (Figure1.3), including transketolase and transaldolase, yielding 5-carbon sugars from 6-carbon plus 3-carbon sugar intermediates, and the sedoheptulose-1,7-bisphosphatase that catalyses the de-phosphorylation of sedoheptulose-1,7-bisphosphate to yield sedoheptulose-7-phosphate. sedoheptulose-1,7-bisphosphatase activity shows a strong correlation with the rate of photosynthetic carbon fixation, thus controlling carbon flux (Harrison et al. 1997). Under EL conditions, the RuBisCO activity rate becomes limiting, and the rate of synthesis of ATP/NADPH from light reactions exceeds their use by CBBc. Depletion of ADP limits ATPase activity in protons' return to the stroma compartment, leading to lumen iper-acidification and triggering excess energy dissipation reactions. This is further enhanced by NADPH accumulation, since CET activation further acidifies the lumen.

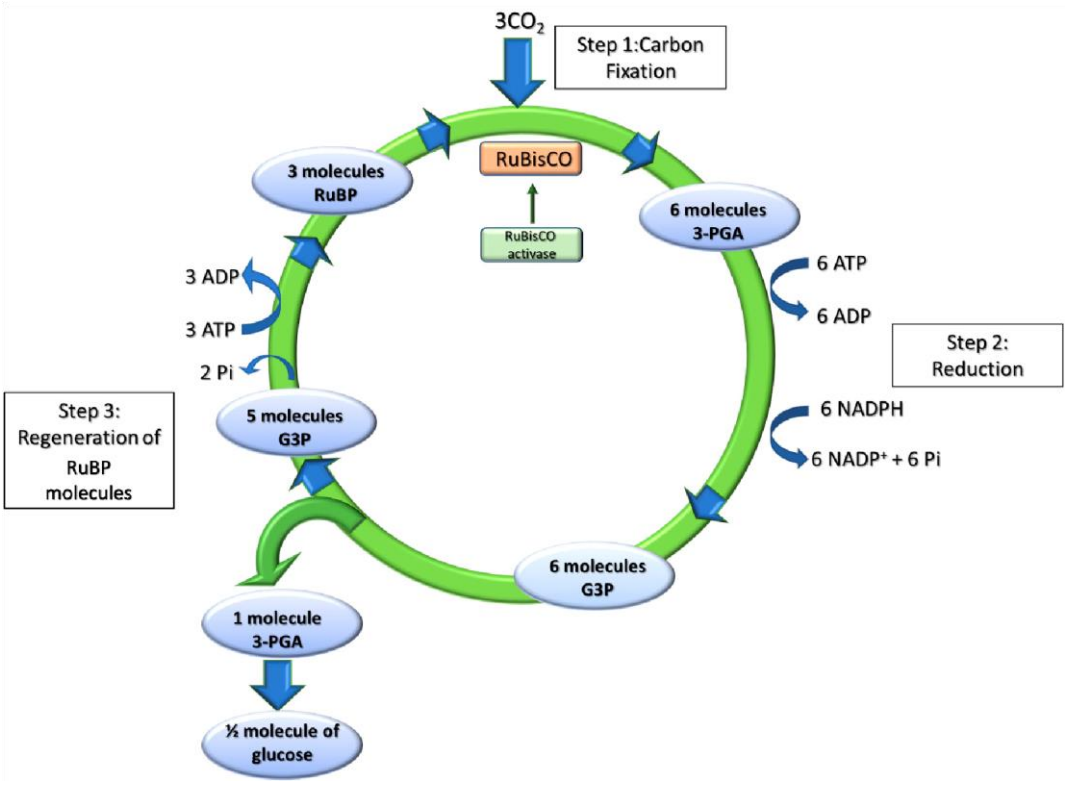

Figure 1.3. The Calvin–Benson–Bassham cycle (CBBc) reactions. The CBBc has three stages. In stage 1, the enzyme RuBisCO incorporates 3 CO_2 molecules into the 5-carbon sugar ribulose-1,5-bisphosphate (RuBP) to form 6 molecules of 3-phosphoglycerate (3-PGA). In stage 2, 6 molecules of 3-PGA are converted into 6 molecules of Glyceraldehyde-3-P (G3P) by using 6 molecules of ATP and 6 molecules of NADPH as reducing power. In stage 3, RuBP is regenerated so that the cycle can continue. Stage 3 includes a complex series of reactions combining 3-, 4-, 5-, 6-, and 7-carbon sugar phosphates, which are not explicitly shown in the diagram.

RuBisCO

In cyanobacteria and plants, along with red, brown and green algae, RuBisCO is found as a large protein complex with a hexadecameric quaternary structures consisting of eight 55-kDa large (L) subunits and eight 15-kDa small (S) subunits (L_8S_8). The RuBisCO crystal structure was determined on complexes purified from *Spinacia oleracea*, *Nicotiana tabacum* (Curmi et al. 1992) and the cyanobacterium *Synechococcus* (Newman et al. 1993). In green algae the crystal structure of *C. reinahardtii* at 1.4 A resolution (Taylor et al. 2001) showed high similarity to the L_8S_8-RuBisCO enzyme assembly from *Spinacia oleracea*. Since RuBisCO evolved in atmosphere with a higher concentration of CO_2 respect to the current one, it has low affinity for CO_2 and low substrate specificity. Thus, it accepts oxygen as substrate at low CO_2, which leads to the loss of fixed carbon as a consequence of feeding a photorespiratory cycle with phosphoglycolate. Although the photorespiratory (C2) cycle recovers part of phosphoglycolate into phosphoglycerate, this reduces the overall light-to-biomass conversion efficiency. In both green algae and higher plants, the ability to fix CO_2 depends in part upon the properties of RuBisCO: While RuBisCO isolated from a few species of red algae have three times higher substrate specificity vs. that from C3 crop species (Uemura et al. 1997), in most of photoautotrophs RuBisCO is operating at no more than 30% of its capacity under standard atmospheric conditions (21% O_2, 0.04% CO_2). Indeed, the chloroplastic abundance of this protein is extremely high. To overcome this drawback, many photosynthetic

organisms have developed different systems to increase the level of CO_2 at the catalytic site in order to enhance the carboxylation while disfavouring the oxygenation reaction. Microalgae absorb HCO_3^- ions, which must be converted to CO_2 before the carbon fixation takes place. Moreover, in green algae RuBisCO is compartmentalized into carbon-concentration sub-compartments of the chloroplast, called pyrenoids, which have been purified from *C. reinhardtii* (Kuchitsu et al. 1991) and shown they consist primarily of RuBisCO. In other algae types including red algae, carboxysomes are present as large molecular architectures including carbonic anhydrase together with RuBisCO, where CO2 level is increased from carbonic anhydrase activity to limit photorespiration and enhance photosynthetic yield (Ryan et al. 2019).

1.2.3 Dynamics of the Photosynthetic Apparatus in Response to Environmental Conditions: Photoprotective Mechanisms

During evolution, photosynthetic organisms are said to have adapted to a wide range of habitats with an extreme variability of light irradiances, water and nutrient abundance and temperature. Abiotic stresses such as drought or nutrient deprivation easily decrease the maximum photosynthetic yield of algae, thus environmental conditions can exacerbate EL stress. In this condition, the energy absorbed exceeds the rate of its utilization by downstream reactions, increases the concentration of Chl-excited singlet states (^{1}Chl *), thus the probability of Chl triplet states (^{3}Chl *) formation together with the release of singlet oxygen ($^1O_2$), a reactive oxygen species (ROS). It comes that a mechanism to dissipate the excitation energy absorbed in excess, is required. Experiencing EL conditions activate the Non-Photochemical Quenching (NPQ) process. This can be experimentally observed as a decrease of fluorescence emitted by PSII upon exposure to over-saturating light. NPQ arises from a number of processes in the thylakoid membranes, and several major components of NPQ can be identified based on the kinetics curves of the relaxation of PSII fluorescence (Horton et al. 1996). The fastest component, immediately triggered upon exposure to EL, is the energy-dependent quenching (qE), which relaxes within approx. one minute upon switching actinic light off.

State transitions (STs) represent changes in the relative antenna sizes of photosystems (Allorent et al. 2013), however although this fluorescence decline (called qT) has been included in NPQ, it is caused by PSI RC activity, and therefore is of the photochemical type. An additional quenching component, that rises and relaxes at a longer time scale than qE, is called qZ (Dall'Osto et al. 2005): This is found in some algae species in which a zeaxanthin-dependent enhancement of NPQ is observed (Quaas et al. 2015). The slowest component, named qI, develops under long lasting (several hours) high light stress (Horton et al. 1996).

The qE response is dependent on a low lumenal pH and requires LhcsR, Chl-xanthophyll-binding proteins found in eukaryotic algae and mosses (Alboresi et al. 2010) and is replaced by the non-pigmented protein PsbS in higher plants (Li et al. 2000; Fan et al. 2015). In *C. reinhardtii*, LhcsR proteins are encoded by three highly homologous genes *LhcsR1*, *LhcsR3.1* and *LhcsR3.2*, while PsbS by two closely linked *PsbS1* and *PsbS2* genes. Both PsbS and LhcsR proteins harbour protonatable residues exposed to the luminal side, which detect low pH and activate the heat dissipation of energy absorbed in excess (Li et al. 2004; Ballottari et al. 2016). In *C. reinhardtii*, accumulation of gene products involved in qE is induced by signals such as high light, blue light and UV light via

increased expression of genes encoding for LhcsR and PsbS. By a forward genetics approach, SPA1 and CUL4 have been identified as components of a putative green algal E3 ubiquitin ligase complex, as critical factors in a signalling pathway that controls light-regulated expression of the dissipative response. The accumulation of two isoforms of LhcsR protein LhcsR1 and LhcsR3 is different. Recently, it has been found that the expression of LhcsR1 protein is constitutive, while the accumulation of LhcsR3 is increased under EL conditions and depends on the activation of the CAS (Petroutsos et al. 2011; Gabilly et al. 2019) calcium sensor. Upon protonation, *C. reinhardtii* LhcsR subunits switch to a quenching conformation. The dynamics of LhcsR proteins transition between unquenched and quenched conformations has been studied in the moss protein LhcsR1 (Pinnola et al. 2016; Kondo et al. 2017; Kondo et al. 2019), showing a 50-fold decrease in lifetime from 3.7 ns lifetime to 80 ps. The physicochemical mechanisms involved were identified to be dual: (i) the transient formation of carotenoid radical cation, thermally recombining to ground state (Holt et al. 2005; Ahn et al. 2008; Bonente et al. 2011), and (ii) the energy transfer from a Chl *a* to lutein S1 state, which thermally relaxes to the ground state within approx. 10 ps (Holt et al. 2005). Thus, the two types of quenching mechanism reported for plants, as localized, respectively, in two different types of LHC subunits (Holt et al. 2005; Ruban et al. 2007; Fuciman et al. 2012), appear to be both active within the single LhcsR subunit (Pinnola et al. 2016). Under EL conditions, lumen acidification triggers the so-called xanthophyll cycle, which involves the xanthophylls violaxanthin (Vio) and zeaxanthin (Zea), and consists of a light-dependent, rapid and reversible de-epoxidation of Vio to Zea. The reaction is catalysed by VDE (violaxanthin de-epoxidase). This enzyme is luminal in plants where it is activated by acidification, while it is stromatic in *Chlamydomonas* (Li et al. 2016b); the xanthophyll cycle of intact *Chlamydomonas* cells is inhibited by the uncoupler nigericin, indicating that the activation of this stromal enzyme also requires the build-up of a pH gradient in EL. The amplitude of qE in plants correlates with the level of Zea though its binding to specific LHC targets, in *C. reinhardtii* NPQ amplitude is Zea-independent (Niyogi 1999). The qT component of NPQ is dependent on ST, i.e., the mechanism of LHCII relocation between PSs, which compensates for PSI/PSII excitation imbalance and optimizes photosynthetic electron transport in response to the light conditions. PSII over-excitation reduces PQ to PQH_2, and activates a thylakoid protein kinase (STT7 in green algae and STN7 in higher plants) which, in turn, phosphorylates LHCII, and leads to its reversible association with the PSI-LHCI complex (Shapiguzov et al. 2016). In *C. reinhardtii*, most of LhcbM proteins get phosphorylated upon ST, including the monomeric antennae CP29 and CP26, which are recruited as a supplementary antenna for PSI. While this mechanism is widespread in green photosynthetic organisms, in plants the amplitude of ST is lower than in *C. reinhardtii*, possibly indicating differences in the regulation of photosynthetic electron transport. The term “qI” refers to all quenching processes relaxing slowly (>10 min), and comprises multiple processes contributing to the down-regulation, inactivation and damaging of PSII. One of the components of the slowly-relaxing NPQ correlates with the synthesis of Zea, was shown as ΔpH-independent, and is possibly related to the binding of Zea to specific antenna proteins (Gilmore and Ball 2000). A second component of NPQ is related to photoinhibition and is enhanced upon prolonged over-excitation. It consists into a light-induced reduction of the quantum yield of PSII, due to the photodamage of the RC protein D1. Thus, quenching relaxation reflects the kinetic of RC repair cycle (Nelson and F Yocum 2006).

The NPQ mechanism is highly relevant for the maintenance of the photosynthetic efficiency which contributes to acclimation to the different light environments. The relative contribution of each of

the NPQ components changes between organisms and irradiances: qE activates based on sudden increases in light intensity, while ST responds to changes in the light spectrum under low light conditions. Thus, LhcsR protein function is synergically with other photoprotective mechanisms, such as CET and ST in shaping the fast response to environmental conditions. Long-term stresses occur on timescales of days and weeks. Photoacclimation mechanisms to such changes involve a rearrangement at the level of chloroplast protein and lipid composition yielding into an adjustment of the stoichiometry of photosynthetic complexes through the modulation of gene expression and synthesis/degradation of individual chloroplast components. A major component of response to excess light consists into down-modulating the size of the PSII antenna (Anderson et al. 1995), and enhancing the stoichiometry of the Cyt b_6f complex, ATPase and RuBisCO with respect to PSII RC. In green algae, EL down-regulates LHCII and LHCI genes transcription, while when under limiting irradiance, the opposite response was shown (Escoubas et al. 1995; Durnford et al. 2003). In *C. reinhardtii* the increase in the Chl *a*/*b* ratio is consistent with decreases in the amount of both LHCI and LHCII in EL (Durnford et al. 2003; Bonente et al. 2012; Mettler et al. 2014); EL stress also induces an accumulation of proteins involved in the NPQ response, such as LhcsR3 in *C. reinhardtii* (Ballottari et al. 2007; Bonente et al. 2012). Moreover, the LhcbM isoforms are expressed differentially depending on growth conditions, which suggests a specific role of different LHC complexes in PSII organization and chloroplast photoprotection (Elrad et al. 2002; Ferrante et al. 2012; Grewe et al. 2014). LhcbM9 is only expressed in stressing conditions and binds to PSII–LHCII complexes, where it protects PSII by inducing an energy-dissipative state with reduced $^1O_2$ formation (Grewe et al. 2014). In *C. reinhardtii*, the transcriptional regulation of *LhcbM* genes is mediated by nucleic acid binding 1 protein (NAB1), a cytosolic protein that prevents the translation of LhcbM by sequestering the corresponding mRNAs into translationally silent ribonucleoprotein complexes (Mussgnug et al. 2005) (Figure 1.4). The relative abundance of NAB1 is regulated by nutrient abundance: Under CO_2 starvation, which hampers the activity of the CBBc, up-regulation of NAB1 promotes an antenna size reduction, thus alleviating the excitation pressure on PSs.

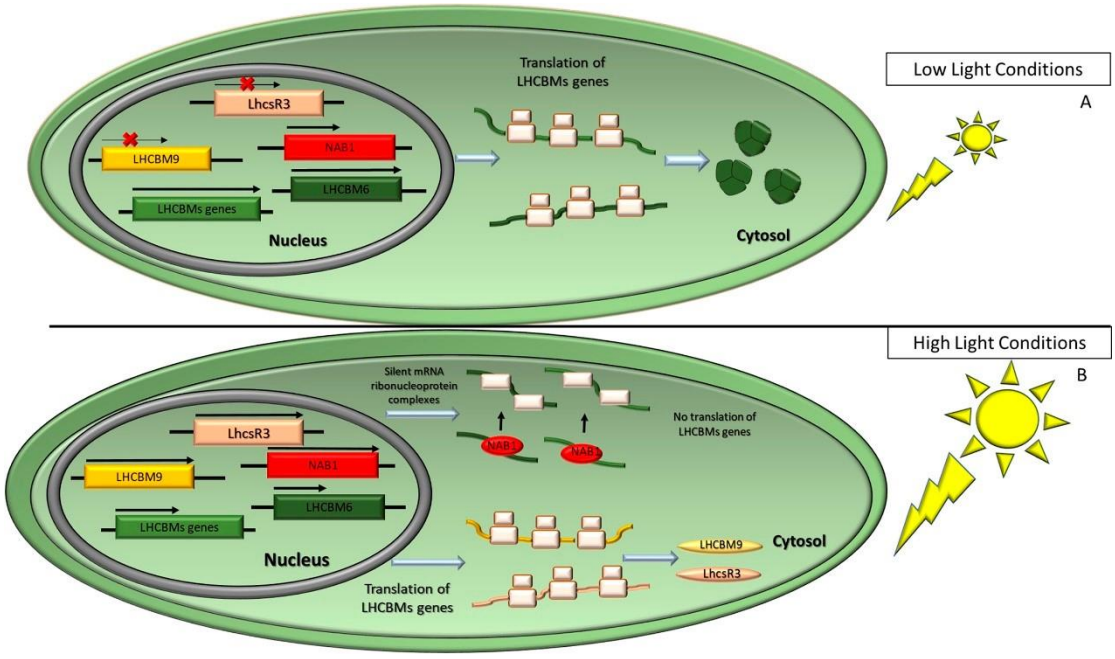

Figure 1.4. Scheme of long-term control mechanisms regulating light harvesting antenna size, as described in the model alga *C. reinhardtii*. (A) In low light conditions, carriers of the photosynthetic electron transport chain are oxidized, and all nuclear genes encoding LhcbMs isoforms associated to the PSII are expressed, except for the isoform 9. LhcbM-encoding mRNAs are translated in the cytosol, then targeted to the chloroplast and inserted in the thylakoid membranes. Under low light conditions, the translational repressor NAB1 is in a less active state. (B) In excess light conditions, ATP and NADPH produced by the light reactions exceed their consumption rate by the CBBc, and the overexcitation of PSII results in the release of reactive oxygen species (ROS). To alleviate excitation pressure, a remodelling of the antenna system is induced by slowing down the transcription of LhcbM genes. Once the translation of NAB1 is promoted, this subunit interacts with LhcbM-encoding mRNAs to form silent mRNA-ribonucleoprotein complexes. In contrast to all other isoforms, the expression of LhcbM9 and LhcsR3 proteins are induced.

1.3 Improving Photosynthetic Yield

1.3.1 Light Harvesting Antenna as Target to Reduce Optical Density in Mass Culture

When grown under mass culture, a condition typical of industrial PBRs, microalgae undergo a progressive drop in productivity as the cell density gradually increases. This can be mainly ascribed to an inhomogeneous light distribution within the culture, due to its high optical density: In this condition, the surface layers of the culture easily reach the saturation of photosynthesis (and possibly photoinhibition), while the inner layers are light-limited. Such steep gradient in light penetration results in a low productivity of the system. Optimization of the light transmittance within the culture volume was proposed as a strategy to alleviate these constraints. A bioengineering approach to decrease the Chl content per cell, thus minimizing the light absorption and enabling a larger fraction of cell suspension to contribute to overall productivity, was first developed in the model alga *C. reinhardtii*. Truncated light-harvesting antenna (*tla*) mutants were obtained by random DNA insertional mutagenesis and selection by Chl fluorescence imaging. Mutant *tla1* showed a significant reduction of Chl content per cell and a lower functional antenna size of both PSI (−50%) and PSII (−65%) vs. wild type (WT) (Polle et al. 2003). In batch culture, *tla1* cells yielded a higher P_{max} at saturating irradiances and higher light-to-biomass conversion efficiency with respect to the WT strain (Polle et al. 2003). Gene *TLA1* was found to participate in the mechanism of Chl antenna size regulation, and indeed its over-expression resulted in a larger antenna size for both photosystems and lower Chl *a*/*b* ratio with respect to WT, while its down-regulation by RNAi resulted in the opposite phenotype (Mitra et al. 2012). Strain *tla2* was mutated in the gene encoding the chloroplast-localized signal recognition particle (CpSRP) receptor CpFTSY, whose deletion was responsible for a pale-green phenotype and a lower Chl *a*/*b* ratio than WT (Kirst et al. 2012). Components of the CpSRP complex, involved in the proper folding of LHCs and targeting of these proteins to the thylakoids, are therefore promising molecular targets to achieve a substantial reduction in Chl antenna size without impairing the photosynthetic electron transport (Figure 1.5) (Kirst and Melis 2014). Moreover, CRISPR-Cas9 technology was recently shown as a reliable approach by which to produce *tla* mutants(Baek et al. 2016; Jeong et al. 2018). Pale-green mutants were obtained in species other than *C. reinhardtii* (Figure 1.5): *N. gaditana* and *C. sorokiniana* mutant strains with truncated antenna were isolated by random mutagenesis and phenotypic selection; once

characterized, they showed higher photosynthetic efficiency than WT and improved photoresistance under EL conditions, in both lab-scale and industrial-scale PBRs (Cazzaniga et al. 2014; Perin et al. 2015). An additional molecular target expected to affect antenna size was *CAO* (encoding for Chlorophyllide *a* oxygenase) (Figure 1.5), encoding for the enzyme responsible for Chl *a* → Chl *b* conversion (Tanaka et al. 1998). In *Chlamydomonas*, both insertional knock-out and point mutations on *CAO* impaired the biogenesis of antenna systems, which were affected in different ways depending on the light conditions (Bujaldon et al. 2017). Moreover, CAO expression was modulated by RNAi, which resulted in knock-down mutants showing a lower Chl *b* content. Therefore, by tuning the Chl *b* relative abundance, corresponding regulation of antennae size can be obtained, and a reduced optical cross-section improves the growth and photosynthetic rate under high light conditions, without impairing other regulatory mechanisms such as ST and NPQ (Perrine et al. 2012).

Additional perspectives towards enhancing the light use efficiency in algae are likely to be developed in the future based on the emerging functional diversity of individual Lhcbm proteins which have been reported to be involved in state1–state2 transitions, NPQ and/or in sustained photoprotection (Ferrante et al. 2012; Grewe et al. 2014) thus opening the perspective of enhancing such functions selectively in industrial strains. Nevertheless, it is not yet clear how engineering antennas can be combined with the well-established enhanced growth efficiency of truncated antenna strain (Cazzaniga et al. 2014; Dall'Osto et al. 2019).

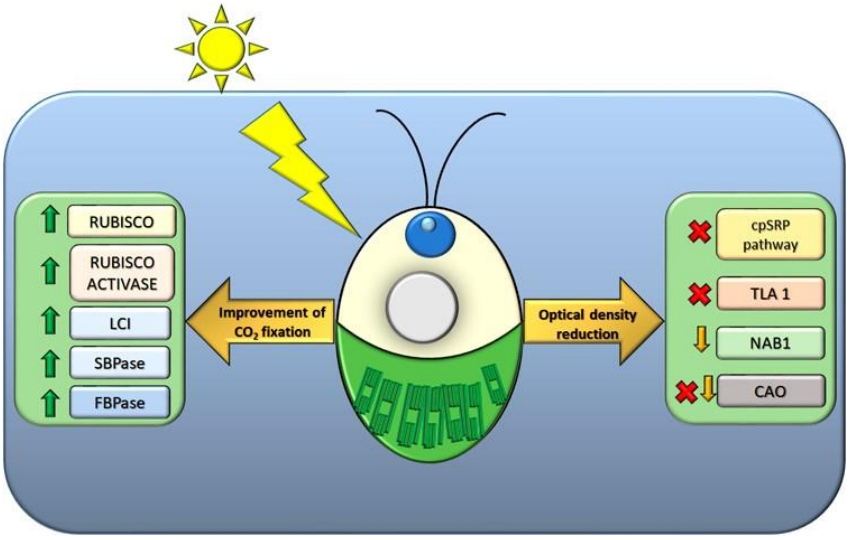

Figure 1.5. Genes successfully targeted in *C. reinhardtii* or other species to improve photosynthetic productivity. Improvement of CO_2 fixation targets: RuBisCO, RuBisCO activase, LCI (Low-CO_2 Inducible protein), SBPase (sedoheptulose1,7-biphosphatase), FBPase (fructose-bisphosphate aldolase). Optical density reduction: cpSRP pathway (chloroplast signal recognition particle), TLA1 (Truncated Light-Harvesting Antenna 1), LhcbM, NAB1 (nucleic acid binding 1 protein) and CAO (Chlorophyllide *a* Oxygenase). Green arrows indicate the over-expressed genes, yellow arrows the down-regulated genes and red crosses indicate the knocked-down genes.

1.3.2 Bioengineering Response to Light Fluctuations and Improving Resistance to Photo-Inhibition

The capacity to counteract EL stress and avoid photoinhibition clearly provide a carbon-gain advantage and therefore represent an important component of productivity. In particular, responses

to fluctuating light conditions are clearly beneficial for photosynthesis since they enhance the 'tracking' of light, thus maintaining high rates of C assimilation, as shown in field crops (Kromdijk et al. 2016). In microalgae, the WT strains show impaired growth when excess irradiance induces photoinhibition, since the repair of photodamage requires metabolic energy. Engineering of the response to EL succeeded in mitigating this loss in efficiency: Very high light resistant (VHL-R) *Chlamydomonas* strains were selected for their ability to grow at irradiances lethal to the control genotype, and found they were affected in the pathways which regulate photoprotective responses, including PSII repair and ROS detoxification (Förster et al. 2005). The *Chlamydomonas* WT strain was UV-mutagenized and selected on a lethal concentration of Red Bengal, a photoreactive chemical releasing $^1O_2$; characterization of tolerant strains identified SOR1 as a factor enhancing resistance to photoinhibition (Fischer et al. 2012). Analogously, UV-mutagenesis and selection under high irradiance (2000 µmol photons $m^{-2}\,s^{-1}$) identified the Light Responsive Signal 1 (LSR1) gene, which conferred improved resistance against exogenous ROS (Schierenbeck et al. 2015). Recently, Dall'Osto and colleagues (Dall'Osto et al. 2019) applied two steps of mutagenesis and phenotypic selection to *Chlorella vulgaris*. First, they selected a strain characterized by a 50% reduction of Chl content per cell and a 30% increased photon-to-biomass conversion efficiency with respect to WT. After a second mutagenesis cycle followed by a selection on Rose Bengal, they selected pale-green genotypes exhibiting higher resistance to singlet oxygen (strains SOR) that showed a further enhancement in biomass productivity with respect to both parental and WT strains (Dall'Osto et al. 2019).

Alternatively to genetic engineering and mutation/phenotypic selection, an alternative approach consists into sampling and evaluating algal biodiversity, particularly in extreme environments which might provide interesting performance when such strains are grown in optimal conditions. An example of this is the case of *Chlorella ohadii*, a *Chlorella* strain from the Sinai desert, which was reported to exhibit high productivity and the robustness of growth (Treves et al. 2013; Treves et al. 2016).

1.3.3. RuBisCO as Target to Improve Carbon Assimilation Efficiency

The rate-limiting step of the CBBc is the fixation of inorganic carbon catalysed by RuBisCO, as the complex has low turnover rate and low substrate specificity. Moreover, it shows affinity for O_2 which leads to futile reactions. The consequences of the wasteful oxygenation reaction are partially alleviated by the photorespiration process which, nevertheless, yields into a partial loss of the CO2, and thus decreases light-to-biomass conversion efficiency (Whitney et al. 2011). Therefore, the engineering of microalgal strains with enhanced RuBisCO catalytic activity would be crucial for improving the efficiency of solar energy conversion. Some species of red algae express isoforms with high specific activity (Uemura et al. 1997). Thus, combining positive mutations from different isoforms has been suggested as a way to obtain RuBisCO with the improved V_{max} of carboxylation catalysis (Karkehabadi et al. 2005). A major constraint to this approach is the high intolerance of the catalytic region to mutations, that made sparsely successful direct evolution strategies (Whitney et al. 2011); nevertheless, some enzymes variants with higher activity have been identified, and their heterologous expression represents a promising approach (Genkov et al. 2010). Other RuBisCO-improved variants were obtained by site directed mutagenesis, targeting either the rbcL gene (RuBisCO large subunit) or the subunit that interacts with Rubisco activase (Larson et al. 1997; Ott et al. 2000). However, their over-expression in *Chlamydomonas* failed to enhance the C fixation

efficiency (Li et al. 2005). On the contrary, the over-expression of endogenous RuBisCO activase in *Nannochloropsis oceanica* increased biomass and lipid productivity up to 40% (Figure 1.5) (Wei et al. 2017c). Consistently, over-expression of RuBisCO in the cyanobacterium *Synechocystis* enhanced photosynthetic efficiency and fatty acid productivity (Figure 1.5) (Ruffing 2014; Liang and Lindblad 2017). In *Chlamydomonas*, a number of strategies were tested to improve carbon assimilation. RuBisCO isoforms with the higher V_{max} of carboxylation catalysis were obtained by the PCR-based gene shuffling of the rbcL gene consisting into a restriction of encoding DNA following low fidelity replication and re-ligating into random assembled sequences with enhanced biochemical variability (Zhu et al. 2010). The site-directed mutagenesis of rbcL resulted in a low-activity RuBisCO variant, which instead triggered a ten-fold higher H_2 production in *Chlamydomonas*, possibly by increasing the pool of reducing equivalents available to the hydrogenase (Pinto et al. 2013). An alternative approach would alter the engineering of cyanobacterial CO_2-concentrating mechanisms, as a possible route to enhance the RuBisCO operating efficiency. Before the approach delivers potential benefits, characterization of algal HCO_3^- transporters and carbonic anhydrases, and identification of factors regulating RuBisCO aggregation into the pyrenoids, is required. Recent advances in dissecting the details of pyrenoid biogenesis in *Chlamydomonas* (Wunder et al. 2018) might guide future redesign of the mechanism, to augment the overall C fixation rate.

Besides RuBisCO, other CBBc enzymes and accessory proteins have been targeted, e.g., sedoheptulose 1,7-bisphosphatase from *C. reinhardtii* has been successfully over-expressed in *D. bardawil*, resulting in a significant enhancement of photosynthetic efficiency (Figure 1.5) (Fang et al. 2012). Over-expression of the fructose 1,6-bisphosphatase in *Synechocystis* enhanced the growth rate with respect to the control genotype under EL conditions (Figure 1.5) (Liang and Lindblad 2016). A strong raise in the photosynthetic productivity of *Synechocystis* was obtained by over-expressing RuBisCO, sedoheptulose1,7-biphosphatase, fructose-bisphosphate aldolase and trans-ketolase (Liang et al. 2018).

Finally, by the over-expression of Low-CO_2 Inducible (LCI) proteins in *C. reinhardtii* maintained at high CO_2 concentration, namely under conditions which repress LCI synthesis, an increase of biomass productivity up to 80% with respect to the control genotype was reported (Figure 1.5) (Spalding 2013).

1.3.4 Engineering of the Lipid Biosynthesis for Renewable Energies Production

The triose phosphate produced by photosynthesis supports the main metabolic pathways of the algal cell, therefore the enhancement of photosynthetic yield potentially results in the enhancement of lipids, proteins and other high value compounds synthesis. Genetic manipulation approaches can generate strains with desirable commercial traits, by either expressing new biosynthetic pathways or enhancing the yield of a product of interest already present in a given strain.

The major research targets is the engineering of strains for a significant increase of total lipid accumulation, and/or the optimization of fatty acid chain-length profile, which can be carried out by targeting single or multiple genes involved in the lipid biosynthesis or by down-regulating competing pathways (Courchesne et al. 2009; Kao and Ng 2017). Saturated and mono-unsaturated C_{14}–C_{20} fatty acids from microalgae are exploited for renewable liquid biofuel production, while the engineering

biosynthesis of long chain-polyunsaturated fatty acids (LC-PUFAs), important components of the human diet, might become a viable option in the market of high-value food additives (Leu and Boussiba 2014). Metabolic engineering reports for redirecting carbon fluxes toward fatty acid production in microalgae, included the up-regulation of key biosynthetic enzymes: (i) acetyl-CoA carboxylase, catalysing the first step for fatty acid biosynthesis, was successfully over-expressed in the chloroplast of *P. tricornutum* (Li et al. 2018a); (ii) malonyl-CoA ACP transacylase enzyme, which catalyses the formation of malonyl-ACP, was over-expressed in both *N. oceanica* and *Schizochytrium spp.*, resulting in 31% and 39.6% total lipid increase with respect to the control genotype, respectively (Chen et al. 2017; Li et al. 2018b); (iii) acyl-ACP thioesterases (TE), involved in the last step of fatty acids biosynthesis, was heterologously expressed in different strains of microalgae (Radakovits et al. 2011; Wei et al. 2017b). In *Dunaliella tertiolecta*, a combinational expression platform involving plant lauric acid-TE (C12TE) and medium-chain fatty acid-specific ketoacyl-ACP synthase was recently engineered, and resulted in a significant increase in lauric acid (C12:0) and myristic acid (C14:0) accumulation (Lin and Lee 2017).

In addition to the strategies for increasing lipid production, fatty acid desaturation could be regulated in order to modify the PUFAs profile, by engineering either the desaturase/elongase pathway or the polyketide synthase pathway (Napier 2002). Both endogenous and exogenous desaturases and elongases have been successfully over-expressed in different oleaginous microalgae such as *N. oceanica* and *P. tricornutum* (Hamilton et al. 2014; Peng et al. 2014; Kaye et al. 2015). In *Chlamydomonas*, over-expression of the endogenous CrΔ4FAD, a monogalactosyl-diacylglycerol Δ4-desaturase, resulted in increased production of the specific product hexadeca-4,7,10,13-tetraenoicacid (16:4) (Zäuner et al. 2012).

Microalgal lipid composition differs among species, more over it isf urthe raffected by the cultivation conditions. The main storage lipids in oleaginous microalgae are triacylglycerols (TAG), which are more desirable for commercial-scale biodiesel processing than polar lipids or free fatty acids (Halim et al. 2012; Liang and Jiang 2013). The first step of TAG biosynthesis is catalysed by acyl-CoA: glycerol-3-phosphate acyl-transferase, whose over-expression in *P. tricornutum* was shown to promote the formation of oil bodies, and led to a significant increase in lipid content (Niu et al. 2016; Zou et al. 2018). A significant increase in lipid productivity was also obtained by up-regulating endogenous lysophosphatidic acid acyltransferase (LPAAT) both in *C. reinhardtii* and in *P. tricornutum*, and by over-expressing the *Brassica napus* LPAAT isoform in *Chlamydomonas*(Yamaoka et al. 2016; Balamurugan et al. 2017; Wang et al. 2018). An additional rate-limiting steps in the TAG biosynthesis of microalgae is catalysed by chloroplastic (DGAT1) and ER (DGAT2) isoforms of diacylglycerol acyltransferase (DGAT) (Cases et al. 1998). Over-expression of DGAT1/DGAT2 in *P. tricornutum* and *Nannochloropsis spp.* resulted in a significant increase of total lipid accumulation (Li et al. 2016a; Wei et al. 2017a; Zou et al. 2018; Cui et al. 2018).

Other enzymes which have been targeted by genetic engineering approaches, and which have succeeded in improving TAG content, included that which was involved in acetyl-CoA synthesis: (i) the *E. coli* isoform of ACS (acetyl-CoA synthetase) was introduced in *Schizochyrium* (Yan et al. 2013); (ii) PDC (pyruvate dehydrogenase complex) abundance was increased by down-regulating pyruvate dehydrogenase kinase (PDK) in *P. tricornutum* (Ma et al. 2014); malic enzyme (ME) and glucose-6-

phosphate dehydrogenase (G6PDH) were over-expressed in *P. tricornutum* (Xue et al. 2015; Xue et al. 2017).

In addition to the modification of fatty acid biosynthesis, competitive pathways e.g., starch synthesis have also been manipulated for generating wider metabolic changes (Sun et al. 2019). The conversion of phosphoenolpyruvate (PEP) to oxaloacetate by PEPC (PEP carboxylase) preferentially diverts the carbon flow towards protein synthesis, and indeed PEPC down-regulation resulted in the over-expression of pyruvate kinase, which increased the levels of pyruvate and acetyl-CoA (Tian et al. 2014). On the other hand, knock-down of a PEPC isoform by either artificial microRNA-mediated technology and CRISPRi in *Chlamydomonas*, and by RNAi in *P. tricornutum*, resulted in higher TAG accumulation (Yang et al. 2016; Kao and Ng 2017; Wang et al. 2017).

Another strategy to improve TAG production is the inhibition of specific lipases. In *Nannochloropsis oceanica* the TAG lipases mutants *tgl1* and *tgl1;2* increased the TAG content by two-fold in early log phase cells (Nobusawa et al. 2019).

Transcription factors represent a suitable target to be manipulated as an alternative to structural genes, since they proved to be more effective for inducing global metabolic changes. Several transcription factors controlling lipid biosynthetic pathways have been identified, and their over-expression resulted into more productive strains. The up-regulation of a Dof-type transcription factor in *Chlamydomonas* doubled the cellular content of TAG (Ibáñez-Salazar et al. 2014; Salas-Montantes et al. 2018). Over-expression of bZIP and bHLH transcription factors in both *N. salina* and *N. oceanica* improved biomass and lipid productivity (Kang et al. 2015; Kang et al. 2017; Kwon et al. 2018; Li et al. 2019). In *N. gaditana*, 20 putative regulators of lipid production, down-regulated by nitrogen deprivation, were identified by RNA-seq; a strategy of selective knock-out by the Crispr-Cas9 system allowed us to identify a homolog of the fungal $Zn(II)_2Cys_6$-encoding gene, which triggered lipid biosynthesis in *Nannochloropsis* and resulted in a 200% increase of C partition to lipids, without significantly affecting the growth rate (Ajjawi et al. 2017). More recently, a Myb-like transcription factor Phosphorus Starvation Response (PtPSR) was identified in *P. tricornutum*; its modulation might represent a good strategy to enhance cell growth and TAG production in limited-phosphorous conditions (Sharma et al. 2019). A MYB DNA binding protein involved in cell cycle regulation was instead targeted in *Chlamydomonas*, showing that the mutants devoid of CrCDC5 accumulate more oil and starch with respect to WT (Torres-Romero et al. 2019).

Integrated, multiomic analysis has been recently performed on different high-lipid productive microalgal strains, in order to pinpoint a range of candidate molecular targets, aimed to enhance oil productivity in different growth conditions (Zhang et al. 2019; Liu et al. 2019).

1.3.5. Endogenous Up-Regulation and Heterologous Expression of Isoprenoid Biosynthetic Pathways in Microalgae

The photoautotrophic nature of microalgae requires the generation of isoprenoids, natural hydrocarbons associated with the photosynthetic apparatus (e.g., carotenoids, plastoquinon, phytol chains) and participating in photon capture and electron transport events. Thus, microalgae own specific isoprenoid biosynthetic pathways that could be manipulated by genetic engineering to

increase the natural capacities for the generation of isoprenoids, or to promote heterologous isoprenoid production. These class of molecules, due to their intensive color, fragrance and antioxidant properties, are in high demand for various applications in animal feed, medicines and nutraceuticals, pest control agents, cosmetics and pigments (D'Adamo et al. 2019).

Regarding the endogenous isoprenoids, carotenoids represent commercially successful products from microalgae: β-carotene from *D. salina* and astaxanthin from *H. pluvialis* are high-price products mainly used in aquaculture, and as food colouring agents and nutraceuticals (Jin et al. 2003). As for zeaxanthin, hyper-accumulating *D. salina* strains were identified (Jin et al. 2001), while a ΔZEP *Chlamydomonas* strain with a far higher zeaxanthin content than WT (56-fold) was shown to have a commercial potential in the production of eggs fortified with carotenoids [(Baek et al. 2016; Baek et al. 2018). In *H. pluvialis*, the endogenous phytoene desaturase was modified by site-directed mutagenesis, enhancing both the resistance to the herbicide norflurazon and the astaxanthin productivity (Steinbrenner and Sandmann 2006). Significant enhancements in carotenoid productivity were obtained by either over-expressing the β-carotene ketolase or expressing the endogenous phytoene desaturase in the chloroplast under the control of the psbA promoter (Kathiresan et al. 2015; Galarza et al. 2018).

In *Chlamydomonas*, the over-expression of *C. zofingiensis* ZEP resulted in an astaxanthin production, reaching values of 0.5 mg g^{-1} DW (Couso et al. 2012). To increase the production of fucoxanthin, employed as an antioxidant agent, the 1-deoxy-d-xylulose 5-phosphate synthase and the phytoene synthase were over-expressed in *Phaeodacthylum* (Eilers et al. 2016).

Two pathways lead to synthesis isoprenoid products: The 2-c-methyl-D-erythritol 4-phosphate/1 deoxy-D-xylulose 5-phosphate (MEP/DOXP) pathway and the mevalonate pathway (MVA). These are localized in different cell compartments but generate the same 5-C precursors, isopentenyl diphosphate (IPP) and dimethylallyl diphosphate (DMAPP). The MVA pathway was lost during evolution in the Chlorophyta and Eustigmatophyceae (Lohr et al. 2012), while it was conserved in other microalgae, e.g., *P. Tricornutum* maintained the cytosolic MVA pathway, thus representing a choice species for isoprenoid engineering and heterologous terpenoid production (Lohr et al. 2012; D'Adamo et al. 2019).

In *Phaeodacthylum*, lupeol synthase isoforms from *A. thaliana* and *L. japonicus* were expressed to produce lupeol, an anti-inflammatory triterpene (D'Adamo et al. 2019). Moreover, co-expression in the diatom of CYP716A12 from *M. truncatula* and its corresponding reductase MtCPR, was aimed to further functionalize lupeol in betulin for the production of the antiretroviral, antimalarial agent betulinic acid (D'Adamo et al. 2019). In *Chlamydomonas*, the fragrance patchoulol was produced by expressing the patchoulol synthase from *Pogostemon cablin* (Lauersen et al. 2016), while the synthesis of bisabolene, a sesquiterpene compound identified as a promising jet fuel candidate, resulted by both over-expressing the bisabolene synthase from *Abies grandis* and down-regulating both the geranylgeranyl diphosphate (GGPP) synthase and the squalene synthase (Wichmann et al. 2018).

Finally, several non-native diterpenoids were successfully produced in *C. reinhardtii*, by the heterologous expression of diterpene synthases targeted to the algal chloroplast, to convert native

GGPP into the diterpenoid products casbene, taxadiene and 13R(+) manoyl oxide (Lauersen et al. 2018).

Notably, besides diatoms and green microalgae, Cyanobacteria represent the most targeted photosynthetic organisms for isoprenoid production, especially terpenoids (Lin and Pakrasi 2019). Cyanobacteria are, indeed, promising platforms for biofuel production (Nozzi et al. 2013), and the knowledge on isoprenoid biosynthetic pathways regulation is instrumental in over-expressing key enzymes toward a higher productivity. To enhance isoprene synthesis, different plant isoprene synthase (IS) genes were expressed in *Synechococcus elongatus*, in particular the IS from *Eucalyptus globulus* was responsible for the most significant productivity enhancement among the isoforms tested (Gao et al. 2016). Moreover, limonene is a terpenoid evaluated as a promising alternative fuel. The limonene synthase from *Mentha spicata* was successfully expressed in different species such as *Synechococcus elongatus* PCC 7942, *Synechocystis* sp. PCC 6803 and *Synechococcus sp.* PCC 7002 (Davies et al. 2014; Wang et al. 2016; Lin et al. 2017).

1.4 Concluding Remarks

Nowadays the technical advance in genetic engineering made it possible to engineer algal strains for enhancing both biomass productivity and the yield of high value products from microalgae. The major efforts are focused on obtaining strains with higher photosynthetic efficiency in order to decrease the unitary cost of algal biomass. The best results have been obtained by enhancing the homogeneity of light distribution within photobioreactors (Kirst and Melis 2014) and by decreasing their susceptibility to photodamage (Dall'Osto et al. 2019). Besides the obvious strategy of targeting antenna systems, photoprotection was also enhanced by increasing photochemical quenching by boosting CO_2 fixation through over-expressing RuBisCO activity, and other rate-liming enzymes in the CBB cycle (Liang and Lindblad 2016) .

Besides productivity, microalgae exploitation targets high value compounds. First, oleaginous strains, especially diatoms, were engineered to optimize the fatty acid chain-length profile for biodiesel production (Sun et al. 2019). Secondly, isoprenoid biosynthesis pathway has been engineered to redirect carbon flux towards specific and high values products for chemical industry and/or as biofuels (Lauersen 2018). While the overall strategies have been well defined, limitations derive mainly from the low number of species that can be engineered to some extent besides the model species *Chlamydomonas reinhardtii* and the efficiency of the expression of the transgenes in different species (Baier et al. 2018).

REFERENCES

Ahmed RA, He M, Aftab RA, Zheng S, Nagi M, Bakri R, Wang C (2017) Bioenergy application of Dunaliella salina SA 134 grown at various salinity levels for lipid production. Sci Rep 7:8118 . https://doi.org/10.1038/s41598-017-07540-x

Ahn TK, Avenson TJ, Ballottari M, Cheng YC, Niyogi KK, Bassi R, Fleming GR (2008) Architecture of a Charge-Transfer State Regulating Light Harvesting in a Plant Antenna Protein. Science (80-) 320:794 LP – 797 . https://doi.org/10.1126/science.1154800

Ajjawi I, Verruto J, Aqui M, Soriaga LB, Coppersmith J, Kwok K, Peach L, Orchard E, Kalb R, Xu W, Carlson TJ, Francis K, Konigsfeld K, Bartalis J, Schultz A, Lambert W, Schwartz AS, Brown R, Moellering ER (2017) Lipid production in Nannochloropsis gaditana is doubled by decreasing expression of a single transcriptional regulator. Nat Publ Gr 35:647–652 . https://doi.org/10.1038/nbt.3865

Alboresi A, Caffarri S, Nogue F, Bassi R, Morosinotto T (2008) In Silico and Biochemical Analysis of Physcomitrella patens Photosynthetic Antenna: Identification of Subunits which Evolved upon Land Adaptation. PLoS One 3:e2033

Alboresi A, Gerotto C, Giacometti GM, Bassi R, Morosinotto T (2010) Physcomitrella patens mutants affected on heat dissipation clarify the evolution of photoprotection mechanisms upon land colonization. Proc Natl Acad Sci U S A 107:11128–11133 . https://doi.org/10.1073/pnas.1002873107

Allorent G, Tokutsu R, Roach T, Peers G, Cardol P, Girard-Bascou J, Seigneurin-Berny D, Petroutsos D, Kuntz M, Breyton C, Franck F, Wollman FA, Niyogi KK, Krieger-Liszkay A, Minagawa J, Finazzi G (2013) A Dual Strategy to Cope with High Light in Chlamydomonas reinhardtii. Plant Cell 25:545–557 . https://doi.org/10.1105/tpc.112.108274

Anderson JM, Chow WS, Park YI (1995) The grand design of photosynthesis: Acclimation of the photosynthetic apparatus to environmental cues. Photosynth Res 46:129–139 . https://doi.org/10.1007/BF00020423

Baek K, Kim DH, Jeong J, Sim SJ, Melis A, Kim JS, Jin E, Bae S (2016) DNA-free two-gene knockout in Chlamydomonas reinhardtii via CRISPR-Cas9 ribonucleoproteins. Sci Rep 6:30620 . https://doi.org/10.1038/srep30620

Baek KL, Yu J, Jeong J, Sim SJ, Bae S, Jin ES (2018) Photoautotrophic production of macular pigment in a Chlamydomonas reinhardtii strain generated by using DNA-free CRISPR-Cas9 RNP-mediated mutagenesis. Biotechnol Bioeng 115:719–728 . https://doi.org/10.1002/bit.26499

Baier T, Wichmann J, Kruse O, Lauersen KJ (2018) Intron-containing algal transgenes mediate efficient recombinant gene expression in the green microalga Chlamydomonas reinhardtii. Nucleic Acids Res 46:6909–6919 . https://doi.org/10.1093/nar/gky532

Balamurugan S, Wang X, Wang HL, An CJ, Li H, Li DW, Yang WD, Liu JS, Li HY (2017) Occurrence of plastidial triacylglycerol synthesis and the potential regulatory role of AGPAT in the model diatom Phaeodactylum tricornutum. Biotechnol Biofuels 10:97 . https://doi.org/10.1186/s13068-017-0786-0

Ballottari M, Dall'Osto L, Morosinotto T, Bassi R (2007) Contrasting Behavior of Higher Plant

Photosystem I and II Antenna Systems during Acclimation. J Biol Chem 282:8947–8958 . https://doi.org/10.1074/jbc.M606417200

Ballottari M, Girardon J, Dall'Osto L, Bassi R (2012) Evolution and functional properties of Photosystem II light harvesting complexes in eukaryotes. Biochim Biophys Acta - Bioenerg 1817:143–157 . https://doi.org/https://doi.org/10.1016/j.bbabio.2011.06.005

Ballottari M, Truong TB, De Re E, Erickson E, Stella GR, Fleming GR, Bassi R, Niyogi KK (2016) Identification of pH-sensing Sites in the Light Harvesting Complex Stress-related 3 Protein Essential for Triggering Non-photochemical Quenching in Chlamydomonas reinhardtii. J Biol Chem 291:7334–7346 . https://doi.org/10.1074/jbc.M115.704601

Barber J (2009) Photosynthetic energy conversion: Natural and artificial. Chem Soc Rev 38:185–196 . https://doi.org/10.1039/b802262n

Basso S, Simionato D, Gerotto C, Segalla A, Giacometti GM, Morosinotto T (2014) Characterization of the photosynthetic apparatus of the Eustigmatophycean Nannochloropsis gaditana: Evidence of convergent evolution in the supramolecular organization of photosystem i. Biochim Biophys Acta - Bioenerg 1837:306–314 . https://doi.org/10.1016/j.bbabio.2013.11.019

Ben-Shem A, Frolow F, Nelson N (2003) Crystal structure of plant photosystem I. Nature 426:630–635 . https://doi.org/10.1038/nature02200

Benedetti M, Vecchi V, Barera S, Dall' Osto L (2018) Biomass from microalgae : the potential of domestication towards sustainable biofactories. Microb Cell Fact 1–18 . https://doi.org/10.1186/s12934-018-1019-3

Bonente G, Ballottari M, Truong TB, Morosinotto T, Ahn TK, Fleming GR, Niyogi KK, Bassi R (2011) Analysis of LhcSR3, a Protein Essential for Feedback De-Excitation in the Green Alga Chlamydomonas reinhardtii. PLOS Biol 9:e1000577

Bonente G, Pippa S, Castellano S, Bassi R, Ballottari M (2012) Acclimation of Chlamydomonas reinhardtii to different growth irradiances. J Biol Chem 287:5833–5847 . https://doi.org/10.1074/jbc.M111.304279

Bowler C, Allen AE, Badger JH, Grimwood J, Jabbari K, Kuo A, Maheswari U, Martens C, Maumus F, Otillar RP, Rayko E, Salamov A, Vandepoele K, Beszteri B, Gruber A, Heijde M, Katinka M, Mock T, Valentin K, Verret F, Berges JA, Brownlee C, Cadoret J-P, Chiovitti A, Choi CJ, Coesel S, De Martino A, Detter JC, Durkin C, Falciatore A, Fournet J, Haruta M, Huysman MJJ, Jenkins BD, Jiroutova K, Jorgensen RE, Joubert Y, Kaplan A, Kröger N, Kroth PG, La Roche J, Lindquist E, Lommer M, Martin–Jézéquel V, Lopez PJ, Lucas S, Mangogna M, McGinnis K, Medlin LK, Montsant A, Secq M-PO, Napoli C, Obornik M, Parker MS, Petit J-L, Porcel BM, Poulsen N, Robison M, Rychlewski L, Rynearson TA, Schmutz J, Shapiro H, Siaut M, Stanley M, Sussman MR, Taylor AR, Vardi A, von Dassow P, Vyverman W, Willis A, Wyrwicz LS, Rokhsar DS, Weissenbach J, Armbrust EV, Green BR, Van de Peer Y, Grigoriev I V (2008) The Phaeodactylum genome reveals the evolutionary history of diatom genomes. Nature 456:239

Bujaldon S, Kodama N, Rappaport F, Subramanyam R, de Vitry C, Takahashi Y, Wollman FA (2017) Functional Accumulation of Antenna Proteins in Chlorophyll b-Less Mutants of Chlamydomonas reinhardtii. Mol Plant 10:115–130 . https://doi.org/10.1016/j.molp.2016.10.001

Cases S, Smith SJ, Zheng YW, Myers HM, Lear SR, Sande E, Novak S, Collins C, Welch CB, Lusis AJ,

Erickson SK, Farese Jr R V (1998) Identification of a gene encoding an acyl CoA:diacylglycerol acyltransferase, a key enzyme in triacylglycerol synthesis. Proc Natl Acad Sci U S A 95:13018–13023

Cazzaniga S, Dall'Osto L, Szaub J, Scibilia L, Ballottari M, Purton S, Bassi R (2014) Domestication of the green alga Chlorella sorokiniana: Reduction of antenna size improves light-use efficiency in a photobioreactor. Biotechnol Biofuels 7:157 . https://doi.org/10.1186/s13068-014-0157-z

Chen J, Liu W, Hu D, Wang X (2017) Identification of a malonyl CoA-acyl carrier protein transacylase and its regulatory role in fatty acid biosynthesis in oleaginous microalga Nannochloropsis oceanica. Biotechnol Appl Biochem 64:620–626 . https://doi.org/10.1002/bab.1531

Courchesne NMD, Parisien A, Wang B, Lan CQ (2009) Enhancement of lipid production using biochemical , genetic and transcription factor engineering approaches. 141:31–41 . https://doi.org/10.1016/j.jbiotec.2009.02.018

Couso I, Cordero BF, Vargas MÁ, Rodríguez H (2012) Efficient Heterologous Transformation of Chlamydomonas reinhardtii npq2 Mutant with the Zeaxanthin Epoxidase Gene Isolated and Characterized from Chlorella zofingiensis. Mar. Drugs 10

Cui Y, Zhao J, Wang Y, Qin S, Lu Y (2018) Characterization and engineering of a dual-function diacylglycerol acyltransferase in the oleaginous marine diatom Phaeodactylum tricornutum. Biotechnol Biofuels 11:32 . https://doi.org/10.1186/s13068-018-1029-8

Curmi PM, Cascio D, Sweet RM, Eisenberg D, Schreuder H (1992) Crystal structure of the unactivated form of ribulose-1,5-bisphosphate carboxylase/oxygenase from tobacco refined at 2.0-A resolution. J Biol Chem 267:16980–16989

D'Adamo S, Schiano di Visconte G, Lowe G, Szaub-Newton J, Beacham T, Landels A, Allen MJ, Spicer A, Matthijs M (2019) Engineering the unicellular alga Phaeodactylum tricornutum for high-value plant triterpenoid production. Plant Biotechnol J 17:75–87 . https://doi.org/10.1111/pbi.12948

Dall'Osto L, Bressan M, Bassi R (2015) Biogenesis of light harvesting proteins. Biochim Biophys Acta 1847:861–871 . https://doi.org/10.1016/j.bbabio.2015.02.009

Dall'Osto L, Caffarri S, Bassi R (2005) A mechanism of nonphotochemical energy dissipation, independent from PsbS, revealed by a conformational change in the antenna protein CP26. Plant Cell 17:1217–1232 . https://doi.org/10.1105/tpc.104.030601

Dall'Osto L, Cazzaniga S, Guardini Z, Barera S, Benedetti M, Mannino G, Maffei ME, Bassi R (2019) Combined resistance to oxidative stress and reduced antenna size enhance light-to-biomass conversion efficiency in Chlorella vulgaris cultures. Biotechnol Biofuels 12:221 . https://doi.org/10.1186/s13068-019-1566-9

Dall'Osto L, Piques M, Ronzani M, Molesini B, Alboresi A, Cazzaniga S, Bassi R (2013) The Arabidopsis nox mutant lacking carotene hydroxylase activity reveals a critical role for xanthophylls in photosystem I biogenesis. Plant Cell 25:591–608 . https://doi.org/10.1105/tpc.112.108621

Davies FK, Work VH, Beliaev AS, Posewitz MC (2014) Engineering Limonene and Bisabolene Production in Wild Type and a Glycogen-Deficient Mutant of Synechococcus sp. PCC 7002 . Front. Bioeng. Biotechnol. 2:21

Drop B, Webber-birungi M, Fusetti F, Kour R, Redding KE, Boekema EJ, Croce R (2011) Photosystem I of Chlamydomonas reinhardtii Contains Nine Light-harvesting Complexes (Lhca) Located on One Side of. 286:44878–44887 . https://doi.org/10.1074/jbc.M111.301101

Drop B, Webber-Birungi M, Yadav SKN, Filipowicz-Szymanska A, Fusetti F, Boekema EJ, Croce R (2014) Light-harvesting complex II (LHCII) and its supramolecular organization in Chlamydomonas reinhardtii. Biochim Biophys Acta - Bioenerg 1837:63–72 . https://doi.org/https://doi.org/10.1016/j.bbabio.2013.07.012

Durnford D, A. Price J, M. McKim S, L. Sarchfield M (2003) Light-harvesting complex gene expression is controlled by both transcriptional and post-transcriptional mechanisms during photoacclimation in Chlamydomonas reinhardtii

Eilers U, Bikoulis A, Breitenbach J, Büchel C, Sandmann G (2016) Limitations in the biosynthesis of fucoxanthin as targets for genetic engineering in Phaeodactylum tricornutum. J Appl Phycol 28:123–129 . https://doi.org/10.1007/s10811-015-0583-8

Elrad D, Niyogi KK, Grossman AR (2002) A Major Light-Harvesting Polypeptide of Photosystem II Functions in Thermal Dissipation. Plant Cell 14:1801 LP – 1816 . https://doi.org/10.1105/tpc.002154

Escoubas JM, Lomas M, LaRoche J, Falkowski PG (1995) Light intensity regulation of cab gene transcription is signaled by the redox state of the plastoquinone pool. Proc Natl Acad Sci U S A 92:10237–10241

Fan M, Li M, Liu Z, Cao P, Pan X, Zhang H, Zhao X, Zhang J, Chang W (2015) Crystal structures of the PsbS protein essential for photoprotection in plants. Nat Struct &Amp; Mol Biol 22:729

Fang L, Lin HX, Low CS, Wu MH, Chow Y, Lee YK (2012) Expression of the Chlamydomonas reinhardtii Sedoheptulose-1,7-bisphosphatase in Dunaliella bardawil leads to enhanced photosynthesis and increased glycerol production. Plant Biotechnol J 10:1129–1135 . https://doi.org/10.1111/pbi.12000

Ferrante P, Ballottari M, Bonente G, Giuliano G, Bassi R (2012) LHCBM1 and LHCBM2/7 polypeptides, components of major LHCII complex, have distinct functional roles in photosynthetic antenna system of Chlamydomonas reinhardtii. J Biol Chem 287:16276–16288 . https://doi.org/10.1074/jbc.M111.316729

Fischer BB, Ledford HK, Wakao S, Huang SG, Casero D, Pellegrini M, Merchant SS, Koller A, Eggen RIL, Niyogi KK (2012) SINGLET OXYGEN RESISTANT 1 links reactive electrophile signaling to singlet oxygen acclimation in Chlamydomonas reinhardtii. Proc Natl Acad Sci 109:E1302–E1311 . https://doi.org/10.1073/pnas.1116843109

Förster B, Osmond CB, Pogson BJ (2005) Improved survival of very high light and oxidative stress is conferred by spontaneous gain-of-function mutations in Chlamydomonas. Biochim Biophys Acta - Bioenerg 1709:45–57 . https://doi.org/10.1016/j.bbabio.2005.05.012

Fuciman M, Enriquez MM, Polívka T, Dall'Osto L, Bassi R, Frank HA (2012) Role of Xanthophylls in Light Harvesting in Green Plants: A Spectroscopic Investigation of Mutant LHCII and Lhcb Pigment–Protein Complexes. J Phys Chem B 116:3834–3849 . https://doi.org/10.1021/jp210042z

Gabilly ST, Baker CR, Wakao S, Crisanto T, Guan K, Bi K, Guiet E, Guadagno CR, Niyogi KK (2019) Regulation of photoprotection gene expression in Chlamydomonas by a putative E3 ubiquitin

ligase complex and a homolog of CONSTANS . Proc Natl Acad Sci. https://doi.org/10.1073/pnas.1821689116

Galarza JI, Gimpel JA, Rojas V, Arredondo-vega BO (2018) Over-accumulation of astaxanthin in Haematococcus pluvialis through chloroplast genetic engineering. Algal Res 31:291–297 . https://doi.org/10.1016/j.algal.2018.02.024

Gao X, Gao F, Liu D, Zhang H, Nie X, Yang C (2016) Engineering the methylerythritol phosphate pathway in cyanobacteria for photosynthetic isoprene production from CO2. Energy Environ Sci 9:1400–1411 . https://doi.org/10.1039/C5EE03102H

García JL, de Vicente M, Galán B (2017) Microalgae, old sustainable food and fashion nutraceuticals. Microb Biotechnol 2783: . https://doi.org/10.1111/1751-7915.12800

Genkov T, Meyer M, Griffiths H, Spreitzer RJ (2010) Functional Hybrid Rubisco Enzymes with Plant Small Subunits and Algal Large Subunits: engineered rbcS cDNA for expression in Chlamydomonas. J Biol Chem 285:19833–19841 . https://doi.org/10.1074/jbc.M110.124230

Georgianna DR, Stephen P (2012) Exploiting diversity and synthetic biology for the production of algal biofuels. Nature 488:329–35 . https://doi.org/10.1038/nature11479

Gilmore AM, Ball MC (2000) Protection and storage of chlorophyll in overwintering evergreens. Proc Natl Acad Sci U S A. https://doi.org/10.1073/pnas.150237697

Grewe S, Ballottari M, Alcocer M, D'Andrea C, Blifernez-Klassen O, Hankamer B, Mussgnug JH, Bassi R, Kruse O (2014) Light-Harvesting Complex Protein LHCBM9 Is Critical for Photosystem II Activity and Hydrogen Production in Chlamydomonas reinhardtii. Plant Cell 26:1598–1611 . https://doi.org/10.1105/tpc.114.124198

Grossman AR (2000) Chlamydomonas reinhardtii and photosynthesis: genetics to genomics. Curr Opin Plant Biol 3:132–137 . https://doi.org/https://doi.org/10.1016/S1369-5266(99)00053-9

Guccione A, Biondi N, Sampietro G, Rodolfi L, Bassi N, Tredici MR (2014) Chlorella for protein and biofuels: From strain selection to outdoor cultivation in a Green Wall Panel photobioreactor. Biotechnol Biofuels 7:1–12 . https://doi.org/10.1186/1754-6834-7-84

Guiry MD (2012) How many species of algae are there? J Phycol 48:1057–1063 . https://doi.org/10.1111/j.1529-8817.2012.01222.x

Halim R, Danquah MK, Webley PA (2012) Extraction of oil from microalgae for biodiesel production: A review. Biotechnol Adv 30:709–732 . https://doi.org/10.1016/j.biotechadv.2012.01.001

Hamilton ML, Haslam RP, Napier JA, Sayanova O (2014) Metabolic engineering of Phaeodactylum tricornutum for the enhanced accumulation of omega-3 long chain polyunsaturated fatty acids. Metab Eng 22:3–9 . https://doi.org/https://doi.org/10.1016/j.ymben.2013.12.003

Harris EH (2001) Chlamydomonas as a model organism. Annu Rev Plant Physiol Plant Mol Biol 52:363–406 . https://doi.org/10.1146/annurev.arplant.52.1.363

Harrison EP, Willingham NM, Lloyd JC, Raines CA (1997) Reduced sedoheptulose-1,7-bisphosphatase levels in transgenic tobacco lead to decreased photosynthetic capacity and altered carbohydrate accumulation. Planta 204:27–36 . https://doi.org/10.1007/s004250050226

Holt NE, Zigmantas D, Valkunas L, Li X-P, Niyogi KK, Fleming GR (2005) Carotenoid Cation Formation and the Regulation of Photosynthetic Light Harvesting. Science (80-) 307:433 LP – 436 .

https://doi.org/10.1126/science.1105833

Horton P, Ruban A V, Walters RG (1996) Regulation Of Light Harvesting In Green Plants. Annu Rev Plant Physiol Plant Mol Biol 47:655–684 . https://doi.org/10.1146/annurev.arplant.47.1.655

Ibáñez-Salazar A, Rosales-Mendoza S, Rocha-Uribe A, Ramírez-Alonso JI, Lara-Hernández I, Hernández-Torres A, Paz-Maldonado LMT, Silva-Ramírez AS, Bañuelos-Hernández B, Martínez-Salgado JL, Soria-Guerra RE (2014) Over-expression of Dof-type transcription factor increases lipid production in Chlamydomonas reinhardtii. J Biotechnol 184:27–38 . https://doi.org/https://doi.org/10.1016/j.jbiotec.2014.05.003

Ip PF, Chen F (2005) Production of astaxanthin by the green microalga Chlorella zofingiensis in the dark. Process Biochem 40:733–738 . https://doi.org/10.1016/j.procbio.2004.01.039

Jans F, Mignolet E, Houyoux P-A, Cardol P, Ghysels B, Cuine S, Cournac L, Peltier G, Remacle C, Franck F (2008) A type II NAD(P)H dehydrogenase mediates light-independent plastoquinone reduction in the chloroplast of Chlamydomonas. Proc Natl Acad Sci. https://doi.org/10.1073/pnas.0806896105

Jeong J, Baek K, Yu J, Kirst H, Betterle N, Shin W, Bae S, Melis A, Jin E (2018) Deletion of the chloroplast LTD protein impedes LHCI import and PSI-LHCI assembly in Chlamydomonas reinhardtii. J Exp Bot 69:1147–1158 . https://doi.org/10.1093/jxb/erx457

Jin E, E W Polle J, Lee HK, Sang M, Man Chang A (2003) Xanthophylls in microalgae: From Biosynthesis to biotechnological mass production and application

Jin E, Polle JEW, Melis A (2001) Involvement of zeaxanthin and of the Cbr protein in the repair of photosystem II from photoinhibition in the green alga Dunaliella salina. Biochim Biophys Acta - Bioenerg 1506:244–259 . https://doi.org/https://doi.org/10.1016/S0005-2728(01)00223-7

Jokel M, Johnson X, Peltier G, Aro EM, Allahverdiyeva Y (2018) Hunting the main player enabling Chlamydomonas reinhardtii growth under fluctuating light. Plant J. https://doi.org/10.1111/tpj.13897

Kang NK, Jeon S, Kwon S, Koh HG, Shin S-E, Lee B, Choi G-G, Yang J-W, Jeong B, Chang YK (2015) Effects of overexpression of a bHLH transcription factor on biomass and lipid production in Nannochloropsis salina. Biotechnol Biofuels 8:200 . https://doi.org/10.1186/s13068-015-0386-9

Kang NK, Kim EK, Kim YU, Lee B, Jeong W-J, Jeong B-R, Chang YK (2017) Increased lipid production by heterologous expression of AtWRI1 transcription factor in Nannochloropsis salina. Biotechnol Biofuels 10:231 . https://doi.org/10.1186/s13068-017-0919-5

Kao PH, Ng IS (2017) CRISPRi mediated phosphoenolpyruvate carboxylase regulation to enhance the production of lipid in Chlamydomonas reinhardtii. Bioresour Technol 245:1527–1537 . https://doi.org/10.1016/j.biortech.2017.04.111

Karkehabadi S, Peddi SR, Anwaruzzaman M, Taylor TC, Cederlund A, Genkov T, Andersson I, Spreitzer RJ (2005) Chimeric small subunits influence catalysis without causing global conformational changes in the crystal structure of ribulose-1,5-bisphosphate carboxylase/oxygenase. Biochemistry 44:9851–9861 . https://doi.org/10.1021/bi050537v

Kathiresan S, Chandrashekar A, Ravishankar GA, Sarada R (2015) Regulation of astaxanthin and its intermediates through cloning and genetic transformation of β-carotene ketolase in

Haematococcus pluvialis. J Biotechnol 196–197:33–41 . https://doi.org/https://doi.org/10.1016/j.jbiotec.2015.01.006

Kaye Y, Grundman O, Leu S, Zarka A, Zorin B, Didi-Cohen S, Khozin-Goldberg I, Boussiba S (2015) Metabolic engineering toward enhanced LC-PUFA biosynthesis in Nannochloropsis oceanica: Overexpression of endogenous Δ12 desaturase driven by stress-inducible promoter leads to enhanced deposition of polyunsaturated fatty acids in TAG. Algal Res 11:387–398 . https://doi.org/https://doi.org/10.1016/j.algal.2015.05.003

Kirst H, García-Cerdán JG, Zurbriggen A, Melis A (2012) Assembly of the light-harvesting chlorophyll antenna in the green alga Chlamydomonas reinhardtii requires expression of the TLA2-CpFTSY gene. Plant Physiol 158:930–945 . https://doi.org/10.1104/pp.111.189910

Kirst H, Melis A (2014) The chloroplast signal recognition particle (CpSRP) pathway as a tool to minimize chlorophyll antenna size and maximize photosynthetic productivity. Biotechnol Adv 32:66–72 . https://doi.org/10.1016/j.biotechadv.2013.08.018

Kondo T, Gordon JB, Pinnola A, Dall'Osto L, Bassi R, Schlau-Cohen GS (2019) Microsecond and millisecond dynamics in the photosynthetic protein LHCSR1 observed by single-molecule correlation spectroscopy. Proc Natl Acad Sci 201821207 . https://doi.org/10.1073/pnas.1821207116

Kondo T, Pinnola A, Chen WJ, Dall'Osto L, Bassi R, Schlau-Cohen GS (2017) Single-molecule spectroscopy of LHCSR1 protein dynamics identifies two distinct states responsible for multi-timescale photosynthetic photoprotection. Nat Chem 9:772

Kromdijk J, Głowacka K, Leonelli L, Gabilly ST, Iwai M, Niyogi KK, Long SP (2016) Improving photosynthesis and crop productivity by accelerating recovery from photoprotection. Science (80-) 354:857 LP – 861 . https://doi.org/10.1126/science.aai8878

Kuchitsu K, Tsuzuki M, Miyachi S (1991) Polypeptide composition and enzyme activities of the pyrenoid and its regulation by CO2 concentration in unicellular green algae. Can J Bot 69:1062–1069 . https://doi.org/10.1139/b91-136

Kwon S, Kang NK, Koh HG, Shin S-E, Lee B, Jeong B, Chang YK (2018) Enhancement of biomass and lipid productivity by overexpression of a bZIP transcription factor in Nannochloropsis salina. Biotechnol Bioeng 115:331–340 . https://doi.org/10.1002/bit.26465

Larson EM, O'Brien CM, Zhu G, Spreitzer RJ, Portis AR (1997) Specificity for activase is changed by a Pro-89 to Arg substitution in the large subunit of ribulose-1,5-bisphosphate carboxylase/oxygenase. J Biol Chem 272:17033–17037 . https://doi.org/10.1074/jbc.272.27.17033

Lauersen KJ (2018) Eukaryotic microalgae as hosts for light-driven heterologous isoprenoid production. Planta. https://doi.org/10.1007/s00425-018-3048-x

Lauersen KJ, Baier T, Wichmann J, Wördenweber R, Mussgnug JH, Hübner W, Huser T, Kruse O (2016) Efficient phototrophic production of a high-value sesquiterpenoid from the eukaryotic microalga Chlamydomonas reinhardtii. Metab Eng 38:331–343 . https://doi.org/https://doi.org/10.1016/j.ymben.2016.07.013

Lauersen KJ, Wichmann J, Baier T, Kampranis SC, Pateraki I, Møller BL, Kruse O (2018) Phototrophic production of heterologous diterpenoids and a hydroxy-functionalized derivative from

Chlamydomonas reinhardtii. Metab Eng 49:116–127 . https://doi.org/https://doi.org/10.1016/j.ymben.2018.07.005

Leu S, Boussiba S (2014) Advances in the Production of High-Value Products by Microalgae. Ind Biotechnol 10:169–183 . https://doi.org/10.1089/ind.2013.0039

Li C, Salvucci ME, Portis AR (2005) Two residues of Rubisco activase involved in recognition of the Rubisco substrate. J Biol Chem 280:24864–24869 . https://doi.org/10.1074/jbc.M503547200

Li DW, Balamurugan S, Yang YF, Zheng JW, Huang D, Zou LG, Yang WD, Liu JS, Guan Y, Li HY (2019) Transcriptional regulation of microalgae for concurrent lipid overproduction and secretion. Sci Adv 5:eaau3795 . https://doi.org/10.1126/sciadv.aau3795

Li DW, Cen SY, Liu YH, Balamurugan S, Zheng XY, Alimujiang A, Yang WD, Liu JS, Li HY (2016a) A type 2 diacylglycerol acyltransferase accelerates the triacylglycerol biosynthesis in heterokont oleaginous microalga Nannochloropsis oceanica. J Biotechnol 229:65–71 . https://doi.org/https://doi.org/10.1016/j.jbiotec.2016.05.005

Li D, Xie W, Hao T, Cai J, Zhou T, Balamurugan S (2018a) Constitutive and Chloroplast Targeted Expression of Acetyl-CoA Carboxylase in Oleaginous Microalgae Elevates Fatty Acid Biosynthesis. 566–572

Li XP, Björkman O, Shih C, Grossman AR, Rosenquist M, Jansson S, Niyogi KK (2000) A pigment-binding protein essential for regulation of photosynthetic light harvesting. Nature 403:391–395 . https://doi.org/10.1038/35000131

Li XP, Gilmore AM, Caffarri S, Bassi R, Golan T, Kramer D, Niyogi KK (2004) Regulation of Photosynthetic Light Harvesting Involves Intrathylakoid Lumen pH Sensing by the PsbS Protein. J Biol Chem 279:22866–22874 . https://doi.org/10.1074/jbc.M402461200

Li Z, Meng T, Ling X, Li J, Zheng C, Shi Y, Chen Z, Li Z, Li Q, Lu Y, He N (2018b) Overexpression of Malonyl-CoA: ACP Transacylase in Schizochytrium sp. to Improve Polyunsaturated Fatty Acid Production. J Agric Food Chem 66:5382–5391 . https://doi.org/10.1021/acs.jafc.8b01026

Li Z, Peers G, Dent RM, Bai Y, Yang SY, Apel W, Leonelli L, Niyogi KK (2016b) Evolution of an atypical de-epoxidase for photoprotection in the green lineage. Nat Plants 2:16140

Liang F, Englund E, Lindberg P, Lindblad P (2018) Engineered cyanobacteria with enhanced growth show increased ethanol production and higher biofuel to biomass ratio. Metab Eng 46:51–59 . https://doi.org/https://doi.org/10.1016/j.ymben.2018.02.006

Liang F, Lindblad P (2017) Synechocystis PCC 6803 overexpressing RuBisCO grow faster with increased photosynthesis. Metab Eng Commun 4:29–36 . https://doi.org/https://doi.org/10.1016/j.meteno.2017.02.002

Liang F, Lindblad P (2016) Effects of overexpressing photosynthetic carbon fl ux control enzymes in the cyanobacterium Synechocystis PCC 6803. Metab Eng 38:56–64 . https://doi.org/10.1016/j.ymben.2016.06.005

Liang M, Jiang J (2013) Progress in Lipid Research Advancing oleaginous microorganisms to produce lipid via metabolic engineering technology. Prog Lipid Res 52:395–408 . https://doi.org/10.1016/j.plipres.2013.05.002

Lin H, Lee YK (2017) Genetic engineering of medium-chain-length fatty acid synthesis in Dunaliella

tertiolecta for improved biodiesel production. 2811–2819 . https://doi.org/10.1007/s10811-017-1210-7

Lin PC, Pakrasi HB (2019) Engineering cyanobacteria for production of terpenoids. Planta 249:145–154 . https://doi.org/10.1007/s00425-018-3047-y

Lin PC, Saha R, Zhang F, Pakrasi HB (2017) Metabolic engineering of the pentose phosphate pathway for enhanced limonene production in the cyanobacterium Synechocystis sp. PCC 6803. Sci Rep 7:17503 . https://doi.org/10.1038/s41598-017-17831-y

Liu J, Sun Z, Mao X, Gerken H, Wang X, Yang W (2019) Multiomics analysis reveals a distinct mechanism of oleaginousness in the emerging model alga Chromochloris zofingiensis. Plant J 98:1060–1077 . https://doi.org/10.1111/tpj.14302

Liu Z, Yan H, Wang K, Kuang T, Zhang J, Gui L, An X, Chang W (2004) Crystal structure of spinach major light-harvesting complex at 2.72 A resolution. Nature 428:287–292 . https://doi.org/10.1038/nature02373

Lohr M, Schwender J, Polle JEW (2012) Isoprenoid biosynthesis in eukaryotic phototrophs: A spotlight on algae. Plant Sci 185–186:9–22 . https://doi.org/https://doi.org/10.1016/j.plantsci.2011.07.018

Ma YH, Wang X, Niu YF, Yang ZK, Zhang MH, Wang ZM, Yang WD, Liu JS, Li HY (2014) Antisense knockdown of pyruvate dehydrogenase kinase promotes the neutral lipid accumulation in the diatom Phaeodactylum tricornutum. Microb Cell Fact 13:100 . https://doi.org/10.1186/s12934-014-0100-9

Melis A (2009) Solar energy conversion efficiencies in photosynthesis : Minimizing the chlorophyll antennae to maximize efficiency. Plant Sci 177:272–280 . https://doi.org/10.1016/j.plantsci.2009.06.005

Mettler T, Mühlhaus T, Hemme D, Schöttler M-A, Rupprecht J, Idoine A, Veyel D, Pal SK, Yaneva-Roder L, Winck FV, Sommer F, Vosloh D, Seiwert B, Erban A, Burgos A, Arvidsson S, Schönfelder S, Arnold A, Günther M, Krause U, Lohse M, Kopka J, Nikoloski Z, Mueller-Roeber B, Willmitzer L, Bock R, Schroda M, Stitt M (2014) Systems Analysis of the Response of Photosynthesis, Metabolism, and Growth to an Increase in Irradiance in the Photosynthetic Model Organism Chlamydomonas reinhardtii. Plant Cell 26:2310 LP – 2350 . https://doi.org/10.1105/tpc.114.124537

Miloslavina Y, de Bianchi S, Dall'Osto L, Bassi R, Holzwarth AR (2011) Quenching in Arabidopsis thaliana Mutants Lacking Monomeric Antenna Proteins of Photosystem II. J Biol Chem 286:36830–36840 . https://doi.org/10.1074/jbc.M111.273227

Mitra M, Kirst H, Dewez D, Melis A (2012) Modulation of the light-harvesting chlorophyll antenna size in Chlamydomonas reinhardtii by TLA1 gene over-expression and RNA interference. Philos Trans R Soc B Biol Sci 367:3430–3443 . https://doi.org/10.1098/rstb.2012.0229

Munekage Y, Hashimoto M, Miyake C, Tomizawa K, Endo T, Tasaka M, Shikanai T (2004) Cyclic electron flow around photosystem I is essential for photosynthesis. Nature 429:579–582 . https://doi.org/10.1038/nature02598

Mussgnug JH, Wobbe L, Elles I, Claus C, Hamilton M, Fink A, Kahmann U, Kapazoglou A, Mullineaux CW, Hippler M, Nickelsen J, Nixon PJ, Kruse O (2005) NAB1 is an RNA binding protein involved in

the light-regulated differential expression of the light-harvesting antenna of Chlamydomonas reinhardtii. Plant Cell 17:3409–3421 . https://doi.org/10.1105/tpc.105.035774.algae

Napier JA (2002) Plumbing the depths of PUFA biosynthesis: a novel polyketide synthase-like pathway from marine organisms. Trends Plant Sci 7:51–54 . https://doi.org/https://doi.org/10.1016/S1360-1385(01)02191-4

Nelson N, F Yocum C (2006) Structure and function of photosystem I and II

Newman J, Branden CI, Jones TA (1993) Structure determination and refinement of ribulose 1,5-bisphosphate carboxylase/oxygenase from Synechococcus PCC6301. Acta Crystallogr D Biol Crystallogr 49:548–560 . https://doi.org/10.1107/S090744499300530X

Niu YF, Wang X, Hu DX, Balamurugan S, Li DW (2016) Molecular characterization of a glycerol - 3 - phosphate acyltransferase reveals key features essential for triacylglycerol production in Phaeodactylum tricornutum. Biotechnol Biofuels 1–11 . https://doi.org/10.1186/s13068-016-0478-1

Niyogi KK (1999) Photoprotection Revisited: Genetic and Molecular Approaches. Annu Rev Plant Physiol Plant Mol Biol 50:333–359 . https://doi.org/10.1146/annurev.arplant.50.1.333

Nobusawa T, Yamakawa-Ayukawa K, Saito F, Nomura S, Takami A, Ohta H (2019) A homolog of Arabidopsis SDP1 lipase in Nannochloropsis is involved in degradation of de novo-synthesized triacylglycerols in the endoplasmic reticulum. Biochim Biophys Acta - Mol Cell Biol Lipids 1864:1185–1193 . https://doi.org/https://doi.org/10.1016/j.bbalip.2019.05.013

Nozzi N, Oliver J, Atsumi S (2013) Cyanobacteria as a Platform for Biofuel Production . Front. Bioeng. Biotechnol. 1:7

Ott CM, Smith BD, Portis AR, Spreitzer RJ (2000) Activase region on chloroplast ribulose-1,5-bisphosphate carboxylase/oxygenase: Nonconservative substitution in the large subunit alters species specificity of protein interaction. J Biol Chem 275:26241–26244 . https://doi.org/10.1074/jbc.M004580200

Peers G, Truong TB, Ostendorf E, Busch A, Elrad D, Grossman AR, Hippler M, Niyogi KK (2009) An ancient light-harvesting protein is critical for the regulation of algal photosynthesis. Nature 462:518–521 . https://doi.org/10.1038/nature08587

Peng K-T, Zheng C-N, Xue J, Chen X-Y, Yang W-D, Liu J-S, Bai W, Li H-Y (2014) Delta 5 Fatty Acid Desaturase Upregulates the Synthesis of Polyunsaturated Fatty Acids in the Marine Diatom Phaeodactylum tricornutum. J Agric Food Chem 62:8773–8776 . https://doi.org/10.1021/jf5031086

Perin G, Bellan A, Segalla A, Meneghesso A, Alboresi A, Morosinotto T (2015) Generation of random mutants to improve light-use efficiency of Nannochloropsis gaditana cultures for biofuel production. Biotechnol Biofuels 8:161 . https://doi.org/10.1186/s13068-015-0337-5

Perrine Z, Negi S, Sayre RT (2012) Optimization of photosynthetic light energy utilization by microalgae. Algal Res 1:134–142 . https://doi.org/10.1016/j.algal.2012.07.002

Petroutsos D, Busch A, Janssen I, Trompelt K, Bergner SV, Weinl S, Holtkamp M, Karst U, Kudla J, Hippler M (2011) The chloroplast calcium sensor CAS is required for photoacclimation in Chlamydomonas reinhardtii. Plant Cell 23:2950–2963 . https://doi.org/10.1105/tpc.111.087973

Pinnola A, Staleva-Musto H, Capaldi S, Ballottari M, Bassi R, Polívka T (2016) Electron transfer between carotenoid and chlorophyll contributes to quenching in the LHCSR1 protein from Physcomitrella patens. Biochim Biophys Acta - Bioenerg 1857:1870–1878 . https://doi.org/https://doi.org/10.1016/j.bbabio.2016.09.001

Pinto TS, Malcata FX, Arrabaça JD, Silva JM, Spreitzer RJ, Esquível MG (2013) Rubisco mutants of Chlamydomonas reinhardtii enhance photosynthetic hydrogen production. Appl Microbiol Biotechnol 97:5635–5643 . https://doi.org/10.1007/s00253-013-4920-z

Polle JEW, Kanakagiri S-D, Melis A (2003) tla1, a DNA insertional transformant of the green alga Chlamydomonas reinhardtii with a truncated light-harvesting chlorophyll antenna size. Planta 217:49–59 . https://doi.org/10.1007/s00425-002-0968-1

Quaas T, Berteotti S, Ballottari M, Flieger K, Bassi R, Wilhelm C, Goss R (2015) Non-photochemical quenching and xanthophyll cycle activities in six green algal species suggest mechanistic differences in the process of excess energy dissipation. J Plant Physiol 172:92–103 . https://doi.org/https://doi.org/10.1016/j.jplph.2014.07.023

Radakovits R, Eduafo PM, Posewitz MC (2011) Genetic engineering of fatty acid chain length in Phaeodactylum tricornutum. Metab Eng 13:89–95 . https://doi.org/10.1016/j.ymben.2010.10.003

Rochaix J-D, Bassi R (2019) LHC-like proteins involved in stress responses and biogenesis/repair of the photosynthetic apparatus. Biochem J 476:581 LP – 593 . https://doi.org/10.1042/BCJ20180718

Ruban A V, Berera R, Ilioaia C, van Stokkum IHM, Kennis JTM, Pascal AA, van Amerongen H, Robert B, Horton P, van Grondelle R (2007) Identification of a mechanism of photoprotective energy dissipation in higher plants. Nature 450:575

Ruffing AM (2014) Improved Free Fatty Acid Production in Cyanobacteria with Synechococcus sp. PCC 7002 as Host. Front Bioeng Biotechnol 2:17 . https://doi.org/10.3389/fbioe.2014.00017

Ryan P, Forrester TJB, Wroblewski C, Kenney TMG, Kitova EN, Klassen JS, Kimber MS (2019) The small RbcS-like domains of the β-carboxysome structural protein CcmM bind RubisCO at a site distinct from that binding the RbcS subunit. J Biol Chem 294:2593–2603 . https://doi.org/10.1074/jbc.RA118.006330

Salas-Montantes CJ, González-Ortega O, Ochoa-Alfaro AE, Camarena-Rangel R, Paz-Maldonado LMT, Rosales-Mendoza S, Rocha-Uribe A, Soria-Guerra RE (2018) Lipid accumulation during nitrogen and sulfur starvation in Chlamydomonas reinhardtii overexpressing a transcription factor. J Appl Phycol 30:1721–1733 . https://doi.org/10.1007/s10811-018-1393-6

Schierenbeck L, Ries D, Rogge K, Grewe S, Weisshaar B, Kruse O (2015) Fast forward genetics to identify mutations causing a high light tolerant phenotype in Chlamydomonas reinhardtii by whole-genome-sequencing. BMC Genomics 16:57 . https://doi.org/10.1186/s12864-015-1232-y

Shah MMR, Liang Y, Cheng JJ, Daroch M (2016) Astaxanthin-Producing Green Microalga Haematococcus pluvialis: From Single Cell to High Value Commercial Products. Front Plant Sci 7:531 . https://doi.org/10.3389/fpls.2016.00531

Shapiguzov A, Chai X, Fucile G, Longoni P, Zhang L, Rochaix JD (2016) Activation of the Stt7/STN7 Kinase through dynamic interactions with the cytochrome b6 f complex. Plant Physiol.

https://doi.org/10.1104/pp.15.01893

Sharma AK, Mühlroth A, Jouhet J, Maréchal E, Alipanah L, Kissen R, Brembu T, Bones AM, Winge P (2019) The Myb-like transcription factor Phosphorus Starvation Response (PtPSR) controls conditional P acquisition and remodeling in marine microalgae. New Phytol. https://doi.org/10.1111/nph.16248

Shen L, Huang Z, Chang S, Wang W, Wang J, Kuang T, Han G, Shen J-R, Zhang X (2019) Structure of a $C_2S_2M_2N_2$-type PSII–LHCII supercomplex from the green alga Chlamydomonas reinhardtii; Proc Natl Acad Sci 201912462 . https://doi.org/10.1073/pnas.1912462116

Simionato D, Block MA, La Rocca N, Jouhet J, Maréchal E, Finazzi G, Morosinotto T (2013) The response of Nannochloropsis gaditana to nitrogen starvation includes de novo biosynthesis of triacylglycerols, a decrease of chloroplast galactolipids, and reorganization of the photosynthetic apparatus. Eukaryot Cell 12:665–676 . https://doi.org/10.1128/EC.00363-12

Spalding MH (2013) Modulation of low carbon dioxide inducible proteins (lci) for increased biomass production and photosynthesis. U.S. Patent Application No. 13/535,842.

Steinbeck J, Ross IL, Rothnagel R, Gäbelein P, Schulze S, Giles N, Ali R, Drysdale R, Sierecki E, Gambin Y, Stahlberg H, Takahashi Y, Hippler M, Hankamer B (2018) Structure of a PSI–LHCI–cyt b6f supercomplex in Chlamydomonas reinhardtii promoting cyclic electron flow under anaerobic conditions. Proc Natl Acad Sci 115:10517 LP – 10522 . https://doi.org/10.1073/pnas.1809973115

Steinbrenner J, Sandmann G (2006) Transformation of the Green Alga Haematococcus pluvialis with a Phytoene Desaturase for Accelerated Astaxanthin Biosynthesis. Appl Environ Microbiol 72:7477 LP – 7484 . https://doi.org/10.1128/AEM.01461-06

Stephenson PG, Moore CM, Terry MJ, Zubkov M V., Bibby TS (2011) Improving photosynthesis for algal biofuels: Toward a green revolution. Trends Biotechnol 29:615–623 . https://doi.org/10.1016/j.tibtech.2011.06.005

Su X, Ma J, Pan X, Zhao X, Chang W, Liu Z, Zhang X, Li M (2019) Antenna arrangement and energy transfer pathways of a green algal photosystem-I–LHCI supercomplex. Nat Plants 5:273–281 . https://doi.org/10.1038/s41477-019-0380-5

Su X, Ma J, Wei X, Cao P, Zhu D, Chang W, Liu Z, Zhang X, Li M (2017) Structure and assembly mechanism of plant C2S2M2-type PSII-LHCII supercomplex. Science (80-) 357:815 LP – 820 . https://doi.org/10.1126/science.aan0327

Sun XM, Ren LJ, Zhao QY, Ji XJ, Huang H (2019) Enhancement of lipid accumulation in microalgae by metabolic engineering. Biochim Biophys Acta - Mol Cell Biol Lipids 1864:552–566 . https://doi.org/https://doi.org/10.1016/j.bbalip.2018.10.004

Tanaka A, Ito H, Tanaka R, Tanaka NK, Yoshida K, Okada K (1998) Chlorophyll a oxygenase (CAO) is involved in chlorophyll b formation from chlorophyll a. Proc Natl Acad Sci 95:12719–12723 . https://doi.org/10.1073/pnas.95.21.12719

Taylor TC, Backlund A, Bjorhall K, Spreitzer RJ, Andersson I (2001) First crystal structure of Rubisco from a green alga, Chlamydomonas reinhardtii. J Biol Chem 276:48159–48164 . https://doi.org/10.1074/jbc.M107765200

Tian QL, Shi DJ, Jia XH, Mi HL, Huang XW, He PM (2014) Recombinant expression and functional

analysis of a Chlamydomonas reinhardtii bacterial-type phosphoenolpyruvate carboxylase gene fragment. Biotechnol Lett 36:821–827 . https://doi.org/10.1007/s10529-013-1418-9

Torres-Romero I, Kong F, Légeret B, Beisson F, Peltier G, Li-Beisson Y (2019) Chlamydomonas cell cycle mutant crcdc5 over-accumulates starch and oil. Biochimie. https://doi.org/https://doi.org/10.1016/j.biochi.2019.09.017

Treves H, Raanan H, Finkel OM, Berkowicz SM, Keren N, Shotland Y, Kaplan A (2013) A newly isolated Chlorella sp. from desert sand crusts exhibits a unique resistance to excess light intensity. FEMS Microbiol Ecol 86:373–380 . https://doi.org/10.1111/1574-6941.12162

Treves H, Raanan H, Kedem I, Murik O, Keren N, Zer H, Berkowicz SM, Giordano M, Norici A, Shotland Y, Ohad I, Kaplan A (2016) The mechanisms whereby the green alga Chlorella ohadii, isolated from desert soil crust, exhibits unparalleled photodamage resistance. New Phytol 210:1229–1243 . https://doi.org/10.1111/nph.13870

Uemura K, Miyachi S, Yokota A (1997) Ribulose-1 , 5-Bisphosphate Carboxylase / Oxygenase from Thermophilic Red Algae with a Strong Specificity for CO 2 Fixation. 571:568–571

Wang C, Chen X, Li H, Wang J, Hu Z (2017) Artificial miRNA inhibition of phosphoenolpyruvate carboxylase increases fatty acid production in a green microalga Chlamydomonas reinhardtii. Biotechnol Biofuels 10:91 . https://doi.org/10.1186/s13068-017-0779-z

Wang C, Li Y, Lu J, Deng X, Li H, Hu Z (2018) Effect of overexpression of LPAAT and GPD1 on lipid synthesis and composition in green microalga Chlamydomonas reinhardtii. J Appl Phycol 30:1711–1719 . https://doi.org/10.1007/s10811-017-1349-2

Wang W, Yu LJ, Xu C, Tomizaki T, Zhao S, Umena Y, Chen X, Qin X, Xin Y, Suga M, Han G, Kuang T, Shen JR (2019) Structural basis for blue-green light harvesting and energy dissipation in diatoms. Science (80-) 363:eaav0365 . https://doi.org/10.1126/science.aav0365

Wang X, Liu W, Xin C, Zheng Y, Cheng Y, Sun S, Li R, Zhu X-G, Dai SY, Rentzepis PM, Yuan JS (2016) Enhanced limonene production in cyanobacteria reveals photosynthesis limitations. Proc Natl Acad Sci 113:14225 LP – 14230 . https://doi.org/10.1073/pnas.1613340113

Wei H, Shi Y, Ma X, Pan Y, Hu H, Li Y, Luo M, Gerken H, Liu J (2017a) A type-I diacylglycerol acyltransferase modulates triacylglycerol biosynthesis and fatty acid composition in the oleaginous microalga, Nannochloropsis oceanica. Biotechnol Biofuels 10:174 . https://doi.org/10.1186/s13068-017-0858-1

Wei K, Tan M, Lee YK (2017b) Expression of the heterologous Dunaliella tertiolecta fatty acyl-ACP thioesterase leads to increased lipid production in Chlamydomonas reinhardtii. J Biotechnol 247:60–67 . https://doi.org/10.1016/j.jbiotec.2017.03.004

Wei L, Wang Q, Xin Y, Lu Y, Xu J (2017c) Enhancing photosynthetic biomass productivity of industrial oleaginous microalgae by overexpression of RuBisCO activase. Algal Res 27:366–375 . https://doi.org/10.1016/j.algal.2017.07.023

Whitney SM, Houtz RL, Alonso H (2011) Advancing Our Understanding and Capacity to Engineer Nature's CO2-Sequestering Enzyme, Rubisco. Plant Physiol 155:27–35 . https://doi.org/10.1104/pp.110.164814

Wichmann J, Baier T, Wentnagel E, Lauersen KJ, Kruse O (2018) Tailored carbon partitioning for

phototrophic production of (E)-α-bisabolene from the green microalga Chlamydomonas reinhardtii. Metab Eng 45:211–222 . https://doi.org/https://doi.org/10.1016/j.ymben.2017.12.010

Wunder T, Cheng SLH, Lai S-K, Li H-Y, Mueller-Cajar O (2018) The phase separation underlying the pyrenoid-based microalgal Rubisco supercharger. Nat Commun 9:5076 . https://doi.org/10.1038/s41467-018-07624-w

Xu Y, Ibrahim I, Wosu C, Ben-Amotz A, Harvey P (2018) Potential of New Isolates of Dunaliella Salina for Natural β-Carotene Production. Biology (Basel) 7:14 . https://doi.org/10.3390/biology7010014

Xue J, Balamurugan S, Li DW, Liu YH, Zeng H, Wang L, Yang WD, Liu JS, Li HY (2017) Glucose-6-phosphate dehydrogenase as a target for highly efficient fatty acid biosynthesis in microalgae by enhancing NADPH supply. Metab Eng 41:212–221 . https://doi.org/https://doi.org/10.1016/j.ymben.2017.04.008

Xue J, Niu YF, Huang T, Yang WD, Liu JS, Li HY (2015) Genetic improvement of the microalga Phaeodactylum tricornutum for boosting neutral lipid accumulation. Metab Eng 27:1–9 . https://doi.org/https://doi.org/10.1016/j.ymben.2014.10.002

Yamaoka Y, Achard D, Jang S, Legéret B, Kamisuki S, Ko D, Schulz-Raffelt M, Kim Y, Song WY, Nishida I, Li-Beisson Y, Lee Y (2016) Identification of a Chlamydomonas plastidial 2-lysophosphatidic acid acyltransferase and its use to engineer microalgae with increased oil content. Plant Biotechnol J 14:2158–2167 . https://doi.org/10.1111/pbi.12572

Yan J, Cheng R, Lin X, You S, Li K, Rong H, Ma Y (2013) Overexpression of acetyl-CoA synthetase increased the biomass and fatty acid proportion in microalga Schizochytrium. Appl Microbiol Biotechnol 97:1933–1939 . https://doi.org/10.1007/s00253-012-4481-6

Yang J, Pan Y, Bowler C, Zhang L, Hu H (2016) Knockdown of phosphoenolpyruvate carboxykinase increases carbon flux to lipid synthesis in Phaeodactylum tricornutum. Algal Res 15:50–58 . https://doi.org/https://doi.org/10.1016/j.algal.2016.02.004

Zäuner S, Jochum W, Bigorowski T, Benning C (2012) A cytochrome b5-containing plastid-located fatty acid desaturase from Chlamydomonas reinhardtii. Eukaryot Cell 11:856–863 . https://doi.org/10.1128/EC.00079-12

Zhang X, Wen F, Xu Z, Sun D, Chew W, Liu J (2019) De novo transcriptomic analysis of the oleaginous alga Botryococcus braunii AC768 (Chlorophyta). J Appl Phycol 31:255–267 . https://doi.org/10.1007/s10811-018-1577-0

Zhu G, Kurek I, Liu L (2010) Chapter 20 Engineering Photosynthetic Enzymes Involved in CO2–Assimilation by Gene Shuffling BT - The Chloroplast: Basics and Applications. In: Rebeiz CA, Benning C, Bohnert HJ, Daniell H, Hoober JK, Lichtenthaler HK, Portis AR, Tripathy BC (eds). Springer Netherlands, Dordrecht, pp 307–322

Zou LG, Chen JW, Zheng DL, Balamurugan S, Li DW, Yang WD, Liu JS (2018) High - efficiency promoter - driven coordinated regulation of multiple metabolic nodes elevates lipid accumulation in the model microalga Phaeodactylum tricornutum. Microb Cell Fact 1–8 . https://doi.org/10.1186/s12934-018-0906-y

CHAPTER 2
Introduction: Biomass from microalgae: the potential of domestication towards sustainable biofactories

This review was published in 2018:

Benedetti, M.; Vecchi, V.; Barera, S.; Dall'Osto, L. Biomass from microalgae: The potential of domestication towards sustainable biofactories. Microb. Cell Fact. 2018, 17, 173.

Abstract: Interest in bulk biomass from microalgae, for the extraction of high-value nutraceuticals, bio-products, animal feed and as a source of renewable fuels, is high. Advantages of microalgal vs. plant biomass production include higher yield, use of non-arable land, recovery of nutrients from wastewater, efficient carbon capture and faster development of new domesticated strains. Moreover, adaptation to a wide range of environmental conditions evolved a great genetic diversity within this polyphyletic group, making microalgae a rich source of interesting and useful metabolites. Microalgae have the potential to satisfy many global demands; however, realization of this potential requires a decrease of the current production costs. Average productivity of the most common industrial strains is far lower than maximal theoretical estimations, suggesting that identification of factors limiting biomass yield and removing bottlenecks are pivotal in domestication strategies aimed to make algal-derived bio-products profitable on the industrial scale. In particular, the light-to-biomass conversion efficiency represents a major constraint to finally fill the gap between theoretical and industrial productivity. In this respect, recent results suggest that significant yield enhancement is feasible. Full realization of this potential requires further advances in cultivation techniques, together with genetic manipulation of both algal physiology and metabolic networks, to maximize the efficiency with which solar energy is converted into biomass and bio-products. In this review, we draft the molecular events of photosynthesis which regulate the conversion of light into biomass, and discuss how these can be targeted to enhance productivity through mutagenesis, strain selection or genetic engineering. We outline major successes reached, and promising strategies to achieving significant contributions to future microalgae-based biotechnology.

Background

Microalgae, a promising feedstock option

Approximately 100,000 terawatts-year (TW-y) power from sunlight reach the surface of our planet. This is a renewable resource exceeding the current human global energy demand (15 TW-y) and the 24 TW-year predicted for anthropic activities by 2030 (Hambourger et al. 2009; Cho 2010) by > 3 orders of magnitude. Sunlight might fully provide for future world energy demand (Chu and Majumdar 2012) and yet its dilute nature represents a major challenge for concentrating, harvesting, storing it efficiently. Oxygenic photosynthesis converts CO_2 into reduced carbon compounds using light and water; through this process photoautotrophic organisms, namely plants, algae and cyanobacteria, store solar energy at a rate of 120 TW-y at the global scale. Therefore, using sunlight and CO_2 to produce a variety of organic molecules and biomass, by the extensive cultivation of photosynthetic organisms, has the potential to cover a significant portion of global energy demand (Stephenson et al. 2011), besides providing for an effective CO_2 capture from e.g. power plants or other large-scale emission sources. As unique feature, photosynthesis allows for direct energy

storage into liquid fuels which can be used in the existing transport systems, while other forms of renewable energy such as hydro-, wind or photovoltaic power, cannot.

Thus, mass culture of microalgae has gained interest in the past few decades. Indeed, beside small-scale traditional cultivations mainly aimed to human feeding, commercial production of algae on a larger scale has been identified in recent years as a renewable and environmentally sustainable strategy for feedstock production. Microalgae include a wide group of photosynthetic, eukaryotic, unicellular organisms: green microalgae, belonging to the class Chlorophyceae, include genera which are among the most widely used for industrial applications, such as *Haematococcus*, *Chlorella* and *Dunaliella*. Diatoms and cyanobacteria, which also represent a valuable biotechnological platform (Huang and Daboussi 2017; Hagemann and Hess 2018), will not be included in this review.

The phyletic group of green microalgae include species which have adapted to diverse environmental conditions, even extreme, of the planet (Tirichine and Bowler 2011). By considering that the unclassified species likely represent the majority of this group (Guiry 2012), it comes that green microalgae are a source of metabolic and genetic diversity (Blunt et al. 2012). Microalgal biomass represents an energy-rich feedstock, which received increasing attention for commercial cultivation in open ponds or closed photobioreactors (PBRs). So far industrial applications include production of bioactive compounds (Borowitzka 2013), recombinant proteins (Scranton et al. 2015), next generation biofuels and wastewater treatment (Sutherland et al. 2015). Once target products extracted, the residual biomass can be further processed into livestock feed, organic fertilizer and biostimulants, or used for energy cogeneration (Passos et al. 2014; Garcia-Gonzalez and Sommerfeld 2016; Dineshkumar et al. 2018); therefore, biorefinery processes applied to mono-species cultivation can yield a large variety of resources.

Although photosynthetic machinery is similar to that of plants, microalgae convert solar energy into biomass and fix CO_2 at efficiencies that are appreciably higher than land plants (Bhola et al. 2014). The maximal conversion efficiencies of solar radiation into biomass are 4.6% for C3 plants and 6.0% for C4 plants at 30 °C, which drops to 2.9% and 4.2% respectively, when measured in the field (Zhu et al. 2010b).

Theoretical quantification of 8–10% in energy conversion efficiency of microalgae (Melis 2009) translates into an expected maximal productivity of 280 ton of algal biomass hectare (ha)$^{-1}$ year^{-1}, while outdoor mass cultivation record yield beyond 100 ton ha^{-1} year^{-1} could not be reached (Rodolfi et al. 2009). This compares to 0.2% of energy conversion efficiency and an average of 10 ton ha^{-1} year^{-1}, reported for sugarcane field trials in the tropics. When considering oil yield extracted from plant vs. algal biomass, palm oil can produce a maximum of 4–5 ton ha^{-1} year^{-1} (Chisti 2007; Mata et al. 2010) vs. 30 ton ha^{-1} year^{-1} (Rodolfi et al. 2009). Thus, record yields of microalgal culture at temperate latitudes is > 5 times higher respect to the case of the best figure for a plant crop.

Multiple reasons contribute to such a feature:

I. When growing in aerated liquid cultures, cells have easy access to light, CO_2 and nutrients. They lack non-productive (heterotrophic) organs to maintain, and the simpler unicellular structure make the whole biomass fully photosynthetically active, irrespective to seasonal life cycle;

II. Algae are metabolically flexible and have a short doubling time. Although most microalgae are primarily photoautotrophs, many species undergo metabolic shift to heterotrophy upon changes in environmental conditions, utilizing organic compounds as C and energy source or to mixotrophy (carrying out photosynthesis as the main energy source, and both organic molecules and carbon dioxide are used as C source). Moreover, under optimal growth conditions, most species have doubling time of a few hours, and cultures reach as much as 10 g l^{-1} of heterotrophic dry weight (DW) biomass and 6 g l^{-1} of photoautotrophic DW biomass (Cuaresma et al. 2009; Mitra et al. 2012a);

III. Microalgae do not require fertile land, and can grow in wastelands, using brackish or wastewater, or even sea water in the case of marine species; hence, their cultivation does not compete with resources for conventional food production, and would be more environmentally sustainable respect to extensive cultivation of crops. Therefore, microalgae offer the opportunity to shift part of unsustainable farming and fishing routines toward unproductive region;

IV. Different species can be selected for specific growth conditions, suited to the local climate, which is more difficult with conventional crops.

Table 1: Noteworthy microalgae species and their biotechnological applications for production of high-value metabolites

Application	**Industrial and medical field**	**Cosmetics and food colorant**	**High-value metabolites**	**Biofuel**	**Dietary supplement and nutraceuticals**
Bioproduct category *Microalgae species* (metabolite)	*Polysaccharides* *Chlorella* spp. (*β-glucans, starch*) *Porphyridium cruentum* *Netrium digitus* *Phycotoxins* *Amphidinium* *Dinophysis* *Prorocentrum* *Phycobiliproteins* Red algae (Phycoerythrin)	*Phycobiliproteins* *Arthrospyra platensis* (phycocyanin) *Carotenoids* *Arthrospyra platensis* *Chlorella vugaris* *Haematococcus pluvialis* *Chlorella zofingiensis* (astaxanthin) *Dunaliella salina* (β-carotene)	*Mycosporine-like amino acids* *Aphanizomenon flosaquae* *Vitamins* *Euglena gracilis* (biotin, α-tocopherol) *Prototheca moriformis* (ascorbic acid) *Arthrospyra platensis* *Chlorella* spp. *Proteins* *Arthrospyra platensis* *Chlorella* spp.	*Oil to biodiesel* *Botryococcus braunii* *Chlorella* spp. *Dunaliella salina* *Monoraphidium contortum* *Scenedesmus* spp. *Carbohydrate to bioethanol* *Spirogyra* spp. *Chlorococum* spp. *Bio-hydrogen* *Chlamydomonas reinhardtii*	*Polyunsaturated fatty acids (PUFAs)* *Parietochloris incisa* *Porphyridium* spp. (arachidonic acid) *Arthrospyra platensis* *Rhodomonas salina* *Tetraselmis uecica* (α-linolenic acid) *Chlorella minutissima* *Monodosus* spp. *Nannochloropsis* spp. *Neochloris oleoabundans* *Pavlova lutheri* (eicosapentaenoic acid) *Crypthecodiuimu* spp. *Isochrysis galbana* *Schizochytrium* spp. *Thalassiosira* spp. *Thraustochytrium* spp. (docosahexaenoic acid)

Main text

2.1 The most promising microalgae species for production of valuable compounds and for biotechnology applications

In this paragraph, the bio-technological applications of best wild type species are reviewed with focus on highvalue production chemicals and biomass for biofuels (Table 1). Currently, the most relevant microalgal species for high-value chemicals production are the cyanobacterium *Arthrospira platensis* (formerly known as Spirulina) and the green microalgae *Chlorella vulgaris*, *Dunaliella salina* and *Haematococcus pluvialis*, which are mainly dedicated to the production of single products in largescale cultivation systems.

Arthrospira platensis is exploited as source of nutraceuticals (Herrera Bravo de Laguna et al. 2015), long-chain polyunsaturated fatty acids (lc-PUFAs) (Al-Dhabi and Valan Arasu 2016), carotenoids (Hynstova et al. 2018) and proteins (Lupatini et al. 2017).

Other applications of Spirulina are in the medical field as a therapeutic (Wu et al. 2016; Lima et al. 2017), as antioxidant (Al-Dhabi and Valan Arasu 2016) and for the extraction of the blue pigment phycocyanin, approved as food colorant by FDA (Rizzo et al. 2015).

Genus *Chlorella* includes a number of species which are widely commercialized for production of nutraceuticals. Besides to the high protein, carotenoids and vitamins content (García et al. 2017), *C. vulgaris* contains also β- and α-glucans, d-glucose polysaccharides which act as immune stimulators, free-radical scavengers and anticancer compounds (Tabarsa et al. 2015). Moreover, *Chlorella* has been successfully used to produce starch, reaching 26% DW yield under mixotrophic condition (Li et al. 2015).

Carotenoids represent the commercial product from microalgae with highest success. Carotenoids are widely used as food colorants, aquaculture feed additives and components for cosmetics and skin care; carotenoids also have biomedical applications, including anti-inflammatory activities which are related to their strong antioxidant properties (Young and Lowe 2018). β-carotene, the first carotenoid successfully marketed at large scale, is produced from the halophilic alga *Dunaliella salina* through both extensive cultivation in ponds and intensive cultivation in PBRs (Bonnefond et al. 2017). Recently, new strains with different ability to accumulate carotenoids and different capacity of photoprotection against high light stress have been isolated; the most promising strain was characterized by a β-carotene productivity of 3.5 g l^{-1} day^{-1} at 1500 µmol m^{-2} s^{-1} (Xu et al. 2018). Currently, various strains of *D. salina* growing at different salinity conditions are available (Ahmed et al. 2017).

Astaxanthin is a high-value, red keto-carotenoid, successfully commercialized by many companies worldwide through cultivation of the green alga *Haematococcus pluvialis*. Under various stress conditions, this alga changes from a thin-wall mobile phase to a red thick-wall resting phase, in which astaxanthin can reach up to 5% DW (Wayama et al. 2013). Astaxanthin is widely employed in the

feed, cosmetic, aquaculture, nutraceutical and pharmaceutical industries because of its antioxidant potential (Shah et al. 2016). Moreover, astaxanthin-rich *Haematococcus* is a popular nutraceutical antioxidant for human diet (Nicoletti 2016). *Chlorella zofingiensis* has been proposed as an alternative astaxanthin source which is more reliable in growth (Liu et al. 2014).

Biosynthesis of fatty acids and triglycerides (TAGs) is relevant for several industrial applications. Microalgae are the primary producers of lc-PUFAs such as eicosapentaenoic acid (EPA) and docosahexaenoic acid (DHA), which accumulate in the oil of many fish species. Aquaculture farming increased demand of lcPUFAs for nutrition, which are currently produced from fish oil, while a more sustainable lc-PUFA supply is seeked. Several marine algal species are rich in lcPUFAs thus have a great potential for biorefinery: these include *Thraustochytrium* sp., *Pavlova lutheri*, *Nannochloropsis gaditana*, *Isochrysis galbana*, *Crypthecodinium cohnii* (rich in DHA and EPA), *Rhodomonas salina* and *Tetraselmis suecica* (α-linolenic acid) (Liu et al. 2013; Ji et al. 2015)and *Parietochloris incisa* (arachidonic acid) (Zorin et al. 2014); these are currently exploited by a number of small companies, marketing biomass of high-values but at small-scale. Lc-PUFAs are important elements for human diet: DHA plays a crucial role as anti-inflammation molecule in allergic diseases and has considerable benefits on visual and cognitive functions; optimization of the ratio of lc-PUFAs in nutraceuticals may contribute to reduce the severity of allergic disease symptoms (Zárate et al. 2017); oil from *Nannochloropsis*, *Rhodomonas* and *Tetraselmis* has higher antioxidant properties respect to fish oil, likely due to the content of valuable carotenoids and polyphenols and is expected to replace fish oils in diets soon (Ryckebosch et al. 2014).

Further species with high potential for large-scale exploitation of extracellular polysaccharides include the microalgae *Porphyridium* and *Desmidiales* spp. Red microalgae *Porphyridium* spp. are fast-growing and accumulate extracellular polysaccharides commercially used in cosmetic and medical field (Arad and van Moppes 2013; Dvir et al. 2015). Amongst *Desmidiales*, *Netrium digitus* has been successfully cultivated in porous substrate bioreactor, reaching a maximum product concentration of 25 g m^{-2} (Ekelhof and Melkonian 2017).

In the last decade, microalgae have received increasing interest as a source of biomass for replacing fossil fuels. Liquid fuels derived from raw biomass are an attractive source of renewable energy, to be used in transport system or energy cogeneration. With respect to the major biofuels currently produced worldwide, namely bio-ethanol from sugar cane and biodiesel from oil crops, the so called "third generation" (microalgal) biofuels, are considered as a promising option, since these organisms are highly productive and provide a solution for the food *vs*. fuel problem (Milano et al. 2016).

Green algae accumulate high levels of polysaccharides both as cell-wall constituents and storage molecules that can be fermented to bioethanol (Shokrkar et al. 2017; Shokrkar et al. 2018). Oil fraction of algal biomass, which range from 20 to 60% DW depending on the species and growth conditions (Rodolfi et al. 2009; Ghasemi Naghdi et al. 2016), is processed by transesterification to produce biodiesel. In this respect, promising species belong to the genus *Chlorella* (Liu et al. 2016), *Scenedesmus* (Breuer et al. 2014) and *Monoraphidium*, the latter showing high productivity and high-quality lipid profile (Bogen et al. 2013). An unusually rich source of TAGs is the green microalga *Botryococcus braunii* (hydrocarbons constituting up to 75% of its DW), however its potential is limited by the slow growth (Gouveia et al. 2017).

Despite great advantages offered by microalgae exploitation, production of third generation biodiesel is still far from being commercially viable (Benvenuti et al. 2017). As an alternative, biogas generation through anaerobic digestion of microalgal biomass has been proposed as a more energetically-favorable process (Gonzalez-Fernandez et al. 2015). The efficiency of biogas production is species-dependent because is based on cell wall degradability and sometime limited by the content in molecules inhibiting growth of methanogenic *Archaea* (Santos-Ballardo et al. 2016). A number of pre-treatment procedures have been tested, including cell wall disruption by chemical/physical methods or enzymatic hydrolysis, which enhanced bio-methane yield (Mahdy et al. 2014; Passos et al. 2014; Mahdy et al. 2016).

Finally, microalgae and cyanobacteria can produce biohydrogen through photo-fermentation, in an anaerobic process involving oxidation of ferredoxin by the hydrogenase enzyme (Khetkorn et al. 2017; Sharma and Arya 2017). Although biological H_2 shows great promise for generating future, large scale sustainable energy, a number of bottlenecks still limit its production (Dubini and Ghirardi 2015); however, recent result (Venkanna et al. 2017) identified in *C. reinhardtii* promising targets for genetic engineering of H_2 production capacity while the use of temperature-sensitive conditional PSII mutants has been proposed in order to separate the oxygenic biomass-accumulating phase from the oxygen sensitive hydrogenase activity (Bayro-Kaiser and Nelson 2016).

Microalgae are gaining importance in the biological offset of polluted matrix, because of their ability to thrive under extreme or polluted condition: they serve for direct carbon capture, a way for reducing CO_2 released by large-scale emission plants (Cheah et al. 2016). Promising species include *Scenedesmus obliquus*, *Chlorella vulgaris*, *Chlorella protothecoides* and *Spirulina* spp., which can grow up to 15–18% CO_2, although highest productivity was observed around 10% C O_2 (Rosa et al. 2015; Assunção et al. 2017). In last years, *N. gaditana* is arising as promising species for CO_2 removal due to a high biofixation rate—more than 1.7 g^{-1} l^{-1} day^{-1} (Adamczyk et al. 2016).

Growth in open ponds is an established technology for bioremediation of wastewater and nutrient recovery in the form of biomass (Sutherland et al. 2015). The effectiveness of microalgae to use inorganic N and P to sustain growth as well as their capacity to sequester heavy metals and toxic compounds, have been demonstrated with a wide range of wastewaters, and at a range of scales (Caporgno et al. 2015; Lv et al. 2017).

2.2 Technical challenges to cost-effective, large-scale microalgae production

Despite a number of industrial applications of microalgae have been proposed and studied in lab-scale, the only successful commercial exploitation of microalgal mass culture is the production of carotenoids, namely β-carotene by *D. salina*, and astaxanthin by *H. pluvialis* (Borowitzka 2013). Other species (*Chlorella* spp., *Spirulina* spp.) produce high-value compounds, however these productions are currently applied at small-scale cultivations, which need significant reduction in operating costs to become competitive with the same molecules extracted from other feedstocks (Leu and Boussiba 2014). A number of species have been identified as promising targets for biorefinery approaches (Chew et al. 2017), which, however, have not yet come to economic viability.

Thus, while microalgae represent a promising source of valuable bio-based products, (1) optimization of both cultivation and processing technologies, together with (2) selection of candidates with high growth rate and cell density, are required to make the process profitable (’t Lam et al. 2018). An overview of the approaches and the major challenges related to point (1) are presented as follows.

In algal biomass pipeline, there are many elements which contribute to the overall cost of the process. Major factors to take into account are (i) the choice of production system, (ii) the strategies to supply nutrients, aeration, mixing, and (iii) how to harvest and process biomass, and (iv) the procedure to avoid infections and contaminants. Different approaches are available, each having benefits and limitations (Fernandes et al. 2015).

Microalgae are mainly cultivated in open ponds, which are cheaper to build, and easier to operate and to scaleup than closed systems. Generally, ponds are raceways at depth of 20–30 cm, in which biomass is mixed by paddles or left unstirred. Drawbacks of these systems include the complication of controlling contaminations, and the difficult of keeping constant growth parameters (e.g. temperature, pH, light); moreover, they suffer of low productivities (< 20 g m^{-2} day^{-1}) due to poor gas exchange and dark zone, therefore low cell density forces to cover extensive areas and requires high costs for harvesting the biomass.

As an alternative to open ponds, closed PBRs allow for higher productivities (~ 0.8–1.5 g l^{-1} day^{-1} (Rodolfi et al. 2009), up to 10 times higher than ponds). Lab-scale PBRs include flat reactors, tubular reactors or vertical plastic bags, with more control over the growth environment, in which biomass is mixed by air-lift or by pumping. These configurations allow higher cell density than ponds, thus improve economic viability of production, however they (i) have high building costs and are difficult to scale-up, (ii) can operate in a sterile mode, which however adds to the management fees, and (iii) require a high energy input for gas exchange (Cuaresma et al. 2011; Münkel et al. 2013). Together with light, CO_2 and nutrients must be supplied to maximize the growth rate, and it significantly affects the economy balance. CO_2 can be delivered through direct bubbling, and its distribution in the culture represents an additional cost factor; another challenge is the removal of excess O_2 which, above air level, inhibits photosynthesis (Wang et al. 2012).

A third production method is the surface-attached algal biofilm, which showed greater yield than suspended culture, and lower land and water requirements, in lab-scale trials. Algal biofilm system thus appears a good option for low-cost productions (Ozkan et al. 2012; Zhang et al. 2017), however more research is needed to move from bench-scale to pilot plant.

Following growth, biomass must be (i) harvested and (ii) processed to dryness. Both steps remain a major obstacle to industrial scale processing and contribute to ~ 1/3 of the final biomass cost. Current harvesting methods include chemical, mechanical and bio-based procedures: electrolytes or polymers are added to flocculate cells; centrifugation or flow filtration are rapid methods, which however implies high investments and operating costs; biological-based methods include auto-flocculation (at high pH, in excess of Ca^{2+} ions), bio-flocculation (caused by secreted polymers) or microbial-induced flocculation (Wrede et al. 2014). Dewatering and drying of biomass is required, and the low biomass concentration (0.1–1% w/w) affects the cost of the final product (Chen et al. 2015). In case the release of the products from cells is required, it should be as more energy-efficient

as possible, avoiding the use of expensive solvents, and costs for treating biomass should be minimized. Novel approaches which limit the use of solvents, e.g. based on enzymatic hydrolysis of the cell wall (Mahdy et al. 2014; Shokrkar et al. 2017), still suffer for expensive enzyme production. To significantly reduce energy penalty of the production process, the waste biomass can be directed to anaerobic digestion and production of biogas, fertilizers, soil amendments or feeds (Yaakob et al. 2014; Mahdy et al. 2016; Dineshkumar et al. 2018).

Figure 2.1 shows the different stages in the production of algal biomass, including the factors to be considered and optimized, which contribute to the price of bioproducts. In consideration of the processing costs at the present state of technology, engineering optimization is necessary to find new, cost-effective methods of producing large quantities of feedstock. However, integration of innovative technical solutions with strains improved by biotechnological approaches, appears essential.

The overall cost of a biomolecule is the results of cellular content of the desired product, and growth rate of the culture, the latter being dependent on the efficiency at which photosynthetically active radiation (PAR) is used to drive photosynthesis. Indeed, an area of promising research aims at improving the light-to-biomass conversion efficiency under mass culture conditions.

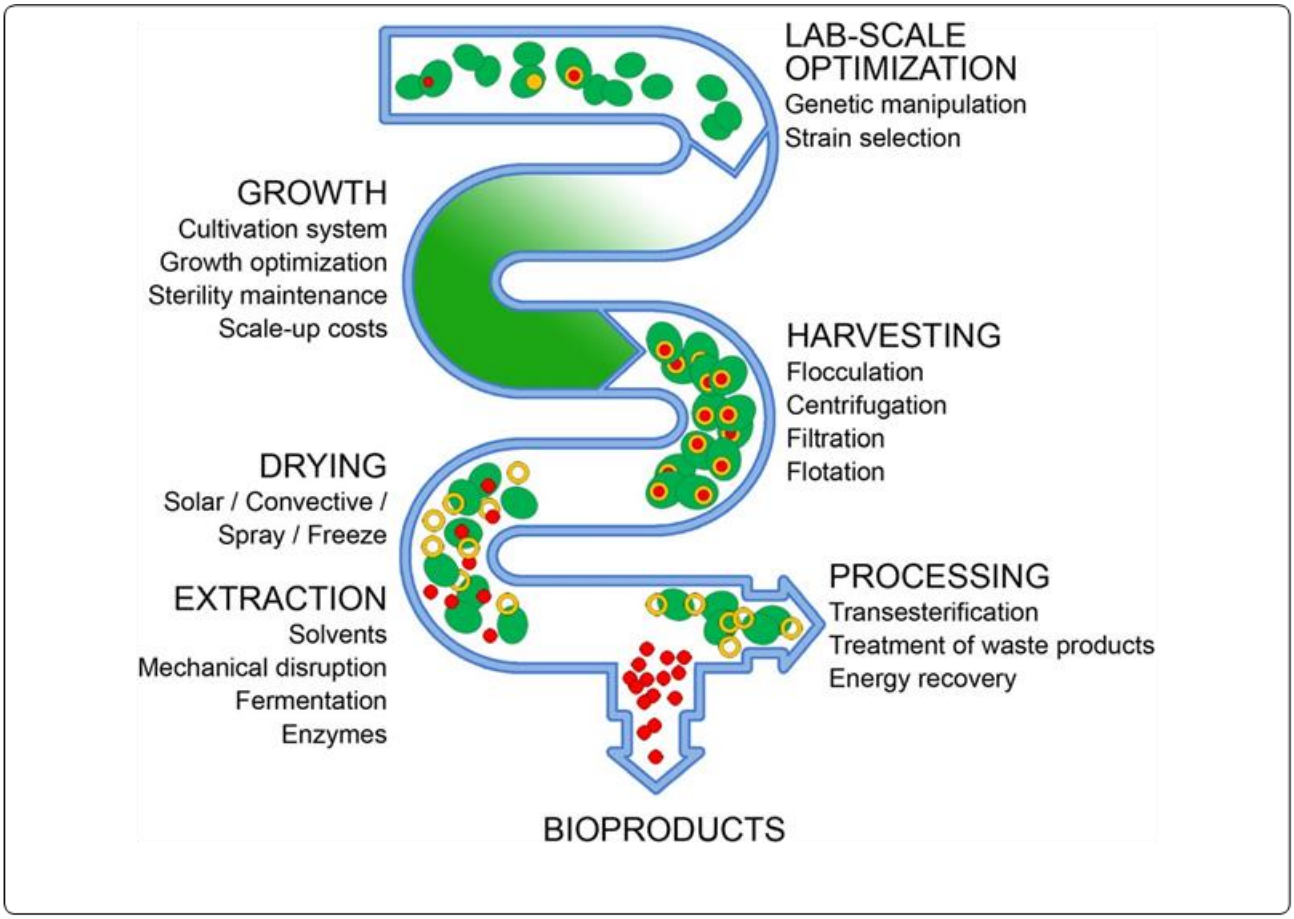

Figure 2.1. General scheme of the algal production chain. A number of factors, including the high cost of the infrastructure and the energy required for growth, harvesting and processing the algal biomass, significantly contribute to the cost of the whole production pipeline.

2.3 Biological constraints in light-to-biomass conversion efficiency

Calculations in (Melis 2009) provided both theoretical maxima of solar energy conversion efficiencies in photosynthesis and productivity yield of microalgae, equal to 8–10% solar-tobiomass and 280 ton of dry biomass ha^{-1} $year^{-1}$, respectively. Instead, outdoor mass cultivation showed that, with the present technology and wild type strains, annual productivities beyond 80–100 ton DW ha^{-1} $year^{-1}$ cannot be maintained at large scale and over long periods (Rodolfi et al. 2009). Overcoming this gap, which limits exploitation of microalgae to their full potential, is therefore essential.

Wild type algal strains suffer of light use inefficiency. Enhancing light-to-biomass conversion efficiency will help counterbalancing the cost of energy and nutrients used in the cultivation system, as well as reducing the costs of downstream biomass processing, making it a target for genetic improvement.

Regulation of light harvesting capacity is crucial for cells in order to balance light reactions and downstream biochemical events of photosynthesis. Indeed, autotrophs have evolved regulatory mechanisms, to fine-tune continuous transitions between “conservative” and “dissipative” state of absorbed energy. In particular, photosynthesis typically displays a light saturation curve (Figure 2.2), in which 3 distinct phases can be identified: (1) at low irradiance, namely when light is the limiting factor, the photosynthetic rate increases linearly with light intensity; (2) at increasing irradiances, the limiting factor becomes CO_2 fixation rate, thus photosynthetic rate increases non-linearly as a function of light; (3) when light intensity overcomes the rate of downstream biochemical reactions, photosystems get rid of energy absorbed in excess, and in this phase photosynthetic rate reaches a plateau. In a dilute culture of *C. vulgaris*, where light attenuation is minimized, light saturation is reached at around 1200 µmol photons m^{-2} s^{-1}. At this irradiance, algae protect themselves from excess illumination by triggering the non-photochemical quenching (NPQ) mechanism, a feedback-regulated de-excitation of Chls that operates in the PSII, to prevent over-excitation of reaction centers (Figure 2.2). Although light-dependent energy quenching is a property of all photosynthetic organisms, large differences in amplitude and kinetics can be observed. Some microalgae, such as *C. zofingiensis*, exhibit constitutively high energy quenching activity (Bonente et al. 2008), while in other species (e.g. *C. reinhardtii*) energy quenching is significantly activated only upon acclimation to excess light conditions (Peers et al. 2009). NPQ activates when light excitation flux exceeds CO_2 fixation rate. However, algae can experience very high light intensity, saturating photoprotective mechanisms. Light in excess of photosynthesis saturation level is dissipated rather than contributing to biomass accumulation, or even causes synthesis of reactive oxygen species (ROS), which damage the photosynthetic machinery and affect biomass yield. *C. reinhardtii* mutant *npq4*, devoid of NPQ response, was indeed more susceptible to photo-oxidation (Peers et al. 2009).

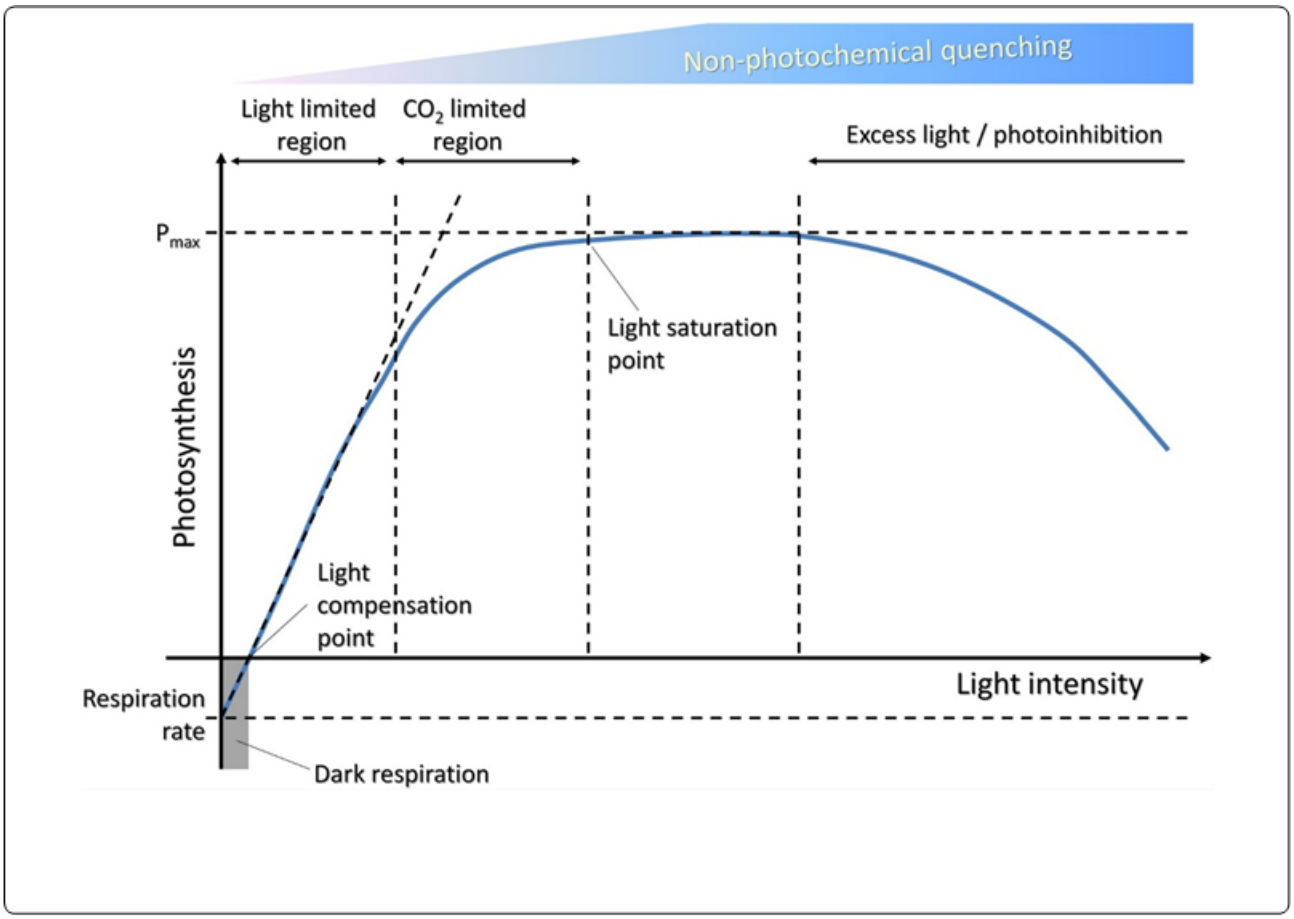

Figure 2.2 Light response curves for photosynthesis. The light compensation point is the minimum light intensity at which the organism shows a gain of carbon fixation. The net photosynthetic rate shows a linear rise in response to increased light, in the range of light limitation. At higher light levels, saturation occurs as the efficiency of the photosynthetic mechanism is reduced due to the activation of energy quenching processes. Under excess light conditions, net photosynthesis can decline as a result of photoxidative stress

Due to the absorption of pigments bound to the large antenna systems in both photosystems, light distribution within the culture is inhomogeneous, and this strongly contributes to the gap between theoretical vs. real productivity. Such large arrays of antenna complexes have been selected by evolution as favorable trait, since they maximize the light-harvesting capacity and therefore the adaptation to a natural water environment where light is often scarce and limits growth, and cell density remains low. Contrary to the natural environment, growth conditions in mass cultures requires high cell biomass per volume of installed facility. However, this results in high optical density and light shortage in the deeper layers of the culture while cells at the surface layers intercept most photons, resulting in saturation of photosynthesis, dissipation of excess energy and/or photoinhibition. The most inner layers easily drop below the compensation point of photosynthesis while active respiration consumes energy. Thus, dense algal cultures suffer both photo-deprivation and photo-inhibition, decreasing the overall light-tobiomass conversion efficiency far below the theoretical score. Rapid mixing of biomass is often suggested as a solution to light gradients, but it is not: rapid light/dark cycles between dark and over-saturating irradiances have a deleterious effect on biomass yield (Külheim et al. 2002). Modeling of the light-response curve of photosynthesis in a culture system (Formighieri et al. 2012) suggests that optimal setting of OD in the culture limits shading while maximizes light absorption and net photosynthesis.

One additional factor which contributes to the inefficiency of photosynthesis is carbon fixation: the enzyme RuBisCO, which catalyzes the carboxylation of Ribulose 1,5-bisphosphate (RuBP), has low affinity for C O_2 and can also use O_2 to give oxygenated substrates (Whitney et al. 2011), which ultimately results in ATP/NADPH consumption and loss of fixed C. To compensate for this, RuBisCO accumulates to as much as 50% of total soluble proteins of the cell. Inefficient light use in mass culture, due to inhomogeneous light distribution, results from limitations in the turnover rate of the Calvin-Benson cycle. The selection of strains with higher RuBP carboxylation activity would therefore be a major goal for the optimization of photosynthesis. Possible strategies include the heterologous expression of variants of RuBisCO with a higher specific activity, or the control of allosteric regulators (e.g. RuBisCO activase) to yield into suppression of oxygenase activity.

Interestingly, many microalgae use biophysical carbon concentrating mechanisms for active retention of inorganic C (Reinfelder 2010) to increase CO_2 availability at the RuBisCO active site within the pyrenoid, a micro-compartment of the chloroplast. Engineering such a mechanism into algal species devoid of pyrenoids might augment the overall C fixation rate and thus photosynthetic efficiency.

In conclusion, results reported in this section suggest that modulation of photosynthetic reactions is a key factor controlling biomass yield at both saturating and subsaturating irradiances, that is worth to be considered for a domestication strategy aimed at improving performances in PBRs.

2.4 Promises of domestication by forward genetic in improving photosynthetic efficiency

According to the previous section, a gap between theoretical and real biomass productivities of microalgae originates from the high OD of cells. With respect to the problem of inhomogeneous light distribution, high density planting of crops is a condition limiting PAR penetration thus productivity, and it is not different than the condition of elevated cell density reachable in a PBR. Moreover, biomass production with wild type algal strains is poorly viable likely as farming with ancestral crop varieties.

The so called ‘Green Revolution’ of agriculture, a domestication based on breeding and phenotypic selection, succeeded in pursuing crop productivities over the past 50 years (Langridge 2014; Gaut et al. 2018). Industrial application of microalgae may take advantage of a domestication approach, analogous to that carried out for modern crops. Thus, selection of strains carrying desired traits, together with implementing new alleles by random mutagenesis or genetic engineering, might improve performances in PBRs.

Random mutagenesis is recognized as a powerful technology in mutation breeding, widely employed for strain improvement and for studying the molecular basis of metabolic processes. Forward genetic approach is of particular relevance for algal biotechnology, since it avoids restrictions to GMO for outdoor production system (Snow and Smith 2012). The most common method for generating genetic variability in a population of microalgae is the mutagenesis induced by either physical

methods (UV-light, γ- and X-rays) or chemical mutagens, e.g. *N*'-nitro-*N* nitrosoguanidine (NTG) and ethyl methanesulfonate (EMS).

Attempts for algae genetic improvement, aimed to enhance light-to-biomass conversion efficiency, relied on random mutagenesis and screening of favorable traits. These approaches, while overcame scarcity of genetic engineering tools in microalgae, needed for efficient screening strategies for strains with higher productivity. Some of these approaches, which succeeded in increasing photosynthetic yield, are presented as follows.

Due to detrimental effect of high OD for mass cultivation, strains carrying truncated antenna size were proposed to perform better in light transmittance than wild type (Nakajima and Ueda 1997). Mutagenesis and screening of *C. reinhardtii* was employed to isolate mutants having a truncated light-harvesting system (Beckmann et al. 2009; Bonente et al. 2011; Kirst et al. 2012; Perrine et al. 2012; Jeong et al. 2017): all of them showed a higher productivity than the wild type in bench-scale growth systems. Cazzaniga and collaborators (Cazzaniga et al. 2014) applied random mutagenesis to a thermotolerant, fast-growing strain of *C. sorokiniana*, and selected pale-green mutants by imaging Chl fluorescence. Mutants were able to perform photosynthesis more efficiently than wild type, minimizing photoinhibition in high light; the positive effect on photosynthetic productivity was confirmed in both lab-scale and outdoor PBRs. Similar results were obtained with *N. gaditana* strains having reduced cellular pigment content (Perin et al. 2015). Finally, simultaneous knock-down of three light-harvesting complex proteins (LHCMB1, 2 and 3) in *C. reinhardtii*, by an RNAi triple knock-down strategy, resulted in improved light-to-H_2 (+ 180% than wild type) and light-to-biomass (+ 165%) conversion efficiencies (Oey et al. 2013).

Implementation of biosynthetic pathway of accessory pigments, e.g. phycobilins or Chls, into genus of industrial interest, has been proposed for improving harvesting efficiency over the full PAR spectrum (Stephenson et al. 2011). Recently, the enzyme responsible for the synthesis of Chl *f*, an oxidized form of Chl *a*, has been isolated from the cyanobacterium *C. fritschii* (Ho et al. 2016); heterologous expression of Chl *f* synthase succeeded in accumulating this chromophore in *Synechococcus* sp. Since Chl *f* expands the spectral range for photosynthesis by absorbing far red light, its expression in microalgae may confer advantages for mass culture in PBRs, which suffers for detrimental sieve-effects at high cell densities. However, the feasibility of this approach, which assumes a correct binding of the new chromophores into the existing pigment-binding complexes, still await experimental confirmation.

CO_2 fixation rate is a major limiting step in biomass yield, which arise from RuBisCO inefficiency. Genetic engineering of RuBisCO to increase its catalytic activity or to enhance its specificity towards CO_2 have been proposed as ways to overcome these limitations (Stephenson et al. 2011). It is worth noting that the natural diversity of RuBisCO is limited, likely because the interactions which support catalytic activity make most of the isoforms of this enzyme intolerant to mutations (Whitney et al. 2011), indeed attempts to overcome its limitations by directed evolution, had scant success. Although variants of RuBisCO with higher activity have been identified (Andrews and Whitney 2003; Tchernov et al. 2008) their heterologous expression in algal strains of industrial potential is still missing. Recently, *E. coli*-based screen of new RuBisCO variants obtained by direct evolution allowed the identification of an unexplored subunit interface with potential of increasing CO_2 fixation rate

(Wilson et al. 2018). Site-directed mutagenesis in such subunit may generate novel variants whose enzymatic characteristics can be subsequently tested in microalgae in terms of enhanced CO_2 fixation. An additional approach may reside in the generation of hybrid RuBisCO by using novel activase isoforms from chemolithoautotroph microorganisms such as *Acidithiobacillus ferrooxidans* (Tsai et al. 2015).

A high photosynthetic efficiency is attainable only in low irradiance and controlled light environments, which allow most absorbed photons can be utilized by the culture; instead in the outdoor, efficiency drops due to fluctuating irradiances, exceeding the photosynthetic capacity. Autotrophs evolved mechanisms for regulating the efficiency of light capture, which can become target of domestication strategies. Several microalgal species e.g. *C. reinhardtii* and *H. pluvialis*, trigger fast phototactic response, for fine-tuning exposure to light. Indeed, phototaxis confers fitness advantage and it is regulated by cytoplasmic redox balance, which in turn is affected by photosynthetic electron transport rate (Wakabayashi et al. 2011). In the attempt of isolating strains with improved light-use-efficiency, Kim and collaborators (Kim et al. 2016) analyzed a *C. reinhardtii* mutant population for rapid phototaxis response and identified mutants with enhanced photoautotrophic growth and lipid production, respectively 1.9- and 8.1fold increases than wild type.

Photosynthetic organisms dynamically regulate the amplitude of NPQ (see "Biological constraints in lightto-biomass conversion efficiency" section): by balancing amplitudes of light harvesting vs. energy dissipation, they maintain optimal fitness in changing light environment. The slow relaxation rate of NPQ upon high- to low-light transition was considered to reduce the overall conversion efficiency of solar to biomass in microalgae, consistent with recent evidences in plants (Kromdijk et al. 2016; Głowacka et al. 2018). Indeed, deletion of the OCP protein, responsible for NPQ response in cyanobacteria, resulted in a 30% higher biomass yield in mass cultures of *Synechocystis* than wild type cells (Peers 2015). Random insertional mutagenesis and Targeting Induced Local Lesions IN Genomes (TILLING) approach on *C. reinhardtii*, following by Chl fluorescence imaging screening, has produced mutants specifically devoid of *lhcsr* genes (Peers et al. 2009; Truong 2011). In their report, (Berteotti et al. 2016) proposed that biomass productivity depends on LHCSR protein accumulation: *C. reinhardtii* strains lacking the two *lhcsr3* genes were more productive than wild type, thus confirming down-regulation of NPQ is a strategy for improving light use efficiency in microalgae. Instead, more recently, (Cantrell and Peers 2017) observed no significant differences in biomass yield between *C. reinhardtii* wild type and the *npq4 lhcsr1* mutant, devoid of all Lhcsr isoforms.

Microalgae growing in mass culture experience rapid changes in the irradiance due to cell mixing into the PBR. The amount of time spent in sub-saturating vs. excess light influences the biomass productivity, which is lower in fluctuating light conditions (Berteotti et al. 2016) possibly due to the metabolic energy needed to repair photodamage. Hence, improving photosynthetic efficiency in excess light conditions is potentially a major goal for establishing efficient outdoor cultivation. Research efforts aimed to obtain non-GMO algal strain tolerant to excess light, mainly focused on the model alga *C. reinhardtii*. Förster et al. (Förster et al. 2005) isolated *very high light resistant* (VHL-R) mutations, which allowed near maximal growth rate at irradiances lethal to the control genotype; characterization of these strains reveals they affected the regulatory pathways which modulate photoprotective response, including PSII repair and ROS detoxification. In (Fischer et al. 2012), wild type strain was UV-mutagenized and plated onto medium containing a lethal concentration of the

photosensitizer Red Bengal; by this approach, SOR1 was identified as a factor enhancing tolerance to photooxidative stress conditions. Schierenbeck and coworkers (Schierenbeck et al. 2015) performed UV-mutagenesis followed by selection under high irradiance (2000 µmol m^{-2} s^{-1}); the two mutations selected, which both mapped in the putative Light Responsive Signal 1 (LSR1) gene, conferred an improved resistance of cells against exogenous ROS. Recent results concern the isolation of pale-green, singlet oxygen resistant mutant by EMS-mutagenized *C. vulgaris*, which showed biomass yield enhancement by 68% than wild type strain (Dall'Osto et al. unpublished results).

2.5 Improving algal biomass productivity by genetic engineering: methods, state of the art and perspectives

Genetic manipulation approaches have the potential to revolutionize industry based on microalgae cultivation. These include transfer of genes isolated from other species to generate strains with desirable commercial traits such as tolerance to excess light and heat stress, resistance to herbivore/pathogen, capacity to outcompete opportunistic organisms, or to express biosynthetic pathways into more productive strains (figure 2.3). Recent progress in genome sequencing, methagenome/ metatranscriptome approaches, and genetic manipulation, yielded into significant advancement in microalgal research. In this paragraph, different strategies of genetic engineering, which revealed effective in improving algal productivity, are discussed. Moreover, additional solutions are proposed.

Organelle	DNA-delivery method	Genetic mechanism	Advantages	Disadvantages	Selection marker
Nucleus	Electroporation gene-gun bombardment *A. tumefaciens*-mediated Glass beads Silicon carbide whiskers and aminoclay nanoparticles	Ectopic recombination (random integration)	Protein can be expressed as secreted protein Post-translational modifications	Identification of high-expressing Transformants gene silencing	Resistance to Paromycin, Zeocin, Hygromycin, Chloramphenicol Auxotrophic complementation (*ARG7*, *NIT1*, *oee1*)
Chloroplast	Gene-gun bombarment Glass beads	Homologous recombination (site-specific integration)	Compartmentalization Lacks gene silencing High expression level	Need to identify homoplasmic transformant Lacks posttranslational modifications	resistance to Spectinomycin Auxotrophic complementation (*atpB, psbH*)

Table 2: Transformation of *C. reinhardtii*
This table displays DNA-delivery methods, genetic mechanism driving the transformation, and the most common selection markers employed so far. Major advantages and disadvantages of nuclear vs. chloroplast transformation are reported.

In the last decades, several efforts have been attempted to optimize the transformation efficiency of different microalgae species. Stable transformation was first developed in *C. reinhardtii*: being able to growth both in autotrophic and heterotrophic conditions, as haploid or diploid cells, *Chlamydomonas* was adopted as powerful genetic system for studying different physiological mechanisms. Nuclear transformation of *C. reinhardtii* may be achieved by several methods such as electroporation (Kang et al. 2015), *Agrobacterium*-mediated transformation (Mini et al. 2018), silicon carbide whiskers and positively-charged aminoclay nanoparticles (Dunahay 1993; Kim et al. 2014)

and glass beads agitation method (Somchai et al. 2016). Both electroporation and *Agrobacterium*mediated transformation also succeeded in transforming algae of economic interest such as *C. vulgaris*, *Neochloris oleoabundans* and *H. pluvialis* (Kathiresan et al. 2015; Chungjatupornchai et al. 2016; Kumar et al. 2018). The introduction of foreign genes into the nuclear genome of microalgae is generally guided by a random integration event (Kindle 1998). Nuclear gene expression is frequently subjected to strong silencing mechanisms due both to position effect and to epigenetic phenomena, similar to those of land plants (Schroda 2006); indeed in microalgae, silenced multicopy transgenes exhibit high levels of DNA methylation as in land plants (Kim and Zilberman 2014; Zhang et al. 2018).

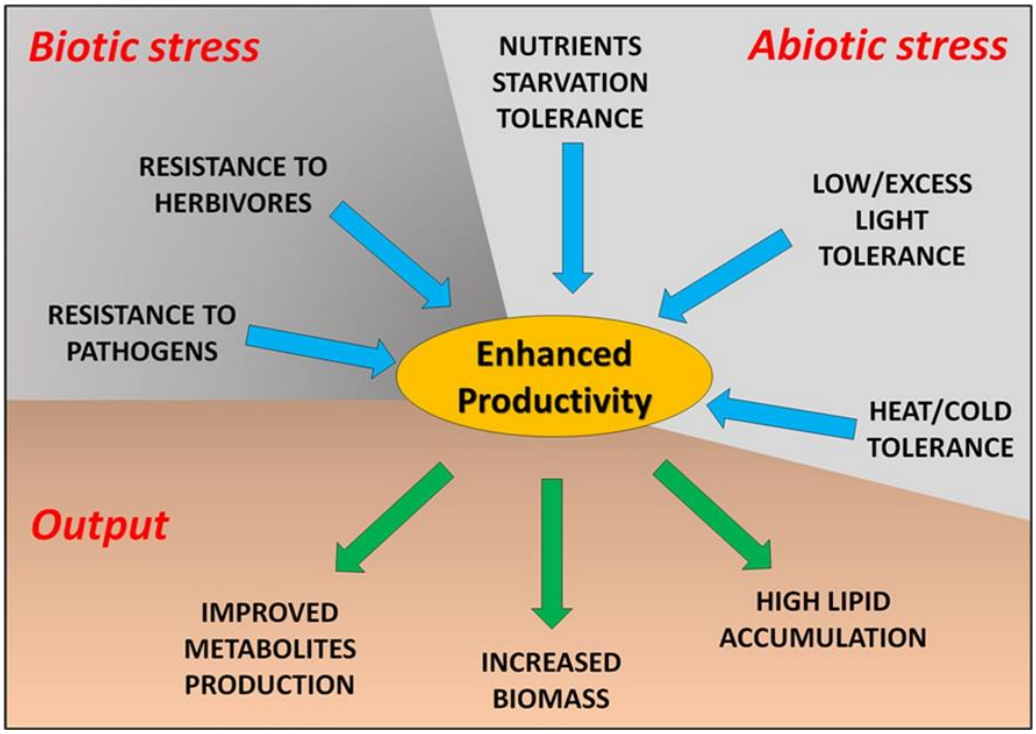

Figure 2.3. Schematic depiction of the major desirable traits to be either implemented or improved, toward higher productivity of microalgae in mass culture.

In last years, many efforts have been attempted to increase the heterologous expression potential of microalgae. Increased expression of transgenes was obtained by fusing the sequences encoding the gene of interest and the selection marker in a unique bicistronic RNA (Rasala et al. 2012; Onishi and Pringle 2016). Recourse to a frequent subset of preferred codons results in elevated transcriptional levels, while the use of codons introducing unintended splicing signals negatively affects the overall expression of transgenes (Weiner et al. 2018), thus a codon usage optimization is mandatory to maximize protein yield. To improve the selection of high-level expressing transformants, last-generation expression vectors exploit the 2A peptide (Kim et al. 2011) to generate transcriptional fusions between selection marker sequence (e.g. antibiotic resistance) and the gene of interest (Rasala et al. 2012). Transcription factors are gaining increasing attention as key regulators of metabolic pathways, in order to enhance yield of high-value molecules or to maximize the production of foreign proteins in microalgae. Over-expression of NsbZIP1, a transcription factor

carrying the basic leucine zipper, resulted in both enhanced growth rate and higher lipid contents in *N. salina* (Kwon et al. 2018).

The biolistic method (particle-gun bombardment) is the elective procedure for chloroplast transformation in microalgae (Doron et al. 2016). The introduction of foreign genes into the plastome is guided by site-specific integration event (i.e. by homologous recombination). Expressing foreign genes in the chloroplast enables to circumvent gene silencing events, which affect the nuclear expression; moreover, it allows for the introduction of operons, encoding several enzymes of a pathway. However, the resulting transformants must undergo several rounds of selection in order to acquire the homoplasmic condition (Wannathong et al. 2016).

Further details concerning nuclear and chloroplast expression in *C. reinhardtii* are summarized in Table 2; moreover, many of these aspects have been covered extensively in a recent review (Doron et al. 2016).

Genome editing technology enables for both gene deletion and gene integration, therefore implementation of these novel genetic tools in microalgae would allow for manipulation of metabolic networks. Recently, a novel approach based on CRISPR–CAS9 genome editing technology have been successfully developed in both the marine diatom *P. tricornutum* (Nymark et al. 2016) and in *C. reinhardtii*, allowing for deletion of specific gene functions (Baek et al. 2016); the latter was achieved by a DNA-free CRISPR–Cas9 method and the outcome was the sequential *FTSY* and *ZEP* double-gene knockout, that resulted in improved photosynthetic productivity. Analogous approach was used to abolish the functions encoded by *MAA7*, *CpSRP43* and *ChlM* genes, which led to pale-green mutants (Shin et al. 2016). In *C. reinhardtii*, the replacement of Cas9 with the Cpf1 ribonucleoprotein achieved a more efficient homologydirected DNA replacement (Ferenczi et al. 2017). However, a common limitation of free-DNA CRISPR–Cas9/Cpf1 methods resides in the lack of selection markers that, in turn, hinders a straightforward selection of the desired mutants; being the genome editing event induced at very low frequency (0.5–0.6%), a visible phenotype makes mutant selection easier. A DNA-based CRISPR–CAS9 method has been developed in the industrial oleaginous microalga *N. oceanica* (Wang et al. 2016) in which nuclear transformation can be efficiently performed by introducing expression cassettes obtained by PCR, making unnecessary the use of expression vectors (Li et al. 2014). Recently, a doubling of the lipid production in *N. gaditana* was obtained by deleting a transcription factor that acts as negative regulator in lipid biosynthesis (Ajjawi et al. 2017).

As previously described, a truncated antenna size yielded into increased productivity in green microalgae (see “Promises of domestication by forward genetic in improving photosynthetic efficiency” section), thus proteins involved in the biogenesis of photosynthetic machinery can be targeted for increasing biomass production. Truncated light-harvesting antenna 1 (*TLA1*), a nuclear gene putatively involved in the regulation of the antenna size of *C. reinhardtii*, was up- and downregulated by overexpression and RNAi, respectively. The strain over-expressing *TLA1* showed a larger antenna size for both photosystems and lower Chl *a*/*b* ration than the wild type, while its down-regulation resulted in the opposite phenotype changes (Mitra et al. 2012b). LHCII, the nucleusencoded light-harvesting proteins associated with PSII, tunes the light harvesting capacity to the prevailing light condition. In *C. reinhardtii*, LHCII translation efficiency is regulated by the

cytosolic RNA-binding protein NAB1, which is subjected to specific nitrosylation in limiting light, thus making such repressor less-active and promoting accumulation of LHC (Berger et al. 2016).

Manipulation of RuBisCO activity, namely the major constraint for C assimilation e.g. under excess light conditions (Ducat and Silver 2012), may improve the photosynthetic yield (Carmo-Silva et al. 2015). Although site-directed mutants in the *rbcL* (RuBisCO large subunit) gene (Larson et al. 1997; Ott et al. 2000) as well as hybrid variants with altered specificity of RuBisCO–RuBisCO activase interaction (Li et al. 2005) have been generated, their over-expression in *C. reinhardtii* did not increase the overall photosynthetic yield.

Recently, biomass productivity as well as lipid yield increased up to 40% in the oleaginous *Nannochloropsis oceanica* by overexpressing endogenous RuBisCO activase (Wei et al. 2017). Conversely, a reduction in the RuBisCO activity by site directed mutagenesis resulted in a tenfold higher H_2 production in *C. reinhardtii* (Pinto et al. 2013), likely because Calvin-Benson cycle competes with Hydrogenase for reducing equivalents.

Further strategies included (i) the PCR-based gene shuffling of *Chlamydomonas* rbcL with sequences representing natural variants of this gene, which yielded isoforms with higher V_{max} of carboxylation catalysis (Zhu et al. 2010a); (ii) regulation of RuBisCO accumulation according to culture conditions, by tuning mRNA level of the nuclear maturation factor MRL1 (Johnson et al. 2010); (iii) overexpression of. sedoheptulose 1,7-bisphosphatase from *C. reinhardtii*, which succeeded in enhancing photosynthetic efficiency in *D. bardawil* (Fang et al. 2012); finally, the over-expression of LowCO_2 Inducible (LCI) proteins in *C. reinhardtii*, under conditions which typically repress their synthesis (i.e. high CO_2 concentration), increased biomass production under elevated C O_2 conditions as much as 80% than control strain (Spalding 2013).

High productivity in open ponds is restricted to species which adapted to high salt concentration (e.g. *Dunaliella*) or high pH (e.g. *Spirulina*), thus outcompeting naturally occurring contaminants. Hence, a trait which confers competitive advantage over undesirable microorganisms, is crucial both to increase the biomass productivity and to reduce the operating costs for maintenance of axenic cultures (Figure 2.1), particularly in either open pond or heterotrophic conditions. In this perspective, non-canonical substrates may be employed for sustaining algal growth. The expression of the phosphite dehydrogenase D (PTXD) from *P. stutzeri* WM88 (Costas et al. 2001) confers to *C. reinhardtii* the capacity of metabolizing phosphite, namely a P source which cannot be utilized by plants, fungi and most bacteria. Transgenic *Chlamydomonas* cells showed higher fitness than *S. obliquus* in competition experiments in which phosphite-repleted/phosphate-depleted medium was used (Loera-Quezada et al. 2016).

Some algal species are strict autotrophs or are highly selective for their C source (e.g. *Chlamydomonas* for acetate), thus trophic conversion by metabolic engineering would be desirable. *Chlamydomonas* cells expressing the hexose transporter HUP1 (monosaccharide-H^+ symporter from *C. kessleri*) metabolized externally supplied glucose for heterotrophic growth and showed higher H_2 production capacity; however, results suggest that glucose cannot fully replace acetate as a C source, for longterm growth in the dark (Doebbe et al. 2007).

Other algal species can metabolize a large array of sugars, and strongly increase their productivity under heterotrophic or mixotrophic growth conditions (Leite et al. 2015); however, heterotrophic growth requires additional costs due to need for exogenous carbon source and maintenance of axenic conditions. Algal strains able of metabolizing raw lignocellulosic biomass scraps, namely cheap agricultural wastes, would certainly contribute to make the whole process economically viable. Foreign genes encoding bacterial and fungal plant Cell Wall Degrading Enzymes (CWDEs), were constitutively expressed in microalgae and addressed to the secretory pathway (Rasala et al. 2012). In *C. reinhardtii*, yield of secreted proteins was improved up to eight-fold by fusing both the putative signal peptide of gametolysin and the repeated serine-proline module, to the N and C terminus of the recombinant protein, respectively (Ramos-Martinez et al. 2017). Contrary to plant cell, some species of unicellular green algae possess a cell wall mainly constituted by proteins (e.g. *C. reinhardtii*) (Imam et al. 1985), thus lack of polysaccharides as major components circumvents the deleterious effects of expressing CWDEs in plants, likely related to hyper-immune responses (Malinovsky et al. 2014; Benedetti et al. 2015). Although some algal spp. synthesizes endogenous CWDEs (Blifernez-Klassen et al. 2012), the native cellulolytic machinery is not efficient enough for degrading hydrolysis-recalcitrant substrates such as lignocellulose. Thus, a promising perspective is the expression of a range of secreted CWDEs, including polygalacturonases, hemicellulases, cellulases and ligninases in a unique algal culture, analogously to the approaches developed in yeasts which yielded into strains able to grow on cellulosic substrates (Kricka et al. 2014).

An overview of the major genetic manipulations which may lead to an improvement of biomass productivity is represented in Figure 2.4.

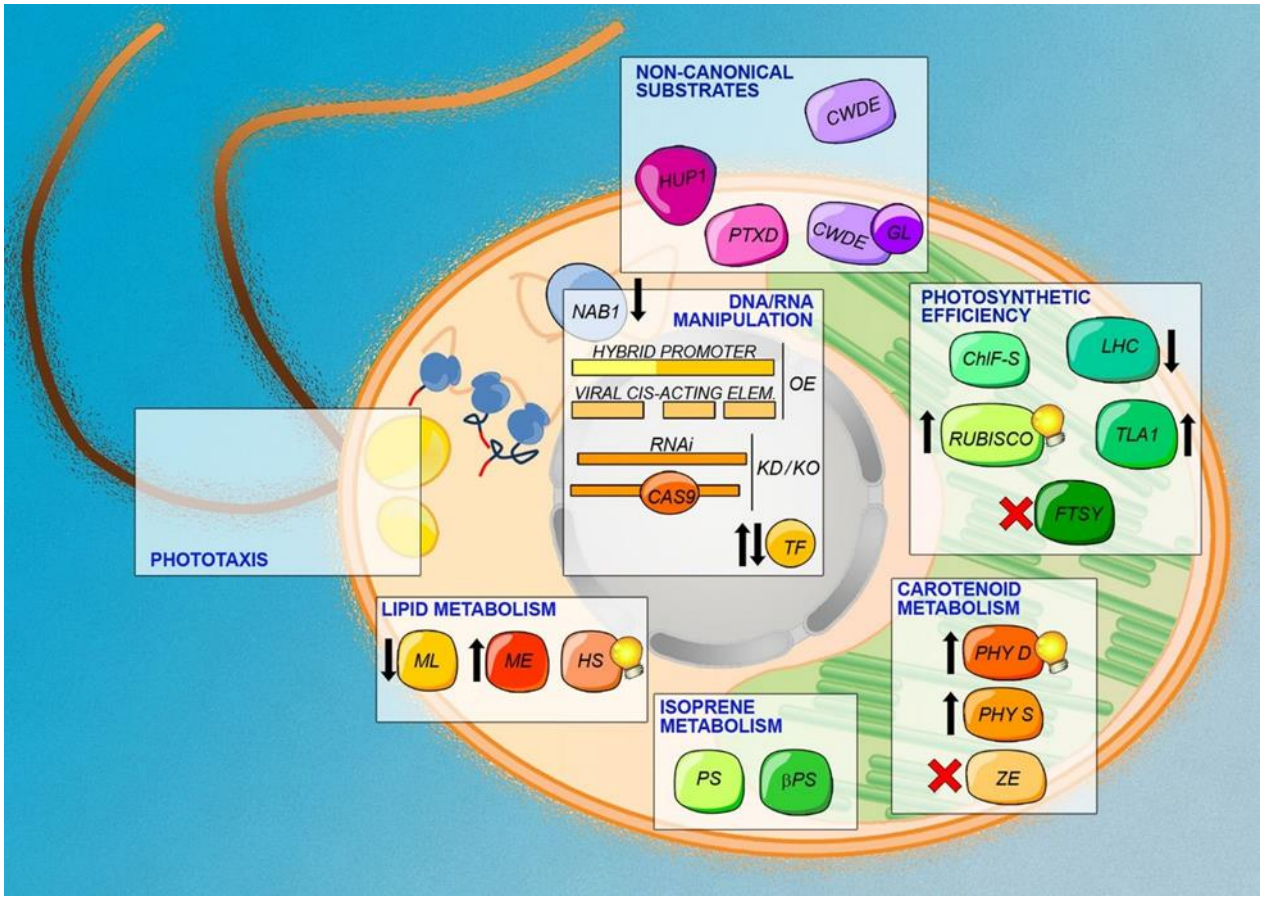

Figure 2.4. Potential traits to be implemented in GM—*C. reinhardtii* cell. The diagram displays a number of genetic strategies, aimed to enhance productivity in mass culture of microalgae. Gene over-expression (OE) using hydrid promoters or viral cis-acting elements and gene disruption/down-regulation (KO/KD) by Crispr–Cas9 and RNAi approaches are indicated. Some traits that may result in higher productivity include an increased photosynthetic efficiency, improved phototaxis, the use of non-canonical substrates, and optimized carotenoid, lipid and isoprene metabolism. Up- and down-ward pointing arrow mean up- and down-regulation, respectively, and are referred to the expression level of the corresponding endogenous enzyme. Bulb and red cross mean enzymatic in vitro improvement and loss of function, respectively. Abbreviations: *Chl-f S* chlorophyll *f* synthase, *CWDE* cell-wall degrading enzyme, *FTSY* chloroplast signal recognition particle, *GL* gametolysin signal peptide, *HS* hydrocarbon-synthase, *HUP1* hexose-proton symporter, *LHC* light harvesting complexes, *ME* malate dehydrogenase, *ML* multifunctional lipase, *NAB1* RNA-binding protein, *PHY D* phytoene desaturase, *PHY S* phytoene synthase, *PS* patchoulol synthase, *PTXD* phosphite dehydrogenase, *β-PS* β-phellandrene synthase, *TF* transcription factor, *TLA1* truncated light-harvesting antenna 1, *ZEP* zeaxanthin epoxidase

2.6 Conclusion

Commercially cultivated for several decades, microalgae are now recognized to offer a great potential for exploitation in different fields including pharmaceuticals, aquaculture and renewable energies. Former efforts in their industrial applications mainly focused in optimizing culture parameters and selecting the best performing wild type strain. However, to promote cultivation of microalgae as a new biotechnological sector, a number of challenges still have to be overcome. Domestication strategies achieved by genetic and metabolic engineering will be crucially important to isolate "*smart strains*" with improved yield, in order to make the production successfully marketed. The opportunities offered by investments in both basic and applied research, are considerable: (i) the rapid evolution of genome sequencing techniques will help defining the gene networks controlling growth, while -omics approaches allow to identify regulatory points of cellular pathways, thus enabling manipulation of key metabolic steps; (ii) prospective redesigns of algal system include light-to-biomass conversion efficiency, oil content/composition, nutrient recovery capacity; (iii) extend the genetic transformation techniques, now carried out successfully in few species only, to the most industrially-relevant species, will offer the opportunity to address the biological constraints limiting growth yield; finally, (iv) the development of reproducible genome editing techniques will permit a fine matching of the primary metabolism to the mass culture conditions, or the development of molecular strategies for strain containment. Encouraging results have recently been obtained by boosting light-use-efficiency or by strengthening specific metabolic pathways. Additional research efforts and funding for implementing innovative biorefineries, will realistically support progress toward next-generation algal biotechnology.

REFERENCES

't Lam GP, Vermuë MH, Eppink MHM, Wijffels RH, van den Berg C (2018) Multi-Product Microalgae Biorefineries: From Concept Towards Reality. Trends Biotechnol 36:216—227 . https://doi.org/10.1016/j.tibtech.2017.10.011

Adamczyk M, Lasek J, Skawińska A (2016) CO2 Biofixation and Growth Kinetics of Chlorella vulgaris and Nannochloropsis gaditana. Appl Biochem Biotechnol 179:1248–1261 . https://doi.org/10.1007/s12010-016-2062-3

Ahmed RA, He M, Aftab RA, Zheng S, Nagi M, Bakri R, Wang C (2017) Bioenergy application of Dunaliella salina SA 134 grown at various salinity levels for lipid production. Sci Rep 7:8118 . https://doi.org/10.1038/s41598-017-07540-x

Ajjawi I, Verruto J, Aqui M, Soriaga LB, Coppersmith J, Kwok K, Peach L, Orchard E, Kalb R, Xu W, Carlson TJ, Francis K, Konigsfeld K, Bartalis J, Schultz A, Lambert W, Schwartz AS, Brown R, Moellering ER (2017) Lipid production in Nannochloropsis gaditana is doubled by decreasing expression of a single transcriptional regulator. Nat Publ Gr 35:647–652 . https://doi.org/10.1038/nbt.3865

Al-Dhabi NA, Valan Arasu M (2016) Quantification of Phytochemicals from Commercial Spirulina Products and Their Antioxidant Activities. Evidence-based Complement Altern Med 2016: . https://doi.org/10.1155/2016/7631864

Andrews TJ, Whitney SM (2003) Manipulating ribulose bisphosphate carboxylase/oxygenase in the chloroplasts of higher plants. Arch Biochem Biophys 414:159–169 . https://doi.org/10.1016/S0003-9861(03)00100-0

Arad SM, van Moppes D (2013) Novel Sulfated Polysaccharides of Red Microalgae: Basics and Applications. Handb. Microalgal Cult. 406–416

Assunção J, Batista AP, Manoel J, da Silva TL, Marques P, Reis A, Gouveia L (2017) CO2 utilization in the production of biomass and biocompounds by three different microalgae. Eng Life Sci 17:1126–1135 . https://doi.org/https://doi.org/10.1002/elsc.201700075

Baek K, Kim DH, Jeong J, Sim SJ, Melis A, Kim JS, Jin E, Bae S (2016) DNA-free two-gene knockout in Chlamydomonas reinhardtii via CRISPR-Cas9 ribonucleoproteins. Sci Rep 6:30620 . https://doi.org/10.1038/srep30620

Bayro-Kaiser V, Nelson N (2016) Temperature-sensitive PSII: a novel approach for sustained photosynthetic hydrogen production. Photosynth Res 130:113–121 . https://doi.org/10.1007/s11120-016-0232-3

Beckmann J, Lehr F, Finazzi G, Hankamer B, Posten C, Wobbe L, Kruse O (2009) Improvement of light to biomass conversion by de-regulation of light-harvesting protein translation in Chlamydomonas reinhardtii. J Biotechnol 142:70–77 . https://doi.org/10.1016/j.jbiotec.2009.02.015

Benedetti M, Pontiggia D, Raggi S, Cheng Z, Scaloni F, Ferrari S, Ausubel FM, Cervone F, De Lorenzo G (2015) Plant immunity triggered by engineered in vivo release of oligogalacturonides, damage-associated molecular patterns. Proc Natl Acad Sci 112:5533–5538 . https://doi.org/10.1073/pnas.1504154112

Benvenuti G, Ruiz J, Lamers PP, Bosma R, Wijffels RH, Barbosa MJ (2017) Towards microalgal triglycerides in the commodity markets. Biotechnol Biofuels 10:188 . https://doi.org/10.1186/s13068-017-0873-2

Berger H, de Mia M, Morisse S, Marchand C, Lemaire SD, Wobbe L, Kruse O (2016) A light switch based on protein S-nitrosylation fine-tunes photosynthetic light-harvesting in the microalga Chlamydomonas reinhardtii. Plant Physiol 171:pp.01878.2015 . https://doi.org/10.1104/pp.15.01878

Berteotti S, Ballottari M, Bassi R (2016) Increased biomass productivity in green algae by tuning non-photochemical quenching. Sci Rep 6:21339 . https://doi.org/10.1038/srep21339

Bhola V, Swalaha F, Ranjith Kumar R, Singh M, Bux F (2014) Overview of the potential of microalgae for CO2 sequestration. Int J Environ Sci Technol 11:2103–2118 . https://doi.org/10.1007/s13762-013-0487-6

Blifernez-Klassen O, Klassen V, Doebbe A, Kersting K, Grimm P, Wobbe L, Kruse O (2012) Cellulose degradation and assimilation by the unicellular phototrophic eukaryote Chlamydomonas reinhardtii. Nat Commun 3:1214 . https://doi.org/10.1038/ncomms2210

Blunt JW, Copp BR, Keyzers RA, Munro MHG, Prinsep MR (2012) Marine natural products. Nat Prod Rep 29:144–222 . https://doi.org/10.1039/C2NP00090C

Bogen C, Klassen V, Wichmann J, Russa M La, Doebbe A, Grundmann M, Uronen P, Kruse O, Mussgnug JH (2013) Identification of Monoraphidium contortum as a promising species for liquid biofuel production. Bioresour Technol 133:622–626 . https://doi.org/https://doi.org/10.1016/j.biortech.2013.01.164

Bonente G, Formighieri C, Mantelli M, Catalanotti C, Giuliano G, Morosinotto T, Bassi R (2011) Mutagenesis and phenotypic selection as a strategy toward domestication of Chlamydomonas reinhardtii strains for improved performance in photobioreactors. Photosynth Res 108:107–120 . https://doi.org/10.1007/s11120-011-9660-2

Bonente G, Passarini F, Cazzaniga S, Mancone C, Buia MC, Tripodi M, Bassi R, Caffarri S (2008) The Occurrence of the psbS Gene Product in Chlamydomonas reinhardtii and in Other Photosynthetic Organisms and Its Correlation with Energy Quenching†. Photochem Photobiol 84:1359–1370 . https://doi.org/https://doi.org/10.1111/j.1751-1097.2008.00456.x

Bonnefond H, Moelants N, Talec A, Mayzaud P, Bernard O, Sciandra A (2017) Coupling and uncoupling of triglyceride and beta-carotene production by Dunaliella salina under nitrogen limitation and starvation. Biotechnol Biofuels 10:25 . https://doi.org/10.1016/0926-860X(93)80133-B

Borowitzka M (2013) High-value products from microalga-their development and commercialisation. J Appl Phycol 25:743–756

Breuer G, de Jaeger L, Artus VG, Martens DE, Springer J, Draaisma RB, Eggink G, Wijffels RH, Lamers PP (2014) Superior triacylglycerol (TAG) accumulation in starchless mutants of Scenedesmus obliquus: (II) evaluation of TAG yield and productivity in controlled photobioreactors. Biotechnol Biofuels 7:70 . https://doi.org/10.1186/1754-6834-7-70

Cantrell M, Peers G (2017) A mutant of Chlamydomonas without LHCSR maintains high rates of photosynthesis, but has reduced cell division rates in sinusoidal light conditions. PLoS One 12:1–26 . https://doi.org/10.1371/journal.pone.0179395

Caporgno MP, Taleb A, Olkiewicz M, Font J, Pruvost J, Legrand J, Bengoa C (2015) Microalgae cultivation in urban wastewater: Nutrient removal and biomass production for biodiesel and methane. Algal Res 10:232–239 . https://doi.org/https://doi.org/10.1016/j.algal.2015.05.011

Carmo-Silva E, Scales JC, Madgwick PJ, Parry MAJ (2015) Optimizing Rubisco and its regulation for greater resource use efficiency. Plant Cell Environ 38:1817–1832 . https://doi.org/https://doi.org/10.1111/pce.12425

Cazzaniga S, Dall'Osto L, Szaub J, Scibilia L, Ballottari M, Purton S, Bassi R (2014) Domestication of

the green alga Chlorella sorokiniana: Reduction of antenna size improves light-use efficiency in a photobioreactor. Biotechnol Biofuels 7:157 . https://doi.org/10.1186/s13068-014-0157-z

Cheah WY, Ling TC, Juan JC, Lee D-J, Chang J-S, Show PL (2016) Biorefineries of carbon dioxide: From carbon capture and storage (CCS) to bioenergies production. Bioresour Technol 215:346–356 . https://doi.org/https://doi.org/10.1016/j.biortech.2016.04.019

Chen C-L, Chang J-S, Lee D-J (2015) Dewatering and Drying Methods for Microalgae. Dry Technol 33:443–454 . https://doi.org/10.1080/07373937.2014.997881

Chew KW, Yap JY, Show PL, Suan NH, Juan JC, Ling TC, Lee DJ, Chang JS (2017) Microalgae biorefinery: High value products perspectives. Bioresour Technol 229:53–62 . https://doi.org/10.1016/j.biortech.2017.01.006

Chisti Y (2007) Biodiesel from microalgae. Biotechnol Adv 25:294–306 . https://doi.org/https://doi.org/10.1016/j.biotechadv.2007.02.001

Cho A (2010) Energy's Tricky Tradeoffs. Science (80-) 329:786 LP – 787 . https://doi.org/10.1126/science.329.5993.786

Chu S, Majumdar A (2012) Opportunities and challenges for a sustainable energy future. Nature 488:294–303 . https://doi.org/10.1038/nature11475

Chungjatupornchai W, Kitraksa P, Fa-aroonsawat S (2016) Stable nuclear transformation of the oleaginous microalga Neochloris oleoabundans by electroporation. J Appl Phycol 28:191–199 . https://doi.org/10.1007/s10811-015-0594-5

Costas AMG, White AK, Metcalf WW (2001) Purification and characterization of a novel phosphorus-oxidizing enzyme from Pseudomonas stutzeri WM88. J Biol Chem 276:17429–17436

Cuaresma M, Janssen M, Vílchez C, Wijffels RH (2009) Productivity of Chlorella sorokiniana in a short light-path (SLP) panel photobioreactor under high irradiance. Biotechnol Bioeng 104:352–359 . https://doi.org/https://doi.org/10.1002/bit.22394

Cuaresma M, Janssen M, Vílchez C, Wijffels RH (2011) Horizontal or vertical photobioreactors? How to improve microalgae photosynthetic efficiency. Bioresour Technol 102:5129–5137 . https://doi.org/https://doi.org/10.1016/j.biortech.2011.01.078

Dineshkumar R, Kumaravel R, Gopalsamy J, Sikder MNA, Sampathkumar P (2018) Microalgae as Bio-fertilizers for Rice Growth and Seed Yield Productivity. Waste and biomass valorization 9:793–800 . https://doi.org/10.1007/s12649-017-9873-5

Doebbe A, Rupprecht J, Beckmann J, Mussgnug JH, Hallmann A, Hankamer B, Kruse O (2007) Functional integration of the HUP1 hexose symporter gene into the genome of C. reinhardtii: Impacts on biological H2 production. J Biotechnol 131:27–33 . https://doi.org/https://doi.org/10.1016/j.jbiotec.2007.05.017

Doron L, Segal N, Shapira M (2016) Transgene Expression in Microalgae—From Tools to Applications . Front. Plant Sci. 7:505 . https://doi.org/10.3389/fpls.2016.00505

Dubini A, Ghirardi ML (2015) Engineering photosynthetic organisms for the production of biohydrogen. Photosynth Res 123:241–253 . https://doi.org/10.1007/s11120-014-9991-x

Ducat DC, Silver PA (2012) Improving carbon fixation pathways. Curr Opin Chem Biol 16:337–344 . https://doi.org/https://doi.org/10.1016/j.cbpa.2012.05.002

Dunahay TG (1993) Transformation of Chlamydomonas reinhardtii with silicon carbide whiskers. Biotechniques 15:452-455,457-458,460

Dvir I, Stark AH, Arad SM (2015) A Foodomics Approach Reveals Hypocholesterolemic Activity of Red Microalgae. Genomics, Proteomics Metabolomics Nutraceuticals Funct. Foods 31–39 . https://doi.org/10.1002/9781118930458.ch3

Ekelhof A, Melkonian M (2017) Enhanced extracellular polysaccharide production and growth by microalga Netrium digitus in a porous substrate bioreactor. Algal Res 28:184–191 . https://doi.org/https://doi.org/10.1016/j.algal.2017.11.003

Fang L, Lin HX, Low CS, Wu MH, Chow Y, Lee YK (2012) Expression of the Chlamydomonas reinhardtii Sedoheptulose-1,7-bisphosphatase in Dunaliella bardawil leads to enhanced photosynthesis and increased glycerol production. Plant Biotechnol J 10:1129–1135 . https://doi.org/10.1111/pbi.12000

Ferenczi A, Pyott DE, Xipnitou A, Molnar A (2017) Efficient targeted DNA editing and replacement in Chlamydomonas reinhardtii using Cpf1 ribonucleoproteins and single-stranded DNA. Proc Natl Acad Sci 114:13567 LP – 13572 . https://doi.org/10.1073/pnas.1710597114

Fernandes BD, Mota A, Teixeira JA, Vicente AA (2015) Continuous cultivation of photosynthetic microorganisms: Approaches, applications and future trends. Biotechnol Adv 33:1228–1245 . https://doi.org/https://doi.org/10.1016/j.biotechadv.2015.03.004

Fischer BB, Ledford HK, Wakao S, Huang SG, Casero D, Pellegrini M, Merchant SS, Koller A, Eggen RIL, Niyogi KK (2012) SINGLET OXYGEN RESISTANT 1 links reactive electrophile signaling to singlet oxygen acclimation in Chlamydomonas reinhardtii. Proc Natl Acad Sci 109:E1302–E1311 . https://doi.org/10.1073/pnas.1116843109

Formighieri C, Franck F, Bassi R (2012) Regulation of the pigment optical density of an algal cell : Filling the gap between photosynthetic productivity in the laboratory and in mass culture. J Biotechnol 162:115–123 . https://doi.org/10.1016/j.jbiotec.2012.02.021

Förster B, Osmond CB, Pogson BJ (2005) Improved survival of very high light and oxidative stress is conferred by spontaneous gain-of-function mutations in Chlamydomonas. Biochim Biophys Acta - Bioenerg 1709:45–57 . https://doi.org/10.1016/j.bbabio.2005.05.012

Garcia-Gonzalez J, Sommerfeld M (2016) Biofertilizer and biostimulant properties of the microalga Acutodesmus dimorphus. J Appl Phycol 28:1051–1061 . https://doi.org/10.1007/s10811-015-0625-2

García JL, de Vicente M, Galán B (2017) Microalgae, old sustainable food and fashion nutraceuticals. Microb Biotechnol 2783: . https://doi.org/10.1111/1751-7915.12800

Gaut BS, Seymour DK, Liu Q, Zhou Y (2018) Demography and its effects on genomic variation in crop domestication. Nat Plants 4:512–520 . https://doi.org/10.1038/s41477-018-0210-1

Ghasemi Naghdi F, González González LM, Chan W, Schenk PM (2016) Progress on lipid extraction from wet algal biomass for biodiesel production. Microb Biotechnol 9:718–726 . https://doi.org/https://doi.org/10.1111/1751-7915.12360

Głowacka K, Kromdijk J, Kucera K, Xie J, Cavanagh AP, Leonelli L, Leakey ADB, Ort DR, Niyogi KK, Long SP (2018) Photosystem II Subunit S overexpression increases the efficiency of water use in a field-grown crop. Nat Commun 9:868 . https://doi.org/10.1038/s41467-018-03231-x

Gonzalez-Fernandez C, Sialve B, Molinuevo-Salces B (2015) Anaerobic digestion of microalgal biomass: Challenges, opportunities and research needs. Bioresour Technol 198:896–906 . https://doi.org/https://doi.org/10.1016/j.biortech.2015.09.095

Gouveia JD, Ruiz J, van den Broek LAM, Hesselink T, Peters S, Kleinegris DMM, Smith AG, van der Veen D, Barbosa MJ, Wijffels RH (2017) Botryococcus braunii strains compared for biomass productivity, hydrocarbon and carbohydrate content. J Biotechnol 248:77–86 . https://doi.org/https://doi.org/10.1016/j.jbiotec.2017.03.008

Guiry MD (2012) How many species of algae are there? J Phycol 48:1057–1063 . https://doi.org/10.1111/j.1529-8817.2012.01222.x

Hagemann M, Hess WR (2018) Systems and synthetic biology for the biotechnological application of cyanobacteria. Curr Opin Biotechnol 49:94–99 . https://doi.org/10.1016/j.copbio.2017.07.008

Hambourger M, Moore GF, Kramer DM, Gust D, Moore AL, Moore TA (2009) Biology and technology for photochemical fuel production. Chem Soc Rev 38:25–35 . https://doi.org/10.1039/B800582F

Herrera Bravo de Laguna I, Toledo Marante FJ, Luna-Freire KR, Mioso R (2015) Extraction of nutraceuticals from Spirulina (blue-green alga): A bioorganic chemistry practice using thin-layer chromatography. Biochem Mol Biol Educ 43:366–369 . https://doi.org/10.1002/bmb.20882

Ho MY, Shen G, Canniffe DP, Zhao C, Bryant DA (2016) Light-dependent chlorophyll f synthase is a highly divergent paralog of PsbA of photosystem II. Science (80-) 353: . https://doi.org/10.1126/science.aaf9178

Huang W, Daboussi F (2017) Genetic and metabolic engineering in diatoms. Philos Trans R Soc B Biol Sci 372: . https://doi.org/10.1098/rstb.2016.0411

Hynstova V, Sterbova D, Klejdus B, Hedbavny J, Huska D, Adam V (2018) Separation, identification and quantification of carotenoids and chlorophylls in dietary supplements containing Chlorella vulgaris and Spirulina platensis using High Performance Thin Layer Chromatography. J Pharm Biomed Anal 148:108–118 . https://doi.org/10.1016/j.jpba.2017.09.018

Imam SH, Buchanan MJ, Shin HC, Snell WJ (1985) The Chlamydomonas cell wall: characterization of the wall framework. J Cell Biol 101:1599–1607 . https://doi.org/10.1083/jcb.101.4.1599

Jeong J, Baek K, Kirst H, Melis A, Jin ES (2017) Loss of CpSRP54 function leads to a truncated light-harvesting antenna size in Chlamydomonas reinhardtii. Biochim Biophys Acta - Bioenerg 1858:45–55 . https://doi.org/10.1016/j.bbabio.2016.10.007

Ji XJ, Ren LJ, Huang H (2015) Omega-3 Biotechnology: A Green and Sustainable Process for Omega-3 Fatty Acids Production. Front Bioeng Biotechnol 3:158 . https://doi.org/10.3389/fbioe.2015.00158

Johnson X, Wostrikoff K, Finazzi G, Kuras R, Schwarz C, Bujaldon S, Nickelsen J, Stern DB, Wollman F-A, Vallon O (2010) MRL1, a Conserved Pentatricopeptide Repeat Protein, Is Required for Stabilization of rbcL mRNA in Chlamydomonas and Arabidopsis. Plant Cell 22:234–248 . https://doi.org/10.1105/tpc.109.066266

Kang S, Kim KH, Kim YC (2015) A novel electroporation system for efficient molecular delivery into Chlamydomonas reinhardtii with a 3-dimensional microelectrode. Sci Rep 5:15835 . https://doi.org/10.1038/srep15835

Kathiresan S, Chandrashekar A, Ravishankar GA, Sarada R (2015) Regulation of astaxanthin and its intermediates through cloning and genetic transformation of β-carotene ketolase in Haematococcus pluvialis. J Biotechnol 196–197:33–41 . https://doi.org/https://doi.org/10.1016/j.jbiotec.2015.01.006

Khetkorn W, Rastogi RP, Incharoensakdi A, Lindblad P, Madamwar D, Pandey A, Larroche C (2017) Microalgal hydrogen production – A review. Bioresour Technol 243:1194–1206 . https://doi.org/https://doi.org/10.1016/j.biortech.2017.07.085

Kim JH, Lee SR, Li LH, Park HJ, Park JH, Lee KY, Kim MK, Shin BA, Choi SY (2011) High Cleavage Efficiency of a 2A Peptide Derived from Porcine Teschovirus-1 in Human Cell Lines, Zebrafish and Mice. PLoS One 6:e18556 . https://doi.org/10.1371/journal.pone.0018556

Kim JYH, Kwak HS, Sung YJ, Choi H Il, Hong ME, Lim HS, Lee JH, Lee SY, Sim SJ (2016) Microfluidic high-throughput selection of microalgal strains with superior photosynthetic productivity using competitive phototaxis. Sci Rep 6:1–11 . https://doi.org/10.1038/srep21155

Kim MY, Zilberman D (2014) DNA methylation as a system of plant genomic immunity. Trends Plant

Sci 19:320–326 . https://doi.org/10.1016/j.tplants.2014.01.014

Kim S, Lee YC, Cho DH, Lee HU, Huh YS, Kim GJ, Kim HS (2014) A Simple and Non-Invasive Method for Nuclear Transformation of Intact-walled Chlamydomonas reinhardtii. PLoS One 9:e101018

Kindle KL (1998) Nuclear Transformation: Technology and Applications BT - The Molecular Biology of Chloroplasts and Mitochondria in Chlamydomonas. In: Rochaix J-D, Goldschmidt-Clermont M, Merchant S (eds). Springer Netherlands, Dordrecht, pp 41–61

Kirst H, Garcia-Cerdan JG, Zurbriggen A, Ruehle T, Melis A (2012) Truncated Photosystem Chlorophyll Antenna Size in the Green Microalga Chlamydomonas reinhardtii upon Deletion of the TLA3-CpSRP43 Gene. Plant Physiol 160:2251–2260 . https://doi.org/10.1104/pp.112.206672

Kricka W, Fitzpatrick J, Bond U (2014) Metabolic engineering of yeasts by heterologous enzyme production for degradation of cellulose and hemicellulose from biomass: a perspective. Front. Microbiol. 5:174 . https://doi.org/10.3389/fmicb.2014.00174

Kromdijk J, Głowacka K, Leonelli L, Gabilly ST, Iwai M, Niyogi KK, Long SP (2016) Improving photosynthesis and crop productivity by accelerating recovery from photoprotection. Science (80-) 354:857 LP – 861 . https://doi.org/10.1126/science.aai8878

Külheim C, Ågren J, Jansson S (2002) Rapid Regulation of Light Harvesting and Plant Fitness in the Field. Science (80-) 297:91 LP – 93 . https://doi.org/10.1126/science.1072359

Kumar M, Jeon J, Choi J, Kim S (2018) Rapid and efficient genetic transformation of the green microalga Chlorella vulgaris. J Appl Phycol 30:1735–1745 . https://doi.org/10.1007/s10811-018-1396-3

Kwon S, Kang NK, Koh HG, Shin S-E, Lee B, Jeong B, Chang YK (2018) Enhancement of biomass and lipid productivity by overexpression of a bZIP transcription factor in Nannochloropsis salina. Biotechnol Bioeng 115:331–340 . https://doi.org/10.1002/bit.26465

Langridge P (2014) Reinventing the Green Revolution by Harnessing Crop Mutant Resources. Plant Physiol 166:1682 LP – 1683 . https://doi.org/10.1104/pp.114.252601

Larson EM, O'Brien CM, Zhu G, Spreitzer RJ, Portis AR (1997) Specificity for activase is changed by a Pro-89 to Arg substitution in the large subunit of ribulose-1,5-bisphosphate carboxylase/oxygenase. J Biol Chem 272:17033–17037 . https://doi.org/10.1074/jbc.272.27.17033

Leite GB, Paranjape K, Abdelaziz AEM, Hallenbeck PC (2015) Utilization of biodiesel-derived glycerol or xylose for increased growth and lipid production by indigenous microalgae. Bioresour Technol 184:123–130 . https://doi.org/10.1016/j.biortech.2014.10.117

Leu S, Boussiba S (2014) Advances in the Production of High-Value Products by Microalgae. Ind Biotechnol 10:169–183 . https://doi.org/10.1089/ind.2013.0039

Li C, Salvucci ME, Portis AR (2005) Two residues of Rubisco activase involved in recognition of the Rubisco substrate. J Biol Chem 280:24864–24869 . https://doi.org/10.1074/jbc.M503547200

Li F, Gao D, Hu H (2014) High-efficiency nuclear transformation of the oleaginous marine Nannochloropsis species using PCR product. Biosci Biotechnol Biochem 78:812–817 . https://doi.org/10.1080/09168451.2014.905184

Li T, Gargouri M, Feng J, Park J-J, Gao D, Miao C, Dong T, Gang DR, Chen S (2015) Regulation of starch and lipid accumulation in a microalga Chlorella sorokiniana. Bioresour Technol 180:250–257 . https://doi.org/https://doi.org/10.1016/j.biortech.2015.01.005

Lima FAV, Joventino IP, Joventino FP, de Almeida AC, Neves KRT, do Carmo MR, Leal LKAM, de Andrade GM, de Barros Viana GS (2017) Neuroprotective Activities of Spirulina platensis in the 6-OHDA Model of Parkinson's Disease Are Related to Its Anti-Inflammatory Effects. Neurochem Res

42:3390–3400 . https://doi.org/10.1007/s11064-017-2379-5

Liu J, Mao X, Zhou W, Guarnieri MT (2016) Simultaneous production of triacylglycerol and high-value carotenoids by the astaxanthin-producing oleaginous green microalga Chlorella zofingiensis. Bioresour Technol 214:319–327 . https://doi.org/https://doi.org/10.1016/j.biortech.2016.04.112

Liu J, Sommerfeld M, Hu Q (2013) Screening and characterization of Isochrysis strains and optimization of culture conditions for docosahexaenoic acid production. Appl Microbiol Biotechnol 97:4785–4798 . https://doi.org/10.1007/s00253-013-4749-5

Liu J, Sun Z, Gerken H, Huang J, Jiang Y, Chen F (2014) Genetic engineering of the green alga Chlorella zofingiensis: a modified norflurazon-resistant phytoene desaturase gene as a dominant selectable marker. Appl Microbiol Biotechnol 98:5069–5079 . https://doi.org/10.1007/s00253-014-5593-y

Loera-Quezada MM, Leyva-González MA, Velázquez-Juárez G, Sanchez-Calderón L, Do Nascimento M, López-Arredondo D, Herrera-Estrella L (2016) A novel genetic engineering platform for the effective management of biological contaminants for the production of microalgae. Plant Biotechnol J 14:2066–2076 . https://doi.org/10.1111/pbi.12564

Lupatini AL, Colla LM, Canan C, Colla E (2017) Potential application of microalga Spirulina platensis as a protein source. J Sci Food Agric 97:724–732 . https://doi.org/10.1002/jsfa.7987

Lv J, Feng J, Liu Q, Xie S (2017) Microalgal Cultivation in Secondary Effluent: Recent Developments and Future Work. Int J Mol Sci 18:79 . https://doi.org/10.3390/ijms18010079

Mahdy A, Mendez L, Blanco S, Ballesteros M, González-Fernández C (2014) Protease cell wall degradation of Chlorella vulgaris: Effect on methane production. Bioresour Technol 171:421–427 . https://doi.org/https://doi.org/10.1016/j.biortech.2014.08.091

Mahdy A, Mendez L, Tomás-Pejó E, del Mar Morales M, Ballesteros M, González-Fernández C (2016) Influence of enzymatic hydrolysis on the biochemical methane potential of Chlorella vulgaris and Scenedesmus sp. J Chem Technol Biotechnol 91:1299–1305 . https://doi.org/https://doi.org/10.1002/jctb.4722

Malinovsky FG, Fangel JU, Willats WGT (2014) The role of the cell wall in plant immunity . Front. Plant Sci. 5:178. DOI: 10.3389/fpls.2014.00178

Mata TM, Martins AA, Caetano NS (2010) Microalgae for biodiesel production and other applications: A review. Renew Sustain Energy Rev 14:217–232 . https://doi.org/https://doi.org/10.1016/j.rser.2009.07.020

Melis A (2009) Solar energy conversion efficiencies in photosynthesis : Minimizing the chlorophyll antennae to maximize efficiency. Plant Sci 177:272–280 . https://doi.org/10.1016/j.plantsci.2009.06.005

Milano J, Ong HC, Masjuki HH, Chong WT, Lam MK, Loh PK, Vellayan V (2016) Microalgae biofuels as an alternative to fossil fuel for power generation. Renew Sustain Energy Rev 58:180–197 . https://doi.org/https://doi.org/10.1016/j.rser.2015.12.150

Mini P, Demurtas OC, Valentini S, Pallara P, Aprea G, Ferrante P, Giuliano G (2018) Agrobacterium-mediated and electroporation-mediated transformation of Chlamydomonas reinhardtii: a comparative study. BMC Biotechnol 18:11 . https://doi.org/10.1186/s12896-018-0416-3

Mitra D, van Leeuwen J (Hans), Lamsal B (2012a) Heterotrophic/mixotrophic cultivation of oleaginous Chlorella vulgaris on industrial co-products. Algal Res 1:40–48 . https://doi.org/https://doi.org/10.1016/j.algal.2012.03.002

Mitra M, Kirst H, Dewez D, Melis A (2012b) Modulation of the light-harvesting chlorophyll antenna size in Chlamydomonas reinhardtii by TLA1 gene over-expression and RNA interference. Philos

Trans R Soc B Biol Sci 367:3430–3443 . https://doi.org/10.1098/rstb.2012.0229

Münkel R, Schmid-Staiger U, Werner A, Hirth T (2013) Optimization of outdoor cultivation in flat panel airlift reactors for lipid production by Chlorella vulgaris. Biotechnol Bioeng 110:2882–2893 . https://doi.org/https://doi.org/10.1002/bit.24948

Nakajima Y, Ueda R (1997) Improvement of photosynthesis in dense microalgal suspension by reduction of light harvesting pigments. J Appl Phycol 9:503–510 . https://doi.org/10.1023/A:1007920025419

Nicoletti M (2016) Microalgae Nutraceuticals. Foods (Basel, Switzerland) 5:54 . https://doi.org/10.3390/foods5030054

Nymark M, Sharma AK, Sparstad T, Bones AM, Winge P (2016) A CRISPR/Cas9 system adapted for gene editing in marine algae. Sci Rep 6:24951

Oey M, Ross IL, Stephens E, Steinbeck J, Wolf J, Radzun KA, Kügler J, Ringsmuth AK, Kruse O, Hankamer B (2013) RNAi Knock-Down of LHCBM1, 2 and 3 Increases Photosynthetic H2 Production Efficiency of the Green Alga Chlamydomonas reinhardtii. PLoS One 8:e61375

Onishi M, Pringle JR (2016) Robust Transgene Expression from Bicistronic mRNA in the Green Alga Chlamydomonas reinhardtii. G3 (Bethesda) 6:4115–4125 . https://doi.org/10.1534/g3.116.033035

Ott CM, Smith BD, Portis AR, Spreitzer RJ (2000) Activase region on chloroplast ribulose-1,5-bisphosphate carboxylase/oxygenase: Nonconservative substitution in the large subunit alters species specificity of protein interaction. J Biol Chem 275:26241–26244 . https://doi.org/10.1074/jbc.M004580200

Ozkan A, Kinney K, Katz L, Berberoglu H (2012) Reduction of water and energy requirement of algae cultivation using an algae biofilm photobioreactor. Bioresour Technol 114:542–548 . https://doi.org/https://doi.org/10.1016/j.biortech.2012.03.055

P**assos F, Uggetti E, Carrère H, Ferrer I** (2014) Pretreatment of microalgae to improve biogas production: A review. Bioresour Technol 172:403–412 . https://doi.org/https://doi.org/10.1016/j.biortech.2014.08.114

Peers G (2015) Enhancement of biomass production by disruption of light energy dissipation pathways. US8940508B

Peers G, Truong TB, Ostendorf E, Busch A, Elrad D, Grossman AR, Hippler M, Niyogi KK (2009) An ancient light-harvesting protein is critical for the regulation of algal photosynthesis. Nature 462:518–521 . https://doi.org/10.1038/nature08587

Perin G, Bellan A, Segalla A, Meneghesso A, Alboresi A, Morosinotto T (2015) Generation of random mutants to improve light-use efficiency of Nannochloropsis gaditana cultures for biofuel production. Biotechnol Biofuels 8:161 . https://doi.org/10.1186/s13068-015-0337-5

Perrine Z, Negi S, Sayre RT (2012) Optimization of photosynthetic light energy utilization by microalgae. Algal Res 1:134–142 . https://doi.org/10.1016/j.algal.2012.07.002

Pinto TS, Malcata FX, Arrabaça JD, Silva JM, Spreitzer RJ, Esquível MG (2013) Rubisco mutants of Chlamydomonas reinhardtii enhance photosynthetic hydrogen production. Appl Microbiol Biotechnol 97:5635–5643 . https://doi.org/10.1007/s00253-013-4920-z

Ramos-Martinez EM, Fimognari L, Sakuragi Y (2017) High-yield secretion of recombinant proteins from the microalga Chlamydomonas reinhardtii. Plant Biotechnol J 15:1214–1224 . https://doi.org/https://doi.org/10.1111/pbi.12710

Rasala BA, Lee PA, Shen Z, Briggs SP, Mendez M, Mayfield SP (2012) Robust Expression and Secretion of Xylanase1 in Chlamydomonas reinhardtii by Fusion to a Selection Gene and

Processing with the FMDV 2A Peptide. PLoS One 7:e43349

Reinfelder JR (2010) Carbon Concentrating Mechanisms in Eukaryotic Marine Phytoplankton. Ann Rev Mar Sci 3:291–315 . https://doi.org/10.1146/annurev-marine-120709-142720

Rizzo RF, dos Santos BDC, de Castro G, Passos TS, Nascimento MD, Guerra HD, da Silva CG, Dias DD, Domingues JR, de Lima-Araujo KG (2015) Production of phycobiliproteins by *Arthrospira platensis* under different lightconditions for application in food products. Food Sci Technol 35:247–252 . https://doi.org/10.1590/1678-457x.6463

Rodolfi L, Zittelli GC, Bassi N, Padovani G, Biondi N, Bonini G, Tredici MR (2009) Microalgae for oil: Strain selection, induction of lipid synthesis and outdoor mass cultivation in a low-cost photobioreactor. Biotechnol Bioeng 102:100–112 . https://doi.org/10.1002/bit.22033

Rosa GM da, Moraes L, Cardias BB, Souza M da RAZ de, Costa JAV (2015) Chemical absorption and CO2 biofixation via the cultivation of Spirulina in semicontinuous mode with nutrient recycle. Bioresour Technol 192:321–327 . https://doi.org/https://doi.org/10.1016/j.biortech.2015.05.020

Ryckebosch E, Bruneel C, Termote-Verhalle R, Goiris K, Muylaert K, Foubert I (2014) Nutritional evaluation of microalgae oils rich in omega-3 long chain polyunsaturated fatty acids as an alternative for fish oil. Food Chem 160:393–400 . https://doi.org/https://doi.org/10.1016/j.foodchem.2014.03.087

Santos-Ballardo DU, Rossi S, Reyes-Moreno C, Valdez-Ortiz A (2016) Microalgae potential as a biogas source: current status, restraints and future trends. Rev Environ Sci Bio/Technology 15:243–264 . https://doi.org/10.1007/s11157-016-9392-z

Schierenbeck L, Ries D, Rogge K, Grewe S, Weisshaar B, Kruse O (2015) Fast forward genetics to identify mutations causing a high light tolerant phenotype in Chlamydomonas reinhardtii by whole-genome-sequencing. BMC Genomics 16:57 . https://doi.org/10.1186/s12864-015-1232-y

Schroda M (2006) RNA silencing in Chlamydomonas: mechanisms and tools. Curr Genet 49:69–84 . https://doi.org/10.1007/s00294-005-0042-1

Scranton MA, Ostrand JT, Fields FJ, Mayfield SP (2015) Chlamydomonas as a model for biofuels and bio-products production. Plant J 82:523–531 . https://doi.org/10.1111/tpj.12780

Shah MMR, Liang Y, Cheng JJ, Daroch M (2016) Astaxanthin-Producing Green Microalga Haematococcus pluvialis: From Single Cell to High Value Commercial Products. Front Plant Sci 7:531 . https://doi.org/10.3389/fpls.2016.00531

Sharma A, Arya SK (2017) Hydrogen from algal biomass: A review of production process. Biotechnol reports (Amsterdam, Netherlands) 15:63–69 . https://doi.org/10.1016/j.btre.2017.06.001

Shin SE, Lim JM, Koh HG, Kim EK, Kang NK, Jeon S, Kwon S, Shin WS, Lee B, Hwangbo K, Kim J, Ye SH, Yun JY, Seo H, Oh HM, Kim KJ, Kim JS, Jeong WJ, Chang YK, Jeong BR (2016) CRISPR/Cas9-induced knockout and knock-in mutations in Chlamydomonas reinhardtii. Sci Rep 6:27810 . https://doi.org/10.1038/srep27810

Shokrkar H, Ebrahimi S, Zamani M (2017) Bioethanol production from acidic and enzymatic hydrolysates of mixed microalgae culture. Fuel 200:380–386 . https://doi.org/https://doi.org/10.1016/j.fuel.2017.03.090

Shokrkar H, Ebrahimi S, Zamani M (2018) Enzymatic hydrolysis of microalgal cellulose for bioethanol production, modeling and sensitivity analysis. Fuel 228:30–38 . https://doi.org/https://doi.org/10.1016/j.fuel.2018.04.143

Snow AA, Smith VH (2012) Genetically Engineered Algae for Biofuels: A Key Role for Ecologists. Bioscience 62:765–768 . https://doi.org/10.1525/bio.2012.62.8.9

Somchai P, Jitrakorn S, Thitamadee S, Meetam M, Saksmerprome V (2016) Use of microalgae

Chlamydomonas reinhardtii for production of double-stranded RNA against shrimp virus. Aquac Reports 3:178–183 . https://doi.org/https://doi.org/10.1016/j.aqrep.2016.03.003

Spalding MH (2013) Modulation of low carbon dioxide inducible proteins (lci) for increased biomass production and photosynthesis. U.S. Patent Application No. 13/535,842.

Stephenson PG, Moore CM, Terry MJ, Zubkov M V., Bibby TS (2011) Improving photosynthesis for algal biofuels: Toward a green revolution. Trends Biotechnol 29:615–623 . https://doi.org/10.1016/j.tibtech.2011.06.005

Sutherland DL, Howard-Williams C, Turnbull MH, Broady PA, Craggs RJ (2015) Enhancing microalgal photosynthesis and productivity in wastewater treatment high rate algal ponds for biofuel production. Bioresour Technol 184:222–229 . https://doi.org/https://doi.org/10.1016/j.biortech.2014.10.074

Tabarsa M, Shin I-S, Lee JH, Surayot U, Park W, You S (2015) An immune-enhancing water-soluble α-glucan from Chlorella vulgaris and structural characteristics. Food Sci Biotechnol 24:1933–1941 . https://doi.org/10.1007/s10068-015-0255-0

Tchernov D, Livne A, Kaplan A, Sukenik A (2008) The kinetic properties of ribulose-1,5-bisphosphate carboxylase/oxygenase may explain the high apparent photosynthetic affinity of Nannochloropsis sp. to ambient inorganic carbon. Isr J Plant Sci 56:37–44 . https://doi.org/10.1560/IJPS.56.1-2.37

Tirichine L, Bowler C (2011) Decoding algal genomes: tracing back the history of photosynthetic life on Earth. Plant J 66:45–57 . https://doi.org/https://doi.org/10.1111/j.1365-313X.2011.04540.x

Truong TB (2011) Investigating the role (s) of LHCSRs in Chlamydomonas reinhardtii. UC Berkeley

Tsai YCC, Lapina MC, Bhushan S, Mueller-Cajar O (2015) Identification and characterization of multiple rubisco activases in chemoautotrophic bacteria. Nat Commun 6:1–10 . https://doi.org/10.1038/ncomms9883

Venkanna D, Südfeld C, Baier T, Homburg S V, Patel A V, Wobbe L, Kruse O (2017) Knock-Down of the IFR1 Protein Perturbs the Homeostasis of Reactive Electrophile Species and Boosts Photosynthetic Hydrogen Production in Chlamydomonas reinhardtii. Front. Plant Sci. 8:1347 . https://doi.org/10.3389/fpls.2017.01347

Wakabayashi K, Misawa Y, Mochiji S, Kamiya R (2011) Reduction-oxidation poise regulates the sign of phototaxis in Chlamydomonas reinhardtii Proc Natl Acad Sci 108:11280 LP – 11284 . https://doi.org/10.1073/pnas.1100592108

Wang B, Lan CQ, Horsman M (2012) Closed photobioreactors for production of microalgal biomasses. Biotechnol Adv 30:904–912 . https://doi.org/https://doi.org/10.1016/j.biotechadv.2012.01.019

W**ang Q, Lu Y, Xin Y, Wei L, Huang S, Xu J** (2016) Genome editing of model oleaginous microalgae Nannochloropsis spp. by CRISPR/Cas9. Plant J 88:1071–1081 . https://doi.org/https://doi.org/10.1111/tpj.13307

Wannathong T, Waterhouse JC, Young REB, Economou CK, Purton S (2016) New tools for chloroplast genetic engineering allow the synthesis of human growth hormone in the green alga Chlamydomonas reinhardtii. Appl Microbiol Biotechnol 100:5467–5477 . https://doi.org/10.1007/s00253-016-7354-6

Wayama M, Ota S, Matsuura H, Nango N, Hirata A, Kawano S (2013) Three-Dimensional Ultrastructural Study of Oil and Astaxanthin Accumulation during Encystment in the Green Alga Haematococcus pluvialis. PLoS One 8:e53618

Wei L, Wang Q, Xin Y, Lu Y, Xu J (2017) Enhancing photosynthetic biomass productivity of industrial oleaginous microalgae by overexpression of RuBisCO activase. Algal Res 27:366–375 .

https://doi.org/10.1016/j.algal.2017.07.023

Weiner I, Atar S, Schweitzer S, Eilenberg H, Feldman Y, Avitan M, Blau M, Danon A, Tuller T, Yacoby I (2018) Enhancing heterologous expression in Chlamydomonas reinhardtii by transcript sequence optimization. Plant J 94:22–31 . https://doi.org/https://doi.org/10.1111/tpj.13836

Whitney SM, Houtz RL, Alonso H (2011) Advancing Our Understanding and Capacity to Engineer Nature's CO2-Sequestering Enzyme, Rubisco. Plant Physiol 155:27–35 . https://doi.org/10.1104/pp.110.164814

Wilson RH, Martin-Avila E, Conlan C, Whitney SM (2018) An improved Escherichia coli screen for Rubisco identifies a protein-protein interface that can enhance CO2-fixation kinetics. J Biol Chem 293:18–27 . https://doi.org/10.1074/jbc.M117.810861

Wrede D, Taha M, Miranda AF, Kadali K, Stevenson T, Ball AS, Mouradov A (2014) Co-Cultivation of Fungal and Microalgal Cells as an Efficient System for Harvesting Microalgal Cells, Lipid Production and Wastewater Treatment. PLoS One 9:e113497

Wu Q, Liu L, Miron A, Klímová B, Wan D, Kuča K (2016) The antioxidant, immunomodulatory, and anti-inflammatory activities of Spirulina: an overview. Arch Toxicol 90:1817–1840 . https://doi.org/10.1007/s00204-016-1744-5

Xu Y, Ibrahim I, Wosu C, Ben-Amotz A, Harvey P (2018) Potential of New Isolates of Dunaliella Salina for Natural β-Carotene Production. Biology (Basel) 7:14 . https://doi.org/10.3390/biology7010014

Yaakob Z, Ali E, Zainal A, Mohamad M, Takriff MS (2014) An overview: biomolecules from microalgae for animal feed and aquaculture. J Biol Res (Thessalonike, Greece) 21:6 . https://doi.org/10.1186/2241-5793-21-6

Young AJ, Lowe GL (2018) Carotenoids-Antioxidant Properties. Antioxidants (Basel, Switzerland) 7:28 . https://doi.org/10.3390/antiox7020028

Zárate R, El Jaber-Vazdekis N, Tejera N, Pérez JA, Rodríguez C (2017) Significance of long chain polyunsaturated fatty acids in human health. Clin Transl Med 6:25 . https://doi.org/10.1186/s40169-017-0153-6

Zhang H, Lang Z, Zhu JK (2018) Dynamics and function of DNA methylation in plants. Nat Rev Mol Cell Biol 19:489–506 . https://doi.org/10.1038/s41580-018-0016-z

Zhang Q, Liu C, Li Y, Yu Z, Chen Z, Ye T, Wang X, Hu Z, Liu S, Xiao B, Jin S (2017) Cultivation of algal biofilm using different lignocellulosic materials as carriers. Biotechnol Biofuels 10:115 . https://doi.org/10.1186/s13068-017-0799-8

Zhu G, Kurek I, Liu L (2010a) Chapter 20 Engineering Photosynthetic Enzymes Involved in CO2–Assimilation by Gene Shuffling BT - The Chloroplast: Basics and Applications. In: Rebeiz CA, Benning C, Bohnert HJ, Daniell H, Hoober JK, Lichtenthaler HK, Portis AR, Tripathy BC (eds). Springer Netherlands, Dordrecht, pp 307–322

Zhu XG, Long SP, Ort DR (2010b) Improving Photosynthetic Efficiency for Greater Yield. Annu Rev Plant Biol 61:235–261 . https://doi.org/10.1146/annurev-arplant-042809-112206

Zorin B, Grundman O, Khozin-Goldberg I, Leu S, Shapira M, Kaye Y, Tourasse N, Vallon O, Boussiba S (2014) Development of a Nuclear Transformation System for Oleaginous Green Alga Lobosphaera (Parietochloris) incisa and Genetic Complementation of a Mutant Strain, Deficient in Arachidonic Acid Biosynthesis. PLoS One 9:e105223

CHAPTER 3
Introduction: *Chlamydomonas* pale mutants

3.1 State of art of *Chlamydomonas* pale mutants

As said in the previous chapters, one of the main limitations in microalgae mass cultivation is the high optical density they reach. Higher plants and green microalgae, indeed, possess a huge light-harvesting system composed by chlorophylls and carotenoids that absorb and transfer the energy of sunlight towards the photochemical reaction centres. The large size of these systems is due to an adaptation in the natural environment, when light is a limiting resource. But, when microalgae grow under direct sunlight in high-density cultures for industrial production, an excess of light absorbance and dissipation by the outer cell layers, causing a shading of the inner layers, can produce a drop in the photosynthetic efficiency and productivity (Melis 2009). Therefore, strains capable of not over-adsorb sunlight are promising for industrial application. Most of these strains, namely pale-green, have a lower chlorophyll content and reduced PSI or/and PSII antenna size (Vecchi et al. 2020). Some of them, affected in antennas structure and not in reactions centres abundance, have a lower chlorophyll *b* content, as this pigment is associated to the peripheral LHCs, in particular to LHCII. At the same time photosensitive pale mutants were also obtained, in order to study the role of specific enzymes in chlorophyll *a* or *b* biosynthetic pathways, in the LHCs (Light Harvesting Complexes) import pathways, or in the assembly of PSI and PSII. Another widely studied pathway is the one of carotenoid production. The biosynthesis of these molecules can be indeed regulated in microalgae, as these molecules not only participate in the widening of the spectral range that chlorophylls can harvest, but also play a role in ROS scavenging and photoprotection of the photosynthetic machinery, by catalysing dissipation of the energy in excess (Edge et al. 1997). Moreover they are widely used for a lot of industrial applications (Safafar et al. 2016). Table 3 summarizes the features of the yet obtained pale-green strains.

Table 3: Most relevant *Chlamydomonas* pale green mutants reported in literature: the table presents the mutants classified based on the affected gene function. The parameters are expressed as % respect to the corresponding wild type values. When they change according to light conditions it is specified in the brackets. When mutants have alternative names, both are specified. When two strains have the same features, they are reported in the same cell and possible differences are reported in the brackets. When more than two strains are reported together it is indicated a parameters variation range. For *tla3* chlorophyll content are reported two different measured performed in two different years by two different groups. Some values were deduced from papers graphs and some ratios were calculated from reported data; therefore, the value could be subjected to small estimation errors. HH: High light LL: Low Light

Mutant	Afftcted gene	Genetic modification	Chl tot %	Chl a/b ratio (%)	Car tot %	Car/ Chl (%)	PSII antenna size (%)	PSI antenna size (%)	Fv/ Fm	Photosensitivity/ photoresistance
SRP pathway										
tla3 (Kirst et al., 2012a; Bujaldon et al., 2020)	*CpSRP43*	Random DNA insertion	16 (2012) 45 (2020)	444 (2012) 200 (2020)	35	240	38	62	70	Saturation at higher light intensities
P71 (Bujaldon et al., 2020)	*CpSRP43*	5-fluorodeoxyuridine mutagenesis	17	222	--	-	13	55	40	-
tla2 (Kirst et al., 2012b)	*CpFTSY*	Random DNA insertion	18	352	35	180	6	60	-	Saturation at higher light intensities
ΔCpFTSY (Baek et al., 2016)	*CpFTSY*	CRISPR-Cas9	30	280	50	180	-	-	-	Photoresitant 700µE
as2 *(Bonente et al.,2011)*	*CpFSTY?*	Random DNA insertion	-	130	190	-	≈80	-	-	Photoresistant
tla4 (Jeong et al., 2017)	*CpSRP54*	Random DNA insertion	57	140	≈80	≈160	78	55	-	Saturation at higher light intensities
ac29 (Bellafiore er al., 2002; Bujaldon et al., 2020)	*Alb3.1*	γ-irradiation mutagenesis	18	420	-	-	-	-	40	-
BF4 (Bujaldon et al., 2020; Olive et al.,1981)	*Alb3.1*	UV mutagenesis	12	300	-	-	13	64	40	-
alb3.2 (Göhre et al., 2006)	*Alb3.2*	RNAi	30	-	-	-	-	-	-	Lethal
Crltd1 (Jeong et al.,2018)	LTD	CRISPR-Cas9	33	100	-	-	55	40	-	Growth similar to WT at 350µE
Antenna size regulators										
tla1 (Polle et al.,2003)	*TLA1*	Random DNA insertion	37.5	270	-	-	65	50	86	Photoresistant
ri6 *(Mitra et al., 2012)*	*TLA1*	RNAi-mediated knock-down	30	231	-	-	74	50	-	Photoresistant
LHCIIs encoding genes and their regulators										
stm3LR3 (Mussgnug et al., 2007)	all LHCII (LHCBM) genes	RNAi-mediated knock-down	32	208	-	-	-	-	-	Photoresistant
stm6Glc4L01 *(Oey et al. ,2013)*	*LHCBM1/2/3* genes	RNAi-mediated knock-down	50	114	-	-	-	-	-	Photoresistant
stm6Glc4T7	*NAB1*	Site-directed mutagenesis	80	106	-	-	85	-	-	Photoresistant
K9 *(Cazzaniga et al., 20020)*	*CP29*	CRISPR-Cas9 mutagenesis	100	87	100	100	144	-	76	Photosensitive
k69	*CP26*	CRISPR-Cas9 mutagenesis	91	70	96	97	258	-	64	Photosensitive
Chl b biosynthesis										
BF3 *(Bujaldon et al., 2017)*	*CAO*	UV-generated mutants	65 (50 µE) 87 (1µE)	∞	-	-	50 (50 µE) 40(1µE)	110 (50 µE) 160(1µE)	60 (50 µE) 37 (1µE)	--
pg27 *(Bujaldon et al., 2017)*	*CAO*	UV-generated mutants	65 (50 µE)	∞	-	-	-	-	40	-

			58 (1µE)							
cbs3 *(Bujaldon et al., 2017)*	*CAO*	DNA deletion	80 (50 µE) 96 (1µE)	∞	-	-	-	-	56	-
yid *(Bujaldon et al., 2017*	*?*	Crossing of yid-BF3 x wt	100 (50 µE) 40 (1µE)	∞	-	-	90 (50 µE) 73 (1µE)	129	95 (50 µE) 85 (1µE)	--
yid-BF3 *(Bujaldon et al., 2017*	*CAO &?*	UV-generated mutants	60 (50 µE) 30(1µE)	∞	-	-	60 (50 µE) 25(1µE)	70	40 (50 µE) 50 (1µE)	--
yid-pg27 *(Bujaldon et al., 2017)*	*CAO &?*	UV-generated mutants	60 (50 µE) 20 (1µE)	∞	-	-	-	-	40 (50µE) 60 (1µE)	-
yid-cbs3 *(Bujaldon et al., 2017)*	*CAO&?*	DNA deletion	60 (50 µE) 34(1µE)	∞	-	-	-	-	55	-
yid-BF3-ftsh1 *(Bujaldon et al., 2017)*	*CAO+ ftsh*	Mutants crossing	16	∞	-	-	31	93	24 (50µE) 1 (1µE)	-
CR118 & CR133 *(Perrine et al., 2012)*	*CAO*	RNAi-mediated knock-down	70	140 (CR188) 180 (CR133)	76 (LL) 100-110 (HL)	-	-	-	-	Photoresistant
NC-7 NC-29 NC-77 *(Negi et al., 2020)*	*CAO*	*cbs3* mutant complemented by *CAO* sequence fused to LRE-NAB1 binding site		120 (LL) 220 (HL)	-	-	78-100	-	97-110	Photoresistant
Chl a biosynthesis										
chl 1& brs1 *(Chekounova et al., 2001; Wang et al., 1974)*	*CHLH*	UV-generated mutants	0.6	-	-	-	-	-	-	Photosensitive
as3/gun4 *(Bonente et al., 2011; Formighieri et al., 2012)*	*GUN4*	Random DNA insertion	50	110	90	174	-	-	-	Photosensitive
chli1/fdx3 *(Brzezowski et al., 2016)*	*CHLI FDX3*	Random DNA insertion	0	0	-	-	-	-	-	Photosensitive
chlM-1 *(Meinecke et al., 2010)*	*MgPMT or PPMT*	UV random mutagenesis	6	-	60	1000	-	-	-	Photosensitive
chlM2 *(Meinecke et al., 2010)*	*MgPMT or PPMT*	UV random mutagenesis	1.5	-	50	3390	-	-	-	Photosensitive
PSII assembly										
ΔpsbO *(Pigolev et al., 2008)*	*psbO*	DNA insertion	50 (HL) 100 (LL)	80 (HL) 100 (LL)	65 (HL) 100 (LL)	125 (HL) 100 (LL)	-	-	7 (HL) 67 (LL)	Photosensitive
A250R *S264K* *(Antonacci et al., 2018)*	*D1*	Particle gun bombardement	60 (A250R) 40 (S264 K)	100	≈7	≈14	-	-	90	Photosensitive
PSI assembly and stability										
ycf3 *(Boudreau et al., 1997)*	*YCF3*	DNA insertion	-	-	-	-	-	-	-	Photosensitive
Ycf4 *(Boudreau et al., 1997)*	*YCF4*	DNA insertion	-	-	-	-	-	-	-	Photosensitive

ΔY3IP1 *(Nellaepalli et al., 2018)*	*Y3IP1*	DNA insertion	-	-	-	-	-	-	-	Photosensitive
Msf1 *(Zhao et al., 2017)*	*MSF1*	DNA insertion	50	110	65	100	-	-	-	Photosensitive
Carotenoid Biosynthesis										
lts1-30 *(Mc Carthy et al., 2004; Chemerilova 1978)*	*PSY*	random mutagenesis	20	-	0	0	-	-	-	Photosensitive
FN68/lts202 *(Forster et al., 1984, Mc Carthy et al., 2004)*	*PSY*	random mutagenesis	16	-	0	0	-	-	-	Photosensitive
w7/lts201 *(Spreitzer & Mets 1981; Mc Carthy et al., 2004)*	*PSY*	random mutagenesis	7.5	-	0	0	-	-	-	Photosensitive
lts1203;204;205;206;207;208;209;210 *(Mc Carthy et al., 2004)*	*PSY*	random mutagenesis	2.5-5.5	*Llts1-210:* 1800 (Tran et al., 2012)	0	0	-	-	-	Photosensitive
Pds1-1 *(Tran et al., 2012)*	*PDS*	UV mutagenesis	12.5	125	4.5	33	-	-	-	Photosensitive
pds1-2, pds 1.3 *(Tran et al., 2012)*	*PDS*	Pds1-2: UV mutagenesis Pds 1-3: random insertion	2.2	640	0	0	-	-	-	Photosensitive
lts1-301pds1-2 *(Tran et al., 2012)*	*PDS and PSY*	Crossing	1.9	660	0	0	-	-	-	Photosensitive
ΔZEP *(Baek et al., 2016)*	*ZEP*	CRISPR-Cas9	85	100	100	140	-	-	-	Photosensitive like WT
ΔZEP ΔCpFTSY *(Baek et al., 2016)*	*ZEP + CPFTSY*	CRISPR-Cas9	36	37	68	196	-	-	-	Photoresistant
npq1 *(Niyogi et al., 1997a; Jahns et al., 2000)*	*VDE*	Random DNA insertion	92	108	103	100	100	-	100	Able to grow in high light
npq2 *(Niyogi et al., 1997a; Jahns et al., 2000)*	*ZEP*	Random DNA insertion	100	116	92	111	100	-	-	Able to grow in high light
Npq2lor1 *(Polle et al., 2001)*	*ZEP & LCYE*	Npq2 spontaneous mutation in lor1 backgroune	70	140	70	100	60	120	86	Photoresistant
Npq1lor1 *(Niyogi et al., 1997 b)*	*VDE* *LCYE*	Crossing	72	150	-	-	-	-	100 (LL) 62 (HL)	Photosensitive
Npq2-2npq1lor1 & *Npq2-3npq1lor1 &* *Npq2-4npq1lor1* (Baroli et al.,2003)	*VDE* *LCYE* *ZEP*	Natural phenotype reversion	70-90 (LL) 60-75 (HL)	115 (LL) 175-200 (HL)	-	-	-	-	100 (LL) ND(HL)	Able to grow in high light
Lor1 *(Niyogi et al., 1997 b; Anwaruzzaman; 2004)*	*LCYE*	UV mutagenesis	-	150	-	-	-	-	100 (HL) 93 (LL)	Able to grow in high light
ELIPs										
ELIP3-OX (Lee et al., 2020)	*ELIP3*	Overexpressing insertional mutant								Photoresistant
ELIP3-RNAi	*ELIP3*	RNAi								Photosensitive

Lee et al., 2020)

3.1.1 Antenna size regulators

As for the LHCs import pathways the main part of the mutants lacked a component of the CpSRP (Chloroplast Signal Recognition Particle) pathway, involved in the protein insertion in thylakoids membrane. They present a reduced antenna size and a lower irradiance at which photosynthesis is saturated (Kirst and Melis 2014). All these mutants will be widely discussed in the following section. Among the genes responsible for the antenna size, *TLA1* (Truncated light harvesting antenna 1) is one of the first identified (Polle et al. 2003). *tla1* mutant showed a reduction of Chl content compared to the WT, PSI and PSII antenna size resulted significantly affected (see Table 1). The *tla1* strain required a higher light intensity to saturate the photosynthesis and showed a greater photosynthetic productivity under mass culture conditions (Polle et al. 2003). Another mutant for this gene, *ri6*, was obtained by modulating its expression by RNAi (Mitra et al. 2012).

3.1.2 LHCIIs encoding genes and their regulator

Interesting pale phenotypes were obtained also targeting LHCII encoding genes (LHCBM) and their regulator. The mutant *stm3LR3* was produced by silencing all these genes via RNA interference. This mutant showed a decreased Chl content and an increased Chla/b ratio compared to his wild type and an improved photon conversion efficiency, producing an increased growth rate (+185% than control genotype, see Mussgnug et al. 2007). By a similar method it was produced also the *stm6Glc4L01* strain, a combined knock-down of three distinct LHCBM isoforms (LHCBM1/2/3). It has a higher rate of light to H_2 (+185% than WT) and to biomass conversion (+165%) under excess light conditions (Oey et al. 2013). Monomeric antenna mutants are instead photosensitive and not significantly pale. The single CP29 KO mutant (k9) and the double CP29 and CP26 KO (K69) are characterized by an increased compensatory LHCII content and functional antenna size of PSII , moreover they are impaired not only in photosynthetic efficiency, but also in state transition and NPQ (Cazzaniga et al. 2020).

3.1.3 Chlorophyll *a* biosynthesis

Other experiments were performed to obtain knock-out and knock-down pale-mutants, missing some enzymes of chlorophyll biosynthetic pathway. In the paragraph 3.3 it will be widely discussed about mutants that are unable to produce chloropyll *b* since devoid of Chlorophyll *a*-oxygenase. Some other interesting mutants have defects in chlorophyll *a* production (Figure 3.1.1). The chlorophyll molecule consists of a magnesium atom in the centre of a porphyrin ring (a cyclic tetrapyrrole); a long carbon–hydrogen side chain (phytol chain) is bounded to the ring. Chlorophyll is present in distinct forms: chlorophylls *a* and *b* are the most present forms in plants and algae. One of the most studied enzymes in its biosynthetic pathway is the Magnesium-chelatase (MgCh), a heteromultimeric complex, responsible for the insertion of the Mg^{++} in the protoporphyrin. It

possesses three subunits D (CHLD), I (CHLI) and H (CHLH). The latter is the real responsible of the chelation step binding the Protoporphyrin IX and the Mg^{++}, while the others play a role in the enzyme activation (Walker and Willows 1997; Lohr et al. 2005). CHLH knock-out mutants, namely *chl1* and *brs1,* were isolated as able to grow only in the dark. They elucidated the light dependence of CHLH biosynthesis (Chekounova et al. 2001). Another important component of the Mg-Chelatase complex is the GUN4 protein, that interacts with CHLH to regulates tetrapyrrole biosynthesis and plays a role in the distribution of porphyrin between MgChelatase (MgCh) and FeChelatase pathways (Sobotka et al. 2008). *Chlamydomonas* mutant *gun4* showed a reduction in chlorophyll content of about 50%, compared to wild type and accumulated Protoporphyrin IX. This mutant therefore was photosensitive and displayed an altered expression of some photosynthetic genes, LHCs and tetrapyrrole pathways encoding genes (Formighieri et al. 2012). This suggested a role of tetrapyrrole synthesis in the regulation of nuclear genes, with a retrograde effect on *gun4* (Leister et al. 2011; Formighieri et al. 2012). Alterations were reported also in the photosynthetic electron transport, due to a strong decrease in PSI-to-PSII ratio (Formighieri et al. 2012). The CHLI subunit of the MgCh has *bona fide* an ATPase activity (Kobayashi et al. 2008). In *Chlamydomonas*, as in plants, there are two isoforms CHLI1 and CHLI2, however their contribution in the biosynthetic pathway is not the same (Brzezowski et al. 2016). As shown in the chlI/fdx3 mutant, CHLI1 is necessary for chlorophyll biosynthesis, while the other isoform has a secondary role and its expression alone does not recover the wild type phenotype (Brzezowski et al. 2016). chlM1 and chlM2 strains were, instead, deprived of Mg-protoporphyrin IX methyltransferase (MgPMT or PPMT). They are photosensitive, yellow in the dark and show a drastic reduction in the abundance of core proteins of photosystems I and II and light-harvesting chlorophyll *a/b*-binding proteins (Meinecke et al. 2010).

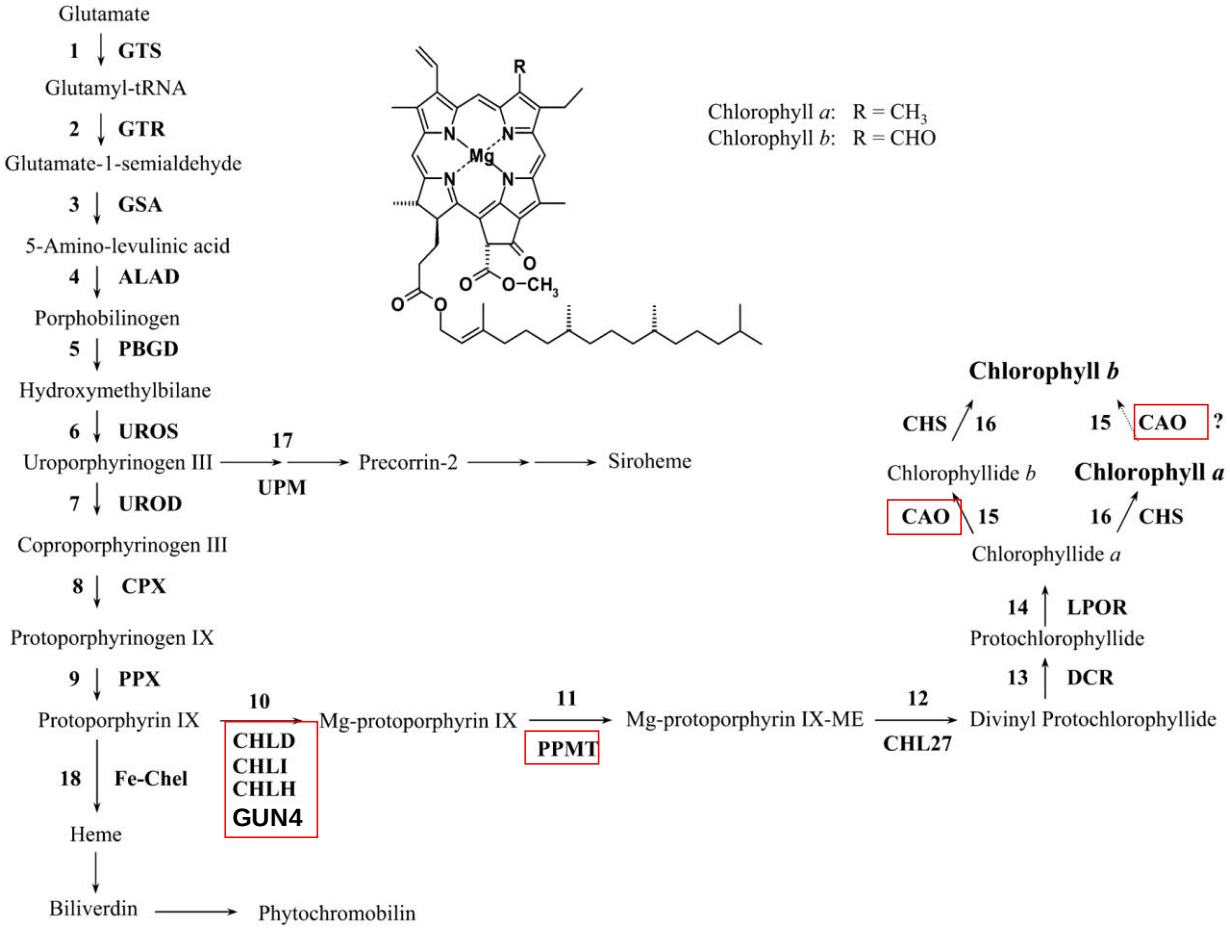

Figure 3.1.1 Chl biosynthetic pathway. Enzyme names are: GTS, glutamyl-tRNA synthetase; GTR, glutamyl-tRNA reductase; GSA, Glu-1-semialdehyde aminotransferase; ALAD, ALA dehydratase; PBGD, porphobilinogen deaminase; UROS, uroporphyrinogen III synthase; UROD, uroporphyrinogen III decarboxylase; CPX, coproporphyrinogen III oxidase; PPX, protoporphyrinogen IX oxidase; CHLD, protoporphyrin IX Mg-chelatase subunit D; CHLI, protoporphyrin IX Mg-chelatase subunit I; CHLH, protoporphyrin IX Mg-chelatase subunit H; GUN4, Tetrapyrrole-binding protein PPMT, Mg-protoporphyrin IX methyltransferase; CHL27, Mg-protoporphyrin IX monomethylester cyclasesubunit; DCR, divinyl protochlorophyllide reductase; LPOR, NADPH:protochlorophyllide oxidoreductase; CAO, chlorophyllide *a* oxygenase; CHS, Chl synthase; UPM, uroporphyrinogen III methyltransferase; and Fe-Chel, ferrochelatase. The red squares indicate the enzymes affected in the cited mutants. (Modified from Lohr et a., 2005)

3.1.4 PSII assembly

The PSII supercomplex has a crucial importance in catalyzing the light phase reactions. The functional role and the importance of each constitutive protein have been widely investigated by direct and reverse genetics. For example, the *ΔpsbO* mutant, missing a component of Oxygen Evolving Complex, is characterized by a photosensitivity to high light. Nevertheless, in the dark, it is capable of assembling stable PSII reaction centers, though is unable to oxidize water, likely because affected in the assembly of the manganese cluster (Pigolev et al. 2009). Interesting results were also derived from the mutagenesis of the highly conserved D1 core protein, which is necessary to sustaining photosynthetic electron transport. Antonacci and colleagues demonstrated that mutants of *Chlamydomonas* carrying Ala250Arg (A250R) and Ser264Lys (S264K) substitutions were differentially affected in electron transport and oxygen production (Antonacci et al. 2018). Moreover they showed different degrees of change in the primary metabolites production, suggesting a role of D1 in metabolic retrograde signalling, that makes it an interesting target for microalgae metabolic switch (Antonacci et al. 2018)

3.1.5 PSI assembly and stability

PSI-deficient mutants were characterized for research purposes, as they were unable to growth photoautotrophically. Reaction centres are indeed necessary to catalyse the electron transfer from plastocyanin to $NADP^+$. Beside mutants devoid of specific PSI subunits, genotypes altered in PSI assembly were isolated, which helped to elucidate the role of some chloroplastic genes. Boudreau and colleagues in 1997 isolated *ycf3*- and *ycf4*-deficient mutants that were able to synthesize PSI subunits, but not to assemble it (Boudreau et al. 1997). These genes are involved in PSI subunits accumulation, belong to the rps9–ycf4–ycf3–rps18 polycistronic transcriptional unit, whose gene products are associated with the thylakoid membrane (Boudreau et al. 1997). Nellaepalli and colleagues observed that Ycf3 and Ycf4 formed modules that mediate PSI assembly, moreover they generated the mutant for the gene Y3IP1, encoding a Ycf3 interacting partner (Nellaepalli et al. 2018). A required factor for the stability and maintenance of PSI is Msf1 (Maintenance factor for photosystem I), identified in 2017 by Zhao and co-workers, which probably interacts with enzymes of the tetrapyrrole biosynthetic pathway. It possibly links chlorophyll biosynthesis with the stability of chlorophyll-binding complexes, in particular PSI. Interestingly, Msf1 is up-regulated under stress conditions (Zhao et al. 2017).

3.1.6 Carotenoid Biosynthetic Pathway

Carotenoids (Car) are poly-isoprenoid compounds which contain 40 carbon atoms and derived from terpenoids biosynthesis pathway. In photosynthesis they are involved in many critical functions, not only as accessory pigments in light harvesting processes. They act also as structural components of LHCs and are involved in photoprotection to dissipate excess energy and to scavenge singlet oxygen (DellaPenna 1999).Carotenoids are classified in two classes, xanthophylls (which contain oxygen) and carotenes. The double carbon-carbon bonds interact in the conjugation process and the π-electrons delocalization in the conjugated double bonds system allow the light absorption in the visible range 400-500 nm.

Therefore, it is not surprising that impairment in the carotenoid biosynthesis (Figure 3.1.2) leads to low photosynthetic efficiency and a pale, and sometimes almost white, phenotype. In 2004 a collection of white *Chlamydomonas* mutants was characterized (McCarthy et al. 2004). They were low in chlorophylls but accumulated about a double amount of tocopherol compared to the wild type, moreover they were able to grow only in the dark, they died also under very low light conditions on acetate-containing medium (McCarthy et al. 2004). All these mutant, named *lts1-30* (Chemerilova 1978), *w7* (Spreitzer and Mets 1981), *fn68* (Förster et al. 2005) and *lts1* from 203 to 210 (McCarthy et al. 2004), were affected in the same allele, encoding for Phytoene Synthase, that converts geranyl geranyl pyrophosphate in phytoene, from which all carotenoids derive. Similar mutants were obtained for the Phytoene desaturase (PDS), catalysing the next step, namely the conversion of Phytoene in ζ-carotene (Tran et al. 2012). The knock down *pds1-1* strain and the knockout *pds1*-2 and *pds 1-3* mutants accumulated only phytoene and no other carotenoids and grow slower also compared to PSY mutants. The same defects were observed in the double mutant *lts1-300-pds1-2* (Tran et al. 2012).

As reported in the first chapter, xanthophyll are carotenoids involved in photoprotective mechanisms and NPQ (Holt et al. 2005; Vecchi et al. 2020). Under excess light conditions, lumen acidification triggers the xanthophyll cycle, consisting of a light-dependent, rapid and reversible de-epoxidation of Vio to Zea, by the action of the lumenal enzyme violaxanthin de-epoxidase (VDE), while the reverse reaction is catalysed by zeaxanthin epoxidase (ZEP). A mutant for ZEP was produced in *Chlamydomonas* by CRISPR-Cas9 system; its growth rate was unaffected with respect to the wild type in high light, however it was used as tool to produce zeaxanthin for industrial and clinical employment (Baek et al. 2016; Baek et al. 2018). The double mutant ΔZEPΔCPFSTY, on the contrary, showed an increased photoresistance, compared to the single ΔCPFTSY (Baek et al. 2016). Mutants for xanthophyll cycle were yet isolated in 1997 by Niyogi and colleagues, they characterized indeed the two random insertional mutants *npq1* and *npq2*, lacking VDE and ZEP respectively (Niyogi et al. 1997a). These mutants didn't present growth defect and have a content of chlorophyll similar to the wild type, in particular *npq1* was able to activate ΔpH-dependent nonphotochemical quenching, suggesting that xanthophyll cycle is not necessary for survival of *Chlamydomonas* in excessive light (Niyogi et al. 1997a; Jahns et al. 2000). *npq2*, instead accumulated zea and had a slower D1 protein degradation in chloramphenicol-treated cells compared to the wild type, thus suggesting a role of zeaxanthin to counteract high light-induced PSII inactivation (Jahns et al. 2000). Besides *npq1* and *npq2*, another paler mutant defective in α-branch of carotenoid biosynthesis was identified: *lor1* (Niyogi et al. 1997b). It was characterized by more defects in chlorophyll synthesis, but nevertheless

it retained NPQ capacity and was still able to grow in high light (Niyogi et al. 1997b). This mutant was then identified as missing lycopene ε-cyclase, that converts lycopene in δ-carotene, which is the precursor of α-carotene and then lutein (Anwaruzzaman et al. 2004). When crossed with *npq1,* produced a mutant defective in the synthesis of lutein, loroxanthin (α-carotene branch), zeaxanthin and antheraxanthin (β-carotene branch), devoid of NPQ and extremely photosensitive (Niyogi et al. 1997b). The double mutant *npq2lor1* was instead investigated to understand the effect of these mutations on the photochemical apparatus assembly and function. It showed a significantly smaller PSII antenna size, but normal PSI antenna size. The most interesting feature is that it needed more light intensity to saturate photosynthesis, as zeaxanthin can replace lutein and violaxanthin in most of the functional light-harvesting antenna (Polle et al. 2001). Finally in 2003 some revertants were isolated among the *npq1lor1* mutants, containing a level of zeaxanthin proportional to their increase in antenna size, compared to the original mutant (Baroli et al. 2003). The zeaxanthin-accumulating revertants had suppression genes that are new alleles of *npq2*, they were able to tolerate higher levels of ROS (Baroli et al. 2003).

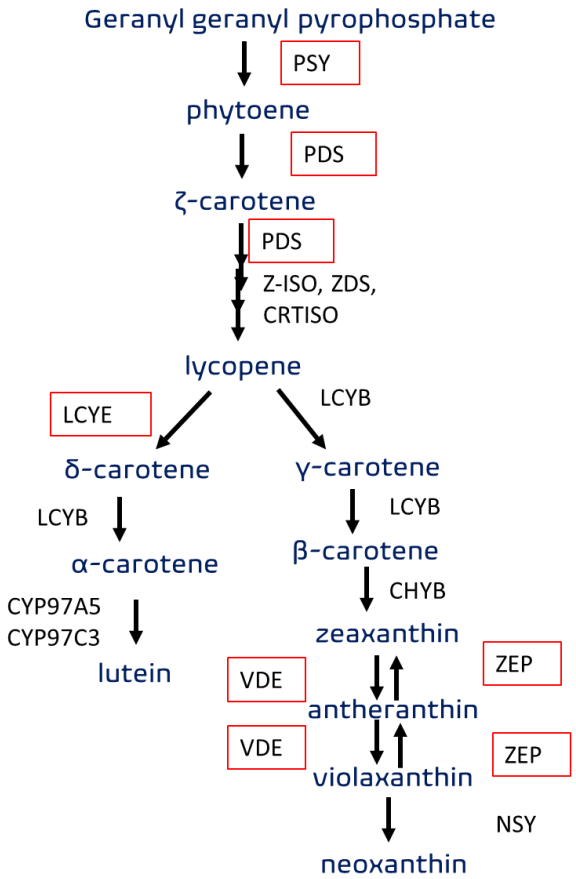

Fig 3.1.2. Simplified carotenoid pathway in algae. PSY, phytoene synthase; PDS, phytoene desaturase; Z-ISO, ζ-carotene isomerase; ZDS, ζ-carotene desaturase; CRTISO, carotenoid isomerase, LCYE, lycopene ε-cyclase; LCYB, lycopene β-cyclase; CYP97A5, cytochrome P450 β-hydroxylase; CYP97C3, cytochrome P450 ε-hydroxylase;CHYB, carotene b-hydroxylase; ZEP, zeaxanthin epoxidase; VDE, violaxanthin de-epoxidase; NSY, neoxanthin synthase. The red square indicates the cited enzymes.

3.1.7 Early Light-Inducible Proteins (ELIPs)

The early light-induced proteins (ELIPs) are part of the multigenic family of pigment-binding light-harvesting complexes (Engelken et al. 2012). They are transiently accumulate when plants are exposed to high light and, due to their photoprotective role, are considered a good genetic target to enhance plant productivity(Grimm and Kloppstech 1987; Tzvetkova-Chevolleau et al. 2007a). ELIPS were proposed to fulfil a chlorophyll sensors role to avoid the over-accumulation of free chlorophyll, which would exacerbate photooxidative stress (Tzvetkova-Chevolleau et al. 2007a). Moreover, they were correlated with the activity of the xanthophyll cycle in severe stress conditions (Rossini et al. 2006). Homologous of these proteins were found also in microalgae (Park et al. 2013; Lee et al. 2020) and are considered promising targets to enhance algae resistance to both high light and low temperature stress (Han and Kim 2013; Lee et al. 2020). Lee and colleagues in 2020 identified in *Chlamydomonas* an *ELIP* homologous, named *ELIP3*, whose expression is induced only when photooxidative and cold stress are combined (Lee et al. 2020). The line over-expressing ELIP3 showed, indeed, an increased resistance to the oxidative stress induced by these conditions, while the RNAi Knock-down strain was far more photosensitive than the WT. Moreover it showed a reduced phototaxis (Lee et al. 2020). It was therefore proposed that ELIP3 could act as a regulator for cell redox state (Lee et al. 2020).

3.2 The SRP pathway as target to improve photosynthesis efficiency

Recently the attention of the researchers was focused on truncated light-harvesting antenna mutants (TLA), that in many cases stood out for the saturation of photosynthesis at higher light intensities than the wild type (Kirst et al. 2012a; Cazzaniga et al. 2014; Dall'Osto et al. 2019). According to Kirst and Melis (Kirst and Melis 2014), one of the most promising pathway to be targeted for TLA mutant generation is the cpSRP pathway.

3.2.1 the CpSRP pathway

In green microalgae, as in higher plants, Light Harvesting Complexes (LHCs) are assembled and inserted by a post- and co-translational insertion into the thylakoid membranes by a mechanism similar to the signal recognition particle (SRP) pathway in bacteria (Pool 2005; Ziehe et al. 2017). In green microalgae these two kinds of insertion process are separate from each other, also thank to two different isoforms of the insertase ALB3 (ALB3.1 and ALB3.2) (Bellafiore et al. 2002; Göhre et al. 2006; Kirst and Melis 2014). The co-translational process leads to the insertion of chloroplast encoded proteins such as subunits of the PSII reaction center (Nilsson and van Wijk 2002; Dewez et al. 2009). According to the model proposed by Melis and Kirst, chloroplast signal recognition particle protein CpSRP54 binds to newly synthesized proteins and to the chloroplast signal recognition receptor CpFTSY, which mediates the interaction of the complex with ALB3.1 and CpSECY (SEC-translocase), the latter being responsible for the insertion in the membrane (Bellafiore et al. 2002; Kirst and Melis 2014). The post-translational integration involves also CpSRP43, a molecular chaperon that dissolves the aggregated light-harvesting proteins. Precursor light-harvesting proteins are imported in the chloroplast upon recognition of a transit peptide via the TOC and TIC envelope-localized complexes, with a role of the LTD protein as intermediary, which as a bias towards PSI antennas apoproteins (Jeong et al. 2018). CpSRP43 interacts with CpSRP54, while CpFTSY (soluble in

algae) recognizes this complex by interacting with CpSRP54 , then the complex reaches ALB3.2 (Moore et al. 2003; Göhre et al. 2006; Kirst and Melis 2014). The integrations occurs upon GTP hydrolysis and the CpSRP complex disassembles (Tu et al. 1999). (figure 3.2.1).

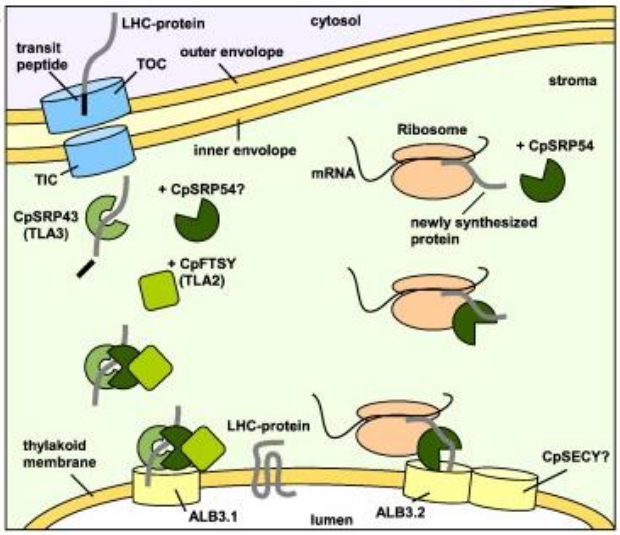

Figure 3.2.1. Model of the CpSRP pathway for protein integration in the developing thylakoid membrane in *Chlamydomonas*. Post-translational (left side) and co-translational (right side). According to the model, chloroplast signal recognition particle protein CpSRP54 binds to newly synthesized proteins and to the chloroplast signal recognition receptor CpFTSY, which mediates the interaction of the complex with ALB3.1 and CpSECY (SEC-translocase), responsible for the insertion in the membrane (Bellafiore et al. 2002; Kirst and Melis 2014). The post-translational integration involves also CpSRP43 that dissolves the aggregated light-harvesting proteins. Precursor light-harvesting proteins are imported in the chloroplast upon recognition of a transit peptide via the TOC and TIC envelope-localized complexes, with a role of the LTD protein as intermediary (Jeong et al. 2018). CpSRP43 interacts with CpSRP54, while CpFTSY (soluble in algae), recognizes this complex, by interaction with CpSRP54 and the complex reaches ALB3.2. (Moore et al. 2003; Göhre et al. 2006; Kirst and Melis 2014) The integration occurs upon GTP hydrolysis and the CpSRP complex disassembles (Tu et al. 1999). (Modified from Kirst and Melis 2014).

3.2.2 *Chlamydomonas* mutants in the CpSRP pathway

Interestingly, *Chlamydomonas* mutants in this pathway (table 3 and 4) are less affected in the growth compared with the corresponding mutants in higher plants (Kirst et al. 2012b; Kirst et al. 2012a; Wang and Grimm 2016) (table 4). These data, accompanied by the evidence that the loss of other proteins enhancing the insertion process did not greatly effect algae fitness and vitality, suggest the existence of alternative pathways involved in this activity (Jeong et al. 2018; Bujaldon et al. 2020).

tla3-cpsrp43 mutant, obtained in *Chlamydomonas* by random insertional mutagenesis (Kirst et al. 2012b) showed a similar reduction of LHCs and a slight reduction in PSI and PSII compared to its correspondent in *Arabidopsis* (*chaos*) (Klimyuk et al. 1999; Amin et al. 1999; Wang and Grimm 2016). Though this mutant displayed an improved solar energy conversion efficiency and photosynthetic productivity in high light massive cultivations (Kirst et al. 2012b), in plants its depletion causes

retarded or defective growth (Lv et al. 2015; Wang and Grimm 2016). This could indicate a specific and conserved role of this chaperon in these organisms, but a different relevance of the role of the whole pathway. However, Bujaldon and collaborators have recently characterized the random mutant p71 of *Chlamydomonas* (Li et al. 2004), missing CpSRP43, that showed a stronger phenotype compared to *tla3*, as this strain showed a less pigment-deficient phenotype than in the previous publication (Bujaldon et al. 2020). They indeed measured a strong decrease in functional PSII (about 85%) in p71, despite the mutant still retained 25% of LHCII than WT, antennae that probably were unable to bind to the core due to the lack of CP26 and CP29. The decrease of PSII antenna size was milder and similar to *tla3*, despite a similar decrease of LHCI content, suggesting a reorganization of LHCs distribution between PSs (Bujaldon et al. 2020). Nevertheless, also their results were consistent with the existence of an alternative pathway with a minor role in LHCs biogenesis, that might explain the partial loss of antenna subunits in these mutants.

As for *tla4-cpsrp54* DNA transposon mutant, it was observed, beside the reduced chl *b* content and the increased photosynthetic productivity, a stronger reduction in LHCI proteins compared to LHCIIs, suggesting a preference of this pathway for sub-classes of LCHc in microalgae (Jeong et al. 2017). The *ffc* mutant in Arabidopsis, lacking the same protein, was instead affected in the insertion of seven over ten LHCs, suggesting some differences in terms of LHC delivery and assembly (Amin et al. 1999; Jeong et al. 2017). Moreover, *ffc* mutants presented an higher content in LHCs respect to *chaos,* indicating that CpSRP43 works predominantly and independently from CpSRP54 in higher plants (Amin et al. 1999; Wang and Grimm 2016). This was confirmed by the characterization of the double mutants *chaos/ffc* (Hutin et al. 2002). However, the same differences in phenotypes strength were observed between *tla4* and *tla3*, suggesting that LHC delivery could occur independently of CpSRP54, via the interaction with other components of the same or of other pathway(s) (Jeong et al. 2017). In addition, while in plants CpSRP54 is responsible for the insertion of other chloroplast encoded proteins, such as psbA/D1 and psbD/D2 PSII reaction center proteins, in *Chlamydomonas* it apparently does not participate to this co-translational assembly pathway (Jeong et al. 2017).

The *CpFTSY* gene in *Chlamydomonas* was identified by Kirst and co-authors in 2012 (Kirst et al. 2012a), by mapping and complementing the *tla2* strain, that missed part of light-harvesting proteins in the thylakoid membrane and showed a mild reduction of the reaction centres. Both PSI and PSII antenna size in this mutant were about 60% than the wild type, moreover *tla2* presented a greater oxygen evolution at saturating irradiances. In 2016, Baek and collaborators reported an enhanced high light resistance of *Δcpftsy*, a strain obtained by CRISPR-Cas9 system, but the higher photoresistance appears controversial (Kirst et al. 2012a; Baek et al. 2016, see chapter 7). Interestingly the deletion of the same subunit in *Arabidopsis* and Maize impaired fitness, light sensitivity and growth rate, and in some case was reported an increased lethality of the knock-out seedlings (Asakura et al. 2004; Tzvetkova-Chevolleau et al. 2007b; Asakura et al. 2008; Wang and Grimm 2016). On the contrary, the same mutation in *Chlorella vulgaris* led to a 44.5 % improvement in biomass productivity under moderate irradiance (200 µmol photons m^{-2} s^{-1}) (Shin et al. 2016).

Moreover, Bujaldon and collaborators characterized an additional mutant, named BF4 (Olive et al. 1981; Bujaldon et al. 2020), lacking Alb3.1 subunit. They observed a phenotype similar to *p71* and to the allelic *ac29* strain, which was previously characterized by Bellafiore et al. (Bellafiore et al. 2002; Ossenbuhl et al. 2004). ALB3.2 was instead targeted by RNAi by Göhre, causing a reduction of both

PSI and PSII content ranging from 25% to 40% respect to wild type. A number of photosynthetic proteins were also lowered by the loss of function of the insertase, whereas the level other proteins increased, implying a role of Alb3.2 on thylakoid protein biogenesis (Göhre et al. 2006).

The LTD protein is a protein involved in the binding and delivery of some LHCP apoproteins to CpSRP43 (Ouyang et al. 2011). Jeong and colleagues in 2018 obtained a genome edited mutant *Crltd*, which lost this protein function (Jeong et al. 2018). It was characterized by a dramatic drop in LHCI and PSI-supercomplex content and it was impaired in chlorophyll content, but the chl a/b ration was similar to the wild type. Moreover, the growth at 350 µE was not significantly impaired, suggesting a not stringent need of LTD for algae and a preference of this protein for the import of LHCI. However some structural changes in grana and vacuoles were observed in *Crltd* as consequences of shortage of LHCI (Jeong et al. 2018).

For the increase of microalgae biomass productivity purpose could be interesting to observe what happen to strains in which these proteins are only downregulated, as it was observed for the *TLA3* mutant in Tobacco plants. (Kirst et al. 2018). Targeting by RNAi the CpSRP43 encoding gene it was indeed possible to obtain enhanced biomass and leaf-to-stem ratio in *Nicotiana tabacum* canopies (Kirst et al. 2018).

Table 4: CpSRP pathway mutants in literature: the table presents the mutants classified based on the affected gene function. The parameters are expressed as % respect to the corresponding wild type values. When they change according to light conditions it is specified in the brackets. When mutants have alternative names, both are specified. When two strains have the same features, they are reported in the same cell and possible differences are reported in the brackets. When more than two strains are reported together it is indicated a parameters variation range. For *tla3* chlorophyll content are reported two different measured performed in two different years by two different groups. Some values were deduced from papers graphs and some ratios were calculated from reported data; therefore, the value could be subjected to small estimation errors. HH: High light LL: Low Light

Mutant And organism	Afftcted gene	Genetic modification	Chl tot %	Chl a/b ratio (%)	Car tot (%)	Car/Chl (%)	PSII antenna size (%)	PSI antenna size (%)	Fv/ Fm	Photosensitivity/ Photoresistance/ Growth phenotype
tla2 *(Kirst et al., 2012b)* *C. reinhardtii*	*CpFTSY*	Random DNA insertion	18	352	35	180	6	60	-	Saturation at higher light intensities
ΔCpFTSY *(Baek et al., 2016)* *C. reinhardtii*	*CpFTSY*	CRISPR-Cas9	30	280	50	180	-	-	-	Photoresitant 700µE
as2 *(Bonente et al.,2011)* *C. reinhardtii*	*CpFSTY?*	Random DNA insertion	-	130	190	-	≈80	-	-	Photoresistant
cpftsy -1 *cpftsy-2* *(Asakura et al., 2008)* *A.thaliana*	*CpFTSY*	Random DNA insertion	6-8		-		-	-	-	Defective growth
csr1-1 *csr1-3* *(Asakura et al., 2004)* *Zea Mays*	*CpFTSY*	Mu transposon-induced non-photosynthetic maize mutants	12 *(csr1-1)* 28 *(csr1.3)*	73 *(csr1-1)* 94 *(csr1.3)*	-	-	-	-	-	Defective growth

cpftsy (Tzvetkova-Chevolleau et al., 2007b; Wang and Grimm 2016) *A: thaliana*	CpFTSY	EMS random chemical mutagenesis	16	87	-	-	-	-	72	Defective growth
tla3 (Kirst et al., 2012a; Bujaldon et al., 2020) *C. reinhardtii*	*CpSRP43*	Random DNA insertion	16 (2012) 45 (2020)	444 (2012) 200 (2020)	35	240	38	62	70	Saturation at higher light intensities
P71 (Bujaldon et al., 2020) *C. reinhardtii*	*CpSRP43*	5-fluorodeoxyuridine mutagenesis	17	222	--	-	13	55	40	-
E5 (Shin et al., 2016) *C. vulgaris*	*CpSRP43*	EMS random chemical mutagenesis	40	180	75	180	-	-	≈110	Photoresistant Increased biomass productivity
chaos (Klimyuk et al., 1999; Amin et al., 1999; Wang and Grimm 2016) *A.thaliana*	*CpSRP43*	Trasposon random insertional mutagenesis	57	130	66	75	-	-	100	Defective growth
TLA3 (Kirst et al., 2018) *N. tabacum*	*CpSRP43*	RNAi-mediated downregulation	67	146	-	-	68	76	-	Increased biomass productivity in canopies
w67 (Lv et al., 2015) *Oryza sativa*	*CpSRP43*	EMS random chemical mutagenesis	45-50 (depends on the stage)	140-157 (depends on the stage)	65-84 (depends on the stage)	130-200 (depends on the stage)	-	-	86	Defective growth and affected photosynthetic capacity
tla4 (Jeong et al., 2017) *C. reinhardtii*	*CpSRP54*	Random DNA insertion	57	140	≈80	≈160	78	55	-	Saturation at higher light intensities
ffc (Hutin et al., 2002; Amin et al., 1999; ; Wang and Grimm 2016) *A.thaliana*	*CpSRP54*	Trasposon random insertionan	≈70	105	-	-	-	-	≈100	Defective growth
chaos/ffc (Hutin et al., 2002; Wang and Grimm 2016) *A.thaliana*	*CpSRP54 & CpSRP43*	Cross between *chaos* and *ffc*	≈30	132	-	-	-	-	-	Defective growth
BF4 (Bujaldon et al., 2020; Olive et al.,1981) *C. reinhardtii*	*Alb3.1*	*UV mutagenesis*	12	300	-	-	13	64	40	-
alb3.2 (Göhre et al., 2006) *C. reinhardtii*	*Alb3.2*	*RNAi*	30	-	-	-	-	-	-	Lethal
Crltd1 (Jeong et al.,2018) *C. reinhardtii*	*LTD*	*CRISPR-Cas9*	33	100	-	-	55	40	-	Growth similar to WT at 350µE
alb3 (Asakura et al., 2008) *A.thaliana*	*alb3*	*Random DNA insertion*	2	-	-	-	-	--		Lethal

3.2.3 The *as2.1* mutant

Bonente and collaborators in 2010, performed a wide random insertional mutagenesis on *Chlamydomonas reinhardtii* and screened the mutated strains to find pale green mutants (Bonente et al. 2011). Among the isolated strains there were two mutants, *as1* and *as2*, characterized by an higher chl a/b ratio respect to the WT, and an higher carotenoids content (Fig.3.2.2 A and B) (Bonente et al. 2011). The latter showed a milder phenotype. When they performed a spectroscopic measure of their antenna size, estimating the kinetic of Fm saturation in the presence of DCMU, it showed a far less impairment respect to *as1* (Fig.3.2.2 C and D) (Bonente et al. 2011). The same happened for PSI antenna size (Fig.3.2.2 E) (Bonente et al. 2011). Mutants were backcrossed with the wild type to exclude the effect of some background mutations and the *as2* derived strain, *as2.1*, showed a higher resistance when grown in high light, compared to the WT (Barera et al., unpublished data). For this reason, after the crossing, in 2011, it was tried to sequence *as 2.1*, it was found a big rearrangement near the insertion, with a wide insertion/deletion in the region including the gene *CpFTSY*, this could explain the pale-green phenotype. However, as the region is rich in G and C bases it was impossible to complete the annotation of the flanking region, that, also according the databases, includes putative genes, not-annotated genes and not properly sequenced BAC (https://phytozome.jgi.doe.gov/pz/portal.html).

a

	β-car	Chl/Car ratio	a/b ratio	Cars	Chl a + b
WT	7.3	3.2	2.7	30.9	100.0
as2	25.7	1.7	3.5	58.5	100.0
as1	34.4	1.5	6.4	66.6	100.0

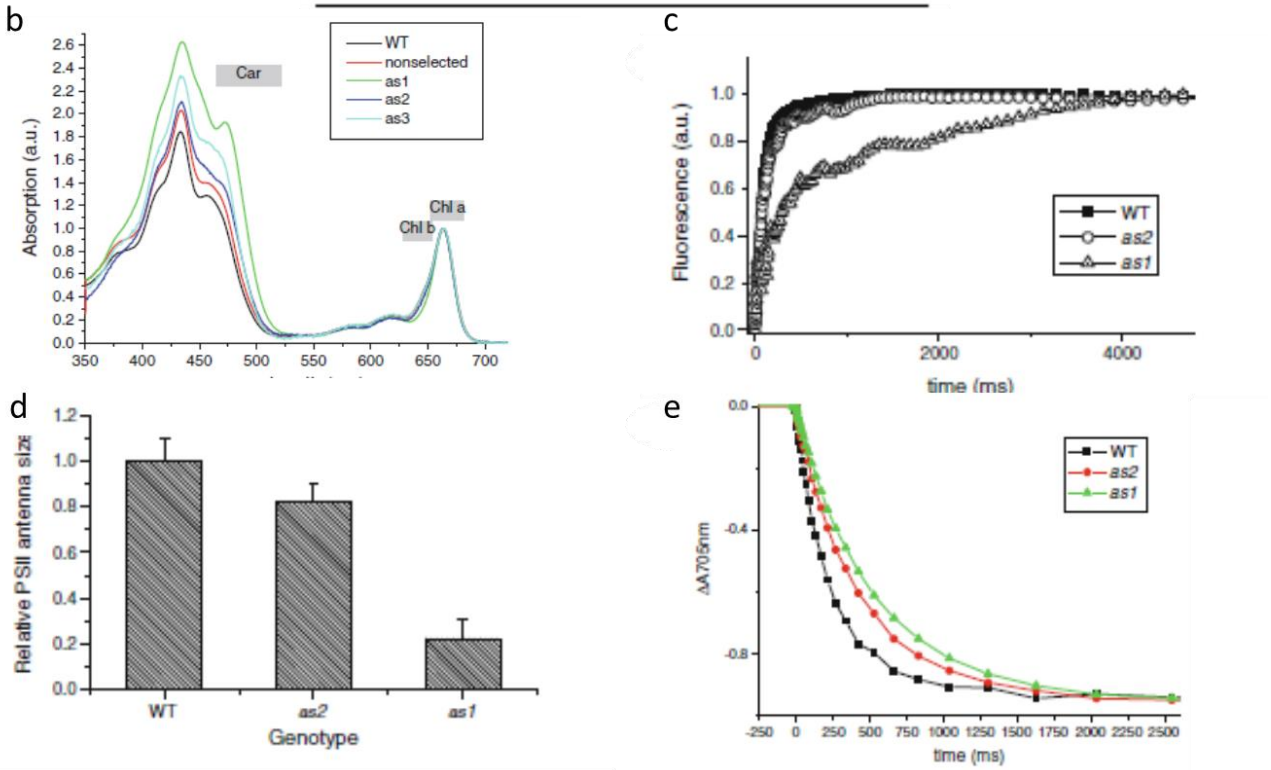

Figure 3.2.2.*as2* mutant features. A) Pigment content (picomoles) of antenna mutant as2 and as1 with respect to WT. B) Absorption spectra in the visible region obtained for WT, as2 and oyher transformants. Data were normalized at Chl a absorption the Qy region (660 nm). Absorption regions where signals from Carotenoids (Car), Chl a and b were detected are also indicated. C and D) Relative PSII functional antenna size of as2 and as1 mutants estimated through fluorescence induction kinetics in the presence of DCMU. C) Fluorescence curved normalized to Fm D) data shown in panel C plotted as (t2/3)-1. Error bars refer to five replicates. E) P700 photo-oxidation kinetic of WT, as2 and as1 at low light intensity to exstimate PSI functional antenna size. (Modified from Bonente et al., 2011).

3.2.4 CpFTSY gene and protein features

As reported in the plant genomes database Phytozome (https://phytozome.jgi.doe.gov/pz/portal.html), the gene is identified by the code Cre05.g241450.t1.1 or g5566.t1 and located in chromosome 5 of *Chlamydomonas*. From Phytozome it was possible to obtain information from other software; according the database Panther (http://www.pantherdb.org/panther/family.do?clsAccession=PTHR11564) it belongs to the protein family of Signal Recognition Particle 54k Protein SRP54 (PTHR11564). As highlighted by Kirst at al. in 2012 (Kirst et al. 2012a), according the KEGG Orthology database this fused signal recognition particle receptor, derived from the bacterial one involved in quorum sensing, protein export and secretion system (https://www.genome.jp/dbget-bin/www_bget?K03110). The domains present in CrCpFTSY protein according Pfam and the analysis performed by Kirst in 2012 are: from amino acids 1 to 36, transit peptide; from 66 to 147 , helical bundle domain (Pfam) SRP54-type; from 162 to 370, GTPase domain (Pfam), SRP54-type; from 164 to 183, P-loop nucleotide binding motif (Kirst et al. 2012a)(fig. 3.2.3 a). As for the genomic region, according to the software the main part of the gene is surrounded by non-annotated genes or putative protein encoding genes, some of them are only annotated by homology analysis and their function has not yet been confirmed *in vivo*. In some cases, there are genes overposed one on another (fig 3.2.3 b). Moreover, if it is taken a look to the genomic sequence of *CpFTSY* the gene has thirteen introns and a very long 3'UTR, and a high G/C content. The coding sequence is, indeed, 1146 base long, while the genomic one is 7312. All these features of the gene and the region made the sequence hard to amplify, analyse, isolate and clone.

a

b

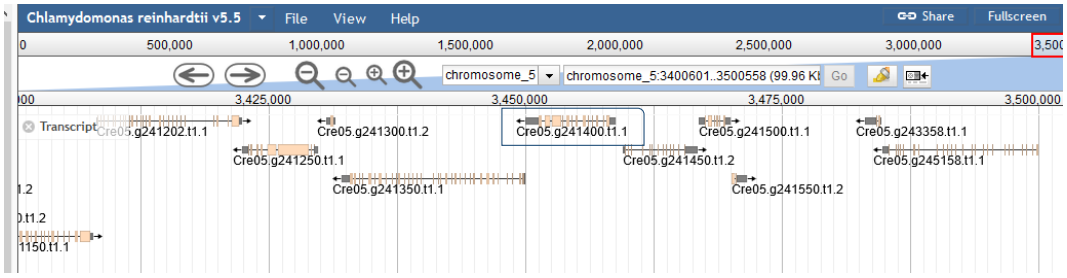

Figure 3.2.3. Predicted structure of CpFTSY and location in the genome of its ecnoding gene. a) Domain composition of the CrCpFTSY protein. cTP, Chloroplast transit peptide; HB, helical bundle domain; GTPase, GTPase domain (modified from Kirst et al., 2012). b) Location of Cre05.g241450.t1.1 gene in the genome, CpFTSY gene is indicated by the blue square. Some of the closest genes are partially overposed to it. (From phytozome.org).

3.3 Chlorophyll *a* oxygenase (CAO)

An alternative method to produce pale-green mutants, characterized by a reduced antenna size, is to act directly on the chlorophyll biosynthetic pathway. As it was seen before the lack of chlorophyll biosynthetic enzymes caused lethal or stunted growth phenotypes to light grown algae. However is possible to obtain more light resistant phenotype by targeting the Chlorophyll *a* oxygenase *(CAO)* biosynthetic enzyme, named also Chlorophyllide *a* oxygenase that acts at the end of the pathway and converts part of chl *a* in chl *b* (Tanaka et al. 1998). In this way the presence of at least chlorophyll *a* allows algae growth in light conditions and compromises less the reaction centers, in which is present only this kind of chlorophyll.

3.3.1 CAO mutants

In 2017, Bujaldon and collaborators characterized three allelic null-mutant for *CAO*, namely *pg27*, *cbs3*, *BF3* that showed a low-fluorescence phenotype when grown under moderate light intensity (Bujaldon et al. 2017). The fluorescence measurement suggested a reorganization of the antenna system, confirmed by emission spectra at 77 K under dim light or moderate light regimes. A reorganization and a different effect on the two supercomplex were easily predictable, if we think that chl b in mainly present in PSII-linked peripherical antennas, the BF3 PSII antenna size was, indeed, two times smaller than that in the wild-type. However, when it was observed the LHC content in BF3 it resulted that it accumulates LHCI proteins to nearly wild-type level and five of these are overaccumulated when grown in dim light, while the LHCII apoprotein remained at the same level. It suggested that the absence of Chl b does not compromise the accumulation of the major Chl *a/b* binding proteins in Chlamy thylakoids but changes their organization, the authors, indeed, hypothesized that the spare LHCIs could occupy alternative sites, probably substituting LHCIIs in distal sites which are normally occupied during state transition (Bujaldon et al. 2017). The three mutants for *CAO*, before the backcrossing performed to eliminate unrelated mutations, showed a so called "*yellow-in the dark*" (*yid*) phenotype, due to a defect in chlorophyll biosynthesis pathway in darkness. The effects of the CAO absence in these mutants, deficient also in Chl *a*, were therefore investigated. The yid-BF3 mutant that accumulates less LHCI proteins compared with the green *BF3* and a yid control, when grown in dim light, while higher levels were produced in moderate light. They hypothesized that the synthesis of Chl *a* in *yid-BF3* cells in the dark is too low to integrate Chl *a* into Chl *b* binding sites in LHC complexes, which results in their degradation. The inactivation of FTSH protease in the mutant *yid-BF3-ftsh1*, indeed, restored a normal level of LHCI, though this didn't happen for LHCII (Bujaldon et al. 2017). Nevertheless, in the growth in moderate light *yid-BF3* cells was observed an impairing in PSI-LHCI supercomplex stability during the solubilization, due to the lack of Chl *b*. Finally, in all the three *BF3*, *yid-BF3* and *yid-BF3-ftsh1* was identified by 77 K fluorescence emission spectrum a new type of chlorophyll–protein complex generated by the Chl *a* binding peripheral antenna protein that accumulate without Chl *b*. The new observed peak

decreased proportionally to LHC contents in the three kind of mutants and seemed that derived from those Chl *a* that occupy Chl *b* binding sites in the PSII peripheral antenna and are loosely bound to the apoproteins (Bujaldon et al. 2017).

As for *CAO* were produced also RNAi mediated knock-down mutants to modulate *Chlamydomonas* antenna size and observed more than a two-fold increase in photosynthetic rate in high light and a 30% increase in growth rate under saturating illumination (Perrine et al. 2012). They showed the capacity to allow a state transitions facilitating enhanced cyclic ATP synthesis and a zeaxanthin–violaxanthin cycles that protects from photoinhibition (Perrine et al. 2012). To modulate the antenna size of *cbs3 CAO*-KO mutant was complemented by a construct designed to control the gene expression by the NAB1-binding sequence LRE (Light Responsive Element) (Negi et al. 2020). NAB1, indeed, recognises this sequence on the mRNA and inhibits the translation in high light conditions. It was observed that the light-regulated antenna sizes conferred to algae a higher photosynthetic rate and a 200% enhance of biomass productivity compared to WT. Moreover, this kind of mutants showed nearly the wild-type ability to carry out state transitions and non-photo-chemical quenching (Negi et al. 2020).

The determinant role of CAO for the modulation of antenna size and its effect on chloroplast structure were already studied In plants (Espineda et al. 1999; Kim et al. 2009; Biswal et al. 2012; Mueller et al. 2012), but in all these organism the lack of this gene caused a delayed development, not observed in *Chlamydomonas* (Mueller et al. 2012). On the contrary the overexpression of this gene leaded to increase biomass productivity in tobacco plants, enhancing antenna size, electron transport rates, carbon dioxide assimilation, starch content, and dry matter accumulation. (Biswal et al. 2012).

Table 5: *CAO* mutants in literature: The parameters are expressed as % respect to the corresponding wild type values. When they change according to light conditions it is specified in the brackets. When mutants have alternative names, both are specified. When two strains have the same features, they are reported in the same cell and possible differences are reported in the brackets. When more than two strains are reported together it is indicated a parameters variation range. Some values were deduced from papers graphs and some ratios were calculated from reported data; therefore, the value could be subjected to small estimation errors. HH: High light LL: Low Light

Mutant And organism	Afftcted gene	Genetic modification	Chl tot %	Chl a/b ratio (%)	Car tot (%)	Car/Chl (%)	PSII antenna size (%)	PSI antenna size (%)	Fv/ Fm	Photosensitivity/ Photoresistance/ Growth phenotype
BF3 *(Bujaldon et al., 2017)* *C. reinhardtii*	*CAO*	UV-generated mutants	65 (50 µE) 87 (1µE)	∞	-	-	50 (50 µE) 40 (1µE)	110 (50 µE) 160 (1µE)	60 (50 µE) 37 (1µE)	--
pg27 *(Bujaldon et al., 2017)* *C. reinhardtii*	*CAO*	UV-generated mutants	65 (50 µE) 58 (1µE)	∞	-	-	-	-	40	-
cbs3 *(Bujaldon et al., 2017)* *C. reinhardtii*	*CAO*	DNA deletion	80 (50 µE) 96 (1µE)	∞	-	-	-	-	56	-
CR118 & CR133 *(Perrine et al., 2012)* *C. reinhardtii*	*CAO*	RNAi-mediated knock-down	70	140 (CR188) 180 (CR133)	76 (LL) 100-110 (HL)	-	-	-	-	Photoresistant

NC-7 NC-29 NC-77 *(Negi et al., 2020) C. reinhardtii*	*CAO*	*cbs3* mutant complemented by *CAO* sequence fused to LRE-NAB1 binding site		120 (LL) 220 (HL)	-	-	78-100	-	97-110	Photoresistant
ch1-2 (Wang & Grimm 2016; Espineda et al., 1999) A.thaliana	*CAO*	X-Ray mutagenesis	60	333	-	-	-	-	-	Defective growth
ch1-3 (Kim et al., 2009;Espineda et al., 1999) A.thaliana	*CAO*	X-Ray mutagenesis	40	∞	100	225	-	-	90	Defective growth
fch2 (Mueller et al., 2012) H. vulgare	CAO	DNA insertional mutant	63	∞	-	-	-	-	-	Delayed development
CAOx (Biswal et al., 2012) N. tabacum	CAO	Overexpressing mutant	128 (HL) 108 (LL)	67 (HL) 85 (LL)	-	-	-	-	100	Increased biomass producitivity

3.3.2 CAO gene and protein features

According to Phytozome database the *CAO* gene (Cre01.g043350) is located in chromosome 1, in a genes dense region, but no genes are overposed to it (fig 3.3.1 a). The gene is quite long, as the major part of *Chlamydomonas* one, among the 4212 bp there are four introns and the coding sequence is 1938 bp long versus the 3428 transcribed. According Pfam software (https://pfam.xfam.org/search/sequence) the significant protein domains are the Rieske [2Fe-2S] domain from aminoacid 305 to 384 and the Pheophorbide a oxygenase domain from 493 to 591 (fig 3.3.1 b).

a

b

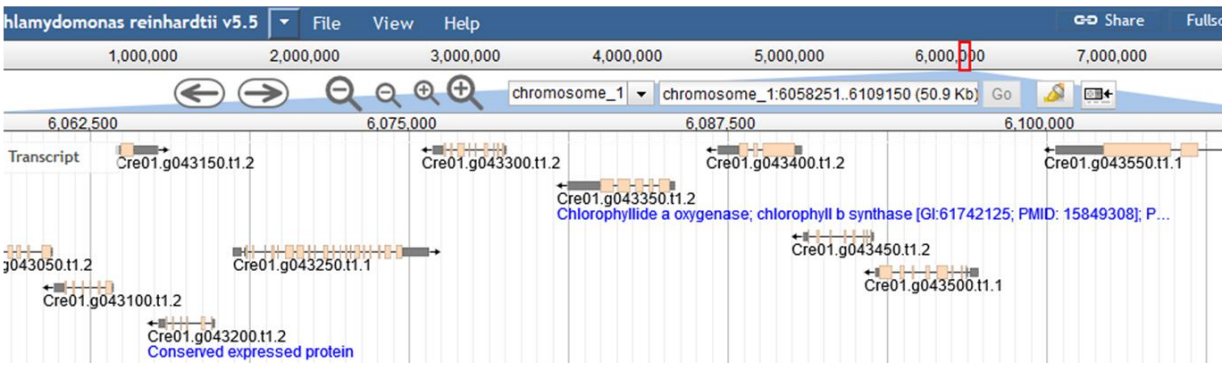

Figure 3.3.1. Predicted structure of CAO and location in the genome of its encoding gene. a) Domain composition of the CAO protein. Rieske, Rieske [2Fe-2S] domain; PaO, Pheophorbide a oxygenase. (From Pfam.org) b) Location of Cre01.g043350 gene in the genome, CAO gene is indicated by the blue square. (From phytozome.org)

3.4 Genetic tools and techniques to obtain mutants in *Chlamydomonas reinhardtii*

As said in the first paragraph, *Chlamydomonas reinhardtii* is the classical model organism for microalgae research. Its haploidy allows the detection of the mutant phenotypes at the first generation without the need for segregation and, at the same time, the sexual reproduction can be induced changing some growth limiting factors (Salomé and Merchant 2019). Moreover, all its genomes (nuclear, chloroplastic and mitochondrial) can be transformed and they were sequenced (Mussgnug 2015). Another great advantage is then the short life cycle, that makes screening procedure faster and the strain manipulation easier, with the possibility to interfere switching some growth conditions with its circadian system that coordinates cell division, photosynthesis, and cilia biogenesis (Noordally and Millar 2015; Strenkert et al. 2019).

In the past were used the so-called classical genetics techniques for strains genetic manipulation, as the induced gametogenesis, mating, and tetrad analysis. They are still useful for forward genetics, to reduce the number of unwanted random mutations by crossing mutants with the respective wt (Harris 2001). Forward genetic was mainly used in the past, when less genetic sequences were available and when sequencing experiments were more expensive. Chemical, physical and random DNA insertion mutagenesis were used to produce large mutants libraries from which phenotypes of interest where time by time isolated. The genes were then mapped by different hybridizations or PCR based tecnhiques. These techniques were subsequently employed for reverse genetics, by TILLING techniques to identify point mutations (Kurowska et al. 2011) or by mutants clusters analysis to found specific DNA insertion. The main disadvantage of these untargeted mutagenesis experiments is the risk of multiple gene mutations in the genome of the strain of interest. For this reason gene targeting tools have been optimized in these years (Salomé and Merchant 2019).

Besides these techniques, the exogenous DNA integration allowed the generation of overexpressing mutants, using strong promoters as hybrid HSP70A-RBCS2 promoter for the nucleus (Schroda et al. 2000), that could be enhanced in combination with enhancing introns (Lauersen et al. 2015). As alternative, to regulate the expression of exogenous genes, different sequences could be used (Quinn et al. 2003), as modulable promoters or regulatory introns (Mussgnug 2015). A classical gene expression construct includes a promoter and eventually regulatory elements, the gene of interest and a transformation marker or reporter, as an antibiotic resistance, a gene to complement a deficient phenotype or a marker allowing colour emission or detection.

3.4.1 Transformation techniques for molecular tools delivery

Since the first *Chlamydomonas* DNA transformation in 1982 (Rochaix, JD; van Dillewijn 1982) a lot of advanced tools and techniques have been developed.

The first Chlamy stable transformation restored chloroplast *atpB* mutants via biolistic tungsten particle bombardment (Boynton et al. 1988). This technique was mainly employed for chloroplast and mitochondria transformation, where it is possible to perform homologous recombination, boosted by optimized plasmids and DNA sequences (Larosa et al. 2012; Esland et al. 2018; Cutolo et al. 2020). For the nuclear genome, on the contrary, it is only possible to perform a random integration (Mussgnug 2015). The advantage of this technique is the possibility to regulate pressions and particles dimensions to be able to successfully transform also in presence of cell wall, but the limit is the cost and the expensive and sophisticated equipment.

The mechanical force transformation method is, instead, performed vortexing algal cell suspension in the presence of exogenous DNA and glass beads or silicon carbide whiskers (Kindle 1990; Dunahay 1993). It allows stable integration of exogenous DNA into the nuclear genome, but it was also used for chloroplastic transformation. The main advantage of this techniques is the low-cost equipment but it is harder to use for cell-wall provided strains, for which the DNA intake could be facilitated by enzymatic treatments (Kindle 1990).

One of the most employed method for nuclear transformation is the electroporation, that leads to a reversible membrane breakdown to allow the uptake of the exogenous DNA. Also, for the cell-wall equipped strains some specific protocol and detergent were optimized, and these procedures work in an efficient way. The main disadvantages are the random insertion of this exogenous DNA and the possible endonucleolytic cleavage of it. Moreover, other DNA molecules can be released from the cells that not survive the electric shock (Zhang et al. 2014).

As for plants also *Agrobacterium tumefaciens* mediated transformation is a feasible way, but it is a labour-intensive technique and it not present advantages over electroporation, except for insertional mutagenesis (Mini et al. 2018).

3.4.2 Gene targeting tools

For targeted gene silencing and knock-down mutant generation the RNA interference (RNAi) techniques are widely used. Small RNA-guided gene silencing is evolutionarily conserved in eukaryotes and occurs by different molecular mechanisms to defend cells from parasites attacks (Kim and Cerutti 2009). Different genetics tools can mimic this system in different organisms to silencing endogenous genes. The Maa7/XIR (NE-537) plasmid tool allowed the application of this system inducing RNAi by the expression of inverted repeat (IR) transgenes in *Chlamydomonas* (Rohr et al. 2004) and it was used also to multiple homologous gene silencing (Mussgnug et al. 2007). Different artificial micro-RNA (amiRNA) gene knockdown tools were then introduced for *C. reinhardtii* (Molnar et al. 2009; Zhao et al. 2009; Perrine et al. 2012; Hu et al. 2014; Charoonnart et al. 2019), with the possibility also to make the silencing inducible (Schmollinger et al. 2010). To obtain specific knockout mutants or to allow specific modification it is necessary a directed endonucleolytic DNA cleavage. If the damage is repaired via error-prone nonhomologous end joining, deletions or insertions are frequent and could cause gene inactivation (Carroll 2014). Specific modification could be achieved by the repair via homologous recombination and addition of a modified homologous fragment (Carroll 2014), but for *Chlamydomonas* this repairing manly occurs in the chloroplast, while in the nucleus the frequency is low, and it is often accompanied by insertions, deletions, and/or rearrangements at

the recombination site (Nour-Eldin et al. 2018). However it was demonstrated that the homologous recombination frequency can be improved synchronizing the cells before the transformation and selecting the right time intervals (Angstenberger et al. 2020).

Before the CRISPR-Cas9 advent the most employed nuclease-based technique was ZFNs, based on fusion of specific DNA-binding protein domains (Zinc-finger) to the FokI nuclease domain (Sizova et al. 2013).

The analogous TALEN techniques, which on the contrary fuses TALE (transcription activator-like effector) proteins domain to FokI was not reported in *Chlamydomonas* (Jeon et al. 2017). However TALE proteins were successfully employed to activate endogenous gene expression by increase nuclear promoter activity (Gao et al. 2015).

3.4.3 CRISPR-Cas9 system in *Chlamydomonas*

The Crispr-Cas9 system brought a revolution for the precise genome editing. This technique was successfully applied to correct genetic errors in human cells and its employment was extended to a wide range of organism and adapted to a lot of purposes. It is based to a natural defence system of some bacteria, which has been evolved to counteract the invasion of alien genomes, as viral one (Doudna and Charpentier 2014). The most used is the Type II CRISPR system, present in *Steptococcus pyogenes* (Sander and Joung 2014). In this bacteria foreign DNA, as soon as enter the cell is cut and incorporated as unique protospacer in the so called “CRISPR array”, composed by CRISPR repeated sequence interrupted by different protospacers. Once the region is transcribed it was processed in single crRNAs composed by one conserved CRISPR repetition and one protospacer, this RNA is partially complementary to another cell transcript, the tracrRNA, that forms a secondary structure recognised by the endonuclease Cas9 protein. This protein can cut foreign sequences complementary to a protospacer, if it is adjacent to a specific three nucleotide “PAM” sequence (in general NGG) (Sander and Joung 2014) (Fig 3.4.1). In this way bacteria have a sort of adaptative immunity. For genome editing purposes the system was optimized designing plasmids containing sequence for the expression of the Cas9 and a single RNA, called “single guide RNA”, composed by the specific protospacer sequence, the CRISPR array repeated sequence and the tracrRNA conserved sequence (fig 3.4.1 c), that is able to form the secondary structure recognised by the protein. The Cas9 of *Streptococcus pyogenes* contains RuvC1- and HNH-like nuclease domains and produces a double strand break in the genome of the expressing organism, near where the sequence complementary to the protospacer is adjacent to a PAM (fig3.4.1b) (Sander and Joung 2014). In this way some of the cut DNAs can be repaired by nonhomologous end joining (NHEJ) or homology-directed repair (HDR) pathways, allowing unspecific or specific mutations respectively in the desired target. For eukaryotic organisms the Cas9 sequence was optimized according the right codon usage and nuclear localization sequences (three in general) were added to allow the entrance in the nucleus (Zuris et al. 2014).

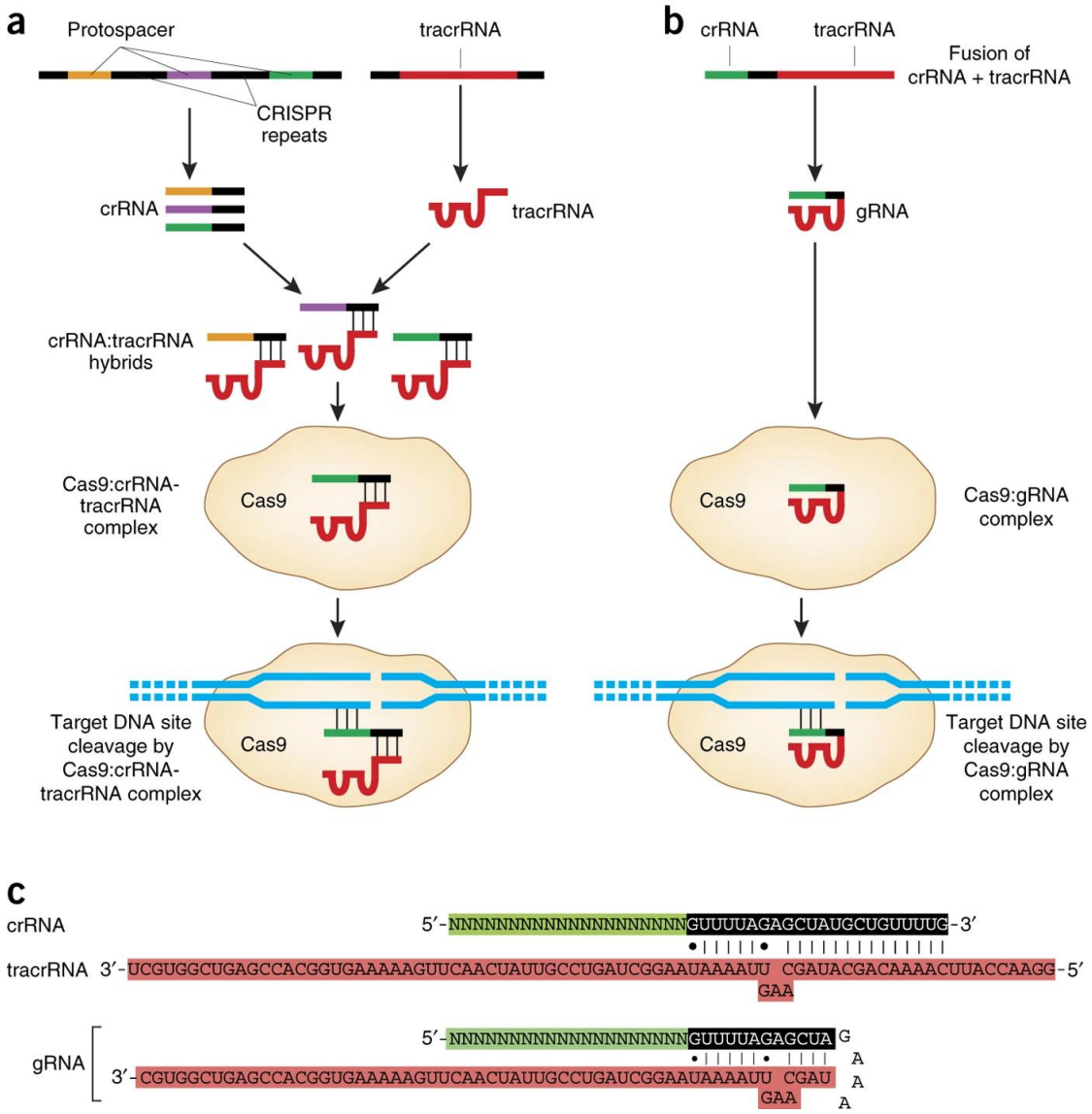

Figure 3.4.1. Comparison between natural and engineered CRISPR-Cas9 system. a) Bacteria CRISPR systems insert foreign DNA sequences into CRISPR arrays, which then is transcribed in crRNAs bearing "protospacer" regions, complementary to the foreign DNA site. crRNAs hybridize to tracrRNAs (also encoded by the CRISPR system) and they can associate with the Cas9 nuclease. crRNA-tracrRNA:Cas9 complexes recognize and cleave foreign DNAs if the protospacer sequences are present. (b) The most widely used engineered CRISPR-Cas system presents a fusion between a crRNA and part of the tracrRNA sequence. This guide RNA complexes with Cas9 to cuts the target DNA sites that are complementary to the 5′ 20 nt of the gRNA and that are adjacent to a PAM sequence. (c) Sequences of a crRNA-tracrRNA hybrid and a gRNA. (From Sanders and Joung, 2014)

The precise delivery of the protein to a target site makes this tool usable for a wide range of applications, by simple Cas9 domain modifications (fig 3.4.2), for example the inactivation of nuclease domains and the insertion of GFP to obtain a probe for a specific sequence, or it can be modified by the insertion of a transcriptional activation domain. In human stem cells or single cell organisms is also possible to directly deliver purified Cas9 ad *in vitro* synthesized sgRNAs by microinjection, electroporation or cationic delivery (Zuris et al. 2014; Baek et al. 2016; Vilarino et al. 2017; Elaswad et al. 2018; Laustsen and Bak 2019).

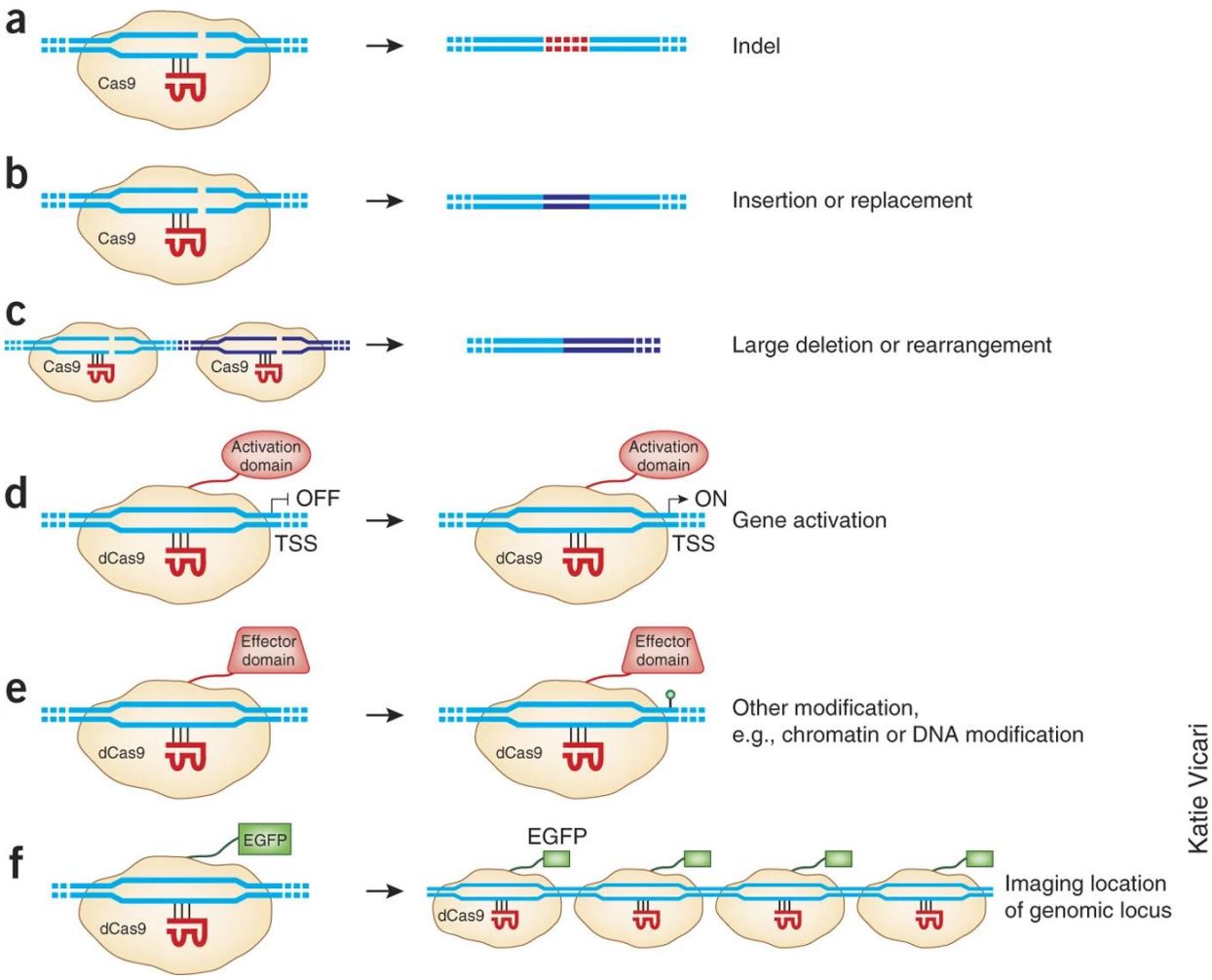

Figure 3.4.2. Different applications of engineered Cas9 protein. a,b) gRNA-guided Cas9 nuclease can produce indel mutations (a) or specific sequence replacement or insertion (b). (c) Pairs of gRNAs that deliver Cas9 nucleases can stimulate large deletions or genomic rearrangements (e.g., inversions or translocations). (d–f) dCas9 can be fused to activation domains (d) to mediate upregulation of specific endogenous genes, heterologous effector domains (e) to alter histone modifications or DNA methylation, or fluorescent proteins (f) to enable imaging of specific genomic loci. TSS, transcription start site. (From Sanders and Joung, 2014)

In microalgae, depending on the species, different Cas9-sgRNA ribonucleoprotein complexes (RNPs) or plasmid delivery were optimized (Patel et al. 2019). In *Chlamydomonas*, the most efficient method is the direct electroporation of the RNP complex in the cell (Baek et al. 2016; Jeong et al. 2018). It was seen an increased transformation efficiency and an easier screening capacity with a co-delivery of a resistance cassette (Fig 3.4.3), that is preferentially inserted in the break produced near the PAM sequence (Shin et al. 2019). Recently the same technique was optimized for the delivery of Cpf1 is an RNA-guided nuclease, similar to Cas9, that recognize different PAM (TTTN**)** sequences and uses shorter RNAs, as it need only crRNA (Ferenczi et al. 2017).

The main possible disadvantage for this technique is the possibility of off-target cuts, that could be overcome by the selection of very specific protospacers using one of the numerous available

software. Those give a specificity score and find possible off-targets in the genome of interest, searching also for the ones that contain mismatches. In *Chlamydomonas* drops of efficiency could be due also to the high G/C content, for G/C rich sequences is more difficult, indeed, to find highly specific targets and the DNA is less accessible to enzymes. Recent improvements of CRISPR-Cas9 technique were obtained transforming cells after their cell cycle synchronization. Depending on the cell cycle stage it is possible indeed to obtain alternatively a better nonhomologous end joining (NHEJ) or homologous recombination (HR) efficiency (Angstenberger et al. 2020).

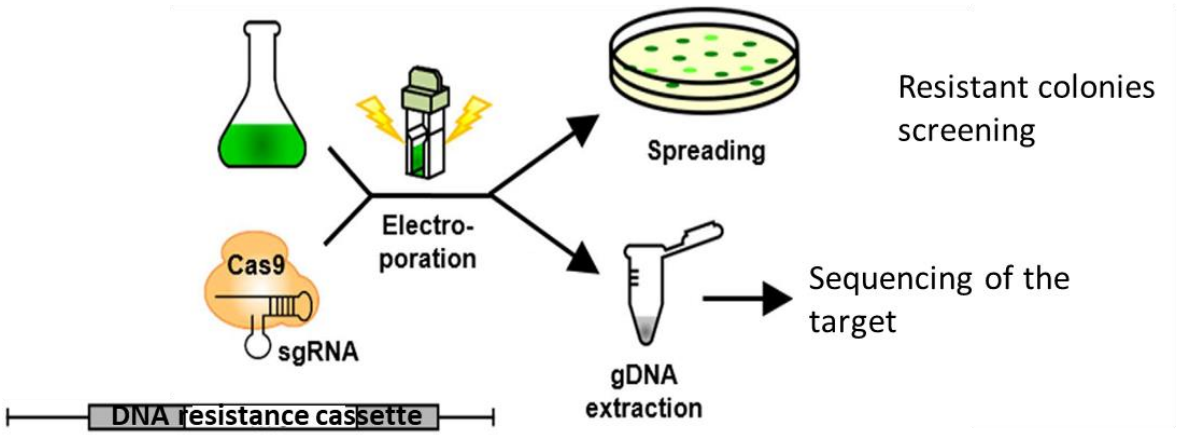

Figure 3.4.3. Example of a widely CRISPR-Cas9 system in *Chlamydomonas*: the Cas9-sgRNA complex and a resistance cassette are co-delivered to the cells by electroporation, the cells were plated on the antibiotic for the phenotype selection, if it is visible, or the screening was performed by the sequencing of the target region. (Modified from Baek et al., 2016)

REFERENCES

Amin P, Sy DAC, Pilgrim ML, Parry DH, Nussaume L, Hoffman NE (1999) Arabidopsis Mutants Lacking the 43- and 54-Kilodalton Subunits of the Chloroplast Signal Recognition Particle Have Distinct Phenotypes. Plant Physiol 121:61 LP – 70 . https://doi.org/10.1104/pp.121.1.61

Angstenberger M, de Signori F, Vecchi V, Dall'Osto L, Bassi R (2020) Cell Synchronization Enhances Nuclear Transformation and Genome Editing via Cas9 Enabling Homologous Recombination in Chlamydomonas reinhardtii. ACS Synth Biol. https://doi.org/10.1021/acssynbio.0c00390

Antonacci A, Lambreva MD, Margonelli A, Sobolev AP, Pastorelli S, Bertalan I, Johanningmeier U, Sobolev V, Samish I, Edelman M, Havurinne V, Tyystjärvi E, Giardi MT, Mattoo AK, Rea G (2018) Photosystem-II D1 protein mutants of Chlamydomonas reinhardtii in relation to metabolic rewiring and remodelling of H-bond network at QB site. Sci Rep 8:14745 . https://doi.org/10.1038/s41598-018-33146-y

Anwaruzzaman M, Chin BL, Li X-P, Lohr M, Martinez DA, Niyogi KK (2004) Genomic analysis of mutants affecting xanthophyll biosynthesis and regulation of photosynthetic light harvesting in Chlamydomonas reinhardtii. Photosynth Res 82:265–276 . https://doi.org/10.1007/s11120-004-2439-y

Asakura Y, Hirohashi T, Kikuchi S, Belcher S, Osborne E, Yano S, Terashima I, Barkan A, Nakai M (2004) Maize Mutants Lacking Chloroplast FtsY Exhibit Pleiotropic Defects in the Biogenesis of Thylakoid Membranes. Plant Cell 16:201 LP – 214 . https://doi.org/10.1105/tpc.014787

Asakura Y, Kikuchi S, Nakai M (2008) Non-identical contributions of two membrane-bound cpSRP components, cpFtsY and Alb3, to thylakoid biogenesis. Plant J 56:1007–1017 . https://doi.org/10.1111/j.1365-313X.2008.03659.x

Baek K, Kim DH, Jeong J, Sim SJ, Melis A, Kim JS, Jin E, Bae S (2016) DNA-free two-gene knockout in Chlamydomonas reinhardtii via CRISPR-Cas9 ribonucleoproteins. Sci Rep 6:30620 . https://doi.org/10.1038/srep30620

Baek KL, Yu J, Jeong J, Sim SJ, Bae S, Jin ES (2018) Photoautotrophic production of macular pigment in a Chlamydomonas reinhardtii strain generated by using DNA-free CRISPR-Cas9 RNP-mediated mutagenesis. Biotechnol Bioeng 115:719–728 . https://doi.org/10.1002/bit.26499

Baroli I, Do AD, Yamane T, Niyogi KK (2003) Zeaxanthin accumulation in the absence of a functional xanthophyll cycle protects Chlamydomonas reinhardtii from photooxidative stress. Plant Cell 15:992–1008 . https://doi.org/10.1105/tpc.010405

Bellafiore S, Ferris P, Naver H, Göhre V, Rochaix JD (2002) Loss of Albino3 Leads to the Specific Depletion of the Light-Harvesting System. Plant Cell 14:2303 LP – 2314 . https://doi.org/10.1105/tpc.003442

Biswal AK, Pattanayak GK, Pandey SS, Leelavathi S, Reddy VS, Govindjee, Tripathy BC (2012) Light Intensity-Dependent Modulation of Chlorophyll b Biosynthesis and Photosynthesis by Overexpression of Chlorophyllide a Oxygenase in Tobacco. Plant Physiol 159:433 LP – 449 . https://doi.org/10.1104/pp.112.195859

Bonente G, Formighieri C, Mantelli M, Catalanotti C, Giuliano G, Morosinotto T, Bassi R (2011) Mutagenesis and phenotypic selection as a strategy toward domestication of Chlamydomonas reinhardtii strains for improved performance in photobioreactors. Photosynth Res 108:107–120 . https://doi.org/10.1007/s11120-011-9660-2

Boudreau E, Takahashi Y, Lemieux C, Turmel M, Rochaix JD (1997) The chloroplast ycf3 and ycf4

open reading frames of Chlamydomonas reinhardtii are required for the accumulation of the photosystem I complex. EMBO J 16:6095–6104 . https://doi.org/10.1093/emboj/16.20.6095

Boynton JE, Gillham NW, Harris EH, Hosler JP, Johnson AM, Jones AR, Randolph-Anderson BL, Robertson D, Klein TM, Shark KB, Sanfrod JC (1988) Chloroplast transformation in Chlamydomonas with high velocity microprojectiles. Science (80-) 240:1534 LP – 1538 . https://doi.org/10.1126/science.2897716

Brzezowski P, Sharifi MN, Dent RM, Morhard MK, Niyogi KK, Grimm B (2016) Mg chelatase in chlorophyll synthesis and retrograde signaling in Chlamydomonas reinhardtii: CHLI2 cannot substitute for CHLI1. J Exp Bot 67:3925–3938 . https://doi.org/10.1093/jxb/erw004

Bujaldon S, Kodama N, Rappaport F, Subramanyam R, de Vitry C, Takahashi Y, Wollman FA (2017) Functional Accumulation of Antenna Proteins in Chlorophyll b-Less Mutants of Chlamydomonas reinhardtii. Mol Plant 10:115–130 . https://doi.org/10.1016/j.molp.2016.10.001

Bujaldon S, Kodama N, Rathod MK, Tourasse N, Ozawa SI, Selles J, Vallon O, Takahashi Y, Wollman F-A (2020) The BF4 and p71 antenna mutants from Chlamydomonas reinhardtii. Biochim Biophys acta Bioenerg 1861:148085 . https://doi.org/10.1016/j.bbabio.2019.148085

Carroll D (2014) Genome Engineering with Targetable Nucleases. Annu Rev Biochem 83:409–439 . https://doi.org/10.1146/annurev-biochem-060713-035418

Cazzaniga S, Dall'Osto L, Szaub J, Scibilia L, Ballottari M, Purton S, Bassi R (2014) Domestication of the green alga Chlorella sorokiniana: Reduction of antenna size improves light-use efficiency in a photobioreactor. Biotechnol Biofuels 7:157 . https://doi.org/10.1186/s13068-014-0157-z

Cazzaniga S, Kim M, Bellamoli F, Jeong J, Lee S, Perozeni F, Pompa A, Jin E, Ballottari M (2020) Photosystem II antenna complexes CP26 and CP29 are essential for nonphotochemical quenching in Chlamydomonas reinhardtii. Plant Cell Environ 43:496–509 . https://doi.org/10.1111/pce.13680

Charoonnart P, Worakajit N, Zedler JAZ, Meetam M, Robinson C, Saksmerprome V (2019) Generation of microalga Chlamydomonas reinhardtii expressing shrimp antiviral dsRNA without supplementation of antibiotics. Sci Rep 9:3164 . https://doi.org/10.1038/s41598-019-39539-x

Chekounova E, Voronetskaya V, Papenbrock J, Grimm B, Beck C (2001) Characterization of Chlamydomonas mutants defective in the H subunit of Mg-chelatase. Mol Genet Genomics 266:363–373 . https://doi.org/10.1007/s004380100574

Chemerilova VI (1978) Investigation of pigmentation modifying mutations in Chlamydomonas reinhardii strains of different ploidy. iI. the lts1 mutation compounds and their use for obtaining the triploid cultures. Genetika

Cutolo E, Tosoni M, Barera S, Herrera-Estrella L, Dall'Osto L, Bassi R (2020) A Phosphite Dehydrogenase Variant with Promiscuous Access to Nicotinamide Cofactor Pools Sustains Fast Phosphite-Dependent Growth of Transplastomic Chlamydomonas reinhardtii. Plants 9, 473 . https://doi.org/10.3390/plants9040473

Dall'Osto L, Cazzaniga S, Guardini Z, Barera S, Benedetti M, Mannino G, Maffei ME, Bassi R (2019) Combined resistance to oxidative stress and reduced antenna size enhance light-to-biomass conversion efficiency in Chlorella vulgaris cultures. Biotechnol Biofuels 12:221 . https://doi.org/10.1186/s13068-019-1566-9

DellaPenna D (1999) Carotenoid Synthesis and Function in Plants: Insights from Mutant Studies in Arabidopsis thaliana BT - The Photochemistry of Carotenoids. In: Frank HA, Young AJ, Britton G, Cogdell RJ (eds). Springer Netherlands, Dordrecht, pp 21–37

Dewez D, Park S, García-Cerdán JG, Lindberg P, Melis A (2009) Mechanism of REP27 Protein Action in the D1 Protein Turnover and Photosystem II Repair from Photodamage. Plant Physiol 151:88 LP

– 99 . https://doi.org/10.1104/pp.109.140798

Doudna JA, Charpentier E (2014) The new frontier of genome engineering with CRISPR-Cas9. Science (80-) 346:1258096 . https://doi.org/10.1126/science.1258096

Dunahay TG (1993) Transformation of Chlamydomonas reinhardtii with silicon carbide whiskers. Biotechniques 15:452-455,457-458,460

Edge R, McGarvey DJ, Truscott TG (1997) The carotenoids as anti-oxidants — a review. J Photochem Photobiol B Biol 41:189–200 . https://doi.org/https://doi.org/10.1016/S1011-1344(97)00092-4

Elaswad A, Khalil K, Cline D, Page-McCaw P, Chen W, Michel M, Cone R, Dunham R (2018) Microinjection of CRISPR/Cas9 Protein into Channel Catfish, Ictalurus punctatus, Embryos for Gene Editing. J Vis Exp 56275 . https://doi.org/10.3791/56275

Engelken J, Funk C, Adamska I (2012) The Extended Light-Harvesting Complex (LHC) Protein Superfamily: Classification and Evolutionary Dynamics BT - Functional Genomics and Evolution of Photosynthetic Systems. In: Burnap R, Vermaas W (eds). Springer Netherlands, Dordrecht, pp 265–284

Esland L, Larrea-Alvarez M, Purton S (2018) Selectable Markers and Reporter Genes for Engineering the Chloroplast of Chlamydomonas reinhardtii. Biology (Basel) 7:46 . https://doi.org/10.3390/biology7040046

Espineda CE, Linford AS, Devine D, Brusslan JA (1999) The AtCAO gene, encoding chlorophyll a oxygenase, is required for chlorophyll b synthesis in Arabidopsis thaliana. Proc Natl Acad Sci 96:10507 LP – 10511 . https://doi.org/10.1073/pnas.96.18.10507

Ferenczi A, Pyott DE, Xipnitou A, Molnar A (2017) Efficient targeted DNA editing and replacement in Chlamydomonas reinhardtii using Cpf1 ribonucleoproteins and single-stranded DNA. Proc Natl Acad Sci 114:13567 LP – 13572 . https://doi.org/10.1073/pnas.1710597114

Formighieri C, Ceol M, Bonente G, Rochaix J-D, Bassi R (2012) Retrograde Signaling and Photoprotection in a gun4 Mutant of Chlamydomonas reinhardtii. Mol Plant 5:1242–1262 . https://doi.org/https://doi.org/10.1093/mp/sss051

Förster B, Osmond CB, Pogson BJ (2005) Improved survival of very high light and oxidative stress is conferred by spontaneous gain-of-function mutations in Chlamydomonas. Biochim Biophys Acta - Bioenerg 1709:45–57 . https://doi.org/10.1016/j.bbabio.2005.05.012

Gao H, Wang Y, Fei X, Wright DA, Spalding MH (2015) Expression activation and functional analysis of HLA3, a putative inorganic carbon transporter in Chlamydomonas reinhardtii. Plant J 82:1–11 . https://doi.org/10.1111/tpj.12788

Göhre V, Ossenbühl F, Crèvecoeur M, Eichacker LA, Rochaix J-D (2006) One of Two Alb3 Proteins Is Essential for the Assembly of the Photosystems and for Cell Survival in Chlamydomonas Plant Cell 18:1454 LP – 1466 . https://doi.org/10.1105/tpc.105.038695

Grimm B, Kloppstech K (1987) The early light-inducible proteins of Barley °. Eur J Biochem 167:493–499 . https://doi.org/https://doi.org/10.1111/j.1432-1033.1987.tb13364.x

Han JW, Kim GH (2013) An ELIP-like gene in the freshwater green alga, Spirogyra varians (Zygnematales), is regulated by cold stress and CO2 influx. J Appl Phycol 1–11 . https://doi.org/10.1007/s10811-013-9975-9

Harris EH (2001) Chlamydomonas as a model organism. Annu Rev Plant Physiol Plant Mol Biol 52:363–406 . https://doi.org/10.1146/annurev.arplant.52.1.363

Holt NE, Zigmantas D, Valkunas L, Li X-P, Niyogi KK, Fleming GR (2005) Carotenoid Cation Formation and the Regulation of Photosynthetic Light Harvesting. Science (80-) 307:433 LP – 436 .

https://doi.org/10.1126/science.1105833

Hu J, Deng X, Shao N, Wang G, Huang K (2014) Rapid construction and screening of artificial microRNA systems in Chlamydomonas reinhardtii. Plant J 79:1052–1064 . https://doi.org/10.1111/tpj.12606

Hutin C, Havaux M, Carde J-P, Kloppstech K, Meiherhoff K, Hoffman N, Nussaume L (2002) Double mutation cpSRP43–/cpSRP54– is necessary to abolish the cpSRP pathway required for thylakoid targeting of the light-harvesting chlorophyll proteins. Plant J 29:531–543 . https://doi.org/https://doi.org/10.1046/j.0960-7412.2001.01211.x

Jahns P, Depka B, Trebst A (2000) Xanthophyll cycle mutants from Chlamydomonas reinhardtii indicate a role for zeaxanthin in the D1 protein turnover. Plant Physiol Biochem 38:371–376 . https://doi.org/https://doi.org/10.1016/S0981-9428(00)00753-1

Jeon S, Lim JM, Lee HG, Shin SE, Kang NK, Park YI, Oh HM, Jeong WJ, Jeong BR, Chang YK (2017) Current status and perspectives of genome editing technology for microalgae. Biotechnol Biofuels 10:267 . https://doi.org/10.1186/s13068-017-0957-z

Jeong J, Baek K, Kirst H, Melis A, Jin ES (2017) Loss of CpSRP54 function leads to a truncated light-harvesting antenna size in Chlamydomonas reinhardtii. Biochim Biophys Acta - Bioenerg 1858:45–55 . https://doi.org/10.1016/j.bbabio.2016.10.007

Jeong J, Baek K, Yu J, Kirst H, Betterle N, Shin W, Bae S, Melis A, Jin E (2018) Deletion of the chloroplast LTD protein impedes LHCI import and PSI-LHCI assembly in Chlamydomonas reinhardtii. J Exp Bot 69:1147–1158 . https://doi.org/10.1093/jxb/erx457

Kim E-H, Li X-P, Razeghifard R, Anderson JM, Niyogi KK, Pogson BJ, Chow WS (2009) The multiple roles of light-harvesting chlorophyll a/b-protein complexes define structure and optimize function of Arabidopsis chloroplasts: A study using two chlorophyll b-less mutants. Biochim Biophys Acta - Bioenerg 1787:973–984 . https://doi.org/https://doi.org/10.1016/j.bbabio.2009.04.009

Kim E-J, Cerutti H (2009) Chapter 5 - Targeted Gene Silencing by RNA Interference in Chlamydomonas. In: King SM, Pazour GJBT-M in CB (eds) Methods in Cell Biology. Academic Press, pp 99–110

Kindle KL (1990) High-frequency nuclear transformation of Chlamydomonas reinhardtii. Proc Natl Acad Sci U S A 87:1228–1232 . https://doi.org/10.1073/pnas.87.3.1228

Kirst H, García-Cerdán JG, Zurbriggen A, Melis A (2012a) Assembly of the light-harvesting chlorophyll antenna in the green alga Chlamydomonas reinhardtii requires expression of the TLA2-CpFTSY gene. Plant Physiol 158:930–945 . https://doi.org/10.1104/pp.111.189910

Kirst H, Garcia-Cerdan JG, Zurbriggen A, Ruehle T, Melis A (2012b) Truncated Photosystem Chlorophyll Antenna Size in the Green Microalga Chlamydomonas reinhardtii upon Deletion of the TLA3-CpSRP43 Gene. Plant Physiol 160:2251–2260 . https://doi.org/10.1104/pp.112.206672

Kirst H, Melis A (2014) The chloroplast signal recognition particle (CpSRP) pathway as a tool to minimize chlorophyll antenna size and maximize photosynthetic productivity. Biotechnol Adv 32:66–72 . https://doi.org/10.1016/j.biotechadv.2013.08.018

Kirst H, Shen Y, Vamvaka E, Betterle N, Xu D, Warek U, Strickland JA, Melis A (2018) Downregulation of the CpSRP43 gene expression confers a truncated light-harvesting antenna (TLA) and enhances biomass and leaf-to-stem ratio in Nicotiana tabacum canopies. Planta 248:139–154 . https://doi.org/10.1007/s00425-018-2889-7

Klimyuk VI, Persello-Cartieaux F, Havaux M, Contard-David P, Schuenemann D, Meiherhoff K, Gouet P, Jones JDG, Hoffman NE, Nussaume L (1999) A Chromodomain Protein Encoded by the Arabidopsis CAO Gene Is a Plant-Specific Component of the Chloroplast Signal Recognition

Particle Pathway That Is Involved in LHCP Targeting. Plant Cell 11:87 LP – 99 . https://doi.org/10.1105/tpc.11.1.87

Kobayashi K, Mochizuki N, Yoshimura N, Motohashi K, Hisabori T, Masuda T (2008) Functional analysis of Arabidopsis thaliana isoforms of the Mg-chelatase CHLI subunit. Photochem Photobiol Sci 7:1188–1195 . https://doi.org/10.1039/B802604C

Kurowska M, Daszkowska-Golec A, Gruszka D, Marzec M, Szurman M, Szarejko I, Maluszynski M (2011) TILLING: a shortcut in functional genomics. J Appl Genet 52:371–390 . https://doi.org/10.1007/s13353-011-0061-1

Larosa V, Coosemans N, Motte P, Bonnefoy N, Remacle C (2012) Reconstruction of a human mitochondrial complex I mutation in the unicellular green alga Chlamydomonas. Plant J 70:759–768 . https://doi.org/10.1111/j.1365-313X.2012.04912.x

Lauersen KJ, Kruse O, Mussgnug JH (2015) Targeted expression of nuclear transgenes in Chlamydomonas reinhardtii with a versatile, modular vector toolkit. Appl Microbiol Biotechnol 99:3491–3503 . https://doi.org/10.1007/s00253-014-6354-7

Laustsen A, Bak RO (2019) Electroporation-Based CRISPR/Cas9 Gene Editing Using Cas9 Protein and Chemically Modified sgRNAs BT - CRISPR Gene Editing: Methods and Protocols. In: Luo Y (ed). Springer New York, New York, NY, pp 127–134

Lee JW, Lee SH, Han JW, Kim GH (2020) Early Light-Inducible Protein (ELIP) Can Enhance Resistance to Cold-Induced Photooxidative Stress in Chlamydomonas reinhardtii . Front. Physiol. 11:1083

Leister D, Wang X, Haberer G, Mayer KFX, Kleine T (2011) Intracompartmental and Intercompartmental Transcriptional Networks Coordinate the Expression of Genes for Organellar Functions. Plant Physiol 157:386 LP – 404 . https://doi.org/10.1104/pp.111.177691

Li Y, Lucas M-G, Konovalova T, Abbott B, MacMillan F, Petrenko A, Sivakumar V, Wang R, Hastings G, Gu F, van Tol J, Brunel L-C, Timkovich R, Rappaport F, Redding K (2004) Mutation of the Putative Hydrogen-Bond Donor to P700 of Photosystem I. Biochemistry 43:12634–12647 . https://doi.org/10.1021/bi036329p

Lohr M, Im C-S, Grossman AR (2005) Genome-Based Examination of Chlorophyll and Carotenoid Biosynthesis in Chlamydomonas reinhardtii Plant Physiol 138:490 LP – 515 . https://doi.org/10.1104/pp.104.056069

Lv X, Shi Y, Xu X, Wei Y, Wang H, Zhang X, Wu J (2015) Oryza sativa Chloroplast Signal Recognition Particle 43 (OscpSRP43) Is Required for Chloroplast Development and Photosynthesis. PLoS One 10:e0143249–e0143249 . https://doi.org/10.1371/journal.pone.0143249

McCarthy SS, Kobayashi MC, Niyogi KK (2004) White mutants of Chlamydomonas reinhardtii are defective in phytoene synthase. Genetics 168:1249–1257 . https://doi.org/10.1534/genetics.104.030635

Meinecke L, Alawady A, Schroda M, Willows R, Kobayashi MC, Niyogi KK, Grimm B, Beck CF (2010) Chlorophyll-deficient mutants of Chlamydomonas reinhardtii that accumulate magnesium protoporphyrin IX. Plant Mol Biol 72:643–658 . https://doi.org/10.1007/s11103-010-9604-9

Melis A (2009) Solar energy conversion efficiencies in photosynthesis : Minimizing the chlorophyll antennae to maximize efficiency. Plant Sci 177:272–280 . https://doi.org/10.1016/j.plantsci.2009.06.005

Mini P, Demurtas OC, Valentini S, Pallara P, Aprea G, Ferrante P, Giuliano G (2018) Agrobacterium-mediated and electroporation-mediated transformation of Chlamydomonas reinhardtii: a comparative study. BMC Biotechnol 18:11 . https://doi.org/10.1186/s12896-018-0416-3

Mitra M, Kirst H, Dewez D, Melis A (2012) Modulation of the light-harvesting chlorophyll antenna

size in Chlamydomonas reinhardtii by TLA1 gene over-expression and RNA interference. Philos Trans R Soc B Biol Sci 367:3430–3443 . https://doi.org/10.1098/rstb.2012.0229

Molnar A, Bassett A, Thuenemann E, Schwach F, Karkare S, Ossowski S, Weigel D, Baulcombe D (2009) Highly specific gene silencing by artificial microRNAs in the unicellular alga Chlamydomonas reinhardtii. Plant J 58:165–174 . https://doi.org/10.1111/j.1365-313X.2008.03767.x

Moore M, Goforth RL, Mori H, Henry R (2003) Functional interaction of chloroplast SRP/FtsY with the ALB3 translocase in thylakoids: substrate not required. J Cell Biol 162:1245–1254 . https://doi.org/10.1083/jcb.200307067

Mueller AH, Dockter C, Gough SP, Lundqvist U, von Wettstein D, Hansson M (2012) Characterization of Mutations in Barley fch2 Encoding Chlorophyllide a Oxygenase. Plant Cell Physiol 53:1232–1246 . https://doi.org/10.1093/pcp/pcs062

Mussgnug JH (2015) Genetic tools and techniques for Chlamydomonas reinhardtii. Appl Microbiol Biotechnol 99:5407–5418 . https://doi.org/10.1007/s00253-015-6698-7

Mussgnug JH, Thomas-Hall S, Rupprecht J, Foo A, Klassen V, McDowall A, Schenk PM, Kruse O, Hankamer B (2007) Engineering photosynthetic light capture: Impacts on improved solar energy to biomass conversion. Plant Biotechnol J 5:802–814 . https://doi.org/10.1111/j.1467-7652.2007.00285.x

Negi S, Perrine Z, Friedland N, Kumar A, Tokutsu R, Minagawa J, Berg H, Barry AN, Govindjee G, Sayre R (2020) Light regulation of light-harvesting antenna size substantially enhances photosynthetic efficiency and biomass yield in green algae†. Plant J 103:584–603 . https://doi.org/https://doi.org/10.1111/tpj.14751

Nellaepalli S, Ozawa S-I, Kuroda H, Takahashi Y (2018) The photosystem I assembly apparatus consisting of Ycf3–Y3IP1 and Ycf4 modules. Nat Commun 9:2439 . https://doi.org/10.1038/s41467-018-04823-3

Nilsson R, van Wijk KJ (2002) Transient interaction of cpSRP54 with elongating nascent chains of the chloroplast-encoded D1 protein; 'cpSRP54 caught in the act.' FEBS Lett 524:127–133 . https://doi.org/10.1016/S0014-5793(02)03016-8

Niyogi KK, Bjorkman O, Grossman AR (1997a) Chlamydomonas Xanthophyll Cycle Mutants Identified by Video Imaging of Chlorophyll Fluorescence Quenching. Plant Cell 9:1369–1380 . https://doi.org/10.1105/tpc.9.8.1369

Niyogi KK, Björkman O, Grossman AR (1997b) The roles of specific xanthophylls in photoprotection. Proc Natl Acad Sci U S A 94:14162–14167 . https://doi.org/10.1073/pnas.94.25.14162

Noordally ZB, Millar AJ (2015) Clocks in Algae. Biochemistry 54:171–183 . https://doi.org/10.1021/bi501089x

Nour-Eldin HH, Specht EA, Ostrand J, Hoang KTD, Karunanithi PS, Mayfield SP (2018) High-throughput system for quantifying and characterizing homologous recombination in Chlamydomonas reinhardtii. Algal Res 31:167–172 . https://doi.org/https://doi.org/10.1016/j.algal.2018.02.005

Oey M, Ross IL, Stephens E, Steinbeck J, Wolf J, Radzun KA, Kügler J, Ringsmuth AK, Kruse O, Hankamer B (2013) RNAi Knock-Down of LHCBM1, 2 and 3 Increases Photosynthetic H2 Production Efficiency of the Green Alga Chlamydomonas reinhardtii. PLoS One 8:e61375

Olive J, Wollman F-A, Bennoun P, Recouvreur M (1981) Ultrastructure of thylakoid membranes in C. reinhardtii: Evidence for variations in the partition coefficient of the light-harvesting complex-containing particles upon membrane fracture. Arch Biochem Biophys 208:456–467 . https://doi.org/https://doi.org/10.1016/0003-9861(81)90532-4

Ossenbuhl F, Gohre V, Meurer J, Krieger-Liszkay A, Rochaix J-D, Eichacker LA (2004) Efficient assembly of photosystem II in Chlamydomonas reinhardtii requires Alb3.1p, a homolog of Arabidopsis ALBINO3. Plant Cell 16:1790–1800 . https://doi.org/10.1105/tpc.023226

Ouyang M, Li X, Ma J, Chi W, Xiao J, Zou M, Chen F, Lu C, Zhang L (2011) LTD is a protein required for sorting light-harvesting chlorophyll-binding proteins to the chloroplast SRP pathway. Nat Commun 2:277 . https://doi.org/10.1038/ncomms1278

Park S, Lee Y, Lee J-H, Jin E (2013) Expression of the high light-inducible Dunaliella LIP promoter in Chlamydomonas reinhardtii. Planta 238:1147–1156 . https://doi.org/10.1007/s00425-013-1955-4

Patel VK, Soni N, Prasad V, Sapre A, Dasgupta S, Bhadra B (2019) CRISPR–Cas9 System for Genome Engineering of Photosynthetic Microalgae. Mol Biotechnol 61:541–561 . https://doi.org/10.1007/s12033-019-00185-3

Perrine Z, Negi S, Sayre RT (2012) Optimization of photosynthetic light energy utilization by microalgae. Algal Res 1:134–142 . https://doi.org/10.1016/j.algal.2012.07.002

Pigolev A V, Zharmukhamedov SK, Klimov VV (2009) The psbO mutant of Chlamydomonas reinhardtii is capable of assembling stable, photochemically active reaction center of photosystem II. Biochem Suppl Ser A Membr Cell Biol 3:33–41 . https://doi.org/10.1134/S199074780901005X

Polle JEW, Kanakagiri S-D, Melis A (2003) tla1, a DNA insertional transformant of the green alga Chlamydomonas reinhardtii with a truncated light-harvesting chlorophyll antenna size. Planta 217:49–59 . https://doi.org/10.1007/s00425-002-0968-1

Polle JEW, Niyogi KK, Melis A (2001) Absence of Lutein, Violaxanthin and Neoxanthin Affects the Functional Chlorophyll Antenna Size of Photosystem-II but not that of Photosystem-I in the Green Alga Chlamydomonas reinhardtii. Plant Cell Physiol 42:482–491 . https://doi.org/10.1093/pcp/pce058

Pool MR (2005) Signal recognition particles in chloroplasts, bacteria, yeast and mammals. Mol Membr Biol 22:3–15 . https://doi.org/10.1080/09687860400026348

Quinn JM, Kropat J, Merchant S (2003) Copper response element and Crr1-dependent Ni(2+)-responsive promoter for induced, reversible gene expression in Chlamydomonas reinhardtii. Eukaryot Cell 2:995–1002 . https://doi.org/10.1128/ec.2.5.995-1002.2003

Rochaix, JD; van Dillewijn J (1982) Transformation of the green alga Chlamydomonas reinhardtii with yeast DNA. Nature 296:70–72

Rohr J, Sarkar N, Balenger S, Jeong B, Cerutti H (2004) Tandem inverted repeat system for selection of effective transgenic RNAi strains in Chlamydomonas. Plant J 40:611–621 . https://doi.org/10.1111/j.1365-313X.2004.02227.x

Rossini S, Casazza AP, Engelmann ECM, Havaux M, Jennings RC, Soave C (2006) Suppression of Both ELIP1 and ELIP2 in Arabidopsis Does Not Affect Tolerance to Photoinhibition and Photooxidative Stress. Plant Physiol 141:1264 LP – 1273 . https://doi.org/10.1104/pp.106.083055

Safafar H, Uldall Nørregaard P, Ljubic A, Møller P, Løvstad Holdt S, Jacobsen C (2016) Enhancement of Protein and Pigment Content in Two Chlorella Species Cultivated on Industrial Process Water. J Mar Sci Eng 4:84 . https://doi.org/10.3390/jmse4040084

Salomé PA, Merchant SS (2019) A Series of Fortunate Events: Introducing Chlamydomonas as a Reference Organism. Plant Cell 31:1682–1707 . https://doi.org/10.1105/tpc.18.00952

Sander JD, Joung JK (2014) CRISPR-Cas systems for editing, regulating and targeting genomes. Nat Biotechnol 32:347–355 . https://doi.org/10.1038/nbt.2842

Schmollinger S, Strenkert D, Schroda M (2010) An inducible artificial microRNA system for

Chlamydomonas reinhardtii confirms a key role for heat shock factor 1 in regulating thermotolerance. Curr Genet 56:383–389 . https://doi.org/10.1007/s00294-010-0304-4

Schroda M, Blöcker D, Beck CF (2000) The HSP70A promoter as a tool for the improved expression of transgenes in Chlamydomonas. Plant J 21:121–131 . https://doi.org/10.1046/j.1365-313x.2000.00652.x

Shin SE, Lim JM, Koh HG, Kim EK, Kang NK, Jeon S, Kwon S, Shin WS, Lee B, Hwangbo K, Kim J, Ye SH, Yun JY, Seo H, Oh HM, Kim KJ, Kim JS, Jeong WJ, Chang YK, Jeong BR (2016) CRISPR/Cas9-induced knockout and knock-in mutations in Chlamydomonas reinhardtii. Sci Rep 6:27810 . https://doi.org/10.1038/srep27810

Shin YS, Jeong J, Nguyen THT, Kim JYH, Jin E, Sim SJ (2019) Targeted knockout of phospholipase A2 to increase lipid productivity in Chlamydomonas reinhardtii for biodiesel production. Bioresour Technol 271:368–374 . https://doi.org/https://doi.org/10.1016/j.biortech.2018.09.121

Sizova I, Greiner A, Awasthi M, Kateriya S, Hegemann P (2013) Nuclear gene targeting in Chlamydomonas using engineered zinc-finger nucleases. Plant J 73:873–882 . https://doi.org/10.1111/tpj.12066

Sobotka R, Dühring U, Komenda J, Peter E, Gardian Z, Tichy M, Grimm B, Wilde A (2008) Importance of the Cyanobacterial Gun4 Protein for Chlorophyll Metabolism and Assembly of Photosynthetic Complexes. J Biol Chem 283:25794–25802 . https://doi.org/10.1074/jbc.M803787200

Spreitzer RJ, Mets L (1981) Photosynthesis-deficient Mutants of Chlamydomonas reinhardii with Associated Light-sensitive Phenotypes. Plant Physiol 67:565 LP – 569 . https://doi.org/10.1104/pp.67.3.565

Strenkert D, Schmollinger S, Gallaher SD, Salomé PA, Purvine SO, Nicora CD, Mettler-Altmann T, Soubeyrand E, Weber APM, Lipton MS, Basset GJ, Merchant SS (2019) Multiomics resolution of molecular events during a day in the life of Chlamydomonas. Proc Natl Acad Sci 116:2374 LP – 2383 . https://doi.org/10.1073/pnas.1815238116

Tanaka A, Ito H, Tanaka R, Tanaka NK, Yoshida K, Okada K (1998) Chlorophyll a oxygenase (CAO) is involved in chlorophyll b formation from chlorophyll a. Proc Natl Acad Sci 95:12719–12723 . https://doi.org/10.1073/pnas.95.21.12719

Tran PT, Sharifi MN, Poddar S, Dent RM, Niyogi KK (2012) Intragenic enhancers and suppressors of phytoene desaturase mutations in Chlamydomonas reinhardtii. PLoS One 7:e42196–e42196 . https://doi.org/10.1371/journal.pone.0042196

Tu C-J, Schuenemann D, Hoffman NE (1999) Chloroplast FtsY, Chloroplast Signal Recognition Particle, and GTP Are Required to Reconstitute the Soluble Phase of Light-harvesting Chlorophyll Protein Transport into Thylakoid Membranes. J Biol Chem 274:27219–27224 . https://doi.org/10.1074/jbc.274.38.27219

Tzvetkova-Chevolleau T, Franck F, Alawady A, Dall'Osto L, Carrière F, Bassi R, Grimm B, Nussaume L, Havaux M (2007a) The light stress-induced protein ELIP2 is a regulator of chlorophyll synthesis. Plant J 50:795–809 . https://doi.org/10.1111/j.1365-313X.2007.03090.x

Tzvetkova-Chevolleau T, Hutin C, Noël LD, Goforth R, Carde JP, Caffarri S, Sinning I, Groves M, Teulon J-M, Hoffman NE, Henry R, Havaux M, Nussaume L (2007b) Canonical Signal Recognition Particle Components Can Be Bypassed for Posttranslational Protein Targeting in Chloroplasts. Plant Cell 19:1635 LP – 1648 . https://doi.org/10.1105/tpc.106.048959

Vecchi V, Barera S, Bassi R, Dall'Osto L (2020) Potential and Challenges of Improving Photosynthesis in Algae. Plants (Basel, Switzerland) 9: . https://doi.org/10.3390/plants9010067

Vilarino M, Rashid ST, Suchy FP, McNabb BR, van der Meulen T, Fine EJ, Ahsan S, Mursaliyev N,

Sebastiano V, Diab SS, Huising MO, Nakauchi H, Ross PJ (2017) CRISPR/Cas9 microinjection in oocytes disables pancreas development in sheep. Sci Rep 7:17472 . https://doi.org/10.1038/s41598-017-17805-0

Walker CJ, Willows RD (1997) Mechanism and regulation of Mg-chelatase. Biochem J 327 (Pt 2:321–333 . https://doi.org/10.1042/bj3270321

Wang P, Grimm B (2016) Comparative Analysis of Light-Harvesting Antennae and State Transition in chlorina and cpSRP Mutants. Plant Physiol 172:1519–1531 . https://doi.org/10.1104/pp.16.01009

Zhang R, Patena W, Armbruster U, Gang SS, Blum SR, Jonikas MC (2014) High-Throughput Genotyping of Green Algal Mutants Reveals Random Distribution of Mutagenic Insertion Sites and Endonucleolytic Cleavage of Transforming DNA. Plant Cell 26:1398–1409 . https://doi.org/10.1105/tpc.114.124099

Zhao L, Cheng D, Huang X, Chen M, Dall'Osto L, Xing J, Gao L, Li L, Wang Y, Bassi R, Peng L, Wang Y, Rochaix J-D, Huang F (2017) A Light Harvesting Complex-Like Protein in Maintenance of Photosynthetic Components in Chlamydomonas Plant Physiol 174:2419 LP – 2433 . https://doi.org/10.1104/pp.16.01465

Zhao T, Wang W, Bai X, Qi Y (2009) Gene silencing by artificial microRNAs in Chlamydomonas. Plant J 58:157–164 . https://doi.org/10.1111/j.1365-313X.2008.03758.x

Ziehe D, Dunschede B, Schunemann D (2017) From bacteria to chloroplasts: evolution of the chloroplast SRP system. Biol Chem 398:653–661 . https://doi.org/10.1515/hsz-2016-0292

Zuris J, Thompson D, Shu Y, Guilinger J, Bessen J, Hu J, Maeder M, Joung J, Chen ZY, Liu D (2014) Cationic lipid-mediated delivery of proteins enables efficient protein-based genome editing in vitro and in vivo. Nat Biotechnol 33: . https://doi.org/10.1038/nbt.3081

CHAPTER 4
Aim of The Thesis

This work is aimed to understand the molecular details of the mechanism(s) regulating light-to-biomass conversion efficiency in unicellular algae under excess light conditions. Indeed, the capacity to counteract photoxidative stress and maintain high assimilation rates is among the major factors which impact on biomass productivity in the artificial condition of a photobioreactor. The output of this research is expected to be of interest for both basic biology and the development of an algae-based industry, for the production of both lipid-rich biomass for biofuels and high value compounds from engineered strains.
The Chlamydomonas reinhardtii as2.1 strain was obtained by backcrossing the *as2* mutant, isolated by Bonente and collaborators in 2011 through random insertional mutagenesis (Bonente et al. 2011). It possessed the typical features of pale green mutants but showed a growth rate far higher than the parental strain, both in high and mild light conditions (Simone Barera, unpublished data). Preliminary analysis showed a great deletion/insertion rearrangement in the region containing CpFTSY encoding gene, a component of the CpSRP pathway which regulates biogenesis of LHC systems. However, it was hard to annotate the complete region, due to high G/C content and its localization at the edge of a sequenced region of the genome. The available details of the mutation are valuable to be used in the construction of fast-growing pale-green mutants by genome editing in different algal strains. Interestingly, the growth rate measured in *as2.1* appeared far higher than other mutants in the SRP pathway (Kirst et al. 2012; Kirst and Melis 2014; Jeong et al. 2017), although a significant growth advantage in high light was reported for this strains respect to the wild type. To verify whether FTSY depletion was related to the enhancement in light-use efficiency in *as2.1*, we produced *CpFTSY* null-mutants by the CRISPR-Cas9 technology. The resulting *CpFTSY* mutants showed, in addition to a pale-green phenotype, a higher sensitivity to excess light stress. In order to investigate the role of *CpFTSY* in the *as2.1* growth phenotype, we carried out a complementation of the mutant strains by expressing CpFTSY under the control of its endogenous promoter.

The genome edited *cpftsy* mutants failed to reproduce the growth phenotype of *as2.1* strain. Rather, they suffered for growth impairment (see the following sections). To further investigate such a controversial output in the context of the biogenesis of LHC system, which should be affected by the lack of CpFTSY, we compared *cpftsy* mutants and a pale green strain blocked on a late step of chlorophyll biosynthesis. In particular we resorted to *cao*, a knockout mutant of *Chlamydomonas* devoid of *Chlorophyll a Oxygenase* (*CAO*) gene, which encodes the enzyme involved in the conversion of chlorophyll *a* into chlorophyll *b*. According to previous reports, such mutant was expected to exhibit a smaller antenna system than WT, since Chl *b* is a chromophores conferring structural stability to antenna complexes and being particularly abundant in LHCII, the major antenna complex of PSII (Bujaldon et al. 2017). The photosynthetic phenotype of *cao* strain has been previously characterized upon growth under dim or moderate light conditions, while only knock-down lines were characterized in high light (Perrine et al. 2012; Bujaldon et al. 2017). To assess the relative importance of CpSRP import pathway vs. Chl *b* biosynthesis pathway in the functional assembly of LHC systems, double mutants *cpftsy-cao* were produced and investigated in term of light-use efficiency.

To obtain an efficient CRISPR-Cas9 procedure to be applied to *Chlamydomonas*, a long work of optimization of the available protocols was carried out. In the second part of the thesis, all the steps are illustrated. The output of this research work have contributed to the publication (Angstenberger et al. 2020), that is reported in chapter 11.

REFERENCES

Angstenberger M, de Signori F, Vecchi V, Dall'Osto L, Bassi R (2020) Cell Synchronization Enhances Angstenberger M, de Signori F, Vecchi V, Dall'Osto L, Bassi R (2020) Cell Synchronization Enhances Nuclear Transformation and Genome Editing via Cas9 Enabling Homologous Recombination in Chlamydomonas reinhardtii. ACS Synth Biol. https://doi.org/10.1021/acssynbio.0c00390

Bonente G, Formighieri C, Mantelli M, Catalanotti C, Giuliano G, Morosinotto T, Bassi R (2011) Mutagenesis and phenotypic selection as a strategy toward domestication of Chlamydomonas reinhardtii strains for improved performance in photobioreactors. Photosynth Res 108:107–120 . https://doi.org/10.1007/s11120-011-9660-2

Bujaldon S, Kodama N, Rappaport F, Subramanyam R, de Vitry C, Takahashi Y, Wollman FA (2017) Functional Accumulation of Antenna Proteins in Chlorophyll b-Less Mutants of Chlamydomonas reinhardtii. Mol Plant 10:115–130 . https://doi.org/10.1016/j.molp.2016.10.001

Jeong J, Baek K, Kirst H, Melis A, Jin ES (2017) Loss of CpSRP54 function leads to a truncated light-harvesting antenna size in Chlamydomonas reinhardtii. Biochim Biophys Acta - Bioenerg 1858:45–55 . https://doi.org/10.1016/j.bbabio.2016.10.007

Kirst H, García-Cerdán JG, Zurbriggen A, Melis A (2012) Assembly of the light-harvesting chlorophyll antenna in the green alga Chlamydomonas reinhardtii requires expression of the TLA2-CpFTSY gene. Plant Physiol 158:930–945 . https://doi.org/10.1104/pp.111.189910

Kirst H, Melis A (2014) The chloroplast signal recognition particle (CpSRP) pathway as a tool to minimize chlorophyll antenna size and maximize photosynthetic productivity. Biotechnol Adv 32:66–72 . https://doi.org/10.1016/j.biotechadv.2013.08.018

Perrine Z, Negi S, Sayre RT (2012) Optimization of photosynthetic light energy utilization by microalgae. Algal Res 1:134–142 . https://doi.org/10.1016/j.algal.2012.07.002

PART I

Genetic and phenotypic analysis of *Chlamydomonas* pale green mutants

CHAPTER 5
Method and Materials

5.1 Strains and culture conditions

The cw15 (mt-), *Chlamydomonas reinhardtii* strain (also named CC-4533, from chlamylibrary.org) was used as a genetic background to generate the genome edited mutants (*cpftsy #1*, *cpftsy#2*, *cao#1*, *cao#2*, cpftsy-cao#1, cpftsy-cao#2, *cpftsyN1*, *cpftsyN2*, *cpftsyN3*, *cpftsyN4*) and the random insertional mutant *as 2.1*. cw 15 is a cell wall-deficient strain, that is easier to transform. *C. reinhardtii* cells were grown in TAP and maintained on TAP-agar medium (Harris et al. 1989; Kropat et al. 2011) at light intensity of 50 µmol/s/m^2, 100 rpm agitation, 25°C controlled temperature, 16 h light/8 h dark photoperiod. irradiance was provided by warm-white LEDs (Epistar 35mil Chip High Power LED, warm white LEDE-P20B-DW, Wayjun Tech., Shenzhen, China). Strains were grown adding 100 µg/ml of ampicillin to avoid contaminations and for each mutant it was added different antibiotics, according to their resistances.

- *cpftsy#1*, *cpftsy #2 cpftsyN1, cpftsyN2, cpftsyN3, cpftsyN4*: Hygromycin 50 µg/ml
- *as2.1*, cao#1 and cao #2: Paromomycin 10 µg/ ml
- *cpftsy-cao#1* and *cpftsy-cao#2*: Hygromycin 50 µg/ml + Paromomycin 10 µg/ ml
- *as2.1 C1 and as2.1 C2*: Paromomycin 10 µg/ml+ Zeocin 20 µg/ml
- CW15+CpFTSY: Zeocin 20 µg/ml
- *cpftsy#1 C1*, *cpftsy#1 C2, cpftsy#2 C1, cpftsy#2 C2:* Hygromicyn 50 µg/ml + Zeocin 20 µg/ml

5.2 Media composition

TAP: Tris-Acetate-Phospate medium (Kropat et al. 2011)

For 1 liter of solution:

Tris-HCl	2.42 g
TAP salts stock solution	25 ml
P-solution (phosphate buffer pH 7.0)	375 µl
Hutner's stock solutions (trace elements)	1 ml for each
Glacial acetic acid	1 ml
Milli q water	Up to 1L

The pH was increased to 6.8-6.9 using HCl.
The medium was autoclaved for 20' at 120 °C.
For solid medium, 1.5 % agar (w/v) was added before autoclaving.

HS (High Salt Medium)

P-solution (phosphate buffer pH 7.0)	5 ml
Beijerinck's solution	5 ml
Hutner's stock solutions (trace elements)	1 ml for each
Milli-q water	Up to 1L

The pH was increased to 6.8-6.9 using HCl.
The medium was autoclaved for 20' at 120 °C.

TAP salts

NH_4Cl	15 g/L
$MgSO_4 \cdot 7\ H_2O$	4 g/L
$CaCl_2 \cdot 2\ H_2O$	2 g/L

P-solution (phosphate buffer pH 7.0)

K_2HPO_4	288 g/L
KH_2PO_4	144 g/L

Beijerinck's solution

NH_4Cl	100 g/L
$MgSO_4 \cdot 7\ H_2O$	4 g/L
$CaCl_2 \cdot 2$ H2O	2 g/L

Hutner's solutions

Solution 1	**EDTA-Na_2 pH 8.0**	**25 mM**
Solution 2	$(NH_4)_6Mo_7O_{23}$	28.5 µM
Solution 3	Na_2SO_3	0.1 mM
Solution 4	$ZnSO_4 \cdot 7H_2O$	25 mM
	EDTA-Na_2 pH 8.0	2.75 mM
Solution 5	$MnCl_2 \cdot 4H_2O$	6 mM
	EDTA-Na_2 pH 8.0	6 mM
Solution 6	$FeCl_3 \cdot 6H_2O$	20 mM
	EDTA-Na_2 pH 8.0	22 mM
	Na_2CO_3	22 mM
Solution 7	$CuCl_2 \cdot 2H_2O$	2 mM
	EDTA-Na_2 pH 8.0	2 mM

TOS medium

TAP	80%
Sucrose	40 mM
Water	20%

LB (Luria-Bertani) medium

For 1 L at pH 7.0:

NaCl	10 g
Yeast extract	5 g
Triptone	10 g
Milliq-water	Up to 1L

The medium was autoclaved for 20' at 20°C
For solid medium, 1.5 % agar (w/v) was added before autoclaving.

Modified high-salt LB

For the recovery of *E. coli* after the electric, or thermal shocks, a high salt LB medium was prepared. In 10 ml of LB were dissolved:

- 125 µl of 1M $MgSO_4$
- 125 µl of 1M $MgCl_2$
- 200 µl of 20% glucose

5.3 Growth in multicultivator

To perform growth experiments was used the Multi-Cultivator MC 1000 (Photon Systems Instruments), composed by two slots of 8 tubes each. The continuous light intensities ranged between 50 and 1000µE, depending on the experiment. The temperature was maintained by a water bath at 25°C. The sensor recorded each hour the absorbance of the cells in the tubes at 720 nm and 680 nm, to monitor the growth curve and the chlorophyll concentration curve. The cells were inoculated in TAP (rich medium) or in HS (minimal medium) at a starting concentration of $5*10^5$ cell/ml.

5.4 Molecular Biology

5.4.1 DNA extraction from *Chlamydomonas*

For the DNA extraction it was used a modified version of a protocol provided by Claire Remacle's laboratory.

- 2-3 ml of fresh culture of about 1x 10^7 cell/ml was pelleted for 5' at 2000 x g at 4°C.
- The pellet was resuspended in 500 µl of TEN (10mM Tris-HCl pH8, 10mM EDTA, 150mM NaCl).
- The suspension was spun down for 2' at 1500 x g at 4°C.
- The pellet was resuspended in 150 µl of water and 300 µl of SDS-EB (2% SDS 400mM NaCl, 40mM EDTA, 100mM Tris HCl pH8) and vortexed.
- 350 µl of phenol:chloroform:isoamyl alcohol (25:24:1) were added to the mixture.
- The sample was vortexed and spun down for 5' at 15000 x g at 4°C.
- The upper phase was collected and 300 µl of Chloroform:isoamyl (24:1) were added to it
- The sample was vortexed and spun down for 5' at 15000 x g at 4°C.

- The upper phase was collected and 2.5V of 100% ethanol and 0.11 V of 3 M pH 5.5 Na acetate 5.5 were added to it.
- The sample was spun down and incubated 30’ at -80°C.
- The sample was spun down for 25’ at 15000 x g at 4°C.
- The supernatant was discarded and resuspended in 1 V of 70% ethanol.
- The sample was spun down for 5’ at 15000 x g and the supernatant was discarded.
- The pellet was dried under hood flux and resuspended in 30 µl of autoclaved milli-q water.

5.4.2 DNA quantification

After the extraction DNA was quantified by NanoDrop (Thermofwasher).
1.5 µl of sample was read using water as reference. The purity of the extraction was evaluated reading the 260 nm /280 nm and the 260 nm /230 nm absorbance ratios. The 260/280 value indicates the ratio between the nucleic acid and the protein content; the 260/230 the ratio between nucleic acid and other organic contaminants likes phenol, ethanol ecc. Both values must be major or equal to 1.8. The quality of DNA was evaluated by 1.5 % (w/v) agarose gel electrophoresis, 100 ng of each sample were loaded, and it was added the 6X TrikTrak loading Dye (Termofisher). As molecular weight marker it was used Gene Ruler 1 kb plus (Termofisher). The gel image was analysed with ChemiDoc (Biorad).

5.4.3 Agarose gel preparation

0.5 or 0.75 g of agarose were dissolved in 50 ml of 0.5X TAE (89 mM Tris-base, 89 mM CH3COOH, 2 mM EDTA pH 8.2) by heating in a microwave oven until boiling and 20000X EuroSafe (Vetroscientifica) was added to detect nucleic acid under ultraviolet (UV) light.

5.4.4 Polymerase Chain Reaction (PCR)

Polymerase chain reaction was used to amplify different kind of genomics sequences. The reaction was performed by using different primers, whose annealing temperature was calculated on the basis of the length and the G/C content [(2°C X n (A/T) + 4°C x n (G/C))-2]. To screen bacterial or algal strain it was used the Go-Taq Green Master Mix (Promega) and the mix in 50 µl was prepared as follows:

2 X Go-Taq Master Mix	25 µl
DMSO	1 µl
100 µM Primer Fw	0.25 µl
100 µM Primer Rev	0.25 µl
Template	100 ng
H_2O	Up to 50 µl

The thermocycler was set as follows:

- 3’ of denaturation at 95°C
- 28-35 cycles:
  - 30’’ of denaturation at 95°C
  - 30’’ of annealing at 56°C-60°C (it depends on the primer length and G/C content)

    - 1 kb/1’ of extension at 72°C
- 3’ of final extension at 72°C

To amplify the templates for the sgRNA, the target sequences for the *in vitro* cut assay and for all sequence that need to be amplify without errors it was used a proof reading taq, namely Phusion Hot Start II DNA Polymerase (Termofisher), and the mix in 50 µl was prepared as follows:

5 X Phusion Buffer	10 µl
10 mM dNTP mix	1 µl
DMSO	1 µl
100 µM Primer Fw	0.25 µl
100 µM Primer Rev	0.25 µl
Template	100 ng
H_2O	Up to 50 µl

The thermocycler was set as follows:

- 30’’ of denaturation at 98°C
- 28-35 cycles:
    - 10’’ of denaturation at 98°C
    - 30’’ of annealing at 56°C-60°C (it depends on the primer length and G/C content)
    - 1 kb/30’’ of extension at 72°C

- 3’ of final extension at 72°C

The PCR product were checked by an electrophoresis analysis on 1-1.5% agarose gel, on the basis of products length.

5.4.5 PCR or DNA reaction products purification

PCR products to sequence, to clone, to use for *in vitro* cut assays and to use as template for *in vitro* transcription were purified using NucleoSpin Gel and PCR Clean-up kit (Macherey-Nagel).

- 100 µl of NTI Binding Buffer were mixed to 50 µl of PCR product.
- The mixture was loaded on a spin column.
- The column was spun down 1’ at 12 000 x g at RT.
- The flowthrough was discarded and 500 µl of NT3 Washing Buffer (containing EtOH) were loaded on the column.
- The column was spun down 1’ at 12 000 x g at RT.
- The flowthrough was discarded and 500 µl of NT3 Washing Buffer were loaded on the column.
- The column was spun down 1’ at 12 000 x g at RT.
- The flowthrough was discarded, and the column was spun down 1’ at 12 000 x g at RT to eliminate the residual EtOH.
- The column was transferred on a new Eppendorf tube and 20 µl of 60°C sterile water were added for the elution.
- The sample was incubated 1’ at RT and spun down 1’ at 12 000 x g at RT.
- The flowthrough was collected in the tube and the column was thrown away.

5.4.6 DNA purification from agarose gel

Fragments of DNA used in cloning procedures were purified using NucleoSpin Gel and PCR Clean-up kit (Macherey-Nagel).

- The gel slice containing the fragment was cut under UV-transilluminator by s scalpel.
- 200 µl of NTI Binding Buffer were added for each 100 mg of agarose.
- The sample was incubated for 10' at 50°C and vortexed every 2-3' to dissolve the gel.
- The mixture was loaded on a spin column.
- The column was spun down 1' at 12 000 x g at RT.
- The flowthrough was discarded and 500 µl of NT3 Washing Buffer (containing EtOH) were loaded on the column.
- The column was spun down 1' at 12 000 x g at RT.
- The flowthrough was discarded and 500 µl of NT3 Washing Buffer were loaded on the column.
- The column was spun down 1' at 12 000 x g at RT.
- The flowthrough was discarded, and the column was spun down 1' at 12 000 x g at RT to eliminate the residual EtOH.
- The column was transferred on a new Eppendorf tube and 20 µl of 60°C sterile water were added for the elution.
- The sample was incubated 1' at RT and spun down 1' at 12 000 x g at RT.
- The flowthrough was collected in the tube and the column was thrown away.

5.4.7 List of used primers

Name	Sequence	Used for:
Cas9REV	AAAAAAAGCACCGACTCGGTGCCAC	SgRNA Template
Sg CAO FWD	GCTCTCCGGGTCCTCAACGAGTTTTAGAGCTAGAAATAGCAAG	SgRNA Template
SgCPFTSY FWD	CGATCTTCAGAGCAGTGCGGGTTTTAGAGCTAGAAATAGCAAG	SgRNA Template
SgCPFTSYNew FWD	GATCGCGTACAAGTACGGCAGTTTTAGAGCTAGAAATAGCAAG	SgRNA Template
PT7CAO FWD	TAATACGACTCACTATAGCTCTCCGGGTCCTCAAC	SgRNA Template
PT7CPFTSY FWD	TAATACGACTCACTATAGCGATCTTCAGAGCAGTGCG	SgRNA Template
PT7CPFTSYNew FWD	TAATACGACTCACTATAGGATCGCGTACAAGTACGGCA	SgRNA Template
CAO FWD	TGTTACCGCATAGAGCAGCC	Fragment for *in vitro* cut
CAO REV	CCCGGCGAGTGAGCATATT	Fragment for *in vitro* cut
CPFTSY FWD	TAGACCTGACGGGTACTGGG	Fragment for *in*

		vitro cut and mutant screening
CPFTSY REV	ACTCCGGTGCTGTTATTGGG	Fragment for *in vitro* cut
CPFTSY REV2	ATGCGGATGCAGTTTCTCCT	Mutant screening
Hyg FWD	GCTACAGCCTGGTGCAAC	Hygromycin resistance cassette insertion screening
PARO FWD	CGGCACCCATCCGGTATAAA	Paromomycin resistance cassette insertion screening
PARO REV	CGTCCAGATCCTCCAAGTCG	Paromomycin resistance cassette insertion screening
M13 REV	ACACTTTATGCTTCCGGCTC	CpFTSY complemented strains screening
CPFTSY UTR FWD	TACTTGCAGTGGAAGCGGAG	CpFTSY complemented strains screening
CPFTSY synt FWD	ACTGTCTTCCGTAGGTGCAG	CpFTSY complemented strains screening
CPFTSY synt rev	TAGCATGTTGAGGCCTGTGG	CpFTSY complemented strains screening

5.4.8 SgRNA DNA- template synthesis

To synthetize the template for a specific sgRNA for a target sequence in the genome it was designed a primer complementary to the target sequence (protospacer) without the PAM and the first part of the conserved sequence of the sgRNA.: Protospacer (20 bp) +GTTTTAGAGCTAGAAATAGCAAG (Primer sgCAO FWD, sgCPFTSY FW1 and sgCPFTSY FWDNew). Then it was designed another fix one complementary to the conserved end of sgRNA sequence: AAAAAAAGCACCGACTCGGTGCCAC (Primer Cas9 rev). As template for the amplification of the conserved parts was used the pDGE5 (Ordon et al. 2017) plasmid, used for the CRISPR-Cas9 technique in plants. The PCR reaction was performed using the proof reading Taq as described in 5.4.4 paragraph, setting 10'' of extension and 58°C as annealing temperature. The result is the complete 76 bp conserved sequence of sgRNA of with the desired 20 bp protospacer.

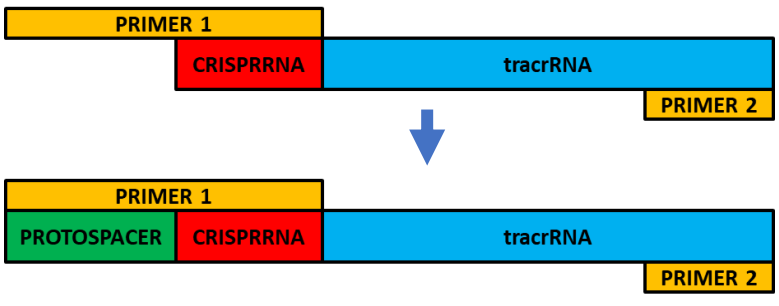

I cycle

From II to last cycle

The product obtained was therefore purified as in 5.4.5 and it was reamplified using a third primer complementary to the protospacer with the adding of the conserved sequence that is recognized from the T7 RNA Polymerase to start the *in vitro* transcription: TAATACGACTCACTATAG+Protospacer (PrimerT7CAO FWD, T7 CPFTSY FWD and T7CPFTSYNew FWD). The reverse primer is the same complementary to the end of sgRNA used before (Cas9 REV). The PCR reaction was performed with the same setting and the final product was the 96 bp sgRNA complete template with the 20-18 bp T7 promoter at the beginning.

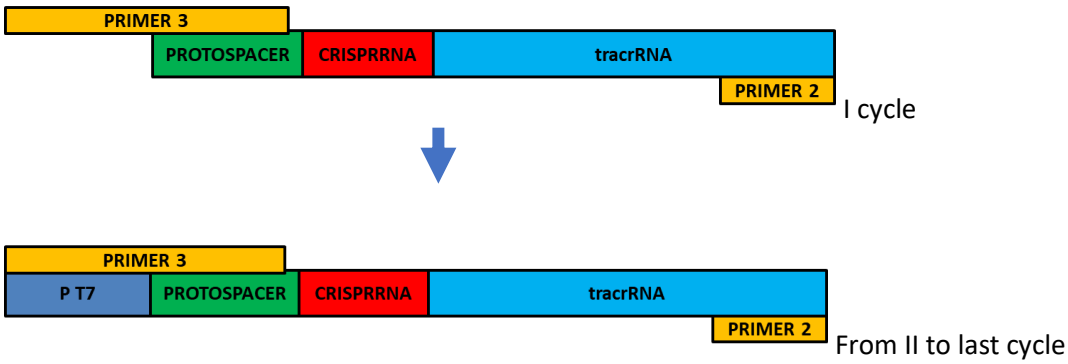

The final product was purified as before and it was used for the *in vitro* transcription.
The two sequences obtained for the following experiment are:

sgCPFTSY template

TAATACGACTCACTATAGGGCGATCTTCAGAGCAGTGCGGGTTTTAGAGCTAGAAATAGCAAGTTAAAATAAG
GCTAGTCCGTTATCAACTTGAAAAAGTGGCACCGAGTCGGTGCTTTTTTT

sgCAO template

TAATACGACTCACTATAGGGGCTCTCCGGGTCCTCAACGAGTTTTAGAGCTAGAAATAGCAAGTTAAAATAAG
GCTAGTCCGTTATCAACTTGAAAAAGTGGCACCGAGTCGGTGCTTTTTTT

sgCPFTSYNew template

TAATACGACTCACTATAGGGGATCGCGTACAAGTACGGCAGTTTTAGAGCTAGAAATAGCAAGTTAAAATAAG
GCTAGTCCGTTATCAACTTGAAAAAGTGGCACCGAGTCGGTGCTTTTTTT

5.4.9 SgRNA *in vitro* synthesis

For the SgRNA *in vitro* synthesis it was used HiScribe™ T7 Quick High Yield RNA Synthesis Kit (NEB) and was used the protocol for sequences smaller than 0.3 kb. The reaction was set as follows:

NTP buffer mix	10 µl
Template DNA	1µg
T7 DNA Polymerase MIX	2 µl
DEPC H_2O	Up to 30 µl

The reaction was incubated 4h at 37°C and the RNA was purified by phenol:chloroform extraction and ethanol precipitation to remove proteins and most of the free nucleotides:

- The reaction volume was adjusted to 180 µl by adding nuclease-free water and 20 µl of 3 M sodium acetate, pH 5.2 were added.
- The extraction was performed with an equal volume of 1:1 phenol:chloroform mixture.
- The sample was vortexed and spun down for 5' at 15000 x g at 4°C.
- Then it was collected the aqueous phase and it was performed an extraction with an equal volume of chloroform.
- The sample was vortexed and spun down for 5' at 15000 x g at 4°C.
- The aqueous phase was collected and transferred to a new tube.
- The RNA was precipitated by adding 2 volumes of ethanol.
- It was incubated at –20°C for at least 30' and the pellet collected by centrifugation for 15' at 15000 x g at 4°C.
- The supernatant was removed, and the pellet was washed with 500 µl of ice cold 70% ethanol.
- The sample was spun down for 5' at 15000 x g at 4°C.
- The RNA was resuspended in 20 µl of DEPC water.
- The RNA was quantified by Nanodrop and stored at –20°C.

5.4.10 *In vitro* sgRNA+Cas9 cut assay

Before transforming *Chlamydomonas* by electroporation to deliver the sgRNA and Cas9 inside the cell it was performed an *in vitro* cut assay in order to check the proper functioning of both molecules. The molecule to cut is a fragment of the target gene, including the sequence that would be cut in *vivo*. If the cut worked, it would be observed on agarose gel two halves of the fragment, instead that the whole one.

- **Fragment amplification:** The PCR reaction was performed using the proof reading Taq as described in 5.4.4 paragraph, setting 40 s of extension and 58°C as annealing temperature.

The selected fragments were between 500 and 700 bp of length and the selected primers were: CAO FWD and CAO REV for *CAO* gene and CPFTSY FWD and CPFTSY REV for *CPFTSY* (see 5.4.7).
As template it was used the cw 15 genomic DNA.

- ***In vitro* cut**: Before the cut 600 ng of Alt-R® S.p. Cas9 Nuclease (IDT) was incubated with 500 ng of the specific sgRNA for 10' at 37°C, in order to allow the assembly of the RNP-Complex. Then 100 ng of the fragment to cut were added in a final volume of 20 µl. The reaction mixture was incubated 1 h at 37°C and 5' at 65°C to interrupt the reaction. The results were checked on 1.5% agarose gel electrophoresis.

5.4.11 Delivery of sgRNA-Cas9 RNP complex in *Chlamydomonas*

To deliver the sgRNA-Cas9 RNP complex in *Chlamydomonas* to produce *cpftsy#1*, *cpftsy#2*, *cao#1*, *cao#2*, *cpftsy-cao#1* and *cpftsy-cao#2* strains it was followed a protocol suggested by Professor Claire Remacle and Dr Gwenaelle Gain (Universitè de Liege), with some modifications.

Chlamydomonas transformation was performed using culture of cw15 (WT cell wall deficient strain) or *cpftsy#1* and *cpftsy #2* strains (for the double mutant construction) at the exponential phase of growth curve (about $1.5*10^6$ cell/ml) in this way:

- 6.5 µg of Alt-R® S.p. Cas9 Nuclease (IDT) was preincubated with 8.33 µg of the specific sgRNA for 30' at 37°C, in order to allow the assembly of the RNP-Complex.
- Meanwhile $1.5* 10^6$ cell/ml culture was pelleted and resuspended up to $2* 10^8$ cell/ml in TOS.
- 500 ng of resistance cassette DNA were added to 250 µl of culture.
- Soon the Cas9-sgRNA complex was added to the cells.
- The mixture was incubated 20' in ice and transferred in an electroporation cuvette.
- The electroporator was set to 600 V 50µF 200Ώ and the cells were subjected to the electric pulse.
- Soon after they were incubated 5' on the bench.
- Then they were transferred in 13 ml of TOS and incubated for 6h.
- After 6 h they were plated on TAP agar plates with the adding of 30% starch and the specific antibiotic.

The screening was then performed by the search of the pale-green phenotype by eye and confirmed by amplification of the gene fragment in which the modification had to be (using CAO FWD and REV and CPFTSY FWD and REV2 primers). Resistance cassettes insertions close to the PAM sequence were detected using a primer on the gene and one on the fragment (Paro rev or Paro fwd+ CAO REV or CAO FWD; Hyg fwd + CPFTSY REV2 or CPFTSY FWD). For PCR screening was used the Go-Taq Green Master Mix (Promega) as in the 5.4.4 section.

cpftsyN1,*cpftsyN2*,*cpftsyN3* and *cpftsyN4* were instead produced by the optimized protocol reported in (Angstenberger et al. 2020).

5.4.12 Resistance cassettes

In order to screen the genome edited mutant easier a resistance cassette was co-delivered in the transformed cells. The Paromomycin resistance cassettes were obtained from the pOpt2_mCerulean3_Paro plasmid, belonging to the pOpt2.0 plasmid series from Professor Kyle J. Lauersen (King Abdullah University of Science and Technology) (Lauersen et al. 2018). The Hygromycin resistance was obtained cutting the pHyg3 plasmid (Berthold et al. 2003). pOpt2_mCerulean3_Paro and pHyg3 were linearized by HF-ScaI (NEB) restriction enzyme.
3 µg of plasmid were cut in 50 µl of reaction:

10 X Cut Smart Buffer (NEB)	5 µl
Plasmid DNA	3 µg
Restriction Enzyme	1.5 µl
H_2O	Up to 50 µl

The reaction was performed for 2 h at 37°C and DNA was purified using NucleoSpin Gel and PCR Clean-up kit (Macherey-Nagel) (see 5.4.5).

5.4.13 Plasmids used in this research

Name	Used for	Antibiotic resistance for bacteria	Antibiotic resistance for algae
pOpt2_mCerulean3_Paro (Lauersen et al., 2018)	Resistance gene insertion in *Chlamydomonas*	Ampicillin	Paromomycin
pHyg3 (Berthold et al., 2003)	Resistance gene insertion in *Chlamydomonas*	Ampicillin	Hygromycin
pOpt2_mRuby2_Ble (Lauersen et al., 2018)	*CpFTSY* synthetic gene cloning for expression in *Chlamydomonas*	Ampicillin	Zeocin
pUC57 (GeneScript) (pUC57_CPFTSY)	*CpFTSY* synthetic gene preservation	Ampicillin	-
pOpt2_CPFTSY_Ble (Obtained in this work)	*Chlamydomonas* complementation	Ampicillin	Zeocin
pDGE5 (Ordon et al., 2017)	Conserved sgRNA sequence amplification	Ampicillin	-

5.4.14 Cut and Paste cloning

To clone the *CPFTSY* gene in an expression vector to transform *Chlamydomonas,* a synthetic gene composed by the CDS and the endogenous promoter and terminator was commissioned to GenScript company. At the start and the end sides were put unique restriction sites for XbaI and SpeI (NEB) enzymes respectively. The received plasmid was used to transform *E. coli* chemically competent Top10 cells (Termofisher) (see the following pragraph) that were plated on ampicillin. Then the plasmid was extracted from a liquid culture as in 5.4.17 and cut by HF-XbaI (NEB) and HF-SpeI (NEB) restriction enzymes at 37°C for 1 h in Cut Smart (NEB) buffer to excide the gene fragment. The fragment was purified cutting it from 1% agarose gel before to proceed. The product was purified using NucleoSpin Gel and PCR Clean-up kit (Macherey-Nagel) (see 5.4.6).
Then the pOpt2_mRuby2_Ble plasmid for algae protein expression was cut by the same enzymes and treated for 1 h at 37°C by FastAP Thermosensitive Alkaline Phosphatase (Thermofisher), in order to prevent the reclosing of the plasmid. Then the reaction product was purified using NucleoSpin Gel and PCR Clean-up kit (Macherey-Nagel) (see 5.4.5). The vector and the fragment in the right proportions were then ligated by T4DNA ligase (NEB) at 16°C overnight. *E. coli* chemically competent Top10 cells (Termofisher) were then transformed with the ligation mixture (5.4.16) and colonies plated on Ampicillin, because the plasmid carried this resistance for Coli. The colonies were screened

by colony PCR by Go-Taq Green Master Mix (Promega) without DMSO (see 5.4.4) using a primer complementary to the plasmid (M13REV) and a primer complementary to the gene (CPFTSYUTR FWD). Then the positive colonies were reinoculated in LB and ampicillin to extract the plasmid for diagnostic cuts and further applications.

5.4.15 Restriction enzymes plasmids cuts

For plasmids cuts were used different restriction enzymes provided by NEB.
To perform diagnostic cut, only to assess if the plasmid in use was the right one, the reaction was set using combinations of two restriction enzymes cutting in unique sites:

10 X Cut Smart Buffer (NEB)	2 µl
Plasmid DNA	100 ng
Restriction Enzyme 1	0.5 µl
Restriction Enzyme 2	0.5 µl
H_2O	Up to 20 µl

The reactions were performed for 1h at 37°C.

In order to cut the vector DNA and the fragment to clone, the reactions were performed in 50 µl and the quantity of starting material depended on the desired proportions between the two elements and on its availability.

10 X Cut Smart Buffer (NEB)	5 µl
DNA	According to the experimental needs
Restriction Enzyme	1.5 µl
H_2O	Up to 50 µl

The reaction was performed for 2 h at 37°C and DNA was purified using NucleoSpin Gel and PCR Clean-up kit (Macherey-Nagel) (see 5.4.5 and 5.4.6).

5.4.16 Transformation of *E. coli* chemically competent cells

To conserve the plasmid for further applications the One Shot TOP 10 chemiocompetent cells (Termofisher) were transformed:

- One 50 µL vial of One Shot® cells for each ligation/transformation was thawed on ice.
- 5 µL of each ligation reaction were pipetted directly into the vial of competent cells and mix by tapping gently.
- The vial was incubated on ice for 30 minutes.
- Then it was incubated for exactly 30 seconds in the 42°C water bath and then left on ice.
- Then 1 ml of modified high-salt LB was added to the cells that were shaken at 37°C for exactly 1 hour at 225 rpm in a shaking incubator.
- Three cell dilutions (in general 1,10 and 100 µl) were plated on LB mixed to the antibiotic for plasmid selection.
- The plates were incubated at 37°C overnight.

5.4.17 Plasmid extraction from E. coli (Miniprep)

All plasmid extractions were performed using NucleoSpin® Plasmid (Macherey-Nagel)

- 5 ml of bacteria saturated culture was spun down 3' at 4000 x g.
- The pellet was resuspended in 250 µL of RNAse containing Buffer A1 and gently mixed.
- Then 250 µL of buffer A2 were added and the sample was incubated 5' at RT after a gentle mixing.
- 300 µL of Buffer A3 were then added and the vial was mixed thoroughly by inverting.
- Then the mixture was centrifuged 5' at 12000 x g.
- The supernatant was loaded on a nucleotide binding column and spun down 5' at 12000 x g.
- The flowthrough was discarded and 600 µl of A4 Washing Buffer were loaded on the column
- The column was spun down 1' at 12 000 x g at RT.
- The flowthrough was discarded, and the column was spun down 2' at 12 000 x g at RT to eliminate the residual EtOH.
- The column was transferred on a new Eppendorf tube and 20 µl of 60°C sterile water were added for the elution.
- The sample was incubated 1' at RT and spun down 1' at 12 000 x g at RT.
- The flowthrough was collected in the tube and the column was thrown away.

5.4.18 *Chlamydomonas* electroporation

Chlamydomonas transformation to deliver exogenous DNA was performed using a culture of cw15, *as2.1*, *cpftsy#1* and *cpftsy #2* cell-wall deficient strains at the exponential phase of growth curve (about $1.5*10^6$ cell/ml) in this way:

- $1.5* 10^6$ cell/ml culture was pelleted and resuspended up to $2* 10^8$ cell/ml in TOS.
- 500 ng of DNA was added to 250 µl of culture.
- The mixture was incubated 20' in ice and transferred in an electroporation cuvette.
- The electroporator was set to 600 V 50µF 200 Ω and the cells were subjected to the electric pulse.
- Soon after they were incubated 5' on the bench.
- Then they were transferred in 13 ml of TOS and incubated for 6h.
- After 6 h they were plated on TAP agar plates with the adding of 30% starch and the specific antibiotic.

5.4.19 *Chlamydomonas* complemented strains screening

To select the *as2.1*, *cpftsy#1* and *cpftsy#2* complemented mutants, dark green colonies were isolated from plates, inoculated in TAP medium and the DNA was extracted as in 5.4.1.
Then, it was performed a PCR with a couple of primers complementary to different exons of *CpFTSY* gene (CPFTSY synt FWD and CPFTSY synt REV) that gave different products for the endogenous and exogenous copies. The PCR was performed with Go-Taq Green Master Mix (Promega) as in 5.4.4. and it was selected a specific elongation time to amplify only the exogenous copy (849 bp), as the endogenous is 5 times longer (4427 bp) due to the introns presence.

5.5 Bioinformatics

5.5.1 Screening primer design

All primers for screening were design using Primer Blast tool (https://www.ncbi.nlm.nih.gov/tools/primer-blast/). Once inserted the sequence of interest, it was chosen the desired amplicon length range and the temperature range (in general between 57 and 63) and it was selected the organism to allow the research of off-target free primers. The software gives the best options calculating also the number nucleotides that could cause self-primer annealing. As the self-annealing or the primer dimers formations can compromise the amplification efficiency, they were *in silico* tested by two software: Multiple Primer Analyzer by Thermofisher (https://www.thermofisher.com/it/en/home/brands/thermo-scientific/molecular-biology/molecular-biology-learning-center/molecular-biology-resource-library/thermo-scientific-web-tools/multiple-primer-analyzer.html) and PCR Primer Stats by Bioinformatics.org (https://www.bioinformatics.org/sms2/pcr_primer_stats.html).

5.5.2 SgRNA protospacer design

The protospacer complementary to the target of the sgRNA was selected by Cas-Designer software: http://www.rgenome.net/cas-designer/ (Park et al., 2015). To obtain a knock-out the target needs to belong to an exon, so the CDS of the gene it was used to find it. After obtained the list of the targets with the PAM included it was selected the target in the desired position, paying attention to the out of frame score (a higher score indicates a higher specificity) and to its belonging to a single exon. To check possible off-targets also with different numbers of mismatches it was used the software Cas-Offinder: http://www.rgenome.net/cas-offinder (Bae et al., 2014)). The selected target sequence without the PAM it was inserted as query and from the research resulted a list of potential off-target sites that differed from the target by up to 3 nucleotides or by up to 2 nucleotides forming a DNA or a RNA bulge.

5.5.3 Sequencing data analysis

All the sample were sequenced by Eurofins genomics. The chromatograms were analysed using Chromas software (Technelysium) and the well sequenced part was exported to DNAMAN software (Lynnon Corporation) to perform alignments between wild type and the sequence of interest.

5.5.4 Restriction enzymes cut prediction *and in silico* cloning

To predict the results of the plasmids cleavages by restriction enzymes it was used the software Serial Cloner (http://serialbasics.free.fr/Serial_Cloner.html). The plasmid sequence was opened in the program and the employed enzymes were selected from a list. It was selected the used DNA ladder to obtain the prediction of the aspect which the reaction product had to have on the agarose gel. The program outputs were then the picture of the *in-silico* agarose gel and the indication of the sizes in base-pairs of the fragments which had to be obtained by the reaction, moreover it was

indicated also their starting and ending points in the whole plasmid. By this program it was also possible to predict the product of a cloning experiment. The sequence of the vector plasmid and of the fragment to insert were opened, it was performed the *in-silico* cleavage by the desired restriction enzymes and the ends of the sequences to join were selected to simulate a ligation reaction. In this way is possible to predict the exact length of the new construct, to better distinguish it *in vivo* from other side-products.

5.5.5 t-test analysis

t- test analysis was performed by the Quick Calcs GraphPad software (https://www.graphpad.com/quickcalcs/ttest1/?Format=SD)

5.5.6 Densitometric measurements

The densitometric analysis was performed by ImageLab software (Biorad). Band intensities were normalized to a reference amount and expressed as a percentage of the corresponding wild-type content.

5.6 Biochemistry

5.6.1 Pigment extraction

Chlorophyll and carotenoid were extracted by a water-solution of 85% acetone buffered by Na_2CO_3. Depending on the intensities of the green colour of the strains, it was taken a cell quantity ranging between 2.5 $*10^6$ and $1*10^7$. The cells were spun down at 2000 *x g* for 5' and the green pellet was resuspended in 1 ml of 85% acetone solution and left for a least 10' on ice in the dark. Then samples were spun down for 10' at 21000 *x g* at 4°C and the supernatant was collected and conserved at -20°C in the dark.

5.6.2 Absorption Spectra and cell pigment content analysis

The absorption spectra in the wavelength range from 350 to 800 nm were obtained at room temperature by double array AMINCO DW2000 spectrophotometer in quartz cuvettes with 1 cm of optical path. The raw data were set to zero by subtracting the value at 720 nm. To obtain the spectra graph the set to zero data were divided for the maximum absorbance value and these normalized data were inserted in a lines and curves dispersion graph. From the set to zero data were extracted the absorbance values at 663.6 nm and 646.6 nm. By Porra method (Porra et al. 1989) was possible to determine Chl *a* and *b* concentrations in mg/ml):
Chl *a*: 12.25 x A663.6 nm - 2.55 x A646.6 nm
Chl *b*: 20.31 x A646.6 nm - 4.91 x A663.6 nm
Chl *a* + Chl *b*: 17.76 x A646.6 nm + 7.43 x A663.6 nm
Chlorophyll *a* to *b* ratio (Chl *a/b*) and Chl/cars ratio were corrected through fitting analysis of the absorption spectrum (Croce et al. 2002).

5.6.3 Tylakoids extraction from *C. reinhardtii*

- About 250 ml of algae culture in the exponential growth phase (about 2* 10^6 cell/ml) were centrifuged for 5' at 1500 *x g*.
- The pellet was resuspended in 25 ml of cold BC1 buffer and from this step the samples were conserved on ice and in the dark.
- The suspension was sonicated 3 times for 10'' on ice.
- The sample was the spun down at 2000 *x g* for 10' and the supernatant was conserved.
- The pellet was the resuspended in 25 ml of cold BC1 and these steps were repeated until the cells pellet was almost completely disrupted.
- The sample was then centrifuged at 10000 *x g* for 10' and the pellet was dissolved in 10 ml of BC3.
- The sample was centrifuged at 10000 x g for 10' and the pellet was resuspended in a quantity of BC4 ranging from 250 µl to 1 ml to obtained almost the same green intensity for all samples.

BC1 Buffer	
Sorbitol	0.4 M
Tricine-KOH pH 8	20 mM
BSA	0.2%
$MgCl_2$	10 mM
Benzamidine	0.2 mM
PMSF	0.2 mM
ε-aminocaproic acid	1 mM

BC3 Buffer	
Hepes-KOH pH 7.6	20 mM
NaCl	15 mM
$MgCl_2$	5 mM
Benzamidine	0.2 mM
PMSF	0.2 mM
ε-aminocaproic acid	1 mM

BC4 Buffer	
Hepes-KOH pH 7.6	20 mM
NaCl	10 mM
$MgCl_2$	5 mM
Sorbitol	20%
Benzamidine	0.2 mM
PMSF	0.2 mM
ε-aminocaproic acid	1 mM

5.6.4 Tylakoids chlorophyll quantity determination

Pigment extraction from 20 µl of extracted thylakoids was performed ad in 5.6.1.
The extract absorption peaks at 720 nm, 663.6 nm and 646.6 nm were red at the spectrophotometer ATI UNICAM and were used to calculate the chlorophyll content according Porra formulae (Porra et al. 1989).

5.6.5 Protein extraction from thylakoids for SDS-Page

For protein western blot analysis, a quantity of thylakoids extract corresponding to the same amount of chlorophyll was collected. It was spun down at 1000 g 5' and resuspended in 1 ml of milli-q water to wash the pellet that could contain residual starch. After another spin-down and water-discard the washing was repeated other two times. The pellet was then resuspended in two fifths of the final volume and one and half volume of LB-tricine denaturing buffer was added. The sample was left to shake in this solution overnight. Before to load the electrophoresis gel, the sample was spun down for 10' at 21000 *x g* and the supernatant was collected.

LB TRICINE	
Tricine superior buffer	1.75 x
Glycerol	10 %
SDS	2%
β-mercaptoethanol	5%

5.6.6 SDS-PAGE protein electrophoresis

(Schägger and von Jagow 1987)

To separate proteins on the basis of their molecular weights was performed an SDS-PAGE analysis. The samples were prepared as in 5.6.5 and their protein, which had been treated by SDS and β-mercaptoethanol, had the same charge/mass ratio and a globular shape.
The tricine gel was prepared as follows:

RUNNING GEL	
Acrylamide 32:1 (32% acrylamide; 1% bis-acrylamide)	15 % (w/v)
Tris-HCl pH 8.45	0.75 M
TEMED	0.047% (v/v)
APS	0.0016% (w/v)
Milli-Q water	Up to the final volume

STACKING GEL		
Acrylamide 32:1 (32 % acrylamide; 1% bis-acrylamide)	4 % (w/v)	
Tris-HCl pH 8.45	0.75 M	
TEMED	0.047% (v/v)	
APS	0.0016% (w/v)	
Milli-Q water	Up to the final volume	

The running buffer for the electrophoresis were prepared as follows:

INFERIOR RUNNING BUFFER 10X	
Tris-HCl pH 8.9	2 M
Milli-Q water	Up to the final volume

SUPERIOR RUNNING BUFFER 10 X	
Tris	1 M
Tricine	1 M
SDS	1% (w/v)
EDTA	10 mM
Milli-Q water	Up to the final volume

The samples were loaded with a molecular weight marker: PiNK Prestained Protein Ladder (GeneDirex).

5.6.7 Coomassie protein staining

(Ball 1986)

To visualize proteins on acrylamide gel, it was used the Coomassie Brilliant Blue R-250 staining, which is able to bind basic aminoacids. Coomassie Brilliant Blue R-250 was eluted in 10% acetic acid and 40% methanol and this solution was poured on the gel and left to act overnight. Then the gel was transferred in a 40% methanol and 10% acetci acid decoloring solution.

5.6.8 Samples preparation for Deriphat-page

Tylakoids were pelleted 10' at 21000 x g at 4°C. Pellet was resuspend in the resuspension solution up to a final chlorophyll concentration of 1 µg/µl, then it was added an equal volume of the solubilization solution, containing β-dodecyl-maltopyranoside (β-DM). The sample was vortexed for 30'' and left on ice for 10'. The sample was centrifuged for 10' at 21000 *x g* to precipitate the insolubilized material and the supernatant was directly loaded on the gel.

RESUSPENSION SOLUTION	
10 X RUNNING BUFFER	1 X
Glycerol	10 %
Milli-Q water	Up to the final volume

1 ml of SOLUBILIZATION SOLUTION	
10 X RUNNING BUFFER	1 X
Glycerol	10 %
β-DM	4%
Milli-Q water	Up to the final volume

5.6.9 Deriphat-PAGE

(Ferguson et al. 1991; Peter et al. 1991)

To analyse the presence and the quantity of the native supercomplex in the thylakoids, it was performed a Deriphat-PAGE analysis by a non-denaturing protein gel. The running gel was prepared pouring two solutions (Light and Heavy) to form a gradient of acrylamide from 4 to 12% and one of glycerol from 6.5 to 12.5%. The stacking gel has, instead, a 3.5% acrylammide concentration and a 6.5% of glycerol. The samples, prepared as in 5.6.8, were loaded and the gel was run at 4°C overnight.

RUNNING GEL

Acrylamide 32:1 (32% acrylamide; 1% bis-acrylamide)	From 4 to 12 % (w/v)
Glycerol	From 6.5 to 12.5% (w/v)
10 X 120 mM Tris, 480 mM Glycine pH 8.5	1 X
TEMED	0.047% (v/v)
APS	0.0016% (w/v)
Milli-Q water	Up to the final volume

STACKING GEL

Acrylamide 32:1 (32 % acrylamide; 1% bis-acrylamide)	3.5 % (w/v)
Glycerol	6.5 % (w/v)
10 X 120 mM Tris, 480 mM Glycine pH 8.5	1 X
TEMED	0.047% (v/v)
APS	0.0016% (w/v)
Milli-Q water	Up to the final volume

INFERIOR RUNNING BUFFER 10X

Tris-HCl pH 8.5	120 mM
Glycine	960 mM
Milli-Q water	Up to the final volume

SUPERIOR RUNNING BUFFER 10 X

Tris-HCl pH 8.3	120 mM
Glycine	960 mM
Deriphat-160	1% (w/v)
Milli-Q water	Up to the final volume

5.6.10 Protein extraction from *Chlamydomonas* cells

Protein extraction from *Chlamydomonas* was performed by harvesting cells that reached the plateau in their growth curve (1-3 $*10^7$ cell/ ml). Cell were pelleted at 2000 x g for 5' and resuspended in an appropriate cell or chlorophyll concentration, depending on the experimental purpose, and 1.5 volume of LB tricine gel (see 5.6.5). The sample was left to shake in this solution overnight. Before to charge the electrophoresis gel, the sample was spun down for 10' at 21000 x g and the supernatant was collected.

5.6.11 Western Blot analysis

To check the presence and the relative quantity of a protein in the mutants strain it was performed a western blot analysis, using specific antibody against proteins of interest (Burnette 1981). Once resolved proteins by SDS-PAGE electrophoresis these were transferred from the gel to a nitrocellulose matrix that binds them (Towbin et al. 1979). The membrane was equilibrated in the transfer buffer before this procedure. The gel and the membrane were left in contact in a chamber full of transfer buffer for 1 h in an electric field with a current of 100 V. The gel and the membrane were put between two layers of filter paper and sponge. The gel was posed towards the negative sites of the transfer chamber, while the membrane towards the positive one. The system was kept frozen by ice. After this period, to check the success of the procedure a Red Ponceau solution was poured on the membrane to see the bound proteins. The stain was washed away by Milli-Q water. The membrane was then left overnight at 4°C in a Blocking Solution containing milk proteins that blocks all the unspecific protein binding sites which could cause false positive results. Then the membrane was left 3h in the primary antibody diluted in the blocking solution. Then it was washed by simple Blocking Solution to remove the excess of the antibody and it was left 2 h in the secondary antibody diluted 1:30000. Then after two washes by the Blocking solution and the last one by the PBS 1X solution the membrane was developed. The secondary antibody was conjugated with the alkaline phosphatase and the developing solution for this molecule was composed by NBT and BCIP. This substrate was converted by the phosphatase in a blue insoluble compound. The reaction was stopped at the desired intensity by water with a drop of hydrocloric acid.

TRANSFER BUFFER

Tris pH 8.3	20 mM
Glycine	152 mM
Methanol	20%
Milli-Q water	Up to the final volume

BLOCKING SOLUTION

Milk powder	5 g/l
PBS 10X pH 7.2	1 X
Tween-20	0.2%
Milli-Q water	Up to the final volume

PBS 10X pH 7.2

NaCl	1.37 M
KCl	27 mM
KH_2PO_4	15 mM
Na_2HPO_4	81 mM
Milli-Q water	Up to the final volume

DEVELOPING SOLUTION

Tris-HCl pH 9.5	100 mM
NaCl	100 mM
$MgCl_2$	5 mM
NBT	0.33 g/l
BCIP	0.15 g/l
Milli-Q water	Up to the final volume

5.6.12 List of used primary antibodies

ANTIBODY	ANIMAL OF ORIGIN
AbCpFTSY (from Professor Anastasios Melis)	Rabbit
AbPsaA (Agrisera AS06-172-100)	Rabbit
AbCP47 (Homemade)	Rabbit
AbLHCII (Homemade)	Rabbit
AbCytF (Agrisera AS06-119)	Rabbit

AbRuBisCO (homemade)	Rabbit

5.6.13 PSII functional antenna size measurement

Relative PSII antenna size has been estimated from Fm (maximal fluorescence) saturation kinetic ($1/t_{2/3}$) in the presence of DCMU 10^{-5} M (Cardol et al. 2008). The kinetic was measured with a home-built apparatus. Fluorescence was excited using a green LED with a peak emission at 520 nm (intensity 20 µmol/s/m^2) and detected in the near infrared.

REFERENCES

Angstenberger M, de Signori F, Vecchi V, Dall'Osto L, Bassi R (2020) Cell Synchronization Enhances Nuclear Transformation and Genome Editing via Cas9 Enabling Homologous Recombination in Chlamydomonas reinhardtii. ACS Synth Biol. doi: 10.1021/acssynbio.0c00390

Bae S, Park J, Kim JS (2014) Cas-OFFinder: a fast and versatile algorithm that searches for potential off-target sites of Cas9 RNA-guided endonucleases. Bioinformatics 30:1473–1475 . https://doi.org/10.1093/bioinformatics/btu048

Ball EH (1986) Quantitation of proteins by elution of Coomassie brilliant blue R from stained bands after sodium dodecyl sulfate-polyacrylamide gel electrophoresis. Anal Biochem 155:23–27. doi: https://doi.org/10.1016/0003-2697(86)90218-6

Berthold P, Schmitt R, Mages W (2003) An Engineered Streptomyces hygroscopicus aph 7''Gene Mediates Dominant Resistance against Hygromycin B in Chlamydomonas reinhardtii. Protist 153:401–412. doi: 10.1078/14344610260450136

Burnette WN (1981) "Western Blotting": Electrophoretic transfer of proteins from sodium dodecyl sulfate-polyacrylamide gels to unmodified nitrocellulose and radiographic detection with antibody and radioiodinated protein A. Anal Biochem 112:195–203. doi: https://doi.org/10.1016/0003-2697(81)90281-5

Cardol P, Bailleul B, Rappaport F, Derelle E, Béal D, Breyton C, Bailey S, Wollman FA, Grossman A, Moreau H, Finazzi G (2008) An original adaptation of photosynthesis in the marine green alga Ostreococcus. Proc Natl Acad Sci U S A 105:7881–7886. doi: 10.1073/pnas.0802762105

Croce R, Canino G, Ros F, Bassi R (2002) Chromophore Organization in the Higher-Plant Photosystem II Antenna Protein CP26. Biochemistry 41:7334–7343. doi: 10.1021/bi0257437

Ferguson L, Halloran E, Hawthornthwaite AM, Cogdel R, Kerfeld C, Peter GF, Thornber JP (1991) The use of non-denaturing Deriphat-polyacrylamide gel electrophoresis to fractionate pigment-protein complexes of purple bacteria. Photosynth Res 30:139–143. doi: 10.1007/BF00042012

Harris EH, Stern DB, Witman GB (1989) The chlamydomonas sourcebook. Academic Press San Diego

Kropat J, Hong-Hermesdorf A, Casero D, Ent P, Castruita M, Pellegrini M, Merchant SS, Malasarn D (2011) A revised mineral nutrient supplement increases biomass and growth rate in Chlamydomonas reinhardtii. Plant J 66:770–780. doi: 10.1111/j.1365-313X.2011.04537.x

Lauersen KJ, Wichmann J, Baier T, Kampranis SC, Pateraki I, Møller BL, Kruse O (2018) Phototrophic production of heterologous diterpenoids and a hydroxy-functionalized derivative from Chlamydomonas reinhardtii. Metab Eng 49:116–127. doi: https://doi.org/10.1016/j.ymben.2018.07.005

Ordon J, Gantner J, Kemna J, Schwalgun L, Reschke M, Streubel J, Boch J, Stuttmann J (2017) Generation of chromosomal deletions in dicotyledonous plants employing a user-friendly genome editing toolkit. Plant J 89:155–168. doi: 10.1111/tpj.13319

Park J, Bae S, Kim JS (2015) Cas-Designer: a web-based tool for choice of CRISPR-Cas9 target sites. Bioinformatics 31:4014–4016 . https://doi.org/10.1093/bioinformatics/btv537

Peter GF, Takeuchi T, Philip Thornber J (1991) Solubilization and two-dimensional electrophoretic procedures for studying the organization and composition of photosynthetic membrane polypeptides. Methods 3:115–124. doi: https://doi.org/10.1016/S1046-2023(05)80203-8

Porra RJ, Thompson WA, Kriedemann PE (1989) Determination of accurate extinction coefficients and simultaneous equations for assaying chlorophylls a and b extracted with four different

solvents: verification of the concentration of chlorophyll standards by atomic absorption spectroscopy. Biochim Biophys Acta - Bioenerg 975:384–394. doi: https://doi.org/10.1016/S0005-2728(89)80347-0

Schägger H, von Jagow G (1987) Tricine-sodium dodecyl sulfate-polyacrylamide gel electrophoresis for the separation of proteins in the range from 1 to 100 kDa. Anal Biochem 166:368–379. doi: https://doi.org/10.1016/0003-2697(87)90587-2

Towbin H, Staehelin T, Gordon J (1979) Electrophoretic transfer of proteins from polyacrylamide gels to nitrocellulose sheets: procedure and some applications. Proc Natl Acad Sci U S A 76:4350–4354. doi: 10.1073/pnas.76.9.4350

CHAPTER 6
Results

6.1 *as 2.1* growth curve

The random insertional mutant *as2.*1, isolated in the laboratory, showed a higher growth rate compared to his wild type cw15 and has a rearrangement in the region containing CpFTSY encoding gene. It was grown in a multicultivator system in HS minimal medium, to see the effects of the photoautotrophic growth, at 1000 µE starting from a concentration of $1*10^5$ cell/ml. The growth curve was obtained measuring the optical density (OD) at 720 nm as at this intensity the chlorophyll doesn't absorb, and it is possible to distinguish the specific signal of the cells. *as2.1* grew faster than the wild type in high light and was more resistant in photoautotrophy.
This feature was attributed to their pale-green cell phenotype due to the lack of *CpFTSY*.

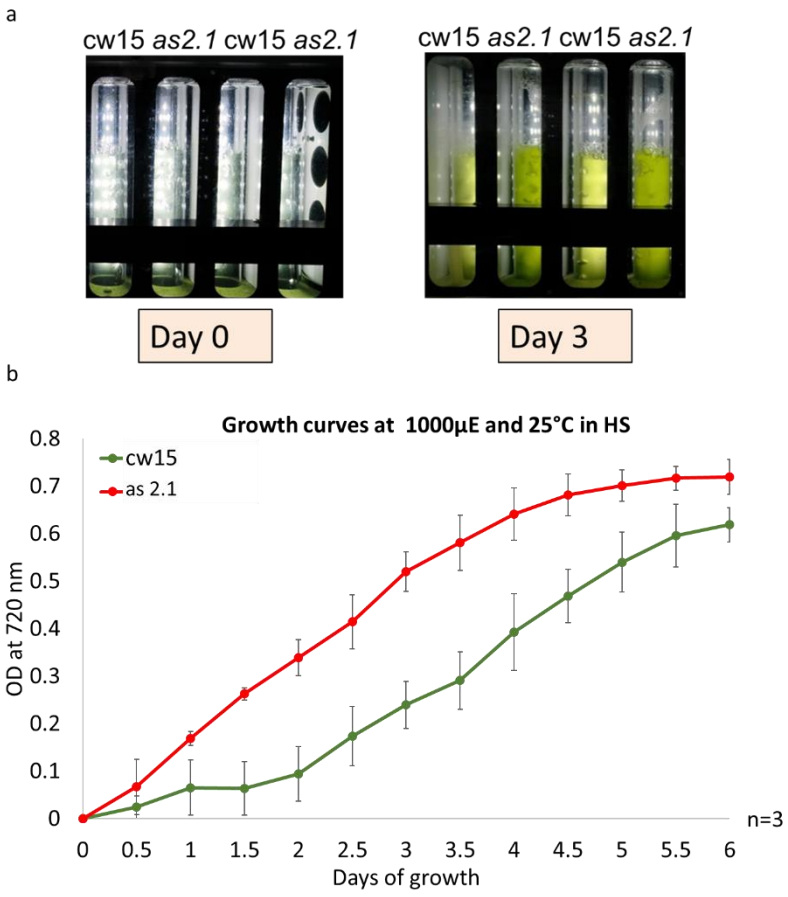

Figure 6.1. Comparison between the growth of *as2.1* and cw15 in minimal medium (HS) with high light conditions (1000µE). a) picture of the multicultivator system tubes at day 0 and after 3 days growth. b) Growth curve obtained from three biological replicates measuring the OD a 720 nm. The growth was performed at 25°C and 1000 µE in HS minimal medium. Points represent the average of the measurements obtained every half day for three biological replicates and the thin black bars show the standard deviation.

6.2 CpFTSY genome-edited mutants production

In order to understand if the mutated *CpFTSY* gene was the reason for the high growth and low pigment phenotype of *as2.1*, it was decided to use the CRISPR-Cas9 system to target this gene directly and compare the phenotype obtained. The CRISPR-Cas9 technique in *Chlamydomonas* was firstly optimized starting from different protocols, (Baek et al. 2016; Ferenczi et al. 2017; Shin et al. 2019) that all required the direct electroporation of the Cas9 protein and the sgRNA into the nucleus of the cells (see 3.6.2). For this purpose, a commercial Cas9 was purchased, the Alt-R® *S.p.* Cas9 Nuclease (IDT), while the sgRNA was synthetized *in vitro*, by transcription of DNA templates. These were produced amplifying the conserved sgRNA sequence from the plasmid pDGE5 (Ordon et al. 2017) and adding to the forward primer the sequence of the protospacer which was selected from the paper of Baek and collaborators (Baek et al. 2016). After the first amplification, a second amplification was performed in order to add the promoter for the T7polymerase which was required for the *in vitro* transcription (figure 6.2.1 a and b).
After the *in vitro* transcription, an *in vitro* cut assay was performed to assess if the complex formed by the Cas9 and the sgRNA worked properly. For this reason, a fragment of the gene including the target sequence, that should be cut *in vivo,* was amplified. The fragment was then incubated with the ribonucleoprotein complex. The result of the reaction with the RNP-complex was that the 555 bp DNA fragment was cut into two fragments of 318 and 237 bp, while in the control reactions, without one or more components, only the signals due to the single components were visible (fig 6.2.1 c).

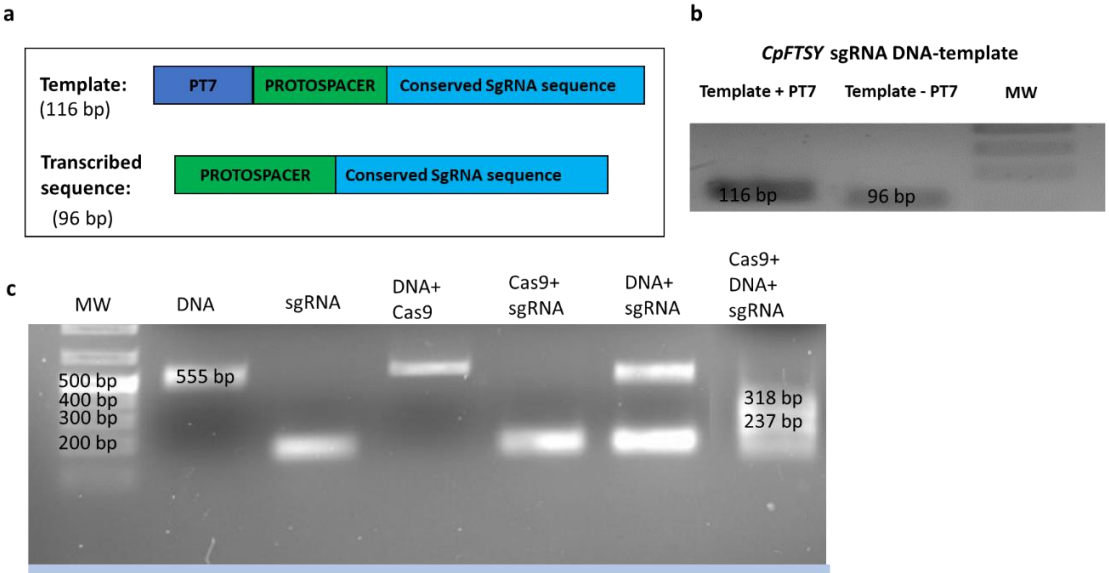

Cas9	No	No	600 ng	600 ng	No	600 ng
sgRNA	No	500 ng	No	500 ng	500 ng	500 ng
DNA *(CpFTSY)*	100 ng	No	100 ng	No	100 ng	100 ng

Figure 6.2.1. DNA template synthesis for *CpFTSY* sgRNA and *in vitro* cut assay. a) Template and transcribed sequence composition schemes. b) PCR products from the two DNA amplification rounds. The template –T7 is the product composed of the protospacer and the conserved sgRNA sequence, the template + T7 is the complete product including PT7 promoter. The products were run on 1.5% agarose gel. MW: molecular weight marker c) *In vitro* cut assay. The cut reaction products and the different controls were checked on a 1.5% agarose gel. The sgRNA alone gave a signal of approximately 100 bp. The test fragment is 555 bp long, while

after incubation with both the sgRNA and Cas9 protein two fragments of 237 and 318 bp were obtained. MW: molecular weight marker.

Once the correct functioning of the ribonucleoprotein complex was assessed, the next step was the transformation of the *Chlamydomonas reinhardtii* cell-wall weakened strain cw15 by electroporation. In addition to the RNP complex, a hygromycin resistance cassette was also introduced, in order to increase the screening and the gene disruption efficiency. As it was previously published that a resistance cassette had a higher probability to be inserted in the region near the cut site, than in any other region of the genome (Shin et al. 2019). The transformed cells were then plated on TAP plates with 50 µg/ml of hygromycin and 30% starch which was required to help the cell-wall weakened cells recover. After 7-10 days the first colonies were visible. Out of over four-hundred colonies two pale green colonies were obtained giving an editing efficiency of 0.5%, which was as expected from the previous work of Baek and collaborators (Baek et al. 2016). The two pale green colonies were selected and inoculated in liquid TAP medium for further analysis (Fig.6.2.2). First, genomic DNA was extracted from these cultures and the fragment containing the target was amplified by PCR, as this reaction worked for the WT genomic DNA, but not for the pale strains, it was hypothesized that the insertion of the resistance cassette made the fragment difficult to amplify due to its increased length. For this reason, another PCR reaction was performed using different pairs of primers, one annealing within the gene and a one within the cassette (figure 6.2.2b). Both mutants were positive for the insertion of the cassette in the target region, this was confirmed by sequencing analysis of the amplified fragments. In *cpftsy#1* the insertion was immediately before target sequence, while in *cpftsy#2* it was after the target, with a small insertion of random bases, probably due to mistakes in the DNA repair mechanism (figure 6.2.2c).

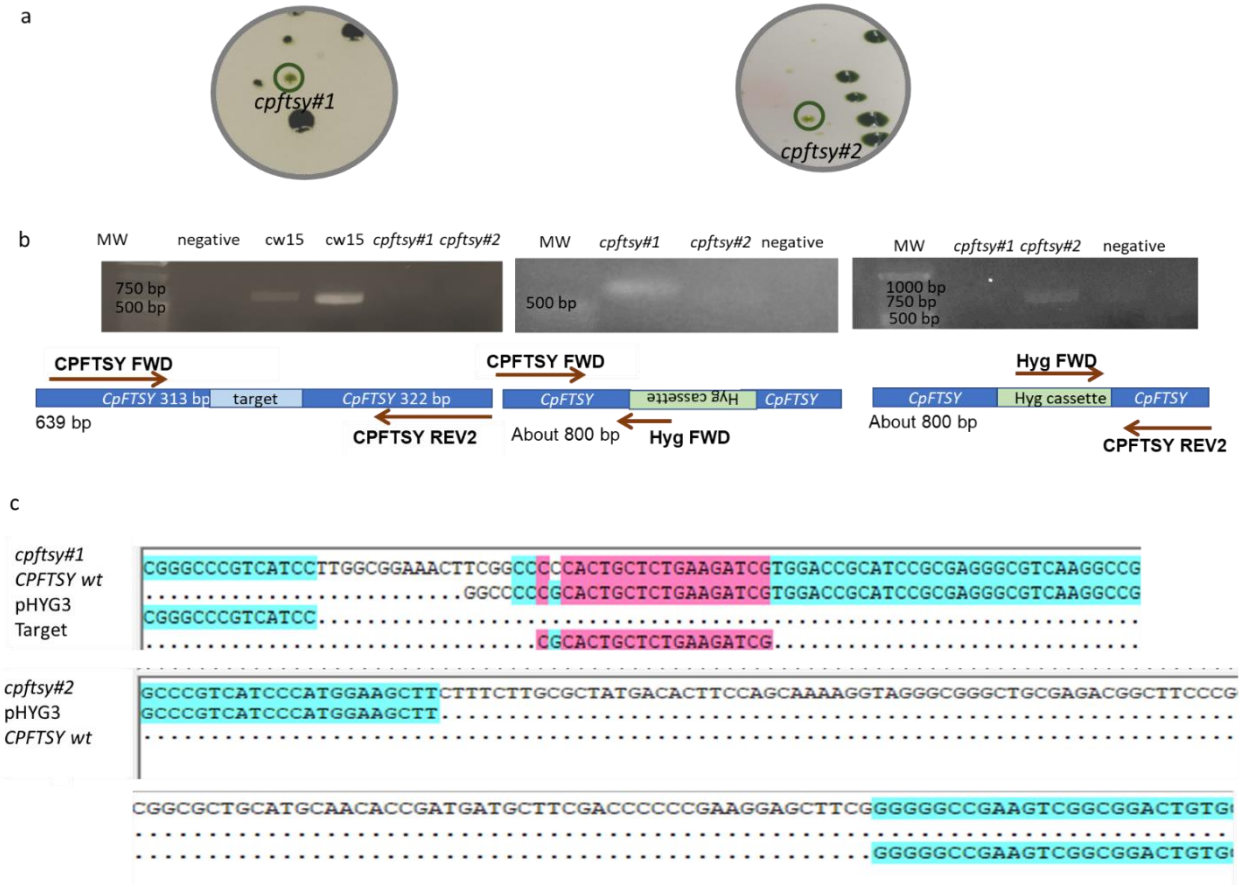

Figure 6.2.2. Phenotype and genomic screening of the *cpftsy* mutants. a) plates pictures. b) PCR analysis of the target region and schematic representations of the amplified fragments. The WT fragment of 639 bp was obtained only in cw15 WT strain, the *cpftsy#1* strain presented an inverted insertion of the pHYG3 cassette, while the cpftsy#2 a straight one. c) portion of fragment sequences of *cpftsy#1* and *cpftsy#2*. In *cpftsy#1* the insertion is immediately before target sequence, while in *cpftsy#2* it is after the target sequence, with a small insertion of random bases, probably due to mistakes in the repair mechanism. Blue colour indicates when only two sequences matched, pink indicates when more sequences matched.

6.3 Comparison between genome edited *cpftsy* mutants and *as2.1*

To understand the role of *CpFTSY* gene in the phenotype of the *as2.1* mutant, the obtained genome edited *cpftsy* mutants were compared to the *as2.1* mutant. First the growth of the mutants and the wild type strains were compared in high light in the multicultivator system. Starting from a concentration of $2*10^5$ cell/ml. In HS minimal medium (to see only the autotrophic growth) at 1000 µE the *as2.1* mutant started to growth earlier in respect to the cw15, reaching a plateau after four days, while the genome edited *cpftsy* mutants little to no grew.

a

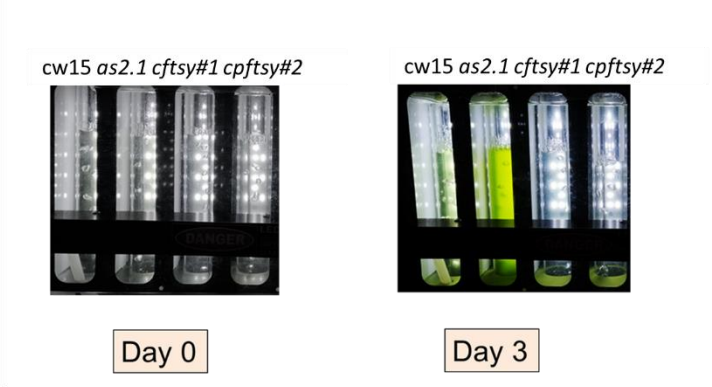

b

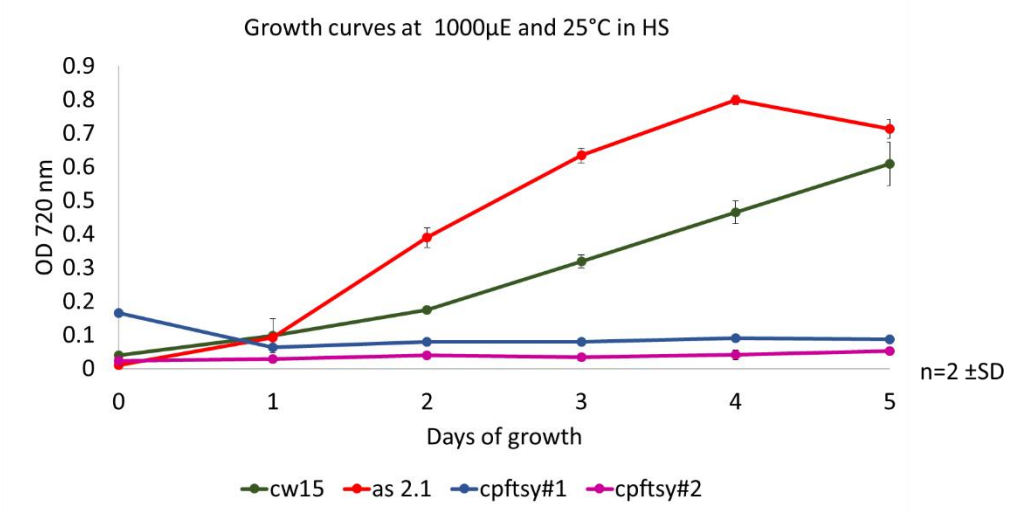

Figure 6.3.1. Comparison between the growth of *as2.1*, *cpftsy#1*, *cpftsy#2* and cw15 in minimal medium (HS) and high light conditions (1000µE): a) pictures of the multicultivator system tubes at day 0 and day 3. b) Growth curve obtained from two biological replicates measuring the OD a 720 nm. The growth was performed at 25°C and 1000 µE in HS minimal medium. Points represents the average of the measurements obtained every day for two biological replicates and the thin black bars the standard deviation.

Mutants in antenna composition can also be characterized by measuring their pigment content by absorption spectra, in particular, Chl *a* versus Chl *b* content and/or Chl versus Cars (carotenoids) content. Chl *b* is, indeed, typical of the antenna complexes, and it is a good indicator of the loss of antennae. Antenna proteins also bind some xanthophylls, for this reason a defect in antenna complexes, could also cause a decrease in carotenoid content.
Then cw15 WT strain, *as2.1* and the two genome edited mutants were grown in liquid culture and their pigments were extracted using 85% acetone. The spectral measurement (6.3.2 a) displayed a large difference between *as2.1* and the genome edited strains. Comparing the *as2.1* and the cw15, the only visible difference is in the region between 450 and 480 nm, in which most of absorption is due to the carotenoids and Chl *b*. Instead of the peak shoulder present in the WT, a small concavity is present in the mutants. In comparison the two genome edited strains had, instead, a stronger phenotype, with a lower signal in the Chl *b* specific region around 646 nm and an higher Chl *a* and carotenoid absorption peak in the region between 420 and 480 nm, with an even larger concavity in the Chl *b* absorption in the region between 450 and 480. From the spectra the chlorophyll content

per cell was derived by Porra formulas (Porra et al. 1989). The averages of the three biological replicates of each mutant were compared with the values obtained from the wild type and the significance of the difference was calculated by t-test analysis (figure 6.3.2 b). The *as2.1* had a significantly lower chlorophyll content in respect to the WT (45% less), but the *cpftsy#1* and *cpftsy#2* mutants displayed even greater differences, with a chlorophyll content that is the 15% and the 22% of the wild type, respectively.
The chlorophyll *a*/*b* ratio was also calculated and corrected through fitting analysis of the absorption spectrum (Croce et al. 2002). *as2.1* had a higher ratio (117%) compared to the wild type, but the two genome edited mutants present a more significant increase of 50% of this ratio (figure 6.3.2 c). As for the Chl/Car ratio the differences between the WT and the *as2.1* mutant were not significant, while between the *cpftsy* genome edited mutants and the cw15 large differences were found. They indeed presented a ratio that was only 43% of the wild type one, indicating a significantly higher carotenoid content (6.3.2 d).

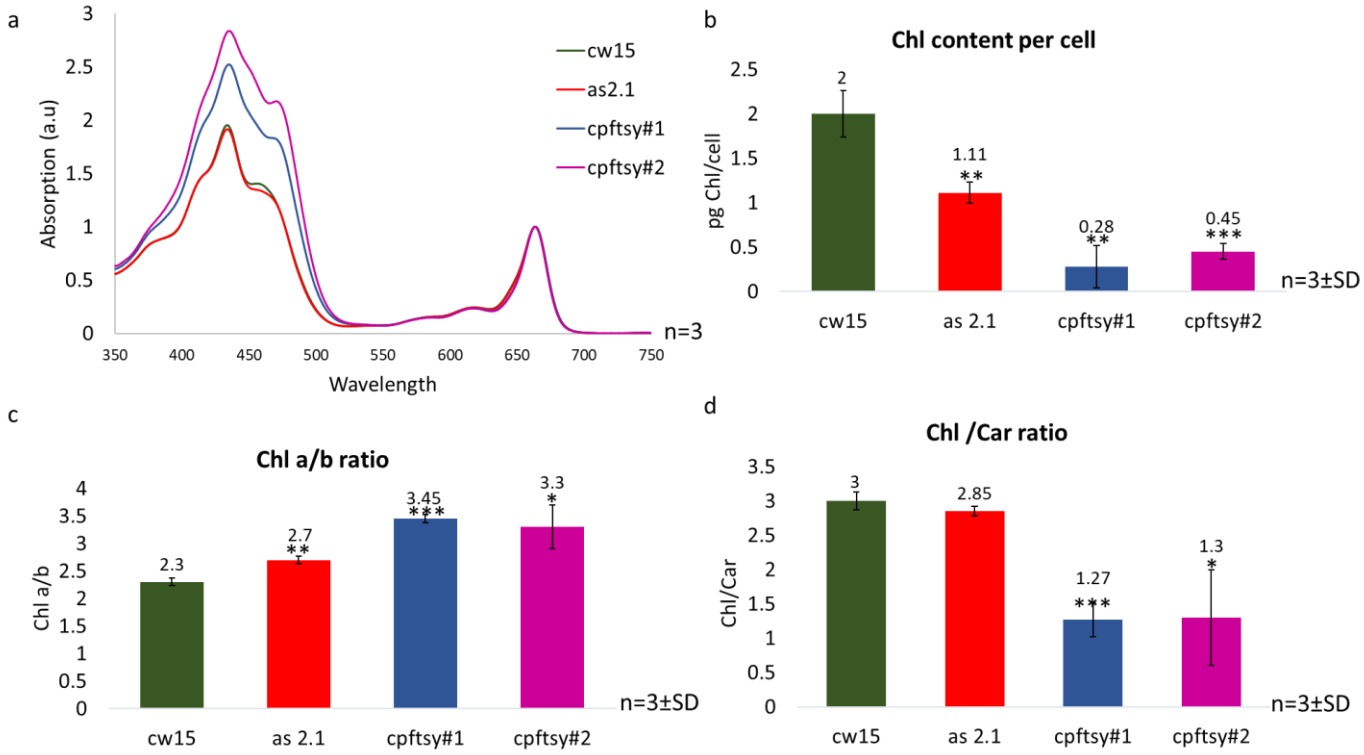

Figure 6.3.2. Absorption spectra of *as2.1*, *cpftsy#1* and *cpftsy#2* and parameters derived by their analysis: a) absorption spectra: data were normalized by set to zero and divided by the maximum absorption value. The data were obtained from three biological replicates. b) chlorophyll content per cell. c) Chl a/b ratio. d) Chl/car ratio. Bars represent the averages of three biological replicates ± standard deviation. Asterisks indicate statistically significant differences between mutant and WT according to Student's t test (*, P < 0.05; **, P < 0.01; ***, P < 0.001).

From the three mutants and the cw15 wild type strain the thylakoids were then extracted, after five days of growth in TAP rich medium and low light conditions (50µE), in order to obtain also the growth of the light sensitive genome edited strains. 25 µg of each sample of chlorophyll were loaded

on the gel to compare these differences. The *as2.1* strain displayed a higher abundance of PSII core and monomeric LHCII compared to the wild type, but a lower abundance of trimeric LHCII, almost a severe decrease in the abundances of the PSII core, PSI-LHCI and PSII-LHCII complexes. The *cpftsy#1* and *cpftsy#2* mutants also displayed a stronger reduction of these complexes but with a higher presence of PSII and monomeric LHCII. This could be due to a stronger reduction in antennas content, underlined also by the lower chlorophyll content and Chl *a*/*b* ratio, respect to both wild type and *as2.1.* Interestingly the two genome edited strains showed a different abundance in trimeric LHCII, suggesting a difference in antennae composition between the two mutants.

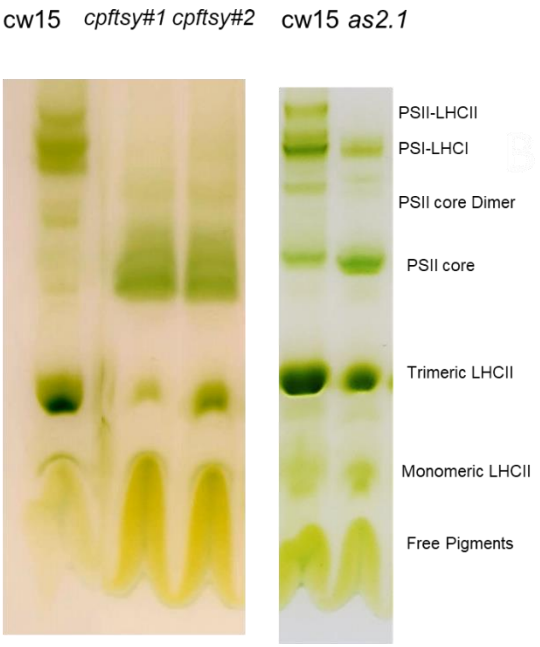

Figure 6.3.3. Non-denaturing Deriphat-PAGE analysis. The thylakoids were extracted from TAP grown cultures at 50 µE. The samples were treated by β-DM detergent. The bands correspondent to the different complexes are indicated in the figure.

6.4 Complementation *of as2.1*, *cpftsy#1* and *cpftsy#2* mutants

After observing the differences between the genome edited strains and *as2.1*, it was decided to complement them with the *CpFTSY* gene, in order to understand the specific role of this gene in the phenotype of *as2.1* and explain the two opposite growth phenotypes. A construct was designed that was composed of the coding sequence (CDS) of CpFTSY with its endogenous promoter and terminator, because the gene complete with introns was to long (fig 6.4.1 a). Anyway, it was hypothesized that the endogenous promoter and terminator should ensure a balanced regulation of gene expression, avoiding an overexpression, which was considered unhelpful for these experimental purposes. The clone was ordered as a synthetic gene from GeneScript so that it contained two new restriction sites for the cloning. The fragment was the excised form the vector pUC57 by the restriction enzymes (REs) SpeI and XbaI and subsequently ligated in the pOpt2_mRuby2_Ble plasmid,

after the excision of its promoter, the Ruby protein encoding sequence and its terminator by the same REs. After *E. coli* transformation a positive colony was selected (fig 6.4.1 d) by PCR using the primers M13 REV (binding within the plasmid) and CPFTSY UTR FWD (binding within the CpFTSY construct). The expected band is 2829 bp long, as control the pUC57_CPFTSY plasmid containing both sequences and the pOpt2_mRuby2_Ble with only the M13 sequence were used. The latter, indeed, gave only unspecific products. A positive colony was the isolated and the plasmid was extracted (pOpt2_CPFTY_Ble), then checked by a diagnostic digest and used for further applications

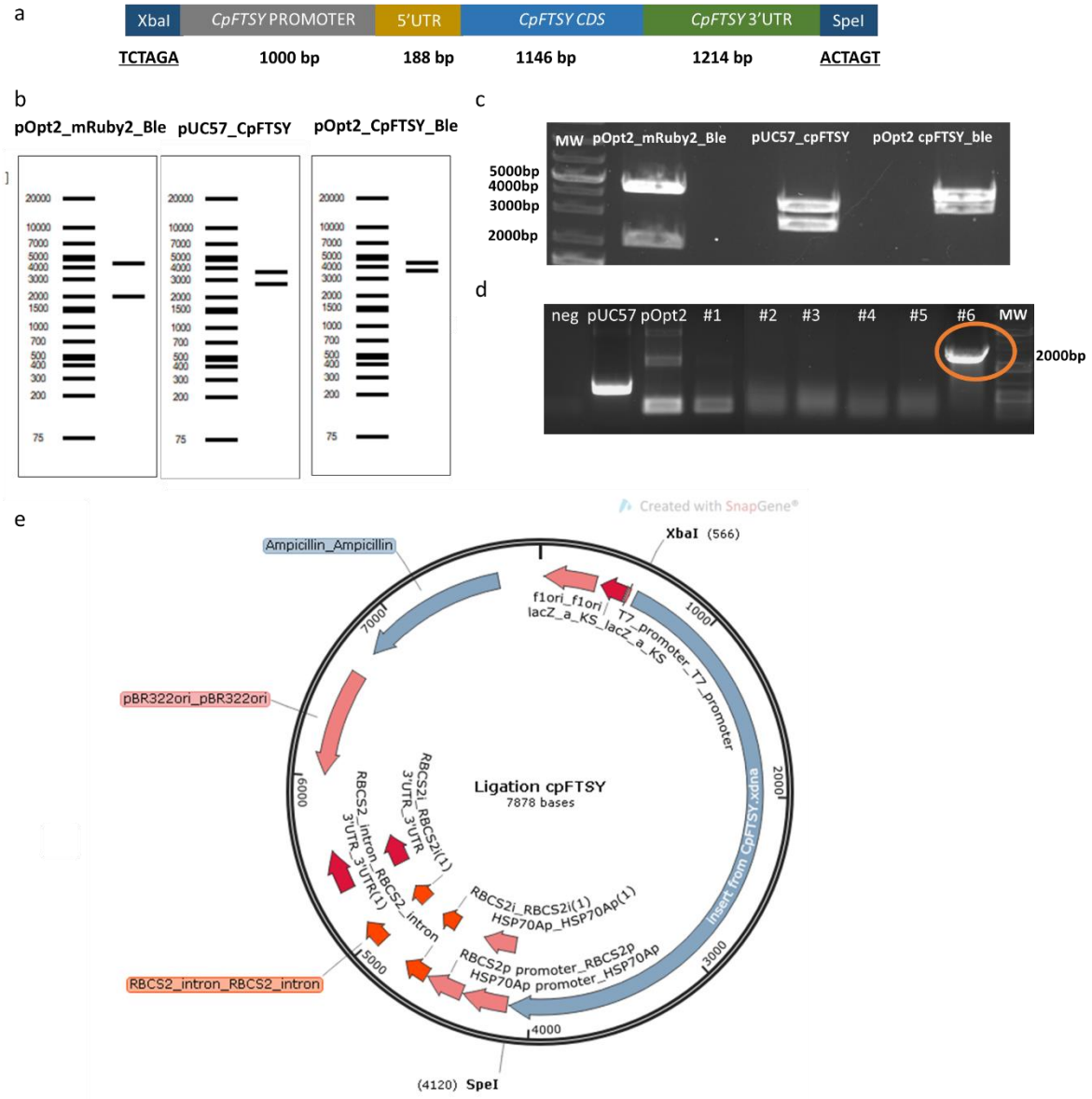

Figure 6.4.1. Cloning of *CpFTSY* gene. a) design of the construct used to complement the three mutants. It contained an XbaI restriction site, the endogenous promoter and 5'UTR of the gene, the CDS of the gene, its endogenous 3'UTR and a SpeI restriction site. b-c) Cut of the plasmids by XbaI and SpeI (c) and their predicted sizes (b). The donor vector PUC57_CpFTSY and the recipient pOpt2_mRuby2_Ble were cut by XbaI and SpeI were compared to the one obtained after the ligation (pOpt2_CpFTSY_Ble), wich was cut with the same REs to check the correct Insertion. The cut predictions were performed by the SerialCloner software. The restriction reactions were run on a 1% agarose gel. d) Colony PCR after *E. coli* transformation with the ligation product. The PCR was performed using a primer on the plasmid M13 sequence (M13 REV) and a plasmid on *CpFTSY* (CPFTSY UTR FWD). Neg is the negative control with the PCR mix without DNA; pUC57 is the positive control (pUC57_CPFTSY) that possesses sequences complementary to both primers, pOpt2 is another control with only the M13 sequence, the numbers from #1 to #6 indicate colonies isolated after the transformation with the ligation mix. The orange circle indicates the positive colony. e) Ligation product prediction. This prediction was performed by SerialCloner and visualized by SnapGene.

The Chlamydomonas strains *as2.1*, *cpftsy#1*, *cpftsy#2* and the WT cw15 were transformed with the pOpt2-CPFTSY-Ble plasmid and as a negative control the pOpt2_mRuby2_Ble empty plasmid. For cw15 as expected there was no difference between the phenotypes resulting from the two transformations. For the genome edited strains some dark green colonies from the transformation were obtained with the construct containing *CpFTSY*, while only pale colonies were obtained from the empty plasmid (figure 6.4.2). For *as2.1* the screening was harder, due to its less pale phenotype and its tendency to form aggregated colonies, composed of multiple cells, that make selection difficult. For this strain the selection of the transformant colonies was ultimately performed by PCR and absorption spectra analysis.

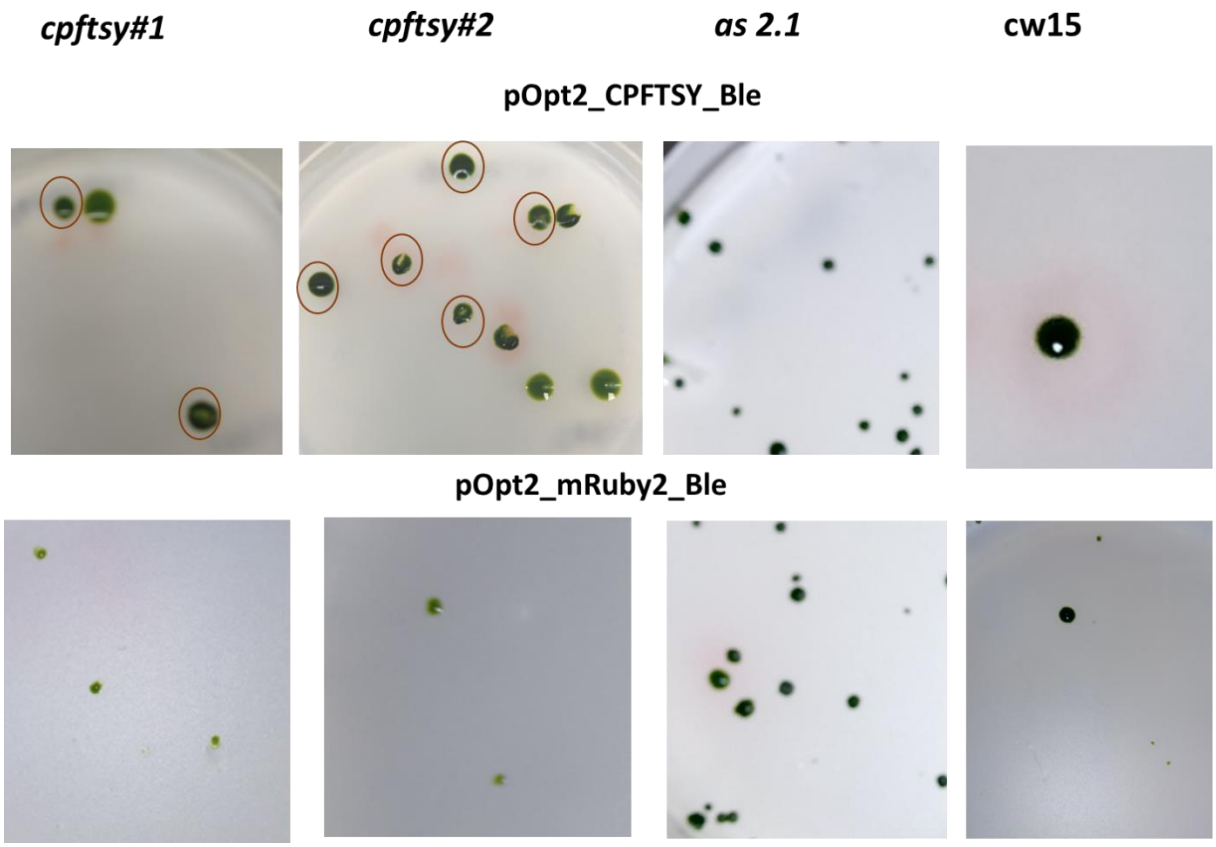

Figure 6.4.2. Chlamydomonas *CpFTSY* transformation results. The four transformed strains are indicated in the upper part of the picture, In the first line there are the pictures of the colonies resulted from the transformation by the plasmid containing *CpFTSY* (pOpt2_CPFTSY_Ble), while in the second line there are the pictures of the control transformation by pOpt2_mRuby2_Ble empty vector. The dark colonies obtained by the complementation of *cpftsy#*1 and*# 2* were underlined by red circles.

To confirm the presence of *CpFTSY* in the dark colonies PCR analysis was performed on their genomic DNA with a primer pair which was complementary to different exons of *CpFTSY* gene (CPFTSY synt FWD and CPFTSY synt REV) that gave different products for the endogenous and exogenous copies. A specific elongation time was selected to only amplify the exogenous copy, which had to be 849 bp long, since

the endogenous copy had to be 4427 bp long due to the presence of introns. As expected, no products resulted from the cw15 and mutant parental strains, while the complemented colonies presented the band. The *as 2.1* parental strain presented some unspecific products, maybe due the gene rearrangement (Figure 6.4.3 b). Two colonies for each of the complemented strains were selected and inoculated in TAP medium to extract proteins for Western Blot analysis by the CpFTSY antibody (Kirst et al. 2012) to confirm the protein expression (figure 6.4.3 c). 1.5 µg of chlorophyll were loaded for each sample. Extracts from both transformed (cw15+ftsy) and untransformed cw15 were used as controls. All the selected complemented colonies presented the 40 kDa band correspondent to the protein, while the parental mutant strains didn't show it.

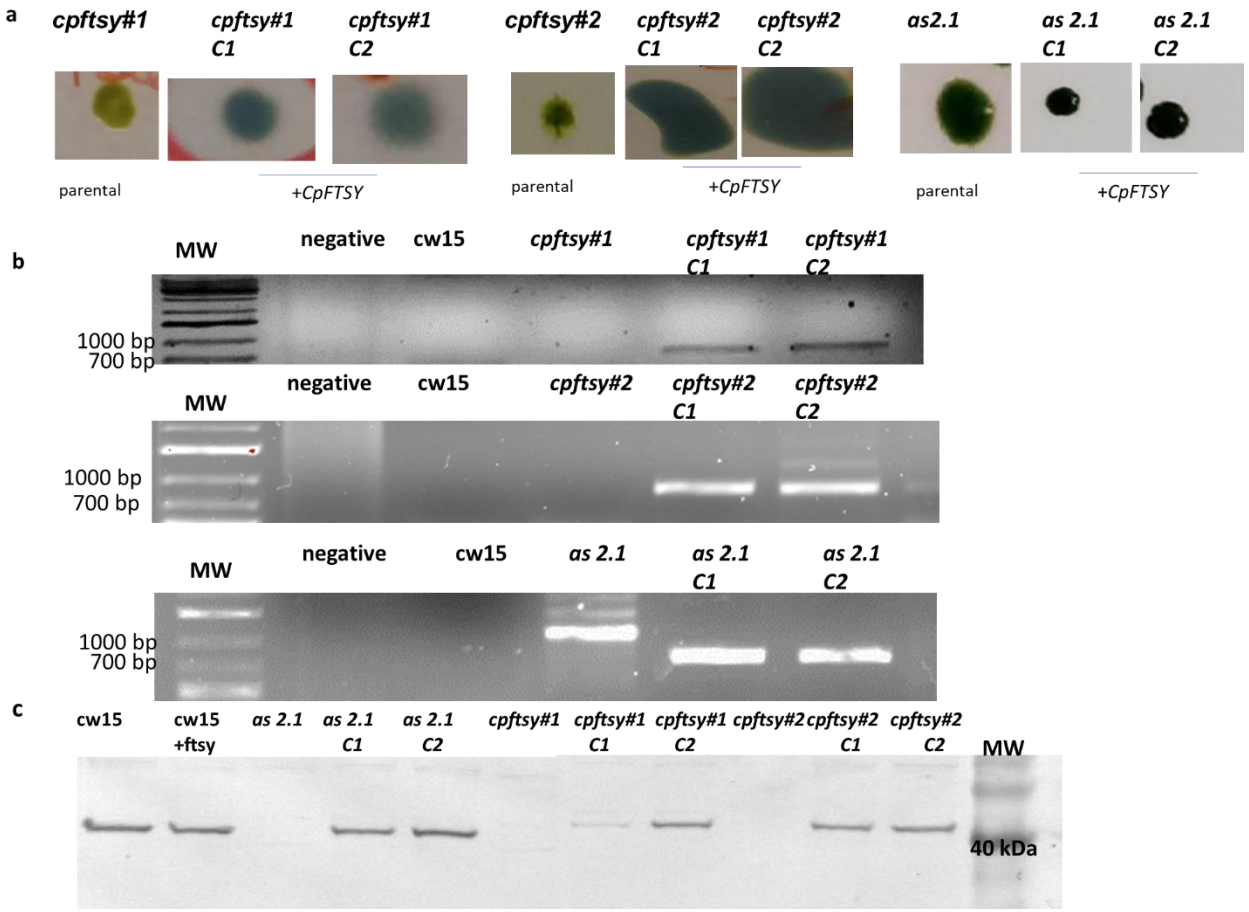

Figure 6.4.3. Complemented strains screening. a) Pictures of the selected dark complemented colonies and their parental strain. b) PCR analysis on the selected dark complemented colonies (*cpftsy#1C1*, *cpftsy#1C2*, *cpftsy#2C1*, *cpftsy#2C2*, *as2.1C1, as2.1C2*) and their parental strains. It was used a negative control(negative), and a wild type control (cw15). The primer used were CPFTSY synt FWD and CPFTSY synt REV. The expected product length was 849 bp. MW: molecular weight marker. c) Western Blot analysis by the antibody against CpFTSY. A quantity of protein extracts, correspondent to 1.5 µg of chlorophyll, was run on 15% tricine gel. The expected band size was 40 kDa. MW: molecular weight marker. C1: complemented strain number one; C2: complemented strains number two.

The absorption spectra of the complemented strains and their parental strains were obtained, after a growth in TAP medium at 50 µE, and compared (figure 6.4.4). All the complemented strains, including the control cw15 transformed with the *CpFTSY* construct showed spectra similar to wild type. In particular, the difference in the region between 450 and 480 nm, mostly due to the carotenoids and the Chl *b*, were non-significant and they lost the lower signal at 646 nm, indicating an increase of Chl *b* content compared to their parental mutant strains. Moreover, the complemented *cpftsy#1* and *#2* strains lost the higher Chl *a* and carotenoids absorption peak in the region between 420 and 480 nm (figure 6.4.4).

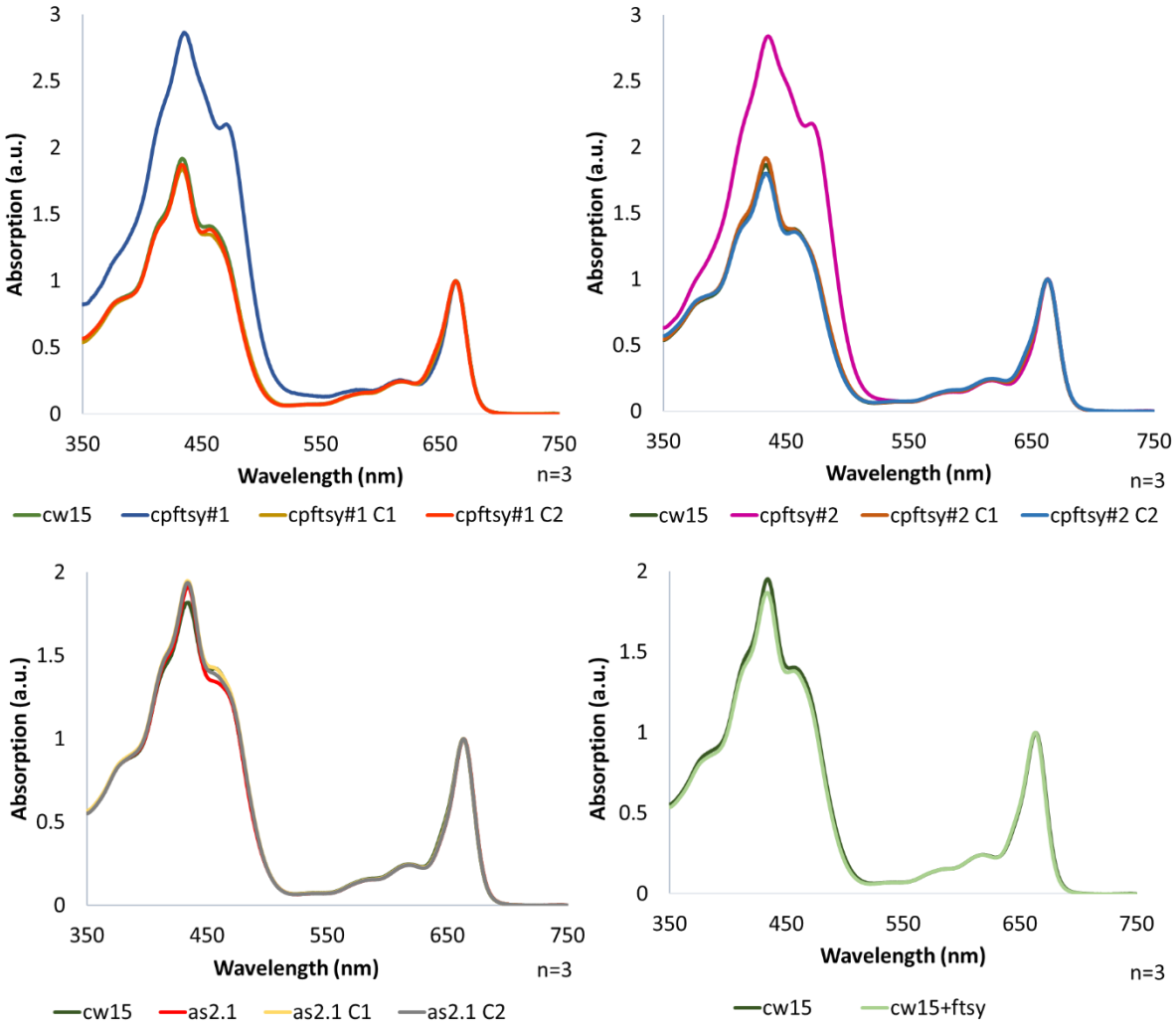

Figure 6.4.4. Absorption spectra of *as2.1*, *cpftsy#1* and *cpftsy#2* mutants compared to their corresponding complemented strains (*cpftsy#1C1, cpftsy#1C2, cpftsy#2C1, cpftsy#2C2, as2.1C1, as2.1C2*) and the WT cw15. To better compare the spectra each mutant and its corresponding complemented strains are presented separately, in comparison with the cw15 WT. As control the cw15 strain transformed by the *CpFTSY* complementation construct (cw15+ ftsy) was used. Data were normalized by set to zero and divide for the maximum absorbance

value. These data were obtained by three biological replicates. C1: complemented strain number one; C2: complemented strains number two.

From the spectra measurement the values of the total chlorophyll content per cell, of the Chl *a* versus Chl *b* content and of the Chl versus Car content were then extrapolated. In the two *as 2.1 C1* and *as2.1 C2* complemented strains there was only a faint increase in chlorophyll content per cell and the difference with the cw15 remained statistically significant, on the contrary there was a lowering in Chl *a*/*b* ratio to value similar to the wild type (figure 6.4.5). For *cpftsy#1 C1* and *cpftsy#1 C2* strains there was a significant increase in chlorophyll content. The *C1* strain reached 1.63 pg of chlorophyll per cell which is still considered statistically different from the WT one, while the *C2* reached a WT level of this pigment (figure 6.4.5). Both of these strains displayed a level similar to the wild type for the Chl *a*/*b* ratio. The same happened to the *cpftsy#2 C1* and *C2* strains and both these strains represented a WT level of chlorophyll. As for Chl/Car ratio the *as2.1* derived strains didn't show any significant differences compared to both WT and their parental strains. It is instead interest to note that the *cpftsy#1 C2* and *cpftsy#2 C2* strains presented a higher ratio compared to the wild type (figure 6.4.5b).

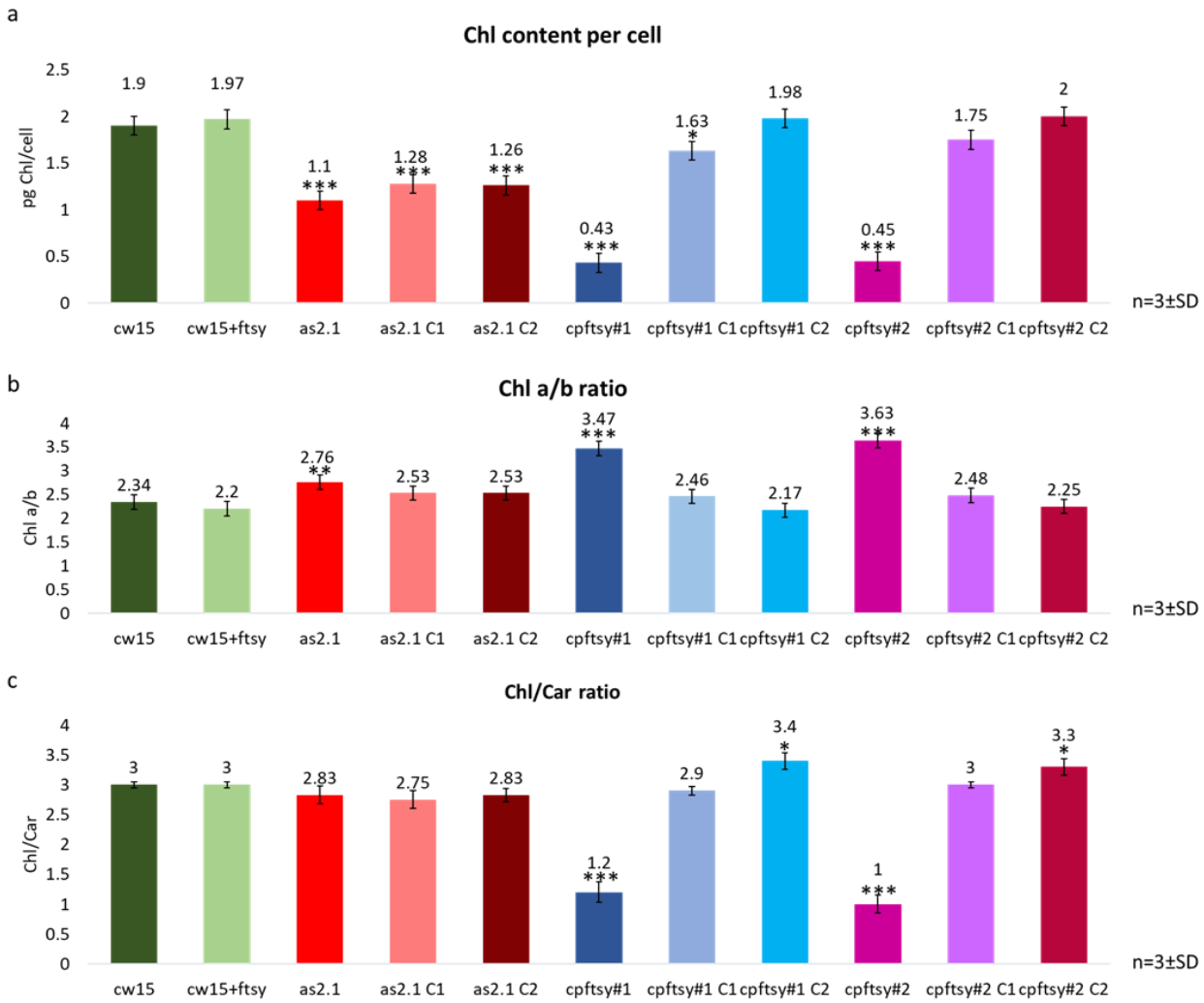

Figure 6.4.5. Photosynthetic parameters derived by absorption spectra analysis. a) chlorophyll content per cell. b) Chl a/b ratio. c) Chl/Car ratio. Bars represent average of three biological replicates ± standard deviation. These data were obtained by three biological replicates. C1: complemented strain number one; C2: complemented strains number two. Asterisks indicate statistically significant differences between mutant and WT according to

Student's t test (*, P < 0.05; **, P < 0.01; ***, P < 0.001).

To monitor the effect of the complementation on the growth each parental strain was compared with the corresponding better complemented mutant. All the strains, including the WT and the transformed cw15 as controls, were grown for five days in the multicultivator system at 1000 µE and 25°C in HS minimal medium to test their light resistance. A concentration of $2*10^5$ cell/ml was inoculated in each tube and the growth was monitored by reading the OD at 720 nm (figure 6.4.6a and b). Moreover, at the end of the growth the dry weight was measured (figure 6.4.6 c). As observed before the *as 2.1* grew faster than the wild type and reached the plateau after three and half days. The *cpftsy* genome edited mutant were instead unable to grow, while all the complemented strains had growth trends similar to the WT, with differences manly due to small fluctuations in the bubbling system (figure 6.4.6 b). At the end of the growth period there were no significant differences in the dry weights between *as2.1*, the cw15 and the complemented strains. This indicates that the most interesting feature of the *as2.1* mutant is the growth speed that allows to obtain the same biomass per growth of the WT in less time. This is interesting for the industrial productivity to reduce the time for obtaining a certain biomass quantity with the same costs. From the complementation data it appears that the loss of *CpFTSY* is only one of the responsible mutations for this phenotype, but is probably not the only one, other close genes, probably not annotated could participate in the determination of this phenotype.

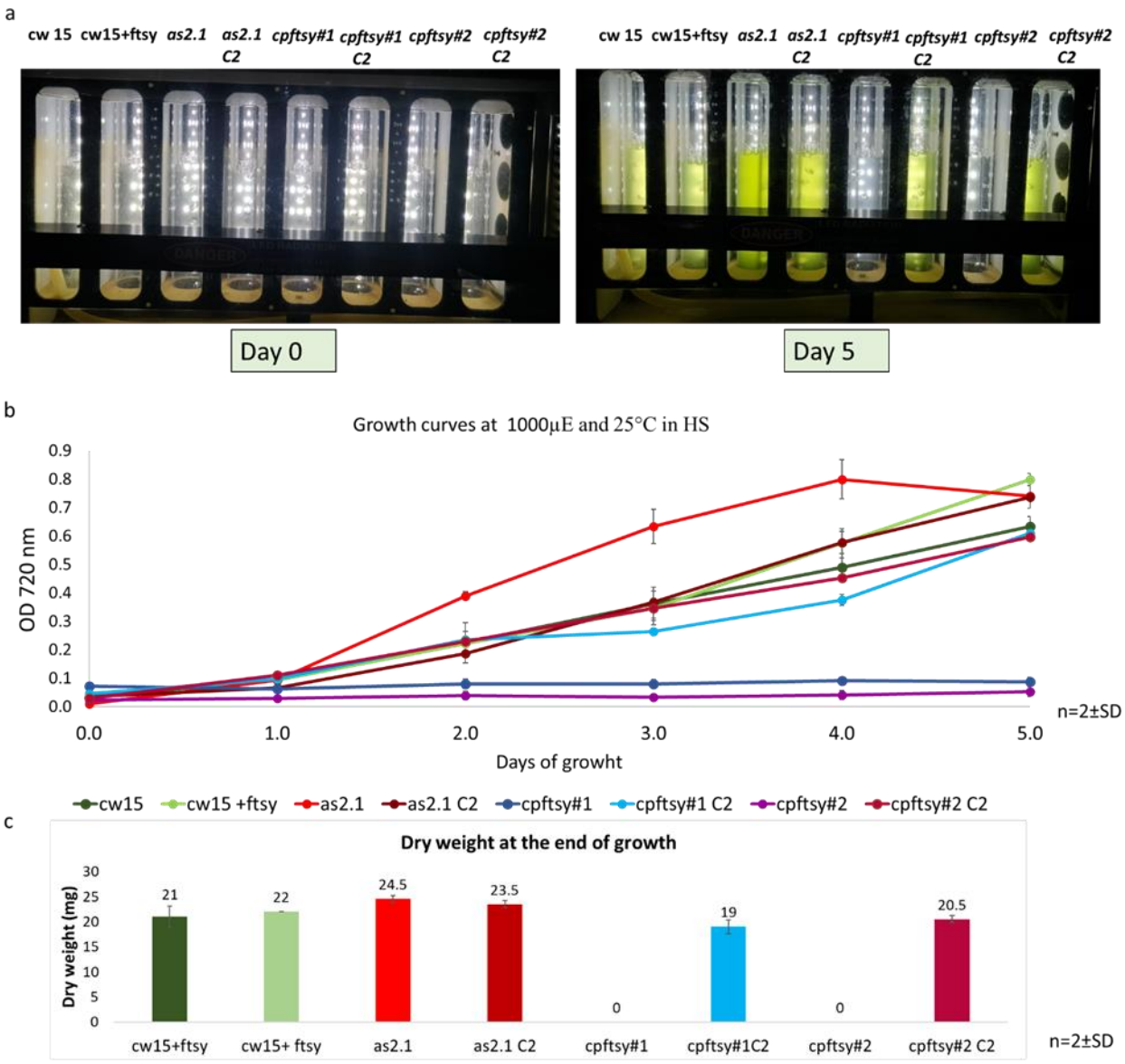

Figure 6.4.6. Parental and complemented mutant growth data. a) Pictures of the multicultivator system tubes at day 0 and day 5. b) Growth curves in high light. The *as2.1*, *cpftsy#1* and *cpftsy#2* mutants and their corresponding complemented strains were grown for five days, together with the cw15 WT and the cw15 transformed controls (cw15+ftsy), at 1000µE in HS medium at 25°C. The growth curves were obtained by measuring the cell optical density at 720 nm at different time points. Points represents the average of the measurements obtained every day for two biological replicates and the thin black bars the standard deviation. c) Dry weights at the end of the growth. The cell cultures grown at 1000µE were pelleted and dried in a lyophilizer machine. Bars represent average of three biological replicates ± standard deviation. No statistical differences were reported according to the Student's t-test analysis. C1: complemented strain number one; C2: complemented strains number two.

From the three mutants *as2.1*, *cpftsy#1*, *cpftsy#2*, their respective completed strains and the cw15 wild type strain the thylakoids were then extracted, after five days of growth in TAP rich medium and low light conditions (50µE). The thylakoidal proteins were extracted by a denaturing Tricine loading buffer and a quantity of samples correspondent to 1.5 µg of chlorophyll were charged on a 15% tricin

gel (figure 6.4.7a). With the same amount of chlorophyll, *cpftsy#1* and *cpftsy#2* mutants presented a higher ATPase and total protein content, compared with WT, complemented strains and *as2.1*, which indicates that it was need more cells to reach this chlorophyll quantity. At the same time both *as2.1* and its complemented strain *as2.1 C2* presented an intermediate protein and ATPase content between cw15 and *cpftsy* mutants, confirming that the complementation failed in restoring the WT chlorophyll content. On the contrary *cpfsty#1C2* and *cpftsy#2C2* complemented strains restored a WT phenotype (figure 6.4.7a). Moreover, for the same amount of chlorophyll all the samples have about the same amount of LHCII compared to the WT, indicating a lower amount of LHCII per cell. In particular taking a look to the three bands between 22 and 29 kDa (fig. 6.4.7), corresponding to LHCII, it resulted a different relative abundance of the lower two between the strains. In all the strains except *cpftsy#1* the lower band (blue arrow in the figure) was more abundant of the upper one (red arrow). *cpftsy#*1 presented, indeed, a similar relative abundance between these two bands, indicating a difference in LHCII composition between the two genome edited strains. The thylakoids extracts were used to perform a Deriphat-PAGE analysis to observe the supercomlexes abundance. A quantity of samples correspondent to 35 µg of chlorophyll were loaded on the gel to compare their differences (fig. 6.4.7b). Unfortunately, LHCII trimers and monomeric LHCII were difficult to distinguish properly, but some differences were still appreciable. *as2.1* and its respective complemented strain *as2.1C2* presented a higher abundance of PSII core and monomeric LHCII compared to the wild type and a lack of PSII core dimer and of PSI-LHCI and PSII-LHCII complexes. This result suggested that the complementation failed in restoring in *as2.1* also a WT photosynthetic protein composition. The *cpftsy#1* and *cpftsy#2* mutants as before showed a stronger reduction of the photosynthetic complexes with a higher presence of PSII and monomeric LHCII and trimeric LHCII, but this time the gel resolution didn't allow to appreciate differences in trimers composition. For their respective complemented strains was instead visible the complete restoration of the WT phenotype.

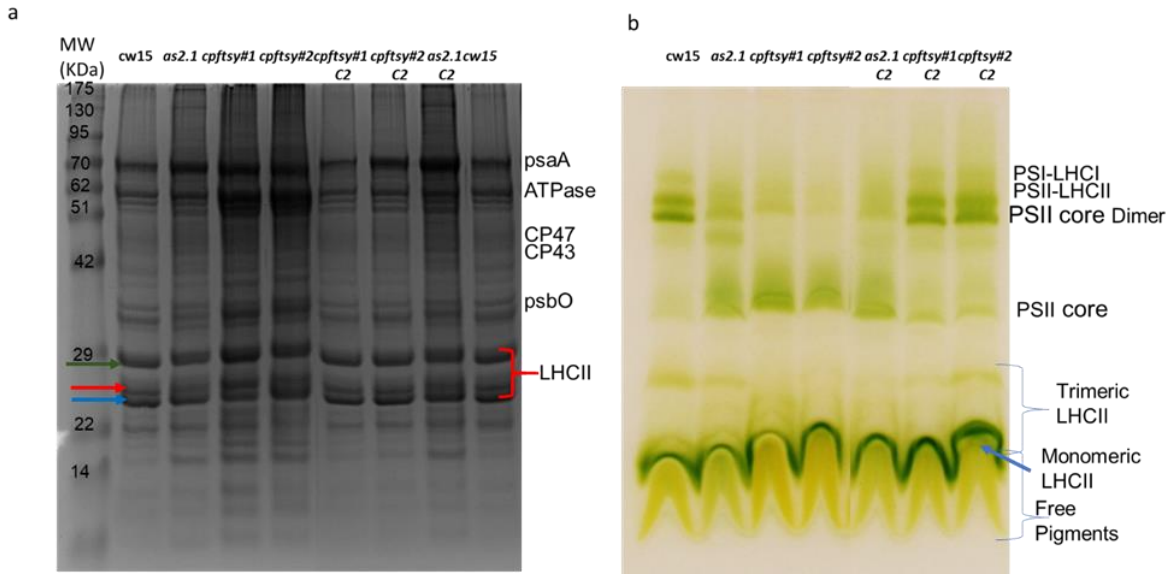

Figure 6.4.7. Denaturing and non-denaturing thylakoidal proteins gel. a) 15% tricine denaturing gel. The thylakoids were extracted from TAP grown cultures at 50 µE. The samples were treated with a denaturing buffer. Blue arrow indicates the lowest band correspondent LHCII, the red arrow the intermediate one and the green the highest one. All the band correspondent to specific photosynthetic proteins are indicated in the figure. b)

Deriphat-PAGE analysis. The thylakoids were extracted from TAP grown cultures at 50 µE. The samples were treated by β-DM detergent. The bands correspondent to the different complexes are indicated in the figure.

6.5 Comparison between *cpftsy* genome edited mutants obtained by different sgRNAs

Analysing *cpftsy#1* and *cpftsy#2* mutants some differences in LHCII antennae composition were detected. It was therefore investigated if this variability was due to a "stechiometric" effect induced by the lack of one of the main LHCPs insertion factor which was not completely compensated by alternative unspecific systems/pathways or if it was due to the effect of side mutations. For this reason it was decided to compared these first genome edited mutants with others strain obtained by another sgRNA targeting the same gene, used during the CRISPR-protocol optimization procedure reported in the publication present in Chapter 9 (Angstenberger et al. 2020). These new strains, already screened by PCR and sequencing, were named *cpftsyN1*, *cpftsyN2*, *cpftsyN3* and *cpftsyN4* and their lacking of CPFTSY were confirmed by WB analysis (figure 6.5.1).

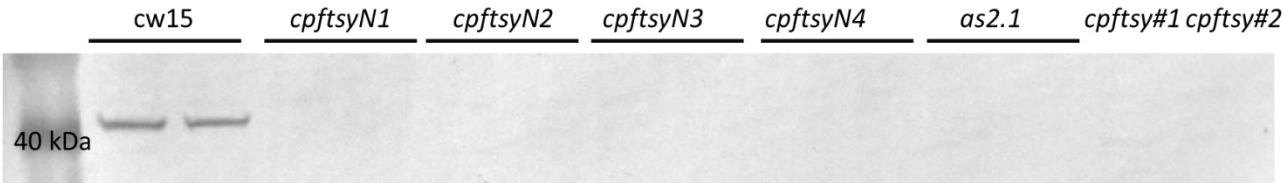

Figure 6.5.1. Western Blot analysis by the antibody against CpFTSY. A quantity of protein extracts, correspondent to 1.5 µg of chlorophyll, was run on 15% tricine gel. The expected band size was 40 kDa. MW: molecular weight marker. N1, N2, N3, N4=New strains obtained by another sgRNA

Then the pigment contents of all the *cpftsy* KO mutants were compared by the spectral measurement (Figure 6.5.2 a). As before it was seen a great difference between *as2.1* and the genome edited strains. Surprisingly the CRISPR-obtained mutants showed a similar spectrum shape, but great differences in carotenoids and chlorophylls regions of the spectra. The variability of the *a*/*b* ratios ranges between 3.4 and 4.9 (figure 6.5.2 b), while the chlorophyll content between the 23% and the 16% compared with the WT (figure 6.5.2 c). The variation is relevant also in carotenoid content, probably indicating a different stress level between the strains (6.5.2.d). The highest a/b ration and the lower chlorophyll content of the new *cpftsy* strains respect to *cpftsy#1* and *cpftsy#2* is explainable by the observation that these mutants after different plating rounds incomed in a sort of auto-selection to compensate the missing of some antennae proteins, with the acquisition of a darker phenotype. This could be due to the selection of mutants able to arrange LHCPs protein in a different way, with the insertion of chlorophyll b in those proteins not dependant on CPFTSY acivity. The "new" mutants were indeed subjected to less plating round and they had less time to autoselect. Moreover a variability between mutants obtained by genome editing was reported also by Baek and colleagues (Baek et al. 2016).

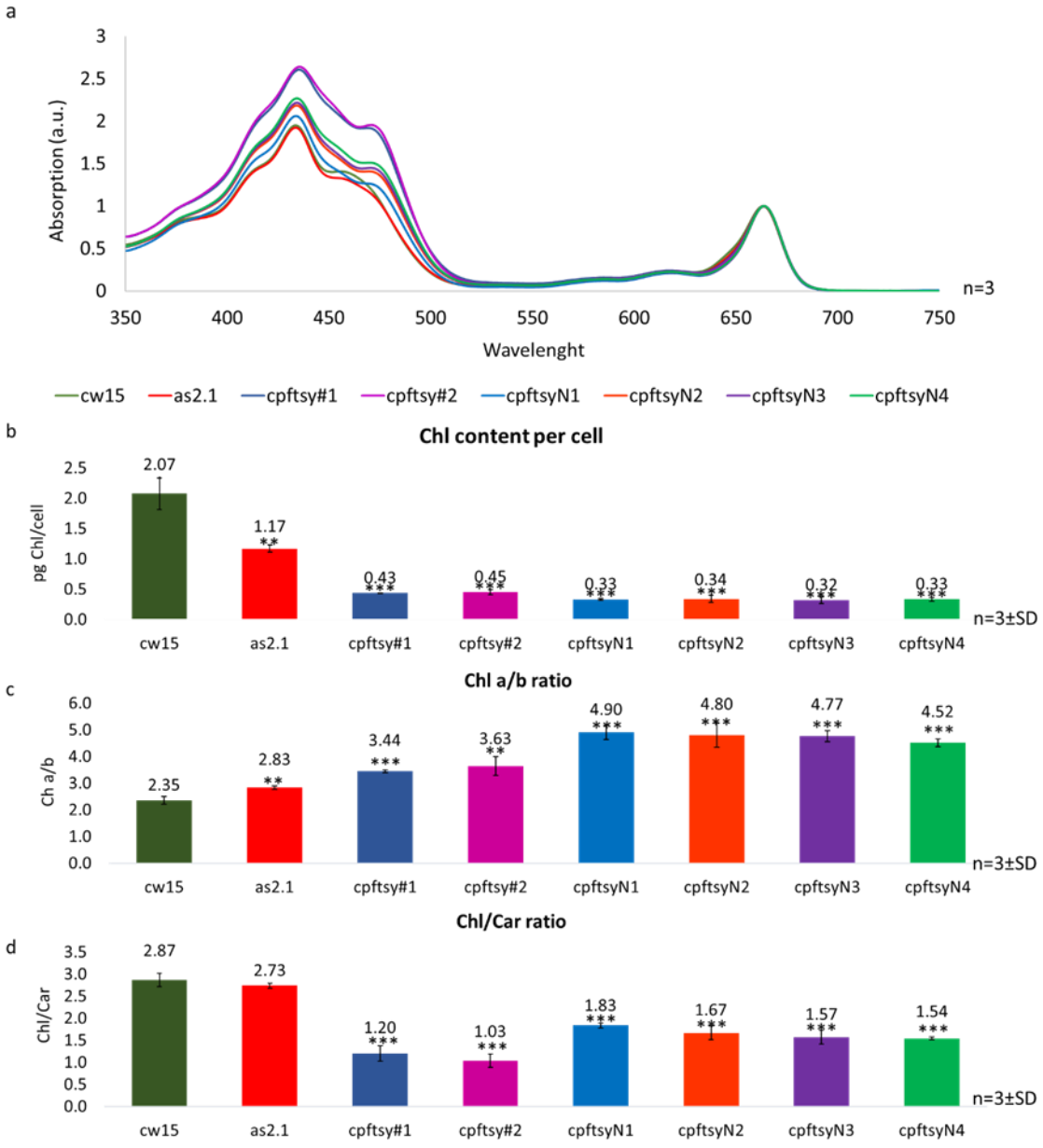

Figure 6.5.2. Absorption spectra of the different *cpftsy* KO mutants and parameters derived by their analysis. a) absorption spectra: data were normalized by set to zero and divide for the maximum absorption value. These data were obtained by three biological replicates. b) chlorophyll content per cell. c) Chl *a*/*b* ratio. d) Chl/Car ratio. Bars represent average of three biological replicates ± standard deviation. Asterisks indicate statistically significant differences between mutant and WT according to Student's t test (*, $P < 0.05$; **, $P < 0.01$; ***, $P < 0.001$).

It was then checked if this different chlorophyll amounts between the *cpftsy* mutants strain corresponded to a different amount of LHCII/cell and if there was variability in their relative abundance also in the new *cpftsy* mutants. Therefore, total protein extracts of the strains,

correspondent to $1*10^6$ cells, were loaded on a 15% tricine gel, to better compare LHCII in relation to cell quantity (figure 6.5.3 a).
A protein quantity for each sample correspondent to $2*10^5$; $4*10^5$; and $8*10^5$ cells was then loaded on another gel to perform a western blot by the antibodies against LHCII and RuBisCO (used as normalizer). The total abundance of LHCII and the relative abundance of the two lowest bands showed a huge variability among the strains and in some cases some bands were difficult to detect by western blot. This observation seems to confirm the hypothesis of a variable organization of the LHCPs protein that remained after the missing of CpFTSY.

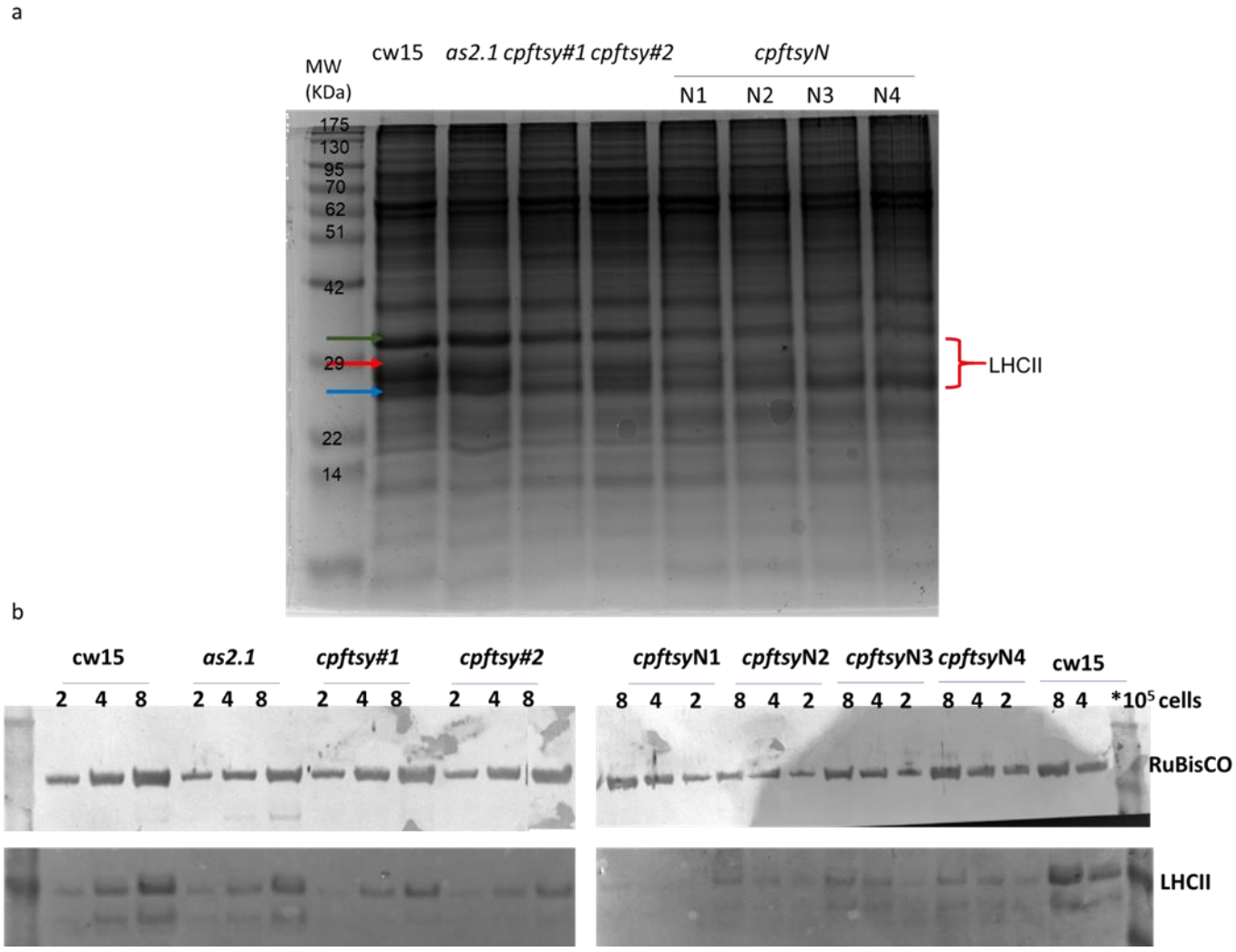

6.5.3. Protein analysis to detect differences in LHCII content. a)15% tricine gel on total extract. A quantity of protein correspondent to $1*10^6$ cell was charged for each sample. Blue arrow indicates the lowest band correspondent to LHCII, the red arrow the intermediate one and the green the highest one. All the band correspondent to specific photosynthetic proteins are indicated in the figure. b) Western blot analysis on LHCII and RuBisCO. Different cell amounts of each strain were charged in the 15% tricine gels ($2*10^5$; $4*10^5$; and $8*10^5$ cells). The different antibodies used are indicated on the right side of the figure.

These differences were observed also extracting thylakoids from all the *cpftsy* KO mutants.

As before a quantity of samples correspondent to 1.5 µg of chlorophyll were loaded on a 15% tricin gel (figure 6.5.4 a). As said before to the same abundance of chlorophyll corresponded a higher ATPase content compared to the wild type in *cpftsy#1* and *cpftsy#2* mutants, but the new genome edited strains showed an even bigger content of this protein, due to their lower chlorophyll quantity per cell. As seen from total extract gel the relative abundance of the lowest LHCII bands was different among GE strains, though all of them showed a lower content of these protein if it is compared with the ATPase.

The Deriphat-PAGE analysis was also performed to observe the supercomplexes content. 35 µg of chlorophyll were loaded on the gel to compare the differences between strains (fig. 6.5.4). Unfortunately, the partial comigration of LHCII trimers and monomeric LHCII made difficult to appreciate some differences in their relative content. However, it was clear that the new mutants contained less of both monomers and trimers also compared to *cpftsy#1* and *cpftsy#2*, and a different content of those seemed to be present among them. N2 and N4 strains seemed to have more trimers than the N1 and N3. What is clear is their supercomplexes level under the detection limit to whom a higher PSII core content corresponds.

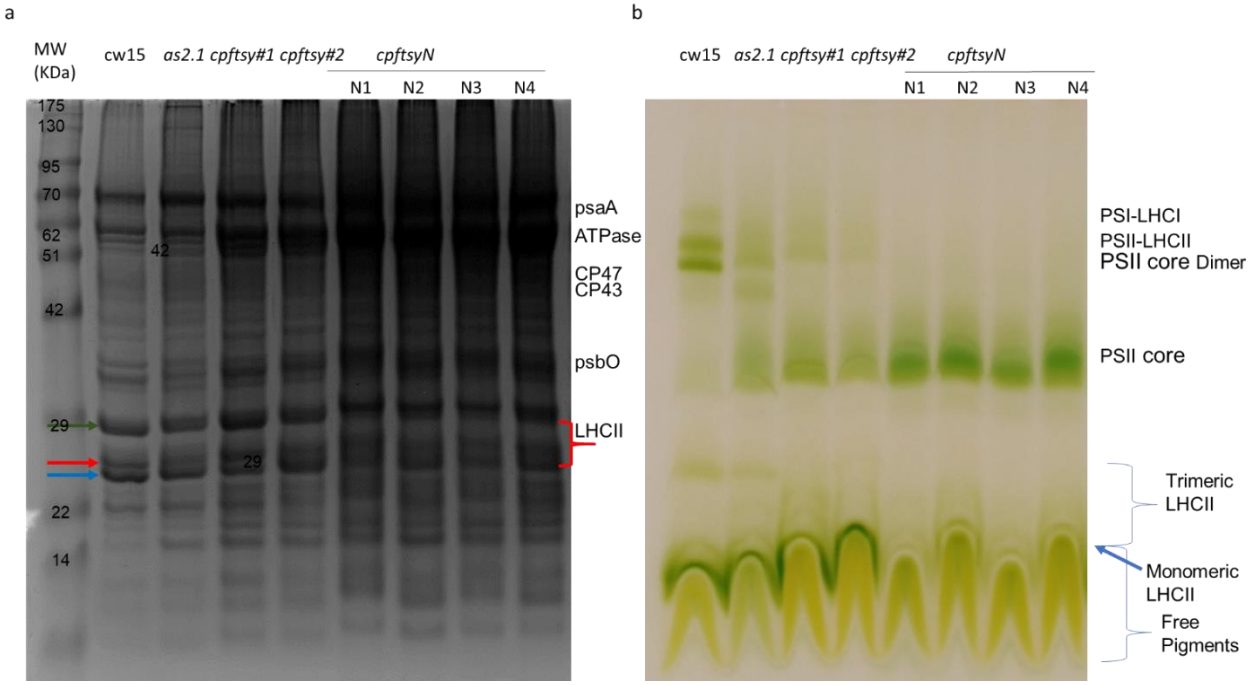

Figure 6.5.4. Denaturing and non-denaturing thylakoidal proteins gel. a)15% tricine denaturing gel. The thylakoids were extracted from TAP grown cultures at 50 µE. The samples were treated with a denaturing buffer. Blue arrow indicates the lowest band correspondent to LHCII, the red arrow the intermediate one and the green the highest one. All the band correspondent to specific photosynthetic proteins are indicated in the figure. b) Deriphat-PAGE analysis. The thylakoids were extracted from TAP grown cultures at 50 µE. The samples were treated by β-DM detergent. The bands correspondent to the different complexes are indicated in the figure.

All this data seemed to confirm a variability of LHCPs content among strains due to an internal rearrangement of antennae complexes and not to the presence of random mutation in some strains. This variable phenotype was revealed also by the PSII functional antenna size measurement. It was

estimated the maximal fluorescence (Fm) saturation kinetic in the presence of DCMU 10^{-5} M, data were normalized and the mutants were compared by calculating the reverse of the time necessary to reach the 2/3 of the maximal fluorescence (Cardol et al. 2008). Each value of $(t2/3)^{-1}$ was then reported relative to the wild type, conventionally set to 1. Since the cell density and the pigments content changed a lot between the *cpftsy* mutants, all the measures were performed changing the instrument parameter to obtain the right sensitivity and each dataset was compared with a WT sample treated by the same conditions. The final data were reported in figure 6.5.5, in which is showed another time the variability among the *cpftsy* mutants. Notably the "oldest" strains (*cpftsy#1*, *cpftsy#2*) showed a higher antenna size (80-85% respect to the WT), suggesting the readaptation of the antenna system that it was hypothesized before.

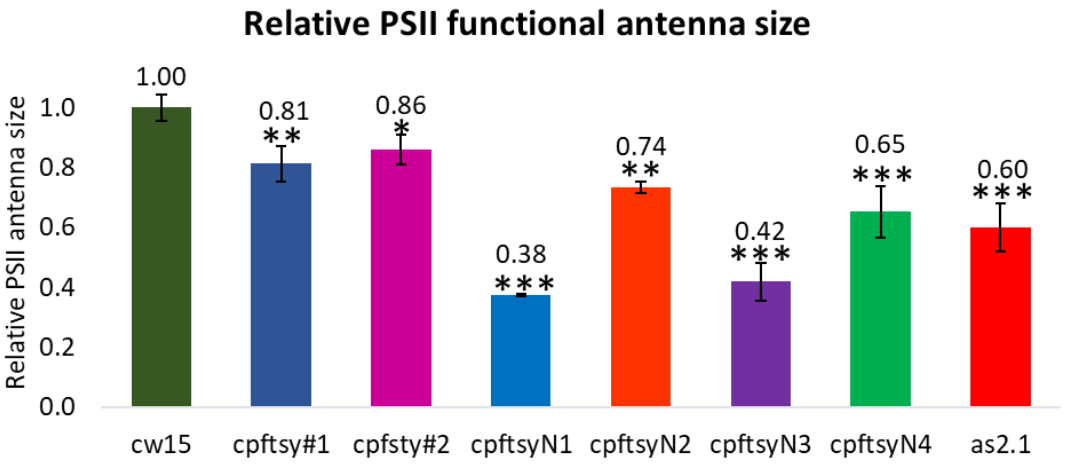

Fig 6.5.5. Relative PSII functional antenna size of *cpftsy* mutants estimated through fluorescence induction kinetics in the presence of DCMU (Cardol et al. 2008). Bars represent average of (t2/3)-1 of three biological replicates normalized to the WT ± standard deviation. Asterisks indicate statistically significant differences between mutant and WT according to Student's t test (*, $P < 0.05$; **, $P < 0.01$; ***, $P < 0.001$).

6.6 Production of *cao* mutants and *cpftsy-cao* double mutants

After observing that the *cpftsy* genome edited mutants were light sensitive and deficient in chlorophyll it was decided to compare the phenotype with a chlorophyll *b* biosynthesis-defective mutant. The aim was to observe which pathway between the antenna insertion and chlorophyll biosynthesis, is the major cause of the photosensitivity and loss of antenna proteins. The *CAO* gene was selected as the target for the CRISPR-Cas9 system. *CAO* encodes for the enzyme Chlorophyll *a* oxygenase, that catalyses the conversion of chlorophyll *a* into chlorophyll *b*, which is a pigment mainly present in peripherical antenna proteins, in particular in the LHCIIs. Random null-mutants and RNAi generated knock-down mutants for this gene had been characterized previously (Perrine et al. 2012; Bujaldon et al. 2017) and for this reason it was reputed also interesting to analyse the features of the gene targeting obtained null-mutants to have a more complete picture of the effect produced by the complete absence of this gene. The same was performed for *cpftsy#1* and *cpftsy#2* genome edited mutants, as the *tla2-cpftsy* random insertional mutant was deeply characterized (Kirst et al.

2012), while the *ΔCpFTSY* mutants produced by Baek and colleagues by CRISPR-Cas9 were only analysed for the pigment content and the ability to grow (Baek et al. 2016).

Moreover, it was decided to produce *cpftsy-cao* double mutants to better understand the importance of the roles of the chlorophyll *b* biosynthetic pathway and the Light Harvesting Antenna protein insertion pathway in the determination of *Chlamydomonas reinhardtii* light harvesting capacity.

The *CAO* sgRNA was designed in the same manner as for the *CpFTSY* gene, but this time the protospacer sequence complementary to the target was selected by using Cas-Designer software(Park et al. 2015). The CDS was used to find an exon-belonging target, situated in the first part of the gene, in order to lead to a truncated gene product. After obtaining the list of the targets with the PAM included it was selected the target with the highest out of frame score (a higher score indicates a higher specificity) and belonging to a single exon. The sequence specificity was tested with the software Cas-OFFinder (Bae et al. 2014) setting the program to obtain a list of the potential off-targets that were different to the target by up to three nucleotides or that could cause a DNA or an RNA bulge (figure 6.6.1b), leading to a mispairing between sgRNA and these sequences, for the difference in up to two nucleotides. The resulted lists (figure 6.6.1a) revealed, the presence of only one site which differentiated from the target by three mismatched nucleotides and a site equal to the target that is the *CAO* gene itself. Among the nineteen DNA or RNA bulge sites it was found only five sequences belonging to genes different from *CAO* and two are in the same position in the genome. These five possible off target sites that differentiate from the target for two or three nucleotides were considered acceptable, considering the difficulties in finding specific sites in the G/C rich *Chlamydomonas* genome and the fact that all the mutants would be sequenced in the *CAO* site (figure 6.6.1c).

a

Cas-Designer

RGEN Target (5' to 3')[?]	Position[?]	Cleavage Position (%)[?]	Direction[?]	GC Contents (%, w/o PAM)[?]	Out-of-frame Score[?]
CGCCTCGACACCCATCGTTGAGG	111	21.2	+	65.0	76.5
GCTCTCCGGGTCCTCAACGATGG	122	21.2	-	65.0	76.5
AGCGGCGGAACTTGCTCTCCGGG	135	23.4	-	65.0	76.1

b

Cas-OFFinder

c

Bulge Type	Target	Chromosome	Position	Direction	Mismatches	Bulge Size
DNA	crRNA: G-CTCTCCGGGTCCTCAACGANGG DNA: tGCTCTCCGGGTCCTCAACGATGG	chromosome_1	5943074	+	1	1
DNA	crRNA: GC-TCTCCGGGTCCTCAACGANGG DNA: tgCTCTCCGGGTCCTCAACGATGG	chromosome_1	5943074	+	2	1
X	crRNA: GCTCTCCGGGTCCTCAACGANGG DNA: GCTCTCCGGGTCCTCAACGATGG	chromosome_1	5943075	+	0	0
RNA	crRNA: GCTCTCCGGGTCCTCAACGANGG DNA: GC-CTCCGGGTCgTCAgCGAAGG	chromosome_16	5115798	+	2	1

Figure 6.6.1.CAO protospacer research. a) Cas-Designer results. The results were filtered to obtain only the target with an out-of-frame score higher than 75 (sixth column). In the first column were reported the selected targets complete of the PAM sequence (NGG), in the second column were indicated the position of the site in the coding sequence, while in the third the column expressed as percentage of the sequence (in this case only 1000 nt over 1938 were inserted as query so this parameter has no sense). In the fourth column it is indicated in which of the two DNA filaments the target is present, in the fifth the G/C percentage of the sequence. The red square indicates the selected target for the genome editing b) visual representation of the RNA and DNA n bulge phenomena. (From http://www.rgenome.net/cas-offinder/) c) example of Cas-OFFinder results. The blue square indicates a real off-target sequence, while the other rules contain sites belonging to the *CAO* gene. In the first column it is indicated the bulge type (X indicates no bulge and simple mismatching), while in the second is reported the target sequence and the sequence of the protospacer (crRNA) indicating the bulge or the mismatch sites. In the third column were reported the chromosomes in which these off-target were collocated, in the fourth the position in the genome and in fifth the strain in which the target is present. The last two columns indicate respectively the number of nucleotides that cause the mismatch and the length in nucleotides of the bulge.

The *CAO* sgRNA was synthesized by two PCR rounds like the *CpFTSY* sgRNA (figure 6.6.2.b), to add the protospacer and the PT7 sequences to the conserved portion of the template (figure 6.6.2.a). After the *in vitro* transcription the *in vitro* cut assay was then performed. The RNP-complex of Cas9 and sgRNA was able to cut a 593 bp *CAO* gene fragment, including the target, in two pieces 379 and 214 base-pair long.

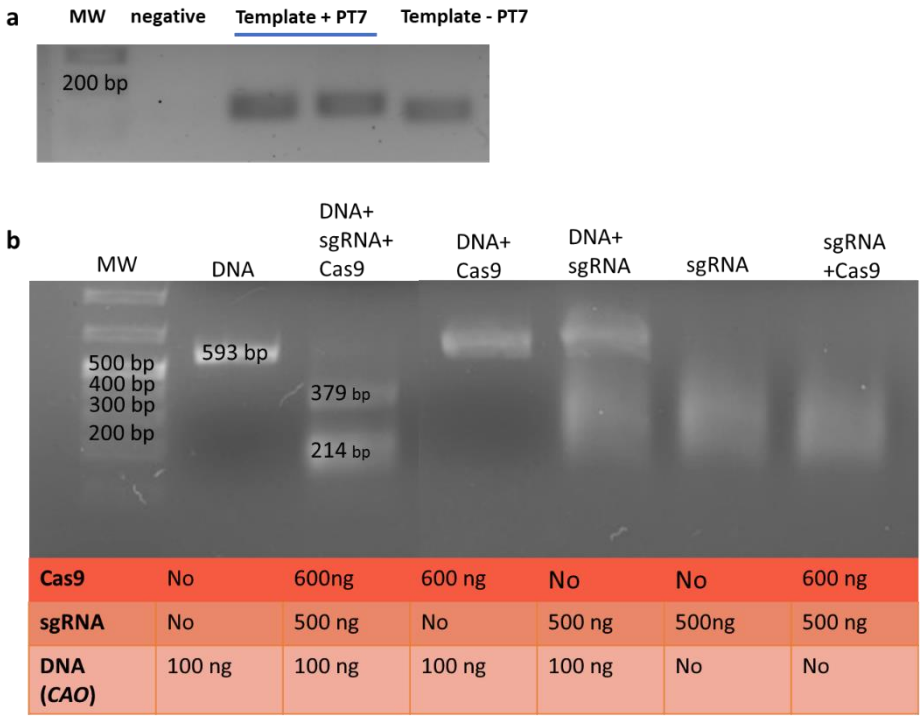

Cas9	No	600ng	600 ng	No	No	600 ng
sgRNA	No	500 ng	No	500 ng	500ng	500 ng
DNA (*CAO*)	100 ng	100 ng	100 ng	100 ng	No	No

Figure 6.6.2. DNA template synthesis for *CpFTSY* sgRNA and *in vitro* cut assay. a) PCR product from the two DNA templates amplification rounds. The template – T7 is the product composed by the protospacer and the conserved sgRNA sequence, the template + T7 is the product complete of the PT7 promoter. The products were run on 1.5% agarose gel. MW: molecular weight marker. b) *In vitro* cut assay. The cut reaction products and the different controls were checked on a 1.5% agarose gel. The sgRNA, alone and combined with Cas9 or DNA only, gave a smear not present when the RNP- complex cuts the DNA. The fragment is 593 bp long, while after the cut with sgRNA and Cas9 were obtained two fragments of 214 and 379 bp. MW: molecular weight marker.

Chlamydomonas reinhardtii cw15 strain was then transformed by electroporation to deliver the RNP-complex formed by Cas9 and *CAO* sgRNA and the Paromomycin resistance, conferred by the plasmid pOpt2_Clover-Paro (Lauersen et al. 2018), to produce *cao* mutant strains. The same was performed on *cpftsy#1* and *cpftsy#2*, to obtain double mutant strains. In this way the double mutants derived from two independent transformations would be obtained reducing the background effect that could be due to specific differences in the two backgrounds, unrelated to the genes of interest. After the transformation the cw15 background cells were plated on solid TAP medium supplemented with 30% starch and 10 µg/ml Paromomycin, while the transformants of *cpftsy#1* or *#2* background on TAP supplement with 30% starch and 10 µg/ml Paromomycin and 50µg/ml Hygromycin. After a week the

colonies were big enough to distinguish phenotypes. The *cao* single mutants were paler compared to cw15 and their colonies were less dense, but the phenotype was not as strong as compared to *cpftsy* single mutants. The *cpftsy-cao* double mutants were instead paler than their background and their colonies grew slower. The transformation efficiency using *CAO* sgRNA was 25%, as it was found that one out four colonies lacked *CAO* expression. By PCR screening with a couple of primers which anneal on the gene larger amplicons were obtained in the mutants *cao#1* and *cao#2* and the double mutants *cpftsy-cao#1* and *cpftsy-cao#2*. This indicated an insertion phenomenon in the region adjacent to the target. This was confirmed by sequencing analysis. *cao#2*, *cpftsy-cao#1* and *cpftsy-cao#2* presented an insertion of part of the plasmid in the target sequence, while *cao#1* had the insertion about 70 nucleotides before.

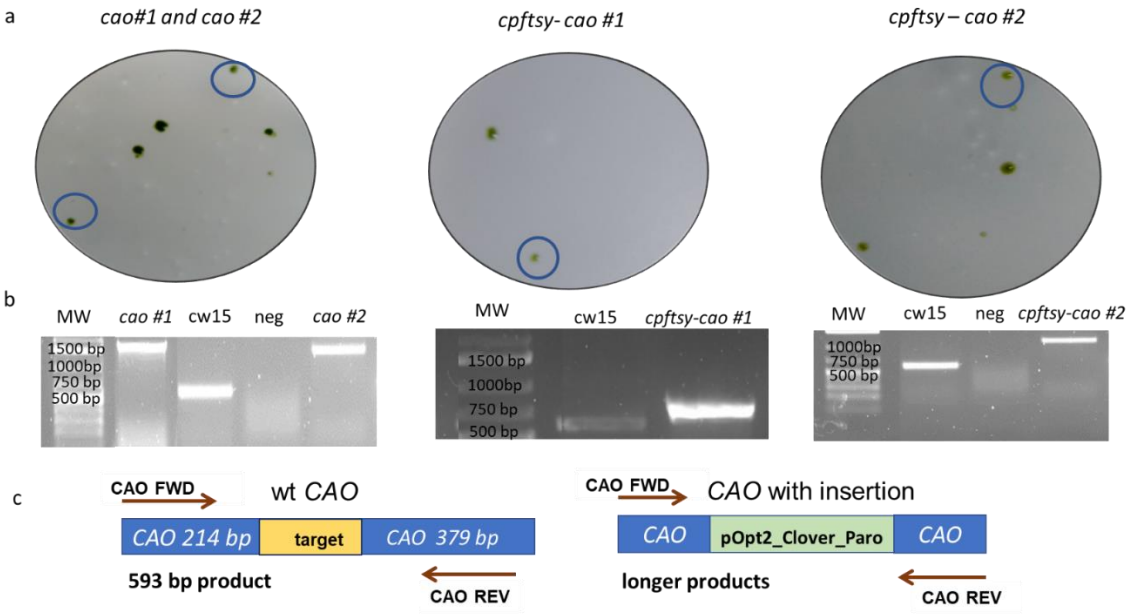

Figure 6.6.3. Screening of the single *cao* mutants and double *cpftsy-cao* mutants. a) Details of the plates 7 days after the transformation. b) PCR analysis of the target region. Samples were run on 1.5% agarose gel. The used primer were CAO FWD and CAO REV, which amplified the target including region. MW: molecular weight marker neg: negative control. c) schematic representations of the amplified fragments. The brown arrows represent the primers the blue square the gene. WT CAO indicates the scheme of the wild type copy of the gene. Target is the region complementary to the protospacer of the sgRNA with two regions of 214 bp and 379 bp amplified at its sides. *CAO* with insertion is a general scheme of the mutant versions of the gene. pOpt2_clover_Paro is the plasmid conferring the resistance, which it was inserted in different ways and allows different PCR products

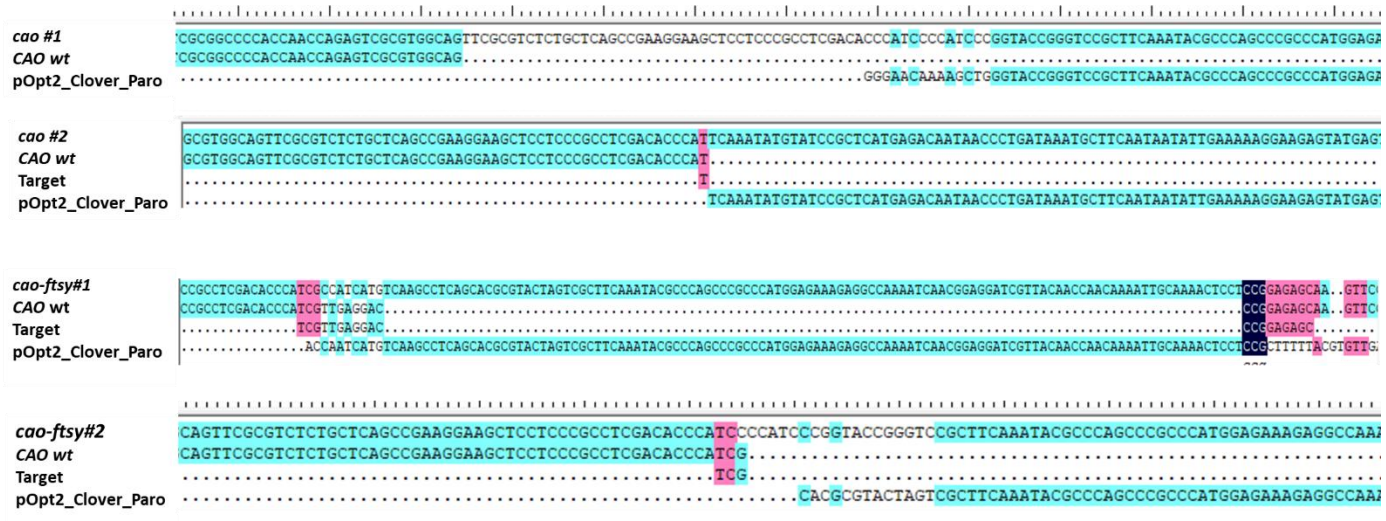

Figure 6.6.4. Sequences of the insertion regions. It is reported the sequencing of the border region between the *CAO* gene sequence and the insertion. For *cao#1* the insertion is about 70 nt before the target. For *cao#2*, cao-*cpftsy#1* and *cao-cpftsy#2* there was an interruption at the beginning of the target region. Light blue colour indicates when only two sequences matched, pink indicates when more sequences matched. Dark blue colour indicates when all the sequences matched together.

6.7 Comparison between *cao#1*, *cao#2*, *cpftsy#1*, *cpftsy#2*, *cpftsy-cao#1 and cpftsy-cao#2.*

The *cao#1*, *cao#2*, *cpftsy#1*, *cpftsy#2*, *cpftsy-cao#1* and *cpftsy-cao#2* strains were then compared for their photosynthesis related features. The spectral measurement of the acetonic extracts of the six mutants and their WT were performed to determine their chlorophyll and carotenoid relative content (figure 6.7.1). The mutants showed that the larger difference was observable in the region between 630 and 650 nm of the spectra, in which the absorption depends on chlorophyll *b*, in the region between 450 and 480 nm, in which it is due to the carotenoids and the Chl *b*, and in the region between 420 and 450 nm, where it is dependent on Chl *a* and carotenoids (figure 6.7.1 a). In the first region *cao* single mutants and *cpftsy-cao* double mutants showed a greater drop in absorption compared not only to the one in cw15, but also *cpftsy* single mutants, as expected for mutants which were unable to convert chlorophyll *a* into chlorophyll *b*. In the region between 450 nm and 480 nm this drop in adsorption was more visible, though in the double mutants there is a more precipitous ascent from the 500 nm region, with a peak at about 420 nm, similar to *cpftsy* single mutants. This indicated that *cpftsy-cao* mutants produced more carotenoids in respect to both cw15 and *cao* single mutants, as for *cpftsy#1* and *cpftsy#2* (figure 6.7.1 a). Looking at chlorophyll content per cell *cao#1* and *cao#2* contained about the 70% of pg of chlorophyll respect to the wild type, while *cpftsy#1* and *#2* and *cpftsy-cao #1* and *#2* strains about the 20%. This could be explained by the fact that *cao* mutants did not produce chlorophyll b and were able to insert chlorophyll *a* into the antenna proteins, the other mutants were unable to insert any antenna proteins at all, so they were defective also in chlorophyll *a* content (figure 6.7.1 b). Obviously as for Chl *a*/*b* ratio in *cao* and *cpfty-cao* mutants it was obtained a value that tends to the infinity (figure 6.7.2 c). The chlorophyll/carotenoids ratio was less affected in *cao* single mutants respect to the others, it was about the 60-65% of the

cw15 level. In *cpftsy* and *cpftsy-cao* mutants it decreased to 32-40% of the wild type value (figure 6.7.1 d)

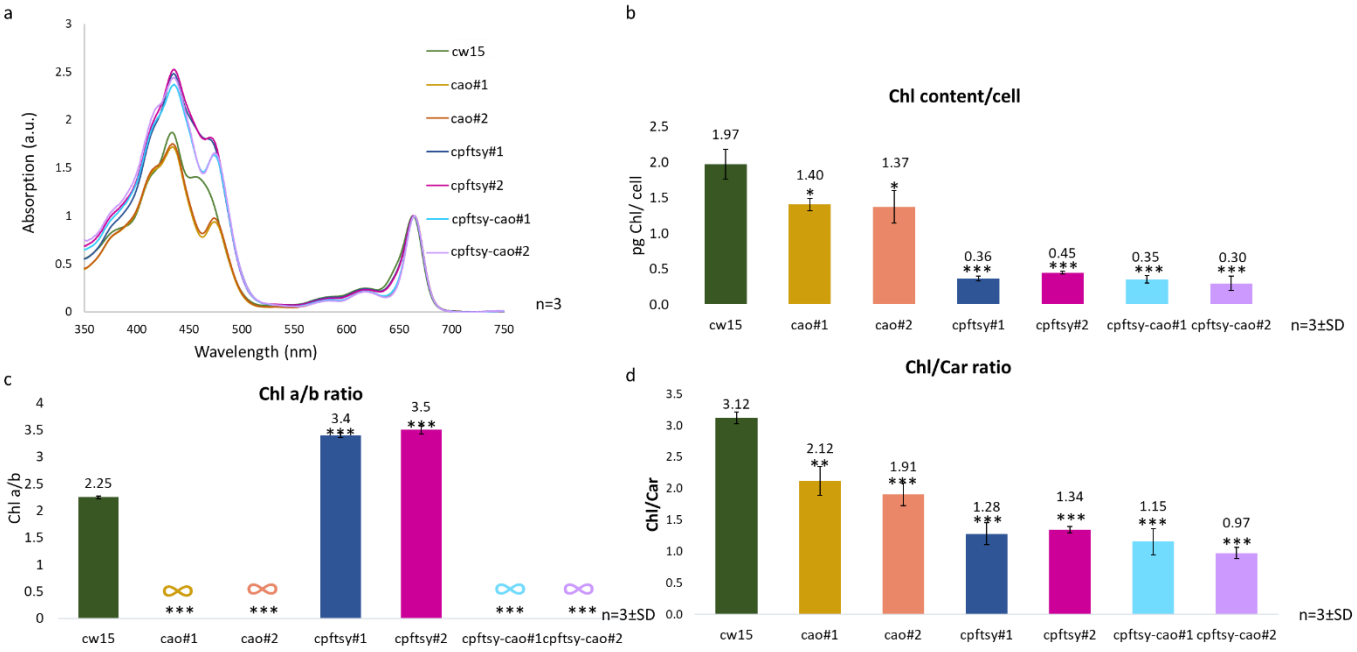

Figure 6.7.1. Absorption spectra of single and double mutants and parameters derived by their analysis.
a) absorption spectra: data were normalized by set to zero and divide for the maximum absorption value. These data were obtained by three biological replicates after a grow in TAP medium at 50 µE at 22°C. b) chlorophyll content per cell. c) Chl *a/b* ratio. d) Chl/car ratio. Bars represent average of three biological replicates ± standard deviation. Asterisks indicate statistically significant differences between mutant and WT according to Student's t test (*, $P < 0.05$; **, $P < 0.01$; ***, $P < 0.001$).

To analyse the differences in growth capacity between cw15, *cpftsy#1*, *cpftsy#2* and the four new strains *cao#1*, *cao#2*, *cpftsy-cao#1* and *cpftsy-cao#2,* they were tested in rich TAP medium and medium light conditions (200 µE). This choice was explained by the fact that *cpftsy* single mutants resulted before unable to grow in minimal medium and high light conditions and the double mutants had difficulties in growing in TAP medium flasks at 50 µE (figure 6.7.2 a). It was chosen also to start from a stronger initial inoculum of $5*10^5$ cell/ml. From this experiment it was observed that *cao#1* and *cao#2* mutants reached the plateau as fast as the wild type and, in this phase, they reached a concentration that is not so different to cw15. *cpftsy#1*, *cpftsy#2* at this light intensity were able to start to grow but they were slower to reach the plateau, however after six days they reached about the same cell density as the *cao* mutants. The double mutants, on the contrary, started to grow slower than the other strains and they stopped their growth at a lower cell concentration, probably this was due to an excess in light stress conditions for the lack of the major part of antenna proteins. On the contrary at 1000 µE all the strains were able to grow and only a small impairment was observed for the double mutants.
When the strains were grown in minimal medium at 1000 µE was clear that the *cao* single mutants were able to start grow earlier compared to the others, suggesting that they are able to rearrange

their antennae system to overcome light stress. However, their final concentration was similar to the WT one, and obviously they reached a lower cell density at the end of the growth in minimal medium compared to the rich one. Using a stronger inoculum than the previous experiments in minimal medium (figure 6.3.1) *cpftsy* single mutants appeared able to start the growth though they reached at lower cell concentration at plateau compared to the *cao* single mutants and cw15. This ability to start the growth could be due also to the autoselection of strains with particular antenna system rearrangement hypothesized from the other experiments. Finally, the double mutants showed to be unable to grow in these conditions, suggesting a too strong affection of their photosynthetic apparatus.

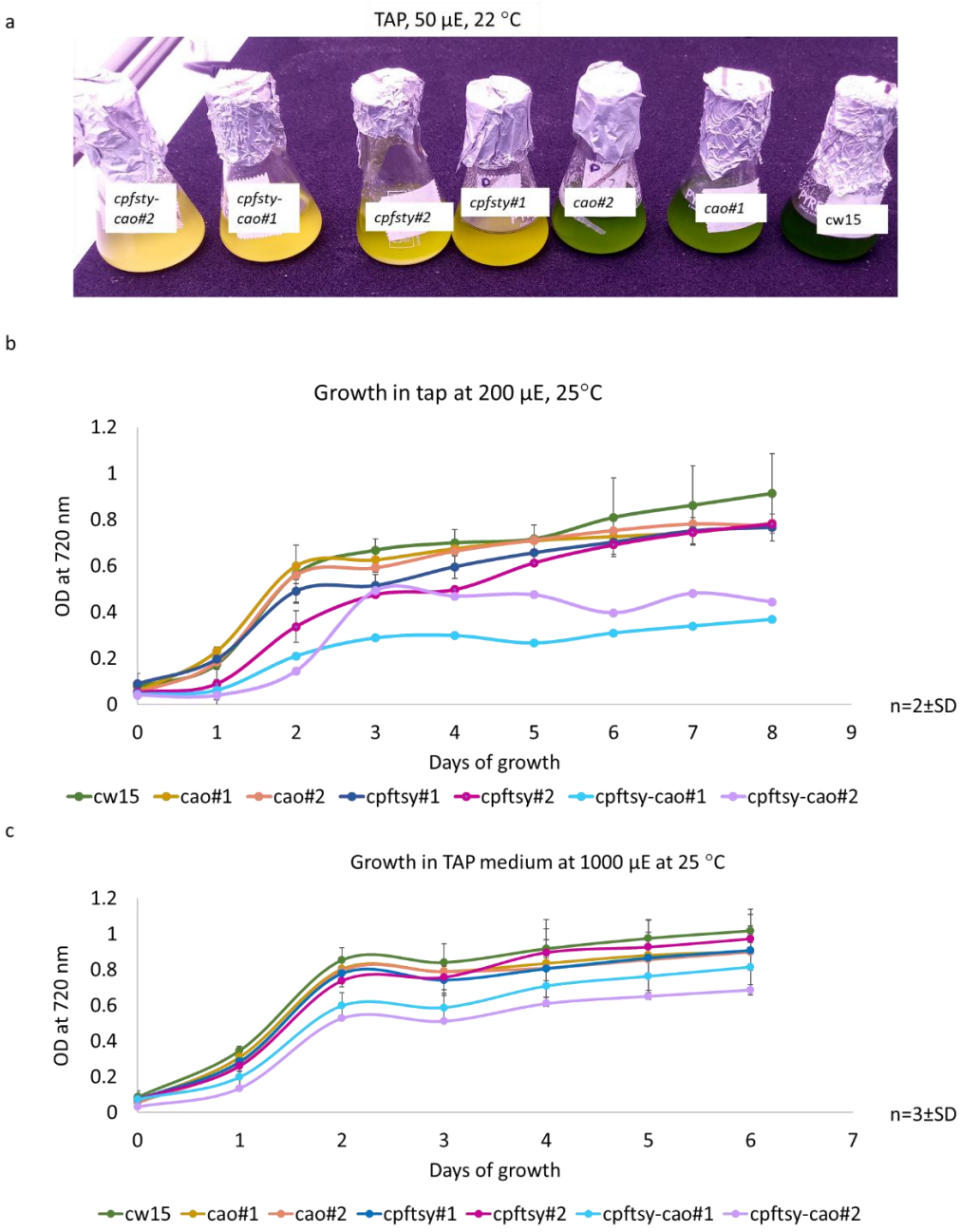

Figure 6.7.2. Growth of mutant strains in rich medium. a) Strains appearance after five days of growth in flasks at 50 µE and 22 °C in TAP medium. b) Growth curves in medium light (200 µE). The strains cw15, *cao#1*, *cao#2*,

cpftsy#1, *cpftsy#2*, *cpftsy-cao#1* and *cpftsy-cao#2* were grown for eight days, at 200µE in TAP medium at 25°C c) Growth curves in high light (1000µE). The strains cw15, *cao#1*, *cao#2*, *cpftsy#1*, *cpftsy#2*, *cpftsy-cao#1* and *cpftsy-cao#2* were grown for eight days, at 1000µE in TAP medium The growth curves were obtained by measuring the cell optical density at 720 nm at different time points. Points represents the average of the measurements obtained every day for two or three biological replicates and the thin black bars the standard deviation.

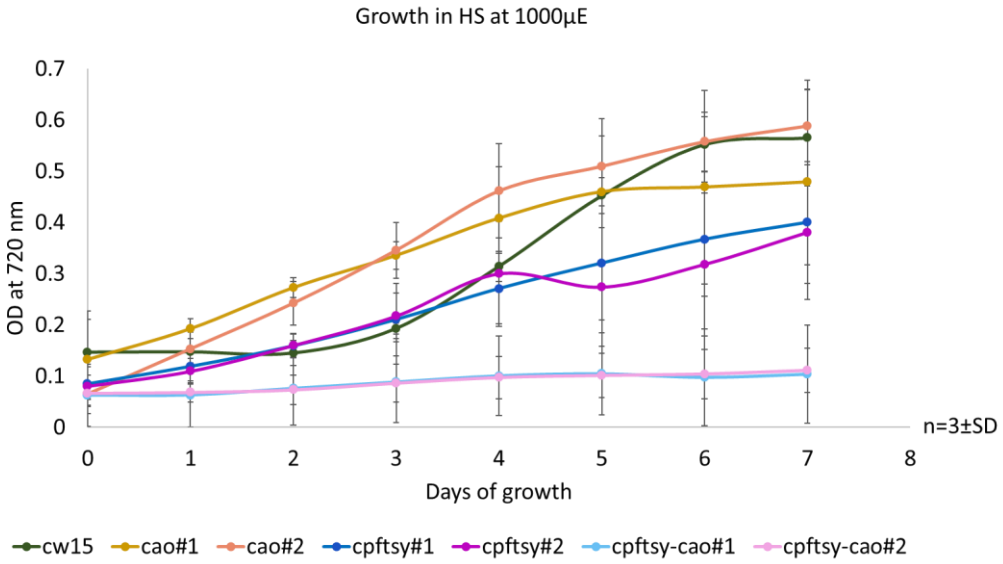

Figure 6.7.3. Growth of mutant strains in minimal medium. The strains cw15, *cao#1*, *cao#2*, *cpftsy#1*, *cpftsy#2*, *cpftsy-cao#1* and *cpftsy-cao#2* were grown for seven days, at 1000µE in HS medium at 25°C. The growth curves were obtained by measuring the cell optical density at 720 nm at different time points. Points represents the average of the measurements obtained every day for three biological replicates and the thin black bars the standard deviation

To better understand the effect of the different mutations on the functionality of antenna proteins the PSII functional antenna size was measured. The estimation of the maximal fluorescence (Fm) saturation kinetic in the presence of DCMU 10^{-5} M was performed by a home-built instrument, after data normalization, the mutants were compared by calculating the reverse of the time necessary to reach the 2/3 of the maximal fluorescence (Cardol et al. 2008). Each value of $(t_{2/3})^{-1}$ was then reported relative to the wild type, conventionally set to 1. For each strain three measurements were performed, and it was selected the average $(t_{2/3})^{-1}$ value (figure 6.7.4).
cpftsy mutants showed a reduction of only 15-20% in antenna size in respect to the wild type. A reduction of 70% was instead observed in *cao* single mutants and *cpftsy-cao #1*, for *cpftsy-cao#2* the estimated reduction was of 80%. The double mutants were close to the instrument sensitivity limit, due to their extremely pale phenotype, so the values obtained were more oscillating compared with the other strains. It was then established to set as $t_{2/3}$ value the point from which the major part of the points values was higher than 0.66.

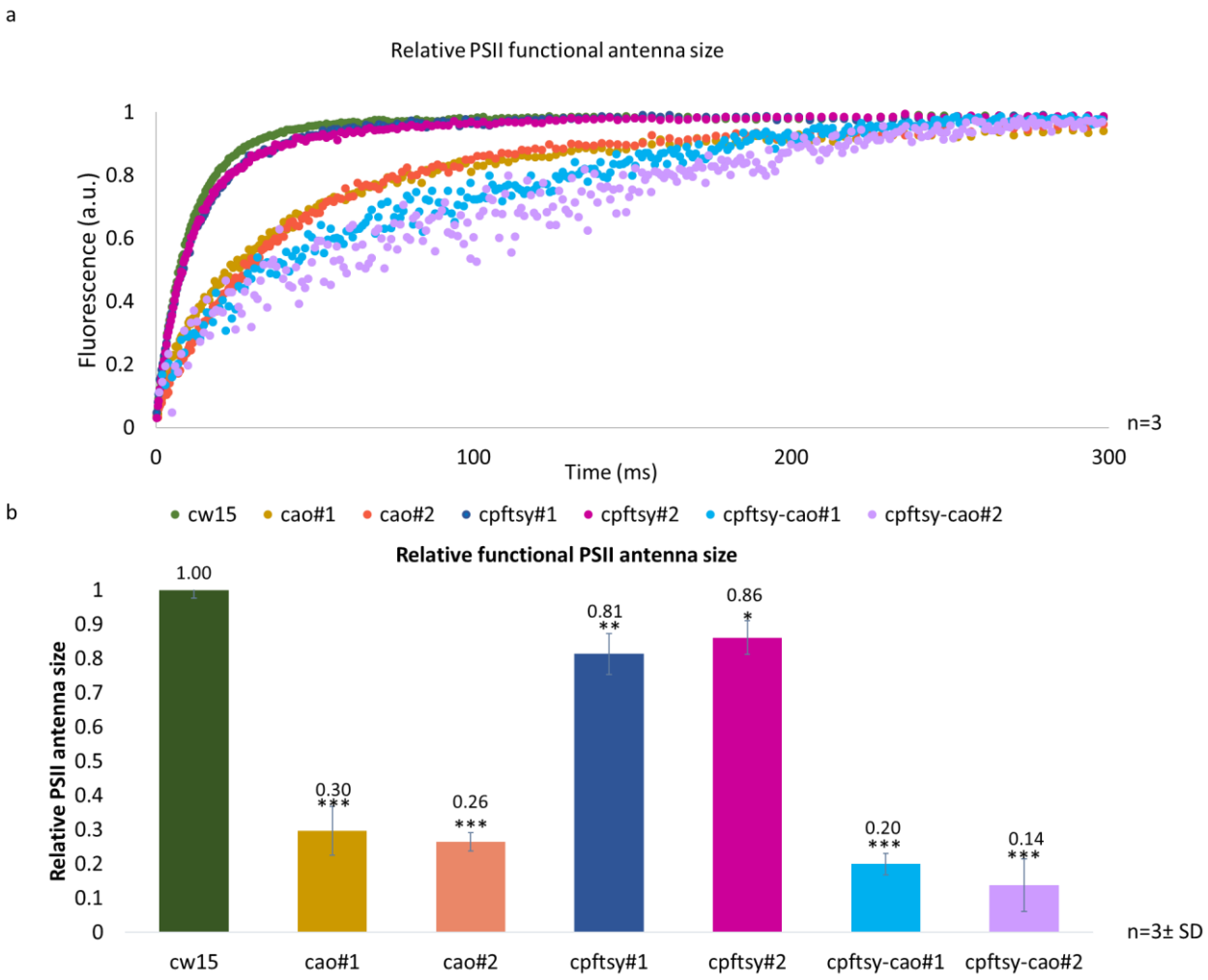

Fig 6.7.4. Relative PSII functional antenna size of *cao#1*, *cao#2*, *cpftsy#1*, *cpftsy#2*, *cpftsy-cao#1* and *cpftsy-cao#2* mutants estimated through fluorescence induction kinetics in the presence of DCMU (Cardol et al. 2008). a) Fluorescence curved normalized to Fm. b) data shown in panel a plotted as $(t_{2/3})^{-1}$. Error bars refer to three replicates. Asterisks indicate statistically significant differences between mutant and WT according to Student's t test (*, P < 0.05; **, P < 0.01; ***, P < 0.001).

From 15% denaturing tricine gel on total extracts, loaded on the basis of cell amounts ($1*10^6$ cells), it resulted as expected a stronger reduction in LHCIIs content in *cao-cpftsy#1* and *cao-cpftsy#2*. *cao* and *cpftsy* mutants also presented a lower content of these antennae, but ,while *cao#1* and *cao#2* showed a similar bands pattern, *cpftsy#1* and *cpftsy#2*, as seen before, showed a different relative abundance of the two lowest bands (figure 6.7.5)

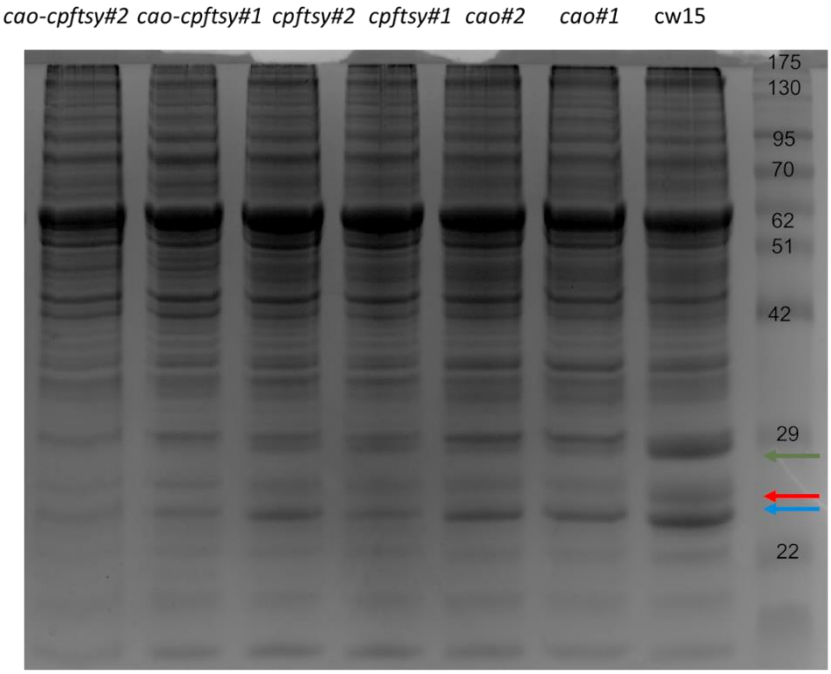

Figure 6.7.5. 15% tricine gel with total protein extract. A quantity of protein correspondent to $1*10^6$ cell was loaded for each sample. Blue arrow indicates the lowest band correspondent to the LHCII, the red arrow the intermediate one and the green the highest one.

To check in more detail the photosynthetic proteins compositions of the six mutants strains a western blot analysis was performed using different antibodies. To better compare the proteins quantity the same gels were cut in different parts and each of them was incubated with an antibody which recognised a protein in this molecular weight range. The proteins were extracted from liquid cultures and for each sample there were loaded on two 15% small tricine gels, amounts of sample proportional to different cells quantities (figure 6.7.6 and 6.7.7). The first two gels were incubated with the antibodies against RuBisCO, and Cytf. The second gels were then incubated with PsaA, CP47 and LHCII antibodies. The RuBisCO quantity in all mutants was proportional to cell quantities and it was used to compare the other proteins by a relative densitometry (figure 6.7.6 and 6.7.7). For the Cytochrome f the amount in the *cpftsy* single mutants was similar to the WT, while *cao#1* and *cao#2* and *cpftsy-cao#1* and *cpftsy-cao#2* showed a reduction of 40% and 65% respectively in its content, probably due to a transcriptional downregulation induced by the reduced light harvesting and the consequent electron transfer capacity (figure 6.7.6). For CP47 PSII core antenna protein a strong reduction (80%) was observed in *cpftsy* single mutants and in the double ones it was hardly detectable. On the contrary its content doubled in *cao#1* and increase 0,8 times in *cao#2* probably to compensate the loss of the chlorophyll b binding antenna proteins (figure 6.7.6). All the strains showed a reduced content also in PSI protein PsaA. For *cao#1* the reduction it was not significant while for *cao#2* it was more evident (60% of the WT). For *cpftsy* single mutants it was detected about the half of the WT content, while a reduction of 70% it was revealed in *cpftsy-cao* double mutants, suggesting a stronger photodamage in these last four strains or an involvement of *CPFTSY* also in core proteins insertion. As expected, all the mutant strains showed a significant reduction in LHCII content. The entity of this difference was higher in *cpftsy-cao#1* and *cpftsy-cao#2* mutants whom

bands were under the detection level. In *cao#1* and *cao#2* only the upper band was detectable, and it was reduced of the 85% compared to cw15. As seen in the green gel these two mutants *cpftsy#1* and *cpftsy#2* showed a different affection in LHCII subunits. *cpftsy#1* had the upper band that is the 50% of the cw15 one, a second band that was the 23% and a third one non detectable. *cpftsy#2* had a lower content of the upper band compared to *cpftsy#1* (the half), a similar amount of band II (24%) and a third band that is the 37% of cw15 one. (figure 6.7.7).

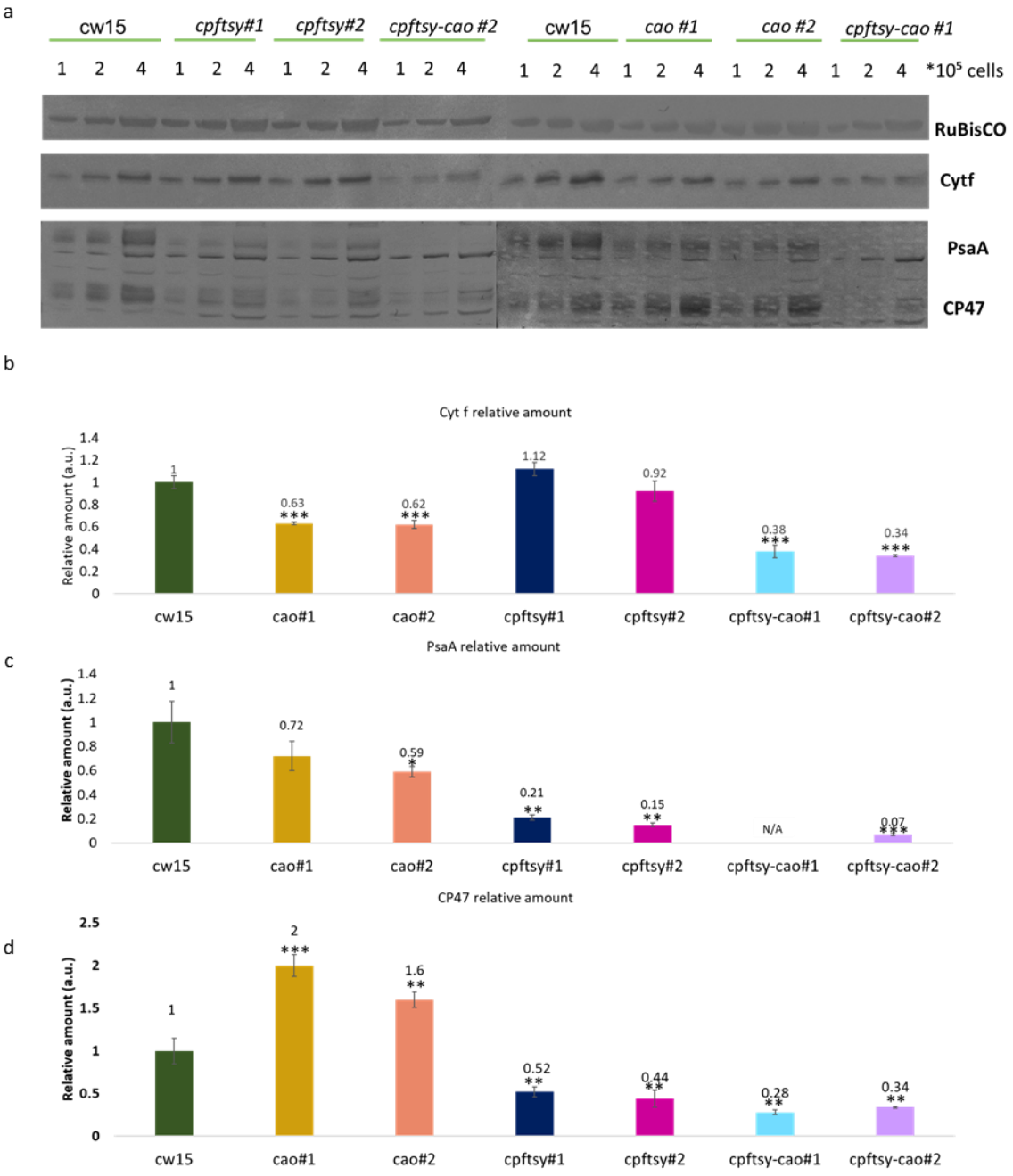

Figure 6.7.6. Western blot and densitometric analysis on Cytochrome f, PsaA and CP47. a) Western blot membranes. sample volumes corresponding to different cell numbers of each strain were loaded in a 15%-acrylammide SDS-PAGE, Tris-Tricine gel system ("1", 1*10^5; "2", 2*10^5; "4", 4*10^5 cells). b-c-d) densitometric analysis on the basis of RuBisCO content. The image analysis was performed by ImageLab software (Biorad). Three different amounts were analysed for each sample. Data of band intensities were normalized to the RuBisCO and expressed as a percentage of the corresponding wild-type content. Asterisks indicate statistically significant differences between mutant and WT according to Student's t test (*, P < 0.05; **, P < 0.01; ***, P < 0.001).. Asterisks indicate statistically significant differences between mutant and WT according to Student's t test (*, P < 0.05; **, P < 0.01; ***, P < 0.001).

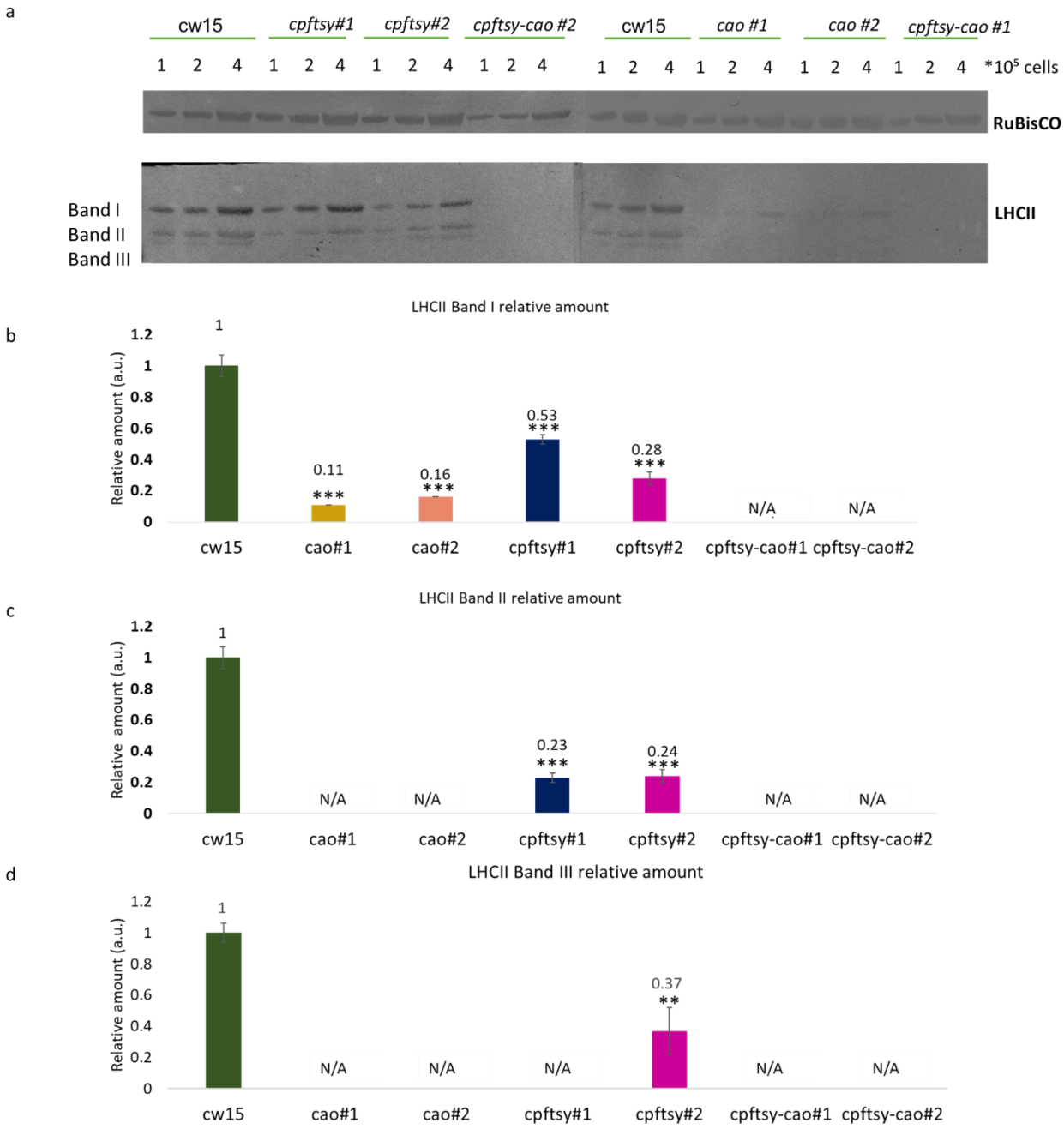

Figure 6.7.7. Western blot and densitometric analysis on LHCIIs content. a) Western blot membranes. sample volumes corresponding to different cell numbers of each strain were loaded in a 15%-acrylammide SDS-PAGE,

Tris-Tricine gel system ("1", $1*10^5$; "2", $2*10^5$; "4", $4*10^5$ cells). b-c-d) densitometric analysis on the basis of RuBisCO content. The image analysis was performed by ImageLab software (Biorad). Three different amounts were analysed for each sample. Data of band intensities were normalized to the RuBisCO and expressed as a percentage of the corresponding wild-type content. Asterisks indicate statistically significant differences between mutant and WT according to Student's t test (*, $P < 0.05$; **, $P < 0.01$; ***, $P < 0.001$).

To observe the differences in antenna proteins and supercomplexes abundance the thylakoids were then extracted from the six mutants and the cw15 wild type strain. They were grown five days in TAP rich medium and low light conditions (50µE), to allow also the growth of the light sensitive genome edited strains. The thylakoids extracts were used to perform a Deriphat-PAGE analysis loading 25 µg of each sample of chlorophyll on the gel (figure 6.7.8). The *cao#1* and *#2* mutants and the double *cpftsy-cao#1* and *#2* showed a higher content in PSII core as expected, because the same amount of chlorophyll means more cells of pale mutants. The other kind of supercomplexes were almost absent. *cpftsy#1* mutant showed a stronger reduction of this complexes with a higher presence of PSII and monomeric LHCII, while *cpftsy #2* showed less monomeric LHCII, but a wild type content in trimeric LHCII, as seen in the previous gel analysis.

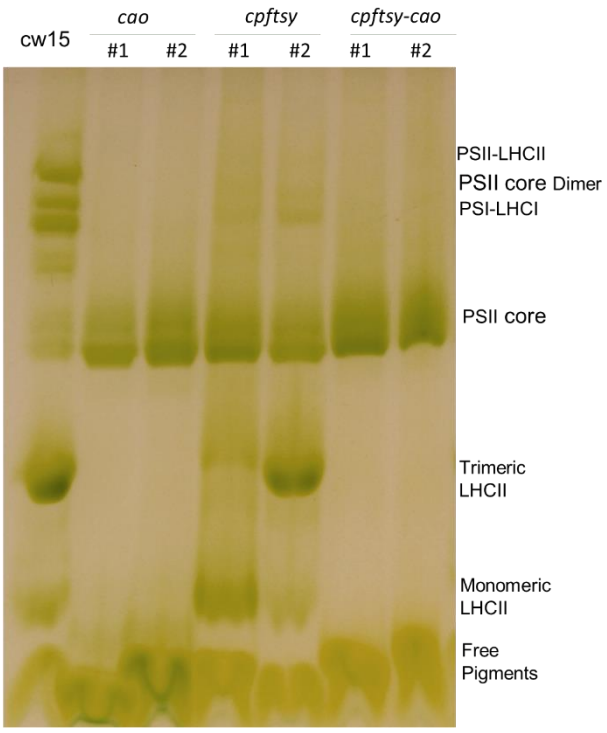

Figure 6.7.8. Deriphat-PAGE analysis. The thylakoids were extracted from TAP grown cultures at 50 µE. The samples were treated by β-DM detergent. The bands correspondent to different kind of complexes are indicated in the figure.

REFERENCES

Angstenberger M, de Signori F, Vecchi V, Dall'Osto L, Bassi R (2020) Cell Synchronization Enhances Nuclear Transformation and Genome Editing via Cas9 Enabling Homologous Recombination in Chlamydomonas reinhardtii. ACS Synth Biol. https://doi.org/10.1021/acssynbio.0c00390

Bae S, Park J, Kim JS (2014) Cas-OFFinder: a fast and versatile algorithm that searches for potential off-target sites of Cas9 RNA-guided endonucleases. Bioinformatics 30:1473–1475 . https://doi.org/10.1093/bioinformatics/btu048

Baek K, Kim DH, Jeong J, Sim SJ, Melis A, Kim JS, Jin E, Bae S (2016) DNA-free two-gene knockout in Chlamydomonas reinhardtii via CRISPR-Cas9 ribonucleoproteins. Sci Rep 6:30620 . https://doi.org/10.1038/srep30620

Bujaldon S, Kodama N, Rappaport F, Subramanyam R, de Vitry C, Takahashi Y, Wollman FA (2017) Functional Accumulation of Antenna Proteins in Chlorophyll b-Less Mutants of Chlamydomonas reinhardtii. Mol Plant 10:115–130 . https://doi.org/10.1016/j.molp.2016.10.001

Cardol P, Bailleul B, Rappaport F, Derelle E, Béal D, Breyton C, Bailey S, Wollman FA, Grossman A, Moreau H, Finazzi G (2008) An original adaptation of photosynthesis in the marine green alga Ostreococcus. Proc Natl Acad Sci U S A 105:7881–7886 . https://doi.org/10.1073/pnas.0802762105

Croce R, Canino G, Ros F, Bassi R (2002) Chromophore Organization in the Higher-Plant Photosystem II Antenna Protein CP26. Biochemistry 41:7334–7343 . https://doi.org/10.1021/bi0257437

Ferenczi A, Pyott DE, Xipnitou A, Molnar A (2017) Efficient targeted DNA editing and replacement in Chlamydomonas reinhardtii using Cpf1 ribonucleoproteins and single-stranded DNA. Proc Natl Acad Sci 114:13567 LP – 13572 . https://doi.org/10.1073/pnas.1710597114

Kirst H, García-Cerdán JG, Zurbriggen A, Melis A (2012) Assembly of the light-harvesting chlorophyll antenna in the green alga Chlamydomonas reinhardtii requires expression of the TLA2-CpFTSY gene. Plant Physiol 158:930–945 . https://doi.org/10.1104/pp.111.189910

Lauersen KJ, Wichmann J, Baier T, Kampranis SC, Pateraki I, Møller BL, Kruse O (2018) Phototrophic production of heterologous diterpenoids and a hydroxy-functionalized derivative from Chlamydomonas reinhardtii. Metab Eng 49:116–127 . https://doi.org/https://doi.org/10.1016/j.ymben.2018.07.005

Ordon J, Gantner J, Kemna J, Schwalgun L, Reschke M, Streubel J, Boch J, Stuttmann J (2017) Generation of chromosomal deletions in dicotyledonous plants employing a user-friendly genome editing toolkit. Plant J 89:155–168 . https://doi.org/10.1111/tpj.13319

Park J, Bae S, Kim JS (2015) Cas-Designer: a web-based tool for choice of CRISPR-Cas9 target sites. Bioinformatics 31:4014–4016 . https://doi.org/10.1093/bioinformatics/btv537

Perrine Z, Negi S, Sayre RT (2012) Optimization of photosynthetic light energy utilization by microalgae. Algal Res 1:134–142 . https://doi.org/10.1016/j.algal.2012.07.002

Porra RJ, Thompson WA, Kriedemann PE (1989) Determination of accurate extinction coefficients and simultaneous equations for assaying chlorophylls a and b extracted with four different solvents: verification of the concentration of chlorophyll standards by atomic absorption spectroscopy. Biochim Biophys Acta - Bioenerg 975:384–394 . https://doi.org/https://doi.org/10.1016/S0005-2728(89)80347-0

Shin YS, Jeong J, Nguyen THT, Kim JYH, Jin E, Sim SJ (2019) Targeted knockout of phospholipase A2

to increase lipid productivity in Chlamydomonas reinhardtii for biodiesel production. Bioresour Technol 271:368–374 . https://doi.org/https://doi.org/10.1016/j.biortech.2018.09.121

CHAPTER 7
Discussion and Conclusion

Sunlight energy exceeds the energy required by anthropic activities by more than 3 orders of magnitude. Therefore, the enhancement of its exploitation represents a major target in the field of renewable energies. Thanks to oxygenic photosynthesis, photoautotrophic organisms (plants, algae and cyanobacteria) convert solar energy into biomass at high rate. Theoretical estimations suggest that large scale cultivation of photoautotrophic organisms could cover a significant portion of global energy demand, in particular the production of liquid fuels which can be used in existing transport systems (Melis 2009). In this scenario, the interest in mass cultivation of microalgae in open ponds or closed photobioreactors (PBRs) has grown in the last decades. Besides small-scale traditional cultivations for nutraceutical purpose, new strategies for feedstock production from these organisms have been proposed in last years (Benedetti et al. 2018). It is worth noting that many algal cultivations are more productive than the best performing energy crops, due to the higher efficiency of converting solar energy into biomass. Microalgae are employed for wastewater treatment and to produce bioactive compounds, recombinant proteins and next generation biofuels (Benedetti et al. 2018; Benedetti et al. 2020). After the extraction of the desired product, residual biomass can be further processed into livestock feed, organic fertilizer and bio-stimulants, or used for energy cogeneration (Garcia-Gonzalez and Sommerfeld 2016; Madeira et al. 2017). Different biotechnological strategies, including forward and reverse genetics, and genetic engineering, are currently employed to increase microalgae productivity, aimed at enhancing light energy conversion efficiency into biomass (Hlavova et al. 2015). Several studies have been focused on the production of high value compounds and recombinant enzymes to be used in industrial processes, whose production costs benefit from the fast growth rate of these organisms (Vingiani et al. 2019; Giovannoni et al. 2020).

However, microalgae industrial exploitation is still limited by economic and technical factors. Such as the high costs required for PBRs construction and maintenance, for water pumping, for biomass harvesting and metabolite extraction and for sterile cultivation. There are also some physiological limitations that affect the productivity of these systems (Dall'Osto et al. 2019). These constrictions limited the light use under high irradiance and mass cultivation conditions (Rodolfi et al. 2009). The largest factors are the light-saturation at the used intensities, the inhomogeneous distribution of light and photoinhibition (Stephenson et al. 2011).

For these reasons a large part of microalgae research community was focused on the obtainment of photosynthetic mutants, both to study photosynthetic mechanisms and to identify more productive strains (Cazzaniga et al. 2014; Kirst and Melis 2014). The so-called pale-green mutants have sparked interest in last few years as they have shorter antenna systems and therefore reduced optical density, making light distribution more homogeneous, can reduce the photoinhibition of the outer cell layers, and moreover they saturate photosynthesis at higher light intensities (Dall'Osto et al. 2019; Vecchi et al. 2020). Not all of these kinds of mutants, of course, are able to growth well, neither in low nor medium light conditions, as the system is fine-tuned and a loss of important

components could lead to a cascade of changes in the regulation of transcription and translation of essential cell components (Formighieri et al. 2012), moreover defects in important pigment biosynthetic pathways lead to semi-lethal phenotypes (Chekounova et al. 2001). Therefore, the study of the loss-of- function mutants for photosynthetic genes allows researchers to discern the differences between interesting mutations for industrial purposes and those useful to deeply understand the regulation mechanisms underlying the metabolic and genetic regulation of this essential process.

In this thesis the effort to find a factor involved in a high growth phenotype leads to the characterization of loss of function mutants, unable to grow in high light, but possessing useful features to understand the importance of some proteins in the regulation of photosynthesis. *as 2.1* is a particular mutant, whose *as2* parental strain obtained in the laboratory where this work was performed (Bonente et al. 2011) and backcrossed with the wild type to clean the genome from on-the-side mutations. *as 2.1* has an interesting phenotype to reproduce for industrial biomass cultivation, as it grows faster than the wild type in high light conditions and in minimal medium, with the possibility to harvest the cell from the saturated bioreactors every 4 days from a proper starting inoculum. This feature was attributed to the moderate pale-phenotype of this mutant, characterized by a lower chlorophyll content and a moderately higher chlorophyll a/b ratio compared to the wild type. This hypothesis was strengthened by the rearrangement in the *CpFTSY* region which was found by previous researches. This gene encodes for a soluble receptor belonging to the SRP pathway, which is required for the insertion of Light Harvesting Chlorophyll Proteins (LHCPs) into thylakoid membranes and its loss could explain the pale phenotype observed.

For this reason, a genome edited mutant, obtained by targeting the *CpFTSY* gene directly by CRISPR-Cas9 system, was considered useful to understand the role of this gene in the understanding of the *as2.1* mutant phenotype. Mutants in this gene were already present in literature, both obtained by random mutagenesis (Kirst et al. 2012a) and genome editing (Baek et al. 2016). Both these mutants had a paler phenotype compared to *as2.1* (see tab 1), but they showed a good productivity, as the mutant *tla2* from Kirst and collaborators saturated photosynthesis at higher light intensity than the wild type (Kirst et al. 2012a), while the mutant ∆cpftsy of Baek seemed to grow faster than the wild type (Baek et al. 2016). To obtain *cpftsy* mutants it was used a protocol that similarly to Baek's one is based on the direct electroporation of the protein and the sgRNA into the cell, but established the codelivery of a resistance cassette both to facilitate the screening and to be sure to a completely interrupt the gene. In following publications it is indeed reported that a linearized DNA sequence is much more likely to be inserted soon after the PAM sequence than in other parts of the genome (Shin et al. 2019). The mutants obtained in this thesis, *cpftsy#1* and *cpftsy#2,* indeed contained a large plasmid insertion either just after or just before the PAM (figure 6.2.2). To be sure of the efficiency of the gene targeting the protospacer selected for the sgRNA was the best of those used by Baek in his publication (Baek et al. 2016). Therefore, these mutants should be similar to those obtained by the other research group. However, when, grown in high light and minimal medium, *cpftsy#*1 and *cpftsy#2* appeared completely unable to start to grow, while *as2.1*, supposedly affected in the same gene, grew faster than the WT cw15 (figure 6.3.1). This difference in respect to the other group's ∆cpftsy mutant could be due to the period of the observation, as they observed the growth for only 40 hours, in such a short period also small fluctuations could be amplified.

To better compare *cpftsy #1* and *cpftsy#2* with *as2.1* the absorption spectra were measured, as indicators of pigment content and consequent loss of antennae. *as 2.1* spectrum showed only minor differences compared to WT, resulting in a reduction of 45% in chlorophyll content and a significatively higher chlorophyll a/b ratio, while the chlorophyll/cars ratio remained the same (figure 6.3.2). *cpftsy#1* and *cpftsy#2* showed on the contrary larger differences in spectra shape compared to the wild type, as confirmed by fitting they presented a lower chlorophyll content (about the 20% of the WT) and a much more higher a/b ratio (figure 6.3.2). Also, the carotenoid content was higher from both the spectra observation and their fitting (figure 6.3.2). The Deriphat-PAGE analysis confirmed this difference between *as 2.1* and the genome edited mutants. *as2.1* presented a lower content in complexes respect to PSII core and monomeric LHCII, with an important reduction in PSII core dimers and PSII LHCII (figure 6.3.3). However, this reduction was more pronounced in *cpftsy#1* and *cpftsy#2*, which in any case presented small differences also among themselves, as *cpftsy#2* presented a higher content in trimeric LHCII compared to the other strains (figure 6.3.3). From this data it would appear that *CpFTSY* was not involved in the *as2.1* high-grow phenotype and that another gene possibly played a role in determining the pale-green phenotype.

To have a better picture of the situation *as2.1*, *cpftsy#1* and *cpftsy#2* were complemented by a plasmid containing the coding sequence of *CpFTSY* under the control of its endogenous promoter and terminator, to avoid background effects due to a different gene regulation (figure 6.4.1). The sequence was able to fully restore the dark green phenotype and the protein expression in all the strains, while for the chlorophyll content the *as2.1* was only partially complemented (figure 6.4.2 and 6.4.5). Moreover, from the Deriphat page analysis emerged that the as2.1C2 complemented strain, conserved the same profile of as2.1 for photosynthetic complexes composition (figure 6.4.7). This indicated that possibly another as yet unknown gene is involved in chlorophyll biosynthesis or in any case not determining a chlorophyll *a*/*b* ratio impairment played a role in the phenotype of this mutant. Taking a look at the grow in high light and minimal medium, the complemented strains derived from *cpftsy* genome edited mutants fully restored the ability to grow similar to WT. At the same time, the *as 2.1* derived complemented strain lost the ability to reach faster the exponential phase, suggesting a partial involvement of *CpFTSY* in the growth phenotype Figure 6.4.6). The protein is absent also in *as2.1*, consequently the phenotype is surely not due to a downregulation of the gene, but another altered factor or a compensation mechanism which activated alternative pathways attenuated the pale green phenotype. It remains to be seen and understood if it is an interactor of the SRP pathway protein or a protein that belongs to a parallel acting pathway or a factor that works in a totally different process which results in the partial softening of the possible consequences of *CpFTSY* loss. Further mapping studies will reveal also if this co-responsible mutation is in the *CpFTSY* poorly annotated flanking region and also if it is present in a gene or in a regulation sequence.

Since in protein gels a variability was observed in *cpfsty*#1 and *cpftsy*#2 mutants for the LHCII content and their arrangement, they were also compared with other genome edited strains *cpftsy*N1,*cpftsy*N2, *cpftsy*N3 and *cpftsy*N4, obtained with another sgRNA against the same gene, during the optimization of the transformation protocol (Angstenberger et al. 2020). The analysis revealed a variability in total chlorophyll and chlorophyll *b* content (figure 6.5.2), as reported by Baek and colleagues (Baek et al. 2016), with different abundances of LHCII proteins, as indicated by the different intensities of their bands in western blot and protein gel analysis (figure 6.5.3 and 6.5.4).

This variability, therefore, it is not due to a side mutation in one of the *cpftsy* mutants, but could be attributed to a different antennae rearrangement. The differences in carotenoids content can therefore be explained by different stress levels depending on the variable connectivity of PSII, that leads to different degrees of photoprotection (figure 6.5.2). The more photosensitive phenotype of the recently isolated strains, that was in part recovered after different plating cycles could be explained by the less connectivity of PSII, that makes the reaction center more exposed to photodamage. According to different authors, the CpSRP pathway is not the only pathway responsible for the insertion of LHCPs into the thylakoid membranes (Kirst et al. 2012b; Kirst et al. 2012a; Bujaldon et al. 2020). Mutations in different proteins involved in this pathway can, indeed, affect the insertion of only some of the LHCPs, and each component seems to have slightly different specificities (Kirst et al. 2012b; Kirst et al. 2012a; Baek et al. 2016; Jeong et al. 2017; Jeong et al. 2018). An alternative receptor or import mechanism could therefore compensate in part for the activity of CpFTSY/CpSRP pathway and among the apoprotein produced, some could be excluded from the insertion and consequently degraded for a saturation of the remaining insertion systems. This could explain the difference abundance of also apoproteins in these strains.

To further understand the mechanisms involved in antenna size determination and, consequently, in light harvesting capacity it was decided to compare *cpftsy* mutants with chlorophyll *b* defective strains. The CRISPR-Cas9 system was employed to obtain both *cao* single and *cpftsy-cao* double mutants (figure 6.6.1;6.6.2;6.6.3;6.6.4) to understand the relative weights of the LHCPs insertion pathway and the chlorophyll *b* biosynthesis pathway in the correct functioning of supercomplexes and antennae connectivity. Other mutants in this gene were previously characterized (Perrine et al. 2012; Bujaldon et al. 2017), but this kind of comparison, which had been already performed in plants (Wang and Grimm 2016) was never done in *Chlamydomonas*. The double mutant was not obtained in plants, probably for the larger defect that this kind of mutation causes in these organisms.
cao single mutants showed, as expected, a chlorophyll *b* deficiency, with large depressions in adsorption spectra in correspondence to the chlorophyll *b* adsorption regions (figure 6.7.1a). The same is true for the *cpftsy-cao* double mutants, that presented, in addition, the large carotenoids peak typical of *cpftsy* mutants (figure 6.7.1a). It also had a lower chlorophyll/carotenoids ratio, because this kind of strain was more light stressed than the single mutants from which it derives (figure 6.7.1d). *cao* single mutants were also less affected in total chlorophyll content and in Chl/Car ratio, probably because they were able to insert chlorophyll *a* also in some Chl *b* binding sites in the PSII peripheral antenna, as suggested by Bujaldon and colleagues in 2017 (Bujaldon et al. 2017). They suggested also that these Chl *a* molecules are only loosely bound to apoproteins, as demonstrated by the Deriphat-PAGE analysis performed in this thesis (figure 6.7.8). Both *cao* and *ftsy-cao* mutants, not only showed a significant deficiency in supercomplexes, but also in monomeric LHCII (figure 6.7.8). Moreover, the western blot analysis showed in *cao* single mutants a doubling in CP47 PSII core antenna protein, suggesting also an increase in Chl *a* binding protein content to compensate the loss Chl *b* (figure 6.7.6). They seemed to be in this way less subjected to light stress and showed the ability to grow faster than the wild type in photoautotrophic condition (figure 6.7.3).
From the western blot also emerged that the defects of the two pathways seem to lead to different alterations in protein expression, probably related to the refined transcriptional regulation mechanism that controls the photosynthesis functioning in plants and algae (figure 6.7.6).
cpftsy mutants were unexpectedly defective in CP47, while *cao* strains in cytochrome f (figure 6.7.6). As expected, the double mutants presented both alterations, further studies can clarify the mechanisms that cause them. Interestingly all the mutants showed a reduction in PsaA content, that

for *cao* single mutants was less significant (according the statistic it was significant only for *cao#2*), but that could explain *cpftsy* and *cpftsy-cao* photosensitivity (figure 6.7.6). Moreover, the decrease of core proteins in *cpftsy* mutants seemed to indicate a previously non reported involvement in the insertion of these protein. The analysis obviously displayed also a reduced amount of LHCIIs apoproteins for all the strains (figure 6.7.7) and the differences that emerged from the western blot correspond to the PSII functional antenna size measurements (figure 6.7.5). *cpftsy* mutants maintained the 80-85% of the function, while *cao* single mutants the 25-30% and *cpftsy-cao* the 15-20% (figure 6.7.5). However, these differences are not directly related to their photosensitivity.
The comparison between single and double mutants grown in medium light and the stronger deficiency in LHCII of the latter seem to confirm the observation of Bujaldon and colleagues for the mutant yid-BF3, a random insertional mutant for *CAO* defective in chlorophyll biosynthesis (Bujaldon et al. 2017). They hypothesized that when Chl *a* biosynthesis is too low is impossible to integrate Chl *a* into Chl *b* binding sites in LHC complexes, allowing their degradation. In the *cpftsy-cao* mutants case the problem is not due to a lower biosynthesis of chlorophyll *a*, but both to the missing of some LHCPs (for the mutation in *CPFTSY*) in thylakoid membranes, which leads consequentially a drop in chlorophyll binding sites of both types, and to the missing of chlorophyll *b* (for *CAO*), that left empty some binding sites of the remaining LHCII inserted with alternative mechanisms, which can be easily degraded. This lack in antennae can explain the extreme photosensitivity of the double mutants.
From these results chlorophyll *b* biosynthetic pathway seems more essential for the organization of the supercomplexes and the peripherical antenna systems, for the balance between LHCII and LHCI and the stability of the LHCPs apoproteins, but is less determinant for photosensitivity/ photoresistance of the cells and for the core functionality. The two *cpftsy* mutants suggest that this pathway has not a unique function in the cell, but as suggested by other authors (Kirst et al. 2012a; Kirst and Melis 2014; Bujaldon et al. 2020), some LHCPs proteins are inserted by other pathways. The differences between *cpftsy#1* and *cpftsy#2* in monomeric and trimeric LHCII content, not only suggested different possible compensation and reorganization mechanisms but also a preference of CpSRP pathway for the LHCII directly bounded to PSII. However, the lower affection of *cpftsy* single mutants in LHCII apoprotein content and the higher antenna size they showed compared to *cao#1* and *cao#2* strains indicate a minor role in antenna size regulation. The lower PsaA and CP47 contents (figure 6.7.6), as said before, also suggest an involvement of this receptor in the core protein insertion. This was observed also by Kirst in 2012, but it was interpretated as an effect of another side mutation (Kirst et al. 2012a). From the Deriphat-PAGE possible effects on PSII core content were not detectable (figure 6.7.8), since it was not loaded on a cell basis. Other measurements and western blots against other core proteins will clarify this aspect.
As final observation an interesting feature of *cao* single mutants is the ability to grow faster than the WT in high light conditions and in minimal medium conditions (figure 6.7.3). Further experiments will reveal if this mutant could be exploitable for industrial applications and if CAO is a good target to produce pale mutants also in other species.

Table 6: Overwiev on *CAO* and *CpFTSY* KO mutants reported in literature and in this work. the table present the mutants classified based on the affected gene function. The parameters values are normalized to the % respect to the respective wild type strain. When they change according light conditions it is specified in the brackets. Some values were deduced from papers graphs and some ratios were calculated from reported data; therefore, the value could be subjected to small estimation errors.

Mutant	Afftcted gene	Genetic modificatio n	Chl tot %	Chl a/b ratio (%)	Car tot (%)	Car/ Chl (%)	PSII antenna size (%)	Fv/ Fm	Photosensitivity/ photoresistance
as2 (Bonente et al.,2011)	*CpFTSY?*	Random DNA insertion	-	130	190	-	About 80	-	Photoresistant
as2.1 (Backcross of as2.1)	*CpFTSY Other gene?*	Random DNA insertion	57	122	-	106	60	-	Photoresistant
as2.1 C1 (this work)	as 2.1 complemented by *CpFTSY* CDS	DNA insertion	68	108	-	106	-	-	Similar to the WT
as2.1 C2 (this work)	as 2.1 complemented by *CpFTSY* CDS	DNA insertion	66	108	-	106	-	-	Similar to the WT
tla2 (Kirst et al., 2012b)	*CpFTSY*	Random DNA insertion	18	352	35	180	63	-	Saturation at higher light intensities
ΔCpFTSY (Baek et al., 2016)	*CpFTSY*	CRISPR-Cas9	30	280	50	180	-	-	Photoresitant 700µE
cpftsy#1 (this work)	*CpFTSY*	CRISPR-Cas9	22	150	-	250	82	-	Photosensitive
cpftsy#2 (this work)	*CpFTSY*	CRISPR-Cas9	22	150	-	250	86	-	Photosensitive
cpftsy#1 C1 (This work)	*cpftsy#1* complemented by *CpFTSY* CDS	DNA insertion	86	108	-	103	-	-	Similar to the WT
cpftsy#1 C2 (this work)	*cpftsy#1* complemented by *CpFTSY* CDS	DNA insertion	104	95	-	88	-	-	Similar to the WT
cpftsy#2 C1 (this work)	*cpftsy#1* complemented by *CpFTSY* CDS	DNA insertion	92	96	-	100	-	-	Similar to the WT
cpftsy#2 C2 (this work)	*cpftsy#1* complemented by *CpFTSY* CDS	DNA insertion	105	108	-	90	-	-	Similar to the WT
cpftsyN1 (this work)	*CpFTSY*	CRISPR-Cas9	16	200	-	64	38	-	Photosensitive
cpftsyN2 (this work)	*CpFTSY*	CRISPR-Cas9	16	200	-	58	74	-	Photosensitive
cpftsyN3 (this work)	*CpFTSY*	CRISPR-Cas9	18	200	-	55	42	-	Photosensitive
cpftsyN4 (this work)	*CpFTSY*	CRISPR-Cas9	16	192	-	55	65	-	Photosensitive
BF3 (Bujaldon et al., 2017	*CAO*	UV-generated mutants	65 (50 µE) 87 (1µE)	∞	-	-	50 (50 µE) 40 (1µE)	60 (50 µE) 37 (1µE)	--
pg27 (Bujaldon et al., 2017)	*CAO*	UV-generated mutants	65 (50 µE) 58	∞	-	-	-	40	-

			(1µE)						
cbs3 (Bujaldon et al., 2017)	*CAO*	DNA deletion	80 (50 µE) 96 (1µE)	∞	-	-	-	56	-
cao#1 (this work)	*CAO*	CRISPR-Cas9	70	∞	-	147	30	-	Photoresistant
cao#2 (this work)	*CAO*	CRISPR-Cas9	70	∞	-	164	26	-	Photoresistant
cpftsy-cao#1 (this work)	*CAO*	CRISPR-Cas9	15	∞	-	270	20	-	Photosensitive
cpftsy-cao#2 (this work)	*CAO*	CRISPR-Cas9	15	∞	-	322	14	-	Photosensitive

REFERENCES

Angstenberger M, de Signori F, Vecchi V, Dall'Osto L, Bassi R (2020) Cell Synchronization Enhances Nuclear Transformation and Genome Editing via Cas9 Enabling Homologous Recombination in Chlamydomonas reinhardtii. ACS Synth Biol. https://doi.org/10.1021/acssynbio.0c00390

Baek K, Kim DH, Jeong J, Sim SJ, Melis A, Kim JS, Jin E, Bae S (2016) DNA-free two-gene knockout in Chlamydomonas reinhardtii via CRISPR-Cas9 ribonucleoproteins. Sci Rep 6:30620 . https://doi.org/10.1038/srep30620

Benedetti M, Barera S, Longoni P, Guardini Z, Herrero Garcia N, Bolzonella D, Lopez-Arredondo D, Herrera-Estrella L, Goldschmidt-Clermont M, Bassi R, Dall'Osto L (2020) A microalgal-based preparation with synergistic cellulolytic and detoxifying action towards chemical-treated lignocellulose. Plant Biotechnol J n/a: . https://doi.org/10.1111/pbi.13447

Benedetti M, Vecchi V, Barera S, Dall' Osto L (2018) Biomass from microalgae : the potential of domestication towards sustainable biofactories. Microb Cell Fact 1–18 . https://doi.org/10.1186/s12934-018-1019-3

Bonente G, Formighieri C, Mantelli M, Catalanotti C, Giuliano G, Morosinotto T, Bassi R (2011) Mutagenesis and phenotypic selection as a strategy toward domestication of Chlamydomonas reinhardtii strains for improved performance in photobioreactors. Photosynth Res 108:107–120 . https://doi.org/10.1007/s11120-011-9660-2

Bujaldon S, Kodama N, Rappaport F, Subramanyam R, de Vitry C, Takahashi Y, Wollman FA (2017) Functional Accumulation of Antenna Proteins in Chlorophyll b-Less Mutants of Chlamydomonas reinhardtii. Mol Plant 10:115–130 . https://doi.org/10.1016/j.molp.2016.10.001

Bujaldon S, Kodama N, Rathod MK, Tourasse N, Ozawa SI, Selles J, Vallon O, Takahashi Y, Wollman FA (2020) The BF4 and p71 antenna mutants from Chlamydomonas reinhardtii. Biochim Biophys acta Bioenerg 1861:148085 . https://doi.org/10.1016/j.bbabio.2019.148085

Cazzaniga S, Dall'Osto L, Szaub J, Scibilia L, Ballottari M, Purton S, Bassi R (2014) Domestication of the green alga Chlorella sorokiniana: Reduction of antenna size improves light-use efficiency in a photobioreactor. Biotechnol Biofuels 7:157 . https://doi.org/10.1186/s13068-014-0157-z

Chekounova E, Voronetskaya V, Papenbrock J, Grimm B, Beck C (2001) Characterization of Chlamydomonas mutants defective in the H subunit of Mg-chelatase. Mol Genet Genomics 266:363–373 . https://doi.org/10.1007/s004380100574

Dall'Osto L, Cazzaniga S, Guardini Z, Barera S, Benedetti M, Mannino G, Maffei ME, Bassi R (2019) Combined resistance to oxidative stress and reduced antenna size enhance light-to-biomass conversion efficiency in Chlorella vulgaris cultures. Biotechnol Biofuels 12:221 . https://doi.org/10.1186/s13068-019-1566-9

Formighieri C, Ceol M, Bonente G, Rochaix JD, Bassi R (2012) Retrograde Signaling and Photoprotection in a gun4 Mutant of Chlamydomonas reinhardtii. Mol Plant 5:1242–1262 . https://doi.org/https://doi.org/10.1093/mp/sss051

Garcia-Gonzalez J, Sommerfeld M (2016) Biofertilizer and biostimulant properties of the microalga Acutodesmus dimorphus. J Appl Phycol 28:1051–1061 . https://doi.org/10.1007/s10811-015-0625-2

Giovannoni M, Gramegna G, Benedetti M, Mattei B (2020) Industrial Use of Cell Wall Degrading Enzymes: The Fine Line Between Production Strategy and Economic Feasibility . Front. Bioeng. Biotechnol. 8:356

Hlavova M, Turoczy Z, Bisova K (2015) Improving microalgae for biotechnology — From genetics to synthetic biology. Biotechnol Adv 33:1194–1203 . https://doi.org/https://doi.org/10.1016/j.biotechadv.2015.01.009

Jeong J, Baek K, Kirst H, Melis A, Jin ES (2017) Loss of CpSRP54 function leads to a truncated light-harvesting antenna size in Chlamydomonas reinhardtii. Biochim Biophys Acta - Bioenerg 1858:45–55 . https://doi.org/10.1016/j.bbabio.2016.10.007

Jeong J, Baek K, Yu J, Kirst H, Betterle N, Shin W, Bae S, Melis A, Jin E (2018) Deletion of the chloroplast LTD protein impedes LHCI import and PSI-LHCI assembly in Chlamydomonas reinhardtii. J Exp Bot 69:1147–1158 . https://doi.org/10.1093/jxb/erx457

Kirst H, García-Cerdán JG, Zurbriggen A, Melis A (2012a) Assembly of the light-harvesting chlorophyll antenna in the green alga Chlamydomonas reinhardtii requires expression of the TLA2-CpFTSY gene. Plant Physiol 158:930–945 . https://doi.org/10.1104/pp.111.189910

Kirst H, Garcia-Cerdan JG, Zurbriggen A, Ruehle T, Melis A (2012b) Truncated Photosystem Chlorophyll Antenna Size in the Green Microalga Chlamydomonas reinhardtii upon Deletion of the TLA3-CpSRP43 Gene. Plant Physiol 160:2251–2260 . https://doi.org/10.1104/pp.112.206672

Kirst H, Melis A (2014) The chloroplast signal recognition particle (CpSRP) pathway as a tool to minimize chlorophyll antenna size and maximize photosynthetic productivity. Biotechnol Adv 32:66–72 . https://doi.org/10.1016/j.biotechadv.2013.08.018

Madeira MS, Cardoso C, Lopes PA, Coelho D, Afonso C, Bandarra NM, Prates JAM (2017) Microalgae as feed ingredients for livestock production and meat quality: A review. Livest Sci 205:111–121 . https://doi.org/https://doi.org/10.1016/j.livsci.2017.09.020

Melis A (2009) Solar energy conversion efficiencies in photosynthesis : Minimizing the chlorophyll antennae to maximize efficiency. Plant Sci 177:272–280 . https://doi.org/10.1016/j.plantsci.2009.06.005

Perrine Z, Negi S, Sayre RT (2012) Optimization of photosynthetic light energy utilization by microalgae. Algal Res 1:134–142 . https://doi.org/10.1016/j.algal.2012.07.002

Rodolfi L, Zittelli GC, Bassi N, Padovani G, Biondi N, Bonini G, Tredici MR (2009) Microalgae for oil: Strain selection, induction of lipid synthesis and outdoor mass cultivation in a low-cost photobioreactor. Biotechnol Bioeng 102:100–112 . https://doi.org/10.1002/bit.22033

Shin YS, Jeong J, Nguyen THT, Kim JYH, Jin E, Sim SJ (2019) Targeted knockout of phospholipase A2 to increase lipid productivity in Chlamydomonas reinhardtii for biodiesel production. Bioresour Technol 271:368–374 . https://doi.org/https://doi.org/10.1016/j.biortech.2018.09.121

Stephenson PG, Moore CM, Terry MJ, Zubkov M V., Bibby TS (2011) Improving photosynthesis for algal biofuels: Toward a green revolution. Trends Biotechnol 29:615–623 . https://doi.org/10.1016/j.tibtech.2011.06.005

Vecchi V, Barera S, Bassi R, Dall'Osto L (2020) Potential and Challenges of Improving Photosynthesis in Algae. Plants (Basel, Switzerland) 9: . https://doi.org/10.3390/plants9010067

Vingiani GM, De Luca P, Ianora A, Dobson ADW, Lauritano C (2019) Microalgal Enzymes with Biotechnological Applications. Mar Drugs 17:459 . https://doi.org/10.3390/md17080459

Wang P, Grimm B (2016) Comparative Analysis of Light-Harvesting Antennae and State Transition in chlorina and cpSRP Mutants. Plant Physiol 172:1519–1531 . https://doi.org/10.1104/pp.16.01009

PART II

CRISPR-Cas9 system optimization in Chlamydomonas

CHAPTER 8
Method and Materials

8.1 Strains and culture conditions

The cw15 (mt-), *Chlamydomonas reinhardtii* strain (named also CC-4533, from chlamylibrary.org) was used as a genetic background to generate the genome edited mutants (*cpftsy#1*, *cpftsy#2*, *cao#1*, *cao#2*) *C. reinhardtii* cells were grown in TAP and maintained on TAP-agar medium (Harris et al. 1989; Kropat et al. 2011) at light intensity of 50 µmol/s/m^2, 100 rpm agitation, 25°C controlled temperature, 16 h light/8 h dark photoperiod. irradiance was provided by warm-white LEDs (Epistar 35mil Chip High Power LED, warm white LEDE-P20B-DW, Wayjun Tech., Shenzhen, China). Strains were grown adding 100 µg/ml of Ampicillin to avoid contaminations and for each mutant it was added different antibiotics, according to their resistances.

- *cpftsy#1* and *cpftsy#2*: Hygromycin 50 µg/ml
- *cao#1* and *cao#2*: Paromomycin 10 µg/ ml

8.2 Media composition

TAP: Tris-Acetate-Phospate medium (Kropat et al. 2011)

For 1 liter of solution:

Tris-HCl	2.42 g
TAP salts stock solution	25 ml
P-solution (phosphate buffer pH 7.0)	375 µl
Hutner's stock solutions (trace elements)	1 ml for each
Glacial acetic acid	1 ml
Milli q water	Up to 1L

The pH was increased to 6.8-6.9 using HCl.
The medium was autoclaved for 20' at 120 °C.
For solid medium, 1.5 % agar (w/v) was added before autoclaving.

TAP salts

NH_4Cl	15 g/L
$MgSO_4 \cdot 7 H_2O$	4 g/L
$CaCl_2 \cdot 2 H_2O$	2 g/L

P-solution (phosphate buffer pH 7.0)

K_2HPO_4	288 g/L
KH_2PO_4	144 g/L

Hutner's solutions

Solution 1	**EDTA-Na_2 pH 8.0**	**25 mM**
Solution 2	$(NH_4)_6Mo_7O_{23}$	28.5 µM
Solution 3	Na_2SO_3	0.1 mM
Solution 4	$ZnSO_4 \cdot 7H_2O$	25 mM
	EDTA-Na_2 pH 8.0	2.75 mM
Solution 5	$MnCl_2 \cdot 4H_2O$	6 mM
	EDTA-Na_2 pH 8.0	6 mM
Solution 6	$FeCl_3 \cdot 6H_2O$	20 mM
	EDTA-Na_2 pH 8.0	22 mM
	Na_2CO_3	22 mM
Solution 7	$CuCl_2 \cdot 2H_2O$	2 mM
	EDTA-Na_2 pH 8.0	2 mM

TOS

TAP	**80%**
Sucrose	40 mM
Water	20%

LB (Luria-Bertani) medium

For 1 L at pH 7

NaCl	10 g
Yeast extract	5 g
Triptone	10 g
Milliq-water	Up to 1L

The medium was autoclaved for 20' at 20°C
For solid medium, 1.5 % agar (w/v) was added before autoclaving.

Modified high-salt LB

For the recovery of E. coli after the electric, or thermal shocks A high salt LB medium was prepared.
In 10 ml of LB were dissolved:

- 125 µl of 1M $MgSO_4$
- 125 µl of 1M $MgCl_2$
- 200 µl of 20% glucose

8.3 Molecular Biology

8.3.1 Polymerase Chain Reaction (PCR)

Polymerase chain reaction was used to amplify different kind of genomics sequences. The reaction was performed by using different primers, whose annealing temperature was calculated on the basis of the length and the G/C content [(2°C X n (A/T) + 4°C x n (G/C))-2]. To screen bacterial or algal strain it was used the Go-Taq Green Master Mix (Promega) and the mix in 50 µl was prepared as follows:

2 X Go-Taq Master Mix	25 µl
DMSO	1 µl
100 µM Primer Fw	0.25 µl
100 µM Primer Rev	0.25 µl
Template	100 ng
H_2O	Up to 50 µl

The thermocycler was set as follows:

- 3' of denaturation at 95°C
- 28-35 cycles:
  - 30'' of denaturation at 95°C
  - 30'' of annealing at 56°C-60°C (it depends on the primer length and G/C content)
  - 1 kb/1' of extension at 72°C
- 3' of final extension at 72°C

To amplify the templates for the sgRNA, the target sequences for the *in vitro* cut assay and for all sequence that need to be amplify without errors it was used a proof reading taq, namely Phusion Hot Start II DNA Polymerase (Termofisher), and the mix in 50 µl was prepared as follows:

5 X Phusion Buffer	10 µl
10 mM dNTP mix	1 µl
DMSO	1 µl
100 µM Primer Fw	0.25 µl
100 µM Primer Rev	0.25 µl
Template	100 ng
H_2O	Up to 50 µl

The thermocycler was set as follows:

- 30'' of denaturation at 98°C
- 28-35 cycles:
  - 10'' of denaturation at 98°C
  - 30'' of annealing at 56°C-60°C (it depends on the primer length and G/C content)
  - 1 kb/30'' of extension at 72°C
- 3' of final extension at 72°C

The PCR products were checked by an electrophoresis analysis on 1-1.5% agarose gel, on the basis of products length.

8.3.2 List of used primers

Name	Sequence	Used for:
Cas9REV	AAAAAAAGCACCGACTCGGTGCCAC	SgRNA Template
Sg CAO FWD	GCTCTCCGGGTCCTCAACGAGTTTTAGAGCTAGAAATAGCAAG	SgRNA Template
SgCPFTSY FWD	CGATCTTCAGAGCAGTGCGGGTTTTAGAGCTAGAAATAGCAAG	SgRNA Template
PT7CAO FWD	TAATACGACTCACTATAGCTCTCCGGGTCCTCAAC	SgRNA Template
PT7CPFTSY FWD	TAATACGACTCACTATAGCGATCTTCAGAGCAGTGCG	SgRNA Template
CAO FWD	TGTTACCGCATAGAGCAGCC	Fragment for *in vitro* cut
CAO REV	CCCGGCGAGTGAGCATATT	Fragment for *in vitro* cut
CPFTSY FWD	TAGACCTGACGGGTACTGGG	Fragment for *in vitro* cut and mutant screening
CPFTSY REV	ACTCCGGTGCTGTTATTGGG	Fragment for *in vitro* cut

CPFTSY REV2	ATGCGGATGCAGTTTCTCCT	Mutant screening
Hyg FWD	GCTACAGCCTGGTGCAAC	Hygromycin resistance cassette insertion screening
PARO FWD	CGGCACCCATCCGGTATAAA	Paromomycin resistance cassette insertion screening
PARO REV	CGTCCAGATCCTCCAAGTCG	Paromomycin resistance cassette insertion screening
XbaINLS FWD	ATTGCTCTAGAAATAATTTTGTTTAACTTTAAGAAGGAGATATAC CATGCCCAAGAAG	NLS amplification and insertion
NLS FWD	ATATACCATGCCCAAGAAGAAGAGGAAGGTGATGGATAAGAAA TACTCAATAGGC	NLS amplification and insertion
NheIRv	TCTTCTTGGCTAGCTCCCC	NLS insertion
Screening fwd	GGAATTGTGAGCGGATAAC	NLS cloning screening

8.3.3 DNA extraction from *Chlamydomonas*

For the DNA extraction it was used a modified version of a protocol provided by Claire Remacle's laboratory.

- 2-3 ml of fresh culture of about 1x 10^7 cell/ml was pelleted for 5' at 2000 x g at 4°C.
- The pellet was resuspended in 500 µl of TEN (10mM Tris-HCl pH8, 10mM EDTA, 150mM NaCl).
- The suspension was spun down for 2' at 1500 x g at 4°C.
- The pellet was resuspended in 150 µl of water and 300 µl of SDS-EB (2% SDS 400mM NaCl, 40mM EDTA, 100mM Tris HCl pH8) and vortexed.
- 350 µl of phenol:chloroform:isoamyl alcohol (25:24:1) were added to the mixture.
- The sample was vortexed and spun down for 5' at 15000 x g at 4°C.
- The upper phase was collected and 300 µl of Chloroform: isoamyl (24:1) were added to it
- The sample was vortexed and spun down for 5' at 15000 x g at 4°C.
- The upper phase was collected and 2.5V of 100% ethanol and 0.11 V of 3 M pH 5.5 Na acetate 5.5 were added to it.
- The sample was spun down and incubated 30' at -80°C.
- The sample was spun down for 25' at 15000 x g at 4°C.
- The supernatant was discarded and resuspended in 1 V of 70% ethanol.
- The sample was spun down for 5' at 15000 x g and the supernatant is discarded.
- The pellet was dried under hood flux and resuspended in 30 µl of autoclaved milli-q water.

8.3.4 DNA quantification

Genomic and plasmid DNA was quantified by NanoDrop (Thermofwasher)
1.5 µl of sample was read using water as reference. The purity of the extraction was evaluated reading the absorbance ratio at 260 nm /280 nm and the 260 nm /230 nm. The 260/280 value indicates the ratio between the nucleic acid and the protein content; the 260/230 the ratio between nucleic acid and other organic contaminants likes phenol, ethanol etc. Both values must be major or equal to 1.8. The quality of DNA was evaluated by 1.5 % (w/v) agarose gel electrophoresis, 100 ng of each sample were loaded, and it was added the 6X TrikTrak loading Dye (Termofisher). As molecular weight marker it was used Gene Ruler 1 kb plus (Termofisher). The gel image was analysed with ChemiDoc (Biorad).

8.3.5 Agarose gel preparation

0.5 or 0.75 g of agarose were dissolved in 50 ml of 0.5X TAE (89 mM Tris-base, 89 mM CH3COOH, 2 mM EDTA pH 8.2) by heating in a microwave oven until boiling and 20000X EuroSafe (Vetroscientifica) was added to detect nucleic acid under ultraviolet (UV) light.

8.3.6 PCR or DNA reaction products purification

Cut plasmid, cut sequences or PCR products to sequence, to clone, to use for *in vitro* cut assays and to use as template for *in vitro* transcription were purified using NucleoSpin Gel and PCR Clean-up kit (Macherey-Nagel).

- 100 µl of NTI Binding Buffer were mixed to 50 µl of PCR product.
- The mixture was loaded on a spin column.
- The column was spun down 1’ at 12 000 x g at RT.
- The flowthrough was discarded and 500 µl of NT3 Washing Buffer (containing EtOH) were loaded on the column.
- The column was spun down 1’ at 12 000 x g at RT.
- The flowthrough was discarded and 500 µl of NT3 Washing Buffer were loaded on the column.
- The column was spun down 1’ at 12 000 x g at RT.
- The flowthrough was discarded, and the column was spun down 1’ at 12 000 x g at RT to eliminate the residual EtOH.
- The column was transferred on a new Eppendorf tube and 20 µl of 60°C sterile water were added for the elution.
- The sample was incubated 1’ at RT and spun down 1’ at 12 000 x g at RT.
- The flowthrough was collected in the tube and the column was thrown away.

8.3.7 SgRNA DNA- template synthesis

To synthetize the template for a specific sgRNA for A target sequence in the genome it was designed a primer complementary to the target sequence (protospacer) without the PAM and the first part of the conserved sequence of the sgRNA.: Protospacer (20 bp) +GTTTTAGAGCTAGAAATAGCAAG (Primer sgCAO FWD and sgCPFTSY FWD). Then it was designed another fix one complementary to the conserved end of sgRNA sequence: AAAAAAAGCACCGACTCGGTGCCAC (Primer Cas9 rev). As template for the amplification of the conserved parts was used the pDGE5 (Ordon et al. 2017) plasmid, used for the CRISPR-Cas9 technique in plants. The PCR reaction was performed using the proof reading Taq as described in 8.3.1 paragraph, setting 10 s of extension and 58°C as annealing temperature. The result is the complete 76 bp conserved sequence of sgRNA of with the desired 20 bp protospacer.

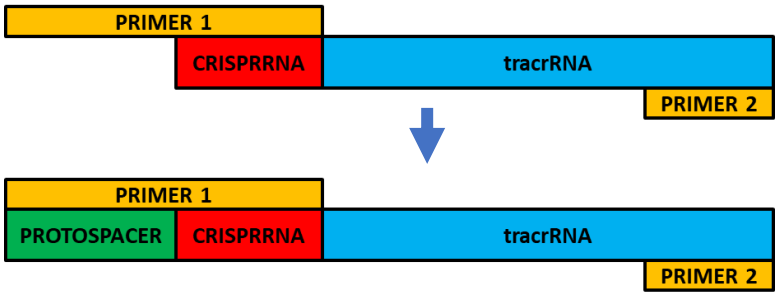

The product obtained was therefore purified as in 8.3.6 and was reamplified using a third primer complementary to the protospacer with the adding of the conserved sequence that is recognized from the T7 RNA Polymerase to start the *in vitro* transcription: TAATACGACTCACTATAG+Protospacer (PrimerT7CAO FWD and T7CPFTSY FWD). The reverse primer is the same complementary to the end of sgRNA used before (Cas9 REV). The PCR reaction was performed with the same setting and the final product was the 96 bp sgRNA complete template with the 20-18 bp T7 promoter at the beginning.

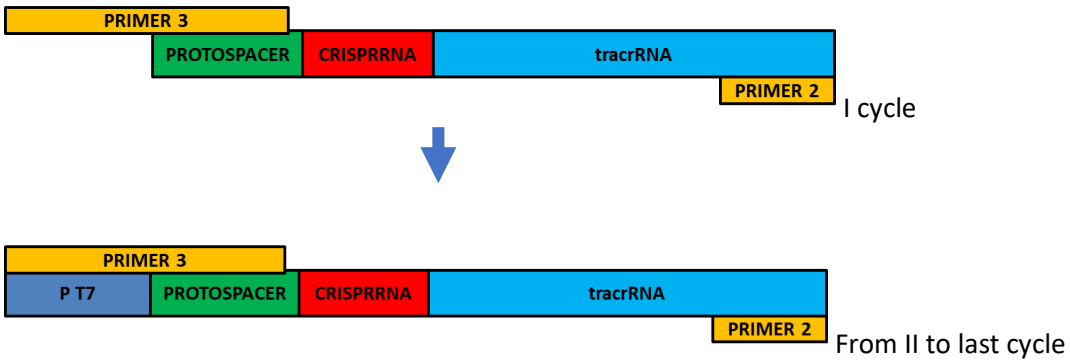

The final product was purified, as before, and it was used for the *in vitro* transcription.
The two sequences obtained for the following experiment are:

sgCPFTSY template

TAATACGACTCACTATAGGGCGATCTTCAGAGCAGTGCGGGTTTTAGAGCTAGAAATAGCAAGTTAAAATAAG
GCTAGTCCGTTATCAACTTGAAAAAGTGGCACCGAGTCGGTGCTTTTTTT

sgCAO template

TAATACGACTCACTATAGGGGCTCTCCGGGTCCTCAACGAGTTTTAGAGCTAGAAATAGCAAGTTAAAATAAG
GCTAGTCCGTTATCAACTTGAAAAAGTGGCACCGAGTCGGTGCTTTTTTT

8.3.8 SgRNA *in vitro* synthesis

For the SgRNA *in vitro* synthesis it was used HiScribe™ T7 Quick High Yield RNA Synthesis Kit (NEB) and was used the protocol for sequences smaller than 0.3 kb. The reaction was set as follows:

NTP buffer mix	10 µl
Template DNA	1µg
T7 DNA Polymerase MIX	2 µl
DEPC H_2O	Up to 30 µl

The reaction was incubated 4h at 37°C and the RNA was purified by phenol:chloroform extraction and ethanol precipitation to remove proteins and most of the free nucleotides:

- The reaction volume was adjusted to 180 µl by adding nuclease-free water and 20 µl of 3 M sodium acetate, pH 5.2 were added.
- The extraction was performed with an equal volume of 1:1 phenol:chloroform mixture.
- The sample was vortexed and spun down for 5’ at 15000 x g at 4°C.
- Then it was collected the aqueous phase and it was performed an extraction with an equal volume of chloroform.
- The sample was vortexed and spun down for 5’ at 15000 x g at 4°C.
- The aqueous phase was collected and transferred to a new tube.
- The RNA was precipitated by adding 2 volumes of ethanol.
- It was incubated at –20°C for at least 30’ and the pellet collected by centrifugation for 15’ at 15000 x g at 4°C.
- The supernatant was removed, and the pellet was washed with 500 µl of ice cold 70% ethanol.
- The sample was spun down for 5’ at 15000 x g at 4°C.
- The RNA was resuspended in 20 µl of DEPC water.
- The RNA was quantified by Nanodrop and stored at –20°C.

8.3.9 Plasmid extraction from E. coli (Miniprep)

All plasmid extractions were performed using NucleoSpin® Plasmid (Macherey-Nagel)

- ml of bacteria saturated culture was spun down 3’ at 4000 x g.
- The pellet was resuspended in 250 µL of RNAse containing Buffer A1 and gently mixed.
- Then 250 µL of buffer A2 were added and the sample was incubated 5’ at RT after a gentle mixing.

- 300 µL of Buffer A3 were then added and the vial was mixed thoroughly by inverting.
- Then the mixture was centrifuged 5’ at 12000 x g.
- The supernatant was loaded on a nucleotide binding column and spun down 5’ at 12000 x g.
- The flowthrough was discarded and 600 µl of A4 Washing Buffer were loaded on the column.
- The column was spun down 1’ at 12 000 x g at RT.
- The flowthrough was discarded, and the column was spun down 2’ at 12 000 x g at RT to eliminate the residual EtOH.
- The column was transferred on a new Eppendorf tube and 20 µl of 60°C sterile water were added for the elution.
- The sample was incubated 1’ at RT and spun down 1’ at 12 000 x g at RT.
- The flowthrough was collected in the tube and the column was thrown away

8.3.10 Restriction enzymes plasmids cuts

For plasmids cuts were used different restriction enzymes provided by NEB.
To perform diagnostic cut, only to assess if the plasmid in use was the right one, the reaction was set using combinations of two restriction enzymes cutting in unique sites:

10 X Cut Smart Buffer (NEB)	2 µl
Plasmid DNA	100 ng
Restriction Enzyme 1	0.5 µl
Restriction Enzyme 2	0.5 µl
H_2O	Up to 20 µl

The reactions were performed for 1h at 37°C.

In order to cut the vector DNA and the fragment to clone the reactions were performed in 50 µl and the quantity of starting material depended on the desired proportions between the two elements and on its availability.

10 X Cut Smart Buffer (NEB)	5 µl
DNA	According to the experimental needs
Restriction Enzyme	1.5 µl
H_2O	Up to 50 µl

The reaction was performed for 2 h at 37°C and DNA was purified using NucleoSpin Gel and PCR Clean-up kit (Macherey-Nagel see below).

8.3.11 Transformation of *E. coli* BL21 electrocompetent cells

For *E. coli* proteins expression, BL21 (DE3) (SIGMA) electrocompetent cells were used.

- Cells were thawed on ice.
- 40 µl of cells were put in an ice-cold 1.5 ml Eppendorf tube and 2 µl of DNA (100 ng) were added.

- The mixture was incubated 1’ on ice.
- The cells were transferred in an ice-cold 0.2 cm cuvette and the pulse was set at 25µF, 200 Ω and 2.5 kV.
- After the pulse the cell suspension was immediately transferred in a 13 ml ice-cold bacteriology tube containing 1 ml of modified LB.
- Cells were incubated 1 h at 37°C. shaking at 225 rpm.
- Cells were plated on LB agar plates with antibiotic.

8.3.12 Cut and Paste cloning

To clone the NLS sequence in pET-Cas9-6xHis (Zuris et al. 2014) plasmid it was synthetized by PCR a sequence containing the XbaI restriction site, the NLS sequence, the first part of the Cas9 gene and the NheI restriction site. The fragment was then purified as in 8.3.6. The plasmid pET-Cas9-6xHis was cut with the HF-XbaI (NEB) and HF-NheI(NEB) and treated for 1 h at 37°C by FastAP Thermosensitive Alkaline Phosphatase (Thermofisher) in order to prevent the reclosing of the plasmid. Then the reaction product was purified using NucleoSpin Gel and PCR Clean-up kit (Macherey-Nagel) (see 8.3.6). The vector and the fragment in the right proportions were then ligated by T4DNA ligase (NEB) at 16°C overnight. *E. coli* chemically competent Top10 cells (Termofisher) where then transformed with the ligation mixture (8.3.13) and colonies plated on ampicillin, because the plasmid carried this resistance for coli. The colonies were screened by colony PCR by Go-Taq Green Master Mix (Promega) without DMSO (see 8.3.1) using a primer complementary to the NLS (Screening fwd) and a primer complementary to the Cas9 gene (NheI rev) and sequenced. The positive colonies were reinoculated in LB and ampicillin to extract the plasmid for diagnostic cuts and to transform BL21 electrocompetent cells.

8.3.13 Transformation of *E. coli* chemically competent cells

To conserve the plasmid for further applications the One-Shot TOP 10 chemically competent cells (Termofisher) were used.

- One 50 µL vial of One Shot® cells for each ligation/transformation was thawed on ice.
- 5 µL of each ligation reaction were pipetted directly into the vial of competent cells and mix by tapping gently.
- The vial was incubated on ice for 30 minutes.
- Then it was incubated for exactly 30 seconds in the 42°C water bath and then left on ice.
- Then 1 ml of modified high-salt LB was added to the cells that were shaken at 37°C for exactly 1 hour at 225 rpm in a shaking incubator.
- Three cell dilutions (in general 1,10 and 100 µl) were plated on LB mixed to the antibiotic for plasmid selection.
- The plates were incubated at 37°C overnight.

8.3.14 Plasmids used in this work

Name	Used for	Antibiotic resistance for	Antibiotic resistance for

		bacteria	algae
pET-Cas9-6xHis (Addgene, Zuris et al.2014)	Cas9 expression in *E. coli*	Ampicillin	-
NLS-pET-Cas9-6xHis (Modified from Addgene plasmid)	Cas9 expression in *E. coli*	Ampicillin	-
pDGE5 (Ordon et al., 2017)	Conserved sgRNA sequence amplification	Ampicillin	-
pHyg3 (Berthold et al., 2003)	Resistance gene insertion in *Chlamydomonas*	Ampicillin	Hygromycin
pOpt2_mCerulean3_Paro (Lauersen et al., 2018)	CPFTSY synthetic gene cloning for expression in *Chlamydomonas*	Ampicillin	Zeocin

8.3.15 In vitro sgRNA+Cas9 cut assay

Before to transform *Chlamydomonas* by electroporation to deliver the sgRNA and Cas9 inside the cell it was performed an *in vitro* cut assay in order to check the proper functioning of both molecules. The molecules to cut is a fragment of the target gene, including the sequence that would be cut in *vivo*. If the cut worked, it would be observed on agarose gel two halves of the fragment, instead that the whole one.

- **Fragment amplification:** The PCR reaction was performed using the proof reading Taq as described in 8.3.1 paragraph, setting 40 s of extension and 58°C as annealing temperature. The selected fragments were between 500 and 700 bp of length and the selected primers were: CAO FWD and CAO REV for *CAO* gene and CPFTSY FWD and CPFTSY REV for *CPFTSY* (see 8.3.2). As template it was used the cw15 genomic DNA.
- ***In vitro* cut**: Before the cut 600 ng of Cas9 Nuclease was incubated with 500 ng of the specific sgRNA for 10' at 37°C, in order to allow the assembly of the RNP-Complex. Then 100 ng of the fragment to cut were added in a final volume of 20 µl. The reaction mixture was incubated 1 h at 37°C and 5' at 65°C to interrupt the reaction. The results were checked on 1.5% agarose gel electrophoresis.

8.3.16 Baek's protocol to deliver sgRNA-Cas9 RNP complex in *Chlamydomonas*

To deliver the sgRNA-Cas9 RNP complex in *Chlamydomonas* it was followed a protocol published by Baek and collaborators (Baek et al. 2016). *Chlamydomonas* transformation was performed using culture of cw15 (WT cell wall deficient strain) at the exponential phase of growth curve (about $1.5*10^6$ cell/ml) in this way:

- 200 µg of home-purified Cas9 Nuclease was preincubated with 140 µg of the specific sgRNA for 10' at 25°C, in order to allow the assembly of the RNP-Complex.
- Meanwhile $1.5* 10^6$ cell/ml culture was pelleted and resuspended up to $2* 10^6$ cell/ml in TOS.
- The Cas9-sgRNA complex was added to 250 µl of cell culture ($5*10^5$ cell).
- The electroporator was settled to 600 V 50µF 200 Ω and the cells were subjected to the electric pulse.
- Then they were transferred in 13 ml of TOS and incubated for 6h.

- After 6 h they were plated on TAP agar plates with the adding of 30% starch and the specific antibiotic.

The screening was then performed by the search of the pale-green phenotype by eye and confirmed by amplification of the gene fragment in which the modification had to be (using CAO FWD and REV and CPFTSY FWD and REV2 primers).

8.3.17 Claire Remacle Protocol to deliver sgRNA-Cas9 RNP complex in *Chlamydomonas*

To deliver the sgRNA-Cas9 RNP complex in *Chlamydomonas* it was followed a protocol suggested by Professor Claire Remacle and Dr Gwenaelle Gain (Universitè de Liege), with some modification. *Chlamydomonas* transformation was performed using culture of cw15 at the exponential phase of growth curve (about $1.5*10^6$ cell/ml) in this way:

- 6.5 µg of Alt-R® S.p. Cas9 Nuclease (IDT) was preincubated with 8.33 µg of the specific sgRNA for 30' at 37°C, in order to allow the assembly of the RNP-Complex.
- Meanwhile $1.5* 10^6$ cell/ml culture was pelleted and resuspended up to $2* 10^8$ cell/ml in TOS.
- 500 ng of resistance cassette DNA were added to 250 µl of culture .
- Soon the Cas9-sgRNA complex was added to the cells.
- The mixture was incubated 20' in ice and transferred in an electroporation cuvette.
- The electroporator was set to 600 V 50µF 200Ώ and the cells were subjected to the electric pulse.
- Soon after they were incubated 5' on the bench.
- Then they were transferred in 13 ml of TOS and incubated for 6h.
- After 6 h they were plated on TAP agar plates with the adding of 30% starch and the specific antibiotic.

The screening was then performed by the search of the pale-green phenotype by eye and confirmed by amplification of the gene fragment in which the modification had to be (using CAO FWD and REV and CPFTSY FWD and REV2 primers). Resistance cassettes insertions close to the PAM sequence were detected using a primer on the gene and one on the fragment (Paro rev or Paro fwd+ CAO REV or CAO FWD; Hyg fwd + CPFTSY REV2 or CPFTSY FWD). For PCR screening was used the Go-Taq Green Master Mix (Promega) as in the 8.3.1.

8.3.18 Resistance cassettes

In order to screen the genome edited mutant easier a resistance cassette was co-delivered in the transformed cell. The paromomycin resistance cassettes were obtained from the pOpt2_mCerulean3_Paro plasmid, belonging to the pOpt2.0 plasmid series from Professor Kyle J. Lauersen (King Abdullah University of Science and Technology) (Lauersen et al. 2018). The hygromycin resistance was obtained cutting the pHyg3 plasmid (Berthold et al. 2003). pOpt2_mCerulean3_Paro and pHyg3 were linearized by HF-ScaI (NEB) restriction enzyme.
3 µg of plasmid were cut in 50 µl of reaction:

10 X Cut Smart Buffer (NEB)	5 µl

Plasmid DNA	3 µg
Restriction Enzyme	1.5 µl
H_2O	Up to 50 µl

The reaction was performed for 2 h at 37°C and DNA was purified using NucleoSpin Gel and PCR Clean-up kit (Macherey-Nagel) (see 8.3.6).

8.4 Bioinformatics

8.4.1 Screening primer design

All primers for screening were design using Primer Blast tool (https://www.ncbi.nlm.nih.gov/tools/primer-blast/). Once inserted the sequence of interest, it was chosen the desired amplicon length range and the temperature range (in general between 57 and 63) and it was selected the organism to allow the research of free from off-target primers. The software gives the best options calculating also the number nucleotides that could cause self-primer annealing. As the self-annealing or the primer dimers formations can compromise the amplification efficiency, they were *in silico* tested by two software: Multiple Primer Analyzer by Thermofisher (https://www.thermofisher.com/it/en/home/brands/thermo-scientific/molecular-biology/molecular-biology-learning-center/molecular-biology-resource-library/thermo-scientific-web-tools/multiple-primer-analyzer.html) and PCR Primer Stats by Bioinformatics.org (https://www.bioinformatics.org/sms2/pcr_primer_stats.html).

8.4.2 SgRNA protospacer design

The protospacer complementary to the target of the sgRNA was selected by the software Cas-Designer software (Park et al. 2015): http://www.rgenome.net/cas-designer/. To obtain a knock-out the target needs to belong to an exon, so the CDS of the gene it was used to find it. After obtained the list of the targets with the PAM included it was selected the target in the desired position paying attention to the out of frame score (an higher score indicates an higher specificity) and to its belonging to a single exon. To check possible off-targets also with different numbers of mismatches it was used the software Cas-Offinder (Bae et al. 2014): http://www.rgenome.net/cas-offinder. The selected target sequence without the PAM it was inserted as query and from the research resulted a list of potential off-target sites that differed from the target by up to 3 nucleotides or by up to 2 nucleotides forming a DNA or a RNA bulge.

8.4.3 Sequencing data analysis

All the sample were sequenced by Eurofins genomics. The chromatograms were analysed using Chromas software (Technelysium) and the well sequenced part was exported on DNAMAN software

(Lynnon Corporation) to perform alignments between wild type and analysed version of the sequence of interest.

8.4.4 Restriction enzymes cut prediction and in silico cloning

To predict the results of the plasmids cleavages by restriction enzymes it was used the software Serial Cloner (http://serialbasics.free.fr/Serial_Cloner.html). The plasmid sequence was opened in the program and the employed enzymes were selected by a list. It was selected the used DNA ladder to obtain the prediction of the aspect which the reaction product had to be on the agarose gel. The program outputs where then this picture of the *in-silico* agarose gel and the indication of the sizes in basepair of the fragments which had to be obtained by the reaction, moreover it was indicated also their starting and ending points in the whole plasmid. By this program it was also possible to predict the product of a cloning experiment. The sequence of the vector plasmid and of the fragment to insert were opened, it was performed the *in-silico* cleavage by the desired restriction enzymes and the ends of the sequences to join were selected to simulation a ligation reaction. In this way is possible to predict the exact length of the new construct to better distinguish it *in vivo* from other side products.

8.5 Biochemistry

8.5.1 Protein extraction protocols trials

To reach a good quality and an efficient Cas9 extraction different total protein extraction protocols were tested changing the buffers composition:

Protocol 1:

- A culture of BL21 *E. coli* cell, containing the plasmid pETCas9-6xHis were grown until it reached 0.6 OD.
- Then the Cas9 expression was induced overnight at 20°C by 500 µM IPTG.
- Then the cell culture was centrifuged at 4000 x g for15’ at 4°C.
- The pellet was resuspended in a quantity **buffer1 (20mM Tris-HCl PH7.4 and 500mM NaCl)** corresponding to 1/40 of the starting culture volume.
- The suspension was sonicated two times for 15’
- Then it was centrifuged 50’ at 4°C t 20000 x g.
- The supernatant was then collected

Protocol 2:

- A culture of BL21 E. coli cell, containing the plasmid pETCas9-6xHis were grown until it reached 0.6 OD.
- Then the Cas9 expression was induced overnight at 20°C by 500 µM IPTG.
- Then the cell culture was centrifuged at 4000 x g for15’ at 4°C.
- The pellet was resuspended in a quantity of **buffer 2 (20mM Tris-HCl PH7.4 and 500mM NaCl, 0.5% Tween 20)** corresponding to 1/40 of the starting culture volume.
- The suspension was sonicated two times for 15’ .

- Then it was centrifuged 50’ at 4°C t 20000 x g.
- The supernatant was then collected

Protocol 3:

- A culture of BL21 E. coli cell, containing the plasmid pETCas9-6xHis were grown until it reached 0.6 OD.
- Then the Cas9 expression was induced overnight at 20°C by 500 µM IPTG.
- Then the cell culture was centrifuged at 4000 x g for 15’ at 4°C.
- The pellet was resuspended in a quantity **of buffer 3 (100mM Tris-HCl PH 6.8, 4% SDS and 20mM EDTA)** corresponding to 1/40 of the starting culture volume.
- The suspension was sonicated two times for 15’.
- Then it was centrifuged 50’ at 4°C t 20000 x g.
- The supernatant was then collected.

Protocol 4

- A culture of BL21 E. coli cell, containing the plasmid pETCas9-6xHis were grown until it reached 0.6 OD.
- Then the Cas9 expression was induced overnight at 20°C by 500 µM IPTG.
- Then the cell culture was centrifuged at 4000 x g for15’ at 4°C.
- Then the cells were resuspended Resuspend 0.8ml/g in 50mM TrisHCl pH 7.5, 100 mM NaCl, 5% Glycerol, 1 mM Caproic acid, 1 mM PMSF, 0.2mM benzamidine.
- The cells were incubated 30’ on ice in 2mg/ml lysozime.
- Then 30’ at Room Temperature in 20 µg/ml Dnase, 10 mM MgCl2 and 1 mM NaCl
- The suspension was sonicated two times for 15’.
- Then it was centrifuged 12’ at 4°C t 12000 x g.
- The supernatant was then collected.

The Cas9 extraction efficiency was tested by western blot. The protocol 1 resulted the most efficient.

8.5.2 Cas9 purification by His-Trap Chromatography

Once performed the total protein extraction the Cas9 was purified by Ni-sepharose chromatography, using a 1 ml HisTrap™ FF crude column (Amersham Bioscience). The procedure was performed as follows:

- The total protein extract was supplemented by 10 mM imidazole
- The His-Trap column was equilibrated by 10 column volumes of Equilibration Buffer at 1ml/min of flow rate
- The extract was then loaded on the column and the flow through was collected
- The column was washed by 10 column volumes of equilibration buffer
- The elution was performed by Elution Buffer, then 1 ml fractions were collected
- The column was then washed by 10 column volumes of Equilibration Buffer
- The flow through was reloaded another time and another cycle was performed as before
- Eluted fractions were dialyzed and concentrated in 20mM HEPES pH 7.5 and 150mM KCl by Vivaspin 6 (Sigma) concentrators with a 100 kDa cut-off

- After the quantification by SDS-Page or Nanodrop the protein concentrated 10 mg/ml was stored in the Cas9 buffer at -80°C.

By this procedure about 1 mg of protein per liter of starting bacteria culture was obtained

EQUILIBRATION BUFFER

Sodiumphosphate pH 7.4	20 mM
NaCl	0.3 M
Imidazole	10 mM
Milli-Q water	Up to the final volume

ELUTION BUFFER

Sodiumphosphate pH 7.4	20 mM
NaCl	0.3 M
Imidazole	300 mM
Milli-Q water	Up to the final volume

Cas9 BUFFER

Hepes pH 7.5	20 mM
Glycerol	5% (w/v)
DTT	1 mM
KCl	150 mM
Milli-Q water	Up to the final volume

8.5.3 SDS-PAGE protein electrophoresis

(Schägger and von Jagow 1987)

To check protein extractions and quantify the Cas9 eluted fractions was performed an SDS-PAGE analysis. The samples were treated by SDS and β-mercaptoethanol to obtain proteins with the same charge/mass ratio and a globular shape that can be separated on the basis of their molecular weights.
The Laemli 7.5% acrylamide gel was prepared as follows:

RUNNING GEL

Acrylamide 37.5:1 (37.5% acrylamide; 1% bis-acrylamide)	7.5 % (w/v)
Tris-HCl pH 8	0.375 M
TEMED	0.047% (v/v)
APS	0.0016% (w/v)
Milli-Q water	Up to the final volume

STACKING GEL

Acrylamide 37.5:1 (37.5 % acrylamide; 1% bis-acrylamide)	4 % (w/v)
Tris-HCl pH 6.8	0.125 M

TEMED	0.047% (v/v)	
APS	0.0016% (w/v)	
Milli-Q water	Up to the final volume	

The running buffer for the electrophoresis were prepared as follows:

INFERIOR RUNNING BUFFER 10X

Tris-HCl pH 8.9	2.5 M
Glycine	2 M
Milli-Q water	Up to the final volume

SUPERIOR RUNNING BUFFER 10 X

Tris	2.5 M
Glycine	2 M
SDS	1% (w/v)
EDTA	10 mM
Milli-Q water	Up to the final volume

The samples were loaded with a molecular weight marker: PiNK Prestained Protein Ladder (GeneDirex).

8.5.4 Coomassie protein staining

(Ball 1986)

To visualize proteins on acrylamide gel, it was used the Coomassie Brilliant Blue R-250 staining, which is able to bind basic aminoacids. Coomassie Brilliant Blue R-250 was eluted in 10% acetic acid and 40% methanol and this solution was poured on the gel and left to act overnight. Then the gel was transferred in a 40% methanol and 10% acetic acid decolouring solution.

8.5.5 Western Blot analysis

To check the presence and the relative quantity of Cas9 protein it was performed a western blot analysis, using specific antibody against His-tag (Burnette 1981). Once resolved proteins by SDS-PAGE electrophoresis these were transferred from the gel to a nitrocellulose matrix that binds them (Towbin et al. 1979). The membrane was equilibrated in the transfer buffer before this procedure. The gel and the membrane were left in contact in a chamber full of transfer buffer for 1 h in an electric field with a current of 100 V. The gel and the membrane were put between two layers of filter paper and sponge. The gel was posed towards the negative sites of the transfer chamber, while the membrane towards the positive one. The system was kept frozen by ice. After this period, to check the success of the procedure a Red Ponceau solution was poured on the membrane to see the bound proteins.
The stain was washed away by Milli-Q water.

The membrane was then left overnight at 4°C in a Blocking Solution containing BSA that blocks all the unspecific protein binding sites which could cause false positive results. Then the membrane was left 3h in the primary antibody diluted in the blocking solution. Then it was washed by simple Blocking Solution to remove the excess of the antibody and it was left 2 h in the secondary antibody diluted 1:30000. Then after two washes by the Blocking solution and the last one by the PBS 1X solution the membrane was developed. The secondary antibody was conjugated with the horseradish peroxidase and the developing of the membrane was performed by ECL (BIO RAD)

TRANSFER BUFFER

Tris pH 8.3	20 mM
Glycine	152 mM
Methanol	20%
Milli-Q water	Up to the final volume

PBS 10X pH 7.2

NaCl	1.37 M
KCl	27 mM
KH_2PO_4	15 mM
Na_2HPO_4	81 mM
Milli-Q water	Up to the final volume

BLOCKING SOLUTION

BSA	3 g/l
PBS 10X pH 7.2	1 X
Tween-20	0.2%
Milli-Q water	Up to the final volume

8.5.6 Dinamic Light Scattering measurement

In order to find the right KCl concentration to conserve the protein properly folded and to prevent the aggregation to not compromise its activity, the Dinamic Light Scattering (DLS) in TOS medium at different salt concentrations was measured by Zetasizer Nano ZS Malvern system.

8.5.7 Pigment extraction

Chlorophyll and carotenoid were extracted by a water-solution of 85% acetone buffered by Na_2CO_3. Depending on the intensities of the green colour of the strains, it was taken a cell quantity of ranging between 2.5 $*10^6$ and $1*10^7$. The cells were spun down at 2000 *x g* for 5' and the green pellet was resuspended in 1 ml of 85% acetone solution and left for a least 10' in ice in the dark. Then samples were spun for 10' at 21000 *x g* at 4°C and the supernatant was collected and conserved at -20°C in the dark.

8.5.8 Absorption Spectra and cell pigment content analysis

The absorption spectra in the wavelength range from 350 to 800 nm were obtained at room temperature by double array AMINCO DW2000 spectrophotometer in quartz cuvettes with 1 cm of optical path. The raw data were set to zero by subtracting the value at 720 nm. To obtain the spectra graph the set to zero data were divided for the maximum absorbance value and these normalized data were inserted in a lines and curves dispersion graph. From the set to zero data were extracted

the absorbance values at 663.6 nm and 646.6 nm. By Porra method (Porra et al. 1989) is possible to determine Chl a and b concentrations in mg/ml):
Chl a: 12.25 x A663.6 nm - 2.55 x A646.6 nm
Chl b: 20.31 x A646.6 nm - 4.91 x A663.6 nm
Chl a + Chl b: 17.76 x A646.6 nm + 7.43 x A663.6 n
Chlorophyll a to b ratio (Chl a/b) and Chl/cars ratio were corrected through fitting analysis of the absorption spectrum (Croce et al. 2002).

REFERENCES

Bae S, Park J, Kim JS (2014) Cas-OFFinder: a fast and versatile algorithm that searches for potential off-target sites of Cas9 RNA-guided endonucleases. Bioinformatics 30:1473–1475. https://doi.org/10.1093/bioinformatics/btu048

Baek K, Kim DH, Jeong J, Sim SJ, Melis A, Kim JS, Jin E, Bae S (2016) DNA-free two-gene knockout in Chlamydomonas reinhardtii via CRISPR-Cas9 ribonucleoproteins. Sci Rep 6:30620. https://doi.org/10.1038/srep30620

Ball EH (1986) Quantitation of proteins by elution of Coomassie brilliant blue R from stained bands after sodium dodecyl sulfate-polyacrylamide gel electrophoresis. Anal Biochem 155:23–27. https://doi.org/https://doi.org/10.1016/0003-2697(86)90218-6

Berthold P, Schmitt R, Mages W (2003) An Engineered Streptomyces hygroscopicus aph 7′′Gene Mediates Dominant Resistance against Hygromycin B in Chlamydomonas reinhardtii. Protist 153:401–412. https://doi.org/10.1078/14344610260450136

Burnette WN (1981) "Western Blotting": Electrophoretic transfer of proteins from sodium dodecyl sulfate-polyacrylamide gels to unmodified nitrocellulose and radiographic detection with antibody and radioiodinated protein A. Anal Biochem 112:195–203. https://doi.org/https://doi.org/10.1016/0003-2697(81)90281-5

Croce R, Canino G, Ros F, Bassi R (2002) Chromophore Organization in the Higher-Plant Photosystem II Antenna Protein CP26. Biochemistry 41:7334–7343. https://doi.org/10.1021/bi0257437

Harris EH, Stern DB, Witman GB (1989) The chlamydomonas sourcebook. Academic Press San Diego

Kropat J, Hong-Hermesdorf A, Casero D, Ent P, Castruita M, Pellegrini M, Merchant SS, Malasarn D (2011) A revised mineral nutrient supplement increases biomass and growth rate in Chlamydomonas reinhardtii. Plant J 66:770–780. https://doi.org/10.1111/j.1365-313X.2011.04537.x

Lauersen KJ, Wichmann J, Baier T, Kampranis SC, Pateraki I, Møller BL, Kruse O (2018) Phototrophic production of heterologous diterpenoids and a hydroxy-functionalized derivative from Chlamydomonas reinhardtii. Metab Eng 49:116–127. doi: https://doi.org/10.1016/j.ymben.2018.07.005

Ordon J, Gantner J, Kemna J, Schwalgun L, Reschke M, Streubel J, Boch J, Stuttmann J (2017) Generation of chromosomal deletions in dicotyledonous plants employing a user-friendly genome editing toolkit. Plant J 89:155–168. doi: 10.1111/tpj.13319Park J, Bae S, Kim J-S (2015) Cas-Designer: a web-based tool for choice of CRISPR-Cas9 target sites. Bioinformatics 31:4014–4016. https://doi.org/10.1093/bioinformatics/btv537

Porra RJ, Thompson WA, Kriedemann PE (1989) Determination of accurate extinction coefficients and simultaneous equations for assaying chlorophylls a and b extracted with four different solvents: verification of the concentration of chlorophyll standards by atomic absorption spectroscopy. Biochim Biophys Acta - Bioenerg 975:384–394. https://doi.org/https://doi.org/10.1016/S0005-2728(89)80347-0

Schägger H, von Jagow G (1987) Tricine-sodium dodecyl sulfate-polyacrylamide gel electrophoresis for the separation of proteins in the range from 1 to 100 kDa. Anal Biochem 166:368–379. https://doi.org/https://doi.org/10.1016/0003-2697(87)90587-2

Towbin H, Staehelin T, Gordon J (1979) Electrophoretic transfer of proteins from polyacrylamide gels to nitrocellulose sheets: procedure and some applications. Proc Natl Acad Sci U S A 76:4350–

4354. https://doi.org/10.1073/pnas.76.9.4350

Zuris JA, Thompson DB, Shu Y, Guilinger JP, Bessen JL, Hu JH, Maeder ML, Joung JK, Chen ZY, Liu DR (2014) Cationic lipid-mediated delivery of proteins enables efficient protein-based genome editing in vitro and in vivo. Nat Biotechnol 33:. https://doi.org/10.1038/nbt.3081

CHAPTER 9
Results

9.1 SgRNA synthesis strategy

To obtain genome edited mutants for the genes *CAO* and *CPFTSY* different procedures were optimized to exploit the CRISPR-Cas9 techniques for this purpose.
First of all it was decided to use the direct codelivery of the sgRNA and the purified Cas9 protein in the cell by electroporation, because, according to previous publications, for Chlamydomonas it was the most efficient strategy (Baek et al. 2016; Shin et al. 2016, 2019; Ferenczi et al. 2017; Jeong et al. 2018). It was decided to select the protospacers for the sgRNAs as suggested by Baek and colleague (Baek et al. 2016). In the case of *CpFTSY* it was selected the most performant sequence present in the paper, while for *CAO* it was designed by two softwares: Cas-Designer and Cas-OFFinder (Bae et al. 2014; Park et al. 2015). *CAO* CDS was used to find an exon-belonging target, at the beginning of the gene, in order to obtain by the *in vivo* targeting a truncated gene product. After obtained the targets list with the PAM included it was selected the one with the highest out of frame score (a higher score indicates a higher specificity) and belonging to a single exon. The sequence specificity was tested with the software Cas-OFFinder (Bae et al. 2014) used to obtain a list of the potential off-target that were different to the target by up to three nucleotides or that could cause a DNA or an RNA bulge (figure 9.1.1.b), to avoid a mispairing between sgRNA and these sequences, for the difference in up to two nucleotides. For *CAO* selected target only one site differentiated from it for a three nucleotides mismatches. Among the nineteen DNA or RNA bulge sites it was individuated only five sequences belonging to genes different from CAO and two are in the same position in the genome.

a

Cas-Designer

RGEN Target (5' to 3')[?]	Position[?]	Cleavage Position (%)[?]	Direction[?]	GC Contents (%, w/o PAM)[?]	Out-of-frame Score[?]
CGCCTCGACACCCATCGTTGAGG	111	21.2	+	65.0	76.5
GCTCTCCGGGTCCTCAACGATGG	122	21.2	-	65.0	76.5
AGCGGCGGAACTTGCTCTCCGGG	135	23.4	-	65.0	76.1

b

Cas-OFFinder

Bulge Type	Target	Chromosome	Position	Direction	Mismatches	Bulge Size
DNA	crRNA: G-CTCTCCGGGTCCTCAACGANGG DNA: tGCTCTCCGGGTCCTCAACGATGG	chromosome_1	5943074	+	1	1
DNA	crRNA: GC-TCTCCGGGTCCTCAACGANGG DNA: tgCTCTCCGGGTCCTCAACGATGG	chromosome_1	5943074	+	2	1
X	crRNA: GCTCTCCGGGTCCTCAACGANGG DNA: GCTCTCCGGGTCCTCAACGATGG	chromosome_1	5943075	+	0	0
RNA	crRNA: GCTCTCCGGGTCCTCAACGANGG DNA: GC-CTCCGGGTCgTCAgCGAAGG	chromosome_16	5115798	+	2	1

Figure 9.1.1 CAO protospacer research: a) Cas-Designer results. The results were filtered to obtain only the target with an out-of-frame score higher than 75 (sixth column). In the first column were reported the selected targets complete of the PAM sequence (NGG), in the second column were indicated the position of the site in the coding sequence, while in the third the column expressed as percentage of the sequence (in this case only 1000 nt over 1938 were inserted as query so this parameter has no sense). In the fourth column it is indicated in which of the two DNA filaments the target is present, in the fifth the G/C percentage of the sequence. The red square indicates the selected target for the genome editing. B) Example of Cas-OFFinder results. The blue square indicates a real off-target sequence, while the other rules contain sites belonging to the CAO gene. In the first column it is indicated the bulge type (X indicates no bulge and simple mismatching), while in the second is reported the target sequence and the sequence of the protospacer (crRNA) indicating the bulge or the mismatch sites. In the third column were reported the chromosomes in which these off-target were collocated, in the fourth the position in the genome and in fifth the strain in which the target is present. The last two columns indicate respectively the number of nucleotides that cause the mismatch and the length in nucleotides of the bulge.

The DNA templates to *in vitro* transcribe the sgRNAs were synthetized by two PCR rounds. The sgRNA conserved sequence was amplified from a plant plasmid pDGE5 (Ordon et al. 2017) and the sequence of the protospacer was added to the forward primer (see 8.3.7 section). After the first amplification it was added to a new forward primer the promoter for the T7polymerase for the in vitro transcription (figure 9.1.2).

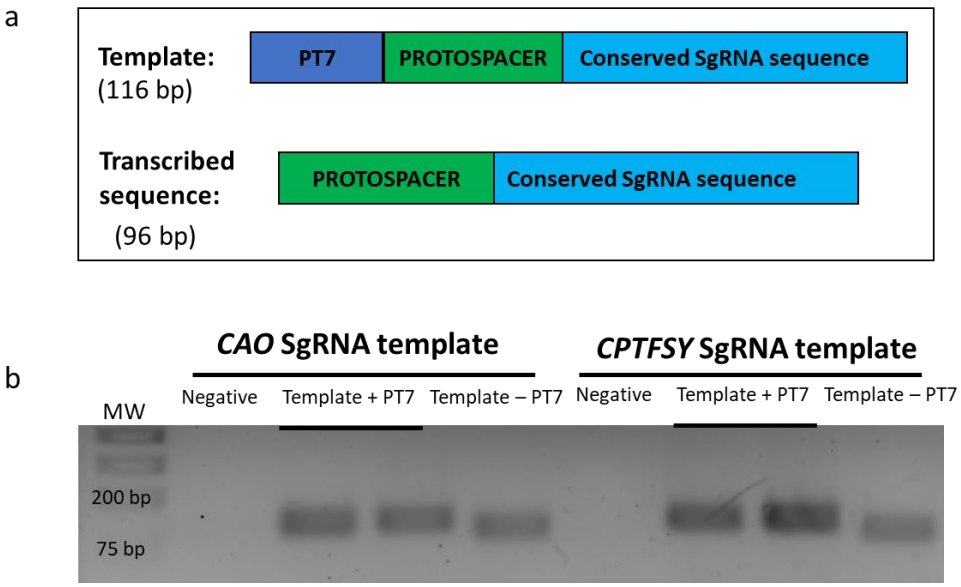

Figure 9.1.2: DNA templates for SgRNAs synthesis: a) Template and transcribed sequence composition schemes. b) PCR products from the two DNA templates amplification rounds. The template –T7 is the product composed by the protospacer and the conserved sgRNA sequence, the template + T7 is the product complete of the PT7 promoter. Negative is the control reaction without DNA. The products were run on 1.5% agarose gel. MW: molecular weight marker.

Once obtained the DNA template the SgRNA were *in vitro* transcribed as described in 6.3.8 section and purified by phenol: chloroform extraction to be employed for the transformation.

9.2 Cas9 purification trials

To obtain a purified Cas9 it was decided to express a tagged protein in *E. coli* and to purify it by affinity chromatography. It was bought from Addgene website the plasmid pET-Cas9-6xHis (Zuris et al. 2014). The bacterial suspension containing the plasmid was plated on ampicillin containing LB plates and then inoculated in liquid LB to extract and check the plasmid by cut with restriction enzyme (figure 9.2.1).

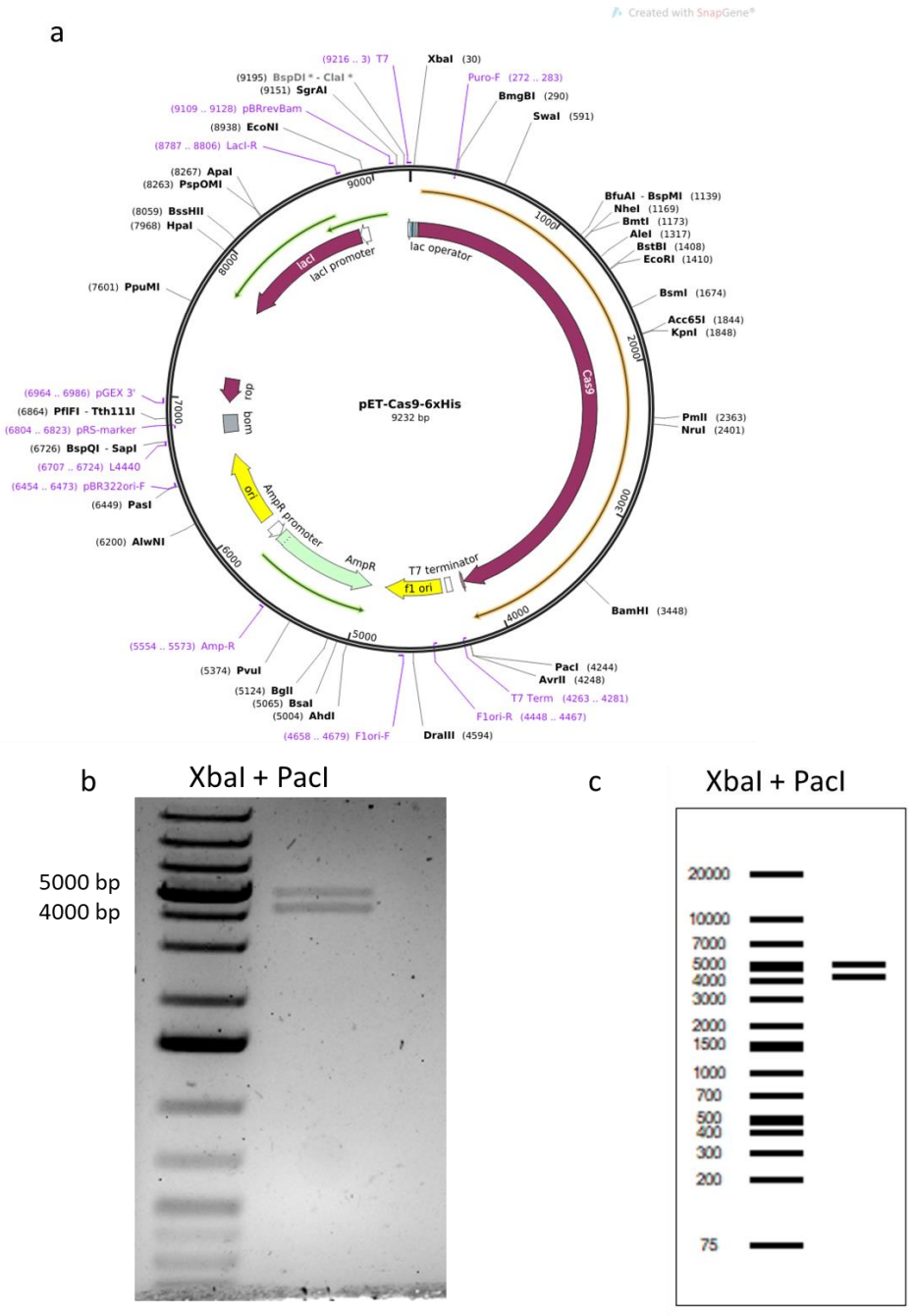

Figure 9.2.1 Plasmid map and plasmid identity control: a)pET-Cas9-6xHis plasmid map (Zuris et al. 2014) (Map visualized by SnapGene software). b) Cut of the plasmid by XbaI and PacI restriction enzyme to assess the identity of the plasmid. The reaction was loaded on 1% agarose gel c) Cut prediction (obtained by SerialCloner).

Once assessed the right structure *E. coli* BL21 (DE3) electrocompetent cells were transformed to express the soluble Cas9 protein. The protein expression was induced at 20°C overnight by 500 µg IPTG in a culture at 0.4-0.8 OD. To test the correct expression of the protein it was tried a first extraction by only sonication, and it was performed a western blot by the antibody against His-Tag, The blot confirmed the presence of the protein at the correct height (160 kDa), but the extraction procedure had to be implemented (figure 9.2.2).

For this reason, different protocols, with different buffer compositions were tried (see 8.5.1 section). The first one was with a only salt and Tris buffer, while the second the Tween 20 was added. The third was only a control of extraction efficiency, because it was based on a denaturing buffer, that was non useful for the obtainment of a properly working protein. The fourth was an adjustment of a protocol used to extract recombinant hemicellulase from BL21 expressing strains (Benedetti et al. 2019). The first protocol showed an efficiency comparable with the third, then it was decided to use it for the total protein extraction before the Ni-affinity chromatography.

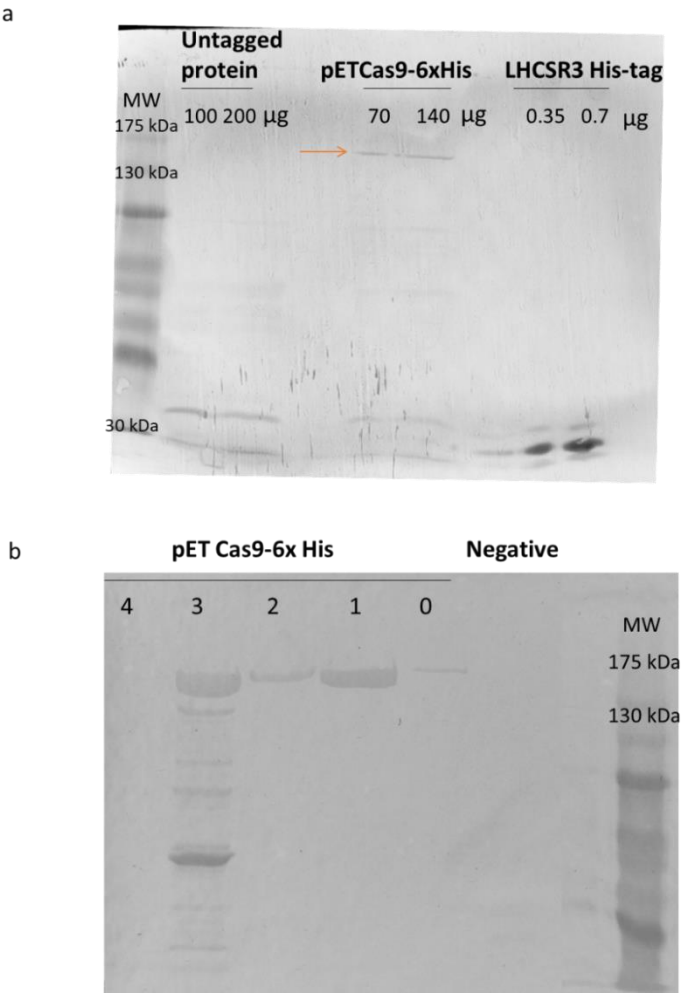

Figure 9.2.2. Protein extraction trials. a) Proteins extraction by sonication only. A wb with antibody against His-Tag was performed using as negative control an untagged protein and as positive control a purified LHCSR3 his-tagged protein. Two different amounts for each protein were loaded. The orange arrow indicates the Cas9 at the

expected molecular weight (160 kDa) b) Proteins extraction by different buffer compositions: 0: old extraction; 1: buffer with 20mM Tris-HCl PH7.4 and 500mM NaCl; 2: 20mM Tris-HCl PH7.4, 0.5% Tween-20 and 500mM NaCl; 3: buffer with 100mM Tris-HCl PH 6.8, 4% SDS and 20mM EDTA; 4: buffer with 50mM TrisHCl pH 7.5, 100 mM NaCl, 5% Glycerol, 1 mM Caproic acid, 1 mM PMSF, 0.2mM benzamidine and procedure described by (Benedetti et al. 2019). An untagged protein was used as negative control.
MW: molecular weight marker. The samples were loaded on a 7.5% Laemmli gel.

Once found the most efficient extraction protocol the protein was purified by Ni-affinity chromatography. By the optimized procedure about 1 mg of protein per litre of starting bacteria culture was obtained (figure 9.2.3). According the protocol of Baek and colleagues (Baek et al. 2016) 200 µg of protein were necessary for each transformation, therefore from each liter of culture the right quantity for five transformations was obtained.

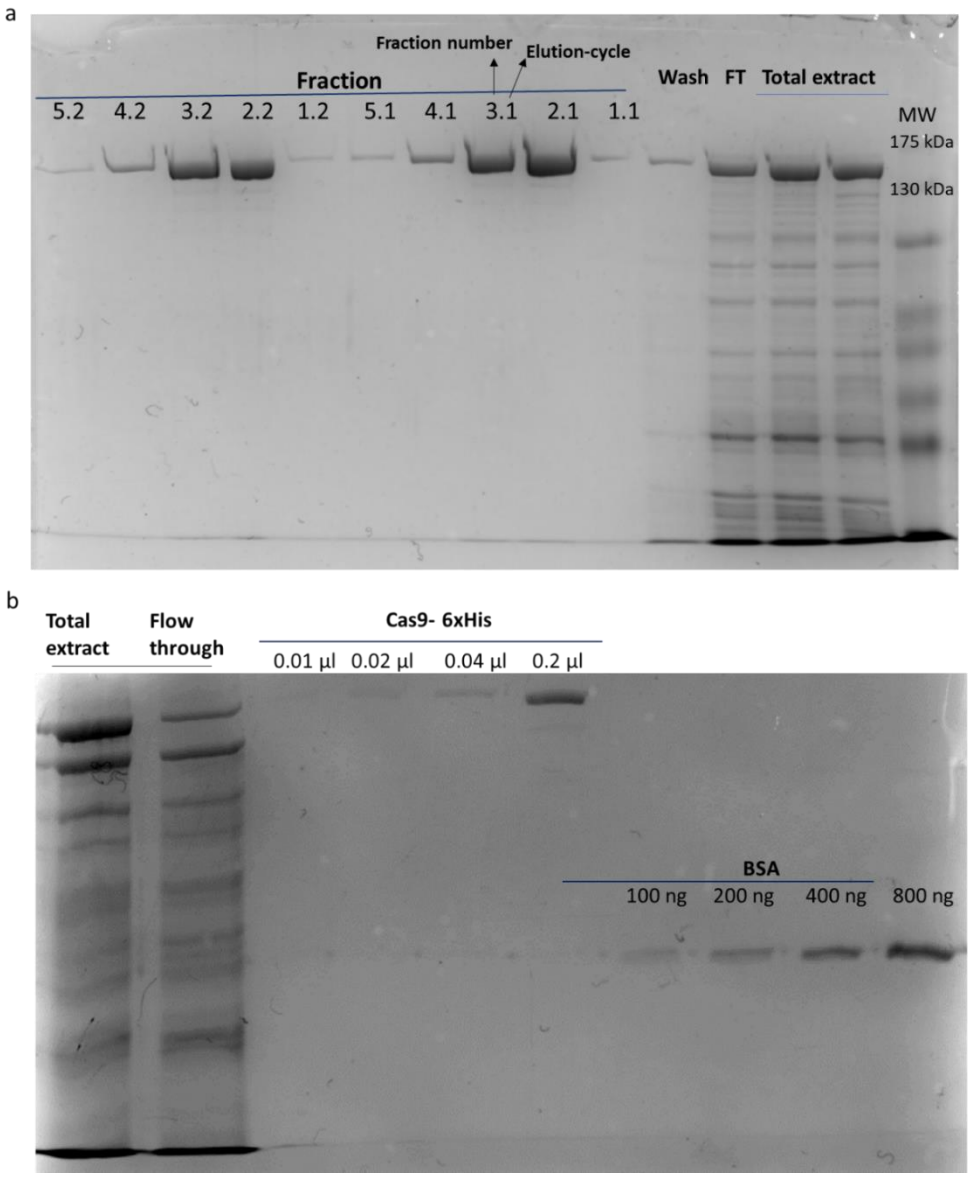

Figure 9.2.3. Cas9 purification check and quantification on Coomassie Blue stained gel. a) Cas9 eluted fractions check. 3 µl of each fraction obtained by the two passages on the column were loaded on a 7.5% Laemmli gel (first number: fraction number; second number: elution cycle) As efficiency control 20 µl of the total extract, of the flow through (FT) and of the column wash residual were loaded. b) Protein quantification on 7.5% Laemmli gel. Different volumes of the concentrated protein were loaded, and the signals were compared with those on different amounts of BSA protein. 20 µl of total extract and flow through were also loaded. MW: molecular weight marker.

9.3 *In vitro* cut assay and first transformation trial

Once purified both the Cas9 and the sgRNA the correct functioning of the Ribonucleoprotein complex was testing by an *in vitro* cut assay (Figure 9.3) as described in the paper of Ferenczi and colleagues (Ferenczi et al. 2017). For this purpose, it was amplified a fragment of the target gene including the sequence that would be cut in vivo, and this DNA was incubated with the ribonucleoprotein complex. The RNP complex seemed to work with a good efficiency, even though it wasn't able to completely cut all the DNA.

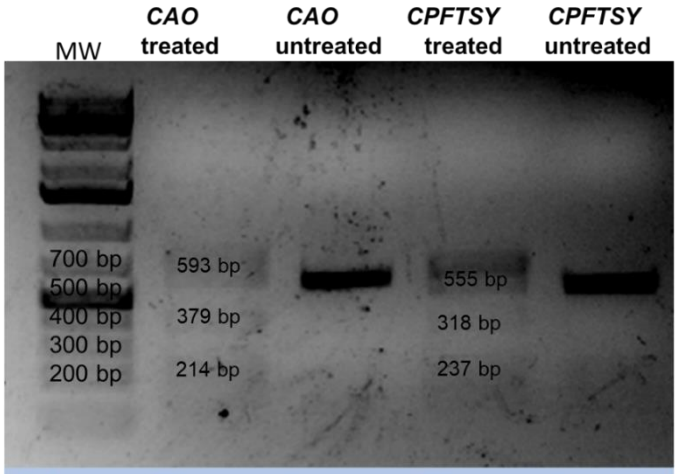

Cas9	600 ng	No	600 ng	No
sgRNA	500 ng	No	500 ng	No
DNA	100 ng	100 ng	100 ng	100 ng

Figure 9.3.In vitro cut assay. The cut reaction products and the controls were checked on a 1.5% agarose gel. The *CPFTSY* fragment is 555 bp long, while after the cut with sgRNA and Cas9 were obtained two fragments of 237 and 318 bp. The *CAO* fragment is 593 bp long, while after the cut with sgRNA and Cas9 were obtained two fragments of 214 and 379 bp MW: molecular weight marker.

The RNP complex was then used to transform *Chlamydomonas reinhardtii* combining the protocols employed by Ferenczi and colleagues and Baek and colleagues (Baek et al. 2016; Ferenczi et al. 2017) (see 9.3.13 section). $5*10^5$ cell cw15 cells were transformed with 200 µg of Cas9 and 140 µg of sgRNA. As not a resistance was used as selection marker the plates were full of colonies and after the screening no pale phenotype were observed for both the target.

9.4 NLS-Cas9 synthesis

Once failed the first transformation trial, it was performed a deeper literature analysis and It resulted that the commercial Cas9 preparations used for *Chlamydomonas* contained the Nuclear Localization Signal, necessary to deliver proteins in the eukaryotic nucleus. It was decided then to insert this sequence in Cas9 plasmid at the N-terminus of the protein encoding sequence It was synthetises by PCR as fragment containing the first part of the protein sequence and the NLS with two restriction enzymes adapters and it was inserted by cut and paste cloning in pET-Cas9-6xHis plasmid (Fig 9.4.1).

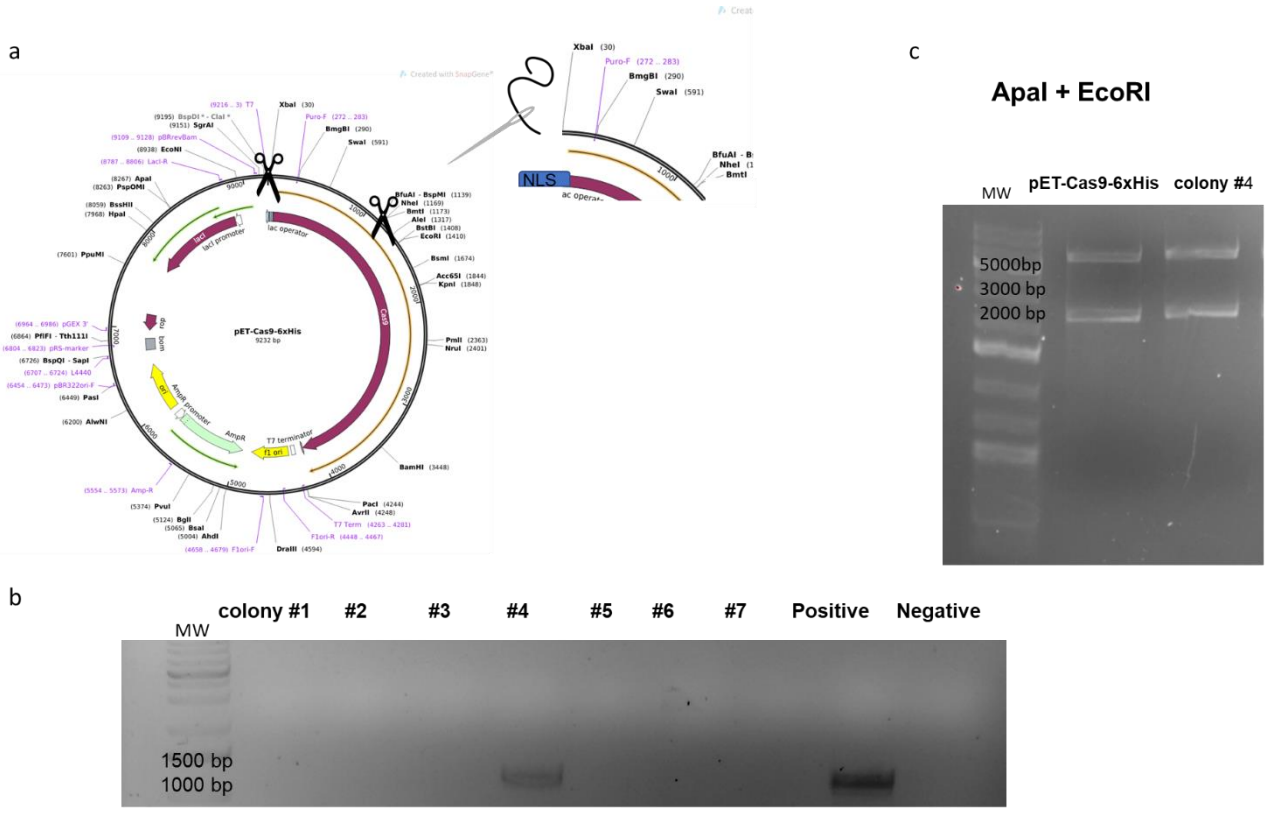

Figure 9.4.1. Cut and paste cloning to insert the NLS sequence at Cas9 N-terminus. a)Schematic representation of the procedure b)Colony PCR on the *E.coli* colonies transformed by the ligation mix. The colony#4 was positive. As positive control pET-Cas9-6xHis plasmid was used. c) Cut assay by ApaI and EcorI restriction enzymes to confirm the identity of the plasmid in the colony #4. As positive control pET-Cas9-6xHis plasmid was used. MW: molecular weight marker

The new plasmid was the used to express the protein in *E.coli* BL21 electrocompetent cell and extracted as shown before. The protein was then used to a new *in vitro* cut assay using *CAO* SgRNA and using as control the Cas9 without NLS and a commercial preparation.

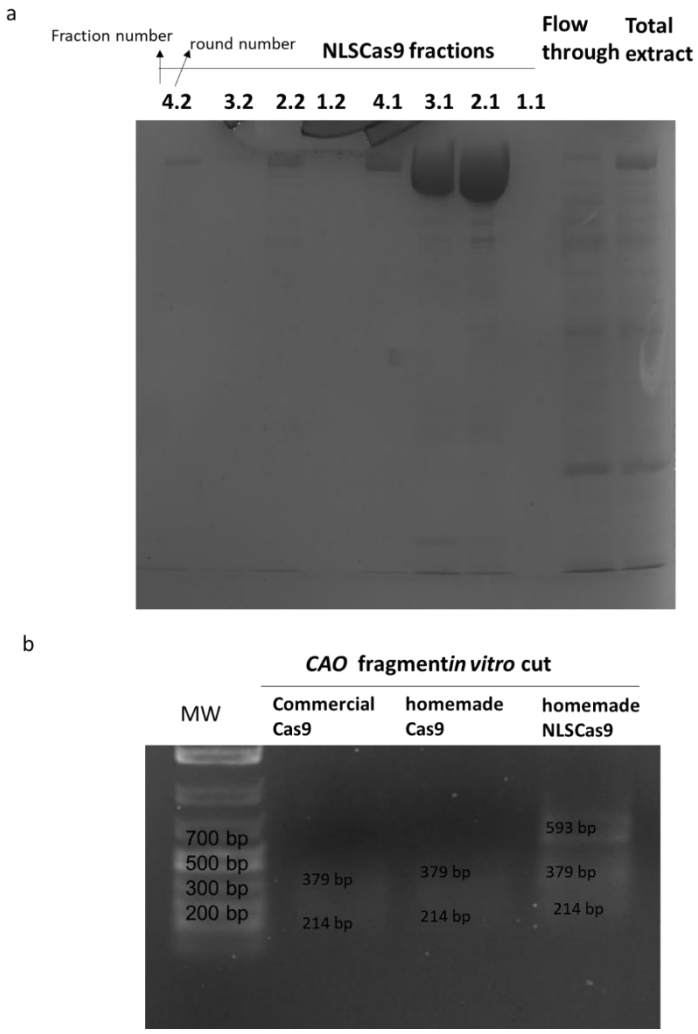

Figure 9.4.2.NLS-Cas9 purification and working trial. a) NLSCas9 eluted fractions check 3 µl of each fraction obtained by the two passages on the column were loaded on a 7.5% Laemmli gel (first number: fraction number; second number: elution cycle) As efficiency control 20 µl of the total extract, of the flow through were loaded. b) NLS-Cas9 *in vitro* cut assay. The cut reaction products and the controls were checked on a 1.5% agarose gel. The CAO fragment wass 593 bp long, while after the cut with sgRNA and Cas9 were obtained two fragments of 214 and 379 bp. As control a commercial Cas9 preparation and the Cas9 without NLS were used. MW: molecular weight marker.

9.5 Cas9 Dynamic Light Scattering at different salt concentrations

As further optimization to improve transformation efficiency Cas9 Dynamic Light Scattering (DLS) was measured at different salt concentration. It was indeed observed that this protein to work properly and to not aggregate had to be conserved in a 150 mM KCl buffer. Moreover, in the first transformation trial, where it was put about 20 µl containing 200 µg of protein in 250 µl of cell suspension, it was observed a precipitation phenomenon. For this reason, it was decided to calculate which was the minimum KCl concentration to maintain the protein functional. As buffer it was used the TOS medium, in which the cells were normally resuspended before the electroporation and it

was observed the DLS at 0, 50, 100, 150, 300 mM KCl. From the graph of the intensities in function of the peaks diameter It was observed that without salt there was only a peak in the righter part of the graph, corresponding to the highly aggregated protein. Adding 50 mM KCl there are a huge peak at lower diameter sizes, but again correspondent to an aggregated form and a second smaller peak corresponding to unaggregated protein, at 100, 150 and 300 mM the peak correspondent to unaggregated protein became huger, and only to smaller peaks, that represent a negligible residual aggregation were present (9.5.1).

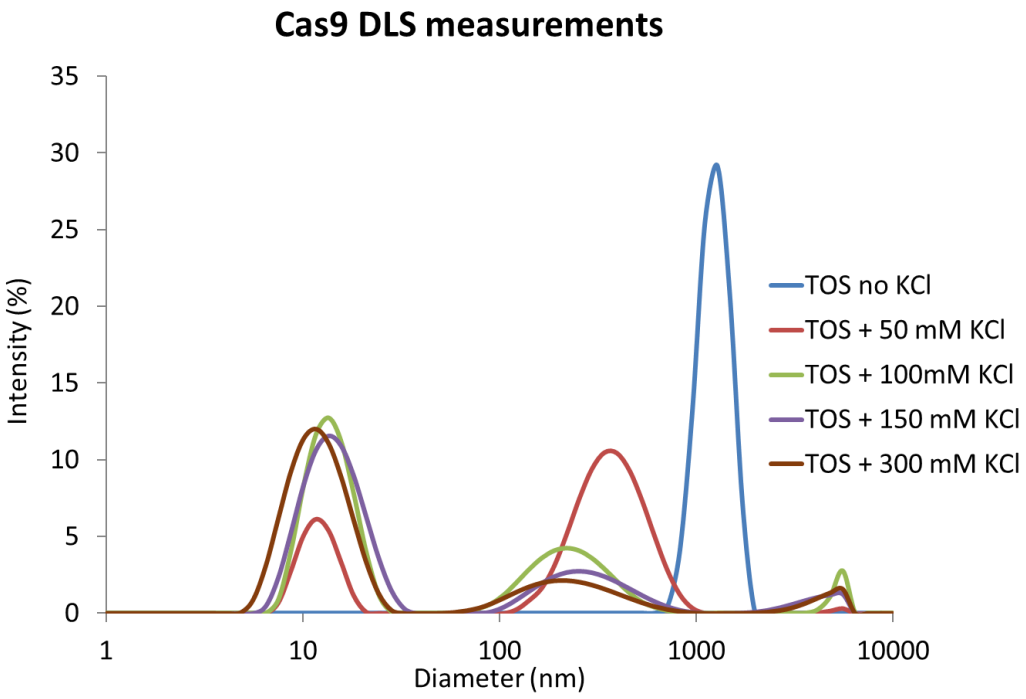

Figure 9.5 Cas9 light scattering data: Dinamic Light Scattering (DLS) in TOS medium at different salt concentrations was measured by Zetasizer Nano ZS Malvern system.

9.6 Transformation by optimized procedure

It was then performed a transformation trial with the new optimizations. The NLS-Cas9 was used to electropore cells which had been resuspended in 150 mM KCl. The procedure was summarized in figure 9.6. Neither this time among the about 2000 colonies screened it was found a pale phenotype.

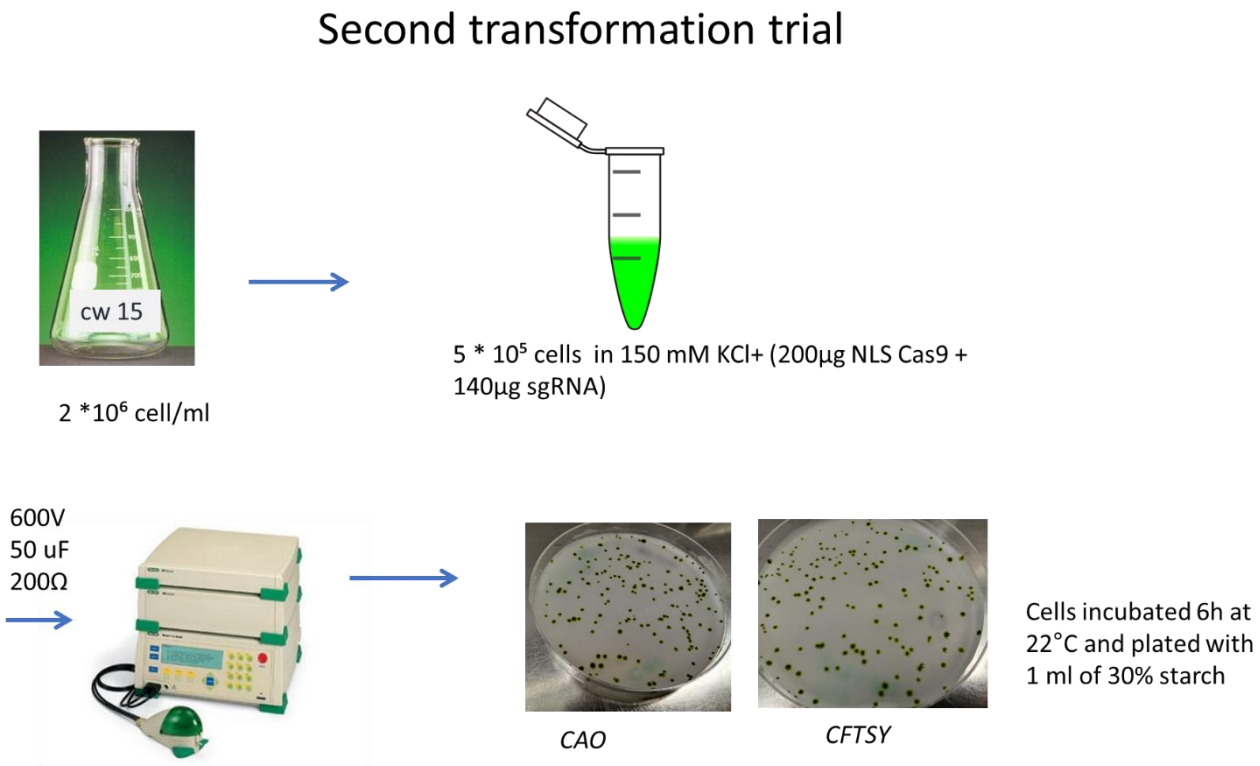

Figure 9.6 Second transformation trial. A culture of cw 15 *Chlamydomonas* strain was grown until a concentration 0f 2* 10^6 cell/ml, 5* 10^5 cells were resuspended in 250 µl of TOS containing 150mM KCl and 200 µg of NLSCas9 plus 140 µg of SgRNA were added. The cells were then electroporated at 600 V 50 µF and 200 Ω and after 6 h of recovery plated on 30% starch plates.

9.7 New transformation protocol trials using homemade and commercial Cas9

To find a new optimized protocol it was tried a procedure suggested by Professor Claire Remacle (University of Liege), who employed an antibiotic resistance cassette to improve the screening procedure and a far less quantity of RNP, using a commercial Cas9 preparation (Alt-R® S.p. Cas9 Nuclease (IDT)). The protein she used had 3NLS signals at the C-terminal, for this reason it was compared the activity of this protein with the homemade NLSCas9.
First it was performed an *in vitro* cut assay for both genes. Both Cas9 revealed efficient in cut the fragments, with a little bit higher efficiency for the commercial Cas9. Obviously, this difference was not due to the NLS presence or the number of NLS, because *in vitro* there is not a cell to enter, but it could be due to different purification techniques.

a

***CpFTSY in vitro* cut**

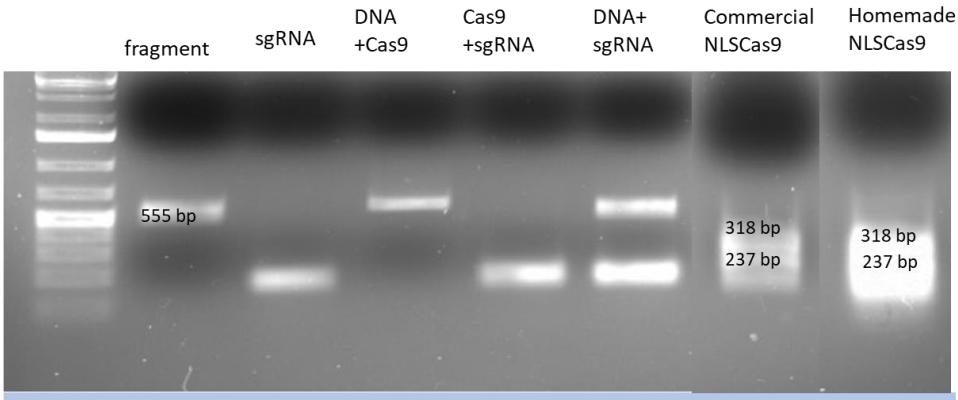

Cas9	No	No	600 ng	600 ng	No	600 ng	600 ng
SgRNA	No	500 ng	No	500 ng	500 ng	500 ng	500 ng
DNA *(CpFTSY)*	100 ng	No	100 ng	No	100 ng	100 ng	100 ng

b

***CAO in vitro* cut**

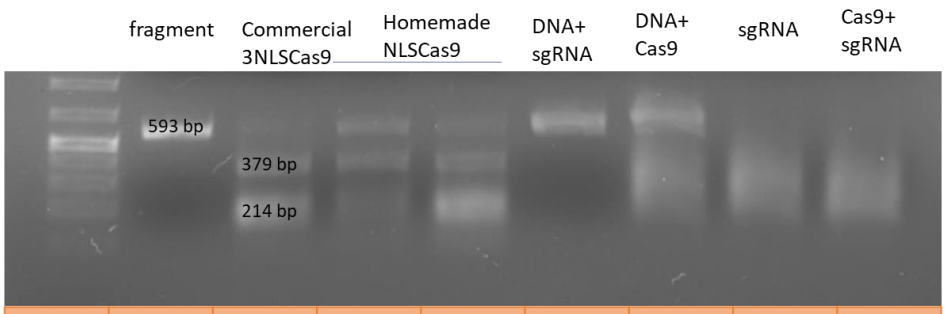

Cas9	No	600ng	600 ng	600 ng	600 ng	No	No	600 ng
sgRNA	No	500 ng	250 ng	500 ng	No	500 ng	500ng	500 ng
DNA (*CAO*)	100 ng	100 ng	100 ng	100 ng	100 ng	100 ng	No	No

Figure 9.7.1: *in vitro* cut assay by homemade and commercial Cas9: a) *CpFTSY in vitro* cut assay. The cut reaction products and the different controls were checked on a 1.5% agarose gel. The sgRNA alone gave a signal of about 100 bp. The fragment is 555 bp long, while after the cut with sgRNA and Cas9 were obtained two fragments of 237 and 318 bp. b) *CAO in vitro* cut assay: The cut reaction products and the different controls were checked on a 1.5% agarose gel. The sgRNA, alone and combined with Cas9 or DNA only, gave a smear not present when the RNP- complex cuts the DNA. The fragment is 593 bp long, while after the cut with sgRNA and Cas9 were obtained two fragments of 214 and 379 bp.

Both Cas9s were then used to perform a *Chlamydomonas* transformation trial by the new protocol (8.3.17).

For *cpftsy* mutant production it was co-delivered an Hygromycin resistance, while for *CAO* a Paromomycin one, obtained by the linearization of pHyg3 (Berthold et al. 2003) and pOpt2_mCerulean3_Paro (Lauersen et al. 2018). There were performed three different

transformations. The first was with the homemade Cas9 followed Baek's protocol with the adding of the resistance cassettes, the second and the third were instead performed according Claire Remacle's procedure, by using homemade or commercial Cas9. The only successfully transformation was the one with the commercial Cas9, and it was supposed that it could be due to the higher number of NLS sequences. For *cao* mutants it was obtained an efficiency of 25% (15 over 60 colonies), while for *cpftsy* of 0.5% (2 over 400 colonies) as expected (Baek et al. 2016). Pale colonies were screened by absorption spectroscopy to check the chlorophyll *a*/*b* ratio and by sequencing of a target containing genomic fragment. The insertion was always present soon after the PAM sequence.

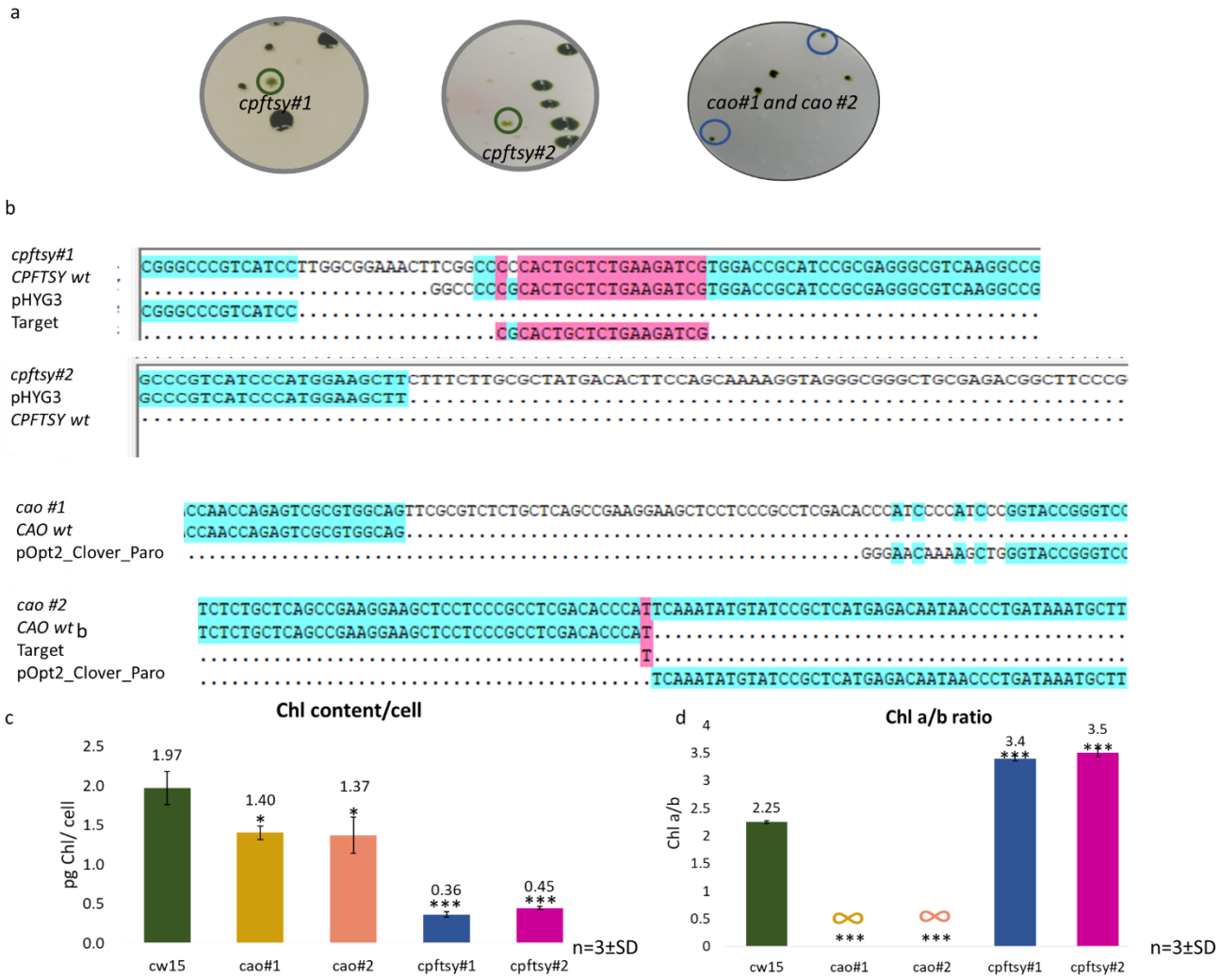

Figure 9.7.2 Phenotypic and sequencing analysis of the mutants obtained by the new protocol. a) Details of the plates 7 days after the transformation. b) Sequences of the insertion regions. In *cpftsy#1* the insertion is immediately before target sequence, while in *cpftsy#2* it is after the target, with a small insertion of random bases, due probably to mistakes in the repair mechanisms. For *cao#1* the insertion is about 70 nt before the target. For *cao#2* there was an interruption at the beginning of the target region. Pink colour represents the matching zone for all sequences and light blue the zone in which only some of them match. c) chlorophyll content per cell. d) chl a/b ratio. Bars represent average of three biological replicates ± standard deviation. Asterisks indicate statistically significant differences between mutant and WT according to Student's t test (*, $P < 0.05$; **, $P < 0.01$; ***, $P < 0.001$).

Further optimizations were then performed to make the homemade Cas9 working. The result of the trials to optimize the homemade Cas9 performances were reported on the paper in the chapter 11 (Angstenberger et al. 2020)

REFERENCES

Angstenberger M, de Signori F, Vecchi V, Dall'Osto L, Bassi R (2020) Cell Synchronization Enhances Nuclear Transformation and Genome Editing via Cas9 Enabling Homologous Recombination in Chlamydomonas reinhardtii. ACS Synth Biol. https://doi.org/10.1021/acssynbio.0c00390

Bae S, Park J, Kim JS (2014) Cas-OFFinder: a fast and versatile algorithm that searches for potential off-target sites of Cas9 RNA-guided endonucleases. Bioinformatics 30:1473–1475 . https://doi.org/10.1093/bioinformatics/btu048

Baek K, Kim DH, Jeong J, Sim SJ, Melis A, Kim JS, Jin E, Bae S (2016) DNA-free two-gene knockout in Chlamydomonas reinhardtii via CRISPR-Cas9 ribonucleoproteins. Sci Rep 6:30620 . https://doi.org/10.1038/srep30620

Benedetti M, Vecchi V, Betterle N, Natali A, Bassi R, Dall'Osto L (2019) Design of a highly thermostable hemicellulose-degrading blend from Thermotoga neapolitana for the treatment of lignocellulosic biomass. J Biotechnol 296:42–52 . https://doi.org/10.1016/j.jbiotec.2019.03.005

Berthold P, Schmitt R, Mages W (2003) An Engineered Streptomyces hygroscopicus aph 7''Gene Mediates Dominant Resistance against Hygromycin B in Chlamydomonas reinhardtii. Protist 153:401–412 . https://doi.org/10.1078/14344610260450136

Ferenczi A, Pyott DE, Xipnitou A, Molnar A (2017) Efficient targeted DNA editing and replacement in Chlamydomonas reinhardtii using Cpf1 ribonucleoproteins and single-stranded DNA. Proc Natl Acad Sci 114:13567 LP – 13572 . https://doi.org/10.1073/pnas.1710597114

Jeong J, Baek K, Yu J, Kirst H, Betterle N, Shin W, Bae S, Melis A, Jin E (2018) Deletion of the chloroplast LTD protein impedes LHCI import and PSI-LHCI assembly in Chlamydomonas reinhardtii. J Exp Bot 69:1147–1158 . https://doi.org/10.1093/jxb/erx457

Lauersen KJ, Wichmann J, Baier T, Kampranis SC, Pateraki I, Møller BL, Kruse O (2018) Phototrophic production of heterologous diterpenoids and a hydroxy-functionalized derivative from Chlamydomonas reinhardtii. Metab Eng 49:116–127 . https://doi.org/https://doi.org/10.1016/j.ymben.2018.07.005

Ordon J, Gantner J, Kemna J, Schwalgun L, Reschke M, Streubel J, Boch J, Stuttmann J (2017) Generation of chromosomal deletions in dicotyledonous plants employing a user-friendly genome editing toolkit. Plant J 89:155–168 . https://doi.org/10.1111/tpj.13319

Park J, Bae S, Kim JS (2015) Cas-Designer: a web-based tool for choice of CRISPR-Cas9 target sites. Bioinformatics 31:4014–4016 . https://doi.org/10.1093/bioinformatics/btv537

Shin SE, Lim JM, Koh HG, Kim EK, Kang NK, Jeon S, Kwon S, Shin WS, Lee B, Hwangbo K, Kim J, Ye SH, Yun JY, Seo H, Oh HM, Kim KJ, Kim JS, Jeong WJ, Chang YK, Jeong BR (2016) CRISPR/Cas9-induced knockout and knock-in mutations in Chlamydomonas reinhardtii. Sci Rep 6:27810 . https://doi.org/10.1038/srep27810

Shin YS, Jeong J, Nguyen THT, Kim JYH, Jin E, Sim SJ (2019) Targeted knockout of phospholipase A2 to increase lipid productivity in Chlamydomonas reinhardtii for biodiesel production. Bioresour Technol 271:368–374 . https://doi.org/https://doi.org/10.1016/j.biortech.2018.09.121

Zuris J, Thompson D, Shu Y, Guilinger J, Bessen J, Hu J, Maeder M, Joung J, Chen ZY, Liu D (2014) Cationic lipid-mediated delivery of proteins enables efficient protein-based genome editing in vitro and in vivo. Nat Biotechnol 33: . https://doi.org/10.1038/nbt.3081

CHAPTER 10
Discussion and Conclusion

Genome editing techniques are the most promising methods to obtain precise mutations in the gene of interest. In this way is possible to study the phenotype associated to specific genes, annotated or not. Once found a target it is possible indeed to design specific molecules to drive a nuclease for the obtainment of the desired mutation.

CRISPR-Cas9 system is nowadays the most used technique for genome editing, as it showed high efficiency and in most cases specificity. According to the model organism the method has to be optimized to guarantee these features. In *Chlamydomonas* this method revealed useful to obtain mutants with an easily screenable phenotype, in particular is widely employed to obtained photosynthesis mutants (Baek et al. 2016; Shin et al. 2016; Ferenczi et al. 2017; Jeong et al. 2018; Cazzaniga et al. 2020). In this thesis it was optimized a transformation protocol to transform *Chlamydomonas reinhardtii* by CRISPR-Cas9 system, starting from Baek's protocol (Baek et al. 2016) and optimizing the steps according the available material and the information collected during the process. It was needed to obtain *cpftsy* mutant strains, similar to those obtained in the paper (Baek et al. 2016), both to check the optimization step and to use this for other research applications previously exposed (Chapter 2,4 and 5). Moreover, *CAO* gene was also targeted to obtain mutants deficient in chlorophyll b production, for both test the efficiency of the optimization for other genes and to compare with *cpftsy* mutants for photosynthesis research purposes.

In Baek's paper it was suggested to electropore *Chlamydomonas* to directly deliver 200 μg of purified Cas9 protein and 140 μg of *in vitro* transcribed sgRNA (Baek et al. 2016). As it was needed this huge amount of protein it was decided to purify a homemade protein. For this reason, it was bought a plasmid for its expression in *E. coli*, and a protocol of purification by Ni-affinity chromatography was set. The first *in vitro* cut trials revealed that the RNP-complex composed by homemade Cas9 and sgRNAs was able to cut both a fragment of the CpFTSY encoding gene and of CAO one. However, when this system was exported *in vivo* it didn't work for none of these genes. For this reason, it was tried to add a nuclear localization signal NLS to the Cas9 encoding sequence in the plasmid. It was reported, indeed, that this sequence is necessary to obtain an efficient protein delivery into the eukaryotic nucleus (Zuris et al. 2014). Moreover it was verified that most of the publication reporting the CRISPR Cas9 in plants used commercial preparations or constructs in which the protein had the NLS (Ordon et al. 2017; Ferenczi et al. 2017; Shin et al. 2019). This sequence was inserted at the N-terminus of the Cas9 sequence in the plasmid, as it was the only site with employable restriction sites to perform the cut and paste cloning. The new protein was successfully expressed and extracted from *E. coli* and was able to cut the target sequences *in vitro* when assembled with a specific sgRNA. However, when it was used to transform *Chlamydomonas*, no mutant clones were obtained. As this protein needs a high salt concentration to maintain the proper folding and a functional structure, different light scattering measurement were performed changing the salt concentration in the algae medium. The measurement revealed a tendency of the Cas9 to aggregate in TOS medium at low salt concentrations. However, neither the addition of 150 mM KCl during the transformation allowed the

transformation success. To understand where the problem was, if in the protein or in the procedure, it was followed a new protocol suggested by Professor Claire Remacle (University of Liege). For this protocol a lower Cas9 concentration was needed, for this reason it was bought a commercial preparation and different transformations were tried, using the commercial or the homemade Cas9. Moreover, to facilitate the screening an antibiotic-containing sequence was introduced with the RNP complex. From the phenotypic screening resulted that only the commercial protein was able to cut the target, as there were obtained colonies with the desired phenotype. The previous difficulties were probably due to some trouble in Cas9 purification. In a first moment it was thought about the necessity for the protein to have more than one NLS at the C-terminal, as the commercial one has three NLS at this side. This was hypothesized, once observed that the homemade NLS Cas9 was active *in vitro*, indicating its structure integrity and its proper folding. In our mind, indeed, the trouble *in vivo* had to be, indeed in the protein ability to reach the nucleus. However, after several successful transformation with the commercial Cas9 preparation, it was decided to retry to use the homemade one, by changing a passage adding EDTA after total protein extraction to eliminate unspecific protein-nucleic acid bonds that cold compromise protein efficiency (Angstenberger et al. 2020). Moreover, it was tried to optimize Chlamydomonas transformation efficiency with the RNP complex, by synchronizing the cell. In this way it was also found a procedure to obtain precise knock-in insertion (Angstenberger et al. 2020). The results of these improvements were published in the paper reported in the next chapter. It is also interesting to note that with the same technique it was obtained a different transformation efficiency between the two target genes. This is not only due to the proper design of sgRNA and in particular to the 20 nt target selection. This is also strongly dependant from the target gene structure and accessibility. *CpFTSY* is a G/C rich gene, difficult also to be amplified, probably for a partialinaccessibility to enzymes. The G/C presence could influence a more cohesive chromatin structure that makes hard for the Cas9 to cut the target. This challenge it was tried to be overcome synchronizing the cell cycle before the transformation as reported in the following paper (Angstenberger et al. 2020).

REFERENCES

Angstenberger M, de Signori F, Vecchi V, Dall'Osto L, Bassi R (2020) Cell Synchronization Enhances Nuclear Transformation and Genome Editing via Cas9 Enabling Homologous Recombination in Chlamydomonas reinhardtii. ACS Synth Biol. https://doi.org/10.1021/acssynbio.0c00390

Baek K, Kim DH, Jeong J, Sim SJ, Melis A, Kim JS, Jin E, Bae S (2016) DNA-free two-gene knockout in Chlamydomonas reinhardtii via CRISPR-Cas9 ribonucleoproteins. Sci Rep 6:30620 . https://doi.org/10.1038/srep30620

Cazzaniga S, Kim M, Bellamoli F, Jeong J, Lee S, Perozeni F, Pompa A, Jin E, Ballottari M (2020) Photosystem II antenna complexes CP26 and CP29 are essential for nonphotochemical quenching in Chlamydomonas reinhardtii. Plant Cell Environ 43:496–509 . https://doi.org/10.1111/pce.13680

Ferenczi A, Pyott DE, Xipnitou A, Molnar A (2017) Efficient targeted DNA editing and replacement in Chlamydomonas reinhardtii using Cpf1 ribonucleoproteins and single-stranded DNA. Proc Natl Acad Sci 114:13567 LP – 13572 . https://doi.org/10.1073/pnas.1710597114

Jeong J, Baek K, Yu J, Kirst H, Betterle N, Shin W, Bae S, Melis A, Jin E (2018) Deletion of the chloroplast LTD protein impedes LHCI import and PSI-LHCI assembly in Chlamydomonas reinhardtii. J Exp Bot 69:1147–1158 . https://doi.org/10.1093/jxb/erx457

Ordon J, Gantner J, Kemna J, Schwalgun L, Reschke M, Streubel J, Boch J, Stuttmann J (2017) Generation of chromosomal deletions in dicotyledonous plants employing a user-friendly genome editing toolkit. Plant J 89:155–168 . https://doi.org/10.1111/tpj.13319

Shin SE, Lim JM, Koh HG, Kim EK, Kang NK, Jeon S, Kwon S, Shin WS, Lee B, Hwangbo K, Kim J, Ye SH, Yun JY, Seo H, Oh HM, Kim KJ, Kim JS, Jeong WJ, Chang YK, Jeong BR (2016) CRISPR/Cas9-induced knockout and knock-in mutations in Chlamydomonas reinhardtii. Sci Rep 6:27810 . https://doi.org/10.1038/srep27810

Shin YS, Jeong J, Nguyen THT, Kim JYH, Jin E, Sim SJ (2019) Targeted knockout of phospholipase A2 to increase lipid productivity in Chlamydomonas reinhardtii for biodiesel production. Bioresour Technol 271:368–374 . https://doi.org/https://doi.org/10.1016/j.biortech.2018.09.121

Zuris J, Thompson D, Shu Y, Guilinger J, Bessen J, Hu J, Maeder M, Joung J, Chen ZY, Liu D (2014) Cationic lipid-mediated delivery of proteins enables efficient protein-based genome editing in vitro and in vivo. Nat Biotechnol 33: . https://doi.org/10.1038/nbt.3081

CHAPTER 11

Cell Synchronization Enhances Nuclear Transformation and Genome Editing via Cas9 Enabling Homologous Recombination in *Chlamydomonas reinhardtii*

This paper was published in September 2020:

Angstenberger M, de Signori F, Vecchi V, Dall'Osto L, Bassi R. Cell Synchronization Enhances Nuclear Transformation and Genome Editing via Cas9 Enabling Homologous Recombination in *Chlamydomonas reinhardtii*. ACS Synth Biol. 2020 Sep 25.

Abstract: In *Chlamydomonas reinhardtii*, the model organism for eukaryotic green algae and plants, the processes of nuclear transformation and genome editing in particular are still marked by a low level of efficiency, and so intensive work is required in order to create and identify mutants for the investigation of basic physiological processes, as well as the implementation of biotechnological applications. In this work, we show that cell synchronization during the stages of the cell cycle, obtained from long- term cultivation under specific growth conditions, greatly enhances the efficiency of transformation and allows the identification of DNA repair mechanisms that occur preferentially at different stages of the cell cycle. We demonstrate that the transformation of synchronized cells at different times was differentially associated with nonhomologous end joining (NHEJ) and/or homologous recombination (HR), and makes it possible to knock-in specific foreign DNA at the genomic nuclear location desired by exploiting HR. This optimization greatly reduces the overall complexity of the genome editing procedure and creates new opportunities for altering genes and their products.

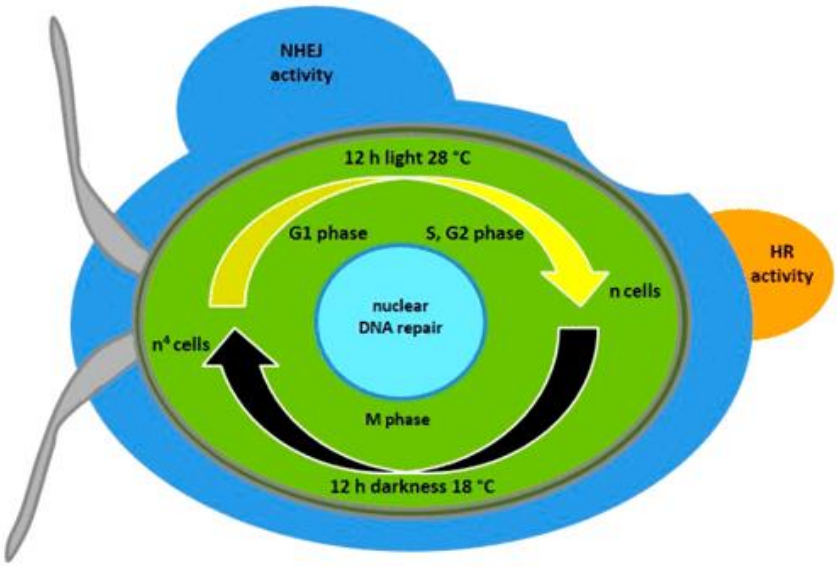

Figure 11.1 Graphical abstract

11.1 Introduction

As the model organism for eukaryotic green algae and plants, *Chlamydomonas reinhardtii* has been widely studied over recent decades, as summarized in ref (Harris 2001). Its fully sequenced (Grossman et al. 2003) haploid genome offers great benefits in establishing techniques for nuclear transformation (Harris 2009) and electroporation, (Shimogawara et al. 1998) as well as genome editing techniques such as the CRISPR/Cas9 system. (Jiang et al. 2014; Ferenczi et al. 2017). Special strains that are even easier to transform are also available, for example, the cw15 strain with a reduced cell wall (Hyams and Davies 1972). Nevertheless, transformation, and specific gene targeting techniques in particular, still need to be further optimized in order to obtain an efficient platform for creating mutants that can be applied to other algae and plant species.

The recent confirmation of the transformation of *C. reinhardtii* using ribonucleoproteins (Baek et al. 2016; Ferenczi et al. 2017) of Cas9 and coupled single-guide RNA (sgRNA) opened the way for the production of gene knockout mutants and, in some cases, the knock-in of foreign DNA delivered in specific sequences (compare figure 11.2).

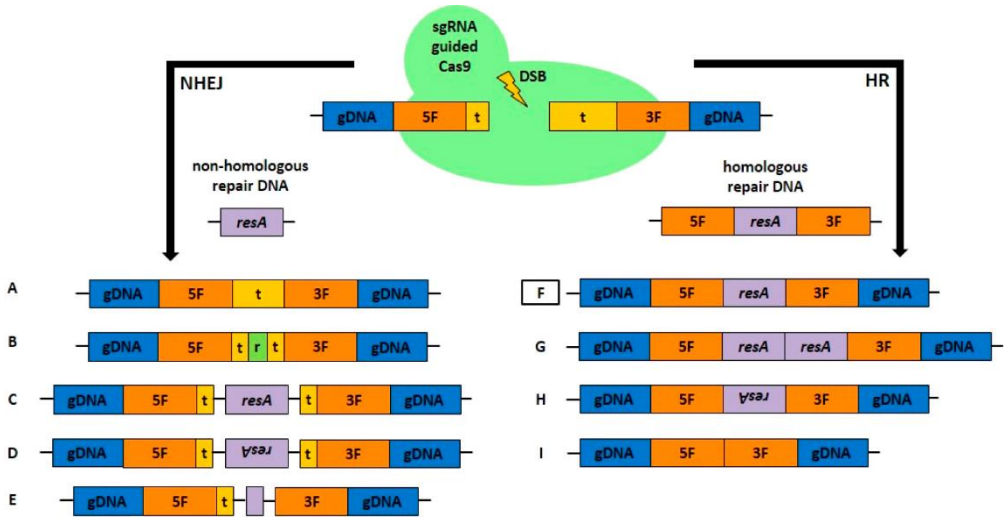

Figure 11.2 Schematic overview of single guide RNA (sgRNA), guided Cas9 introduced DNA double-strand breaks (DSB), and possible DNA repair pathways in eukaryotes. Repair mechanisms include nonhomologous end joining (NHEJ) and homologous recombination (HR), the possible outcomes of which depend on the provision of DNA repair and the respective active repair mechanism. In the uppermost part, the selected exemplary nuclear (gDNA) target sequence (t) and 5′ and 3′ flanking regions (5F, 3F) are depicted. Using sgRNA-guided Cas9, a DSB can be introduced in the target region, but the process is not entirely predictable. As long as a nonhomologous repair template confers antibiotic resistance (*resA* cassette), an active NHEJ pathway can lead to several results: (A) target sequence repair with error-prone sequence modifications, (B) insertion of random (r) sequences, (C) insertion of DNA clockwise, and anticlockwise in (D), and (E) insertion of truncated repair DNA. As a consequence, there are likely to be remnants of the chosen target sequence. In contrast, the provision of homologous repair DNA containing the flanking regions can lead to different results in an active HR pathway: the most desirable outcome is shown in (F), that is, the sequence-specific replacement of the target sequence with *resA*. Other options are multiple insertions of *resA* (G), inverted insertions (H) and deletions (I).

The latter was recently confirmed (Kim et al. 2020) as enabling unspecific knock-ins *via* nonhomologous end-joining (NHEJ), which displayed the disadvantage of sequence changes often observed during DNA integration (Figure 11.2 C,E) which, together with low transformation efficiency, makes identification of specific genotypes problematic and requiring extensive sequencing procedures. Therefore, specific knock-ins caused by HR (Figure 11.2 F–I), with a high probability of complete and sequence-specific DNA integration, display great potential in altering gene structures and therefore altering protein sequences, to implement protein tagging systems, (Lechtreck et al. 2009) for example, or to replace genes with copies containing single point mutations. Significantly, such specific knock-ins created through the HR pathway (Figure 11.2 F), that is, replacing a target sequence using homologous flanking regions, only appear naturally at very low frequencies in *C. reinhardtii*; (Sodeinde and Kindle 1993; Gumpel et al. 1994; Nelson and Lefebvre 1995; Zorin et al. 2009) instead, random DNA integration is dominant and mediated by NHEJ (Zhang et al. 2014). Inducing DNA double-strand breaks (DSB) using the Cas9 nuclease at specific sequences and providing homologous repair templates were shown to increase the probability of specific knock-ins in various species (Sizova et al. 2013; Irion et al. 2014). HR activity is often suppressed by the NHEJ pathway in eukaryotes (Frit et al. 2014) and is only present in certain stages of the eukaryotic cell cycle, (Lin et al. 2014) that is, in the late DNA synthesis phase (S phase) and early mitotic phase (M phase). In addition, HR activity is well-known from the recombination of parental DNA in meiosis.

Various attempts to improve HR efficiency in microalgae as well as in other species have been reported in recent years, including, for example, by interfering with the NHEJ-specific DNA-Ligase IV,(Schorsch et al. 2009; Angstenberger et al. 2019) inducing DSBs, or taking advantage of synchronized cells in order to access HR specific stages of the cell cycle for transformation, for example, using a zinc-finger nuclease (Sizova et al. 2013). However, the level of HR efficiency so far obtained is still lower than that required to make these procedures part of the daily routine of the genetic modification of *C. reinhardtii*. Therefore, a more profound synchronization of cells in a culture during the eukaryotic cell cycle stages at the same time display a promising advantage to optimize genome editing in *C. r.* by exploiting the differentially present DNA integration mechanisms during the cell cycle and though could serve as a model system for similar strategies in other algae species. It was our hypothesis that a relaxed chromatin structure, present during the interphase in all synchronized cells of *C. r.* before entering the mitotic prophase with associated chromatin condensation,(Buffaloe 1958) could enhance DNA integration. Moreover, such chromatin state is expected to offer a more accessible target for the Cas9 nuclease in order to introduce a DSB for repair by NHEJ or HR. The latter mechanism, which could be displayed at a specific cell cycle stage, could lead to a specific knock-in of a transformed DNA molecule containing homologous flanking regions to a defined target site (Figure 11.2 F).

Cell synchronization depends on light and temperature (12 h of light at 28 °C and 12 h of darkness at 18 °C) and was shown to be obtained during short-term cultivation,(Strenkert et al. 2019) leading to one cell division per night (M phase) and cell growth during the day (interphase) in *C. reinhardtii*. Moreover, depending on specific growth conditions, *C. r.* can even undergo multiple cell divisions consisting of S and M phases (Coleman 1982) including chromatin decondensation (Johnson and Porter 1968). Further, cells enter the interphase again starting with the G1 phase that can last for several hours (Craigie and Cavalier-Smith 1982) and includes an extended decondensed chromatin

structure. Between S and M phase, eukaryotes generally exhibit a second growth phase G2, that is either not present or difficult to detect in *C. r.* (Jones 1970). In order to reach optimal cell synchronization, long-term cultivation in such conditions (Strenkert et al. 2019) was therefore chosen to investigate the possibility of maximizing genome editing (GE) efficiency by accessing each stage of the cell cycle for transformation and so define specific properties for DNA integration depending on NHEJ which is dominant in the G1 phase in eukaryotes (Hinz et al. 2005) and/or HR, that is present in S and early M phase. Determining the transformation efficiency (obtained clones/used ng DNA for transformation/transformed cells) at certain stages of the cell cycle, using either nonhomologous or homologous transformation constructs, should therefore provide information about the ongoing DNA repair mechanisms (NHEJ/HR), while target sequence analysis could confirm the occurrence of specific knock-ins.

For the prompt detection of transformation events, the gene *cpftsy* (Kirst et al. 2012; Baek et al. 2016; Kim et al. 2020) was chosen as the target. The associated protein is involved in the assembly of the light-harvesting system in the thylakoid membranes. When absent due to a knockout, mutants display a pale green phenotype that is easily detected by the naked eye on plates during growth after transformation. This approach made it possible for the knockout frequency to be quickly determined by counting the pale green colonies as compared to the native green ones, created by random mutations. Interestingly, the knockout frequency of *C. r. cpftsy* was very low in earlier experiments (0.5–1%) compared to knockouts of other target genes, for example, the chlorophyllide-a oxygenase (*CAO*, ∼20%, data not shown), which also leads to a pale phenotype, though less pronounced. Nevertheless, analyzing the low knockout frequency of the *cpftsy* gene offers the advantage of showing the full effect of an optimized GE frequency, avoiding saturation. To enable specific recombination events by HR at the *cpftsy* locus, a construct with 2 kb flanking regions surrounding the sgRNA guided target sequence was created. Large flanking regions were previously shown to enhance HR events in *C. reinhardtii* (Plecenikova et al. 2013) and in other microalgae,(Angstenberger et al. 2019) increasing the probability of such events.

11.2 Results and Discussion

C. r. cw15 Cell Synchronization under Long-Term Cultivation

As reported by ref (Strenkert et al. 2019), cell synchronization of *C. r.* can be achieved by applying a temperature of 28 °C during the light phase (resulting in cell growth) and 18 °C in the dark phase (leading to an exact doubling of cell numbers). We observed the growth behaviour of cw15 in similar light-dark and warm-cool cycles, as carried out by ref (Strenkert et al. 2019), in a multicultivator system that measured the optical density over several days (not shown). Interestingly, under these growth conditions (12 h light at 28 °C and 12 h darkness at 18 °C), we observed a change in growth behaviour during prolonged cultivation, leading to a higher daily cell number than expected, if two daughter cells were being generated by each mother cell. In order to further characterize such growth behaviour, a batch culture of cw15 was maintained under these conditions and after 3 to 4 days of growth, cells were used to inoculate a new culture, in order to achieve a long-term adaptation (2 weeks of preculturing with ongoing cultivation). Following a subsequent inoculation, the cell number was determined continuously using a cell counter (Figure 11.3 A, B).

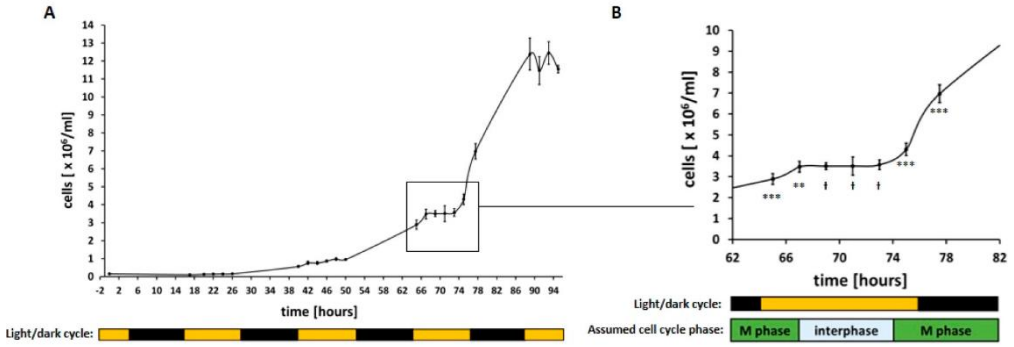

Figure 11.3. Growth curves of synchronized *C. r.* cw15 cultures. The number of cells of *C. r.* cw15 grown at 28 °C during the light phase (12 h, 200 µmol photons m^{-2} s^{-1}) and at 18 °C (12 h) during the dark phase (as indicated by bars) was determined using a cell counter after 2 weeks of preculturing under the same conditions. Each data point represents an average of three technical replicates that were each counted twice. (A) Overview of cell number during growth for 4 days. (B) Enlarged view of the curve after 3 days of growth. Assumed cell cycle phases are shown as bars. A one-sided *t* test was performed, and the statistical confidence level is shown in relation to the previous data point as two asterisks for $p < 0.01$, three asterisks for $p < 0.001$, while a hash represents insignificant values of $p > 0.05$.

As expected, a pretty constant cell number was measured during the light phases (Figure 11.3 A), but a significant cell number increase was observed during each dark phase. In addition to the previous report (Strenkert et al. 2019) in which the cultivation was short-term, we saw higher cell division rates after long-term cultivation with approximately 2 cell divisions during each dark phase, as previously described by (Coleman 1982) to be possible in *C. r*.

On the third day after inoculation in particular (Figure 11.3 B), the expected synchronization of the culture could be observed. After 3 h of light, cell division stopped and the cell number remained constant for about 6 h before cell division resumed. In the following 4.5 h, the cell number doubled, from 3.57×10^6 cells/mL to 6.97×10^6 cells/mL (a factor of 1.95), implying synchronized cell division was underway in the culture. A second cell division occurred during this dark phase, resulting in 12.4×10^6 cells/mL the next day (a factor of 1.78). On the basis of general knowledge of the eukaryotic cell cycle, we could assume that the two major phases (interphase and M phase, Figure 11.3 B) were underway in the vast majority of the cw15 cells at different points of time during this cultivation procedure. Due to the occurrence of two subsequent cell divisions in the dark phase, a second interphase (though shorter) occurred, as described by ref (Matsumura et al. 2010). This shorter interphase was not examined further and so is not displayed in the M phase in Figure 11.3 B.

Determination of Transformation Efficiency in Synchronized *C. r.* cw15 Cultures

Using cw15 synchronized cultures made it possible to investigate the effect on transformation efficiency and the occurrence of different DNA repair mechanisms (NHEJ/HR) by using a nonhomologous (pHyg3, Figure 11.4) or homologous linearized transformation construct (HCP, containing homologous flanking regions of *cpftsy*, Figure 11.4) at different time points during cultivation. Random DNA integration by NHEJ was therefore expected to lead to hygromycin-

resistant, normal green colonies, whereas HR-mediated recombination events at *cpftsy* should generate pale green clones.

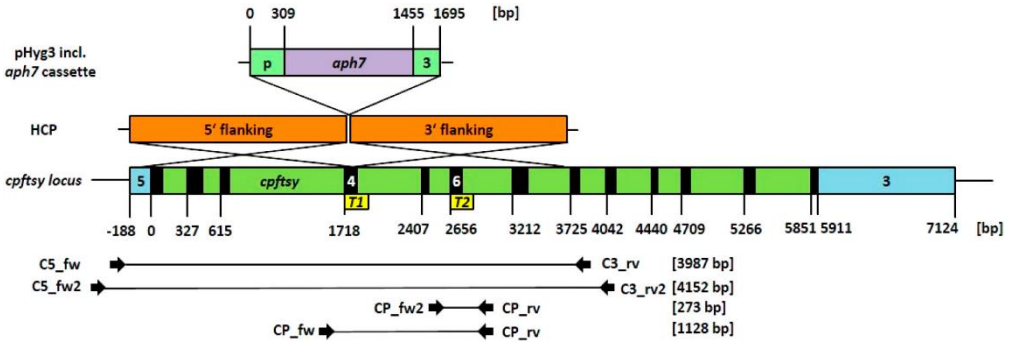

Figure 11.4. Overview of used transformation constructs and the target locus of *cpftsy* depicted as true-to-scale schematic representations of different elements. (Top) The standard transformation vector pHyg3 for *C. r.* contains the antibiotic resistance cassette, consisting of the promoter (p) of the β-Tubulin gene, the hygromycin resistance gene *aph7* and the 3′ UTR (3) of the RubisCO small subunit 2 gene. (Middle) The knock-in construct HCP (homologous recombination for *cpftsy*) targeting the *cpftsy* locus was created by cloning the *aph7* cassette of pHyg3 in between two homologous flanking regions (5′ and 3′ flanking, surrounding a first target sequence T1) into the bluescript vector KS-. (Bottom) The *cpftsy* locus included the 5′ UTR (5), coding exons depicted in black and the 3′ UTR (3). Both target sequences used for creating sgRNA (T1, T2) are shown, as well as the primer binding sites and the sizes of the expected amplification products.

First, we defined an optimized transformation protocol aimed at minimizing false positive clones and simplifying the procedure based on (Shimogawara et al. 1998). The final optimized protocol is described in detail in the Methods section (see also Table S11.1) and includes the reduction of materials, working time and a more stringent selection using a higher hygromycin concentration. Once optimized conditions on synchronized cw15 had been established, the analysis of transformations at different time points on the third day of cultivation with respective constructs (Figure 11.5 A) displayed a strong enhancement of the transformation efficiency (TE).

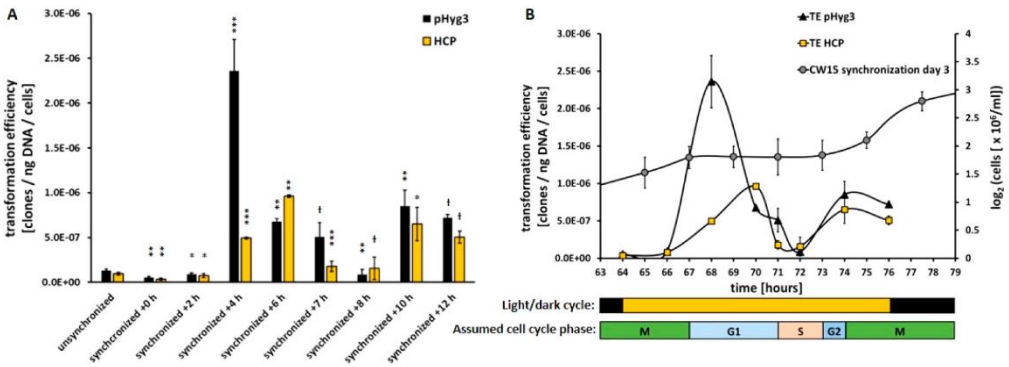

Figure 11.5. Analysis of transformation efficiency of unsynchronized and synchronized cell cultures of *C. r.* cw15. (A) TE was measured at different time points (h, hours after illumination start) after 3 days of cultivation under synchronizing conditions. Each data point shows mean ± SD, *n* = 3. Transformations by linearized construct pHyg3 (nonhomologous) are depicted in black, and those by linearized construct HCP (homologue to *cpftsy*) are

shown in yellow. A one-sided *t* test was performed and the statistical confidence level is shown in relation to the previous related data point as one asterisk for $p < 0.05$, two asterisks for $p < 0.01$, three asterisks for $p < 0.001$, while a hash represents insignificant values of $p > 0.05$. (B) TE data is displayed in comparison with the corresponding cell number (shown as $\log_2$, gray circles) on the third day of growth under synchronizing conditions (compare Figure 11.3 B). Below, the illumination cycle is depicted as bars, as well as the assumed cell cycle phases.

Compared to the TE of unsynchronized cells, the TE using synchronized cells and pHyg3 remained rather low during the first hours of illumination (around 10^{-7} clones/ng DNA/cells) but was drastically enhanced to a maximum at +4 h of illumination (+1800%). In the following hours, TE decreased to a pronounced minimum at +8 h, but increased again at the end of illumination period to around 5×10^{-7} clones/ng DNA/cells. TE using HCP displayed a similar pattern, but interestingly reached a maximum at +6 h ($\sim 10^{-6}$ clones/ng DNA/cells), although less pronounced compared to that for pHyg3. No pale colonies could be found after all those transformations, confirming the before mentioned inefficiency of the HR pathway in *C. r*. Nevertheless, the different maxima of TE using pHyg3 and HCP point to the recognition by the cell of homologous foreign DNA, which cannot be used for HR-mediated recombination in this physiological state, probably due to missing DNA DSBs in the target sequence *cpftsy* and/or an inactive HR pathway caused by a lack of necessary proteins.

By combining the TE values of synchronized cw15 cells with the cell number on day 3 after inoculation (Figure 11.5 B), it was possible to associate the defined cell cycle stages based on TE tendency. As with the G1 phase, NHEJ is the dominant DNA repair pathway, reflected in the maximal TE using pHyg3 at +4 h of illumination. The following minimum of TE at +8 h can be explained by cells entering the S phase, in which DNA integration must be avoided in order to protect the karyome from the random rearrangement of the newly synthesized DNA. Nevertheless, the possibility that HR could be active at this stage was further investigated. Before entering the M phase, eukaryotic cells undergo a shorter G2 phase, although not described by the literature (Jones 1970; Matsumura et al. 2010; Strenkert et al. 2019) for *C. r.*, which we associated with around +9 h after illumination. Cells then re-enter the M phase at around +10 h of light and begin to divide. HR activity was therefore expected to be present during the last hours of illumination in order to enable sequence-specific DNA repair to take place before cell division. These results strongly suggest the need for the Cas9 nuclease to introduce DNA DSBs enabling recombination events.

Genome Editing of Synchronized cw15 Using the Cas9 Nuclease

The Cas9 nuclease was expressed in *E. coli* and purified using Ni-affinity chromatography. The presence of recombinant enzyme was evaluated by SDS-PAGE in the eluted fractions (Figure S11.1 A), which showed a high degree of purity. Another critical feature for a high activity was the removal of bacterial nucleic acids, achieved by EDTA incubation and subsequent washing to remove the chelating agent. The concentrated Cas9 preparation (Figure S11.1B) was further evaluated by immunodecoration analysis using an α-His tag antibody (Figure S11.1C). An *in vitro* assay proved the capability of restricting the defined target DNA sequence of *cpftsy* (Figure S11.1D) in the presence of the respective sgRNA (T1, T2). Since both target sequences are close to the end of the DNA molecule (Figure 11.4), little change in size occurred, but it nevertheless proved to be a functional Cas9 nuclease.

Interestingly, while testing different target sequences as sgRNA for *cpftsy* in transformations (not shown), we saw that not all events led to the creation of a pale phenotype, suggesting the inefficiency of *cpftsy* related sequences in genome editing. The defined target sequence 1 (T1, (Baek et al. 2016), Figure 11.4) was therefore maintained and an additional target sequence (T2, Figure 11.4) was chosen. Both sgRNAs led to the creation of pale mutants and so were used together for genome editing experiments. Although T2 is also present in HCP (Figure 11.4), a restriction of the homologous template was not thought to interfere with putative HR activity, since about half of the homologous flanking region would still be present and because there was no incubation of Cas9 ribonucleoproteins together with HCP at activating temperatures prior to transformation.

When transforming synchronized cw15 at different time points using Cas9, pale green mutants were obtained in all cases at higher percentages than for unsynchronized cultures (Figure 11.6 A, C–E), underlining once again the advantage of synchronization. Interestingly, TE increased only at +4 h when using HCP together with Cas9 ribonucleoproteins (HCP-GE) compared to the use of HCP alone, underscoring the dominance of the NHEJ pathway in leading to random mutants. In all other cases, TE decreased or was unchanged when additionally using Cas9, pointing to more specific DNA repair, that is, HR.

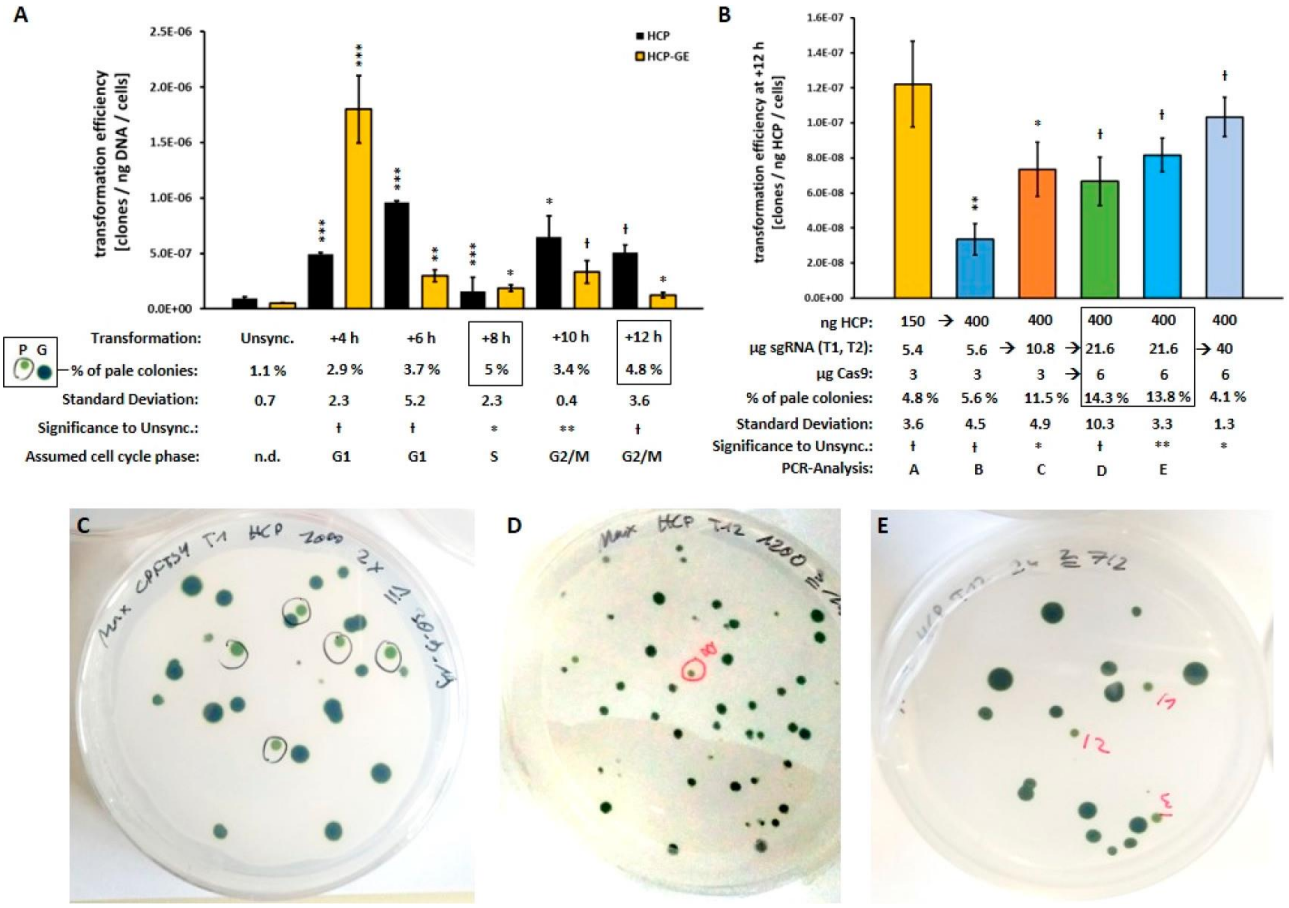

Figure 11.6. Transformation efficiency of unsynchronized and synchronized cell cultures of *C. r.* cw15. Effect of ribonucleoprotein Cas9 on the transformation efficiency. (A) TE were determined for unsynchronized (unsync.) and synchronized cell cultures of *C. r.* cw15, using the linearized *cpftsy* homologous HCP construct only (black bars) or together with ribonucleoproteins (yellow bars, HCP-GE containing Cas9, sgRNAs T1 and T2) at different time points after the start of illumination. Data is shown as mean ± SD, $n = 3$. Below, the determined percentage of the total pale green colonies obtained for HCP-GE (P, of green colonies G) is given: maximal values are surrounded by black boxes. A one-sided *t* test was performed, and the statistical confidence level is shown in relation to the data of unsynchronized cells (unsync.) as one asterisk for $p < 0.05$, two asterisks for $p < 0.01$, three asterisks for $p < 0.001$, with a hash representing insignificant values of $p > 0.05$. This was calculated in the same way as (B). Assumed cell cycle phases are also shown below. (B) Transformation efficiencies of further variations of HCP-GE trials at time point +12 h are shown as mean ± SD, $n = 3$. The amounts used of HCP, sgRNAs T1, T2, and Cas9, as well as the percentage of pale colonies and the numbers for PCR analysis, are given below. The determined optimal ratio of components is marked by a black box. Representative pictures of transformation results, *i.e.*, pale mutants (marked black and red) *vs* normal green mutants are shown as a general example in (C), of transformation using HCP at +4 h (D, compare A), as well as of transformation D at +12 h (E, compare B).

The maximal efficiencies for creating pale mutants (around 5%) occurred at +8 h and +12 h of illumination, which were associated with the S phase and the G2/M phase respectively, since HR activity has a higher efficiency for functional knockouts and was assumed to be present at these time points. This hypothesis was further supported by the rather low percentage of pale mutants at time point +4 h, which was attributed to the G1 phase with high NHEJ activity. Since TE at +8 h (S phase) was very low (Figure 11.5 B), time point +12 h was chosen for further optimization experiments to test different amounts of the components used (Figure 11.6 B) due to quite a high TE and a high percentage of pale mutants accompanied by the expected HR activity.

Interestingly, the provision of more plasmid DNA (150 to 400 ng HCP) decreased the TE but resulted in a similar percentage of pale mutants, confirming the recognition of the homologous template and, moreover, that the introduction of the DSB was the limiting step. This conclusion was further confirmed when using double the amount of sgRNA (5.4 µg to 10.8 µg) because the TE increased again (+100%) and the percentage of pale mutants was more than doubled (factor 2.1). A further increase of sgRNA (21.6 µg) and Cas9 (6 µg) resulted in the highest percentage of pale mutants observed (14.3% and 13.8%), with an average of 14%. A further increase of sgRNA to 40 µg decreased the yield of pale green clones, which confirms the optimal ratio previously determined. Overall, the efficiency of creating pale mutants could be increased by about 1300% by switching from unsynchronized cells (1.1% of pale green clones) to synchronized cells at +12 h (14%). In principle, this could be optimized even further by using different combinations of components.

Determination of HR-Mediated Knock-Ins in Pale Mutants

A major advantage of knock-ins caused by HR is the easy detection of functional knockout mutants by means of PCR screening. Indeed, large insertions can be easily detected and a functional knockout is the highly probable consequence. Since NHEJ-mediated gene disruption in most cases results in only a few base changes, (Gonzalez-Ballester et al. 2011) sequencing of the corresponding target sequence products is required and the function of the knockout has to be determined by other means, for example, by the analysis of the protein content. In order to analyze pale mutants

obtained from different time points (+1 h and +12 h of illumination, Figure 11,7 A), PCR was performed using primers for *cpftsy* that bind to the exterior of the flanking regions (Figure 11.4) in order to avoid false positive PCR artifacts (Won and Dawid 2017). Interestingly, the native PCR amplicon could not be detected in most clones from synchronized cultures, indicating a relatively high knock-in frequency (either unspecific, by NHEJ, or specific, by HR) of larger DNA molecules (for example, plasmid) into the *cpftsy* target itself. Clones derived from transformation at +1 h were devoid of the expected HR-mediated recombination product (target sequence replacement) of about 5.8 kb, as had been expected due to the inactive HR pathway. On the other hand, two out of four clones from transformation at +12 h did show the 5.8 kb recombination product, so supporting the presence of HR in the assumed G2/M phase. The total occurrence of HR-mediated recombination events could be even higher at this time point or at others, since there are different outcomes (Figure 11.2 F–I) from recombination-like events, for example, multiple insertions and deletions (Angstenberger et al. 2019). Interestingly, the sought-after knock-ins of HCP into *cpftsy* could not be identified at any time point other than +12 h (tested for +1, +2, +4, +6, +8, and +10 h with about 40 pale clones in total, data not shown).

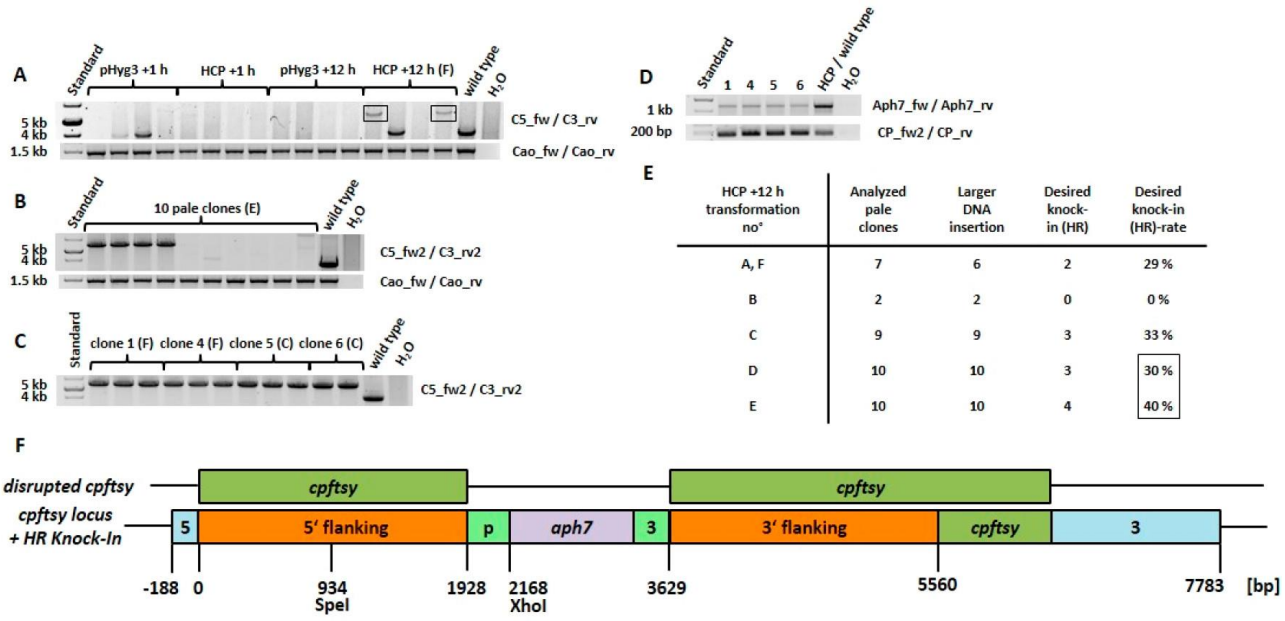

HCP +12 h transformation no°	Analyzed pale clones	Larger DNA insertion	Desired knock-in (HR)	Desired knock-in (HR)-rate
A, F	7	6	2	29 %
B	2	2	0	0 %
C	9	9	3	33 %
D	10	10	3	30 %
E	10	10	4	40 %

Figure 11.7. Target sequence analysis of selected pale mutants of *C. r.* cw15 from different transformation approaches. (A) PCR analysis carried out by the flanking region surrounding primers (C5_fw/C3_rv) for locus *cpftsy*. Four pale mutants for each construct (pHyg3, HCP) at two different time points (+1 h, + 12 h) were analyzed together with the wild type; the amplicons expected after HR-mediated knock-in of about 5.8 kb are surrounded by black boxes. (B) Similar PCR analysis were carried out with optimized primers (C5_fw2, C3_rv2) for 10 pale clones from transformation E (see Figure 11.6 B). As positive controls for each cell line, additional PCRs were performed using primers Cao_fw and Cao_rv and are shown in the lower part of the A–B panels. (C) Selected pale mutants from transformations C, F at +12 h (see Figure 11.6 B) were used for the amplification of sufficient amounts of recombinant knock-in fragments of *cpftsy* for purification and further analysis, as shown in (D), that is, Nested-PCRs were performed using the purified fragments as template and primers Aph7_fw/Aph7_rv for detection of the inserted *aph7* gene, in addition to primers CP_fw2/Cp_rv for detection of the target sequence T2 of *cpftsy* as a control. (E) Summary of results of additional PCR analysis performed on pale clones from corresponding transformations of *C. r.*cw15 at +12 h after the start of illumination (see

also Figure 11.6 B), showing the numbers of analyzed pale clones, the larger DNA insertions in *cpftsy* detected, the desired HR-mediated knock-ins (flanking-based target sequence replacement) and its occurrence rate. (F) Schematic representation of knock-ins of the *aph7* cassette into *cpftsy* detected, based on HR-mediated recombination, which was confirmed by sequencing the corresponding XhoI and SpeI restricted amplicons (cloned into bluescript vector KS-) from clones 1F and 4F (see Figure S11.2). The disrupted genomic sequence of *cpftsy* is depicted at the top, showing the occurrence of the gene disruption that leads to the pale phenotype. For the numbering, compare with Figure 11.6 B, except for transformation F, which is not shown in detail.

Pale clones derived from the transformations shown in Figure 11.6 B (as indicated for PCR analysis) were analyzed with optimized primers. In all 10 pale clones from transformation E (Figure 11.7B), the native sequence of *cpftsy* could not be amplified, indicating larger DNA insertions in all of them. The first four clones displayed the expected HR-mediated knock-in product of about 5.8 kb. When several clones carrying the same mutation had been identified, four of them were chosen for further analysis, as shown in Figure 11.7 C (clone number and respective transformation number as indicated, compare with Figure 11.6 B).

All clones displayed the recombinant PCR product expected after HR-mediated knock-in of HCP into *cpftsy* and were amplified in triplets and a doublet for further analysis. After gel extraction and purification of the respective fragments, Nested-PCR was performed (Figure 11.7 D), which showed the abundance of the inserted *aph7* gene, as well as the T2 sequence of *cpftsy* used as a control. In Figure 11.7 E, the results of all tested clones are displayed, showing the maximal yield of specific knock-ins into *cpftsy* from transformations D and E (compare with Figure 11.6 B), on average 35%. To further verify the specific knock-ins and provide smaller molecules for easy cloning and subsequent sequencing, PCR was again performed, as described above, using gDNA from clones 1(F) and 4(F) and partially digested thereafter with XhoI and SpeI (see Figure S11.2). This revealed the expected products of about 3.5 kb and 2.3 kb (XhoI), the latter digested further to 1.1 kb and 1.2 kb (SpeI) respectively. Final sequencing confirmed the HR-mediated sequence-specific knock-in in those clones, which is shown schematically in Figure 11.7 E.

11.3 Conclusion

Overall, the demonstrated synchronization of *C. r.* cw15 cultures is a powerful option for enhancing the efficiency of nuclear transformation, also confirmed in mammalian cells (Cervia et al. 2018) and, in particular for precise genome editing *via* HR, as demonstrated, for example, in different yeast species (Tsakraklides et al. 2015). Furthermore, this type of cell synchronization makes future in-depth research possible into the cell cycle of *C. r.* and could be very useful for further research into DNA damage responses (Čížková et al. 2019) during the cell cycle. The phases of the latter could be more precisely defined by using antibodies for cell cycle relevant proteins, for example, cyclins or by determining cyclin-dependent protein kinase activity (Bertoni 2018). We demonstrated that access to certain cell cycle stages makes possible the genetic manipulation of the nuclear genome in different ways, depending on the desired outcome. When simple random DNA integration is sufficient, usage of the dominance of NHEJ at +4 h after illumination is the best option, since it enables the highest transformation efficiency, as also described by ref (Olmo et al. 2018) for the eukaryotic parasite *Trypanosoma cruzi*.

With regard to genome editing strategies, avoiding NHEJ as much as possible and favoring HR-mediated DNA integration offers multiple benefits, including the reduction of unspecific DNA integration (Zhu et al. 2015) and enhanced gene targeting (Ishibashi et al. 2006). A time point in the cell cycle of *C. r.* was identified (+12 h of illumination, Figures 11.5B and 11.7) offering a higher HR/NHEJ ratio and used to create mutants with an HR-based knock-in. Further research is required to evaluate the additional possibility of inactivating the NHEJ pathway in *C. r.*, which could reduce or even eliminate unspecific DNA integration (Ishibashi et al. 2006; Schorsch et al. 2009; Angstenberger et al. 2019) accompanied by specific knock-ins using cell synchronization. Furthermore, the greatest efficiency of gene targeting in producing knockouts could be observed at this time point (+12 h), which confirms the advantage of HR-based gene disruption in leading to a higher probability of functional knockouts of genes. Such knockout mutants also offer the benefit of being easily identified by PCR, due to the high frequency of knock-in events using larger DNA molecules. Additional PCR analysis (Won and Dawid 2017) of targeted loci also enables the identification of the desired knock-in events (target sequence replacement by HR) that were shown to happen at acceptable rates. The actual efficiency of HR as identified in this work might be even higher, given the different outcomes of HR, as described by (Steiner et al. 1995) for the fungus *Ashbya gossypii*.
Specific knock-ins make advanced genome editing possible, for example, eliminating native genes and replacing them with altered sequences for specific purposes, such as point mutated (Rubinstein et al. 1993) or extended (Wang et al. 2017) gene copies leading to tagged proteins (Yu et al. 2020). Thus, 5% of colonies growing on selective medium will display a desired mutant knock-in sequence even in the absence of a visible phenotype. Since *cpftsy* displays a rather inefficient target for genome editing and was mainly chosen as the optimal phenotype of a knockout, our improved strategy should increase the efficiency of genome editing for more easily accessible targets and so provide high frequencies of the creation of knockouts and specific knock-ins. Finally, valuable information concerning the nuclear HR pathway in *C. r.* could be obtained, that is, its identification in special phases (G2/M) of the cell cycle, which is consistent with other eukaryotes (Lin et al. 2014).

11.4 Outlook

Further optimization of HR usage could be achieved by identifying the optimal length of the homologous regions (Plecenikova et al. 2013) and the additional determination of optimal Cas9, sgRNA, and plasmid amounts (Kim et al. 2020) as well as other types of DNA nucleases like Cas12a (Schindele and Puchta 2020). Moreover, the strategy presented should be applicable to other algae species, when conditions of synchronization have been identified and nuclear transformation is possible, (Meyer et al. 1985; Menges and Murray 2006) especially if the genetic handling of species is problematic, enabling more efficient nuclear transformation and genome editing strategies, necessary for basic research and biotechnological applications.

11.5 Methods

Chemicals, Reagents, and Enzymes

If not otherwise stated, all the chemicals and reagents used were provided by Sigma-Aldrich and AppliChem and all the enzymes used were supplied by New England Biolabs, Promega and Thermo Fisher Scientific.

Gene Identity

The phytozome database (https://phytozome.jgi.doe.gov) was used for *C. r*. relevant data. Database entry for *cpftsy* is Cre05.g241450.

Strains, Cell Culture, and Transformation

The *Chlamydomonas reinhardtii* strain cw15 (Hyams and Davies 1972) was used in all the experiments described and was cultivated in 20 mL flasks containing TAP-medium (Andersen 2005), supplemented with 100 µg/mL of ampicillin. Normal growth conditions were set to 25 °C with 200 µmol photons m^{-2} s^{-1} of white light for 16 and 8 h of darkness. Synchronizing growth conditions were adjusted to ref (Strenkert et al. 2019) with 200 photons m^{-2} s^{-1} of white light for 12 h at 28 °C, followed by 12 h of darkness at 18 °C. Cell number was determined using a Countess II FL cell counter (Life Technologies) and the results were divided by a calibration factor of 2.

Transformation

For optimized transformation of *C. r*.cw15 based on ref (Shimogawara et al. 1998), the respective number of cells (unsynchronized: 5×10^6; synchronized: 10^6) were harvested at 8000*g* for 7 min and resuspended in 50 µL of TOS-Medium (80% v/v TAP, 40 mM Sucrose). The suspension was mixed with different amounts of linearized plasmid DNA (pHyg3: NdeI; HCP: XbaI; for unsynchronized cells: 250 ng; for synchronized cells: in general 150 ng, 60 ng for time point +4 HCP-GE (see Figure 11.6 A) and 400 ng for time points +8 h as well as +12 h (see Figure 11.6 A, B). For genome editing experiments, a further 3 µg Cas9 (deviating amounts see Figure 11.6 B) and 5.4 µg sgRNA, each consisting of 50% sgRNA for *cpftsy* target1 and target2 (deviating amounts see Figure 11.6 B), were added and the mixture incubated on ice for 5 min. Transformation was carried out in 0.4 cm spaced cuvettes by electroporation using a Gene Pulser II (Bio-Rad) set to 200 Ω, 50 µF and 0.6 kV. Recovery was achieved in 1.5 mL TOS-Medium containing reaction tubes kept in darkness overnight on a mixing rotator. After subsequent centrifugation at 8000*g* for 7 min, cells were resuspended in 1 mL 30% starch containing TAP-Medium, supplemented with 60 µg/mL hygromycin and 100 µg/mL ampicillin. This solution was distributed on two 60 µg/mL hygromycin and 100 µg/mL ampicillin containing 1.5% Agar-TAP-plates to obtain selection.

E. coli strain Top10 (Thermo Fisher Scientific) and BL21 (Stratagene) were transformed with constructs using the standard heat shock method and selection was achieved by using 100 µg/mL ampicillin on 1.3% Agar-LB-plates (1% tryptone, 0.5% yeast extract and 0.5% NaCl). Subsequent cultivation was carried out at 37 °C for 16 h in LB-medium.

Isolation of Nucleic Acids

Plasmid isolation from *E. coli* was carried out using the GeneJet Miniprep Kit (Thermo Scientific). Contrary to the supplier's instructions, the elution buffer was prewarmed to 55 °C and elution was repeated once using the eluate.

Isolation of genomic DNA from *C. reinhardtii* cw15 was carried out after ref (Kira et al. 2016) . Harvested cells (12 000*g* for 30 s) of 1–2 weeks old cultures grown in plastic multiwells of 2–3 mL TAP-Medium each were resuspended in 700 µL 2× CTAB buffer, supplemented with 100 µg Proteinase K and 50 µg RnaseA. After incubation for 2–5 h at 60 °C, genomic DNA was extracted using 1 unit of chloroform/isoamyl alcohol (24:1) after centrifugation at 12 000*g* for 5 min. This step was repeated with 1 unit of phenol (10 mM Tris-HCl buffered at pH 8)/chloroform/isoamyl alcohol (25:25:1) and 1 unit of chloroform. Precipitation was achieved using 0.3 M sodium acetate pH 5 and the addition of 1 unit of isopropanol at −20 °C for 1 h. After centrifugation at 12 000*g* for 15 min, the supernatant was removed and the sediment was washed twice with 70% ethanol at 12 000*g* for 5 min. Sediments were dried at 42 °C for 1 h and resuspended in 20–50 µL 10 mM Tris-HCL pH 8.

Isolation of *in vitro* transcribed sgRNA was carried out in the same way as described for genomic DNA, starting by increasing the final volume after the reaction to 1 mL with DEPC-H_2O and continuing with phenol (Tris-HCl buffered pH 5)/chloroform/isoamyl alcohol (25:25:1) extraction.

Concentration of nucleic acids was determined using a Nanodrop One (Thermo Scientific). In the case of plasmid DNA for transformation of *C. reinhardtii*, concentration was precisely determined on 1% agarose gels compared to the marker GeneRuler 1kb Plus (Thermo Scientific) using the ImageJ software (https://imagej.nih.gov/ij/).

Amplification, *In Vitro* Transcription, Restriction, and Cloning

Taq polymerase was expressed in *E. coli* Bl21 and isolated according to the literature (Desai and Pfaffle 1995). As a general buffer, 10 mM Tris-HCl pH 8.3, 50 mM KCl and 4 mM $MgCl_2$ were chosen, while special amplifications based on GC rich templates like those present in *cpftsy* (5' Flanking region, see Figure 11.4) were performed using 75 mM Tris-HCl pH 8.3, 20 mM $(NH_4)_2SO_4$ and 4 mM $MgCl_2$. Reactions also contained 10 pmol of each primer, 0.53 mM dNTPs (each) and 0.26 M Betain. Annealing temperatures 2–5 degrees below the supplier's reported melting temperature of primers were chosen, with elongation to 1 min/kb at 72 °C. All amplifications for cloning were achieved by using Hybrid Polymerase (EURX) in accordance with the supplier's instructions. In addition, target sequence analysis of *cpftsy* using flanking regions surrounding primers (see Figure 11.4) was carried out using the same buffer, containing $(NH_4)_2SO_4$, as that for Taq amplifications of GC rich templates.

Amplification of template DNA for *in vitro* transcription of sgRNA was obtained using Taq polymerase with the NH_4 buffer, as mentioned above, using primers (see Table S2) sg_CP_fw1 and T7_CP_fw1 (for target T1, see Figure 11.4) as well as sg_CP_fw2 and T7_CP_fw2 (for target T2, designed using www.e-crisp.org, see Figure 11.4). As a first step, target sequence (5') elongated primers binding the Cas9 required RNA sequence (sg_CP_fw1, sg_CP_fw2) on plasmid pDGE277 (Ordon et al. 2020) were used. After dilution of the PCR products obtained to about 0.1–1 ng/µL, a second amplification was performed with primers binding the target sequence and containing a 5' addition

of the T7 polymerase motif (T7_CP_fw1, T7_CP_fw2). After determining the concentration of the PCR products obtained, 1 µg of template DNA was used for *in vitro* transcription, using the Hi Scribe T7 Quick High Yield RNA Synthesis Kit (New England Biolabs) at 37 °C overnight, with subsequent purification of sgRNA as mentioned above. Recombinant Cas9 activity was tested at 37 °C for 1 h using 100 ng of PCR product created with Primers Cp_fw and Cp_rv (see Figure 11.4), 400 ng sgRNA for *cpftsy* target 1 and 2 (see Figure 11.4) and 750 ng of recombinant Cas9 (see chapter below) in cleavage buffer (20 mM Tris-HCl pH 7.5, 20 mM KCl, 5 mM $MgCl_2$).

Plasmid DNA was restricted using the enzymes XhoI, SpeI, NdeI, XbaI, NheI, and EcoRV at 37 °C for 3–16 h, with subsequent heat inactivation at 65 °C for 10 min. Isolation of PCR products for cloning was achieved using the GeneJET Gel Extraction Kit (Thermo Scientific) and initially cloned into Blueskript KS- (Snapgene) for sequencing (Eurofins), subsequent restriction and ligation using T4 Ligase into final constructs.

Expression and Purification of Recombinant Cas9

E. coli strain BL21 was transformed with the Cas9 nuclease (160 kDa) encoding plasmid pET- NLS-Cas9-6xHis (Addgene). After expression, the recombinant Cas9 contained a nuclear localization signal and a C-terminal his-tag for purification using nickel affinity chromatography. After overnight cultivation of a 5 mL culture containing 25 µg/mL chloramphenicol and 100 µg/mL ampicillin, 1 L LB-Medium containing the same antibiotics was inoculated and the culture grown to an OD_{600} of 0.5. Expression of recombinant Cas9 was induced with 0.5 mM isopropyl β-d-1-thiogalactopyranoside, and cultivation continued overnight at 20 °C. Cells were harvested at 5000*g* for 10 min and purified in accordance with ref (Zuris et al. 2014) using Nickel NTA affinity chromatography. In order to remove nucleic acids from *E. coli* from the protein solution, the latter was supplemented with 10 mM EDTA and incubated for 1 h. Subsequent concentration using centricons (10 kDa cutoff) was carried out twice to a small volume and again diluted in order to remove nucleic acids and EDTA, achieving a final volume of 750 µL. Thereafter, the protein solution was analyzed on SDS-page (Laemmli 1970) and immunoblotting was carried out. Protein concentration was determined using a Nanodrop One with an extinction coefficient at 280_{nm} of 120.450 M^{-1} cm^{-1}.

Construction of Knock-In Construct HCP

All the elements necessary for creating HCP (5’ flanking (5F): chromosome_5:3459480–3461402, *aph7* cassette, 3’ flanking (3F): chromosome_5:3461425–3463347; see Figure 11.4) were amplified as described above using 5F_fw/rv (5F), pBT_fw/rbsc2_rv (*aph7* cassette) and 3F_fw/rv (sequences see Table S11.2), cloned into bluescript vector KS- and sequenced. The 5’ flanking region (5F) was amplified using a reverse primer (5F_rv) that also carried nucleotides for an in-frame stop codon after sequence-specific knock-in into *cpftsy*. The *aph7* cassette from the transformation vector pHyg3, (Berthold et al. 2003) conferring resistance to hygromycin, consisted of the promoter from the β-tubulin gene, the *aph7* gene itself and the 3’ UTR of the RubisCO small subunit 2 gene. Further sequence extension of used primers provided restriction motifs for *Eco*RI and XbaI (5F) as well as NheI and XbaI (*aph7* cassette and 3F). All elements were cloned again into bluescript KS- in the order shown (Figure 11.4), leading to the HCP construct.

11.6 Supporting information

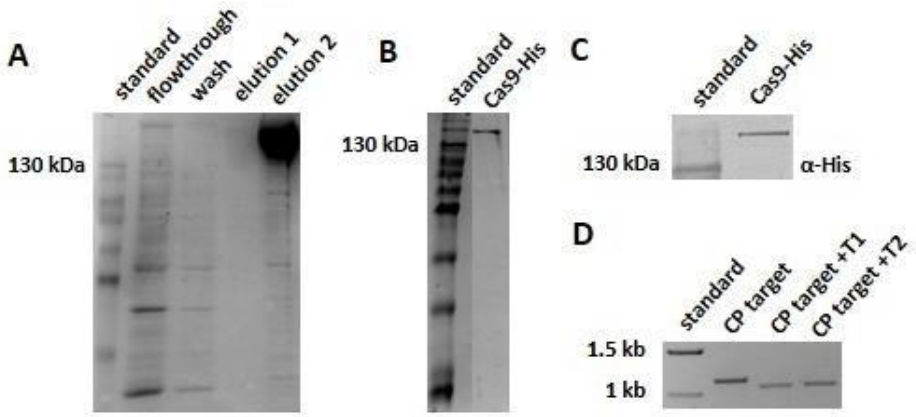

Figure S11.1. Result of expression and purification of nuclease Cas9 from *E. coli*. (A) SDS- PAGE analysis after expression and purification of recombinant Cas9-His in *E. coli*, carried out on eluted fractions from Ni-affinity chromatography. (B) SDS-PAGE analysis of Cas9-His after EDTA treatment, washing and concentration by centricons. (C) Immunoblot using an α-His antibody for detection of Cas9-His. (D) *In vitro* restriction assay using Cas9-His, amplified and purified target DNA of *cpftsy* (CP target, see Fig. 11.4: CP_fw/CP_rv) and sgRNA for target T1 and T2.

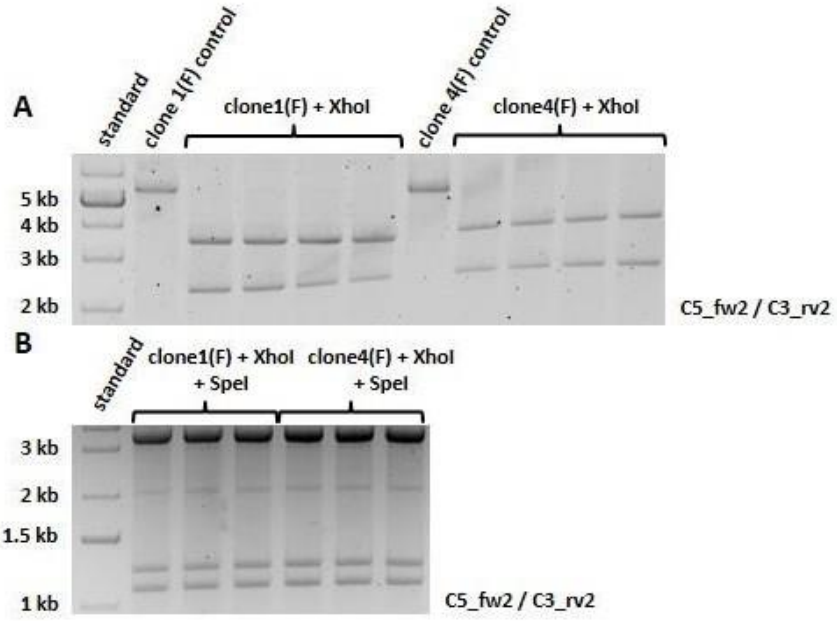

Fig. S11.2 Agarose gels showing restriction analysis of cpftsy knock-in amplification products. After amplification of the recombinant *cpftsy* sequence containing the desired knock-in of the aph7 cassette using the primers C5_fw2 and C3_rv2 (see Fig. 11.4 and 11.7), in one reaction for clones 1F and 4F (A), one part was loaded as a control (5.8 kb), while the rest was digested with XhoI and loaded onto 4 lanes, leading to the restricted fragments of 2.3 kb and 3.5 kb as expected. In a second reaction, also using SpeI (Fig. 11.7), the fragment of 2.3 kb was further digested into one fragment of 1.1 kb and another of 1.2 kb. Fragments of 3.5 kb, 1.2 kb and 1.1 kb were purified by gel extraction and cloned into the bluescript vector KS- for sequencing, which confirmed the occurrence of sequence-specific knock- in, as shown in Figure 11.7 F.

Table S11.1 Transformation procedure overview. Shown are the original and optimized transformation protocols for *C. r.cw15* used in this study, showing an overall optimization and an especially marked reduction of the necessary compounds due to the use of synchronized cell cultures with a very high transformation efficiency.

	Original protocol unsynchronized cells [based on Shimogawara *et al.*, 1998[4]]	**Optimized protocol unsynchronized cells**	**Optimized protocol synchronized cells**
Light / Temperature	24 °C; 16 h light, 8 h darkness	24 °C; 16 h light, 8 h darkness	28°C 12 h light; 18 °C 12 h darkness
Doubling time	8 - 10 h	8 - 10 h	24h
Transformation culture	0.5 x 10^6 cells/ml; 3-4 days	10^5 cells/ml; 3 days	10^5 cells/ml; 3 days
Cells / transformation	5 x 10^7	5 x 10^6	10^6
Linearized DNA	1 µg	250 ng	60 – 400 ng
Transformation volume	250 µl	50 µl	50 µl
Recovery volume	20 ml	1.5 ml	1.5 ml
Plates / Transformation	6	2	2
Cas9	5 µg – 15 µg	3 µg	3 µg – 6 µg
sgRNA	8 – 12 µg	5.4 µg	5.4 µg – 40 µg
Timepoint of transformation [hours after illumination start]	+4	+4	0, +1, +2, +4, +6, +8, +10, +12
Hygromycin [µg/ml]	25	60	60

Table S11.2 Primers used in this study.

Primer	Sequence (5‘ -> 3‘)
CP_fw	GTCACCTCGAATCACACAC
CP_fw2	GAAGGAGTGAGATGACTTGGAC
CP_rv	CTCCTCCACCTCTTCTGCTC
C5_fw	TGGAGATCCAGGTCGGTTGC
C5_fw2	TTGTAAAGTGAGGTCCAGAGGAGC
C3_rv	CCAGGTTCTGTTGGTTGGC
C3_rv2	TGCCGTGTCTACCAGAATGAGGTC
5F_fw	GCGAATTCCGCTTGAGGAACACATAC
5F_rv	GCTCTAGATTAGCCGAAGTCGGCGGACTG
pBT_fw	CTATGCTAGCCTTGCGCTATGACACTTC
Aph7_fw	ATGCGCTAGCATGACACAAGAATCCCTG
Aph7_rv	TCTAGATTATCAGGCGCCGGGGGCGG
rbsc2_rv	GCTCTAGACGCTTCAAATACGCCCAG
3F_fw	TATAGCTAGCACCGCATCCGCGAGGG
3F_rv	CGTCTAGAGTGGTAGTTGGTGTACG
Cao_fw	TGTTACCGCATAGAGCAGCC
Cao_rv	CGCTACTCACCGCTGAGAAC
sg_CP_fw1	CGATCTTCAGAGCAGTGCGGGTTTTAGAGCTAGAAATAGCAAG
T7_CP_fw1	TAATACGACTCACTATAGCGATCTTCAGAGCAGTGCG
sg_CP_fw2	GATCGCGTACAAGTACGGCAGTTTTAGAGCTAGAAATAGCAAG
T7_CP_fw2	TAATACGACTCACTATAGGATCGCGTACAAGTACGGCA
Cas9_rv	AAAAAAAGCACCGACTCGGTGCCAC

REFERENCES

Andersen RA (2005) Algal Culturing Techniques. Elsevier Academic Press, New York

Angstenberger M, Krischer J, Aktaş O, Büchel C (2019) Knock-Down of a ligIV Homologue Enables DNA Integration via Homologous Recombination in the Marine Diatom Phaeodactylum tricornutum. ACS Synth Biol 8:57–69 . https://doi.org/10.1021/acssynbio.8b00234

Baek K, Kim DH, Jeong J, Sim SJ, Melis A, Kim JS, Jin E, Bae S (2016) DNA-free two-gene knockout in Chlamydomonas reinhardtii via CRISPR-Cas9 ribonucleoproteins. Sci Rep 6:30620 . https://doi.org/10.1038/srep30620

Berthold P, Schmitt R, Mages W (2003) An Engineered Streptomyces hygroscopicus aph 7''Gene Mediates Dominant Resistance against Hygromycin B in Chlamydomonas reinhardtii. Protist 153:401–412 . https://doi.org/10.1078/14344610260450136

Bertoni G (2018) Cell Cycle Regulation by Chlamydomonas Cyclin-Dependent Protein Kinases. Plant Cell, 30(2), 271. https://doi.org/10.1105/tpc.18.00103

Buffaloe ND (1958) A Comparative Cytological Study of Four Species of Chlamydomonas. Bull Torrey Bot Club 85:157–178 . https://doi.org/10.2307/2483212

Cervia LD, Chang CC, Wang L, Mao M, Yuan F (2018) Enhancing Electrotransfection efficiency through improvement in nuclear entry of plasmid DNA. Mol Ther Acids 11:263–271 . https://doi.org/10.1016/j.omtn.2018.02.009

Čížková M, Slavková M, Vítová M, Zachleder V, Bišová K (2019) Response of the green alga Chlamydomonas reinhardtii to the DNA damaging agent zeocin. Cells 8:735 . https://doi.org/10.3390/cells8070735

Coleman AW (1982) The Nuclear Cell Cycle in Chalmydomonas (Chlorophyceae). J Phycol 18:192–195 . https://doi.org/https://doi.org/10.1111/j.1529-8817.1982.tb03172.x

Craigie RA, Cavalier-Smith T (1982) Cell volume and the control of the Chlamydomonas cell cycle. J Cell Sci 54:173–191

Desai UJ, Pfaffle PK (1995) Single-step purification of a thermostable DNA polymerase expressed in Escherichia coli. Biotechniques 19:780-782,784

Ferenczi A, Pyott DE, Xipnitou A, Molnar A (2017) Efficient targeted DNA editing and replacement in Chlamydomonas reinhardtii using Cpf1 ribonucleoproteins and single-stranded DNA. Proc Natl Acad Sci 114:13567 LP – 13572 . https://doi.org/10.1073/pnas.1710597114

Frit P, Barboule N, Yuan Y, Gomez D, Calsou P (2014) Alternative end-joining pathway(s): Bricolage at DNA breaks. DNA Repair (Amst) 17:81–97 . https://doi.org/https://doi.org/10.1016/j.dnarep.2014.02.007

Gonzalez-Ballester D, Pootakham W, Mus F, Yang W, Catalanotti C, Magneschi L, de Montaigu A, Higuera JJ, Prior M, Galván A (2011) Reverse genetics in Chlamydomonas: a platform for isolating insertional mutants. Plant Methods 7:24 . https://doi.org/10.1186/1746-4811-7-24

Grossman AR, Harris EE, Hauser C, Lefebvre PA, Martinez D, Rokhsar D, Shrager J, Silflow CD, Stern D, Vallon O, Zhang Z (2003) Chlamydomonas reinhardtii at the crossroads of genomics. Eukaryot Cell 2:1137–1150 . https://doi.org/10.1128/ec.2.6.1137-1150.2003

Gumpel NJ, Rochaix JD, Purton S (1994) Studies on homologous recombination in the green alga Chlamydomonas reinhardtii. Curr Genet 26:438–442 . https://doi.org/10.1007/BF00309931

Harris EH (2001) Chlamydomonas as a model organism. Annu Rev Plant Physiol Plant Mol Biol 52:363–406 . https://doi.org/10.1146/annurev.arplant.52.1.363

Harris EH (2009) The Chlamydomonas Sourcebook: Introduction to Chlamydomonas and Its Laboratory Use: Volume 1. Academic press

Hinz JM, Yamada NA, Salazar EP, Tebbs RS, Thompson LH (2005) Influence of double-strand-break repair pathways on radiosensitivity throughout the cell cycle in CHO cells. DNA Repair (Amst) 4:782–792

Hyams J, Davies DR (1972) The induction and characterisation of cell wall mutants of Chlamydomonas reinhardi. Mutat Res Mol Mech Mutagen 14:381–389 . https://doi.org/https://doi.org/10.1016/0027-5107(72)90135-2

Irion U, Krauss J, Nüsslein-Volhard C (2014) Precise and efficient genome editing in zebrafish using the CRISPR/Cas9 system. Development 141:4827 LP – 4830 . https://doi.org/10.1242/dev.115584

Ishibashi K, Suzuki K, Ando Y, Takakura C, Inoue H (2006) Nonhomologous chromosomal integration of foreign DNA is completely dependent on MUS-53 (human Lig4 homolog) in Neurospora. Proc Natl Acad Sci 103:14871–14876

Jiang W, Brueggeman AJ, Horken KM, Plucinak TM, Weeks DP (2014) Successful Transient Expression of Cas9 and Single Guide RNA Genes in Chlamydomonas reinhardtii Eukaryot Cell 13:1465 LP – 1469 . https://doi.org/10.1128/EC.00213-14

Johnson UG, Porter KR (1968) Fine structure of cell division in Chlamydomonas reinhardi. Basal bodies and microtubules. J Cell Biol 38:403–425 . https://doi.org/10.1083/jcb.38.2.403

Jones RF (1970) Physiological and biochemical aspects of growth and gametogenesis in Chlamydomonas reinhardtii. NY Acad Sci Ann

Kim J, Lee S, Baek K, Jin E (2020) Site-Specific Gene Knock-Out and On-Site Heterologous Gene Overexpression in Chlamydomonas reinhardtii via a CRISPR-Cas9-Mediated Knock-in Method. Front. Plant Sci. 11:306 . https://doi.org/10.3389/fpls.2020.00306

Kira N, Ohnishi K, Miyagawa-Yamaguchi A, Kadono T, Adachi M (2016) Nuclear transformation of the diatom Phaeodactylum tricornutum using PCR-amplified DNA fragments by microparticle bombardment. Mar Genomics 25:49–56 . https://doi.org/https://doi.org/10.1016/j.margen.2015.12.004

Kirst H, García-Cerdán JG, Zurbriggen A, Melis A (2012) Assembly of the light-harvesting chlorophyll antenna in the green alga Chlamydomonas reinhardtii requires expression of the TLA2-CpFTSY gene. Plant Physiol 158:930–945 . https://doi.org/10.1104/pp.111.189910

Laemmli UK (1970) Cleavage of Structural Proteins during the Assembly of the Head of Bacteriophage T4. Nature 227:680–685 . https://doi.org/10.1038/227680a0

Lechtreck K-F, Luro S, Awata J, Witman GB (2009) HA-tagging of putative flagellar proteins in Chlamydomonas reinhardtii identifies a novel protein of intraflagellar transport complex B. Cell Motil Cytoskeleton 66:469–482 . https://doi.org/10.1002/cm.20369

Lin S, Staahl BT, Alla RK, Doudna JA (2014) Enhanced homology-directed human genome engineering by controlled timing of CRISPR/Cas9 delivery. Elife 3:e04766–e04766 . https://doi.org/10.7554/eLife.04766

Matsumura K, Yagi T, Hattori A, Soloviev M, Yasuda K (2010) Using single cell cultivation system for on-chip monitoring of the interdivision timer in Chlamydomonas reinhardtii cell cycle. J Nanobiotechnology 8:23. https://doi.org/10.1186/1477-3155-8-23

Menges M, Murray JAH (2006) Synchronization, Transformation, and Cryopreservation of Suspension-Cultured Cells BT - Arabidopsis Protocols. In: Salinas J, Sanchez-Serrano JJ (eds). Humana Press, Totowa, NJ, pp 45–61

Meyer P, Walgenbach E, Bussmann K, Hombrecher G, Saedler H (1985) Synchronized tobacco protoplasts

are efficiently transformed by DNA. MGG Mol. Gen. Genet. 201:513–518

Nelson JA, Lefebvre PA (1995) Targeted disruption of the NIT8 gene in Chlamydomonas reinhardtii. Mol Cell Biol 15:5762 LP – 5769 . https://doi.org/10.1128/MCB.15.10.5762

Olmo F, Costa FC, Mann GS, Taylor MC, Kelly JM (2018) Optimising genetic transformation of Trypanosoma cruzi using hydroxyurea-induced cell-cycle synchronisation. Mol Biochem Parasitol 226:34–36. https://doi.org/10.1016/j.molbiopara.2018.07.002

Ordon J, Bressan M, Kretschmer C, Dall'Osto L, Marillonnet S, Bassi R, Stuttmann J (2020) Optimized Cas9 expression systems for highly efficient Arabidopsis genome editing facilitate isolation of complex alleles in a single generation. Funct Integr Genomics 20:151–162 . https://doi.org/10.1007/s10142-019-00665-4

Plecenikova A, Mages W, Andrésson ÓS, Hrossova D, Valuchova S, Vlcek D, Slaninova M (2013) Studies on Recombination Processes in two Chlamydomonas reinhardtii Endogenous Genes, NIT1 and ARG7. Protist 164:570–582 . https://doi.org/https://doi.org/10.1016/j.protis.2013.05.004

Rubinstein M, Japón MA, Low MJ (1993) Introduction of a point mutation into the mouse genome by homologous recombination in embryonic stem cells using a replacement type vector with a selectable marker. Nucleic Acids Res 21:2613–2617

Schindele P, Puchta H (2020) Engineering CRISPR/LbCas12a for highly efficient, temperature-tolerant plant gene editing. Plant Biotechnol J 18:1118–1120 . https://doi.org/10.1111/pbi.13275

Schorsch C, Köhler T, Boles E (2009) Knockout of the DNA ligase IV homolog gene in the sphingoid base producing yeast Pichia ciferrii significantly increases gene targeting efficiency. Curr Genet 55:381–389 . https://doi.org/10.1007/s00294-009-0252-z

Shimogawara K, Fujiwara S, Grossman A, Usuda H (1998) High-efficiency transformation of Chlamydomonas reinhardtii by electroporation. Genetics 148:1821–1828

Sizova I, Greiner A, Awasthi M, Kateriya S, Hegemann P (2013) Nuclear gene targeting in Chlamydomonas using engineered zinc-finger nucleases. Plant J 73:873–882 . https://doi.org/10.1111/tpj.12066

Sodeinde OA, Kindle KL (1993) Homologous recombination in the nuclear genome of Chlamydomonas reinhardtii. Proc Natl Acad Sci U S A 90:9199–9203 . https://doi.org/10.1073/pnas.90.19.9199

Steiner S, Wendland J, Wright MC, Philippsen P (1995) Homologous recombination as the main mechanism for DNA integration and cause of rearrangements in the filamentous ascomycete Ashbya gossypii. Genetics 140:973–987

Strenkert D, Schmollinger S, Gallaher SD, Salomé PA, Purvine SO, Nicora CD, Mettler-Altmann T, Soubeyrand E, Weber APM, Lipton MS, Basset GJ, Merchant SS (2019) Multiomics resolution of molecular events during a day in the life of Chlamydomonas. Proc Natl Acad Sci 116:2374 LP – 2383 . https://doi.org/10.1073/pnas.1815238116

Tsakraklides V, Brevnova E, Stephanopoulos G, Shaw AJ (2015) Improved gene targeting through cell cycle synchronization. PLoS One 10:e0133434 . https://doi.org/10.1371/journal.pone.0133434

Wang Q, Xue H, Li S, Chen Y, Tian X, Xu X, Xiao W, Fu YV (2017) A method for labeling proteins with tags at the native genomic loci in budding yeast. PLoS One 12:e0176184 . https://doi.org/10.1371/journal.pone.0176184

Won M, Dawid IB (2017) PCR artifact in testing for homologous recombination in genomic editing in zebrafish. PLoS One 12:e0172802 . https://doi.org/10.1371/journal.pone.0172802

Yu J, Cho E, Choi YG, Jeong YK, Na Y, Kim JS, Cho SR, Woo JS, Bae S (2020) Purification of an Intact Human Protein Overexpressed from Its Endogenous Locus via Direct Genome Engineering. ACS Synth Biol 9:1591–1598

Zhang R, Patena W, Armbruster U, Gang SS, Blum SR, Jonikas MC (2014) High-Throughput Genotyping of

Green Algal Mutants Reveals Random Distribution of Mutagenic Insertion Sites and Endonucleolytic Cleavage of Transforming DNA. Plant Cell 26:1398–1409 . https://doi.org/10.1105/tpc.114.124099

Zhu L, Mon H, Xu J, Lee JM, Kusakabe T (2015) CRISPR/Cas9-mediated knockout of factors in non-homologous end joining pathway enhances gene targeting in silkworm cells. Sci Rep 5:18103 . https://doi.org/10.1038/srep18103

Zorin B, Lu Y, Sizova I, Hegemann P (2009) Nuclear gene targeting in Chlamydomonas as exemplified by disruption of the PHOT gene. Gene 432:91–96 . https://doi.org/https://doi.org/10.1016/j.gene.2008.11.028

Zuris J, Thompson D, Shu Y, Guilinger J, Bessen J, Hu J, Maeder M, Joung J, Chen ZY, Liu D (2014) Cationic lipid-mediated delivery of proteins enables efficient protein-based genome editing in vitro and in vivo. Nat Biotechnol 33: . https://doi.org/10.1038/nbt.3081

APPENDIX

Sustainable production of cellulolytic enzymes in different model organisms

CHAPTER 12
Appendix: Design of a highly thermostable hemicellulose-degrading blend from *Thermotoga neapolitana* for the treatment of lignocellulosic biomass

This paper was published in March 2019.

Benedetti M, Vecchi, V., Betterle, N., Natali, A., Bassi, R., Dall'Osto, L. Design of a highly thermostable hemicellulose-degrading blend from *Thermotoga neapolitana* for the treatment of lignocellulosic biomass. J Biotechnol 2019, 296:42–52.

Abstract: The biological conversion of lignocellulose into fermentable sugars is a key process for the sustainable pro-duction of biofuels from plant biomass. Polysaccharides in plant feedstock can be valorized using thermostable mixtures of enzymes that degrade the cell walls, thus avoiding harmful and expensive pre-treatments. (Hyper) thermophilic bacteria of the phylum Thermotogae provide a rich source of enzymes for such industrial appli-cations. Here we selected *T. neapolitana* as a source of hyperthermophilic hemicellulases for the degradation of lignocellulosic biomass. Two genes encoding putative hemicellulases were cloned from T. *neapolitana* genomic DNA and expressed in Escherichia coli. Further characterization revealed that the genes encoded an endo-1,4-β-galactanase and an α-L-arabinofuranosidase with optimal temperatures of ˜90 °C and high turnover numbers during catalysis (k_{cat} values of ˜177 and ˜133 s^{-1}, respectively, on soluble substrates). These enzymes were combined with three additional T. neapolitana hyperthermophilic hemicellulases – endo-1,4-β-xylanase (XynA), endo-1,4-β-mannanase (ManB/Man5A) and β-glucosidase (GghA) – to form a highly thermostable hemi-cellulolytic blend. The treatment of barley straw and corn bran with this enzymatic cocktail resulted in the solubilization of multiple hemicelluloses and boosted the yield of fermentable sugars by up to 65% when the complex substrates were further degraded by cellulases.

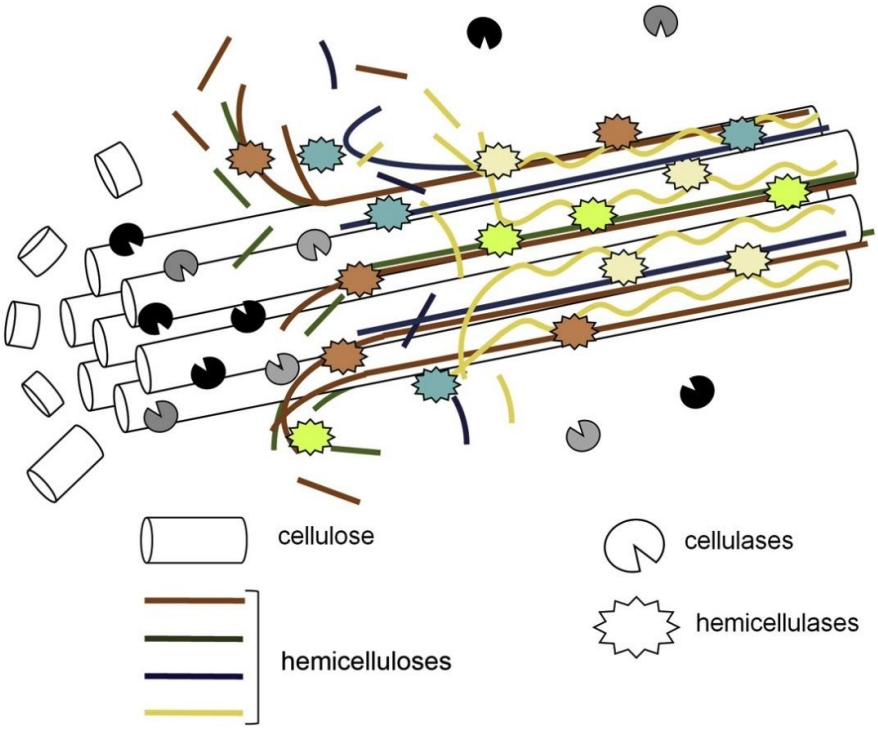

Figure 12.1 Graphical Abstract

Abbreviations: αAF, α-L-arabinofuranosidase; βG, endo-14-β-galactanase; CBM, carbohydrate binding modules; CWDE, cell-wall degrading enzyme; DW, dry weight; HCWDE, hyperthermophilic CWDE; GH, glycosyl-hydrolytic domains; HH, hyperthermophilic hemicellulases; pNPAF, p-nitrophenyl-α-L-arabinofuranoside; pNPG, p-nitrophenyl-β-glucopyranoside; XynA, endo-14-β-xylanase; ManB/Man5A, endo-14-β-mannanase; GghA, β-glucosidase

12.1. Introduction

Lignocellulose in plant cell walls represents more than 90% of the dry weight (DW) of plant biomass and is the most abundant carbon source on Earth, providing a rich feedstock for the production of renewable fuels. The industrial exploitation of lignocellulose as an energy feedstock requires the efficient and economically viable hydrolysis of the substrate to form soluble sugars that can be fermented by industrial microbes (Sanderson 2011; Saini et al. 2015). Lignocellulose is a complex and heterogeneous material whose primary role is to form the structure of plant cell walls, providing mechanical resistance and protection against pathogens (Keegstra 2010). It comprises three major polymers: cellulose (30–60%), hemicelluloses (20–40%) and lignin (10–25%). Cellulose fibers interact via hydrogen bonds with hemicelluloses, a branched and heterogeneous group of polysaccharides, and this assembly is in turn occluded by lignin to increase its overall robustness and hydrophobicity, forming a reservoir of energy and reducing power locked in by the complex structure and diverse composition (Bajpai 2016).

Physical, chemical or enzymatic treatments can be used to convert lignocellulosic biomass into fermentable sugars suitable for the production of biofuels and other renewable chemicals (Kumar et al. 2009; Chiaramonti et al. 2012). However, physical and chemical treatments are harmful to the

environment and increase the production costs, whereas the use of microbial cell wall degrading enzymes (CWDEs) is limited by both the cost of the enzymes and their low hydrolytic efficiency (Kumar et al. 2009; Brodeur et al. 2011). Three major factors limit the enzymatic degradation of lignocellulose: the hydrophobic nature of the substrate, which hiders access by CWDEs; the chemical heterogeneity of hemicelluloses, which requires diverse CWDEs for efficient degradation (Scheller and Ulvskov 2010); and the fact that certain oligosaccharides and phenolic compounds released during the degradation of cell walls act as CWDE inhibitors (Jönsson and Martín 2016). For example, long-chain oligomers derived by the partial hydrolysis of xylan, an abundant hemicellulose in monocots, are potent inhibitors of cellobiohydrolases (Baumann et al. 2011; Momeni et al. 2015).

The pre-treatment or co-treatment of lignocellulosic biomass with hemicellulase-enriched enzyme mixtures can improve the industrial saccharification of cellulosic biomass by releasing monosaccharides from hemicelluloses and enhancing cellulase activity (Gao et al. 2011; Juturu and Wu 2012). Accordingly, the identification of novel hemicellulases may enlarge the panel of available CWDEs and hence the number of enzymatic combinations with diverse substrate specificities. Hyperthermophilic CWDEs (HCWDEs) have recently attracted interest for lignocellulose-based bioprocesses because they are synthesized by hyperthermophiles, i.e. bacteria and archaea with optimal growth temperatures exceeding 80 °C (Vieille and Zeikus 2001). Hyperthermophilic hemicellulases are highly desirable for the saccharification of plant biomass because thermostable enzymes demonstrate superior hydrolytic activity compared to their mesophilic counterparts (Yeoman et al. 2010; Anitori 2012; Peng et al. 2015) and tend to remain stable even in the presence of surfactants and under extreme pH conditions (de Miguel Bouzas et al. 2006; Souza et al. 2016) that facilitate the hydrolysis of lignocellulose (Ooshima et al. 1986; Li et al. 2016). Furthermore, high temperatures promote the partial detachment of lignin from the hemicellulose–cellulose assembly and therefore prevent contamination by mesophilic microbes, thus increasing the saccharification yield (Sarmiento et al. 2015). Finally, CWDE-inhibiting proteins, which are widely distributed in the plant cell wall as a defense mechanism (York et al. 2004; Juge 2006; Kalunke et al. 2015; Benedetti et al. 2018a), are inactivated at high temperatures, preventing them from interfering with the industrial degradation process.

Thermotoga is a genus of (hyper)thermophilic bacteria of the phylum *Thermotogae* (Frock et al. 2010), which includes the species *T. maritima* and *T. neapolitana* known for their ability to degrade cellulose and xylan, respectively. The *T. neapolitana* genome (https://www.ncbi.nlm.nih.gov/genome/genomes/534) encodes an arsenal of hyperthermophilic glycoside hydrolases including hemicellulases, cellulases and αamylases, which could be suitable for industrial applications (Duffaud et al. 1997; King et al. 1998; Bok et al. 1998; Park et al. 2010; Cheng et al. 2011). We therefore selected *T. neapolitana* as a source of additional hyperthermophilic hemicellulases for the pre-treatment or co-treatment of lignocellulosic biomass. Two genes encoding putative hemicellulases were identified by homology analysis and cloned for heterologous expression in *Escherichia coli* and subsequent biochemical characterization. We analyzed the optimal temperature conditions and substrate preferences, and pooled them with three already-characterized hemicellulases from *T. neapolitana* to form a hyperthermophilic cocktail for the pre-treatment of lignocellulose to facilitate the activity of cellulases. As proof of concept, we applied this mixture of five enzymes in combination with a commercial cellulolytic cocktail for the

enzymatic hydrolysis of barley straw and corn bran as model substrates representing agricultural waste.

12.2 Materials and methods

Cloning and expression of HCWDEs

Thermotoga neapolitana strain DSM 4359 was used as the source of genomic DNA. *Escherichia coli* strains DH5α and BL21(DE3) were used as cloning and expression hosts, respectively. Selected genes were amplified from *T. neapolitana* genomic DNA using the primers listed in Supplementary Table S12.1, which contained terminal restriction enzyme sites. The resulting products were inserted into the vector pGEM-T easy (Promega) using the corresponding restriction sites, and all recombinant vectors were sequenced to ensure the integrity of the inserts. The enzyme sequences were transferred to vector pRSFDuet (Novagen) allowing the inducible expression of each enzyme in *E. coli* BL21 cells as His_6 tag fusions for the detection and purification of the products by immuno-decoration and Ni-affinity chromatography, respectively. The transformed cells were grown in super broth (SB) containing 50 μg mL^{-1} kanamycin and 50 μg mL^{-1} chloramphenicol, and expression was induced by adding 100 μM isopropyl β-d-1-thiogalactopyranoside (IPTG) when optical density at 720 nm reached 0.6 OD.

Partial purification of HCWDEs

Following the induction of recombinant enzyme expression, the cultures were centrifuged (4000 × *g*, 5 min, 10 °C) and the pellet was resuspended in lysis buffer (50 mM Tris−HCl pH 8.8, 100 mM NaCl, 5% (v/v) glycerol, 1 mM ε-aminocaproic acid, 1 mM phenylmethylsulfonyl fluoride, 0.2 mM benzamidine). The resuspended cells were incubated with lysozyme (30 min, 4 °C) then sonicated for 30 min and centrifuged (12,000 × *g*, 15 min, 10 °C). The supernatant was enriched for thermophilic proteins by heating to 70 °C for 30 min, promoting the aggregation of mesophilic proteins (Patchett et al. 1989). After centrifugation to remove the mesophilic protein pellet (12,000 × *g*, 30 min, 10 °C), the supernatant was dialyzed against 5 mM imidazole, 500 mM NaCl and 50 mM Tris−HCl (pH 7.4). The dialyzed sample was passed through a pre-equilibrated Ni-affinity chromatography column and, after extensive washing, was eluted in buffer containing 250 mM imidazole. HCWDEs in the elution fractions were detected by immuno-decoration using antibody H-15 specific for the His_6 tag (Santa Cruz Biotechnology). Fractions containing HCWDEs were concentrated and dialyzed using Vivaspin 500 polyethersulfone (PES) columns with a molecular weight cut-off (MWCO) of 30,000 Da (Sartorius). Enzyme purity and concentration were assessed by sodium dodecylsulfate polyacrylamide gel electrophoresis (SDS-PAGE) followed by Coomassie Brilliant Blue staining and comparison to bovine serum albumin standards (BSA Fraction V, Sigma-Aldrich).

Biochemical characterization of HCWDEs

The pH optimum of each enzyme was determined using citrate–phosphate (CP) buffer (pH 3.0–8.0) supplemented with 50 mM NaCl. The temperature optimum was determined by conducting assays in the temperature range 20–100 °C for 15 min with the substrates 1% (w/v) potato galactan, 1% (w/v) galactomannan, 5 mM *p*-nitrophenyl-β-glucopyranoside (*p*NPG), 5 mM *p*-nitrophenyl-α-

arabinofuranoside (*p*NPAF), 1% (w/v) beechwood xylan, 1% (w/v) wheat flour arabinoxylan, and 1% (w/v) pectic galactan from lupin. Xylan (Xylose ≥ 90%) and *p*NPG were purchased from Sigma-Aldrich. Galactomannan (24:76 Gal:Man), *p*NPAF, arabinoxylan (38:62 Ara:Xyl), potato galactan (88:2:3:7 Gal:Ara:Rha:GalA) and pectic galactan (77:14:3:0.6:5.4 Gal:Ara:Rha:Xyl:GalA) were purchased from Megazyme. Thermostability was determined by evaluating the residual activity of the enzymes at pH 6.0 following incubation for 3 h at temperatures in the range 60–100 °C. For enzymatic assays, HCWDEs were used at a concentration of 5 nM (i.e. between 0.25 and 0.6 µg mL^{-1}, depending on the molar mass of the enzyme). For substrate specificity analysis, reactions were carried out at pH 6.0 and 75 °C using arabinoxylan and arabinogalactan as substrates. The kinetic parameters of α-l-arabinofuranosidase (αAF) and endo-1,4-β-galactanase (βG) were determined under optimal pH and temperature conditions using the pure enzyme (5 nM) and different substrate concentrations ranging from 3×10^{-2} to 15 mM for *p*NPAF, and from 0.01%–3% (w/v) for galactan. K_M and V_{max} were calculated using the "Very Simple K_M V_{max} Tool Kit" software (http://www.ic50.tk/kmvmax.html) and reported values are means of three independent replicates. To compare the activity of *T. maritima* isoenzymes, the kinetic parameters of αAF and βG were also evaluated under the reaction conditions described in earlier reports, specifically pH 7.0/80 °C for αAF (Miyazaki 2005) and pH 7.0/70 °C with 0.5% potato galactan for βG (Yang et al. 2006). Thermally-inactivated enzymes (autoclaved at 120 °C for 5 h) were used as negative controls. The quantity of reducing ends released during the hydrolysis of galactan, galactomannan, xylan, arabinogalactan and arabinoxylan was determined in µmol as previously described, using d-galactose, d-mannose, d-xylose, d-galactose and d-xylose to construct the corresponding calibration curves (Lever 1972). Glycoside hydrolases can degrade polymeric substrates in endo-mode, thus generating oligomers with different degrees of polymerization. Accordingly, enzymatic activity should not be determined by measuring the total sugars released during hydrolysis because this may overestimate number of enzymatic conversions, whereas the quantity of reducing ends is proportional to the number of enzymatic conversions. The quantity of *p*-nitrophenol released during the hydrolysis of *p*NPAF and *p*NPG was determined using different amounts of *p*-nitrophenol to construct the calibration curve.

Bioinformatics

Fourteen genes encoding glycoside hydrolases (EC 3.2.1.-) were selected from the *T. neapolitana* DSM 4359 genome sequence (https://www.genome.jp/dbget-bin/www_bget?refseq + NC_011978) according to their substrate specificities. Conserved domains were detected using CD-Search (Marchler-Bauer et al. 2017) (https://www.ncbi.nlm.nih.gov/Structure/cdd/wrpsb.cgi) with the putative amino acid sequence of each enzyme as the query. The output (accession numbers from the list of domain hits) was used to search the UniProt database (https://www.uniprot.org/) to identify the substrate-binding and catalytic domains of each enzyme according to CAZy conventions (http://www.cazy.org/). We used Protein BLAST to find similar sequences (https://blast.ncbi.nlm.nih.gov/Blast.cgi?PAGE=Proteins), and signal peptides were predicted (Petersen et al. 2011) using the SignalP v4.1 Server (http://www.cbs.dtu.dk/services/SignalP/). Amino acid alignments were generated using DNAMAN v4.15 (Lynnon Biosoft).

Degradation of lignocellulosic material

Straw from barley (*Hordeum vulgare*) was kindly provided by Prof. Felice Cervone (Department of Biology and Biotechnology, Sapienza, University of Rome). Raw bran from corn (*Zea mays*) was provided by Prof. David Bolzonella (Department of Biotechnology, University of Verona). In both cases, the lignocellulosic material was pre-treated with a mild alkaline solution as previously described (Chen et al. 2013) with modifications. The material was homogenized in liquid nitrogen and mixed with 0.1 g NaOH per g DW of substrate in the appropriate volume of water to yield a 4% NaOH solution. The samples were incubated at 75 °C for 2 h (Chen et al. 2013; Zheng et al. 2014; Xu et al. 2016) and the insoluble solid fraction was then washed several times with ultrapure water before freeze-drying and storing at room temperature. For the enzymatic assays, this insoluble solid fraction (1.5% w/v) was incubated in 50 mM CP buffer (pH 6.0) with either 0.5% (v/v) Celluclast/Cellobiase (CC mixture) or 0.1 mg mL^{-1} of the hyperthermophilic hemicellulase cocktail supplemented with 0.02% NaN_3 (HH mixture). The CC mixture comprised 0.4% (v/v) *Trichoderma* reseei cellulase (Celluclast) and 0.1% (v/v) *Aspergillus niger* cellobiase (Cellobiase) from Sigma-Aldrich. The HH mixture comprised equimolar amounts of each *T. neapolitana* HCWDE. A two-step enzymatic degradation was also carried out in which the sample was incubated first at 75 °C for 24 h with the HH mixture and then at 37 °C for another 24 h with the CC mixture. Inactivated enzymatic mixtures were added at the same time points as negative controls. The yield of soluble sugars was evaluated at the end of the reaction using the phenol–sulfuric acid assay (Dubois et al. 1956). Substrate hydrolysis was reported as the quantity of sugars (g) released as a proportion of the mass of insoluble alkaline-treated lignocellulosic material (g) and was expressed as a percentage. Glucose in the neutralized acid-treated filtrates was quantified using the glucose oxidase/peroxidase (GOPOD) assay kit (Megazyme). The monosaccharide composition of alkaline-treated lignocellulosic materials and reaction filtrates was determined in neutralized acid-treated samples by high-performance anionic exchange chromatography coupled with pulsed amperometric detection (HPAEC-PAD) as previously described (Gigli Bisceglia et al. 2018).

12.3 Results

Sequence analysis for the selection of putative *T. neapolitana* hemicellulases

We prepared an effective cocktail of HCWDEs suitable for the degradation of lignocellulose by selecting genes encoding a range of hemicellulases from the biomass-decomposing hyperthermophilic bacterium *T. neapolitana*. At least seven *T. neapolitana* genes encoding HCWDEs have been already been identified (Zverlov et al. 1996; King et al. 1998; Bok et al. 1998; Yernool et al. 2000; Parker et al. 2001) and they are listed in Table 7. Four of them encode cellulases (Bok et al. 1998; Yernool et al. 2000) and two encode hemicellulases (Zverlov et al. 1996; Parker et al. 2001). Other *T. neapolitana* hemicellulases have been purified but the corresponding genes are unknown (McCutchen et al. 1996; Duffaud et al. 1997). We therefore selected 14 *T. neapolitana* genes encoding putative or known glycosyl hydrolases (EC 3.2.1.-) for sequence analysis, identifying carbohydrate binding modules (CBMs)and glycosyl hydrolase domains. This allowed us to select the minimal number of CWDEs with the widest potential substrate range, and to discard enzymes with redundant and/or unnecessary activities (Supplementary Table S12.2). Within this group, we found that the products of genes CTN_RS01985 and CTN_RS06855 were highly similar to glycosyl hydrolases involved in the degradation of arabinose -branched

hemicelluloses and galactans, respectively. They were accordingly designated as a putative α-l-arabinofuranosidase (αAF) and arabinogalactan endo-1,4-β-galactanase (βG), respectively, based on the NCBI Conserved Domain Database (Marchler-Bauer et al. 2017). The alignment of these proteins with the corresponding *T. maritima* isoenzymes (Miyazaki 2005; Yang et al. 2006) revealed 84.8% identify for βG and 90.6% identity for αAF (Figure 12.2). *T. neapolitana* αAF featured a signal peptide 28 amino acids in length, which was not present in the *T. maritima* ortholog.

Table 7: CWDEs isolated from *T. neapolitana.* The preferential substrate of each CWDE is reported. nd, not determined.

CWDE	Substrate	Gene	Gene locus	References
endoglucanase A	cellulose, 1,4-β-glucan	*CelA*	CTN_RS05505	(Bok et al. 1998)
endoglucanase B	cellulose, 1,4-β-glucan	*CelB*	CTN_RS05510	
β-glucosidase	β-glucosides	*GghA*	CTN_RS03850	(Yernool et al. 2000)
cellobiose phosphorylase	cellobiose	*CbpA*	CTN_RS03855	
endo-1,4-β-xylanase	1,4-β-xylan	*XynA*	CTN_RS03160	(Zverlov et al. 1996)
endo-1,4-β-mannanase	1,4- β-mannan	*ManB/Man5A*	CTN_RS06730	(Parker et al. 2001)
β-mannosidase	1,4-β-dimannosides	*Man2*	CTN_RS04100	
β-mannosidase	1,4-β-dimannosides	nd	nd	(Duffaud et al. 1997)
α-galactosidase	α-galactosides	nd	nd	(McCutchen et al. 1996)
β-mannosidase	1,4-β-dimannosides	nd	nd	

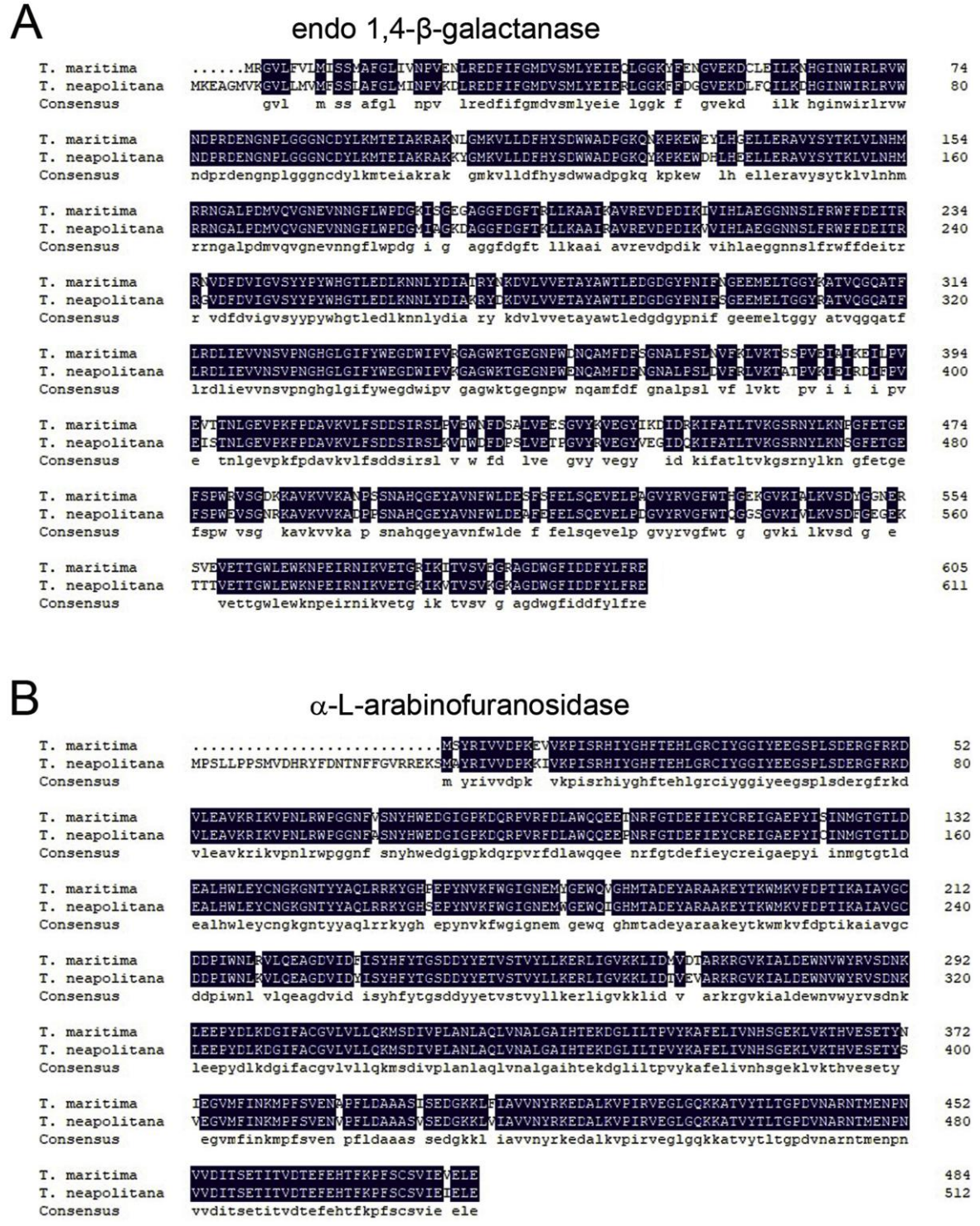

Fig. 12.2 Amino acid alignment of the *T. neapolitana* hemicellulases βG and αAF and their *T. maritima* orthologs. The alignments of (A) endo1,4-galactanase (βG) and (B) α-l-arabinofuranosidase (αAF) showed amino acid sequence identities of 84.8% and 90.6%, respectively. Identical amino acids are highlighted with a dark background. The consensus sequence is also shown

Enzymes with αAF and βG activities have not been reported in *T. neapolitana* before, so a mixture including these enzymes might enhance the degradation of galactan and arabinose - branched polysaccharides such as arabinogalactan and arabinoxylan (Figure 12.3). We therefore

expressed both enzymes in *E. coli* for biochemical characterization, and prepared a mixture containing both enzymes in addition to *T. neapolitana* endo-1,4-β-xylanase XynA, β-glucosidase GghA and endo-1,4-β-mannnase ManB/Man5A (Zverlov et al. 1996; Yernool et al. 2000; Parker et al. 2001), to improve the capacity of the mixture for lignocellulose hydrolysis (Figure 12.3). XynA and GghA can degrade xylan and several β-disaccharides, including cellobiose, which inhibits the cellobiohydrolase activity of cellulases through a product-inhibition mechanism (Zhao et al. 2004). Indeed, the lack of β-glucosidase activity in most commercial enzymatic blends is a major bottleneck that reduces the efficiency of industrial lignocellulose degradation (Sørensen et al. 2013). The inclusion of ManB/Man5A broadened the spectrum of digestible hemicelluloses to include mannans and galactomannans (figure 12.3).

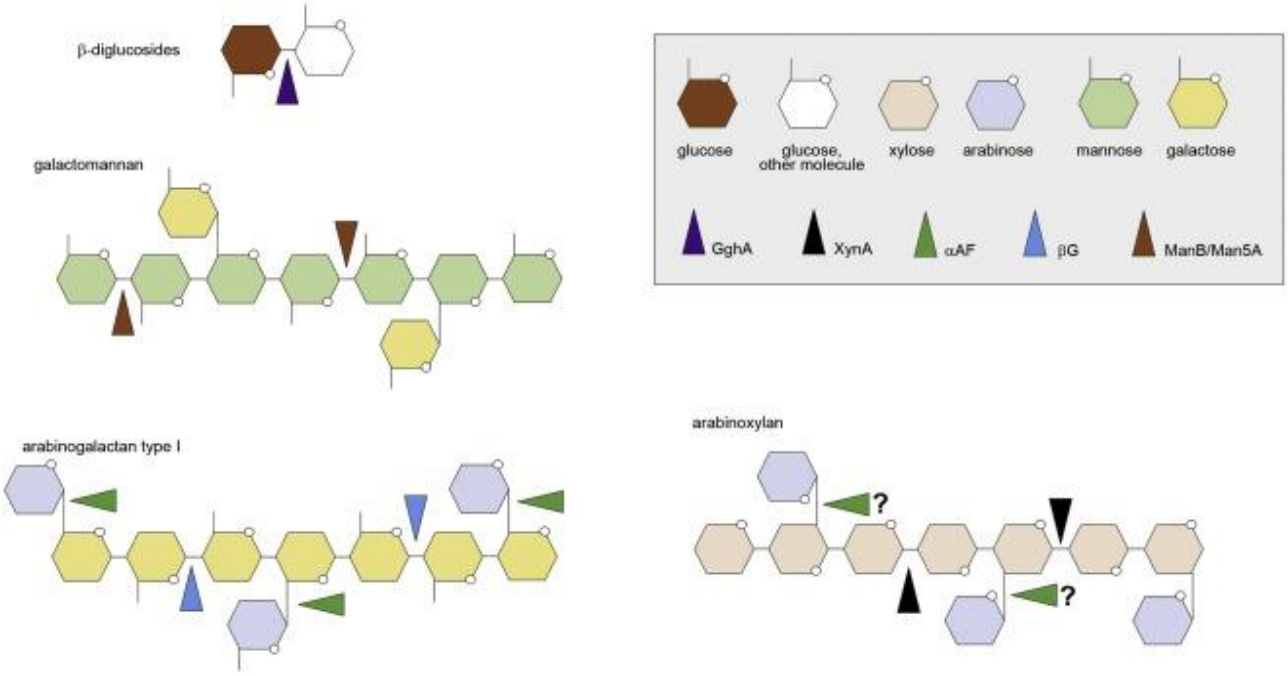

Fig. 12.3 Substrate specificity of the HH mixture. Schematic representation showing the major classes of hemicelluloses targeted by the HH mixture. The cleavage sites of the hemicellulolytic enzymes used in this study are also reported. Question marks show the potential cleavage of α-1,2 and α-1,3 glycosidic bonds in arabinoxylan by αAF.

Cloning, expression and partial purification of HCWDEs

The five HCWDE genes described above were amplified from the genomic DNA of *T. neapolitana* DSM 4359. The presence of signal peptides in the five proteins was excluded by SignalP4 software analysis, although the cloned αAF gene included an upstream sequence of 84 bp encoding an unpredicted signal peptide 28 amino acids in length. All five genes were appended with a 5' His_6 tag sequence allowing the immunological detection and Ni-affinity purification of the enzymes. For biochemical characterization, the recombinant enzymes βG, αAF and GghA were expressed in *E. coli* at 37 °C because they remained predominantly soluble and active, whereas XynA and ManB/Man5A aggregated at 37 °C (data not shown) and were therefore expressed at 16 °C. The five HCWDEs were extracted from *E. coli* by sonication and purified from the lysates using a two-step procedure involving the heat precipitation of labile host cell proteins (Patchett et al. 1989) followed by Ni- affinity chromatography to capture the His_6 tag. Extraction and heat precipitation alone

achieved substantial purification as shown by SDS-PAGE analysis (Figure 12.4 A) but affinity chromatography removed all residual host cell proteins and prevented their interference with subsequent enzyme characterization (Figure 12.4 B). SDS-PAGE analysis of the affinity-purified βG revealed a clear doublet, with both bands representing βG given their recognition by a specific antibody (Figure 12.4 B). The presence of two variants may reflect the partial denaturation of the protein in the buffer due to its high stability (Vieille and Zeikus 2001) or a proteolytic degradation of the C-terminal portion lacking the His_6 tag. The molecular masses of αAF, XynA, GghA, βG and ManB/Man5A as determined by SDS-PAGE were 55, 120, 50, 67 and 65 kDa respectively, consistent with the expected values (Figure 12.5 A).

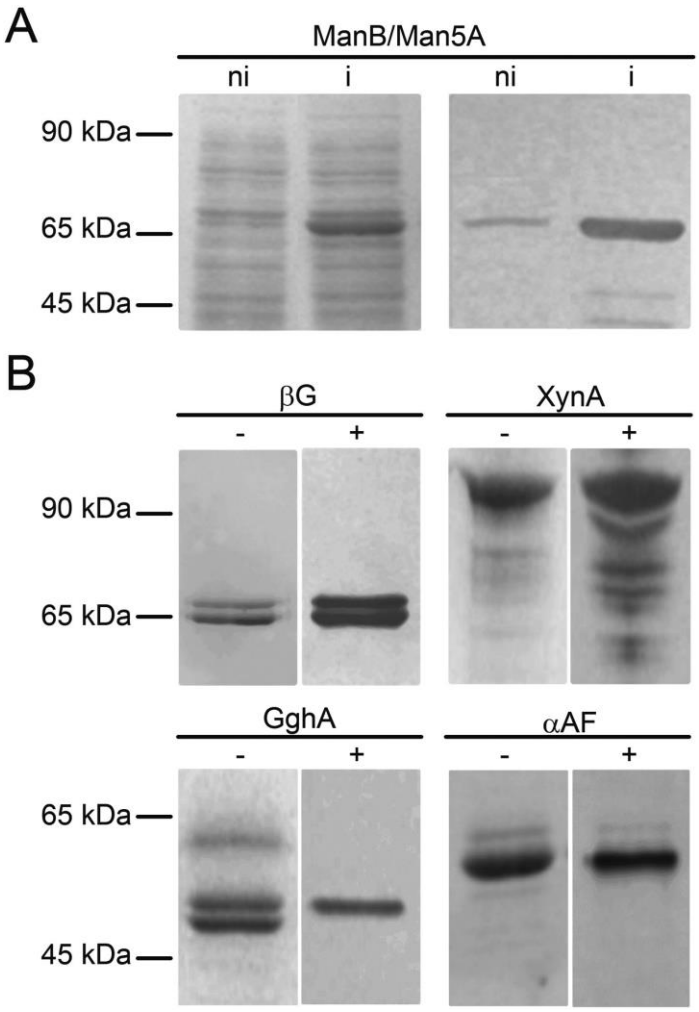

Figure 12.4. Expression and purification of HCWDEs in *E. coli*. A. Expression of βM in *E. coli* cell extracts before induction (ni) and after induction (i) as determined by SDS-PAGE (left panel) and immuno-decoration (right panel). B. SDS-PAGE (–) and immuno-decoration analysis (+) of the eluted fraction of βG, XynA, GghA and αAF from the Ni-NTA affinity chromatography step. Abbreviations: αAF = α-l-arabinofuranosidase, XynA=endoxylananse A, GghA = β-glucosidase, βG = β-galactanase, ManB/Man5A = β-mannanase.

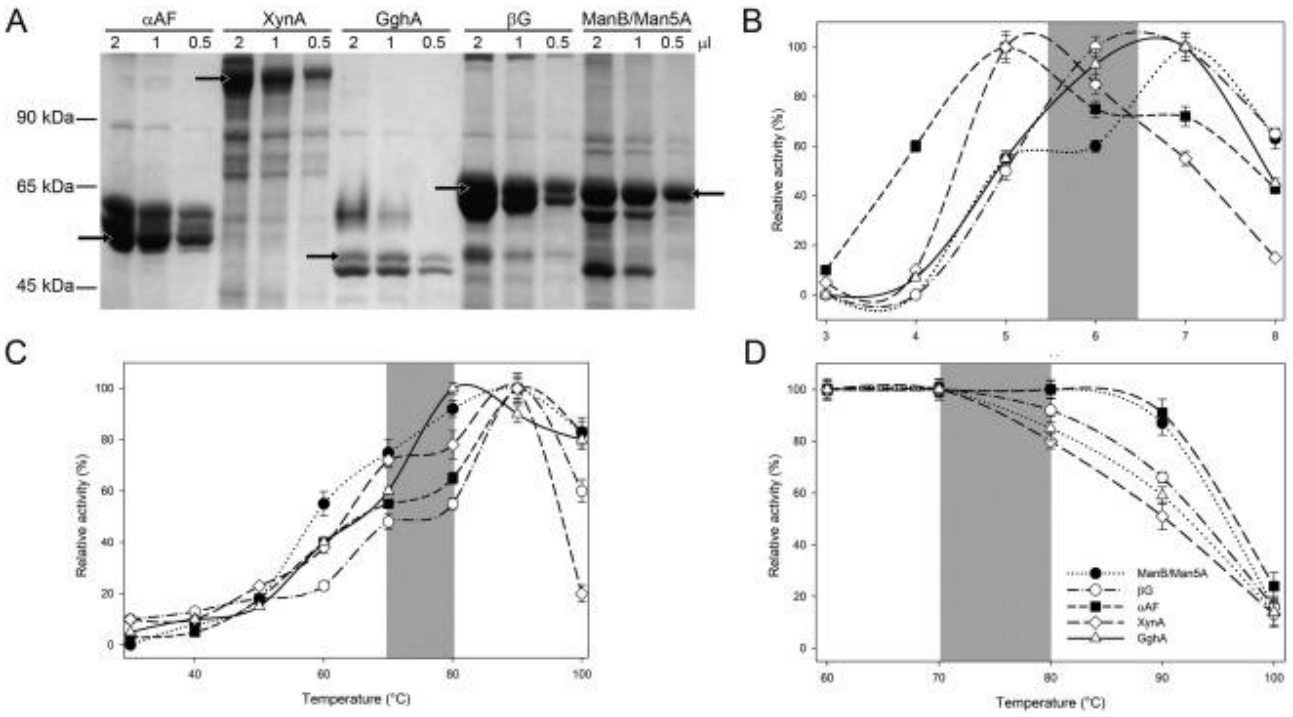

Figure 12.5. Determination of the optimal temperature and pH conditions of the HH mixture. A. SDS-PAGE analysis of the fractions eluted from the Ni-NTA affinity chromatography step. Three volumes of each fraction were evaluated (0.5, 1 and 2 µl). Black arrow indicates the corresponding enzyme band. B, C. Effect of pH (B) and temperature (C) on the activity of each HCWDE in the mixture, expressed as relative activity (%). D. Residual activity (%) following a 3-h incubation at temperatures of 60–100 °C. Gray area indicates the range of pH and temperatures suitable for the HH mixture. Abbreviations: αAF = α-l-arabinofuranosidase, XynA = endoxylananse A, GghA = β-glucosidase, βG = β-galactanase, ManB/Man5A = β-mannanase.

Enzymatic activity of purified HCWDEs and determination of reaction conditions for the cocktail

Following purification, the activities of the HCWDEs were investigated using either chromogenic reagents or plant cell wall polysaccharides as substrates. We found that ManB/Man5A, βG, αAF, GghA and XynA were active against galactomannan, galactan, *p*NPAF, *p*NPG and xylan, respectively. The ability to function and remain stable at high temperatures over a broad pH range enhances the efficiency of an HH mixture, so the optimal pH and temperature were determined for each enzyme in turn. All HCWDEs showed maximum activity within the pH range 5–7 (Figure 12.5 B) and at temperatures close to 90 °C (Figure 12.5 C) thus confirming their hyperthermophilic nature. As expected, the activity of all five HCWDEs fell significantly at temperatures below 30 °C (Figure 11.5 C). However, the enzymes differed considerably in terms of thermostability. XynA was the least stable, retaining only half of its initial activity after 3 h at 90 °C, whereas αAF was the most stable, retaining ˜90% of its initial activity under the same conditions (Figure 12.5 D).

The pH and temperature optima determined for βG (6.5, 90 °C) and αAF (5.0, 90 °C) were similar to the values reported for the orthologs in *T. maritima* (Miyazaki 2005; Yang et al. 2006). The K_M and k_{cat} values for *T. neapolitana* βG in the presence of potato galactan were 0.7 ± 0.1% and 177.6 ± 13.5 s^{-1}, respectively; similarly, the values for *T. neapolitana* αAF in the presence of *p*NPAF were

0.15 ± 0.05 mM and 134.85 ± 11.26 s^{-1}, respectively (Supplementary Fig. S12.1). To compare the activities of the *T. neapolitana* enzymes with their *T. maritima* orthologs, the kinetic parameters were also evaluated under the reaction conditions previously used to analyze the *T. maritima* enzymes (Miyazaki 2005; Yang et al. 2006). Whereas the activity of *T. neapolitana* βG against galactan was comparable to value reported for *T. maritima* βG (0.36 µmol s^{-1} mg^{-1}), *T. neapolitana* αAF showed a three-fold higher affinity for *p*NPAF and a three-fold higher activity (Figure 12.6 A).

A

ORGANISM	UNIPROT	ENZYME	K_M (mM)	kcat (sec^{-1})	Reference
T. maritima	Q9WYB7	αAF	0.42	21.7	*Miyazaki et al., 2005*
T. neapolitana	B9KC33		0.13 ± 0.02	74.8 ± 0.4	*This work*
				Specific activity (µmol s^{-1} mg^{-1})	
T. maritima	Q9X0S8	βG		0.36	*Yang et al., 2006*
T. neapolitana	B9K9B3			0.35 ± 0.04	*This work*

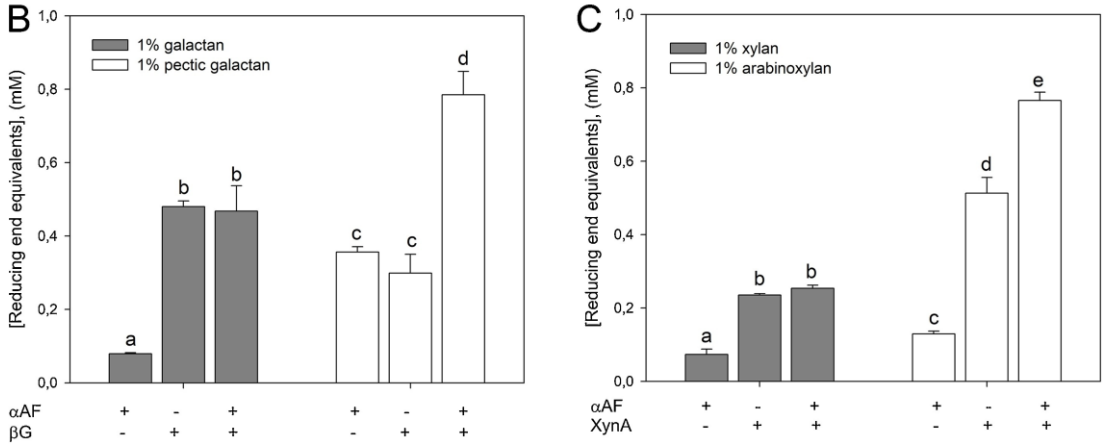

Figure 12.6 Enzymatic characterization of *T. neapolitana* αAF and βG. **A**. The kinetic parameters of αAF and βG were determined under the same reaction conditions as those used for the characterization of the corresponding isoenzymes from *T. maritima*, using *p*NPAF and potato galactan as substrates. **B**. The activity of αAF, βG and the combination of both enzymes against 1% galactan (gray bars) and 1% pectic galactan (white bars). **C**. The activity of αAF, XynA and the combination of both enzymes against 1% xylan (gray bars) and 1% arabinoxylan (white bars). Each enzyme was used at 5 nM. +/- indicates presence/absence of the corresponding enzyme. Activity is expressed as reducing ends equivalents (mM) after 20 min. Data are expressed as means ± SD, n = 3. Values marked with the same letters (a-e) are not significantly different from each other (ANOVA test, $P < 0.05$). Abbreviations: αAF = α-l-arabinofuranosidase, XynA = endoxylananse A, βG = β-galactanase.

The analysis of thermal properties showed that all five enzymes were thermostable at temperatures below 80 °C, so we decided on a working temperature of 75 °C for the HH mixture, slightly lower than the optimum in order to maintain stability during the prolonged reaction required to digest a recalcitrant substrate such as raw lignocellulose. We therefore used these reaction conditions to test

the activity of the αAF-βG combination against pectic galactan (mainly comprising arabinogalactan type I) and of the αAF-XynA combination against arabinoxylan. Although the arabinose content of wheat arabinoxylan (38% mol/mol) is higher than that of pectic galactan (17% mol/mol), the release of more arabinose from pectic galactan indicated that αAF was more efficient at cleaving α-1,6-linked l-arabinofuranose residues from arabinogalactan than α-1,2/α-1,3-linked l-arabinofuranose residues from arabinoxylans (Figure 11.6 B–C). Surprisingly, despite the high similarity between the αAF orthologs, the *T. maritima* αAF was unable to cleave arabinofuranose residues from wheat arabinoxylan and arabinogalactan (Miyazaki 2005). We also found that βG was less active against pectic galactan than galactan, indicating that l-arabinofuranose residues hindered the activity of βG, as observed for the *T. maritima* ortholog (Yang et al. 2006). Notably, we observed synergistic activity between αAF and the endo-acting glycosyl hydrolases (βG and XynA) towards the arabinose-substituted polysaccharides (Figure 11.6 B-C), thus highlighting the ability of αAF to support the action of βG and XynA in the HH mixture.

Testing the HH mixture as a supplement for cellulolytic cocktails

We prepared an enzyme cocktail containing equimolar amounts of the five recombinant hemicellulases and tested the HH mixture using barley straw and corn bran as model substrates representing the agricultural waste typically used for the conversion of plant biomass to fuel. Both substrates are predominantly cellulose embedded in various hemicelluloses including xylans, arabinoxylans and arabinogalactans, plus different quantities of lignin: 1–2% in corn bran and 15–20% in barley straw (Viëtor et al. 1991; Gibeaut et al. 2005; Palmarola-Adrados et al. 2005; Rose et al. 2010). Notably, compositional analysis of the non-cellulosic polysaccharides in barley straw revealed xylose as the main component plus smaller but significant amounts of arabinose and traces of uronic acids, indicating that barley straw hemicelluloses are mainly composed of acidic arabinoxylans, similar to those found in the straws of other plants (Sun et al. 2002). Arabinoxylan is also a major component of corn bran (Agger et al. 2010).

The raw materials were pre-treated with a mild alkaline solution to remove lignin while preserving a portion of the hemicelluloses and most of the cellulose (Zheng et al. 2014). Untreated lignocellulosic material is extremely hydrophobic and therefore a poor substrate for cellulases, whereas the pre-treated material not only lacks the lignin component but also has a looser cellulose crystalline matrix, thus facilitating enzyme access (Chen et al. 2013; Zheng et al. 2014). Chemical treatments may alter the composition and structure of lignocellulosic substrates, so we investigated the monosaccharide composition of the pre-treated barley straw and corn bran by HPAEC-PAD chromatography. The alkaline-treated feedstocks contained similar proportions of cellulose and hemicelluloses, and xylan was the most prominent non-cellulosic polysaccharide in both cases (48% and 36% mol/mol in bran and straw, respectively). Arabinoxylan and (arabino)galactan were more abundant in corn bran than barley straw (Supplementary Fig. S12.2) whereas glucuronic acid was present in trace amounts in both materials (data not shown). Despite the lack of β-mannans in these materials, ManB/Man5A was included in the HH mixture because we envisaged the cocktail as a generic blend suitable for diverse lignocellulosic materials.

Enzymatic degradation of the bran and straw involved two consecutive reactions: in the first step, the biomass was heated to 75 °C for 24 h in the presence of the HH mixture, and in the second step

the partially digested products were cooled to 37 °C and incubated for 24 h with the CC mixture, comprising a preparation of the commercial cellulase cocktails Celluclast and Cellobiase. The separate phases were necessary because the CC enzymes are purified form the mesophilic organisms *T. reseei* and *A. niger*, and they would be denatured at 75 °C. The reaction was carried out at pH 6.0, which was the optimal pH for both the HH and CC mixtures, thus avoiding the need for pH adjustment. The same substrates were also digested with the CC mixture alone and with the HH mixture alone in order to compare the efficiency of the single and combined enzymatic treatments.

When the reactions were complete, the quantity of soluble sugars was measured in each sample. In the alkaline-treated barley straw, the HH mixture alone yielded approximately the same quantity of soluble sugars as the CC mixture alone (Figure 12.7 A) whereas the HH mixture alone was less efficient than the CC mixture alone when the substrate was corn bran (Figure 12.7 B). However, the combined treatments indicated synergistic interactions between the two enzyme mixtures against both substrates, reflecting the ability of the HH mixture to make the lignocellulosic material more accessible to the cellulases. In the alkaline-treated barley straw, the combined treatment released 65% more glucose than the CC mixture alone (Figure 12.7 A), and in the alkaline-treated corn bran, the combined treatment resulted in a 35% improvement (Figure 12.7 B). The treatment of either substrate with the HH mixture alone predominantly led to the release of xylose, arabinose and galactose, as expected given the substrate specificity of the enzymes (Figure 12.7 C). The presence of more arabinose and galactose in the filtrates prepared from alkaline-treated corn bran was consistent with the higher content of arabino-substituted polysaccharides in this substrate (Supplementary Fig. S12.2). Accordingly, the improved release of glucose from the substrates subjected to the two-phase process with both enzyme mixtures was associated with the solubilization of xylose-derived polysaccharides (Supplementary Fig. S12.3).

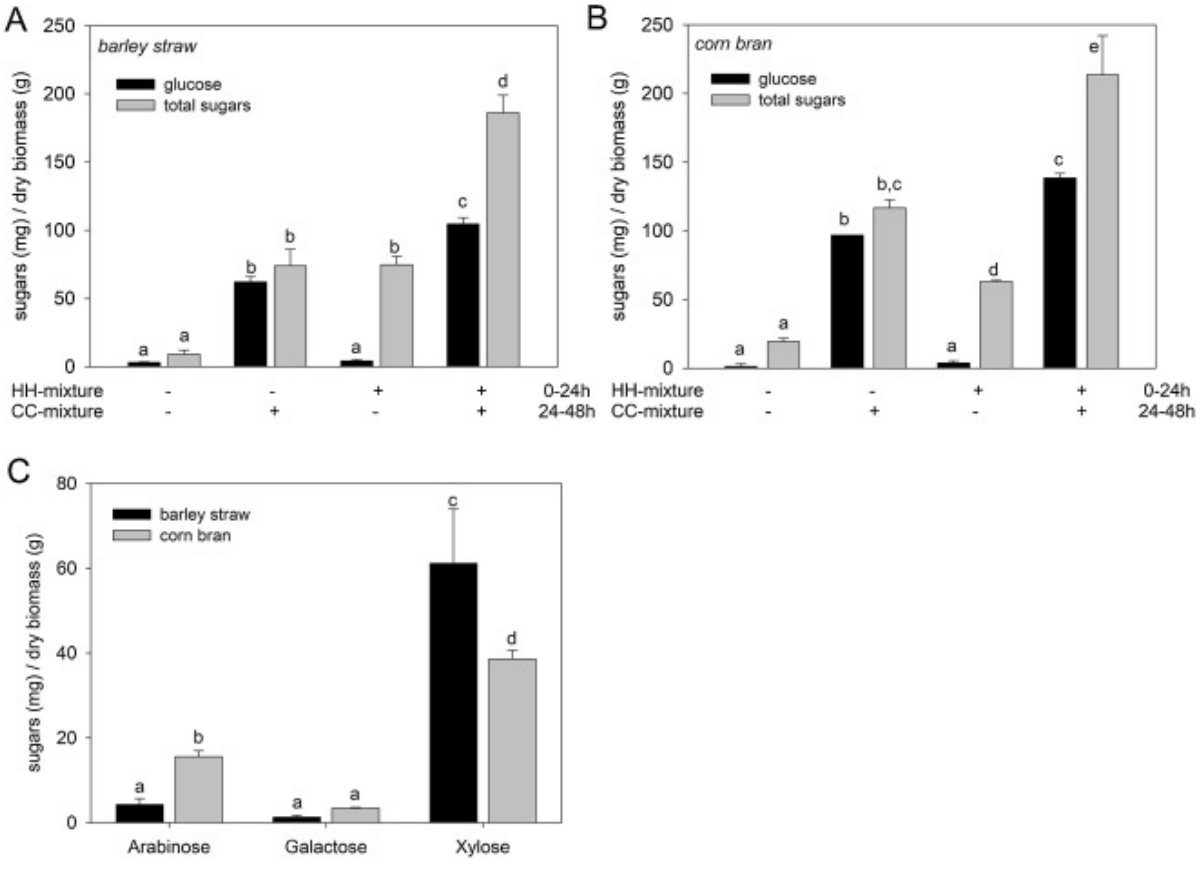

Figure 12.7. Hydrolysis by cellulases with and without the HH mixture for the conversion of lignocellulose substrates. A, B. Sugars released from alkaline-treated barley straw (A) and alkaline-treated corn bran (B) after different enzymatic treatments. Glucose (black bars) and total sugars (gray bars) in the acid-treated filtrates were determined by GO-POD and phenol-sulfuric acid assays, respectively. C. Monosaccharide composition analysis of the acid-treated filtrates from barley straw (black bars) and corn bran (gray bars) following treatment with the HH mixture, as determined by HPAEC-PAD. +/- indicate treatment with active/autoclaved enzymatic mixture. Data are expressed as means±SD, n=3. Values marked with the same letters (a–e) are not significantly different (ANOVA test, $P<0.05$). CC mixture=Celluclast+Cellobiase, HH mixture = αAF+βG+ManB/5A+XynA+GghA.

12.4 Discussion

The genus *Thermotoga* is a rich source of HCWDEs. Xylanolytic enzymes from *T. maritima* have already been used successfully for the production of food, paper and biofuels (Frock et al. 2010). Furthermore, among the HCWDEs characterized thus far, glycosyl hydrolases from *T. neapolitana* showed both high activity and remarkable thermostability, marking this species as an excellent source of enzymes for industrial applications (Zverlov et al. 1996; McCutchen et al. 1996; Duffaud et al. 1997; King et al. 1998; Bok et al. 1998; Yernool et al. 2000). *T. neapolitana* has also received considerable interest due to its ability to produce biohydrogen from waste (Ngo et al. 2011).

The *T. neapolitana* genome contains many genes encoding candidate HCWDE genes, and here we sought novel hemicellulases for the treatment of plant biomass to remove hemicelluloses and thus facilitate the activity of cellulases. Hemicelluloses are abundant in lignocellulosic biomass, accounting for 20–40% of the DW depending on the plant species. Both the heterogeneous composition and the branched structure of hemicelluloses limit the digestion of cellulose by restricting access, so hemicellulose depolymerization is necessary for efficient lignocellulose degradation (Hayashi and Kaida 2011). Furthermore, the inefficient degradation of hemicelluloses generates oligosaccharides that inhibit CWDEs and the microbes that convert sugars into biofuels (Baumann et al. 2011; Jönsson and Martín 2016).

We selected two *T. neapolitana* candidate hemicellulase genes (CTN_RS01985 and CTN_RS06855) and expressed them in *E. coli*. Analysis of their substrate specificity revealed that CTN_RS01985 encoded an αAF with high activity against *p*NPAF, whereas CTN_RS06855 encoded a βG with high activity against galactan, although lower activity against pectic galactan probably due to the presence of arabinose residues protecting the main backbone (Figure 12.3). Whereas *T. neapolitana* βG was similar in activity to its ortholog in *T. maritima*, the *T. neapolitana* αAF was three times more active against *p*NPAF than its ortholog, reflecting the three-fold higher affinity for this substrate (Figure 12.6 A), and also showed a different substrate specificity (Figure 12.6 B–C). Intriguingly, most of the sequence differences between the αAF orthologs were found at the N-terminus, because the *T. neapolitana* enzyme carries an N-terminal extension 28 amino acids in length. We speculate that the presence of this peptide may affect the substrate-binding capacity or stability of αAF. The characterization of truncated versions of *T. neapolitana* αAF would be necessary to determine the precise role of this peptide.

Our preliminary data indicated that T. neapolitana αAF and βG are versatile candidates for

the enzymatic degradation of lignocellulose, and to test this hypothesis we created a novel hemicellulolytic blend (the HH mixture) comprising five different T. neapolitana hemicellulases, and tested its ability to support the activity of cellulolytic cocktails. The five components of the HH mixture targeted different substrates, allowing the degradation of different hemicelluloses (Figure 12.3).

ManB/Man5A hydrolyzes mannans and galactomannans (Nascimento et al., 2014), αAF hydrolyzes terminal non-reducing α-l-arabinofuranoside residues in the α-l-arabinosides found in arabinoxylan and arabinogalactan, βG hydrolyzes 1,4-β-d-galactosidic linkages that form the structural motif of type I arabinogalactan, xylanase degrades linear β-1,4-xylans (Beg et al. 2001), and GghA hydrolyzes β-glycosidic bonds in glucose derivatives, thus increasing the saccharification yield and reducing the inhibitory effects of by-products. Notably, the HH mixture was active against two different alkaline-treated lignocellulosic substrates (Figure 12.7), thus confirming the effectiveness of the blend for the enzymatic conversion of lignocellulose in typical agricultural waste. The quality of the soluble sugars was dependent on the starting composition of the substrate, suggesting that the optimization of enzymatic ratios could help to improve the efficiency of the HH mixture.

Our results clearly showed that the solubilization of hemicelluloses promoted the release of glucose by the CC mixture, thus suggesting that the removal of hemicelluloses facilitates enzyme access. The concentration of enzymes in our CC mixture is sufficient for the rapid hydrolysis of Arabidopsis leaf tissue, achieving a saccharification efficiency greater than 50%, but it is below the optimal concentration required for the efficient hydrolysis of other types of plant biomass, such as tobacco and durum wheat (Lionetti et al. 2010). In our experiments, the hydrolysis of xylan played a prominent role in increasing the activity of cellulases against the alkaline-treated barley straw and corn bran. Given that the CC mixture was composed of mesophilic enzymes, a two-step reaction was necessary to ensure the cellulases were not denatured. It is possible that a cocktail containing hyperthermophilic hemicellulases and cellulases in a combined single-step reaction would be more efficient by promoting synergy between the components, and this will be addressed in future experiments.

In this study, we selected barley straw and corn bran as model substrates representing agricultural waste with different cell-wall compositions. Barley contains less starch than corn and the mash created while converting it into ethanol is viscous, making the industrial process more energy-demanding. Even so, barley and other grains such as wheat, pearl millet, sorghum and field peas could play a role in bridging the gap between current *and* next-generation bioethanol production methods. In the US alone, barley residues could provide up to 3.8 billion liters of ethanol per year, thus highlighting the need for innovative technologies to exploit this resource. However, corn bran has the potential to generate higher yields of bioethanol than bran from wheat and barley (Gibreel et al. 2009). Thus, strategies focused on improving the yield of fermentable sugars from the non-starch polysaccharide fraction of raw biomass may enhance their potential as energy feedstocks for biofuel production. It is notable that the alkaline-treated barley straw and corn bran mainly contained xylan and arabinoxylan hemicelluloses, but the HH mixture could be modified to work optimally with lignocellulosic substrates containing different types of hemicellulose such as mannans, which are prominent components of hardwood and softwood (Brigham et al. 2018).

Recently, a hyperthermophilic xylanase and endoglucanase were overexpressed in Arabidopsis and targeted to the apoplast targeting without adverse effects on plant growth (Mir et al. 2014; Mir et al. 2017). HCWDEs generally show low activity at the normal growth temperatures of land plants, so they can accumulate in the apoplast without hampering plant development. In contrast, stunted growth and morphological defects are common among transgenic plants that accumulate mesophilic CWDEs into the apoplast (Capodicasa et al. 2004; Sticklen 2008). This probably reflects the degradation of cell-wall polysaccharides, and the consequential triggering of plant defense responses (Aziz et al. 2007; Ferrari 2013; Souza et al. 2017). Such fragments are known as damage-associated molecular patterns (DAMPs), and if not promptly inactivated they severely impair plant growth (Benedetti et al. 2015; Benedetti et al. 2018a). Notably, transgenic plants over-expressing hyperthermophilic xylanase and endoglucanase showed accelerated lignocellulosic digestion, indicating that the accumulation of HCWDEs in the cell wall is a viable strategy to enhance the saccharification of plant biomass. In this perspective, the novel HCWDEs identified here could be used to generate transgenic, autocatalytic plants with increased saccharification efficiency. Alternatively, microalgae may provide a convenient bio-factory for the production of hyperthermophilic hemicellulases because they produce more biomass than land plants and they grow on inexpensive media such as wastewater and agro-industrial waste (Brasil et al. 2017; Benedetti et al. 2018b). The cell walls of most of microalgae are devoid of hemicelluloses, so the algal production of hemicellulases would bear no risk of toxic effects in the production host (Imam et al. 1985; Gerken et al. 2013).

12.5 Conclusions

We have confirmed that the rational incorporation of a set of enzymes with diverse substrate specificities in an HH mixture enhanced the ability of cellulase to degrade alkaline-treated lignocellulosic material at high temperatures. This ultimately led to a higher yield of fermentable sugars in cellulase-treated raw biomass.

12.6 Supporting Information

Figure S12.1

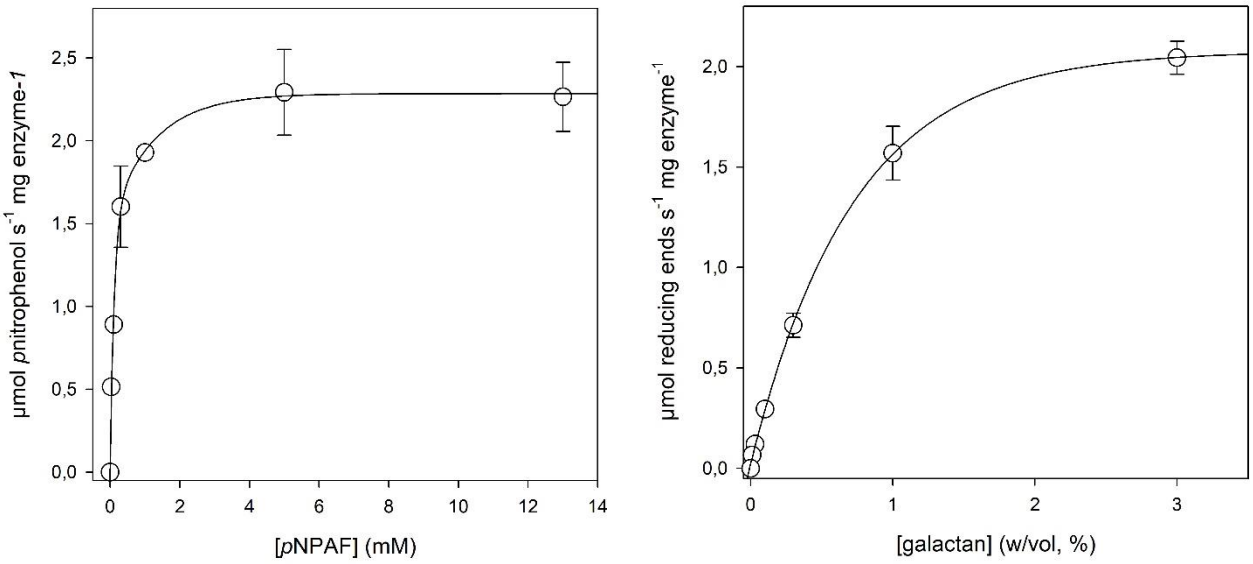

Supplementary Figure S12.1. Enzymatic activity of αAF and βG at different substrate concentrations. The enzymatic activity of αAF (left) and of βG (right) was evaluated at 90°C under optimal pH conditions using *p*NPAF and galactan substrates, respectively. K_M and V_{max} were calculated by interpolation using the "Very Simple K_M V_{max} Tool Kit" software. Values are from two independent replicates are expressed as means ± SD.

Figure S12.2

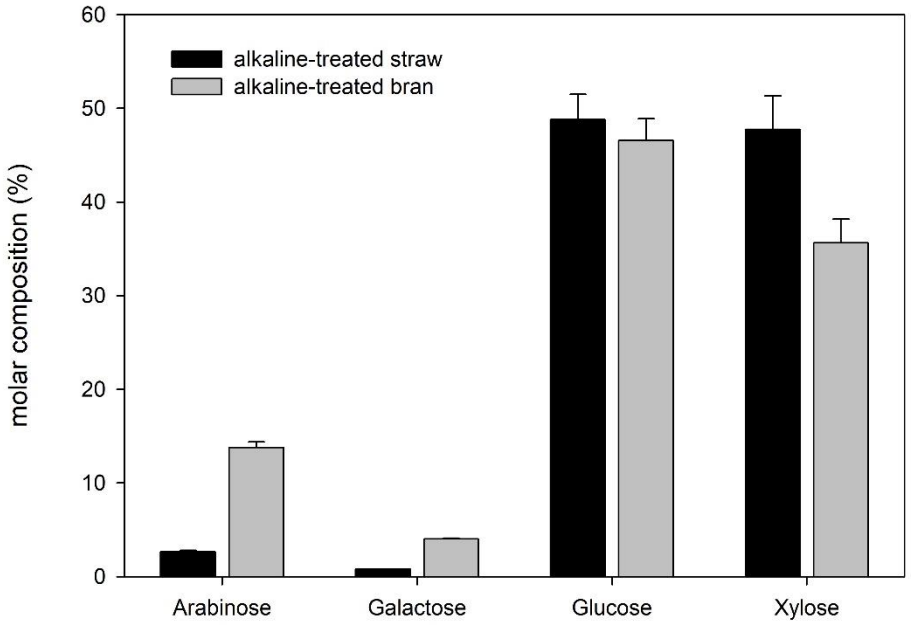

Supplementary Figure S12.2. Monosaccharide composition analysis of alkaline-treated barley straw (black bars) and corn bran (gray bars) as determined by HPAEC-PAD. Glucuronic acid was found in trace amounts in all samples. Fucose, rhamnose, mannose and galacturonic acid were not detected. Data are expressed as means ± SD, n = 2.

Figure S12.3

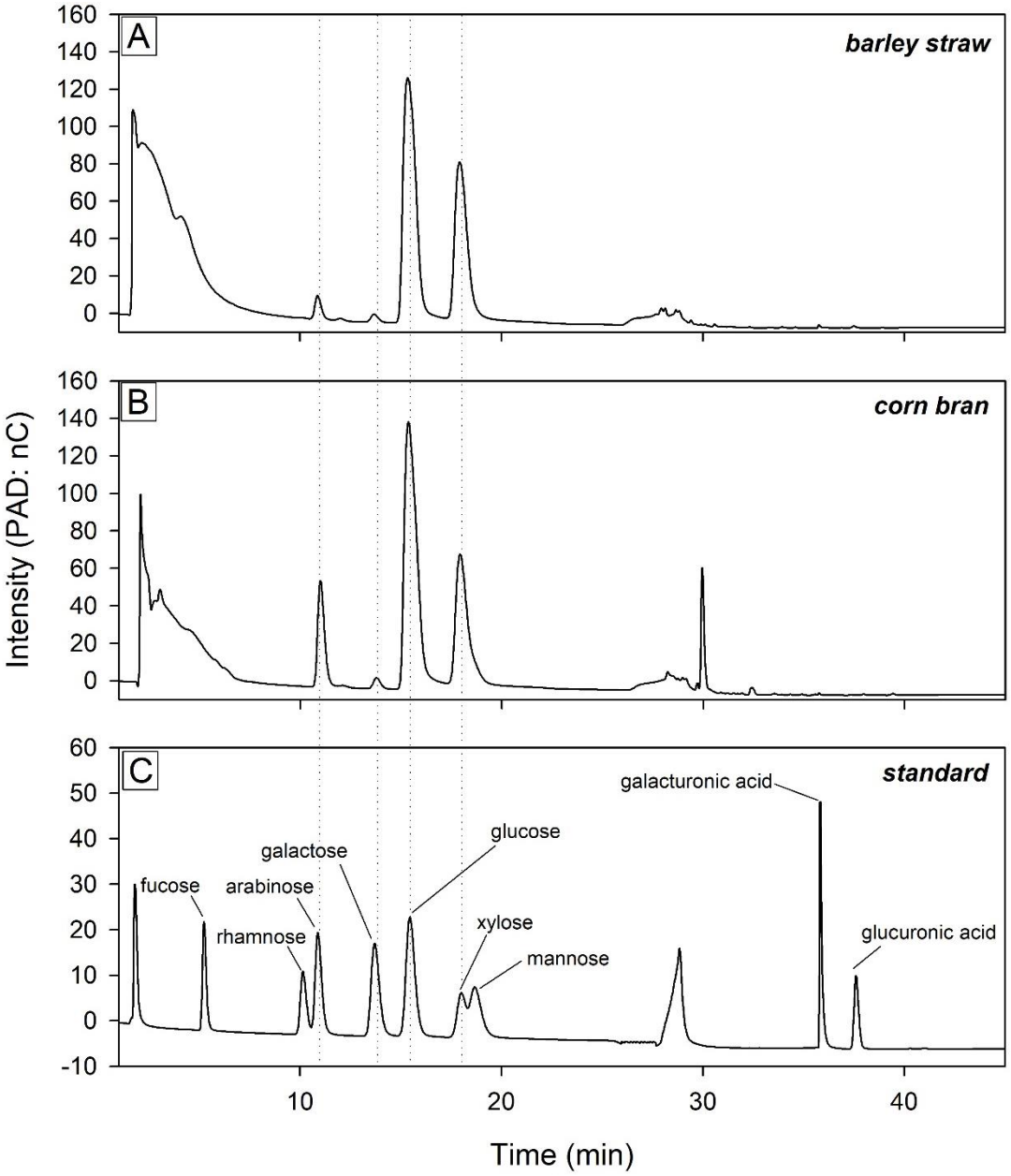

Supplementary Figure S12.3. Monosaccharide composition analysis of acid-treated filtrates, from alkaline-treated barley straw and corn bran, at the end of the enzymatic reaction as determined by HPAEC-PAD. Representative chromatographic (HPAEC-PAD) analyses of acid-treated filtrates from barley straw (**A**) and corn bran (**B**) following treatment with the HH and CC mixtures (**C**) Chromatographic analysis of standard monosaccharides. CC mixture = Celluclast + Cellobiase, HH mixture = αAF + βG + ManB/5A + XynA + GghA.

Supplementary Table S12.1. Sequences of oligonucleotides used for the construction of cassettes for HCWDE expression in *E. coli.* The restriction sites used for cloning are underlined.

Gene locus	CWDE	Sequences
CTN_RS01985	α-L-arabinofuranosidase	Fw ATGGATCCACCTTCACTTCTTCCGCC Rv ATGTCGACCTCCAATTCTATCTCAATCAC
CTN_RS03160	1,4-β-xylanase	Fw TAGTCGACTGTGGGTTCATGCGAAAG Rv ATAAGCTTCTTGATG AGCCTGAGAT TTC
CTN_RS06855	endo-β-1,4-galactanase	Fw TAGGATCCAAGGAGGCTGGTATGGTGAAAG Rv ATAAGCTTCTCCTCCCTGAACAGATAGAAATC
CTN_RS06730	β-mannanase	Fw ATCTGCAGAGAAAACTTGTGTTCTCATTTTTG Rv GAAAGCTTTCAAGAAGATTTTTTATAGAGCCTC
CTN_RS03850	β-glucosidase	Fw TAGAATTCATCGTGAAAAAGTTTCCCG Rv ATGTCGACATCTGTTAGTCCGTTG

Table S12.2. Selection of 14 *T. neapolitana* HCWDEs. Fourteen HCWDEs were individually selected on the basis of their diverse substrate specificities. Enzymes already characterized are indicated in bold. HCWDEs selected for the expression in *E. coli* are highlighted in gray. For each enzyme, carbohydrate binding modules (CBM) and catalytic domains (GH) are indicated.

CWDE	Gene	Gene locus	Conserved domain
peptidoglycan hydrolase		CTN_RS00115	GH73
α-L-arabinofuranosidase	*AbfA*	CTN_RS01985	GH51
β-glucosidase	*BglX*	CTN_RS03085	GH3
endo-1,3-β-xylanase	*XylC*	CTN_RS03090	GH26
endo-1,4-β-xylanase	*XylB*	CTN_RS03120	GH10
endo-1,4-β-xylanase	***XynA***	**CTN_RS03160**	**GH10/CBM9/CBM4_9**
β-glucosidase	*Bgl3B*	CTN_RS03345	GH3
β-glucosidase/laminaribiasi	*BglB*	CTN_RS03350	GH3/CBM4
β-glucosidase	***GghA/Bgl***	**CTN_RS03850**	**GH1**
Glycoside hydrolase, protein precursor		CTN_RS03795	GH13/CBM48
endo-1,4-β-xylanase		CTN_RS06515	GH10/CBM9/CBM22
endo-1,4-β-galactanase	*GanB*	CTN_RS06855	GH1/GH53/CBM61
endo-1,4-β-mannanase	***ManB/Man5A***	**CTN_RS06730**	**GH5/CBM27**
Lytic transglycosylase		CTN_RS08255	GH23

REFERENCES

Agger J, Viksø-Nielsen A, Meyer AS (2010) Enzymatic Xylose Release from Pretreated Corn Bran Arabinoxylan: Differential Effects of Deacetylation and Deferuloylation on Insoluble and Soluble Substrate Fractions. J Agric Food Chem 58:6141–6148 . https://doi.org/10.1021/jf100633f

Anitori RP (2012) Extremophilesmicrobiology and biotechnology

Aziz A, Gauthier A, Bézier A, Poinssot B, Joubert J-M, Pugin A, Heyraud A, Baillieul F (2007) Elicitor and resistance-inducing activities of beta-1,4 cellodextrins in grapevine, comparison with beta-1,3 glucans and alpha-1,4 oligogalacturonides. J Exp Bot 58:1463–72 . https://doi.org/10.1093/jxb/erm008

Bajpai P (2016) Pretreatment of Lignocellulosic Biomass for Biofuel Production. Springer Briefs in Molecular Science

Baumann MJ, Borch K, Westh P (2011) Xylan oligosaccharides and cellobiohydrolase I (TrCel7A) interaction and effect on activity. Biotechnol Biofuels 4:45 . https://doi.org/10.1186/1754-6834-4-45

Beg Q, Kapoor M, Mahajan L, Hoondal G (2001) Microbial xylanases and their industrial applications: a review. Appl Microbiol Biotechnol 56:326–338 . https://doi.org/10.1007/s002530100704

Benedetti M, Pontiggia D, Raggi S, Cheng Z, Scaloni F, Ferrari S, Ausubel FM, Cervone F, De Lorenzo G (2015) Plant immunity triggered by engineered in vivo release of oligogalacturonides, damage-associated molecular patterns. Proc Natl Acad Sci 112:5533–5538 . https://doi.org/10.1073/pnas.1504154112

Benedetti M, Vecchi V, Barera S, Dall' Osto L (2018a) Biomass from microalgae : the potential of domestication towards sustainable biofactories. Microb Cell Fact 1–18 . https://doi.org/10.1186/s12934-018-1019-3

Benedetti M, Verrascina I, Pontiggia D, Locci F, Mattei B, De Lorenzo G, Cervone F (2018b) Four Arabidopsis berberine bridge enzyme-like proteins are specific oxidases that inactivate the elicitor-active oligogalacturonides. Plant J. https://doi.org/10.1111/tpj.13852

Bok JD, Yernool DA, Eveleigh DE (1998) Purification, Characterization, and Molecular Analysis of Thermostable Cellulases CelA and CelB fromThermotoga neapolitana Appl Environ Microbiol 64:4774 LP – 4781 . https://doi.org/10.1128/AEM.64.12.4774-4781.1998

Brasil B dos SAF, de Siqueira FG, Salum TFC, Zanette CM, Spier MR (2017) Microalgae and cyanobacteria as enzyme biofactories. Algal Res 25:76–89

Brigham JS, Adney WS, Himmel ME (2018) Hemicellulases: diversity and applications. In: Handbook on Bioethanol. Routledge, pp 119–141

Brodeur G, Yau E, Badal K, Collier J, Ramachandran KB, Ramakrishnan S (2011) Chemical and physicochemical pretreatment of lignocellulosic biomass: a review. Enzyme Res 2011:787532 . https://doi.org/10.4061/2011/787532

Capodicasa C, Vairo D, Zabotina O, McCartney L, Caprari C, Mattei B, Manfredini C, Aracri B, Benen J, Knox JP, De Lorenzo G, Cervone F (2004) Targeted modification of homogalacturonan by transgenic expression of a fungal polygalacturonase alters plant growth. Plant Physiol 135:1294–304 . https://doi.org/10.1104/pp.104.042788

Chen Y, Stevens MA, Zhu Y, Holmes J, Xu H (2013) Understanding of alkaline pretreatment parameters for corn stover enzymatic saccharification. Biotechnol Biofuels 6:8 . https://doi.org/10.1186/1754-6834-6-8

Cheng YS, Ko TP, Wu TH, Ma Y, Huang CH, Lai HL, Wang AHJ, Liu JR, Guo RT (2011) Crystal structure and substrate-binding mode of cellulase 12A from Thermotoga maritima. Proteins Struct Funct Bioinforma 79:1193–1204 . https://doi.org/https://doi.org/10.1002/prot.22953

Chiaramonti D, Prussi M, Ferrero S, Oriani L, Ottonello P, Torre P, Cherchi F (2012) Review of pretreatment processes for lignocellulosic ethanol production, and development of an innovative method. Biomass and Bioenergy 46:25–35 . https://doi.org/https://doi.org/10.1016/j.biombioe.2012.04.020

de Miguel Bouzas T, Barros-Velázquez J, Gonzalez Villa T (2006) Industrial applications of hyperthermophilic enzymes: a review. Protein Pept Lett 13:645–651

Dubois M, Gilles KA, Hamilton JK, Rebers PA, Smith F (1956) Colorimetric Method for Determination of Sugars and Related Substances. Anal Chem 28:350–356 . https://doi.org/10.1021/ac60111a017

Duffaud GD, McCutchen CM, Leduc P, Parker KN, Kelly RM (1997) Purification and characterization of extremely thermostable beta-mannanase, beta-mannosidase, and alpha-galactosidase from the hyperthermophilic eubacterium Thermotoga neapolitana 5068. Appl Environ Microbiol 63:169 LP – 177

Ferrari S (2013) Oligogalacturonides: plant damage-associated molecular patterns and regulators of growth and development. Front Plant Sci 4: . https://doi.org/10.3389/fpls.2013.00049

Frock AD, Notey JS, Kelly RM (2010) The genus Thermotoga: recent developments. Environ Technol 31:1169–1181

Gao D, Uppugundla N, Chundawat SPS, Yu X, Hermanson S, Gowda K, Brumm P, Mead D, Balan V, Dale BE (2011) Hemicellulases and auxiliary enzymes for improved conversion of lignocellulosic biomass to monosaccharides. Biotechnol Biofuels 4:5

Gerken HG, Donohoe B, Knoshaug EP (2013) Enzymatic cell wall degradation of Chlorellavulgaris and other microalgae for biofuels production. Planta 237:239–253 . https://doi.org/10.1007/s00425-012-1765-0

Gibeaut DM, Pauly M, Bacic A, Fincher GB (2005) Changes in cell wall polysaccharides in developing barley (Hordeum vulgare) coleoptiles. Planta 221:729–738 . https://doi.org/10.1007/s00425-005-1481-0

Gibreel A, Sandercock JR, Lan J, Goonewardene LA, Zijlstra RT, Curtis JM, Bressler DC (2009) Fermentation of Barley by Using Saccharomyces cerevisiae: Examination of Barley as a Feedstock for Bioethanol Production and Value-Added Products. Appl Environ Microbiol 75:1363 LP – 1372 . https://doi.org/10.1128/AEM.01512-08

Gigli Bisceglia N, Savatin D V, Cervone F, Engelsdorf T, De Lorenzo G (2018) Loss of the Arabidopsis Protein Kinases ANPs Affects Root Cell Wall Composition, and Triggers the Cell Wall Damage Syndrome. Front Plant Sci 8:

Hayashi T, Kaida R (2011) Hemicelluloses as recalcitrant components for saccharification in wood. In: Routes to Cellulosic Ethanol. Springer, pp 45–52

Imam SH, Buchanan MJ, Shin HC, Snell WJ (1985) The Chlamydomonas cell wall: characterization of the wall framework. J Cell Biol 101:1599–1607 . https://doi.org/10.1083/jcb.101.4.1599

J**önsson LJ, Martín C** (2016) Pretreatment of lignocellulose: Formation of inhibitory by-products and strategies for minimizing their effects. Bioresour Technol 199:103–112 . https://doi.org/https://doi.org/10.1016/j.biortech.2015.10.009

Juge N (2006) Plant protein inhibitors of cell wall degrading enzymes. Trends Plant Sci 11:359–367 . https://doi.org/https://doi.org/10.1016/j.tplants.2006.05.006

Juturu V, Wu JC (2012) Microbial xylanases: engineering, production and industrial applications. Biotechnol Adv 30:1219–1227

Kalunke RM, Tundo S, Benedetti M, Cervone F, De Lorenzo G, D'Ovidio R (2015) An update on polygalacturonase-inhibiting protein (PGIP), a leucine-rich repeat protein that protects crop plants against pathogens. Front. Plant Sci.6:146. https://doi.org/ 10.3389/fpls.2015.00146.

Keegstra K (2010) Plant Cell Walls. Plant Physiol 154:483–486 . https://doi.org/http://dx.doi.org/10.1104/pp.110.161240

King MR, Yernool DA, Eveleigh DE, Fine BM (1998) Thermostable α-galactosidase from Thermotoga neapolitana: cloning, sequencing and expression. FEMS Microbiol Lett 163:37–42 . https://doi.org/10.1111/j.1574-6968.1998.tb13023.x

Kumar P, Barrett DM, Delwiche MJ, Stroeve P (2009) Methods for Pretreatment of Lignocellulosic Biomass for Efficient Hydrolysis and Biofuel Production. Ind Eng Chem Res 48:3713–3729 . https://doi.org/10.1021/ie801542g

Lever M (1972) A new reaction for colorimetric determination of carbohydrates. Anal Biochem 47:273–279 . https://doi.org/10.1016/0003-2697(72)90301-6

Li Y, Sun Z, Ge X, Zhang J (2016) Effects of lignin and surfactant on adsorption and hydrolysis of cellulases on cellulose. Biotechnol Biofuels 9:20 . https://doi.org/10.1186/s13068-016-0434-0

Lionetti V, Francocci F, Ferrari S, Volpi C, Bellincampi D, Galletti R, D'Ovidio R, De Lorenzo G, Cervone F (2010) Engineering the cell wall by reducing de-methyl-esterified homogalacturonan improves saccharification of plant tissues for bioconversion. Proc Natl Acad Sci 107:616–621 . https://doi.org/10.1073/pnas.0907549107

Marchler-Bauer A, Bo Y, Han L, He J, Lanczycki CJ, Lu S, Chitsaz F, Derbyshire MK, Geer RC, Gonzales NR, Gwadz M, Hurwitz DI, Lu F, Marchler GH, Song JS, Thanki N, Wang Z, Yamashita RA, Zhang D, Zheng C, Geer LY, Bryant SH (2017) CDD/SPARCLE: functional classification of proteins via subfamily domain architectures. Nucleic Acids Res 45:D200–D203 . https://doi.org/10.1093/nar/gkw1129

McCutchen CM, Duffaud GD, Leduc P, Petersen ARH, Tayal A, Khan SA, Kelly RM (1996) Characterization of extremely thermostable enzymatic breakers (α-1,6-galactosidase and β-1,4-mannanase) from the hyperthermophilic bacterium Thermotoga neapolitana 5068 for hydrolysis of guar gum. Biotechnol Bioeng 52:332–339 . https://doi.org/https://doi.org/10.1002/(SICI)1097-0290(19961020)52:2<332::AID-BIT13>3.0.CO;2-L

Mir BA, Mewalal R, Mizrachi E, Myburg AA, Cowan DA (2014) Recombinant hyperthermophilic enzyme expression in plants: A novel approach for lignocellulose digestion. Trends Biotechnol. 32:281–289

Mir BA, Myburg AA, Mizrachi E, Cowan DA (2017) In planta expression of hyperthermophilic enzymes as a strategy for accelerated lignocellulosic digestion. Sci Rep 7: . https://doi.org/10.1038/s41598-017-11026-1

Miyazaki K (2005) Hyperthermophilic α-L-arabinofuranosidase from Thermotoga maritima MSB8: molecular cloning, gene expression, and characterization of the recombinant protein. Extremophiles 9:399–406

Momeni MH, Ubhayasekera W, Sandgren M, Ståhlberg J, Hansson H (2015) Structural insights into the inhibition of cellobiohydrolase Cel7A by xylo-oligosaccharides. FEBS J 282:2167–2177 . https://doi.org/https://doi.org/10.1111/febs.13265

Ngo TA, Kim M-S, Sim SJ (2011) High-yield biohydrogen production from biodiesel manufacturing waste by Thermotoga neapolitana. Int J Hydrogen Energy 36:5836–5842 . https://doi.org/https://doi.org/10.1016/j.ijhydene.2010.11.057

Ooshima H, Sakata M, Harano Y (1986) Enhancement of enzymatic hydrolysis of cellulose by surfactant. Biotechnol Bioeng 28:1727–1734

Palmarola-Adrados B, Galbe M, Zacchi G (2005) Pretreatment of barley husk for bioethanol production. J Chem Technol Biotechnol 80:85–91 . https://doi.org/https://doi.org/10.1002/jctb.1161

Park K-M, Jun S-Y, Choi K-H, Park K-H, Park C-S, Cha J (2010) Characterization of an exo-acting intracellular α-amylase from the hyperthermophilic bacterium Thermotoga neapolitana. Appl Microbiol Biotechnol 86:555–566

P**arker KN, Chhabra SR, Lam D, Callen W, Duffaud GD, Snead MA, Short JM, Mathur EJ, Kelly RM** (2001) Galactomannanases Man2 and Man5 from Thermotogaspecies: Growth physiology on galactomannans, gene sequence analysis, and biochemical properties of recombinant enzymes. Biotechnol Bioeng 75:322–333

Patchett ML, Neal TL, Schofield LR, Strange RC, Daniel RM, Morgan HW (1989) Heat treatment purification of thermostable cellulase and hemicellulase enzymes expressed in E. coli. Enzyme Microb Technol 11:113–115 . https://doi.org/10.1016/0141-0229(89)90069-0

Peng X, Qiao W, Mi S, Jia X, Su H, Han Y (2015) Characterization of hemicellulase and cellulase from the extremely thermophilic bacterium Caldicellulosiruptor owensensis and their potential application for bioconversion of lignocellulosic biomass without pretreatment. Biotechnol Biofuels 8:131

Petersen TN, Brunak S, von Heijne G, Nielsen H (2011) SignalP 4.0: discriminating signal peptides from transmembrane regions. Nat Methods 8:785–786 . https://doi.org/10.1038/nmeth.1701

Rose DJ, Inglett GE, Liu SX (2010) Utilisation of corn (Zea mays) bran and corn fiber in the production of food components. J Sci Food Agric 90:915–924 . https://doi.org/https://doi.org/10.1002/jsfa.3915

Saini JK, Saini R, Tewari L (2015) Lignocellulosic agriculture wastes as biomass feedstocks for second-generation bioethanol production: concepts and recent developments. 3 Biotech 5:337–353 . https://doi.org/10.1007/s13205-014-0246-5

Sanderson K (2011) Lignocellulose: A chewy problem. Nature 474:S12–S14 . https://doi.org/10.1038/474S012a

Sarmiento F, Peralta R, Blamey JM (2015) Cold and Hot Extremozymes: Industrial Relevance and Current Trends. Front Bioeng Biotechnol 3: . https://doi.org/10.3389/fbioe.2015.00148

Scheller HV, Ulvskov P (2010) Hemicelluloses. Annu Rev Plant Biol 61:263–289 . https://doi.org/10.1146/annurev-arplant-042809-112315

Sørensen A, Lübeck M, Lübeck PS, Ahring BK (2013) Fungal beta-glucosidases: a bottleneck in industrial use of lignocellulosic materials. Biomolecules 3:612–631

Souza C de A, Li S, Lin AZ, Boutrot F, Grossmann G, Zipfel C, Somerville SC (2017) Cellulose-Derived Oligomers Act as Damage-Associated Molecular Patterns and Trigger Defense-Like Responses. Plant Physiol 173:2383–2398 . https://doi.org/10.1104/pp.16.01680

Souza T V, Araujo JN, da Silva VM, Liberato M V, Pimentel AC, Alvarez TM, Squina FM, Garcia W (2016) Chemical stability of a cold-active cellulase with high tolerance toward surfactants and chaotropic agent. Biotechnol Reports 9:1–8 . https://doi.org/https://doi.org/10.1016/j.btre.2015.11.001

Sticklen MB (2008) Plant genetic engineering for biofuel production: towards affordable cellulosic ethanol. Nat Rev Genet 9:433–443

Sun R, Sun XF, Liu GQ, Fowler P, Tomkinson J (2002) Structural and physicochemical characterization

of hemicelluloses isolated by alkaline peroxide from barley straw. Polym Int 51:117–124 . https://doi.org/https://doi.org/10.1002/pi.815

Vieille C, Zeikus GJ (2001) Hyperthermophilic enzymes: sources, uses, and molecular mechanisms for thermostability. Microbiol Mol Biol Rev 65:1–43

Viëtor RJ, Voragen AGJ, Angelino SAGF, Pilnik W (1991) Non-starch polysaccharides in barley and malt: a mass balance of flour fractionation. J Cereal Sci 14:73–83 . https://doi.org/https://doi.org/10.1016/S0733-5210(09)80019-2

Xu H, Li B, Mu X (2016) Review of Alkali-Based Pretreatment To Enhance Enzymatic Saccharification for Lignocellulosic Biomass Conversion. Ind Eng Chem Res 55:8691–8705 . https://doi.org/10.1021/acs.iecr.6b01907

Yang H, Ichinose H, Yoshida M, Nakajima M, Kobayashi H, Kaneko S (2006) Characterization of a thermostable endo-β-1, 4-D-galactanase from the hyperthermophile Thermotoga maritima. Biosci Biotechnol Biochem 70:538–541. https://doi.org/10.1271/bbb.70.538

Yeoman CJ, Han Y, Dodd D, Schroeder CM, Mackie RI, Cann IK (2010) Chapter 1 - Thermostable Enzymes as Biocatalysts in the Biofuel Industry. In: Advances in Applied Microbiology. Academic Press, pp 1–55

Yernool DA, McCarthy JK, Eveleigh DE, Bok JD (2000) Cloning and Characterization of the Glucooligosaccharide Catabolic Pathway β-Glucan Glucohydrolase and Cellobiose Phosphorylase in the Marine HyperthermophileThermotoga neapolitana J Bacteriol 182:5172 LP – 5179 . https://doi.org/10.1128/JB.182.18.5172-5179.2000

York WS, Qin Q, Rose JKC (2004) Proteinaceous inhibitors of endo-β-glucanases. Biochim Biophys Acta (BBA)-Proteins Proteomics 1696:223–233. https://doi.org/10.1016/j.bbapap.2003.07.003

Zhao Y, Wu B, Yan B, Gao P (2004) Mechanism of cellobiose inhibition in cellulose hydrolysis by cellobiohydrolase. Sci China Ser C Life Sci 47:18–24 . https://doi.org/10.1360/02yc0163

Zheng Y, Zhao J, Xu F, Li Y (2014) Pretreatment of lignocellulosic biomass for enhanced biogas production. Prog Energy Combust Sci 42:35–53 . https://doi.org/https://doi.org/10.1016/j.pecs.2014.01.001

Zverlov V, Piotukh K, Dakhova O, Velikodvorskaya G, Borriss R (1996) The multidomain xylanase A of the hyperthermophilic bacterium Thermotoga neapolitana is extremely thermoresistant. Appl Microbiol Biotechnol 45:245–247 . https://doi.org/10.1007/s002530050678

CHAPTER 13
Appendix: Expression of a Hyperthermophilic Cellobiohydrolase in Transgenic *Nicotiana tabacum* by Protein Storage Vacuole Targeting

This paper was published in December 2020:

Benedetti, M.; Vecchi, V.; Guardini, Z.; Dall'Osto, L.; Bassi, R. Expression of a Hyperthermophilic Cellobiohydrolase in Transgenic *Nicotiana tabacum* by Protein Storage Vacuole Targeting. *Plants* 2020, *9*, 1799.

Abstract: Plant expression of microbial Cell Wall Degrading Enzymes (CWDEs) is a valuable strategy to produce industrial enzymes at affordable cost. Unfortunately, the constitutive expression of CWDEs may affect plant fitness to variable extents, including developmental alterations, sterility and even lethality. In order to explore novel strategies for expressing CWDEs in crops, the cellobiohydrolase CBM3GH5, from the hyperthermophilic bacterium *Caldicellulosiruptor saccharolyticus*, was constitutively expressed in *N. tabacum* by targeting the enzyme both to the apoplast and to the protein storage vacuole. The apoplast targeting failed to isolate plants expressing the recombinant enzyme despite a large number of transformants being screened. On the opposite side, the targeting of the cellobiohydrolase to the protein storage vacuole led to several transgenic lines expressing CBM3GH5, with an enzyme yield of up to 0.08 mg g DW^{-1} (1.67 Units g DW^{-1}) in the mature leaf tissue. The analysis of CBM3GH5 activity revealed that the enzyme accumulated in different plant organs in a developmental-dependent manner, with the highest abundance in mature leaves and roots, followed by seeds, stems and leaf ribs. Notably, both leaves and stems from transgenic plants were characterized by an improved temperature-dependent saccharification profile.

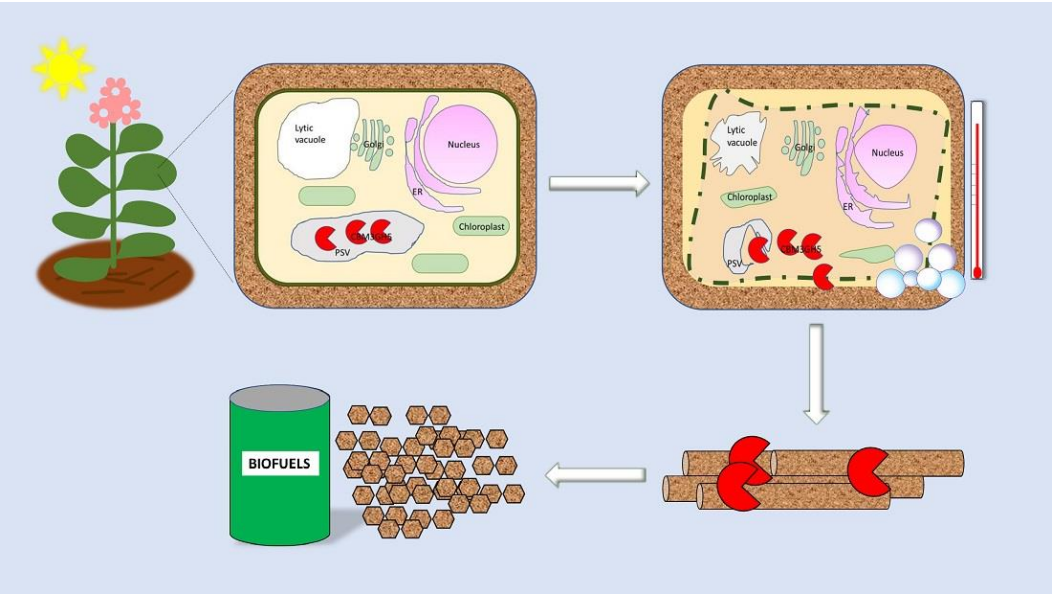

Figure 13.1. Graphical abstract

13.1 Introduction

In recent years, the request for sustainable fuels has promoted research toward the use of plant biomass, an abundant source of renewable energy, for production of biofuels. Biological conversion into fermentable sugars requires production of large amounts of microbial Cell Wall Degrading Enzymes (CWDEs), whose expression in planta might provide a low-cost production platform together with a direct contact with their natural substrates—i.e., plant cell wall polysaccharides. The in muro targeting of CWDEs does enhance the hydrolysis of cell wall polysaccharides into fermentable sugars (Li et al. 2014) and yet often leads to undesired side effects (Benedetti et al. 2019a). Indeed, CWDEs are produced by phytopathogens to dismantle the cell wall integrity, thus supporting the infection process (Kubicek et al. 2014) and providing carbon sources for the microbe (Lagaert et al. 2009). Conversely, plants evolved a system of plant pattern-recognition receptors (PPRRs) to promptly perceive CWDEs secreted by pathogens—e.g., by sensing the products of their activity (Damage Associated Molecular Patterns, DAMPs) (Boudart et al. 2003; Benedetti et al. 2015; de Azevedo Souza et al. 2017) or by recognizing specific epitopes in CWDEs (Poinssot et al. 2003; Ma et al. 2015) such as Microbe Associated Molecular Patterns (MAMPs) (Choi and Klessig 2016). For example, a number of endo-xylanases characterized by the glycoside-hydrolase domain GH11 (see http://www.cazy.org/Glycoside-Hydrolases.html for further details on glycoside-hydrolase (GH) families) triggered an activity-independent immune response in plants, through recognition of a conserved 25-residue peptide (Frías et al. 2019). Such events mainly occur at the apoplast/outer membrane interface, where PPRRs are located (Zipfel 2014). Even though the defence responses protect plants against microbial infections, a hyperactivation of immunity response negatively impacts the plant development, likely due to the growth–defence trade-off (Benedetti et al. 2015; Benedetti et al. 2018). Therefore, the uncontrolled in planta expression of CWDEs may result into developmental alterations and reduced productivity (Capodicasa et al. 2004). The constitutive expression of cellulases in *N. tabacum* resulted in a wide range of enzyme yields and plant phenotypes, depending on (i) the expression strategy adopted, (ii) the substrate specificity and (iii) the catalytic domain of the expressed enzyme (Dai et al. 1999; Ziegelhoffer et al. 1999; Harrison et al. 2011; Petersen and Bock 2011; Jin et al. 2011; Castiglia et al. 2016; Giovannoni et al. 2020).

In this work, we explored the possibility of expressing CWDEs in crops by a novel expression strategy. To this aim, the cellobiohydrolase (CBH) portion of cellulosome CelB from the hyperthermophilic bacterium *Caldicellulosiruptor saccharolyticus*, formerly known as CBM3GH5 (Park et al. 2011), was constitutively expressed in *N. tabacum* by targeting the enzyme to the protein storage vacuole (PSV) which is an organelle developed ad hoc for protein storage (Jiang et al. 2001). In plant cells, PSVs and lytic vacuoles (LVs) are distinct organelles which are served by distinct transport vesicles. Accordingly, their membranes are marked by the presence of distinct tonoplast intrinsic proteins (Hinz 1999) with both storage and defence proteins stably accumulating in PSVs at high levels. Interestingly, the C-terminal Pro-Peptide (CTPP) of Chitinase 1 from *N. tabacum* (NtChitinase1), a protein involved in plant defence against fungi (Neuhaus et al. 1991a), was shown to be sufficient for efficient redirecting an apoplast-targeted protein to the PSV (Neuhaus et al. 1991b; Claude et al. 2005). Therefore, the CTTP sorting signal from NtChitinase1 was fused to the sequence encoding the highly thermostable CBM3GH5 and transformed into tobacco in order to generate a transgenic plant in which the transgenic enzyme activity was controlled by both the cell compartmentalization and the

temperature. The effect of this transgenesis strategy was compared to that of expressing CBM3GH5 with a target signal to the apoplast as for enzyme yield and the impact on the plant fitness.

13.2. Results

Design and Transient Expression of CBM3GH5-HA and CBM3GH5-HA-VAC in N. tabacum

In order to target the recombinant protein to the PSV, the CBH portion of cellulosome CelB from *Caldicellulosiruptor saccharolyticus*, previously known as CBM3GH5 (Park et al. 2011), was codon-optimized for the nuclear expression in *N. tabacum* and fused at the C-terminus to the sequence encoding the HA-epitope (-YPYDVPDYA--) and the C-terminal Pro-Peptide of Chitinase 1 from *N. tabacum* (--GNGLLVDTM) (Neuhaus et al. 1991b; Claude et al. 2005; Stigliano et al. 2014). Additionally, the protein CBM3GH5 was capped with the sequence encoding the signal peptide of PGIP2 from *Phaseolus vulgaris* (MTQFNIPVTMSSSLSIILVILVSLRTALSE-) for targeting the enzyme to the apoplast (Capodicasa et al. 2004; D'Ovidio et al. 2004; Benedetti et al. 2015) since the entry in the secretory pathway is required for an efficient vacuole sorting (Neuhaus et al. 1991b; Park et al. 2004); the CBM3GH5-encoding sequence devoid of the C-terminal Pro-Peptide was used to redirect the enzyme to the apoplast (Figure 13.2 A). Vacuolar and apoplastic versions of CBM3GH5 were named as CBM3GH5-HA-VAC and CBM3GH5-HA, respectively. The entire gene sequences used to generate the fusion proteins CBM3GH5-HA-VAC and CBM3GH5-HA are reported in Data S13.1. Expression of CBM3GH5 was performed in *N. tabacum* as an example of crop plant whose scraps can be used in the bioethanol industry. At the beginning, transient expression in *N. tabacum* was employed to validate the functioning of both the constructs. At 2 days post-infiltration (2 dpi), CMB3GH5-HA-VAC was detected in leaves by immuno-decoration analysis. CBM3GH5-HA-VAC was efficiently extracted from leaf tissue by using heat (70 °C) and a Tween 20-supplemented buffer (0.4% *v/v*), while NaCl-supplemented buffer (0.8 M) failed at extracting CBM3GH5-HA-VAC (Figure 13.2 B). CBM3GH5-HA-VAC was detected as a doublet at molecular weight around 90 kDa in SDS-PAGE gels. Agroinfiltration with the empty vector was also performed as a control. Unlike CBM3GH5-HA-VAC, the apoplastic version of CBM3GH5 was extracted as a single 90 kDa band by NaCl-supplemented buffer (Figure 13.2 C). In these experiments, the chloroplast-expressed CBM3GH5-HA from *C. reinhardtii* was used as reference (Figure 13.2 C) (Benedetti et al. 2020). Both the CBM3GH5 isoforms expressed in tobacco showed a slightly higher molecular weight than the recombinant enzyme from *C. reinhardtii*, suggesting either an event of glycosylation or a partially processed protein. Since the chloroplast translational machinery cannot introduce glycosylation, we expect the algal-expressed enzyme is not glycosylated. All these results suggest that CBM3GH5-HA was expressed as secreted protein, while CBM3GH5-HA-VAC was retained in the cell since the combined use of nondenaturing detergent and heat was required for efficient extraction. Activity assays carried out on the leaf extracts confirmed the presence of the enzyme in the same samples which were shown to contain cross-reactivity towards the α-HA probe: the enzymatic activity was proportional to the relative abundance of the immunotitration signals (Figure 13.2 C).

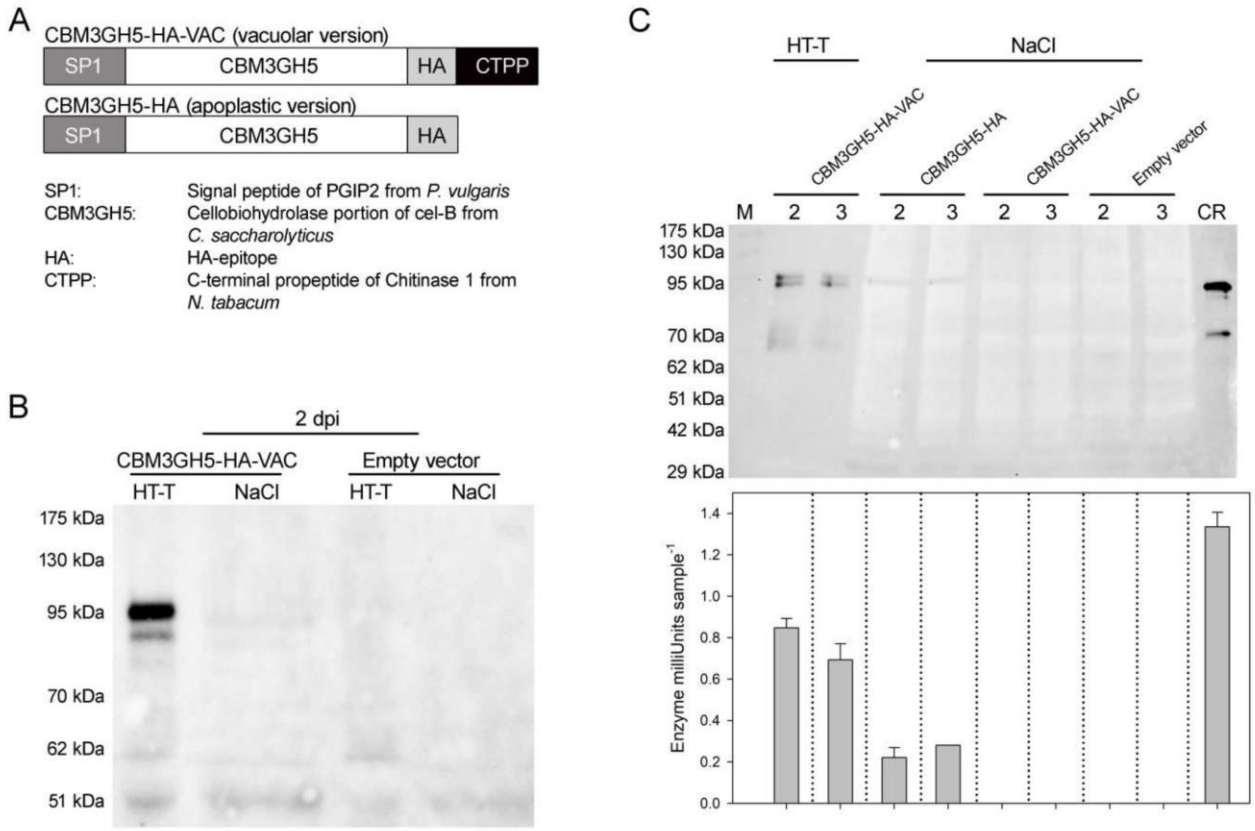

Figure 13.2 Transient expression of CBM3GH5 in *Nicotiana tabacum*. (A) Schematic representation of the vacuolar and apoplast version of CBM3GH5, referred to as CBM3GH5-HA-VAC and CBM3GH5-HA, respectively. Expected molecular weights: 80 kDa. (B) Immuno-decoration analysis of leaf extracts from CBM3GH5-HA-VAC-agroinfiltrated plants, using α-HA as primary antibody. Extraction was performed 2 days post-agro-infiltration (dpi) using a Tween 20-supplemented buffer plus heat (HT-T) or a NaCl-supplemented buffer (NaCl). Agroinfiltration with the empty vector was used as negative control. (C) (Upper panel) α-HA immuno-decoration analysis of leaf extracts from agroinfiltrated leaves. Extraction was performed two and three days post-agro-infiltration (2, 3) using the same buffers described in (B). In total, 70 ng of recombinant CBM3GH5-HA from *C. reinhardtii* (CR) was used as reference. (Lower panel) Activity of CBM3GH5 in the same extracts, determined by activity assay and expressed as Enzyme milliUnits (nmol reducing ends released from carboxy-methylcellulose (CMC) min^{-1}) per sample.

Stable Expression of CBM3GH5-HA and CBM3GH5-HA-VAC in N. tabacum

Agrobacterium-mediated transformation of leaf tissue was used to generate stable tobacco plants constitutively expressing CBM3GH5-HA and CBM3GH5-HA-VAC. As revealed by transformation efficiency analysis, the isolation of transgenic lines constitutively expressing CBM3GH5-HA was not possible (Figure 13.3 A). Although the presence of the transgene in the genome was confirmed by PCR in the regenerated plants (Figure S13.1), both gene expression and enzyme activity were not detected in such lines (data not shown), thus suggesting gene-silencing events in the antibiotic-resistant plants (Eamens et al. 2008). This result is consistent with the evidence (Capodicasa et al. 2004; Benedetti et al. 2015) that apoplastic accumulation of CWDEs may compromise plant development, since the cell wall fragments derived from the residual hydrolytic activity (Aziz et al. 2007; Ferrari et al. 2013; de Azevedo Souza et al. 2017) as well as CWDEs themselves behave as powerful elicitors of plant defence (Lee and West 1981; Ma 2008; Ma et al. 2015). It is worth noting that such recognition events occur in the apoplast—namely, the compartment to which CBM3GH5-

HA was targeted (Choi and Klessig 2016). Instead, five independent T1 CBM3GH5-HA-VAC-expressing plants were successfully identified by the activity assay performed on 1-month-old transgenic plants (Figure 13.3 B). This result is consistent with CBM3GH5-HA-VAC being retained in the symplast, thus avoiding the detrimental effect that CBM3GH5 exerted in the apoplast. The ratio of nondenaturing extraction buffer per gram of fresh weight (FW) leaf tissue was optimized, and (2 mL extraction buffer: 1 g FW leaf) was selected as the ratio which allows the highest CBM3GH5-HA-VAC recovery yield (Figure 13.3 C). The five independent expressing transformants were grown for seed production and stable plant selection. After segregation analysis, CBM3GH5-HA-VAC#4 and #6 were identified as 3:1 segregating lines. Activity assay performed on 1-month-old T2 CBM3GH5-HA-VAC#4 plants revealed that the enzyme content ranged from 0.4 to 0.7 U g DW^{-1}, thus suggesting the homozygous condition increased the CBH content (Figure 13.3 D). CBM3GH5-HA-VAC#4-11 and #6-7 were selected as two independent single-insertion homozygous lines and used for subsequent characterization.

A

CONSTRUCT	Nr. ROUNDS TRANSFORMATION (50 leaf disks transformation^{-1})	Nr. CALLI	Nr. ROOTED CALLI	T1 PLANTS WITH ACTIVITY
CBM3GH5-HA	4	87	9	0 *
CBM3GH5-HA-VAC	1	21	7	5 *
EMPTY VECTOR	1	18	14	n/a

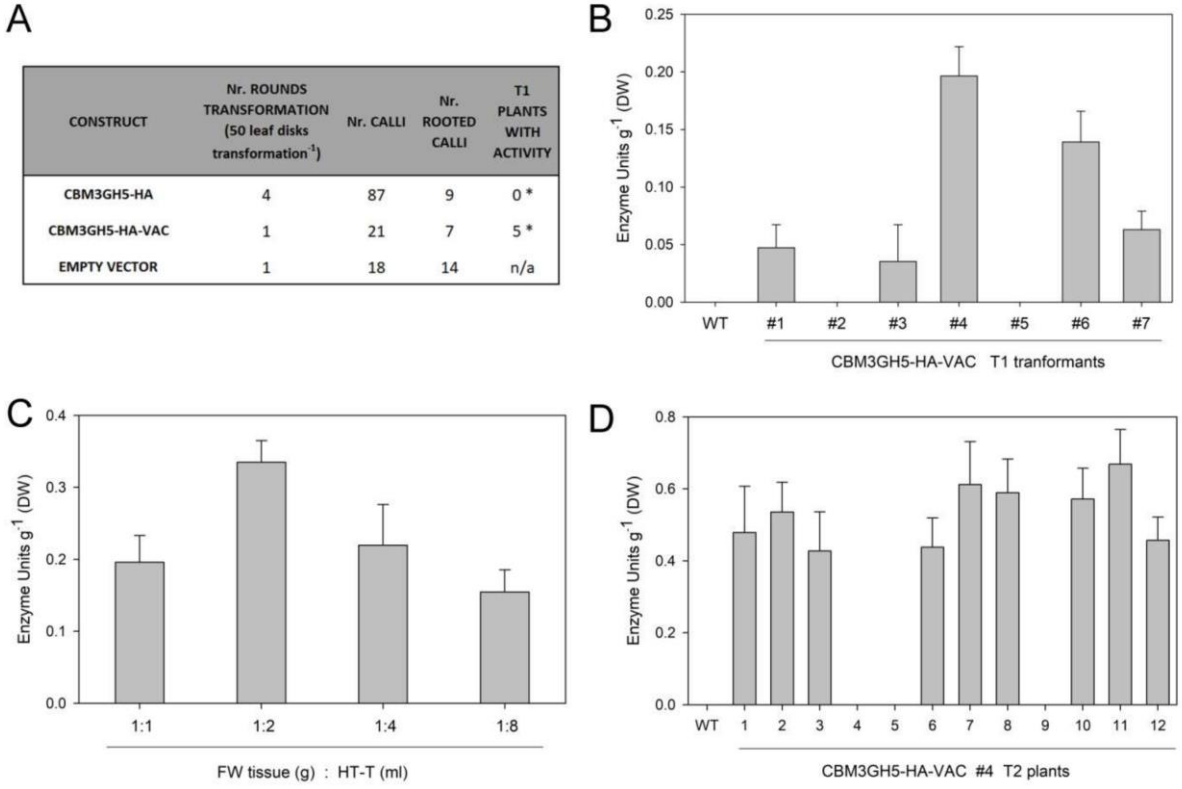

Figure 13.3 Stable transformation of CBM3GH5 in *Nicotiana tabacum*. (A) Comparison of the transformation efficiency of different constructs on Agrobacterium-mediated *N. tabacum* transformation. Numbers of regenerated plants and activity in T1 transformants are reported. The association between groups (N rooted calli and T1 plants with activity) and the CBM3GH5 version is statistically significant according to Fischer's exact test (* p value < 0.05). n/a, not available. (B) Activity of CBM3GH5 in leaf extract from 30-day-old T1 CBM3GH5-HA-VAC plants, as determined by activity assay. (C) Activity of CBM3GH5 in leaf extracts from 30-day-old T1 CBM3GH5-HA-VAC#4 using different ratios of Tween 20-supplemented buffer per gram of tissue. (D) Activity of CBM3GH5 in leaf extract from 30-day-old T2 CBM3GH5-HA-VAC#4 plants as determined by activity assay. Enzyme activity is expressed as Enzyme Units (µmol reducing ends released from CMC min−1) per gram dry weight (DW) leaf.

Spatial and Temporal Accumulation Pattern of CBM3GH5-HA-VAC in Transgenic Plants

CBM3GH5-HA-VAC-expressing plants grew without morphological defects or significant loss in biomass with respect to the control genotype, thus implying that PSV expression of CBM3GH5 did not affect plant development (Figure 13.4 A). Gene expression and enzyme activity analyses were performed on leaves L5–L10 from 55-day-old CBM3GH5-HA-VAC #4-11 and #6-7 transgenic plants (Figure 13.4 A). Both gene expression (Figure 13.4 B) and enzymatic activity (Figure 13.4 C) were higher in the #4-11 than in #6-7 transgenic line, in accordance with the previous result (Figure 2B) with line #4-11, showing 45% higher activity with respect to #6-7 plant (Figure 13.4 C). Therefore, CBM3GH5-HA-VAC #4-11 plant was used to investigate the spatial and temporal distribution of CBM3GH5-HA-VAC during plant development. The expression of a transgene under control of the constitutive 35S promoter is expected to be homogeneous through the different plant tissues. Indeed, tracking the constitutive expression of the Green Fluorescent Protein (GFP) in transgenic tobacco revealed that GFP was uniformly distributed in all the organs, with slightly higher abundance in vascular tissue, whereas it was absent in seeds (Hraška et al. 2008). However, protein targeting to PSV may alter the expected spatial and temporal distribution of a constitutively expressed protein. In order to investigate this point, the activity of CBM3GH5 was measured during plant development. CBM3GH5 activity in leaves reached a maximum level at the preflowering and flowering stages (Figure 13.4 D). The highest activity was observed in the most expanded leaves of each developmental stage, while the activity was lower in young leaves and gradually decreased proceeding from mature to senescent leaf (Figure 13.4 D). Thus, the expression of CBM3GH5-HA-VAC was dependent on a developmental regulation consistent with a previous report for a recombinant protein targeted to the LVs (Harrison et al. 2014). As additional information, the activity of CBM3GH5 was evaluated in different organs of the flowering plant: the higher level of activity was detected in leaves, roots and seeds, while activity was significantly lower in stem and leaf ribs (−60% than leaves, Figure 13.4 E). Therefore, the spatial analysis of cellulolytic activity supported the vacuole sorting of CBM3GH5-HA-VAC, since PSVs have been reported to accumulate in seeds and storage organs such as roots (Herman and Larkins 1999); it is noteworthy that the evaluation of enzymatic activity in the different plant organs suggested a mapping of PSV distribution, pointing to the presence of PSVs in the root apparatus of N. tabacum. Notably, the highest abundance of CBM3GH5 activity per gram of total soluble proteins (TSP) was detected in roots in accordance with the TSP content of seed (200 mg TSP g DW−1), leaf (70 mg TSP g DW−1), stem and root extracts (18 mg TSP g DW−1) (Figure 13.4 F).

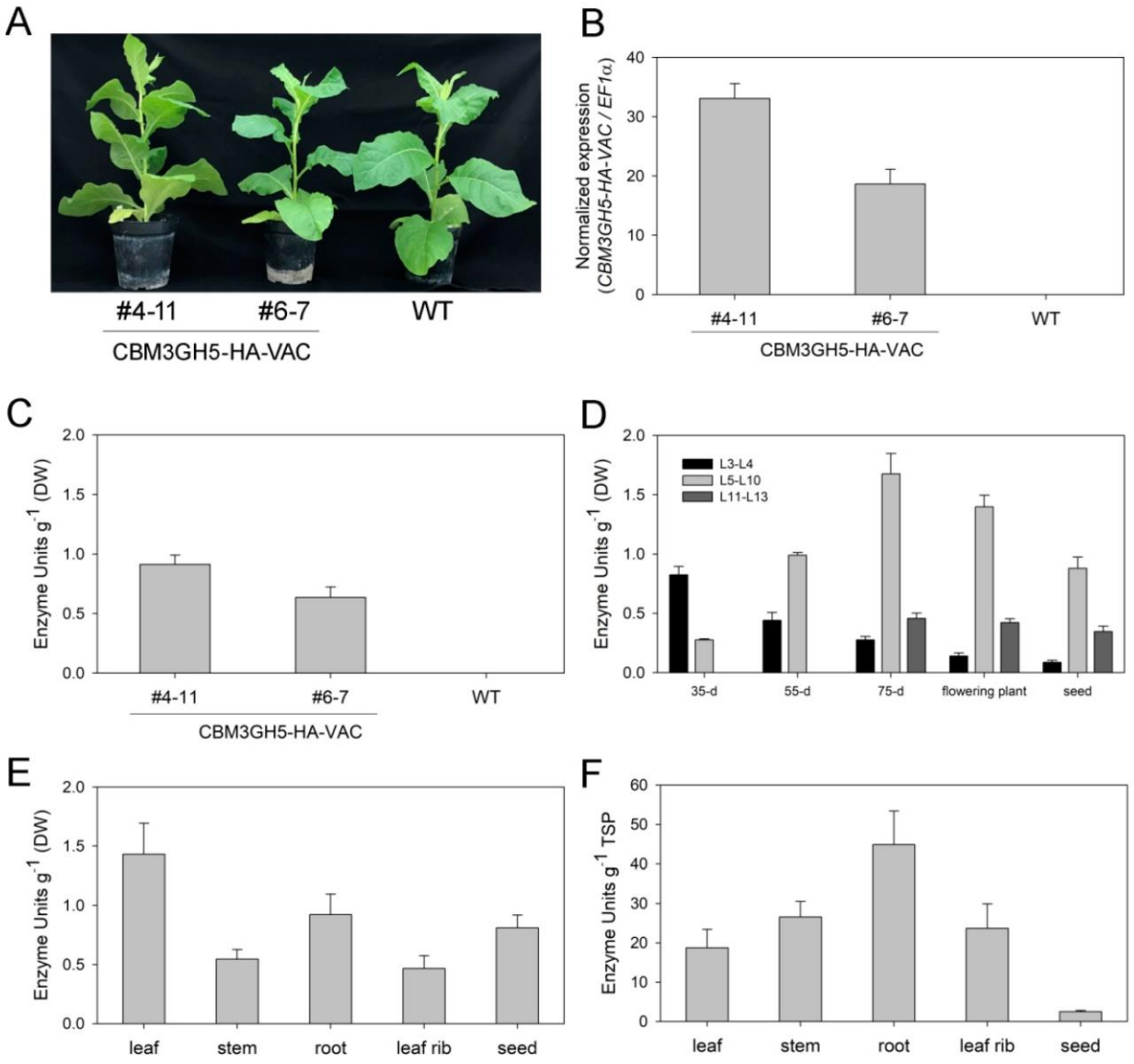

Figure 13.4 Spatial and temporal accumulation of CBM3GH5-HA-VAC in T3 transgenic plants. (A) Representative picture of 55-day-old CBM3GH5-HA-VAC#4-11, CBM3GH5-HA-VAC#6-7 and wild-type (WT) plants. (B,C) Relative expression (B) and activity (C) of CBM3GH5 in leaves (L5–L10) from 55-day-old CBM3GH5-HA-VAC#4-11 and #6-7 plants. (D) Activity of CBM3GH5 in leaf extracts from CBM3GH5-HA-VAC#4-11 at five different developmental stages (35-d: 35-day-old plant, 55-d: 55-day-old plant, 75-d: 75-day-old plant, flowering plant and seed—i.e., plant upon seed maturation). (E,F) Activity of CBM3GH5 in different tissue extracts from flowering CBM3GH5-HA-VAC#4-11 plants (i.e., L5–L10 leaf, stem, root and leaf rib) plus seeds per gram DW (E) and per gram of total soluble proteins (TSP) (F); data are from two independent experiments with consistent results.

Biochemical Characterization of CBM3GH5-HA Purified from the Transgenic Plants

Different from evidence of transient expression (Figure 13.2), CBM3GH5-HA-VAC could not be detected by immuno-decoration analysis in stable transgenic plants (data not shown) despite the enzymatic activity being clearly detectable (Figure 13.3 and Figure 13.4). This evidence could be ascribed to the maturation process of CBM3GH5-HA-VAC upon PSV sorting. We hypothesize an

unpaired cleavage of the C-terminal Pro-Peptide, affecting the integrity of HA-epitope, thus compromising detection by α-HA. In order to further characterize the expression of the recombinant enzyme, we purified CBM3GH5-HA-VAC from mature leaves of transgenic *N. tabacum* and performed a biochemical characterization. Purification was performed by a two-step procedure consisting of a heat-mediated enrichment of the total protein extract (Patchett et al. 1989) followed by an anionic exchange chromatography (AEC) (Park et al. 2011; Benedetti et al. 2020). Extraction was carried out by using both the Tween 20-supplemented buffer and heat, following the optimized conditions of Figure 13.3 C. The elution of CBM3GH5-HA-VAC from AEC was performed by a stepwise NaCl gradient. The activity co-eluted with a single 80 kDa band as revealed by enzymatic assay and SDS-PAGE analysis (Figure 13.5 A,B), thus confirming that CBM3GH5-HA-VAC was expressed in mature tobacco leaves, displaying the same molecular weight of the recombinant CBM3GH5-HA from *C. reinhardtii* (Benedetti et al. 2020) (Figure 13.5 A). The evaluation of specific activity towards 1% carboxy-methylcellulose (CMC) revealed that both plant and microalgal versions of the enzyme showed similar specific activities (Figure 13.5 B); the activities at different temperatures upon prolonged reaction time also revealed similar enzymatic properties of the two enzymes (Figure 13.5 C). Despite both preparations being hyperthermophilic, the enzyme produced in microalgae showed a temperature-dependent peak shifted towards higher temperature by 10 °C. Treatment of the eluted protein from AEC with PNGase A did not alter the electrophoretic mobility, which was the same in the isoforms expressed in plant and in alga (Figure S13.2), thus suggesting the recombinant protein was not modified by *N*-glycosylation. Together, these results suggest that the fusion of SP1 and CTPP at the N- and C-termini of CBM3GH5, respectively, allowed the vacuole compartmentalization of CBH in a non-*N*-glycosylated form.

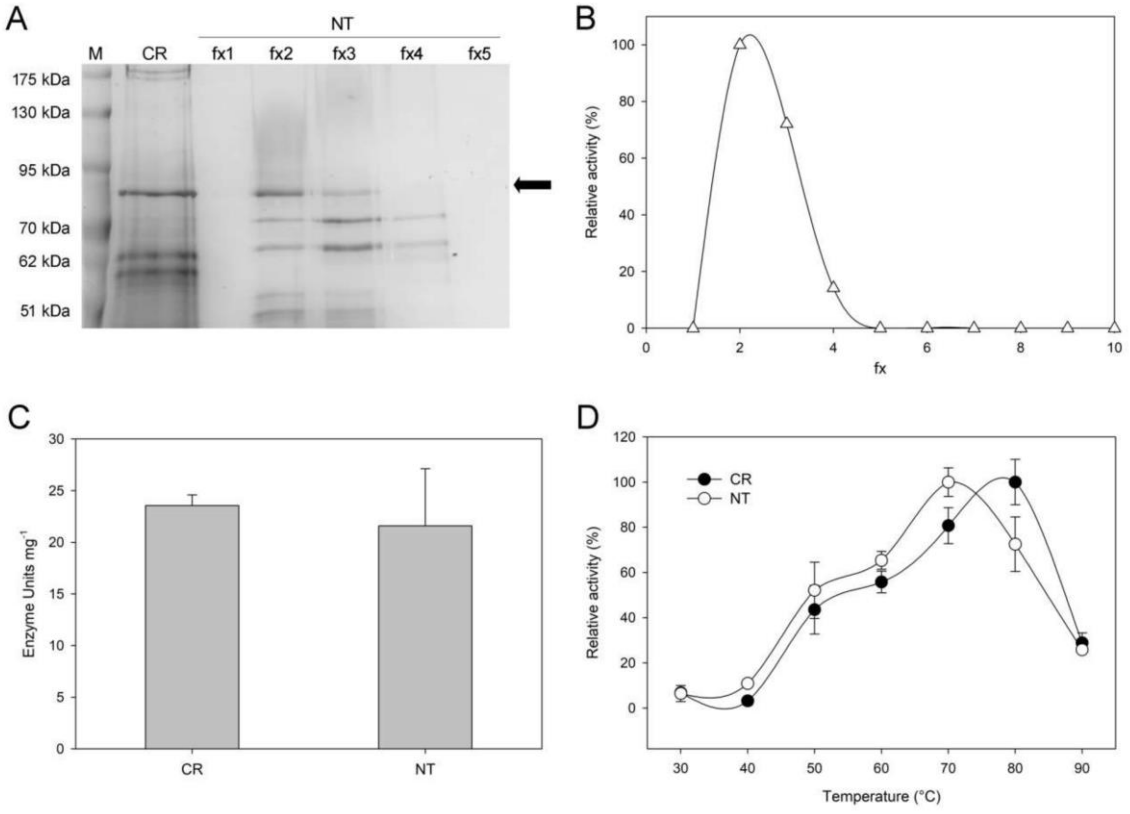

Figure 13.5 Biochemical characterization of CBM3GH5-HA-VAC purified from mature leaves of CBM3GH5-HA-VAC#4-11 plants. (A) SDS-PAGE analysis of fractions (fx) eluted from anionic exchange chromatography (AEC).

Black arrow points to CBM3GH5-HA. Recombinant CBM3GH5-HA from *C. reinhardtii* (CR) was used as reference. (B) Activity of CBM3GH5-HA-VAC in the same fractions (fx) shown in (A), expressed as relative activity (%). (C) Specific activity of CBM3GH5 from *C. reinhardtii* (CR) and *N. tabacum* (NT) towards 1% CMC; specific activity was expressed as Enzyme Units per mg of enzyme (pH 5.5, 75 °C). (D) Relative activity (%) of CBM3GH5 from *N. tabacum* protein storage vacuole (NT) and *C. reinhardtii* chloroplast (CR) towards 1% CMC, after 7 h incubation at different temperatures.

Leaves and Stems from CBM3GH5-HA-VAC-Expressing Plant Showed an Increased Temperature-Dependent Saccharification Yield

Plant expression of CWDEs can be used for generating plants with enhanced saccharification efficiencies. To evaluate if the vacuole accumulation of CBM3GH5 affected the sugar release from *N. tabacum* cell walls, saccharification efficiency was assessed on stems and leaves with the highest enzyme contents (i.e., L5–L10), and expressed as the ratio (%) between solubilized reducing sugars and total sugars in the starting tissue (Lionetti et al. 2010). Determination of total carbohydrates of tobacco leaves and stems confirmed that both wild-type and transgenic plants had the same sugar content (Figure 13.6 A). In the saccharification experiment, the commercial cellulolytic blend Celluclast was supplemented in the incubation medium at mid-high temperature (55 °C), since Celluclast retains ~95% of starting activity after a 1-day incubation at 50 °C (Gama et al. 2015); thus, treatments at 55 °C are a good compromise between the activity of the commercial cellulolytic blend and CBM3GH5 specific activity vs. temperature (Park et al. 2011). The saccharification efficiency of leaf and stem biomass from transgenic lines #4-11 and #6-7 was 13% to 16% (as absolute values) higher than wild-type samples (Figure 13.6 B,C), thus indicating that CBM3GH5 synergistically acted in supporting the cellulolytic activity of the commercial blend. The release of reducing sugars was proportional to the activity of CBM3GH5-HA-VAC as indicated by the increased release in the higher-expressing CBM3GH5-HA-VAC plant—i.e., #4-11; interestingly, the increased enzymatic saccharification of CBM3GH5-HA-VAC line #4-11, with respect to line #6-7, was statistically significant towards stems—i.e., a highly hydrolysis-recalcitrant material (Figure 13.6 C). On the opposite side, at the lower temperature (25 °C), saccharification efficiency of transgenic plants decreased at the same level as wild-type plant (Figure 13.6 D), thus indicating that the release of sugars was temperature-dependent, and suggesting that no major changes in the cell wall architecture occurred in the transgenic lines. As expected from the synergistic action between Celluclast and CBM3GH5, the reducing sugars released from leaf material upon 48 h of incubation were mainly constituted by glucose (i.e., 65–70%)—i.e., the monosaccharide constituting cellulose (Figure S13.3).

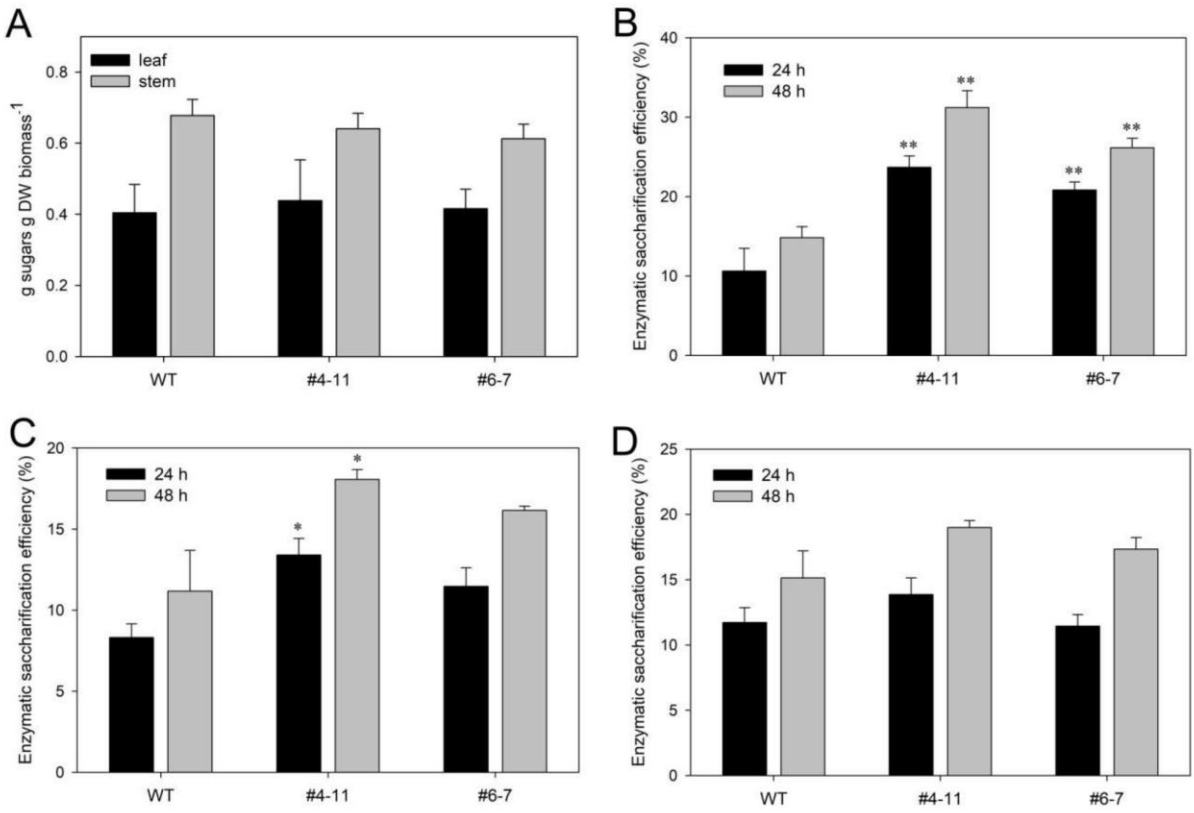

Figure 13.6 CBM3GH5-HA-VAC plants showed an increased temperature-dependent saccharification efficiency. (A) Sugars released upon acid-hydrolysis of leaf (black bar) and stem (grey bar) material from wild-type and transgenic CBM3GH5-HA-VAC plants, as determined by phenol–sulfuric acid assay. (B,C) Saccharification efficiency of leaf (B) and stem (C) material from CBM3GH5-HA-VAC#4-11, CBM3GH5-HA-VAC#6-7 and WT plants after 24 (black bar) and 48 (grey bar) hours of incubation with 1% Celluclast at 55 °C. (D) Saccharification efficiency of leaf material from CBM3GH5HAVAC#4-11, CBM3GH5HAVAC#6-7 and WT plants after 24 (black bar) and 48 (grey bar) hours of incubation with 1% Celluclast at 25 °C. Data are expressed as mean ± SD (N ≥ 3). Asterisks indicate statistically significant difference against control (WT) according to Student's t test (* $p < 0.05$; ** $p < 0.01$).

13.3 Discussion

Plant cell wall structures can be successfully altered by using focused transgenic-based strategies for increasing the saccharification efficiency of plant biomass: alterations in cell wall structures may be achieved by either modifying the level of endogenous enzymes involved in the metabolism of plant cell wall polysaccharides or accumulating recombinant CWDEs into the apoplast. The outcome of such strategies is not easily predictable, resulting in a wide range of different plant phenotypes. For example, transgenic plants with altered pectin structures or with altered hemicellulose and lignin contents (Bindschedler et al. 2007; Weng et al. 2008) resulted in higher enzymatic saccharification, as expected by the more relaxed cell wall matrix which favored the accessibility of cellulolytic enzymes to cellulose fibers (Lionetti et al. 2010); however, the alteration of cell wall structures resulted in altered phenotypes and morphological defects (Capodicasa et al. 2004). In other cases, the altered expression of endogenous enzymes of cell wall synthesis resulted in both higher saccharification and biomass productivity, as observed by downregulating the expression of the galacturonosyl-transferase 4 (*GAUT4*)-encoding gene in switchgrass and poplar (Biswal et al. 2018). Biological

conversion by CWDEs is limited by high costs and low efficiency, and should be compared to chemical methods which are harmful for the environment. The cost-effectiveness of microbial CWDEs and Cell Wall Modifying Enzymes (CWMEs) produced in transgenic plants depends on enzymatic activity and level of accumulation in the plant tissue; however, avoiding growth defects related to the CWDE carbohydrate-degrading activity remains a major challenge. In order to circumvent such undesired phenotypes, plant expression of CWDEs can be controlled by ad hoc expression strategies (Benedetti et al. 2019a; Giovannoni et al. 2020). In this regard, compartmentalized expression was attempted to selectively accumulate CWDEs in organelles such as chloroplasts (Petersen and Bock 2011; Castiglia et al. 2016) , LVs (Harrison et al. 2011) or in the cytoplasm (Dai et al. 1999; Ziegelhoffer et al. 1999), thus avoiding the interaction with the cell wall polysaccharides and PPRRs. It is worth noting that N- and O-linked glycosylation can be critical for stability of certain fungal cellulases (Greene et al. 2015), and since these post-translation modifications mainly occur in endoplasmic reticulum (ER) and Golgi apparatus, they cannot be operated on plastid-expressed enzymes. Although delivery of recombinant proteins to LVs was successfully achieved (Marin Viegas et al. 2017), vacuole sorting of CWDEs was dependent on the development of LVs in each plant tissue (Harrison et al. 2014). Control of CWDE-encoding gene expression was attempted by using synthetic promoters induced by ethanol (Klose et al. 2013) and β-estradiol (Zuo et al. 2000) or by endogenous pathogen-induced (e.g., *PR1* (At2g14610), *RetOx* (AT1G26380)) (Benedetti et al. 2015) and senescence-induced promoters (e.g., *SAG12* (AT5G45890)) (Tomassetti et al. 2015). However, endogenous promoters are often affected by transcriptional leakiness (Benedetti et al. 2015) or are not ideal for supporting a robust transgene expression (Tomassetti et al. 2015). Last but not least, by expressing enzyme isoforms with high (>70 °C) temperature-dependent activities, such as those from hyperthermophiles, the activity of CWDEs can be quenched during plant development (Mir et al. 2014; Mir et al. 2017).

In our study, the thermostable cellobiohydrolase CBM3GH5 was expressed in transgenic *N. tabacum* plants by targeting the enzyme to the PSV. When developing a technology for engineering plants producing CWDEs, the choice of a highly thermostable CBH has several advantages: (i) the low activity of CBM3GH5 at the growth-temperature of *N. tabacum* should prevent side-effects on plant health, in the event PSV sorting may suffer for leakiness; (ii) the heat treatment can promote both the release of the enzyme from PSV as well as the relaxation of the polysaccharide matrix, further increasing hydrolyzation efficiencies (Sarmiento et al. 2015); (iii) the temperature-dependent activity of CBH can be used to pinpoint the enzyme in the different organs during plant development. The latter point is crucial having been the first attempt, to our knowledge, of targeting a recombinant protein to PSV in a crop species; (iv) CBHs, together with β-glucosidases, are key-enzymes for the degradation of cellulose (Benedetti et al. 2019a; Giovannoni et al. 2020). In this regard, the presence of carbohydrate binding module (CBM) in CBM3GH5 was expected to enhance the hydrolysis of crystalline cellulose (Poole et al. 1992; Carrard et al. 2000).

In order to pursue this issue, CBM3GH5 was overexpressed by either apoplast or PSV targeting, and the effects of the two different strategies were investigated. Surprisingly, we failed to isolate stable transgenic lines expressing the apoplastic version of CBM3GH5, although the transient expression analysis confirmed the apoplast-targeted enzyme was efficiently translated (Figure 13.2 C). The lack of stable CBM3GH5-expressing transformants was statistically significant, pointing to the apoplastic localization of the hydrolase as a negative selection trait in tobacco plants (Figure 13.3 A). This result

was unexpected since the hyperthermophilic nature of CBM3GH5 should, in principle, prevent any cellulolytic activity at the growth temperature of tobacco, thus preserving plant fitness. To explain the potential "lethal" phenotype, it seems conceivable that in muro CBM3GH5 expression exerts its deleterious effects by a residual hydrolyzing activity at greenhouse temperature (Figure 13.5 D). Alternatively, the recombinant enzyme could be recognized as a MAMP by tobacco PPRR, thus affecting plant development. According to this hypothesis, expression of GH5 cellulases resulted in plants with morphological defects or with low cellulolytic activities, despite the enzymes being compartmentalized or endowed with a temperature-inducible activity (Castiglia et al. 2016; Faè et al. 2017; Benedetti et al. 2020). Alternatively, the lack of stable transformants accumulating CBM3GH5 in the apoplast could be a consequence of a reduced stability of CBM3GH5-HA with respect to CBM3GH5-HA-VAC. Such reduced stability may be ascribed to endogenous proteolysis, which is expected to lack in ad hoc compartment evolved to store proteins—i.e., the PSV. Additionally, unwanted glycosylation may affect enzyme stability; indeed, opposite to that expected for the apoplastic isoform, CBM3GH5-HA-VAC was expressed in a nonglycosylated form, which appears favorable since unnecessary glycosylation could impair the stability of bacterial enzymes (Figure 13.5 A and Figure S13.2). Based on the specific activity of tobacco-expressed CBM3GH5-HA-VAC, the yield of the enzyme in PSV was about 0.08 mg g^{-1} DW in the mature leaves of *N. tabacum* (see figure 13.4 D and Figure 13.5 B: yield calculated as (1.67 U g DW^{-1})/(21.59 U mg^{-1})) whereas the percentage abundance ranged from 0.09% to 0.2% of TSP in leaf and root tissues, respectively (see Figure 13.4 F—i.e., percentage abundance in leaf extract calculated as (18.7 U g TSP^{-1})/(21,590 U g^{-1}) × 100%; percentage abundance in root extract calculated as (44.8 U g TSP^{-1})/(21,590 U g^{-1}) × 100%). As observed for expression in LVs, the plant developmental stage is crucial for accumulation of CBM3GH5-HA-VAC (Harrison et al. 2014): the highest level was detected in the most expanded leaves of the preflowering and flowering stages while a 50–80% reduction was measured in senescent leaves (Figure 13.4 D). Interestingly, a relevant activity of CBM3GH5 was also detected in roots and seeds, indicating PSV sorting as an additional tool for accumulating recombinant proteins in bulb-plants and seeds (Figure 13.4 E,F).

Notably, PSV sorting of CBM3GH5 resulted in transgenic plants with an improved saccharification efficiency of both leaves and stems, which (i) was proportional to the expression level of CBM3GH5 (Figure 13.6 B,C), and (ii) increased in transgenic plants in a temperature-dependent manner (Figure 13.6 D), thus confirming the involvement of CBM3GH5. However, the improved saccharification yield is still too low to sustain biofuel production in a cost-effective manner; therefore, further optimizations will be required to support progress toward biofuel from plants. For example, the use of a highly thermostable CWDE blend is likely to further improve the saccharification efficiency, as suggested by the observation that biomass treatment at 70–75 °C boosted the activity of CBM3GH5 up to 40% (Figure 13.5 D) (Benedetti et al. 2019b). Other strategies aimed at improving the enzyme yield of CBM3GH5 may include the use of tissue-specific and age-regulated promoters to drive the expression of PSV-targeted CWDE—i.e., by maximizing the amount of CBM3GH5 in PSVs at the desired developmental stage. Moreover, in order to explain the low yield of recombinant CBM3GH5-HA-VAC, the yield analysis of other categories of PSV-targeted CWDEs is necessary to exclude the possibility that CBM3GH5 was a particularly problematic enzyme to produce in tobacco. Lastly, opposite to the apoplastic targeting of CBM3GH5, the compartmentalized accumulation of CBM3GH5 into PSVs allowed the isolation of stable expressing plants, pointing to the PSV targeting-based technology as a valuable option when other expression strategies are not effective.

13.4. Materials and Methods

Synthesis In Vitro and Cloning of the Gene Encoding CBM3GH5

The cellobiohydrolase portion of CelB from *C. saccharolyticus,* formerly known as CBM3GH5 (UniprotKB: P10474, aa 380-1039) (Park et al. 2011), was reverse-translated into the codon-optimized sequence for nuclear expression in *N. tabacum* by using the software OPTIMIZER (http://genomes.urv.es/OPTIMIZER/) (Puigbò et al. 2007). The codon-optimized sequence encoding the signal peptide (SP1) of Polygalacturonase-Inhibiting Protein 2 from *Phaseolus vulgaris* (MTQFNIPVTMSSSLSIILVILVSLRTALSE) and the sequences encoding the HA-epitope (underlined amino acids) and the C-terminal Pro-Peptide of Chitinase 1 (CTPP) from *N. tabacum* (YPYDVPDYAGNGLLVDTM) were added in frame to the 5^{I} and 3^{I} ends of CBM3GH5-encoding sequence, respectively. The sequences encoding the restriction sites XbaI and SacI were added at the 5^{I} and 3^{I} ends of the sequence. The entire sequence was synthesized by GeneArt (Life Technologies, Regensburg, Germania) (Data S13.1). The synthetic gene was cloned downstream of the 35S promoter into the binary vector pBI121 (Clonetech) using the restriction sites XbaI and SacI. For the apoplastic CBM3GH5-HA version, the same sequence was readapted by PCR amplification using the primers Apo Fw and Apo Rv (Table S13.1), in order to eliminate the sequence encoding the CTPP (Data S13.1), and then cloned in the same vector by using the same restriction sites. *E. coli* strain XL10gold (Agilent Technologies) was transformed with these constructs and used for plasmid propagation. Sequencing of the genes was performed in order to exclude the presence of undesired mutations using the primers Apo Fw, CBH785 Fw, CBH1565 Fw and CBH240 Rv (Table S13.1). The CBM3GH5-HA was heterologously expressed in the *C. reinhardtii* chloroplast as reported in (Benedetti et al. 2020).

Transient and Stable Expression of CBM3GH5 in N. tabacum by Agrobacterium-Mediated Transformation

A. tumefaciens GV3101 and *N. tabacum* cv. Petit Havana SR1, here referred as wild type (WT), were used to generate transgenic tobacco plants. The pBI121 binary vector containing the synthetic gene was introduced into *Agrobacterium tumefaciens* strain GV3101 by electroporation. For transient expression, agroinfiltration was performed according to (Yang et al. 2000) with some modifications. Bacterial suspension in infiltration buffer (10 mM MES, 10 mM $MgCl_2$, 100 µM acetosyringone, pH 5.6) at a final Abs_{600} of 0.8 was used for syringe infiltration of 6-week-old *N. tabacum* plants. Three leaves were infiltrated for each plant and for each construct. Protein extraction was performed from infiltrated leaves at 2- and 3-days post-infiltration (dpi). Stable transformation of *N. tabacum* was carried out by co-cultivating *Agrobacterium* and tobacco leaf disks according to (Horsch et al. 1985; Rogers et al. 1986); about 50 leaf disks were used for each transformation cycle. Selection of transformants was performed using the appropriate concentration of plant hormones and kanamycin (150 µg mL^{-1}) as selection marker. Carbenicillin (250 µg mL^{-1}) and cefotaxime (250 µg mL^{-1}) were added to selective medium in order to eliminate residual *Agrobacterium* cells upon the co-cultivation step.

Growth and Selection of Transgenic Tobacco Plants

Regenerated plants were transferred to a mist bed for a week before being moved to a bench in the greenhouse. When plants reached 15 cm in height, they were moved to 2 gal containers (7.6 L) to allow for further growth until reaching maturity. Regenerated plants were screened by PCR and subsequently by an activity assay. T1 plants that showed to be positive from the activity assay were grown until maturation and their seeds were harvested. About 100 seeds from each T1 transformant were surface-sterilized and plated on MS medium containing kanamycin as selective agent for segregation analysis. About 10–15 T2 plants from 2 independent 3:1 segregating lines (i.e., CBM3GH5-HA-VAC#4 and #6) were grown and used for further characterization.

Immuno-Decoration Analysis and Activity Assay Using Protein Extract from Transgenic Tobacco Plants

Protein extraction was performed by using Tween 20- and NaCl-supplemented buffers. Tween 20-supplemented buffer: 20 mM Na Citrate pH 5.5, 0.5% Tween 20. NaCl-supplemented buffer: 20 mM Na Citrate pH 5.5, NaCl 0.8 M. Leaves, stems, roots and seeds from transgenic plants or agroinfiltrated leaves were homogenized in liquid nitrogen and the resulting powders were quickly suspended in the extraction buffer at the ratio (1 mL buffer: 1 g FW grinded tissue). After optimizing the ratio [mL extraction buffer: g FW tissue], the subsequent extractions were performed by using 2 mL Tween 20-supplemented buffer per g FW tissue. Protein extraction by Tween 20-supplemented buffer was carried out by incubating the resuspended sample for 1 h at 70 °C, under gentle shaking, followed by extraction with NaCl-based buffer by incubating the resuspension for 30 min at 4 °C, under gentle shaking. After incubation, the sample was centrifuged at 14,000× *g* 10 min and the supernatant was used for downstream applications. Protein extracts from 10 mg FW of plant materials were either loaded onto SDS-PAGE for immuno-decoration analysis using a primary α-HA antibody (HA7 clone, Sigma-Aldrich) or used for enzymatic assays. Determination of the protein content was performed by Pierce™ BCA Protein Assay Kit (Thermo-Fisher Scientific). For enzymatic assays, the protein extracts (1/10 of the total reaction volume) were incubated in a buffer containing 50 mM Na Acetate pH 5.5 and 1% Azo-CM-Cellulose (Megazyme) as substrate. Alternatively, the protein extracts were dialyzed using Vivaspin 10,000 MWCO PES (Sartorius) and used for enzymatic assays using a buffer containing 50 mM Na Acetate pH 5.5 and 1% CMC (Sigma-Aldritch) as substrate. The conditions for the enzymatic reaction were set at 75 °C and pH 5.5, on the basis of the previous characterization (Park et al. 2011). Activity was expressed as Enzyme Units per gram dry weight (DW) tissue. Enzyme Units were expressed as µmol (reducing) ends released per minute, unless otherwise stated. Determination of µmol reducing ends released upon hydrolysis of CMC was performed according to (Lever 1972) using different amounts of glucose as the calibration curve. Values of Enzyme Units were calculated as mean of two different time-points; the same reaction performed by using autoclaved extract was used as a negative control. Sampling of leaf material was performed according to the nomenclature reported in (Faè et al. 2017). Leaves were named starting from cotyledons. Numeration started from the dicotyledonous leaves, classified as first and second leaves, respectively. For enzymatic assays, similar amount of each leaf was sampled and gathered into 3 groups: L3–L4, L5–L10, L11–L13.

Gene Expression Analysis in N. tabacum

Gene expression analysis of *CBM3GH5-HA-VAC* was performed on 55-day-old plants using leaves at the similar developmental stage (L5–L6). Gene expression was analysed using *EF1α* as internal reference according to (Schmidt and Delaney 2010). Primers used for q-RT-PCR analysis are reported in Table S13.1 (CBHRT Fw/Rv, EFRT Fw/Rv). Experimental design and procedures were performed according to (Benedetti et al. 2018).

Purification of Recombinant Cellobiohydrolase from CBM3GH5-HA-VAC#4-11 Plants

Extraction in nondenaturing condition was performed from 5 g FW CBM3GH5-HA-VAC#4-11 leaf material, by a modified buffer (10 mM Tris-HCl pH 7.5, 0.4% Tween 20) at the optimized ratio [2 mL extraction buffer: 1 g FW leaf]. After 1 h incubation at 70 °C, the sample was centrifuged at 14,000× *g* 10 min to promote the precipitation of thermal-denaturated protein (Patchett et al. 1989). Supernatant was loaded on a Q-sepharose column (Amersham) equilibrated with 20 mM Tris-HCl pH 7.5. Elution was performed by using a stepwise NaCl gradient (from 0 to 1 M NaCl, with 0.1 M increments). Fractions eluted from the Q-sepharose column were tested by enzymatic assay and analyzed by SDS-PAGE for determination of enzyme concentration using different amount of BSA as calibration standard. Protein concentration was assessed using the Quantity-One software (Biorad). The specific activity of the enzyme (Units mg enzyme^{-1}) was used for determining the amount of recombinant enzyme in CBM3GH5HAVAC#4-11 plants. Deglycosylation of purified CBM3GH5 isoforms was performed by using PNGase A according to the manufacturer's instructions (P0707, New England Biolabs).

Saccharification Assay on Plant Materials

Saccharification of plant materials was performed according to (Lionetti et al. 2010) with some modifications. Before sampling, plants were incubated in the dark for 1 day in order to minimize the starch content. L5–L10 leaves and stems (delimited by the second and fifth internodes) were collected from 75-day-old tobacco plants. Samples were sterilized in a 1% sodium hypochlorite solution for 5 min and cut into 0.2-cm thin stripes with a razor blade; leaf and stem stripes were washed three times with sterile water. Plant samples (150–250 mg FW) were incubated in a filter-sterilized solution containing 50 mM Na Acetate pH 5.5, 0.4% (*v*/*v*) Tween-20, 0.02% (*w*/*v*) NaN_3 and 1% (*v*/*v*) Celluclast® 1.5 L (cellulase from *Trichoderma reesei* ATCC 26921). The incubation of leaf and stem stripes was carried out at either 55 or 25 °C. The enzymatic saccharification efficiency was determined as released reducing sugars vs. total sugars measured in the untreated plant material.

Determination of Total Carbohydrates in the Incubation Medium and in the Leaf Material

Determination of μmol reducing ends released upon hydrolysis was performed according to (Lever 1972) using difference amounts of glucose as calibration curve. Total carbohydrates in plant material were determined upon acid-hydrolysis in accordance with the Laboratory Analytical Procedure of the National Renewable Energy Laboratory (**https://www.nrel.gov/**): sample was first hydrolyzed in 72% (*v*/*v*) sulfuric acid at 30 °C for 1 h and then in 4% (*v*/*v*) sulfuric acid at 120 °C for 1 h. Total sugars were estimated spectrophotometrically by using the phenol–sulfuric acid assay (Dubois et al. 1956). Glucose released upon the enzymatic hydrolysis was quantified by a glucose-oxidase/peroxidase

assay (GOPOD assay kit, Megazyme) and expressed as released glucose vs. total sugars measured in the untreated plant material. Values are reported as mean of three different replicates.

13.5 Supplementary Materials

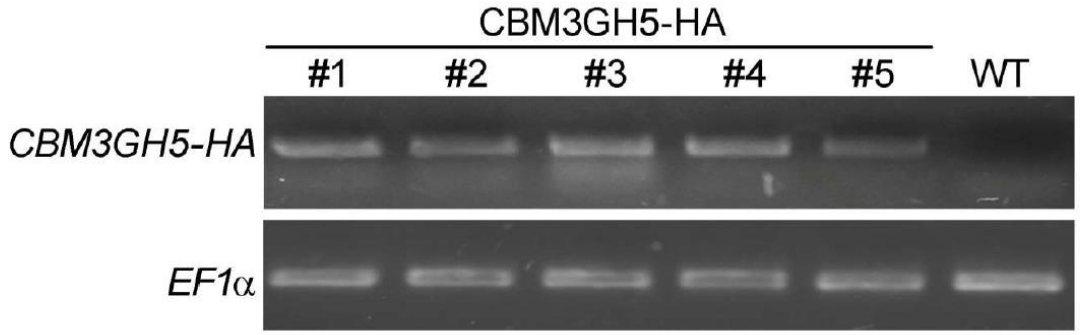

Figure S13.1. Presence of CBM3GH5-HA gene sequence in five representative T1 independent tobacco transformants. PCR analysis of CBM3GH5-HA was performed using 0.5 µg of gDNA from five T1 transformants. PCR analysis using 0.5 µg gDNA from WT plants was used as negative control. Amplification of EF1α (Eukaryotic Translation Elongation Factor 1 alpha) was used as internal reference.

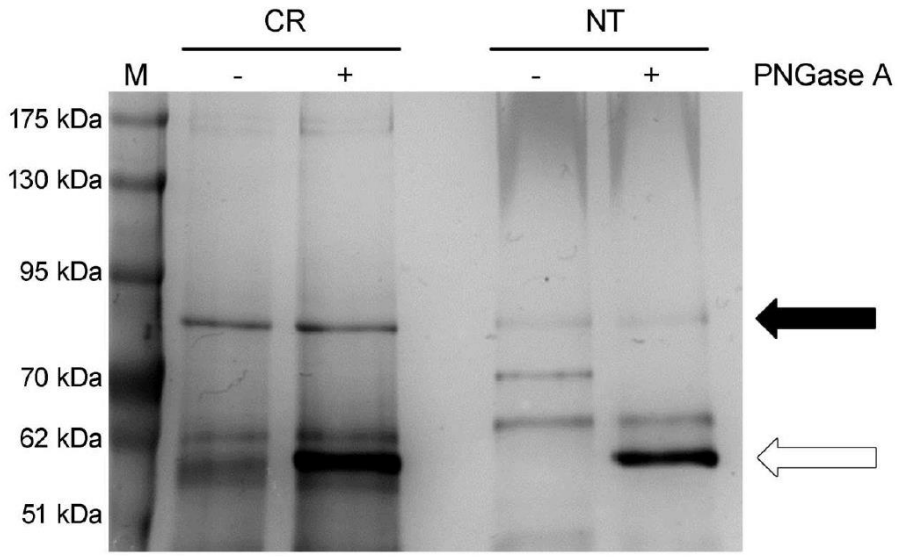

Figure S13.2. Deglycosylation of the partially purified CBM3GH5-HA-VAC by PNGase A treatment. SDS-PAGE analysis of fractions from AEC, before (-) and after (+) treatment with PNGase A. Analysis of Fx3 (see Figure 4b) is reported as representative result. Analysis of recombinant CBM3GH5-HA from C. reinhardtii (CR) is reported as control. Black and white arrow point to CBM3GH5-HA and PNGase A, respectively.

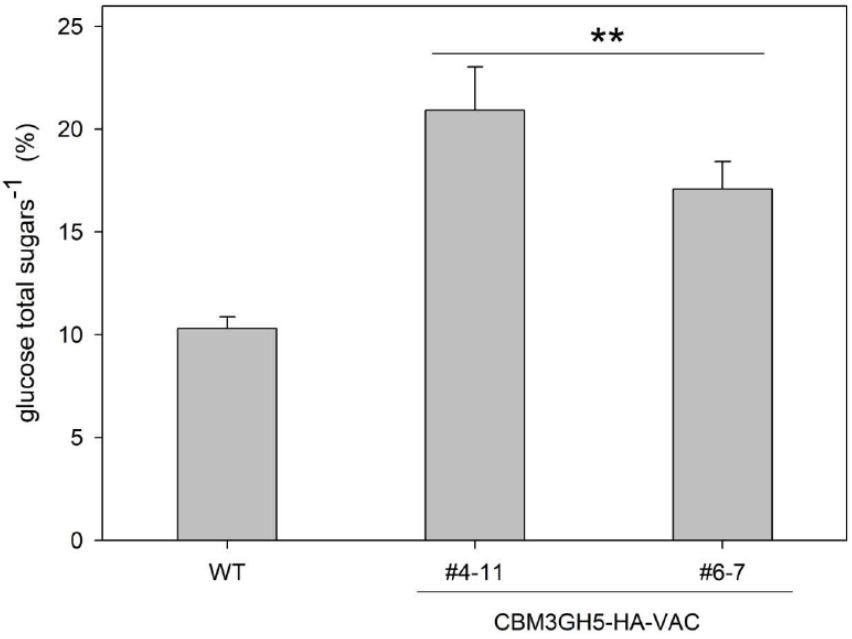

Figure S13.3. Transgenic CBM3GH5-HA-VAC plants release more glucose than WT upon the enzymatic hydrolysis. Glucose released from leaf tissues in the incubation medium by Celluclast treatment, upon 48 h of reaction at 55°C, as determined by GO-POD assay. The percentage is expressed as ratio between released glucose vs. total sugars measured in the untreated plant material. Data are expressed as mean ± SD (n≥3). Asterisks indicate statistically significant difference against control (WT) according to Student's t test (**, P <0.01).

Table S13.1. Primers used in this study. Primers used for the construction of the expression cassette CBM3GH5-HA in N. tabacum (Apo Fw, Apo Rv), gene sequencing (CBH785 Fw, CBH1565 Fw, CBH240 Rv) and gene expression analysis (CBHRT Fw, CBHRT Rv, EFRT Fw, EFRT Rv) are reported.

Primers	Sequence
Apo Fw	CTAAGTCTAGATGACTCAATTTAATATTCC
Apo Rv	CTAAGGAGCTCTTAAGCATAATCTGGAACATCATATG
CBH785 Fw	CCAGATGATACTAATGATGATTGGC
CBH1565 Fw	TGGGGAGGAAATCTTAGAGG
CBH240 Rv	CCAGTAGCTGGAGTAGAAACTGG
CBHRT Fw	GCTGGACAACTTCAACCAGG
CBHRT Rv	AGCCAAGACCAATCATTTCCT
EFRT Fw	GGTATCCGCTCCCAGAGTT
EFRT Rv	TTCTGAGCCACCTTGGAAAAC

Data S13.1. Gene sequences encoding CBM3GH5-HA and CBM3GH5-HA-VAC. Codon-optimized sequence of (A) CBM3GH5-HA and (B) CBM3GH5-HA-VAC used for the nuclear expression in Nicotiana tabacum. Underlined sequences: restriction sites used for cloning; green sequence: START codon; yellow sequence: signal peptide of Polygalacturonase Inhibiting Protein 2 from Phaseolus vulgaris encoding sequence; grey sequence: CBM3GH5 from *Caldicellulosiruptor saccharolyticus* encoding sequence; blue sequence: HA epitope encoding sequence; turquoise sequence: C-Terminal Pro-Peptide of Chitinase 1 from N. tabacum encoding sequence; red sequence: STOP codon.

A

TCTAGATGACTCAATTTAATATTCCAGTTACTATGTCTTCTTCTCTTTCTATTATTCTT
GTTATTCTTGTTTCTCTTAGAACTGCTCTTTCTGAAGGAGTTACTACTTCTTCTCC
AACTCCAACTCCAACTCCAACTGTTACTGTTACTCCAACTCCAACTCCAACTCCA
ACTCCAACTGTTACTGCTACTCCAACTCCAACTCCAACTCCAGTTTCTACTCCAG
CTACTGGAGGACAAATTAAGGTTCTTTATGCTAATAAGGAAACTAATTCTACTA
CTAATACTATTAGACCATGGCTTAAGGTTGTTAATTCTGGATCTTCTTCTATTGA
TCTTTCAAGGGTTACTATTAGATATTGGTATACTGTTGATGGAGAAAGGGCACA
ATCTGCTGTTTCTGATTGGGCTCAAATTGGAGCTTCTAATGTTACTTTTAAGTTT
GTTAAACTTTCTTCTTCTGTTTCTGGAGCTGATTATTATCTTGAAATTGGATTTAA
GTCTGGAGCTGGACAACTTCAACCAGGAAAGGATACTGGAGAAATTCAAATTA
GATTTAATAAGTCTGATTGGTCTAATTATAATCAAGGAAATGATTGGTCTTGGCT
TCAATCTATGACTTCTTATGGAGAAAATGAAAAGGTTACTGCTTATATTGATGG
AGTTCTTGTTTGGGGACAAGAACCATCTGGAGCTACTCCAGCTCCAACTATGAC
TGTTGCTCCAACTGCTACTCCAACTCCAACTCTTTCTCCAACTGTTACTCCAACT
CCAGCTCCAACTCAAACTGCTATTCCAACTCCAACTCTTACTCCAAATCCAACTC
CAACTTCTTCTATTCCAGATGATACTAATGATGATTGGCTTTATGTTTCTGGAAA
TAAGATTGTTGATAAGGATGGAAGACCAGTTTGGCTTACTGGAATTAATTGGTT
TGGATATAATACTGGAACTAATGTTTTTGATGGAGTTTGGTCTTGTAATCTTAAG
GATACTCTTGCTGAAATTGCTAATAGAGGATTTAATCTTCTTAGAGTTCCAATTT
CTGCTGAACTTATTCTTAATTGGTCTCAAGGAATTTATCCAAAGCCAAATATTAA
TTATTATGTTAATCCAGAACTTGAAGGAAAGAATTCTCTTGAAGTTTTTGATATT
GTTGTTCAAACTTGTAAGGAAGTTGGACTTAAGATTATGCTTGATATTCATTCTA
TTAAGACTGATGCTATGGGACATATTTATCCAGTTTGGTATGATGAAAAGTTTAC
TCCAGAAGATTTTTATAAGGCTTGTGAATGGATTACTAATAGATATAAGAATGA
TGATACTATTATTGCTTTTGATCTTAAGAATGAACCACATGGAAAGCCATGGCA
AGATACTACTTTTGCTAAGTGGGATAATTCTACTGATATTAATAATTGGAAGTAT
GCTGCTGAAACTTGTGCTAAGAGAATTCTTAATATTAATCCAAATCTTCTTATTG
TTATTGAAGGAATTGAAGCATATCCAAAGGATGATGTTACTTGGACTTCTAAGT
CTTCTTCTGATTATTATTCTACTTGGTGGGGAGGAAATCTTAGAGGAGTTAGAAA
GTATCCAATTAATCTTGGAAAGTATCAAAATAAGGTTGTTTATTCTCCACATGAT
TATGGACCATCTGTTTATCAACAACCATGGTTTTATCCAGGATTTACTAAGGAAT
CTCTTCTTCAAGATTGTTGGAGACCAAATTGGGCTTATATTATGGAAGAAAATA
TTGCTCCACTTCTTATTGGAGAATGGGGAGGACATCTTGATGGAGCTGATAATG
AAAAGTGGATGAAGTATCTTAGAGATTATATTATTGAAAATCATATTCATCATA
CTTTTTGGTGTTTTAATGCTAATTCTGGAGATACTGGAGGACTTGTTGGATATGA
TTTTACTACTTGGGATGAAAAGAAGTATTCTTTTCTTAAGCCAGCTCTTTGGCAA
GATTCTCAAGGAAGATTTGTTGGACTTGATCATAAGAGACCACTTGGAACTAAT
GGAAAGAATATTAATATTACTACTTATTATAATAATAATGAACCAGAACCAGTT

CCAGCTTCTAAGTATCCATATGATGTTCCAGATTATGCTTAAGAGCTC

B

TCTAGATGACTCAATTTAATATTCCAGTTACTATGTCTTCTTCTCTTTCTATTATTCTT
GTTATTCTTGTTTCTCTTAGAACTGCTCTTTCTGAAGGAGTTACTACTTCTTCTCC
AACTCCAACTCCAACTCCAACTGTTACTGTTACTCCAACTCCAACTCCAACTCCA
ACTCCAACTGTTACTGCTACTCCAACTCCAACTCCAACTCCAGTTTCTACTCCAG
CTACTGGAGGACAAATTAAGGTTCTTTATGCTAATAAGGAAACTAATTCTACTA
CTAATACTATTAGACCATGGCTTAAGGTTGTTAATTCTGGATCTTCTTCTATTGA
TCTTTCAAGGGTTACTATTAGATATTGGTATACTGTTGATGGAGAAAGGGCACA
ATCTGCTGTTTCTGATTGGGCTCAAATTGGAGCTTCTAATGTTACTTTTAAGTTT
GTTAAACTTTCTTCTTCTGTTTCTGGAGCTGATTATTATCTTGAAATTGGATTTAA
GTCTGGAGCTGGACAACTTCAACCAGGAAAGGATACTGGAGAAATTCAAATTA
GATTTAATAAGTCTGATTGGTCTAATTATAATCAAGGAAATGATTGGTCTTGGCT
TCAATCTATGACTTCTTATGGAGAAAATGAAAAGGTTACTGCTTATATTGATGG
AGTTCTTGTTTGGGGACAAGAACCATCTGGAGCTACTCCAGCTCCAACTATGAC
TGTTGCTCCAACTGCTACTCCAACTCCAACTCTTTCTCCAACTGTTACTCCAACT
CCAGCTCCAACTCAAACTGCTATTCCAACTCCAACTCTTACTCCAAATCCAACTC
CAACTTCTTCTATTCCAGATGATACTAATGATGATTGGCTTTATGTTTCTGGAAA
TAAGATTGTTGATAAGGATGGAAGACCAGTTTGGCTTACTGGAATTAATTGGTT
TGGATATAATACTGGAACTAATGTTTTTGATGGAGTTTGGTCTTGTAATCTTAAG
GATACTCTTGCTGAAATTGCTAATAGAGGATTTAATCTTCTTAGAGTTCCAATTT
CTGCTGAACTTATTCTTAATTGGTCTCAAGGAATTTATCCAAAGCCAAATATTAA
TTATTATGTTAATCCAGAACTTGAAGGAAAGAATTCTCTTGAAGTTTTTGATATT
GTTGTTCAAACTTGTAAGGAAGTTGGACTTAAGATTATGCTTGATATTCATTCTA
TTAAGACTGATGCTATGGGACATATTTATCCAGTTTGGTATGATGAAAAGTTTAC
TCCAGAAGATTTTTATAAGGCTTGTGAATGGATTACTAATAGATATAAGAATGA
TGATACTATTATTGCTTTTGATCTTAAGAATGAACCACATGGAAAGCCATGGCA
AGATACTACTTTTGCTAAGTGGGATAATTCTACTGATATTAATAATTGGAAGTAT
GCTGCTGAAACTTGTGCTAAGAGAATTCTTAATATTAATCCAAATCTTCTTATTG
TTATTGAAGGAATTGAAGCATATCCAAAGGATGATGTTACTTGGACTTCTAAGT
CTTCTTCTGATTATTATTCTACTTGGTGGGGAGGAAATCTTAGAGGAGTTAGAAA
GTATCCAATTAATCTTGGAAAGTATCAAAATAAGGTTGTTTATTCTCCACATGAT
TATGGACCATCTGTTTATCAACAACCATGGTTTTATCCAGGATTTACTAAGGAAT
CTCTTCTTCAAGATTGTTGGAGACCAAATTGGGCTTATATTATGGAAGAAAATA
TTGCTCCACTTCTTATTGGAGAATGGGGAGGACATCTTGATGGAGCTGATAATG
AAAAGTGGATGAAGTATCTTAGAGATTATATTATTGAAAATCATATTCATCATA
CTTTTTGGTGTTTTAATGCTAATTCTGGAGATACTGGAGGACTTGTTGGATATGA
TTTTACTACTTGGGATGAAAAGAAGTATTCTTTTCTTAAGCCAGCTCTTTGGCAA
GATTCTCAAGGAAGATTTGTTGGACTTGATCATAAGAGACCACTTGGAACTAAT
GGAAAGAATATTAATATTACTACTTATTATAATAATAATGAACCAGAACCAGTT
CCAGCTTCTAAGTATCCATATGATGTTCCAGATTATGCTGGAAATGGACTTCTTG
TTGATACTATGTAAGAGCTC

REFERENCES

Aziz A, Gauthier A, Bézier A, Poinssot B, Joubert J-M, Pugin A, Heyraud A, Baillieul F (2007) Elicitor and resistance-inducing activities of beta-1,4 cellodextrins in grapevine, comparison with beta-1,3 glucans and alpha-1,4 oligogalacturonides. J Exp Bot 58:1463–72 . https://doi.org/10.1093/jxb/erm008

Benedetti M, Barera S, Longoni P, Guardini Z, Herrero Garcia N, Bolzonella D, Lopez-Arredondo D, Herrera-Estrella L, Goldschmidt-Clermont M, Bassi R, Dall'Osto L (2020) A microalgal-based preparation with synergistic cellulolytic and detoxifying action towards chemical-treated lignocellulose. Plant Biotechnol J n/a: . https://doi.org/10.1111/pbi.13447

Benedetti M, Locci F, Gramegna G, Sestili F, Savatin DV (2019a) Green production and biotechnological applications of cell wall lytic enzymes. Appl Sci 9:5012. https://doi.org/10.3390/app9235012

Benedetti M, Pontiggia D, Raggi S, Cheng Z, Scaloni F, Ferrari S, Ausubel FM, Cervone F, De Lorenzo G (2015) Plant immunity triggered by engineered in vivo release of oligogalacturonides, damage-associated molecular patterns. Proc Natl Acad Sci 112:5533–5538 . https://doi.org/10.1073/pnas.1504154112

Benedetti M, Vecchi V, Betterle N, Natali A, Bassi R, Dall'Osto L (2019b) Design of a highly thermostable hemicellulose-degrading blend from Thermotoga neapolitana for the treatment of lignocellulosic biomass. J Biotechnol 296:42–52 . https://doi.org/10.1016/j.jbiotec.2019.03.005

Benedetti M, Verrascina I, Pontiggia D, Locci F, Mattei B, De Lorenzo G, Cervone F (2018) Four Arabidopsis berberine bridge enzyme-like proteins are specific oxidases that inactivate the elicitor-active oligogalacturonides. Plant J. https://doi.org/10.1111/tpj.13852

Bindschedler L V., Tuerck J, Maunders M, Ruel K, Petit-Conil M, Danoun S, Boudet AM, Joseleau JP, Bolwell GP (2007) Modification of hemicellulose content by antisense down-regulation of UDP-glucuronate decarboxylase in tobacco and its consequences for cellulose extractability. Phytochemistry 68:2635–2648 . https://doi.org/10.1016/j.phytochem.2007.08.029

Biswal AK, Atmodjo MA, Li M, Baxter HL, Yoo CG, Pu Y, Lee Y-C, Mazarei M, Black IM, Zhang J-Y, Ramanna H, Bray AL, King ZR, LaFayette PR, Pattathil S, Donohoe BS, Mohanty SS, Ryno D, Yee K, Thompson OA, Rodriguez M, Dumitrache A, Natzke J, Winkeler K, Collins C, Yang X, Tan L, Sykes RW, Gjersing EL, Ziebell A, Turner GB, Decker SR, Hahn MG, Davison BH, Udvardi MK, Mielenz JR, Davis MF, Nelson RS, Parrott WA, Ragauskas AJ, Neal Stewart C, Mohnen D (2018) Sugar release and growth of biofuel crops are improved by downregulation of pectin biosynthesis. Nat Biotechnol 36:249–257 . https://doi.org/10.1038/nbt.4067

Boudart G, Charpentier M, Lafitte C, Martinez Y, Jauneau A, Gaulin E, Esquerré-Tugayé M-T, Dumas B (2003) Elicitor activity of a fungal endopolygalacturonase in tobacco requires a functional catalytic site and cell wall localization. Plant Physiol. https://doi.org/10.1104/pp.011585

Capodicasa C, Vairo D, Zabotina O, McCartney L, Caprari C, Mattei B, Manfredini C, Aracri B, Benen J, Knox JP, De Lorenzo G, Cervone F (2004) Targeted modification of homogalacturonan by transgenic expression of a fungal polygalacturonase alters plant growth. Plant Physiol 135:1294–304 . https://doi.org/10.1104/pp.104.042788

C**arrard G, Koivula A, Soderlund H, Beguin P** (2000) Cellulose-binding domains promote hydrolysis of different sites on crystalline cellulose. Proc Natl Acad Sci. https://doi.org/10.1073/pnas.160216697

Castiglia D, Sannino L, Marcolongo L, Ionata E, Tamburino R, De Stradis A, Cobucci-Ponzano B, Moracci M, La Cara F, Scotti N (2016) High-level expression of thermostable cellulolytic enzymes

in tobacco transplastomic plants and their use in hydrolysis of an industrially pretreated Arundo donax L. biomass. Biotechnol Biofuels. https://doi.org/10.1186/s13068-016-0569-z

Choi HW, Klessig DF (2016) DAMPs, MAMPs, and NAMPs in plant innate immunity. BMC Plant Biol.

Claude SJD, Marie-Agnès G, Catalina R, Nadine P, Marie-Christine KM, Jean-Marc N, Loïc F, Véronique G (2005) Targeting of proConA to the plant vacuole depends on its nine amino-acid C-terminal propeptide. Plant Cell Physiol. https://doi.org/10.1093/pcp/pci176

D'Ovidio R, Raiola A, Capodicasa C, Devoto A, Pontiggia D, Roberti S, Galletti R, Conti E, O'Sullivan D, De Lorenzo G (2004) Characterization of the complex locus of bean encoding polygalacturonase-inhibiting proteins reveals subfunctionalization for defense against fungi and insects. Plant Physiol. https://doi.org/10.1104/pp.104.044644

Dai Z, Quesenberry RD, Gao J, Hooker BS (1999) Expression of Trichoderma reesei exo-cellobiohydrolase I in transgenic tobacco leaves and calli. Appl Biochem Biotechnol. https://doi.org/ABAB:79:1-3:689 [pii]

de Azevedo Souza C, Li S, Lin AZ, Boutrot F, Grossmann G, Zipfel C, Somerville SC (2017) Cellulose-derived oligomers act as damage-associated molecular patterns and trigger defense-like responses. Plant Physiol 173:2383–2398 . https://doi.org/10.1104/pp.16.01680

Dubois M, Gilles KA, Hamilton JK, Rebers PA, Smith F (1956) Colorimetric Method for Determination of Sugars and Related Substances. Anal Chem 28:350–356 . https://doi.org/10.1021/ac60111a017

Eamens A, Wang M-B, Smith NA, Waterhouse PM (2008) RNA silencing in plants: yesterday, today, and tomorrow. Plant Physiol 147:456–68 . https://doi.org/10.1104/pp.108.117275

Faè M, Accossato S, Cella R, Fontana F, Goldschmidt-Clermont M, Leelavathi S, Reddy VS, Longoni P (2017) Comparison of transplastomic Chlamydomonas reinhardtii and Nicotiana tabacum expression system for the production of a bacterial endoglucanase. Appl Microbiol Biotechnol 101:4085–4092 . https://doi.org/10.1007/s00253-017-8164-1

Ferrari S, Savatin D V., Sicilia F, Gramegna G, Cervone F, De Lorenzo G (2013) Oligogalacturonides: Plant damage-associated molecular patterns and regulators of growth and development. Front. Plant Sci. 4 . https://doi.org/10.3389/fpls.2013.00049

Frías M, González M, González C, Brito N (2019) A 25-Residue Peptide From Botrytis cinerea Xylanase BcXyn11A Elicits Plant Defenses. Front. Plant Sci. 10:474 . https://doi.org/10.3389/fpls.2019.00474

Gama R, Van Dyk JS, Pletschke BI (2015) Optimisation of enzymatic hydrolysis of apple pomace for production of biofuel and biorefinery chemicals using commercial enzymes. 3 Biotech 5:1075–1087 . https://doi.org/10.1007/s13205-015-0312-7

Giovannoni M, Gramegna G, Benedetti M, Mattei B (2020) Industrial Use of Cell Wall Degrading Enzymes: The Fine Line Between Production Strategy and Economic Feasibility . Front. Bioeng. Biotechnol. 8:356

Greene ER, Himmel ME, Beckham GT, Tan Z (2015) Glycosylation of Cellulases. In: Advances in carbohydrate chemistry and biochemistry. pp 63–112

Harrison MD, Geijskes J, Coleman HD, Shand K, Kinkema M, Palupe A, Hassall R, Sainz M, Lloyd R, Miles S, Dale JL (2011) Accumulation of recombinant cellobiohydrolase and endoglucanase in the leaves of mature transgenic sugar cane. Plant Biotechnol J. https://doi.org/10.1111/j.1467-7652.2011.00597.x

Harrison MD, Geijskes RJ, Lloyd R, Miles S, Palupe A, Sainz MB, Dale JL (2014) Recombinant Cellulase Accumulation in the Leaves of Mature, Vegetatively Propagated Transgenic Sugarcane.

Mol Biotechnol 56:795–802 . https://doi.org/10.1007/s12033-014-9758-9

Herman E, Larkins B (1999) Protein storage bodies and vacuoles. Plant Cell 11:601–14

Hinz G (1999) Vacuolar Storage Proteins and the Putative Vacuolar Sorting Receptor BP-80 Exit the Golgi Apparatus of Developing Pea Cotyledons in Different Transport Vesicles. Plant Cell Online. https://doi.org/10.1105/tpc.11.8.1509

Horsch RB, Fry JE, Hoffmann NL, Eichholtz D, Rogers SG, Fraley RT (1985) A simple and general method for transferring genes into plants

Hraška M, Rakouský S, Čurn V (2008) Tracking of the CaMV-35S promoter performance in GFP transgenic tobacco, with a special emphasis on flowers and reproductive organs, confirmed its predominant activity in vascular tissues. In: Plant Cell, Tissue and Organ Culture

Jiang L, Phillips TE, Hamm CA, Drozdowicz YM, Rea PA, Maeshima M, Rogers SW, Rogers JC (2001) The protein storage vacuole: a unique compound organelle. J Cell Biol 155:991–1002 . https://doi.org/10.1083/jcb.200107012

Jin S, Kanagaraj A, Verma D, Lange T, Daniell H (2011) Release of Hormones from Conjugates: Chloroplast Expression of β-Glucosidase Results in Elevated Phytohormone Levels Associated with Significant Increase in Biomass and Protection from Aphids or Whiteflies Conferred by Sucrose Esters. Plant Physiol 155:222 LP – 235 . https://doi.org/10.1104/pp.110.160754

Klose H, Günl M, Usadel B, Fischer R, Commandeur U (2013) Ethanol inducible expression of a mesophilic cellulase avoids adverse effects on plant development. Biotechnol Biofuels 6:53 . https://doi.org/10.1186/1754-6834-6-53

Kubicek CP, Starr TL, Glass NL (2014) Plant Cell Wall–Degrading Enzymes and Their Secretion in Plant-Pathogenic Fungi. Annu Rev Phytopathol 52:427–451 . https://doi.org/10.1146/annurev-phyto-102313-045831

Lagaert S, Beliën T, Volckaert G (2009) Plant cell walls: Protecting the barrier from degradation by microbial enzymes. Semin. Cell Dev. Biol.

Lee SC, West CA (1981) Polygalacturonase from Rhizopus stolonifer, an Elicitor of Casbene Synthetase Activity in Castor Bean (Ricinus communis L.) Seedlings. Plant Physiol 67:633–9

Lever M (1972) A new reaction for colorimetric determination of carbohydrates. Anal Biochem 47:273–279 . https://doi.org/10.1016/0003-2697(72)90301-6

Li Q, Song J, Peng S, Wang JP, Qu G-Z, Sederoff RR, Chiang VL (2014) Plant biotechnology for lignocellulosic biofuel production. Plant Biotechnol J 12:1174–1192 . https://doi.org/10.1111/pbi.12273

Lionetti V, Francocci F, Ferrari S, Volpi C, Bellincampi D, Galletti R, D'Ovidio R, De Lorenzo G, Cervone F (2010) Engineering the cell wall by reducing de-methyl-esterified homogalacturonan improves saccharification of plant tissues for bioconversion. Proc Natl Acad Sci 107:616–621 . https://doi.org/10.1073/pnas.0907549107

Ma CJ (2008) Cellulase elicitor induced accumulation of capsidiol in Capsicum annumm L. suspension cultures. Biotechnol Lett 30:961–965 . https://doi.org/10.1007/s10529-007-9624-y

Ma Y, Han C, Chen J, Li H, He K, Liu A, Li D (2015) Fungal cellulase is an elicitor but its enzymatic activity is not required for its elicitor activity. Mol Plant Pathol 16:14–26 . https://doi.org/10.1111/mpp.12156

Marin Viegas VS, Ocampo CG, Petruccelli S (2017) Vacuolar deposition of recombinant proteins in plant vegetative organs as a strategy to increase yields. Bioengineered

Mir BA, Mewalal R, Mizrachi E, Myburg AA, Cowan DA (2014) Recombinant hyperthermophilic enzyme expression in plants: A novel approach for lignocellulose digestion. Trends Biotechnol.

32:281–289

Mir BA, Myburg AA, Mizrachi E, Cowan DA (2017) In planta expression of hyperthermophilic enzymes as a strategy for accelerated lignocellulosic digestion. Sci Rep 7: . https://doi.org/10.1038/s41598-017-11026-1

Neuhaus JM, Ahl-Goy P, Hinz U, Flores S, Meins F (1991a) High-level expression of a tobacco chitinase gene in Nicotiana sylvestris. Susceptibility of transgenic plants to Cercospora nicotianae infection. Plant Mol Biol. https://doi.org/10.1007/BF00017924

Neuhaus JM, Sticher L, Meins F, Boller T (1991b) A short C-terminal sequence is necessary and sufficient for the targeting of chitinases to the plant vacuole. Proc Natl Acad Sci U S A 88:10362–6

Park JI, Kent MS, Datta S, Holmes BM, Huang Z, Simmons BA, Sale KL, Sapra R (2011) Enzymatic hydrolysis of cellulose by the cellobiohydrolase domain of CelB from the hyperthermophilic bacterium Caldicellulosiruptor saccharolyticus. Bioresour Technol 102:5988–5994 . https://doi.org/10.1016/j.biortech.2011.02.036

Park M, Kim SJ, Vitale A, Hwang I (2004) Identification of the protein storage vacuole and protein targeting to the vacuole in leaf cells of three plant species. Plant Physiol 134:625–39 . https://doi.org/10.1104/pp.103.030635

Patchett ML, Neal TL, Schofield LR, Strange RC, Daniel RM, Morgan HW (1989) Heat treatment purification of thermostable cellulase and hemicellulase enzymes expressed in E. coli. Enzyme Microb Technol 11:113–115 . https://doi.org/10.1016/0141-0229(89)90069-0

Petersen K, Bock R (2011) High-level expression of a suite of thermostable cell wall-degrading enzymes from the chloroplast genome. Plant Mol Biol. https://doi.org/10.1007/s11103-011-9742-8

Poinssot B, Vandelle E, Bentéjac M, Adrian M, Levis C, Brygoo Y, Garin J, Sicilia F, Coutos-Thévenot P, Pugin A (2003) The endopolygalacturonase 1 from Botrytis cinerea activates grapevine defense reactions unrelated to its enzymatic activity. Mol Plant Microbe Interact. https://doi.org/10.1094/MPMI.2003.16.6.553

Poole DM, Morag E, Lamed R, Bayer EA, Hazlewood GP, Gilbert HJ (1992) Identification of the cellulose-binding domain of the cellulosome subunit S1 from Clostridium thermocellum YS. FEMS Microbiol Lett. https://doi.org/10.1111/j.1574-6968.1992.tb05563.x

Puigbò P, Guzmán E, Romeu A, Garcia-Vallvé S (2007) OPTIMIZER: a web server for optimizing the codon usage of DNA sequences. Nucleic Acids Res 35:W126–W131 . https://doi.org/10.1093/nar/gkm219

Rogers SG, Horsch RB, Fraley RT (1986) Gene transfer in plants: Production of transformed plants using Ti plasmid vectors. Methods Enzymol 118:627–640 . https://doi.org/10.1016/0076-6879(86)18105-5

S**armiento F, Peralta R, Blamey JM** (2015) Cold and hot extremozymes: Industrial relevance and current trends. Front. Bioeng. Biotechnol. 3 . https://doi.org/10.3389/fbioe.2015.00148

Schmidt GW, Delaney SK (2010) Stable internal reference genes for normalization of real-time RT-PCR in tobacco (Nicotiana tabacum) during development and abiotic stress. Mol Genet Genomics. https://doi.org/10.1007/s00438-010-0511-1

Stigliano E, Di Sansebastiano GP, Neuhaus JM (2014) Contribution of chitinase A's C-terminal vacuolar sorting determinant to the study of soluble protein compartmentation. Int J Mol Sci 15:11030–9 . https://doi.org/10.3390/ijms150611030

Tomassetti S, Pontiggia D, Verrascina I, Reca IB, Francocci F, Salvi G, Cervone F, Ferrari S (2015) Controlled expression of pectic enzymes in Arabidopsis thaliana enhances biomass conversion

without adverse effects on growth. Phytochemistry 112:221–230 . https://doi.org/10.1016/j.phytochem.2014.08.026

Weng JK, Li X, Bonawitz ND, Chapple C (2008) Emerging strategies of lignin engineering and degradation for cellulosic biofuel production. Curr. Opin. Biotechnol. 19(2):166-72 https://doi.org/10.1016/j.copbio.2008.02.014

Yang Y, Li R, Qi M (2000) In vivo analysis of plant promoters and transcription factors by agroinfiltration of tobacco leaves. Plant J 22:543–51 .

Ziegelhoffer T, Will J, Austin-Phillips S (1999) Expression of bacterial cellulase genes in transgenic alfalfa (Medicago sativa L.), potato (Solanum tuberosum L.) and tobacco (Nicotiana tabacum L.). Mol Breed 5:309–318 . https://doi.org/10.1023/A:1009646830403

Zipfel C (2014) Plant pattern-recognition receptors. Trends Immunol 35:345–351 . https://doi.org/10.1016/j.it.2014.05.004

Zuo J, Niu QW, Chua NH (2000) An estrogen receptor-based transactivator XVE mediates highly inducible gene expression in transgenic plants. Plant J 24:265–273 . https://doi.org/https://doi.org/10.1046/j.1365-313x.2000.00868.x